CILIATE BIODIVERSITY AND EVOLUTION FROM MORPHOLOGICAL, GENOMIC AND EPIGENOMIC VIEWS

EDITED BY: Xiao Chen, Lifang Li, Hongbo Pan and Xiaoshou Liu
PUBLISHED IN: Frontiers in Marine Science

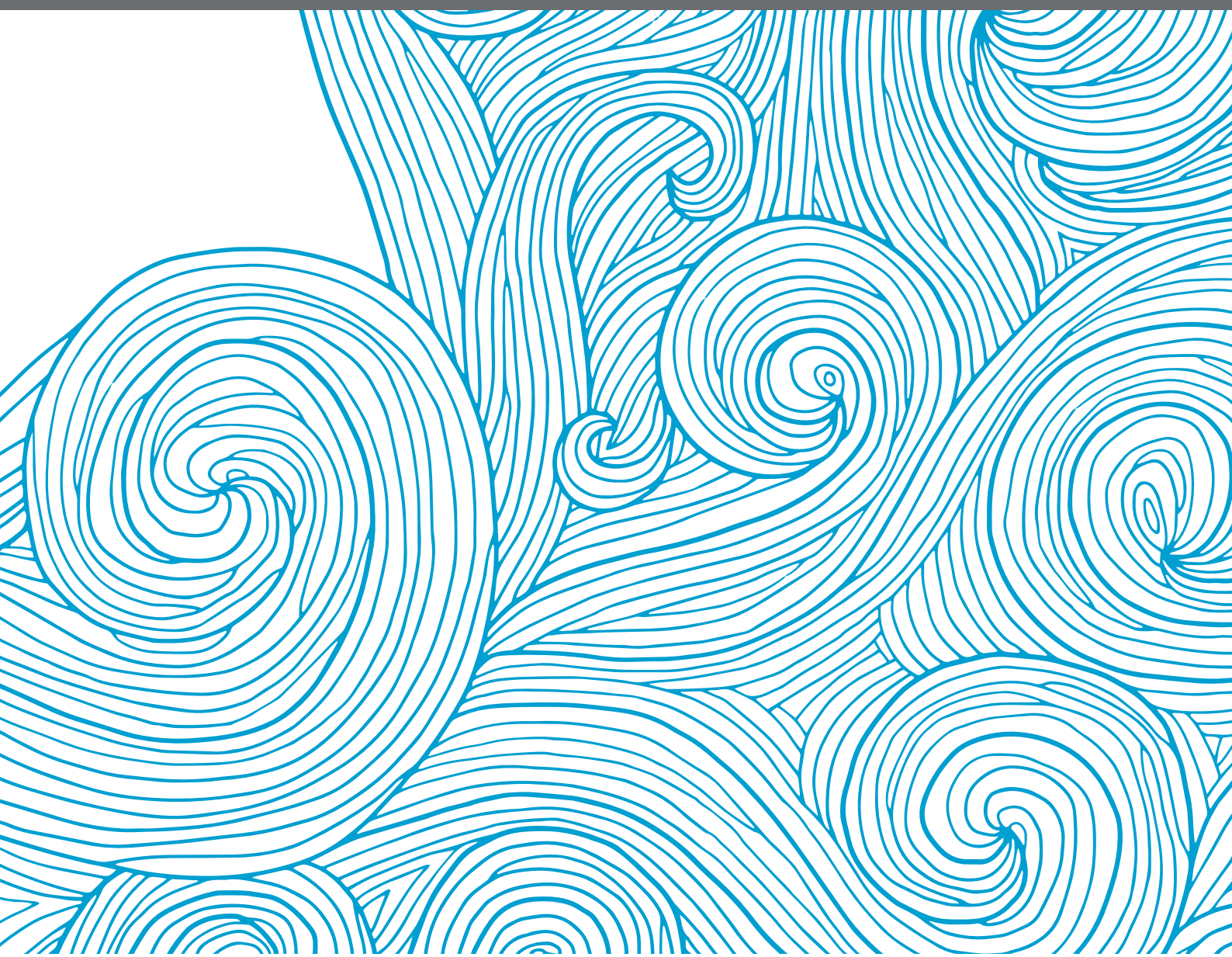

frontiers Research Topics

frontiers

ISSN 1664-8714
ISBN 978-2-88966-845-8
DOI 10.3389/978-2-88966-845-8

About Frontiers

Frontiers is more than just an open-access publisher of scholarly articles: it is a pioneering approach to the world of academia, radically improving the way scholarly research is managed. The grand vision of Frontiers is a world where all people have an equal opportunity to seek, share and generate knowledge. Frontiers provides immediate and permanent online open access to all its publications, but this alone is not enough to realize our grand goals.

Frontiers Journal Series

The Frontiers Journal Series is a multi-tier and interdisciplinary set of open-access, online journals, promising a paradigm shift from the current review, selection and dissemination processes in academic publishing. All Frontiers journals are driven by researchers for researchers; therefore, they constitute a service to the scholarly community. At the same time, the Frontiers Journal Series operates on a revolutionary invention, the tiered publishing system, initially addressing specific communities of scholars, and gradually climbing up to broader public understanding, thus serving the interests of the lay society, too.

Dedication to Quality

Each Frontiers article is a landmark of the highest quality, thanks to genuinely collaborative interactions between authors and review editors, who include some of the world's best academicians. Research must be certified by peers before entering a stream of knowledge that may eventually reach the public - and shape society; therefore, Frontiers only applies the most rigorous and unbiased reviews.
Frontiers revolutionizes research publishing by freely delivering the most outstanding research, evaluated with no bias from both the academic and social point of view. By applying the most advanced information technologies, Frontiers is catapulting scholarly publishing into a new generation.

What are Frontiers Research Topics?

Frontiers Research Topics are very popular trademarks of the Frontiers Journals Series: they are collections of at least ten articles, all centered on a particular subject. With their unique mix of varied contributions from Original Research to Review Articles, Frontiers Research Topics unify the most influential researchers, the latest key findings and historical advances in a hot research area! Find out more on how to host your own Frontiers Research Topic or contribute to one as an author by contacting the Frontiers Editorial Office: frontiersin.org/about/contact

CILIATE BIODIVERSITY AND EVOLUTION FROM MORPHOLOGICAL, GENOMIC AND EPIGENOMIC VIEWS

Topic Editors:
Xiao Chen, Columbia University Irving Medical Center, United States
Lifang Li, Shandong University, Weihai, China
Hongbo Pan, Shanghai Ocean University, China
Xiaoshou Liu, Ocean University of China, China

Citation: Chen, X., Li, L., Pan, H., Liu, X., eds. (2021). Ciliate Biodiversity and Evolution from Morphological, Genomic and Epigenomic Views. Lausanne: Frontiers Media SA. doi: 10.3389/978-2-88966-845-8

Table of Contents

05 ***Environmental Factors and Pollution Stresses Select Bacterial Populations in Association With Protists***
Songbao Zou, Qianqian Zhang, Xiaoli Zhang, Christine Dupuy and Jun Gong

24 ***Ontogeny and Phylogeny of a New Hypotrichous Ciliate (Protista, Ciliophora),* Metaurostylopsis alrasheidi *n. sp., With Establishment of a New Genus* Monourostylopsis *n. gen.***
Wenya Song, Yu Qiao, Jingyi Dong, William A. Bourland, Tengteng Zhang and Xiaotian Luo

38 ***Taxonomy and Molecular Phylogeny of Three Species of Scuticociliates From China:* Citrithrix smalli *gen. nov., sp. nov.,* Homalogastra binucleata *sp. nov. and* Uronema orientalis *Pan et al., 2015 (Protozoa, Ciliophora, Oligohymenophorea), With the Proposal of a New Family, Citrithrixidae fam. nov.***
Mingjian Liu, Chundi Wang, Xiaozhong Hu, Zhishuai Qu, Limin Jiang, Saleh A. Al-Farraj, Hamed A. El-Serehy, Alan Warren and Weibo Song

53 ***Single-Cell Genomic Sequencing of Three Peritrichs (Protista, Ciliophora) Reveals Less Biased Stop Codon Usage and More Prevalent Programmed Ribosomal Frameshifting Than in Other Ciliates***
Xiao Chen, Chundi Wang, Bo Pan, Borong Lu, Chao Li, Zhuo Shen, Alan Warren and Lifang Li

61 ***Novel Contributions to the Taxonomy of the Ciliates Genus* Euplotes *(Ciliophora, Euplotida): Redescription of Two Poorly Known Species, With a Brief Note on the Distributions of This Genus in Coastal Waters of Southern China***
Weiwei Liu, Jiamei Jiang, Yehui Tan and Xiaofeng Lin

73 ***Systematics and Multi-Gene Phylogeny of the Subfamily Nothoholostichinae (Ciliophora, Hypotrichia), With Integrative Description of a New Marine Species* Nothoholosticha luporinii *n. sp.***
Tengyue Zhang, Yurui Wang, Ting Cheng, Jiyang Ma, Peter Vd'ačný, Weibo Song and Chen Shao

90 ***Ultrastructural Features of an Abundant and Ubiquitous Marine Ciliate,* Uronychia binucleata *(Protista, Ciliophora, Euplotida)***
Jingyi Dong, Xinpeng Fan, Tengyue Zhang, Saleh A. Al-Farraj, Thorsten Stoeck, Honggang Ma and Lifang Li

103 ***Morphogenesis of the Ciliature During Sexual Process of Conjugation in the Ciliated Protist* Euplotes raikovi**
Usman Asghar, Yong Chi, Yunyi Gao, Borong Lu, Yaohan Jiang Ruitao Gong, Honggang Ma, Khaled A. S. Al-Rasheid and Feng Gao

112 ***Morphology and Molecular Phylogeny of Four Trachelocercid Ciliates (Protozoa, Ciliophora, Karyorelictea) Found in Marine Coastal Habitats of Northern China, With Description of a New Genus, Two New Species and a New Combination***
Mingzhen Ma, Yuqing Li, Honggang Ma, Khaled A. S. Al-Rasheid, Alan Warren, Yurui Wang and Ying Yan

127 *Taxonomy of Three Oxytrichids (Protozoa, Ciliophora, Hypotrichia), With Establishment of the New Species* **Rubrioxytricha guangzhouensis** *spec. nov.*
Xiaotian Luo, Jie Huang, William A. Bourland, Hamed A. El-Serehy, Saleh A. Al-Farraj, Xumiao Chen and Weibo Song

144 *A New Record of* **Oxytricha granulifera granulifera** *Foissner and Adam, 1983 (Protozoa, Ciliophora, Oxytrichidae) From a Hot Spring in Iceland, With Notes on Its Abnormal Form During Cultivation*
Rong Zhu, Zhishuai Qu, Qi Zhang, Sabine Filker, Thorsten Stoeck, Fengchao Li and Xiaozhong Hu

155 *Species Diversity of the Pleurostomatid Ciliate Genus* **Amphileptus** *(Ciliophora, Haptoria), With Notes on the Taxonomy and Molecular Phylogeny of Three Species*
Lei Wu, Jiqiu Li, Alan Warren and Xiaofeng Lin

171 *Gastronautidae Deroux, 1994 and* **Trithigmostoma** *Jankowski, 1967: Evolutionary Links Among Cyrtophorian Ciliates (Protista, Ciliophora, and Phyllopharyngea)*
Zhishuai Qu, Hongbo Pan, Congcong Wang, Honggang Ma, Thorsten Stoeck and Xiaozhong Hu

185 *Genetic Diversity in Marine Planktonic Ciliates (Alveolata, Ciliophora) Suggests Distinct Geographical Patterns – Data From Chinese and European Coastal Waters*
Maximilian H. Ganser, Dominik Forster, Weiwei Liu, Xiaofeng Lin, Thorsten Stoeck and Sabine Agatha

207 *Molecular Evolutionary Analyses of* **Euplotes** *Species Living in Freshwater and Marine Habitats: A Mitogenomic Perspective*
Ning Huang, Shuai Chen, Ming He, Qi Song, Lina Hou, Yan Zhao, Shuo Zhao and Miao Miao

frontiers in Marine Science

ORIGINAL RESEARCH
published: 07 August 2020
doi: 10.3389/fmars.2020.00659

Environmental Factors and Pollution Stresses Select Bacterial Populations in Association With Protists

*Songbao Zou[1,2,3], Qianqian Zhang[1], Xiaoli Zhang[1], Christine Dupuy[4] and Jun Gong[3,5]**

[1] Yantai Institute of Coastal Zone Research, Chinese Academy of Sciences, Yantai, China, [2] University of Chinese Academy of Sciences, Beijing, China, [3] School of Marine Sciences, Sun Yat-sen University, Zhuhai, China, [4] Littoral Environnement et Sociétés (LIENSs) UMR 7266 CNRS, University of La Rochelle, La Rochelle, France, [5] Southern Marine Science and Engineering Guangdong Laboratory (Zhuhai), Zhuhai, China

Digestion-resistant bacteria (DRB) refer to the ecological bacterial group that can be ingested, but not digested by protistan grazers, thus forming a specific type of bacteria-protist association. To test the hypothesis that the environment affects the assembly of DRB in protists, a mixotrophic ciliate, *Paramecium bursaria*, and a heterotrophic ciliate, *Euplotes vannus*, were reared at different temperatures, light conditions, and concentration gradients of antibiotic oxytetracycline and heavy metals. Community profiling indicated that the composition of DRB in both species varied significantly across the manipulated conditions, except for in *P. bursaria* under light/dark treatments. Clone library analysis of bacterial 16S rRNA genes showed that DRB were diverse. *Pseudomonas* became more abundant during the warmer treatment of *P. bursaria*, whereas the dominance of *Pseudoalteromonas* weakened and *Vibrio* became more abundant in *E. vannus* at a higher temperature. During the treatment of diel light:dark cycles, *Aestuariibacter* and *Alteromonas* were selected for in *E. vannus* but not *Pseudoalteromonas*, which was highly represented in the all-light and all-dark treatments. In contrast, *P. bursaria* consistently hosted *Nevskia*, *Curvibacter*, and *Asticcacaulis* under all light conditions. There were many bacterial species co-resistant to oxytetracycline and to protistan digestion, in which *Sphingomonas, Alteromonas*, *Aestuariibacter*, *Puniceicoccaceae* (Verrucomicrobia), *Pseudomonas*, and *Sulfitobacter* were frequently abundant. *Flectobacillus* and *Aestuariibacter* were major lead-resistant bacteria associated with the studied protists. *Acinetobacter* and *Hydrogenophaga* were abundant in the *P. bursaria* treated with a high dose of mercury. *Aestuariibacter* was found as a dominant group of DRB in *E. vannus* across all cadmium treatments. In summary, this study demonstrates for the first time that environmental stress selects for bacterial populations associated with protists and that there are diverse bacterial species that not only are resistant to pollution stresses but can also survive protistan predation. This work highlights that bacteria-protists associations need to be taken into account in understanding ecological and environmental issues, such as resilience of bacterial community and function, microbial co-occurrence, and quantity and distribution of antibiotic resistant bacteria and genes.

Keywords: antibiotic resistance, interkingdom interaction, light, metal resistance, protozoa, warming

OPEN ACCESS

Edited by:
Hongbo Pan,
Shanghai Ocean University, China

Reviewed by:
Martina Schrallhammer,
University of Freiburg, Germany
Zhenzhen Yi,
South China Normal University, China

***Correspondence:**
Jun Gong
gongj27@mail.sysu.edu.cn

Specialty section:
This article was submitted to Marine Evolutionary Biology, Biogeography and Species Diversity, a section of the journal Frontiers in Marine Science

Received: *15 June 2020*
Accepted: *21 July 2020*
Published: *07 August 2020*

Citation:
Zou S, Zhang Q, Zhang X, Dupuy C and Gong J (2020) Environmental Factors and Pollution Stresses Select Bacterial Populations in Association With Protists. Front. Mar. Sci. 7:659. doi: 10.3389/fmars.2020.00659

INTRODUCTION

Bacteria and protists are major players in the microbial food web of aquatic environments, in which heterotrophic bacteria incorporate dissolved organic matter and nutrients for growth and transfer carbon and energy to higher trophic levels as a consequence of predation by small protists (Azam et al., 1983). In the last two decades, much efforts have been made to understand how and why protists selectively graze on bacteria or how bacteria become resistant to protistan predation. It has been demonstrated that changes in bacterial cell size, morphology, movement, cell-cell configuration in space, and chemical resistance contribute to their anti-predation (Matz and Kjelleberg, 2005; Pernthaler, 2005; Jousset, 2012). Furthermore, recent studies have provided evidence for another strategy of anti-predation—some bacterial populations in aquatic environments can be ingested, but not digested by protistan grazers, thus potentially forming microbial associations with the protistan hosts (e.g., First et al., 2012; Šimek et al., 2013; Gong et al., 2014). When protistan isolates and assemblages are exposed in natural bacterial communities, the detected digestion-resistant bacteria (DRB) can be prevalent and diverse, showing a common trait in taxonomic composition where Gammaproteobacteria and Alphaproteobacteria usually dominate in marine samples (Martinez-Garcia et al., 2012; Pucciarelli et al., 2015; Farnelid et al., 2016; Gong et al., 2016). From an ecological point of view, the existence of DRB could prevent organic matter and energy from being transferred to protistan grazers and higher trophic levels via the microbial loop, adding another layer of complexity in the structure and functions of microbial webs.

Despite the ecological importance of DRB, associations between DRB and protists remain poorly understood. One issue is how environment and host affect the diversity and assemblage composition of the DRB associated with protistan populations. There are indications that pre-culture conditions would affect the ingestion and digestion of heterotrophic nanoflagellates (Boenigk et al., 2001). In our previous studies of DRB in ciliated protists cultivated in the laboratory or isolated directly from natural environments, we also observed that the DRB assemblage could substantially differ among host species and even for populations of the same species isolated at separate time points at an identical location, suggesting that the DRB diversity and assemblage composition can be both host- and environment-dependent (Gong et al., 2014, 2016). These relationships seem straightforward, since numerous studies have demonstrated that changes in physical and chemical factors drive bacterial abundance and community composition in bulk environmental samples via bottom-up controls or due to effects of pollutants (e.g., Storesund et al., 2015; Ibekwe et al., 2016).

It is well known that environmental factors play important roles in shaping the diversity and dynamic of the bacteria in a natural aquatic environment (Alonso-Sáez et al., 2006; Adams et al., 2010; Darriba et al., 2012; Hu et al., 2014). When the diversity of source bacteria shifts via environmental filtering, it is likely that different sets of bacterial populations are ingested by the protists and retained inside the cells for at least a short-term period, resulting in different assemblage structures of DRB accordingly. However, when the ingested bacteria escape from lysosomes, they enter into the cytoplasm of host cells, a relatively stable physical and chemical environment (due to cellular homeostasis), which may select for a specific group of DRB. However, it remains to be investigated if and how DRB assemblage associated with bacterivorous protists varies with environmental changes and under chemical stresses.

In this study, we performed microcosm experiments using two bacterivorous protist species, *Euplotes vannus*, a marine heterotrophic ciliate, and *Paramecium bursaria*, a freshwater ciliate with endosymbiotic green algae (*Chlorella* sp.). We aimed to test the following hypotheses: (1) warming, light condition, antibiotic, and heavy metal treatments would individually lead to significant changes in DRB assemblages of both ciliate species; (2) the changes in DRB assemblages in both ciliates were greater than the free-living bacterioplankton in the media; and (3) there were diverse bacteria co-resistant to antibiotics/metals and protistan digestion. We believe that the exploration of the diversity and variation pattern of DRB will improve our understanding of bacteria-protist interactions and the dynamics of microbial food webs.

MATERIALS AND METHODS

Source Organisms and Cultivation

The freshwater ciliate species *P. bursaria*, collected from a pond on the campus of Yantai University (Yantai, Shandong, China) in 2014, and the marine species *E. vannus*, isolated from the estuarine water of the Guangdang River (Yantai, China) in 2013, were investigated. The water used for cultivation was collected on site and treated by passing through a GF/C glass fiber filter (1822-047 grade, pore size: 1.2 μm, Whatman, United Kingdom), such that most pico-, nano-, and larger-sized organisms were removed, and the raw bacterioplankton was largely retained as food for the testing protists. The ciliate cells were observed under a stereoscope (XLT-400, Guilin Guiguang, Guangxi, China), individually selected with a micropipette, and washed for at least 3 times in sterile water to remove other protists and attaching bacteria. A few (3 to 5) cleaned cells were then inoculated into filtered water, allowing the stock cultures to develop. The stock cultures (each in 15 mL volume) were maintained in glass Petri dishes at 16°C for 2 weeks, with several rice grains to enrich bacterial prey (**Supplementary Figure S1**).

Experimental Settings

Different temperatures, illuminations, and stresses of antibiotics and heavy metals were set up to investigate the effects of environmental factors and pollution stresses on the diversity of DRB. For each treatment, about 30 ciliate individuals were picked up from the stock cultures and transferred into a Petri dish containing 20 ml aliquote of the filtered water, in which we assumed there was a bacterial community initially identical in quantity and community composition but subsequently being selectively grazed under various treatment conditions (**Supplementary Figure S1**). Effects of each factor were investigated independently, and each treatment was performed in

triplicate. To investigate the effect of temperature, the Petri dishes with stock ciliate cultures were incubated in three chemostats, which were set at a temperature of 16°C, 21°C, and 25°C, with other factors kept constant (e.g., with 12 h:12 h alternation of light and dark and good gas exchange). The experiments testing the effects of light and pollutant stresses were performed at a constant temperature of 25°C. Light treatments were maintained in consistently illuminated (LL), completely dark (DD), and 12 h:12 h alternation of light and dark conditions (LD).

The effects of pollution stresses on the DRB assemblage were carried out along gradients of the pollutants. To examine the effects of antibiotics, oxytetracycline, one of the most widely used antibiotics in farming industrials, was used in this study. The stock solution (100 mg/L) of oxytetracycline (OTC, Sigma, St. Louis, MO, United States) was added, drop-by-drop, to the ciliate cultures and gently mixed, resulting in final concentrations of 1, 10, and 20 mg/L (hereafter referred to as OTC1, OTC10, and OTC20, respectively). Three types of heavy metals, lead chloride ($PbCl_2$), cadmium chloride ($CdCl_2$), and mercury chloride ($HgCl_2$; AR grade; Sinopharm, Shanghai, China) were used at final concentrations as follows: 10, 30, and 50 mg/L for $PbCl_2$ (hereafter referred to as Pb10, Pb30, and Pb50); 0.01, 0.05, and 0.1 mg/L for $HgCl_2$ (hereafter referred to as Hg0.01, Hg0.05, and Hg0.1); and 0.1, 0.5, and 1 mg/L for $CdCl_2$ (hereafter referred to as Cd0.1, Cd0.5, and Cd1). Since neither *P. bursaria* in the Cd treatments nor *E. vannus* in the Hg treatments survived, these treatments were not included in the subsequent analyses. The cultures without any amendments of antibiotic and heavy metals (i.e., the treatments OTC0, Pb0, Hg0, and Cd0) were taken as the controls.

For molecular assays of DRB inside the protistan cells, approximately 20-30 ciliate cells in all of these treatments were isolated during their exponential growth stages, which usually took place within 8 days of cultivation according to our pilot studies. In order to minimize the contamination from the bacteria attached to the cell surface and the cilia, protistan cells from these treatments were washed repeatedly (at least three times) by transferring to a series of sterilized seawater (for *E. vannus*) or autoclaved Milli-Q water (for *P. bursaria*) with a clean micropipette. These cleaned ciliates were then maintained in the sterilized water for two or three days, allowing the ingested bacteria to be digested as much as possible. The remaining bacteria inside these ciliate cells were considered DRB. Since the free-living bacteria in the culture medium were apparently sources for the DRB, the diversity of the former might be altered under different conditions, which was a potential mechanism modulating the diversity of the latter. To investigate this, therefore the ciliate-free culture medium was also collected for analyzing the free-living bacterial community composition and structure in each treatment.

DNA Extraction, Clone Libraries, and Sequencing

Three to five ciliate individuals with a minimum volume of water were transferred to a microfuge tube for DNA extraction using a REDExtract-N-Amp Tissue PCR Kit (Sigma, St. Louis, MO, United States), according to the modified protocol (Gong et al., 2014). Furthermore, the DNA of bacterioplankton was prepared by taking 3 μL of ciliate-free culture medium from each treatment using the same method.

The identities of the DRB were revealed using PCR amplification, clone library construction, and sequencing of bacterial 16S rRNA genes. PCR was carried out in a Applied Biosystems Veriti® 96-Well thermal cycler (Foster City, CA, United States), with universal bacterial 16S rRNA gene primers 27F1 (5′-AGAGTTTGATCCTGGCTCAG-3′) and 1492R (5′-GGTTACCTTGTTACGACTT-3′) (Lane, 1991), or 63F (5′-CAGGCCTAACACATGCAAGTC-3′) and 1389R (5′-ACGGGCGGTGTGTACAAG-3′) (Osborn et al., 2000). Each PCR reaction cocktail contained 1 μL of 10 μM forward and reverse primers, 1 μL of template DNA, 2.5 μL of 10 × PCR buffer, 2.5 μL of 25 mmol/μL $MgCl_2$, 0.5 μL of 10 mmol/μL dNTP, and 0.2 μL of 1 U *Taq* DNA polymerase (Fermentas, Thermo Scientific, Waltham, MA, United States), and deionized water was added to a final volume of 25 μL. The PCR reactions were programmed as follows: an initial denaturation step at 94°C for 3 min, followed by 35 cycles of 30 s denaturation at 94°C, 1 min annealing (primers 27F/1492R at 50°C, and primers 63F/1389R at 52°C), and a 2 min elongation at 72°C, with a final extension step of 72°C for 7 min. Subsequently, all PCR products were visualized on 1% agarose gels, which contained GoldView (Solarbio, Beijing, China). The target bands were excised, purified by a TIANquick Midi Purification Kit (Tiangen, Beijing, China), inserted into PTZ57 R/T vectors using the InsTAclone PCR Clone Kit (Fermentas), and transferred to the competent cells Trans5α (TransGen Biotech, Beijing, China) in order to construct the clone libraries. A total of 108 clone libraries were constructed, with about 50 positive clones randomly selected for pre-screening, which was conducted using restriction fragment length polymorphism (RFLP) analysis with *Taq* and *Hha*I, two FastDigest restriction enzymes (Thermo Scientific, Waltham, MA, United States). About 20–30 clones in each library were sequenced on an automated ABI 373 DNA sequencer (Applied Biosystems) in a commercial sequencing service company (Sangon Biotech, Shanghai, China).

The 16S rRNA gene sequences (about 1300 bp in length) obtained from cloning and sequencing were aligned using MAFFT v.7.0 with default parameters (Katoh and Standley, 2013). Potential chimeras were identified using Bellerophon (Huber et al., 2004) and Mallard 1.02 (Ashelford et al., 2006) and discarded before subsequent analysis. The cleaned sequences were clustered into operational taxonomic units (OTUs) at 97% identity using Mothur v.1.17 (Schloss et al., 2009). Taxonomic identities and systematic placements of the OTUs were assigned using the RDP Classifier (release 11.5) (Wang et al., 2007). The 16S rRNA gene sequences have been deposited in the GenBank databases with accession numbers MH555909 to MH556816.

Phylogenetic Analyses

For several sequences that assigned into unclassified Bacteroidetes and Verrucomicrobia by the RDP classifier, phylogenetic analyses were carried out using both maximum

likelihood (ML) and Bayesian inference (BI) algorithms to further resolve their taxonomic ranks. Reference sequences of previously described species were retrieved from the GenBank database and aligned with the sequences in question using MAFFT. The alignment was refined manually using SeaView4 (Galtier et al., 1996). The models of nucleotide substitution were estimated using jModeltest2 (Darriba et al., 2012) based on Akaike information criterion (AIC) and Bayesian information criterion (BIC). The ML analysis was conducted using PhyML v.3.3 (Guindon et al., 2009) with a best-fit GTR + I + G evolutionary model and 1000 bootstrap replicates. The BI trees were generated using MrBayes 3.2.7 with selected parameters (rates = invgamma, number of substitution types = 6, ncat = 4) corresponding to the best model selected (GTR + I + G) (Ronquist and Huelsenbeck, 2003), implemented using Markov Chain Monte Carlo simulations and four chains running for 3,000,000 generations. The first 25% of generations were discarded as burn-in.

Profiling of Bacterial Assemblages

Variations in the assemblage structure of both the DRB associated with the protists and the bacterioplankton in the culture medium (but outside the ciliate cells) among the treatments were assessed using terminal restriction fragment length polymorphism (T-RFLP). Bacterial 16S rRNA genes were amplified as described above, except that the forward primer 63F was labeled with a fluorescent dye, 6-carboxyfluorescein, at its 5′ end. The PCR products were purified with the TIAN Quick Midi Purification Kit (Tiangen, Beijing, China). The DNA yield was quantified using a NanoDrop 2000C spectrophotometer (Thermo Fisher, Wilmington, DE, United States). A 15 μL digestion mixture containing 7.5 μL of purified PCR product (each with about 20 ng of DNA) and 7.5 μL of digestion buffers with restriction endonuclease *Hha*I (Fermentas) were incubated at 37°C for 1 h. Sizes of the terminal restriction fragments (T-RFs) were determined using an ABI 3730 DNA analyzer (Sangon Biotech, Shanghai, China). The baseline threshold for signal detection was set to 50 fluorescence intensity units to eliminate any background interference. Only the peaks with T-RF lengths ranging from 40 to 400 bp were included in the subsequent analysis. The relative abundance of each T-RF was calculated as the peak area ratio of the T-RF to all T-RFs detected for a given sample. Minor peaks with a relative abundance of < 1% of the total were excluded, and the remaining peaks were presumed to represent bacterial phylotypes.

The assemblage information generated from the T-RFLP profiling was analyzed using the software package PRIMER v.6 (Primer-E, Plymouth, United Kingdom). In order to test the differences in DRB assemblages, relative abundances of T-RFs were log-transformed, and a matrix of assemblage similarities was generated using the Bray-Curtis index. Non-metric multidimensional scaling (MDS) was executed to visualize the differences in DRB assemblage structure among the treatments of each factor. To test the hypotheses that a given factor would affect the assemblage structure of the DRB and the bacterioplankton in the waters, analysis of similarity (ANOSIM) was performed.

RESULTS

Community Profiling of Bacterioplankton in the Culture Media

The T-RFLP profiling and ANOSIM results of global tests showed that all environmental factors investigated in this study, i.e., temperature ($R \geq 0.71$, $P \leq 0.014$), light ($R \geq 0.38$, $P \leq 0.039$), OTC ($R \geq 0.47$, $P = 0.001$), Pb ($R \geq 0.75$, $P \leq 0.002$), Hg ($R = 1.00$, $P = 0.001$), and Cd ($R = 0.76$, $P = 0.001$), significantly affected the community structure of bacterioplankton in the culture media for the tested ciliate species (**Table 1**). From the point view of the *R* statistic values of global tests, the effects of the tested heavy metals on the bacterioplankton community structure seem to be stronger than those of temperature, OTC antibiotics, and light.

Community Profiling of DRB

The DRB assemblages were clearly separated into three groups by temperature in *E. vannus*, which was well-illustrated in the MDS plots (**Figure 1B**), while the temperature-specific clusters somewhat overlapped in *P. bursaria* (**Figure 1A**). The analysis of the assemblage structure of the DRB generally showed similar results of the bacterioplankton, namely, the effects of temperature (global test, $R \geq 0.50$, $P = 0.001$), OTC ($R \geq 0.49$, $P = 0.001$), and Pb ($R \geq 0.80$, $P = 0.001$) were significant for the DRB in both species. Testing on a single species also illustrated that Hg ($R = 0.73$, $P = 0.001$) was an influential factor in the assemblage structure of DRB in *P. bursaria*, and Cd for that in *E. vannus* ($R = 0.79$, $P = 0.001$). The only exception was the light treatments in *P. bursaria*, in which the assemblage of DRB was not significantly different among the LL, LD, and DD treatments ($R = 0.05$, $P = 0.362$) (**Figure 1C** and **Table 1**).

The MDS plots showed that, within the same range of a given environmental factor, the DRB assemblages were clearly separated into three groups in the marine species but overlapped somewhat in the freshwater form (**Figure 1**). These patterns were also supported by the results of ANOSIM: the *R*-value of the DRB assemblage was consistently lower than that of the bacterioplankton community in all treatments of *P. bursaria* (i.e., $\Delta R_{mean} = R_{DRB} - R_{water} = -0.22$; $n = 5$) but higher in those of *E. vannus* (i.e., $\Delta R_{mean} = R_{DRB} - R_{water} = 0.15$; $n = 5$; **Table 1**). This indicated that the DRB assemblage was less variable in *P. bursaria* but more variable in *E. vannus* as compared with their surrounding bacterial prey under varying temperature, light, OTC, Pb, Hg, and Cd concentrations. The DRB and bacterioplankton community were also significantly different in a given treatment, especially under highly stressed conditions (e.g., at 25°C or in OTC20, see **Supplementary Table S1**).

Identity and Classification of Digestion-Resistant Bacteria

A total of 1018 raw sequences of 16S rRNA genes were obtained from 108 clone libraries and sequencing. After removing 110 chimeras, 908 remained (**Figure 2** and **Table 2**). Overall, most of these DRB belonged to the phylum Proteobacteria (61.3% for *P. bursaria* and 87.4% for *E. vannus*). The phylotypes belonging to Bacteroidetes (25.7%), Actinobacteria (13.8%),

TABLE 1 | Analysis of similarities (ANOSIM) statistics shows the differences in the community structures of digestion-resistant bacteria (DRB) in ciliates *Paramecium bursaria* and *Euplotes vannus*, as well as the bacterioplankton in their culture medium subjected to environmental changes.

Comparison	*P. bursaria*				*E. vannus*			
	Bacterioplankton		DRB		Bacterioplankton		DRB	
	R	*P*	*R*	*P*	*R*	*P*	*R*	*P*
Temperature (global test)	**0.77**	**0.014**	**0.50**	**0.001**	**0.71**	**0.004**	**0.86**	**0.001**
16°C vs. 21°C	0.04	0.400	0.15	0.071	0.96	0.100	**0.44**	**0.008**
21°C vs. 25°C	1.00	0.100	0.21	0.087	0.48	0.100	**1.00**	**0.008**
16°C vs. 25°C	1.00	0.100	0.11	0.127	0.93	0.100	**0.88**	**0.008**
Light (global test)	**0.41**	**0.014**	0.05	0.362	**0.38**	**0.039**	**0.87**	**0.001**
LL vs. DD	0.33	0.400	0.19	0.400	−0.30	0.900	**0.59**	**0.008**
LL vs. LD	0.56	0.100	0.33	0.300	0.89	0.100	**0.96**	**0.008**
DD vs. LD	0.33	0.400	0.00	0.700	0.52	0.100	**1.00**	**0.008**
OTC (global test)	**0.57**	**0.001**	**0.53**	**0.001**	**0.47**	**0.001**	**0.49**	**0.001**
OTC0 vs. OTC1	0.56	0.100	0.12	0.214	0.11	0.300	0.07	0.214
OTC0 vs. OTC10	0.56	0.100	**0.62**	**0.008**	0.67	0.100	0.17	0.103
OTC0 vs. OTC20	0.59	0.100	0.66	0.600	1.00	0.100	**0.35**	**0.008**
OTC1 vs. OTC10	0.93	0.100	0.05	0.706	0.30	0.100	**0.51**	**0.016**
OTC1 vs. OTC20	1.00	0.100	**0.23**	**0.048**	0.37	0.100	**0.52**	**0.016**
OTC10 vs. OTC20	-0.15	0.100	0.20	0.103	0.63	0.100	**0.32**	**0.016**
Pb^{2+} (global test)	**1.00**	**0.001**	**0.83**	**0.001**	**0.75**	**0.002**	**0.80**	**0.001**
Pb0 vs. Pb10	1.00	0.100	**0.63**	**0.029**	0.93	0.100	0.24	0.086
Pb0 vs. Pb30	1.00	0.100	**0.38**	**0.029**	0.56	0.100	**0.84**	**0.005**
Pb0 vs. Pb50	1.00	0.100	**0.56**	**0.029**	1.00	0.100	**0.46**	**0.005**
Pb10 vs. Pb30	1.00	0.100	0.42	0.057	0.70	0.200	1.00	**0.029**
Pb10 vs. Pb50	1.00	0.100	−0.01	0.486	0.59	0.100	0.40	0.057
Pb30 vs. Pb50	1.00	0.100	0.33	0.086	0.74	0.100	**0.71**	**0.029**
Hg^{2+} (global test)	**1.00**	**0.001**	**0.73**	**0.001**	–	–	–	–
Hg0 vs. Hg0.01	1.00	0.100	**0.25**	**0.029**	–	–	–	–
Hg0 vs. Hg0.05	1.00	0.100	**0.51**	**0.029**	–	–	–	–
Hg0 vs. Hg0.1	1.00	0.100	0.09	0.400	–	–	–	–
Hg0 vs. Hg0.05	1.00	0.100	−0.01	0.514	–	–	–	–
Hg0.01 vs. Hg0.1	1.00	0.100	0.16	0.057	–	–	–	–
Hg0.05 vs. Hg0.1	1.00	0.100	**0.42**	**0.029**	–	–	–	–
Cd^{2+} (global test)	–	–	–	–	**0.76**	**0.001**	**0.79**	**0.001**
Cd0 vs. Cd0.1	–	–	–	–	0.85	0.100	0.26	0.076
Cd0 vs. Cd0.5	–	–	–	–	0.52	0.100	0.25	0.114
Cd0 vs. Cd1	–	–	–	–	1.00	0.100	**0.85**	**0.005**
Cd0.1 vs. Cd0.5	–	–	–	–	0.63	0.100	0.02	0.429
Cd0.1 vs. Cd1	–	–	–	–	1.00	0.100	0.46	0.057
Cd0.5 vs. Cd1	–	–	–	–	1.00	0.100	**0.77**	**0.029**

Significant differences ($P < 0.05$) are highlighted in bold. Bacterial community differences are based on the Bray–Curtis dissimilarities. Consistently illuminated, completely dark, and 12 h:12 h alternation of light and dark conditions referred to as LL, DD and LD; oxytetracycline concentrations of 0, 1, 10, and 20 mg/L referred to as OTC0, OTC1, OTC10, and OTC20, respectively; lead concentrations of 0, 10, 30, and 50 mg/L referred to as Pb0, Pb10, Pb30, and Pb50, respectively; mercury concentrations of 0, 0.01, 0.05, and 0.1 mg/L referred to as Hg0, Hg0.01, Hg0.05, and Hg0.1, respectively; cadmium concentrations of 0, 0.1, 0.5, and 1 mg/L referred to as Cd0, Cd0.1, Cd0.5, and Cd1, respectively.

Verrucomicrobia (11.3%), and Firmicutes (0.53%) were relatively minor. The proteobacterial DRB belonged to proteobacterial classes (Gammaproteobacteria, Alphaproteobacteria, and Betaproteobacteria), of which Gammaproteobacteria was the most abundant in *P. bursaria* and *E. vannus*, accounting for 37.1 and 71.9%, respectively. The DRB of Alphaproteobacteria showed similar proportions in these two ciliates (10.3 and 13.4%), whereas the relative abundance of Betaproteobacteria was much higher in the *P. bursaria* (13.8%) than in *E. vannus* (2.1%) (**Figure 2**).

A total of 84 OTUs were obtained for the DRB of these two ciliate species, of which 72 OTUs showed high sequence identity (97–100%) with described species, and the remaining 15 OTUs had sequence similarities lower than 97% (**Table 2**). The Proteobacteria OTUs were prevalent in the DRB assemblages of both ciliates, accounting for 81% of the OTUs observed (**Figure 2**

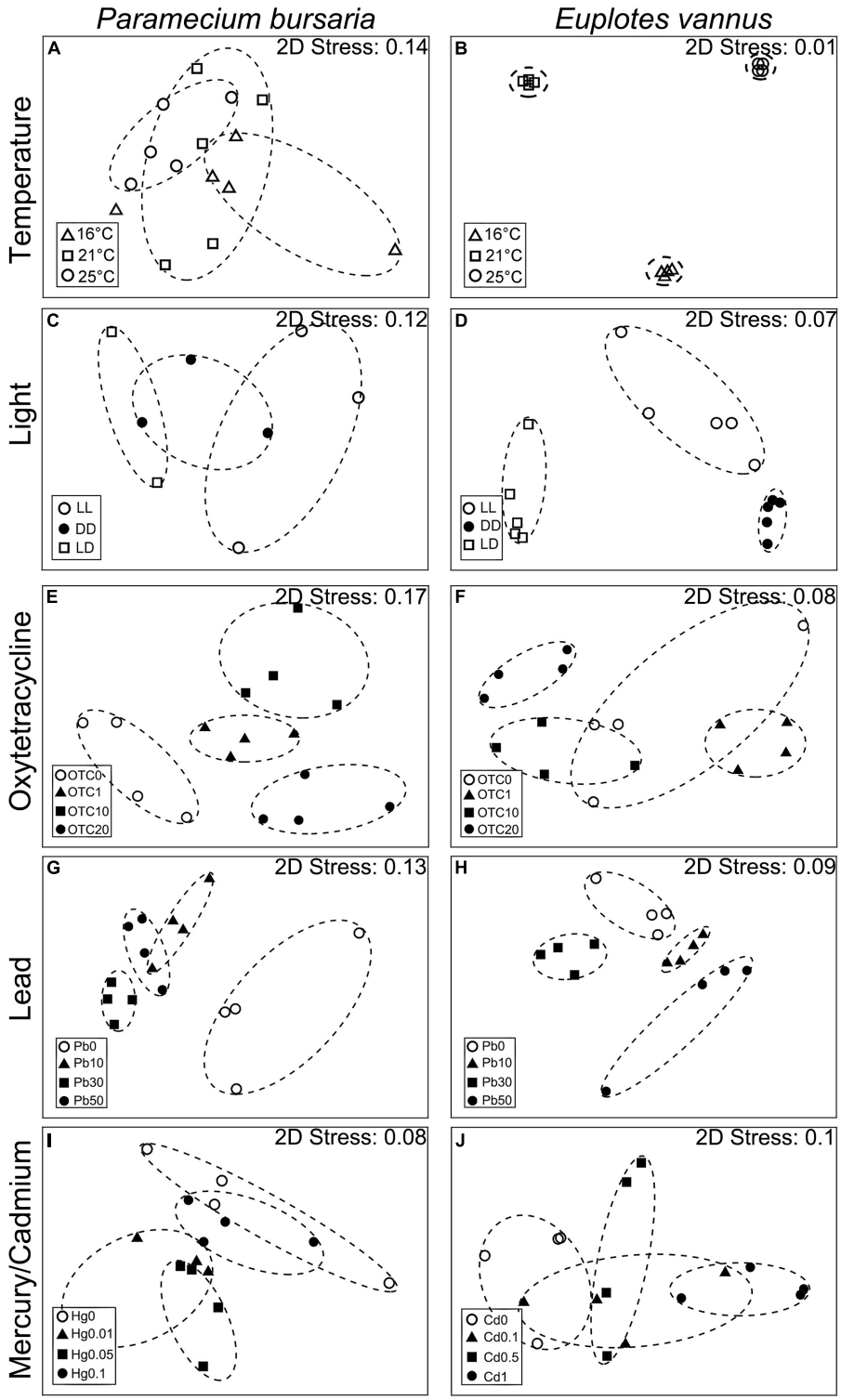

FIGURE 1 | Plots of multi-dimensional scaling ordinations based on Bray-Curtis similarities of the assembly of digestion-resistant bacteria (DRB) in the ciliates *Paramecium bursaria* **(A,C,E,G,I)** and *Euplotes vannus* **(B,D,F,H,J)** reared under different conditions. **(A,B)** At temperatures of 16°C, 21°C, and 25°C; **(C,D)** under three light conditions: consistently illuminated (LL), completely dark (DD), and diel light and dark cycles (LD); **(E,F)** under antibiotic treatments (OTC0, OTC1, OTC10, and OTC20) with the oxytetracycline concentrations of 0 mg/L (OTC0), 1 mg/L (OTC1), 10 mg/L (OTC10), and 20 mg/L (OTC20), respectively; **(G,H)** under lead treatments (Pb0, Pb10, Pb30, and Pb50) with the concentration of 0 mg/L (Pb0), 10 mg/L (Pb10), 30 mg/L (Pb30), and 50 mg/L (Pb50), respectively; **(I)** under mercury treatments (Hg0, Hg0.01, Hg0.05, and Hg0.1) for *P. bursaria* at 0 mg/L (Hg0), 0.01 mg/L (Hg0.01), 0.05 mg/L (Hg0.05), and 0.1 mg/L (Hg0.1), respectively; and **(J)** under cadmium treatments (Cd0, Cd0.1, Cd0.5, and Cd1) for *E. vannus* at 0 mg/L (Cd0), 0.1 mg/L (Cd0.1), 0.5 mg/L (Cd0.5), and 1 mg/L (Cd1), respectively.

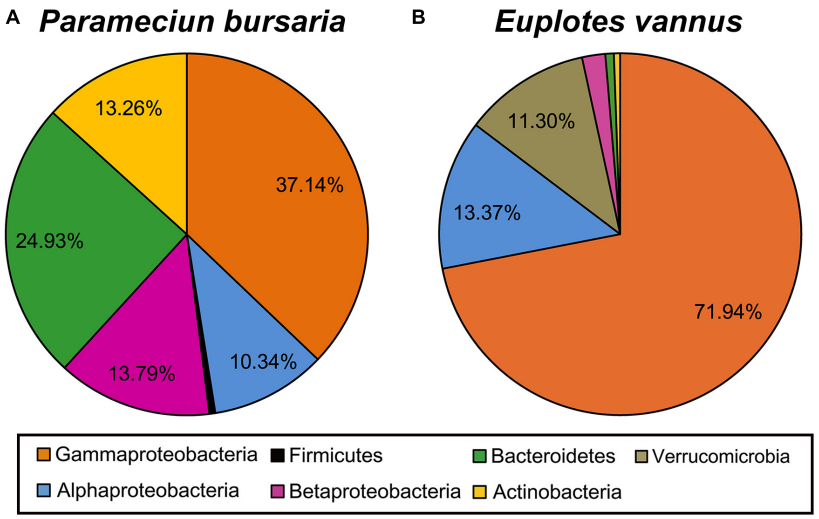

FIGURE 2 | A pie chart showing the phylogenetic composition of digestion-resistant bacteria (DRB) in association with the ciliated protozoa *Paramecium bursaria* **(A)** and *Euplotes vannus* **(B)**.

and **Table 2**). Gammaproteobacteria (41) also dominated in terms of OTU number, which was about three times the amount of Alphaproteobacteria (14) and Betaproteobacteria (13).

A majority of Gammaproteobacteria OTUs were mostly affiliated with the genera *Pseudoalteromonas* (13 OTUs), *Aestuariibacter* (5 OTUs), *Alteromonas* (5 OTUs), and *Pseudomonas* (5 OTUs). The phylotypes of the former three genera were exclusively detected in the marine ciliate *E. vannus*, whereas the phylotypes of *Pseudomonas* were detected in the DRB assemblages of *both P. bursaria* and *E. vannus* (**Table 2**). *Nevskia* (2 OTUs) and *Spongiibacter* (2 OTUs) had fewer OTUs, and *Aeromonas*, *Acinetobacter*, *Alcanivorax*, *Escherichia*, *Haemophilus*, *Psychrosphaera*, *Serratia*, and *Vibrio* were each represented with a single OTU (**Table 2**).

The most frequently occurring OTUs from DRB in the Alphaproteobacteria were affiliated with the family *Rhodobacteraceae* (5 OTUs, with five genera *Thalassococcus, Nautella, Ruegeria, Paracoccus*, and *Sulfitobacter*) (**Table 2**). The phylotypes of the family *Caulobacteraceae* were represented by 4 OTUs and two genera, *Caulobacter* and *Asticcacaulis*, which were abundant in the DRB assemblages of *P. bursaria* under the light treatments (**Table 2**). Two OTUs belonged to the genus *Sphingomonas* and occurred in both ciliates. The remaining three alphaproteobacterial OTUs were *Methylobacterium*, *Phyllobacterium*, and *Agrobacterium,* which were all associated with the *P. bursaria*. Nearly all of the Betaproteobacteria OTUs were recovered from *P. bursaria,* except for one OTU (*Pelomonas* sp.) detected in both two ciliate species (**Table 2**). Other OTUs were affiliated with the genera *Aquabacterium*, *Curvibacter*, *Hydrogenophaga*, *Janthinobacterium*, *Methylophilus*, *Polynucleobacter*, *Limnobacter*, *Ralstonia*, and *Variovorax* (**Table 2**).

There were 10 OTUs of DRB affiliated with the phylum Bacteroidetes. These included two OTUs of *Arcicella* and another two of *Flectobacillus*, both of which are members of the family *Cytophagaceae* (**Table 2**). Three OTUs of *Flavobacteriaceae* were closely related to *Ochrovirga* and *Flavobacterium*. Two OTUs were members of *Cryomorphaceae*: one was affiliated with *Fluviicola,* and the other could represent a new genus within this family (**Figure 3A**), exhibiting a 90% similarity with the 16S rRNA gene of *Vicingus serpentipes* (**Table 2**). The OTU sharing an 88% sequence similarity with *Crocinitomix catalasitica* was confirmed to be a member of the order Flavobacteriales but remained unresolved at the family level in the ML and Bayesian trees (**Figure 3A**). The remaining OTU of this phylum was closely related to *Algoriphagus* (**Table 2**).

The actinobacterial DRB were represented by two OTUs affiliated with *Micrococcus* and *Propionibacterium* (**Table 2**). Another two OTUs were related to *Anaerocolumna* and *Peptoniphilus* (phylum Firmicutes), which were only detected in the freshwater ciliate (**Table 2**). A single verrucomicrobial OTU, which was associated with the marine ciliate *E. vannus*, shared a low sequence similarity (89%) with *Ruficoccus amylovorans* (family *Puniceicoccaceae*), likely representing a new genus (**Figure 3B** and **Table 2**).

Warming Effect on the Assemblage Structure of DRB

Analysis of the clone libraries indicated that the DRB assemblage in *P. bursaria* was dominated by *Pseudomonas* spp., of which the relative abundance gradually increased from 50% to 65% and 76% with increasing temperature (**Table 2** and **Figure 4A**). *Flavobacterium*, *Peptoniphilus*, and *Micrococcus*, though not abundant, were only detected in the warmest treatment for the freshwater ciliate. In contrast, the DRB assemblage in *E. vannus* was generally dominated by *Pseudoalteromonas* spp., of which the relative abundance decreased from 74% to 40% with temperature. The relative abundance of *Vibrio* sp. was minor (2.7%) during the treatment at 16°C but became abundant (50%) at 25°C (**Table 2**

TABLE 2 | Detection and classification of digestion-resistant bacteria (DRB) in *Paramecium bursaria* (P) and *Euplotes vannus* (E) in various temperature, light, antibiotic, and heavy metal treatments.

OTU ID	Accession number	Closest matched species (accession number)	Coverage (%)	Identity (%)	Classification	Treatment	Ciliate
OTU1	MH556452	*Aestuariibacter* sp. strain 12C24 (KU963301)	100	99–100	*Gamma, Alteromonadaceae*	25°C; LD; OTC0, OTC1, OTC10; Pb10, Pb30, Pb50; Cd0, Cd0.1, Cd0.5, Cd1.0	E
OTU2	MH556787	*Aestuariibacter halophilus* (LC221844)	100	99	*Gamma, Alteromonadaceae*	LD; OTC1, OTC20	E
OTU3	MH556783	*Aestuariibacter* sp. Bh22 (LN897328)	100	94	*Gamma, Alteromonadaceae*	OTC20	E
OTU4	MH556703	*Aestuariibacter aggregatus* strain WH169 (MH414455)	100	97	*Gamma, Alteromonadaceae*	OTC20	E
OTU5	MH556467	*Aestuariibacter* sp. strain 12C24 (KU963301)	100	97–98	*Gamma, Alteromonadaceae*	OTC0; Cd0.1	E
OTU6	MH556726	*Alteromonas* sp. H86 (FJ903192)	100	98	*Gamma, Alteromonadaceae*	OTC1	E
OTU7	MH556162	*Alteromonas* sp. M71_D24 (FM992713)	100	95	*Gamma, Alteromonadaceae*	LD	E
OTU8	MH556150	*Alteromonas* sp. SPB-8 (DQ412077)	93	98	*Gamma, Alteromonadaceae*	LD	E
OTU9	MH556135	*Alteromonas* sp. AKA07-1 (AB571941)	100	97–98	*Gamma, Alteromonadaceae*	LD; OTC0, OTC1	E
OTU10	MH556153	*Alteromonas tagae* strain BCRC 17571 (NR_043977)	100	97–99	*Gamma, Alteromonadaceae*	LD, LL	E
OTU11	MH556079	*Pseudoalteromonas phenolica* strain JCM 21460 (NR_113299)	100	96–97	*Gamma, Pseudoalteromonadaceae*	LL, DD	E
OTU12	MH556080	*Pseudoalteromonas* sp. 03/034 (AJ874351)	100	96–98	*Gamma, Pseudoalteromonadaceae*	LL	E
OTU13	MH556095	*Psychrosphaera saromensis* strain DL8-2 (KF146527)	100	97–98	*Gamma, Pseudoalteromonadaceae*	LL, DD, LD	E
OTU14	MH556118	*Pseudoalteromonas* sp. 03/034 (AJ874351)	100	99	*Gamma, Pseudoalteromonadaceae*	16°C; DD, LL	E
OTU15	MH556233	*Pseudoalteromonas piscicida* strain MCCB 201 (KF880965)	100	98–99	*Gamma, Pseudoalteromonadaceae*	25°C	E
OTU16	MH556167	*Pseudoalteromonas* sp. 01/121 (AJ874345)	100	98–100	*Gamma, Pseudoalteromonadaceae*	16°C, 21°C; DD, LL	E
OTU17	MH556181	*Pseudoalteromonas* sp. A28 (AF227238)	100	95	*Gamma, Pseudoalteromonadaceae*	16°C	E
OTU18	MH556191	*Pseudoalteromonas* sp. BSw21650 (JF697294)	100	98–99	*Gamma, Pseudoalteromonadaceae*	16°C, 21°C	E
OTU19	MH556216	*Pseudoalteromonas* sp. CF6-1 (FJ169996)	100	96	*Gamma, Pseudoalteromonadaceae*	21°C	E
OTU20	MH556254	*Pseudoalteromonas* sp. HK41 (HQ343275)	100	97–98	*Gamma, Pseudoalteromonadaceae*	25°C	E
OTU21	MH556169	*Pseudoalteromonas* sp. KASP34 (KU647930)	99	99	*Gamma, Pseudoalteromonadaceae*	16°C	E
OTU22	MH556210	*Pseudoalteromonas* sp. S1649 (FJ457154)	100	98–99	*Gamma, Pseudoalteromonadaceae*	16°C, 21°C; LL, DD	E
OTU23	MH556188	*Pseudoalteromonas* sp. S511-1 (AB029824)	100	97–98	*Gamma, Pseudoalteromonadaceae*	16°C, 21°C	E
OTU24	MH556236	*Pseudoalteromonas viridis* (AB681561)	100	95	*Gamma, Pseudoalteromonadaceae*	25°C	E
OTU25	MH556186	*Algicola bacteriolytica* strain MR32e (HQ439519)	99	95	*Gamma, Pseudoalteromonadaceae*	16°C	E
OTU26	MH555990	*Pseudomonas synxantha* strain NBRC 3913 (NR_113583)	100	98–99	*Gamma, Pseudomonadaceae*	16°C; OTC1	E, P
OTU27	MH555987	*Pseudomonas psychrophila* strain P270 (KC904093)	100	99–100	*Gamma, Pseudomonadaceae*	16°C, 21°C, 25°C; OTC1, OTC10, OTC20	P

(Continued)

TABLE 2 | Continued

OTU ID	Accession number	Closest matched species (accession number)	Coverage (%)	Identity (%)	Classification	Treatment	Ciliate
OTU28	MH556036	*Pseudomonas* sp. K3R3.1A (KC433646)	100	99	*Gamma, Pseudomonadaceae*	21°C, 25°C; Hg0.01; OTC0, OTC10, OTC20	P
OTU29	MH556031	*Pseudomonas fluorescens* strain ex17 (KF317887)	100	99–100	*Gamma, Pseudomonadaceae*	16°C, 21°C, 25°C; OTC0, OTC1, OTC10; Pb10; Hg0, Hg0.01, Hg0.1	E, P
OTU30	MH556663	*Pseudomonas* sp. R02 (KT890300)	100	98	*Gamma, Pseudomonadaceae*	OTC20	P
OTU31	MH555949	*Nevskia ramosa* strain Soe1 (NR_025269)	99	98–99	*Gamma, Sinobacteraceae*	DD, LD, LL	P
OTU32	MH555974	*Nevskia ramosa* (AJ001343)	99	95	*Gamma, Sinobacteraceae*	DD	P
OTU33	MH556800	*Spongiibacter marinus* (AB985586)	100	96–97	*Gamma, Spongiibacteraceae*	OTC10	E
OTU34	MH556747	*Spongiibacter marinus* (AB985580)	100	99	*Gamma, Spongiibacteraceae*	OTC10, OTC20; LD	E
OTU35	MH556281	*Escherichia coli* strain Y38 (JN578647)	100	99	*Gamma, Enterobacteriaceae*	Hg0, Hg0.05, Hg0.1	P
OTU36	MH556409	*Serratia proteamaculans* strain PW172 (JF494823)	100	99	*Gamma, Enterobacteriaceae*	Pb50	P
OTU37	MH556249	*Vibrio neocaledonicus* strain MS1 (KJ841877)	100	99	*Gamma, Vibrionaceae*	16°C, 25°C	E
OTU38	MH556000	*Aeromonas caviae* strain AH08 (KU975030)	100	99	*Gamma, Aeromonadaceae*	16°C	P
OTU39	MH556788	*Alcanivorax* sp. MCCC 1A00973 (KU681505)	100	99	*Gamma, Alcanivoracaceae*	OTC20	E
OTU40	MH556230	*Acinetobacter junii* strain B2w (KX058411)	100	99	*Gamma, Moraxellaceae*	21°C; LD; Hg0.01, Hg0.05; OTC0, OTC10	E, P
OTU41	MH556303	*Haemophilus* sp. oral (AY005034)	100	99	*Gamma, Pasteurellaceae*	Hg0.01	P
OTU42	MH556285	*Asticcacaulis excentricus* strain CB 48 (NR_114730)	98–100	99	*Alpha, Caulobacteraceae*	Hg0, Hg0.1	P
OTU43	MH555955	*Asticcacaulis* sp. clone Sa4_4.4 (GQ181156)	100	98	*Alpha, Caulobacteraceae*	LD, DD, LL	P
OTU44	MH555978	*Caulobacter* sp. BBCT11 (DQ337547)	100	96	*Alpha, Caulobacteraceae*	DD	P
OTU45	MH555956	*Caulobacter* sp. DNA (AJ227760)	100	99	*Alpha, Caulobacteraceae*	LL	P
OTU46	MH556716	*Thalassococcus* sp. KU27F5 (AB636146)	100	99	*Alpha, Rhodobacteraceae*	OTC1	E
OTU47	MH556768	*Nautella* sp. A04V (LC094988)	100	97–99	*Alpha, Rhodobacteraceae*	LL; OTC0, OTC1, OTC10	E
OTU48	MH556144	*Ruegeria pelagia* strain NBRC 102038 (NR_114024)	100	99–100	*Alpha, Rhodobacteraceae*	LL, LD	E
OTU49	MH556262	*Paracoccus* sp. I7 (KR108387)	100	99	*Alpha, Rhodobacteraceae*	Hg0	P
OTU50	MH556666	*Sulfitobacter* sp. QD214-NF102 (KC689801)	100	99	*Alpha, Rhodobacteraceae*	OTC20	P
OTU51	MH555995	*Sphingomonas abaci* strain SS1-08 (KU341393)	100	99	*Alpha, Sphingomonadaceae*	LD; 16°C; OTC0, OTC1, OTC10, OTC20	E, P
OTU52	MH556759	*Sphingomonas roseiflava* strain MK341 (NR_117716)	100	97	*Alpha, Sphingomonadaceae*	OTC10	E
OTU53	MH556325	*Methylobacterium* sp. 20 (JF905619)	100	99	*Alpha, Methylobacteriaceae*	Hg0.05	P
OTU54	MH556314	*Phyllobacterium myrsinacearum* isolate OTU-a22 (KJ147062)	100	99	*Alpha, Phyllobacteriaceae*	16°C; Hg0.05	P

(Continued)

TABLE 2 | Continued

OTU ID	Accession number	Closest matched species (accession number)	Coverage (%)	Identity (%)	Classification	Treatment	Ciliate
OTU55	MH556037	*Agrobacterium rhizogenes* strain IV (HM582866)	100	99	*Alpha, Rhizobiaceae*	21°C	P
OTU56	MH556569	*Pelomonas* sp. clone 35Fe00 (KF287732)	100	99	*Beta, Comamonadaceae*	Pb30, Pb50; Hg0.01; Cd0.1, Cd1.0	E, P
OTU57	MH556333	*Hydrogenophaga* sp. 7B-224 (KF441666)	99	98	*Beta, Comamonadaceae*	Hg0.1	P
OTU58	MH555972	*Curvibacter lanceolatus* strain NBRC 103051 (NR_114201)	100	98–99	*Beta, Comamonadaceae*	LL, LD, DD	P
OTU59	MH555959	*Variovorax paradoxus* (HQ845986)	100	99	*Beta, Comamonadaceae*	LL, LD	P
OTU60	MH556621	*Ralstonia* sp. S1SM82 (KT183537)	100	99	*Beta, Burkholderiaceae*	OTC0	P
OTU61	MH556271	*Polynucleobacter acidiphobus* (AB599874)	100	99	*Beta, Burkholderiaceae*	Hg0	P
OTU62	MH556312	*Limnobacter* sp. KNF002 (AB426551)	100	99	*Beta, Burkholderiaceae*	Hg0.05	P
OTU63	MH556310	*Aquabacterium commune* strain B8 (NR_024875)	100	98–99	*Beta, Burkholderiales*	Hg0.01, Hg0.05	P
OTU64	MH556265	*Aquabacterium fontiphilum* strain K10 (KT345664)	100	99	*Beta, Burkholderiales*	Hg0	P
OTU65	MH556313	*Aquabacterium fontiphilum* strain CS-6 (NR_044322)	98	98	*Beta, Burkholderiales*	Hg0.05	P
OTU66	MH556272	*Limnobacter* sp. strain DRY11W (MH463959)	100	94	*Beta, Burkholderiales*	Hg0	P
OTU67	MH556266	*Methylophilus methylotrophus* strain NCIMB 10515 (NR_041257)	99	99	*Beta, Methylophilaceae*	Hg0	P
OTU68	MH556063	*Janthinobacterium* sp. TP-Snow-C76 (KC987006)	100	99	*Beta, Oxalobacteraceae*	16°C, 25°C	P
OTU69	MH556619	*Arcicella aquatica* strain NO-502 (NR_029000)	100	99	*Bacteroidetes, Cytophagaceae*	OTC0	P
OTU70	MH556411	*Arcicella rigui* strain HMF3820 (KT983986)	100	96	*Bacteroidetes, Cytophagaceae*	Pb50	P
OTU71	MH556371	*Flectobacillus* sp. WG3 (FN547417)	100	98–99	*Bacteroidetes, Cytophagaceae*	Pb10, Pb30, Pb50; Hg0, Hg0.05	P
OTU72	MH556345	*Flectobacillus rhizosphaerae* strain JC289 (NR_137382)	96	95	*Bacteroidetes, Cytophagaceae*	Pb10	P
OTU73	MH556228	*Ochrovirga pacifica* (JN596241)	97	95	*Bacteroidetes, Flavobacteriaceae*	21°C	E
OTU74	MH556330	*Flavobacterium fontis* strain MIC3010 (NR_109522)	96	99	*Bacteroidetes, Flavobacteriaceae*	Hg0.1	P
OTU75	MH556040	*Flavobacterium* sp. T3L.05.LWF.W.Kidney.D (JX287789)	98	99–100	*Bacteroidetes, Flavobacteriaceae*	25°C	P
OTU76	MH556400	*Fluviicola hefeinensis* strain MYL-8 (NR_133750)	100	98	*Bacteroidetes, Cryomorphaceae*	Pb50	P
OTU77	MH556320	*Vicingus serpentipes* strain ANORD5 (NR_159281)	100	90	*Bacteroidetes, Cryomorphaceae*	Hg0.05	P

(Continued)

TABLE 2 | Continued

OTU ID	Accession number	Closest matched species (accession number)	Coverage (%)	Identity (%)	Classification	Treatment	Ciliate
OTU78	MH556294	*Algoriphagus aquatilis* strain NBRC 104237 (NR_114262)	100	99	*Bacteroidetes, Cyclobacteriaceae*	Hg0.01	P
OTU79	MH556315	*Crocinitomix catalasitica* IFO 15977 (NR_040905)	95	88	*Bacteroidetes*	Hg0.05	P
OTU80	MH556064	*Micrococcus* sp. ce2 (JN082244)	99	99	*Actino, Micrococcaceae*	25°C	P
OTU81	MH556002	*Propionibacterium acnes* strain ChDC KB81 (KF933807)	99	99	*Actino, Propionibacteriaceae*	LD; 16°C, 21°C, 25°C; Hg0; Pb50	E, P
OTU82	MH556282	*Anaerocolumna* sp. CBA3638 (CP048000)	99	93	*Firmicutes, Lachnospiraceae*	Hg0	P
OTU83	MH556048	*Peptoniphilus* sp. EL1 (LN867000)	99	99	*Firmicutes, Peptoniphilaceae*	25°C	P
OTU84	MH556212	*Ruficoccus amylovorans* CC-MHH0563 (NR_156844)	99	89	*Verrucomicrobia, Puniceicoccaceae*	16°C, 21°C, 25°C; LD;OTC0, OTC1, OTC10; Cd0, Cd0.1, Cd0.5	E

Notes: Consistently illuminated, completely dark, and 12 h:12 h alternation of light and dark conditions referred to as LL, DD and LD; oxytetracycline concentrations of 0, 1, 10, and 20 mg/L referred to as OTC0, OTC1, OTC10, and OTC20, respectively; lead concentrations of 0, 10, 30, and 50 mg/L referred to as Pb0, Pb10, Pb30, and Pb50, respectively; mercury concentrations of 0, 0.01, 0.05, and 0.1 mg/L referred to as Hg0, Hg0.01, Hg0.05, and Hg0.1, respectively; cadmium concentrations of 0, 0.1, 0.5, and 1 mg/L referred to as Cd0, Cd0.1, Cd0.5, and Cd1, respectively.

and **Figure 4A**). *Ruficoccus*-like species (Verrucomicrobia) were consistently present, accounting for a small portion (3.3–13.5%) of the DRB in association with *E. vannus*. Nevertheless, warming induced a gradual decrease in its relative abundance. *Aestuariibacter* and *Pseudomonas* spp. were present only in the warmest treatment of the *Euplotes* (**Figure 4A**).

Variations in the Bacterial Assemblages Under Photoperiod Conditions

E. vannus under the condition of LD hosted 9 bacterial genera, which was much more diverse than that in both LL and DD. Structurally, *Pseudoalteromonas* spp. and *Psychrosphaera saromensis* dominated under conditions of both LL and DD, whereas *Aestuariibacter* spp. were the most abundant (31%) in the LD treatment. Phylotypes of *Aestuariibacter*, *Propionibacterium*, *Sphingomonas*, *Spongiibacter*, and *Ruficoccus*-like were detected only under the LD treatment (**Figure 4B**). In contrast, *P. bursaria* consistently hosted *Nevskia* sp. (38–44%), *Curvibacter* (25–29%), and *Asticcacaulis* (6–25%). Interestingly, *Caulobacter* and *Variovorax* were present but not in LD and DD, respectively (**Figure 4B**).

Bacteria Co-resistant to Antibiotic and Digestion

Sphingomonas and *Arcicella* species occurred in the DRB of *P. bursaria*, accounting for 73% in the control (OTC0). However, these two taxa were not detectable in the OTC treatments. *Pseudomonas* in the control *P. bursaria* had a low abundance (19%) but a high abundance (50%–100%) after OTC applications. Also, *Sulfitobacter* was absent in the control and at a lower dose of OTC but represented 47% of the DRB in the OTC20 treatment (**Figure 5A**).

The bacteria associated with *E. vannus* treated with OTC included *Aestuariibacter*, *Acinetobacter*, *Alcanivorax*, *Alteromonas*, *Pseudomonas*, *Nautella*, *Thalassococcus*, *Sphingomonas*, *Spongiibacter*, and *Ruficoccus*-like Verrucomicrobia (**Figure 5A**). In contrast to the non-detection of *Sphingomonas* in *P. bursaria* at high doses of OTC, this genus occurred with high relative abundance in *E. vannus* treated with 10 and 20 mg/L of OTC. Both the *Aestuariibacter* and *Ruficoccus*-like phylotypes were abundant at the low-dose treatment but were reduced or disappeared at the higher doses (**Figure 5A**).

DRB Assemblages Changed With the Concentrations of Heavy Metals

The DRB in the control *P. bursaria* (Pb0) were represented by nine bacterial genera, of which only four were detected in the Pb-treated treatments, including *Flectobacillus*, *Pseudomonas*, *Fluviicola*, and *Serratia*. *Flectobacillus* was the most dominant, accounting for 83%, 100%, and 64% in Pb10, Pb30, and Pb50, respectively. *Fluviicola* and *Serratia* together represented 36% sequences in Pb50 (**Table 2** and **Figure 5B**).

There were many DRB persisting in the Hg treatments. These included *Acinetobacter*, *Aquabacterium*, *Escherichia*, *Flavobacterium*, *Hydrogenophaga*, *Pelomonas*, *Phyllobacterium*, and *Pseudomonas*. The most abundant at the high dose

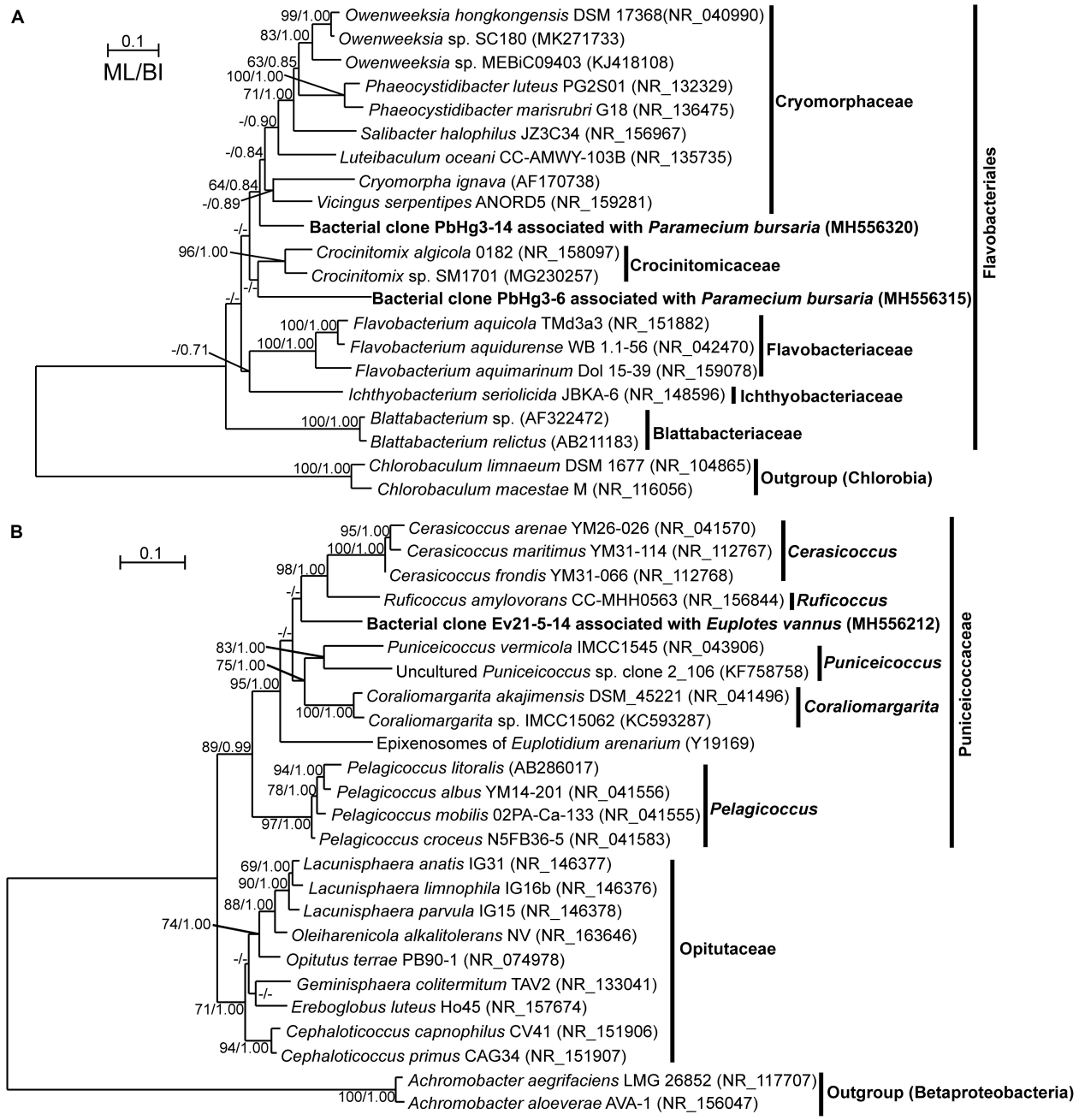

FIGURE 3 | Maximum likelihood (ML) trees based on 16S rRNA genes showing the phylogenetic positions of digestion-resistant bacterial (DRB) phylotypes affiliated with the order *Flavobacteriales* **(A)** and with the family *Puniceicoccaceae* **(B)**. The trees generated using Bayesian Inference (BI) showed similar topologies with the ML trees. The newly obtained sequences are highlighted in bold. The numbers at the nodes show the bootstrap values and posterior probabilities; only the bootstrap values not lower than 50% and the posterior probabilities not lower than 0.8 are shown. Accession numbers are provided for all sequences.

of $HgCl_2$ were *Hydrogenophaga* (42%) and *Escherichia* (25%), whereas *Acinetobacter* (54%) and *Pseudomonas* (13%) dominated the assemblage in the low dose treatment (**Table 2** and **Figure 5C**).

The DRB assemblage in *E. vannus* was consistently dominated by a single genus, *Aestuariibacter*, in both Pb and Cd treatments (**Table 2** and **Figures 5B,C**). Nevertheless, *Pelomonas* (11%) occurred in Pb30 and increased to 17% in Pb50 (**Figure 5B**). Furthermore, in the treatments of Cd0.1 and Cd1.0, *Pelomonas* was also present but with minor proportions (3 and 8%, respectively). *Ruficoccus*-like Verrucomicrobia was minor (3.6%) in the control but abundant (∼35%) in both Cd0.1 and Cd0.5 treatments (**Table 2** and **Figure 5C**).

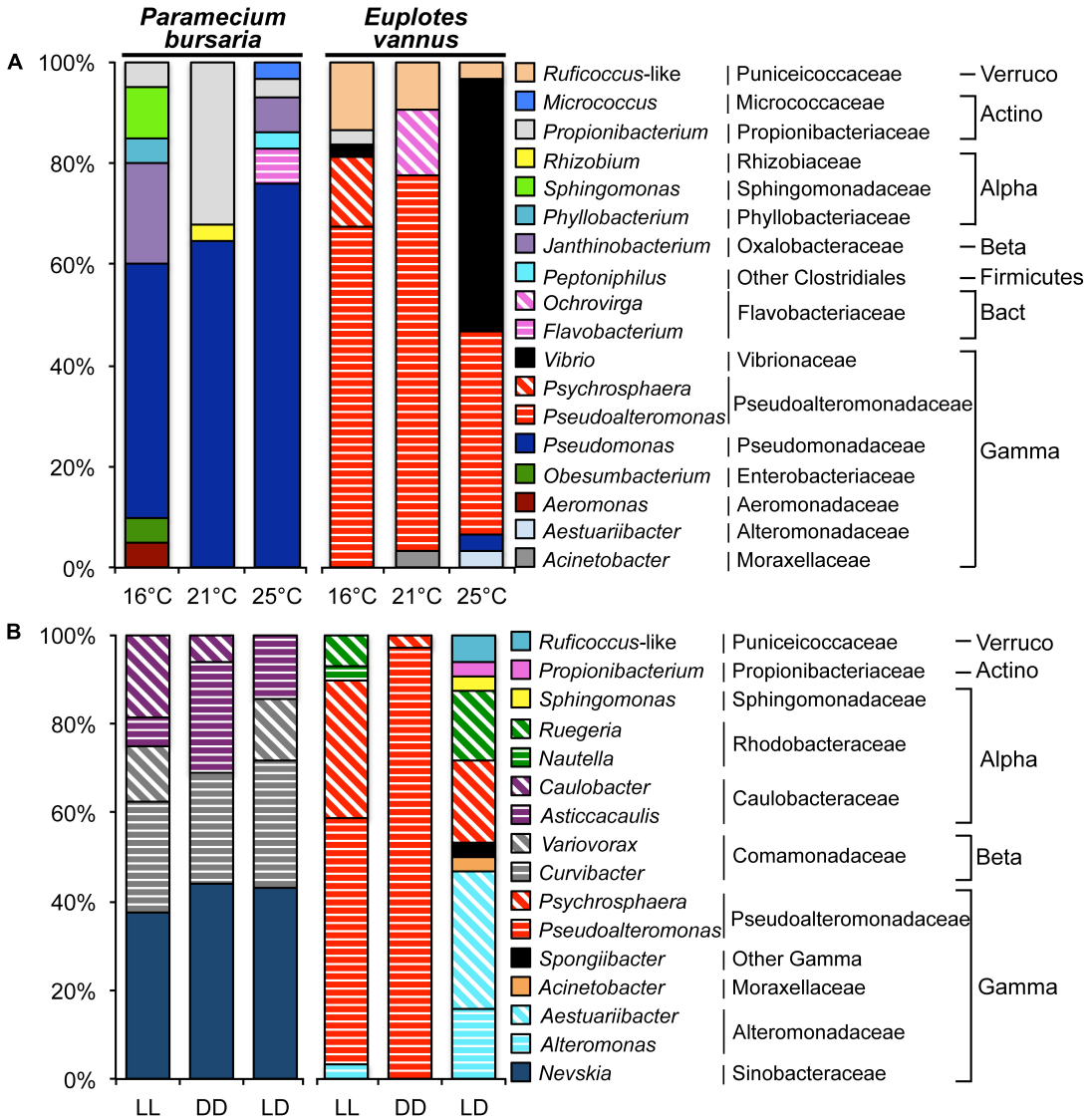

FIGURE 4 | Variations in the assemblage structure of digestion-resistant bacteria (DRB) in association with two ciliates *Paramecium bursaria* and *Euplotes vannus* in different treatments. **(A)** A temperature gradient (16°C, 21°C, and 25°C); and **(B)** light conditions (LL, DD, and LD represent consistently illuminated, completely dark, and 12 h:12 h alternation of light and dark conditions, respectively). Note that *Pseudomonas* and *Pseudoalteromonas* dominated the DRB assemblages in *P. bursaria* and *E. vannus*, with increasing and decreasing relative abundance with temperature, respectively. In different light environments, the composition of DRB in *P. bursaria* was rather similar, whereas *Aestuariibacter* and *Alteromonas* in *E. vannus* became more important under the condition of light-dark diel cycle. Abbreviations: Actinobacteria (Actino), Alphaproteobacteria (Alpha), Bacteroidetes (Bact), Betaproteobacteria (Beta), Gammaproteobacteria (Gamma), and Verrucomicrobia (Verruco).

DISCUSSION

By using *E. vannus* and *P. bursaria* as models, this study is the first to explicitly investigate how the composition and structure of DRB assemblages vary along various physical and chemical gradients. Overall, our molecular profiling of these two protist species indicated that experimentally manipulated warming, irradiance, antibiotic, and heavy metal stresses significantly influenced the structure of DRB assemblages. This provides evidence that the association between DRB and protists is highly dependent on environmental conditions.

It was conceivable that there were consistently larger variations in the assemblage structure of DRB, relative to those in the environmental bacterioplankton across the treatments of *E. vannus* (**Table 1**). This is likely related to the fact that the variations in the environmental factors caused the shifts in the bacterioplankton community structure first (**Supplementary Table S1**), and then selective ingestion and differential digestion of the engulfed bacterial taxa took place next, which further screened out digestible populations, resulting in the altered assemblage structure of the bacteria (i.e., DRB) that resided in the protistan cells (**Table 1** and **Figures 4**, **5**). However,

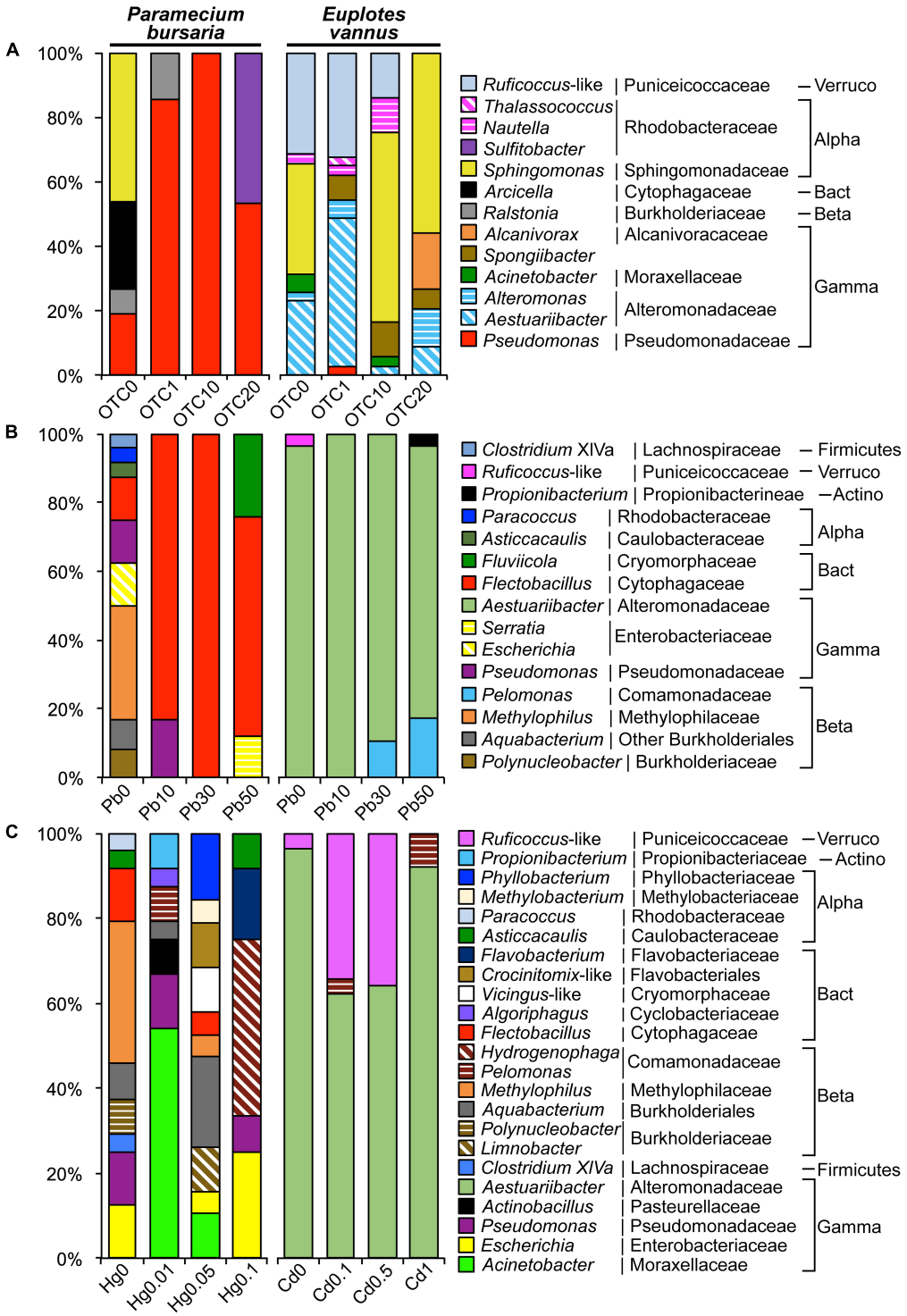

FIGURE 5 | Variations in the assemblage structure of digestion-resistant bacteria (DRB) in *Paramecium bursaria* and *Euplotes vannus* **(A)** under antibiotic treatments (OTC0, OTC1, OTC10, and OTC20) with the oxytetracycline concentrations of 0 mg/L (OTC0), 1 mg/L (OTC1), 10 mg/L (OTC10), and 20 mg/L (OTC20), respectively; **(B)** under the lead treatments (Pb0, Pb10, Pb30, and Pb50) with the concentration of 0 mg/L (Pb0), 10 mg/L (Pb10), 30 mg/L (Pb30), and 50 mg/L (Pb50), respectively; **(C)** under mercury treatments (Hg0, Hg0.01, Hg0.05, and Hg0.1) for *P. bursaria* at 0 mg/L (Hg0), 0.01 mg/L (Hg0.01), 0.05 mg/L (Hg0.05), and 0.1 mg/L (Hg0.1), respectively; **(C)** and under cadmium treatments (Cd0, Cd0.1, Cd0.5, and Cd1) for *E. vannus* at 0 mg/L (Cd0), 0.1 mg/L (Cd0.1), 0.5 mg/L (Cd0.5), and 1 mg/L (Cd1), respectively. Note that *Pseudomonas*, *Sulfitobacter,* and *Sphingomonas* were highly antibiotic-resistant. *Flectobacillus* and *Fluviicola* were highly Pb-resistant. *Hydrogenophaga* was Hg-resistant, and both *Aestuariibacter* and *Pelomonas* were co-resistant to Pb and Cd. Abbreviations: Actinobacteria (Actino), Alphaproteobacteria (Alpha), Bacteroidetes (Bact), Betaproteobacteria (Beta), Gammaproteobacteria (Gamma), and Verrucomicrobia (Verruco).

this reasoning cannot explain the results for *P. bursaria*, in which the assemblage structure of DRB across multiple environmental gradients appeared to be less variable than that of environmental bacterioplankton. The contrasting variability of DRB in *P. bursaria* and *E. vannus* may be related to their nutritional models (mixotrophy vs. heterotrophy), in which the mixotrophs have a highly flexible physiology to cope with the changing environment by shifting between phototrophic and phagotrophic lifestyles. The characteristic intracellular environment of mixotrophs thus selects a narrow spectrum of bacterial species to reside intracellularly.

The selection of DRB in all the treatments investigated in this study may be related to the direct influence of environmental factors and pollution stresses on the physiology and biochemistry of the protists, which may affect the interactions between the predators and preys. At a higher temperature (not higher than the optimal temperature), a protist usually has a high growth rate (Montagnes and Weisse, 2000), ingestion rate (Izaguirre et al., 2012), and digestion rate (Sherr et al., 1988). Compared to the light condition, protozoan ingestion rate determined by using fluorescently labeled prey was lower under the dark conditions (Izaguirre et al., 2012). Light availability is important for mixotrophs. For example, *Chlorella* symbionts provide photosynthetic products to their host under light conditions (Shibata et al., 2016), but they lost their ability to resist host digestion in darkness (Kodama and Fujishima, 2014). Heavy metals also affect protistan ingestion rates (Al-Rasheid and Sleigh, 1994) and physiology (Kim et al., 2011).

The bacterial species associated with the protistan grazers may be related to not only the life stage and physiology of ciliates (Xu et al., 2020), but also depend on the biological nature (e.g., digestibility) of these bacteria (Zou et al., 2020), which are more or less reflected by their phylogenetic classification. Our analyses of clone libraries revealed that the overall DRB assemblage composition in *E. vannus* across all treatments was dominated by Gamma- and Alphaproteobacteria, which was consistent with previous reports for a range of marine ciliate species and picoeukaryotes (Farnelid et al., 2016; Gong et al., 2016). However, this compositional trait of DRB was not applicable for the DRB in the freshwater species *P. bursaria*, in which Gammaproteobacteria, Bacteroidetes, and Betaproteobacteria were the most abundant three taxa. The high proportions of Bacteroidetes and Betaproteobacteria could be due to their generally high abundance in freshwater systems (Newton et al., 2011). The phylum Bacteroidetes is well known for its high abundance in the gut microbiota (Mahowald et al., 2009) and for having a special protein secretion system (Type IX Secretion System, T9SS) that ensures cell survival and fitness in response to its habitat (Lasica et al., 2017). It is likely that habitat (freshwater-marine) distinctness in higher taxonomic composition of DRB exists, but it is a notion that needs to be further investigated for more freshwater protist species. At lower taxonomic ranks, the DRB assemblage composition and structure along different environmental gradients and pollutant stresses showed many interesting characteristics, many of which are reported for the first time in this study, and the underlying mechanisms are discussed below.

Warming Selected Specific Bacterial Species in Association With Protists

It is interesting to observe that *Pseudomonas* spp., as a dominant group in *P. bursaria*, had higher relative abundances at higher temperatures (**Figure 4A**). It was possible that the endosymbiotic green algae *Chlorella* sp. became more carbon-rich at higher temperatures (Serra-Maia et al., 2016), which could supply more organic matter to the symbiotic *Pseudomonas* species (Yao et al., 2019). An opposite trend was observed for the dominant DRB group in the algae-free ciliate *E. vannus*, in which the relative abundance of *Pseudoalteromonas* species decreased progressively with the increase of temperature (**Figure 4A**). The cellular chemical composition of *E. vannus* could be altered with temperature, with decreasing carbon to nitrogen ratio or phosphorus ratio at higher temperatures, according to the ecological stoichiometry theory (Woods et al., 2003; Fu and Gong, 2017). This temperature-driven stoichiometric shift in the host could select against specific heterotrophic DRB populations, such as *Pseudoalteromonas* spp. The lower relative abundance of *Pseudoalteromonas* occurred at a higher temperature (25°C), which could be attributed to the mechanism whereby *Pseudoalteromonas* kills other bacterial competitors, such as *Vibrio,* by secreting pseudoalterin, a thermolabile protease (Richards et al., 2017; Tang et al., 2020), which might lower the killing activity at a higher temperature, resulting in a higher proportion of co-occurring *Vibrio* in the DRB assemblage. Also, a higher temperature might enrich the type III secretion system (T3SS) of *Vibrio* in association with protists (Matz et al., 2011).

Light-Driven DRB Assemblage in the Heterotrophic Protist, but Light-Independent DRB in the Mixotroph

The DRB assemblage significantly responded to the light conditions, which occurred only in the heterotrophic *E. vannus* but not in the mixotrophic *P. bursaria*, indicating that the mixotroph could select specific bacterial populations. Interestingly, the DRB detected in the *P. bursaria*, i.e., the gammaproteobacterial *Nevskia* and the alphaproteobacterial *Caulobacter* and *Asticcacaulis*, share a common morphological character in having a stalk or holdfast at certain life stages, with which cells are able to attach onto a water-air interface or substrate surface (Stürmeyer et al., 1998; Purcell et al., 2007; Persat and Gitai, 2014). Typical species of the former two genera have also been demonstrated to be light-sensitive. For example, *Nevskia ramosa* often inhabit at the air-water interface and is capable of DNA reparation against UV damage (Stürmeyer et al., 1998). Visible light can act to regulate a sensory module in *Caulobacter crescentus* in order to increase the biochemical activity and cellular signaling for cell–surface and cell–cell attachment (Purcell et al., 2007). *Asticcacaulis* was detected in the microbial consortium of the oil-rich green alga *Botryococcus braunii* (Sambles et al., 2017). In the constant light treatment, continuous uptake of nutrients by the autotrophs, which included those in medium and the *Chlorella* symbionts inside the *P. bursaria*, probably lead to nutrient limitation to heterotrophic bacteria in the medium. Attachments to, or residue

of these bacteria inside the ciliate cell may facilitate themselves to immediately "capture" the nutrients regenerated by the protist. In constant darkness, *P. bursaria* might sustain by bacterivory, and the bacteria-protist association might reduce bacterial mortality. Therefore, our study based on light manipulation and single cell analysis of protists provides evidence that mixotrophic protists are previously unrecognized hosts and micro-niches of these attaching bacteria in natural environments.

The *Curvibacter* phylotype occurred as DRB of the *P. bursaria* in all-light, all-dark, and diel-cycle treatments. Cultivation in constant darkness or at night might lower the concentration of dissolved oxygen, which provides an ecological advantage to microaerobic bacteria, such as *Curvibacter* sp. (Ding and Yokota, 2010). It has been demonstrated that members of this genus are able to inhibit fungal infection by interacting with other commensal bacterial species in the cnidarian *Hydra* (Fraune et al., 2015). In fact, at least filament fungi were recognizable via the naked eye at later periods of the cultures supplied with rice grains, indicating a risk of fungal infection of the *P. bursaria*. In this sense, it is possible for these bacterial consortiums to function in anti-fungal activity. The *Variovorax* phylotypes were only detected in both LL and LD treatments of the *P. bursaria*. This adaptive ability in such contrasting light environments is consistent with a previous study, which showed a combination of autotrophic and heterotrophic features in the genome of *Variovorax paradoxus* (Han et al., 2011).

The DRB in the heterotrophic ciliate *E. vannus* were photoperiod-dependent. *Alteromonas* sp. was dominant in the treatment of the diel light:dark cycles, suggesting a role of light (or darkness) in selecting these bacteria in association with the protistan cell. A similar mechanism was proposed by a previous study (Biller et al., 2018), which stated that *Alteromonas* may provide energy or organic compounds to cyanobacteria *Prochlorococcus* under the stress of darkness. The *Pseudoalteromonas* phylotypes were consistently present in the DRB assemblages under the conditions having a photic period, probably contributing to anti-fungal infection by more actively producing antifungal polyketide alteramides during the dark period (Moree et al., 2014). Thus, the co-occurrence of these two bacterial taxa may be of benefit to the host for a balance between rapid growth and low pathogenic infection under a natural diel light-dark condition (Liu et al., 2019).

Evidence for Prevalent Antibiotic-Resistant Bacteria Sheltered in Protistan Cells

Gomiero and Viarengo (2014) showed that the antibiotic OTC (3.2 μM to 32 mM) treatments induced changes in the growth, survival, endocytosis rate, and lysosomal membrane stability of the marine ciliate *Euplotes crassus*. Such physiological shifts might have also occurred in these two species we investigated. Apart from that, we found the dominant DRB in the OTC-treated marine ciliate *E. vannus* were affiliated with the members of the genus *Sphingomonas* and the family *Alteromonadaceae* (*Alteromonas* and *Aestuariibacter*) (**Figure 5A**), which is in line with previous findings that both *Sphingomonas* and *Alteromonas* species were resistant to antibiotics, such as OTC (Miranda and Zemelman, 2002; Dang et al., 2007). However, the relative abundance of the phylotype of the family *Puniceicoccaceae* (phylum Verrucomicrobia) decreased in OTC10 and was non-detectable in OTC20, indicating it is sensitive to OTC.

Both *Pseudomonas* and *Sulfitobacter* phylotypes prevailed in the DRB assemblage of mixotrophic *P. bursaria* reared in media with an antibiotic concentration up to 20 mg/L, indicating high antibiotic resistance of these bacteria and that the intracellular environment may provide a favorable habitat for their survival. Indeed, it has been demonstrated that many *Pseudomonas* species could degrade antibiotics via efflux pumps (e.g., Jiang et al., 2014), and consortiums of these bacterial species with algae could enhance the efficiency of degrading antibiotics (Leng et al., 2020). Similarly, genes involved in aromatic compound catabolism and a type IV secretion system are present in the genome of a strain of *Sulfitobacter* (Ankrah et al., 2014), and *Sulfitobacter* in the diatom phycosphere could supply indole acetic acid to the algae in exchange for organosulfur compounds (Amin et al., 2015). Furthermore, *Sulfitobacter* strains isolated from marine hydrothermal vent fields were found to be antibiotic-resistant (Farias et al., 2015). All these suggest that the mixotrophic protist bearing endosymbiotic microalgae (e.g., *Chlorella* sp.) could play a role in accommodating these antibiotic-resistant bacteria, which represent a previously unrecognized scenario in the antibiotic resistance of environmental bacterial populations.

Bacterial Co-resistance to Heavy Metals and to Protistan Digestions

It is well known that short-rod cells of *Flectobacillus* form long filaments and chains of several cells, a morphology-based strategy to protect themselves from being ingested by nanoflagellates predators (Corno and Jürgens, 2006). We detected these bacteria as a member of DRB in *P. bursaria*, suggesting an effect of predator size in the prey-predator interactions, i.e., enlarged bacterial cell size may be effective to avoid being engulfed by small protists but not necessarily for large-celled protists, such as ciliates with wide or highly contractile cytostomes. Furthermore, the *Flectobacillus* phylotypes became dominant in the Pb-treated cultures, demonstrating they are co-resistant to Pb and protistan digestion. However, *Flectobacillus* spp. were found to be a dominant bacterial group in the riverbed sediments spiked with high concentrations of metals, including Cd and Cu, but not in the Pb and Cr treatments (Du et al., 2018). In the Hg-treated *P. bursaria* culture, we also found that *Flectobacillus* phylotypes only accounted for a minor portion of DRB. This suggests a strain-level differentiation in the heavy metal resistance of *Flectobacillus*.

Acinetobacter junii is able to form biofilms on surfaces to resistant to mercury (Sarkar and Chakraborty, 2008), which is in line with our observation of its survival in *P. bursaria* under Hg stresses. In addition, our results point to the non-digestible nature of this bacterial species in ciliated protozoa, highlighting its ecological success in natural environments. Furthermore, *Hydrogenophaga* was also abundant in *P. bursaria* treated with a

high dose of Hg. It remains to be investigated how this hydrogen-oxidizing species interacts with the host and endosymbiotic green alga within the *P. bursaria* under Hg stress, though it is known that As (III) could be oxidized by a strain of this genus under aerobic conditions (Terry et al., 2015).

Not much is known about the ecology and microbial association of *Aestuariibacter*, except for our recent report of this genus as a DRB in four marine and one freshwater species of ciliates (Gong et al., 2016). In the present study, we once again found this genus as a dominant group of DRB in *E. vannus* across all Pb^{2+} and Cd^{2+} treatments and under low-dose antibiotic treatment, indicating *Aestuariibacter* is a previously unrecognized superstar in co-resistance to heavy metals, antibiotics, and protistan digestion. This is probably due to their resident habitats of high-pollution stresses, such as coastal seawater and tidal flats (Yi et al., 2004; Wang et al., 2010). *Pelomonas* was present in the DRB of *E. vannus* treated with high doses of Pb^{2+} and Cd^{2+} but absent in the controls, indicating the metal tolerance of this group. Phylotypes of this genus were also detected in Cd- and Cu-treated activated sludge using DGGE and sequencing (Bhat et al., 2020). Strains of Verrucomicrobia have been isolated as gut symbionts from sea cucumber, marine sponges, clamworm (Wertz et al., 2012), and the marine ciliate *Euplotidium* (Petroni et al., 2000). Our study showed the association between a possible new genus of the family *Puniceicoccaceae* with the ciliate *E. vannus* and for the first time their differential resistance to metals Pb and Cd.

CONCLUDING REMARKS

As major players in the microbial loop and biogeochemical cycle within ecosystems, both bacteria and protists are ecologically linked not only through prey-predator food chains but also via collaboration in facing multiple stresses. Our study reveals for the first time that the assemblage composition and structure of ingested but inedible bacteria in two protists vary significantly in response to stresses of temperature, light, antibiotics, and heavy metals, indicating that the environment plays an important role in selecting specific bacterial populations in protist-bacteria associations. Our results for these two ciliate species also provide an indication that trophic mode of protists (mixotrophs vs. heterotrophs) could be a factor influencing the bacteria-protist interactions, a notion warrants further investigation considering their increasingly recognized importance in marine food webs (Stoecker et al., 2017). Furthermore, bacterial antibiotic resistance and metal resistance have been extensively studied in the past several decades. The ecological interactions between these resistant bacteria and protists remain poorly understudied (Nguyen et al., 2020). Our findings in this study provide evidence that there are diverse bacterial stains, which are not only resistant to antibiotics and/or heavy metals in natural environments but have also survived protistan digestion, suggesting some bacterial species/strains could use protistan cells as shelters in facing of pollution stresses.

DATA AVAILABILITY STATEMENT

The datasets presented in this study can be found in online repositories. The names of the repositories and accession numbers can be found in the article/**Supplementary Material**.

AUTHOR CONTRIBUTIONS

SZ did the data curation-equal, formal analysis-equal, investigation-equal, methodology-equal, resources-equal, software-equal, validation-equal, visualization-equal, and wrote the original draft-lead. QZ performed the resources-supporting and validation-supporting. XZ and CD performed the validation-supporting. JG performed the conceptualization-lead, data curation-supporting, funding acquisition-lead, methodology-equal, project administration-lead, resources-equal, supervision-equal, validation-equal, and wrote, reviewed and edited the manuscript-lead. All authors contributed to the article and approved the submitted version.

FUNDING

This work was supported by the Marine S&T Fund of Shandong Province for Pilot National Laboratory for Marine Science and Technology (Qingdao) (No. 2018SDKJ0406-4), the Key Research Project of Frontier Science, CAS (No. QYZDB-SSW-DQC013-1), and a NSFC-CNRS Collaboration Project (No. 41311130107).

SUPPLEMENTARY MATERIAL

The Supplementary Material for this article can be found online at: https://www.frontiersin.org/articles/10.3389/fmars.2020.00659/full#supplementary-material

FIGURE S1 | A general scheme of research methodology.

REFERENCES

Adams, H. E., Crump, B. C., and Kling, G. W. (2010). Temperature controls on aquatic bacterial production and community dynamics in arctic lakes and streams. *Environ. Microbiol.* 12, 1319–1333. doi: 10.1111/j.1462-2920.2010.02176.x

Alonso-Sáez, L., Gasol, J. M., Lefort, T., Hofer, J., and Sommaruga, R. (2006). Effect of natural sunlight on bacterial activity and differential sensitivity of natural bacterioplankton groups in northwestern mediterranean coastal waters. *Appl. Environ. Microbiol.* 72, 5806–5813. doi: 10.1128/AEM.00597-06

Al-Rasheid, K. A. S., and Sleigh, M. A. (1994). The effects of heavy metals on the feeding rate of *Euplotes mutabilis* (Tuffrau, 1960). *Eur. J. Protistol.* 30, 270–279. doi: 10.1016/S0932-4739(11)80073-8

Amin, S. A., Hmelo, L. R., Van Tol, H. M., Durham, B. P., Carlson, L. T., Heal, K. R., et al. (2015). Interaction and signalling between a cosmopolitan phytoplankton and associated bacteria. *Nature* 522, 98–101. doi: 10.1038/nature14488

Ankrah, N. Y. D., Lane, T., Budinoff, C. R., Hadden, M. K., and Buchan, A. (2014). Draft genome sequence of *Sulfitobacter* sp. *CB*2047, a member of the *Roseobacter clade* of marine bacteria, isolated from an *Emiliania huxleyi* bloom. *Genome Announc.* 2:e001125-14. doi: 10.1128/genomeA.01125-14

Ashelford, K. E., Chuzhanova, N. A., Fry, J. C., Jones, A. J., and Weightman, A. J. (2006). New screening software shows that most recent large 16S rRNA gene clone libraries contain chimeras. *Appl. Environ. Microbiol.* 72, 5734–5741. doi: 10.1128/AEM.00556-06

Azam, F., Fenchel, T., Field, J. G., Gray, J. S., Meyer-Reil, L. A., and Thingstad, F. (1983). The ecological role of water-column microbes in the sea. *Mar. Ecol. Prog. Ser.* 10, 257–263. doi: 10.3354/meps010257

Bhat, S. A., Cui, G., Li, W., Wei, Y., and Li, F. (2020). Effect of heavy metals on the performance and bacterial profiles of activated sludge in a semi-continuous reactor. *Chemosphere* 241:125035. doi: 10.1016/j.chemosphere.2019.125035

Biller, S. J., Coe, A., Roggensack, S. E., and Chisholm, S. W. (2018). Heterotroph interactions alter *Prochlorococcus* transcriptome dynamics during extended periods of darkness. *mSystems* 3:e0040-18. doi: 10.1128/mSystems.00040-18

Boenigk, J., Matz, C., Jürgens, K., and Arndt, H. (2001). The influence of preculture conditions and food quality on the ingestion and digestion process of three species of heterotrophic nanoflagellates. *Microb. Ecol.* 42, 168–176. doi: 10.1007/s002480000116

Corno, G., and Jürgens, K. (2006). Direct and indirect effects of protist predation on population size structure of a bacterial strain with high phenotypic plasticity. *Appl. Environ. Microbiol.* 72, 78–86. doi: 10.1128/AEM.72.1.78-86.2006

Dang, H., Zhang, X., Song, L., Chang, Y., and Yang, G. (2007). Molecular determination of oxytetracycline-resistant bacteria and their resistance genes from mariculture environments of China. *J. Appl. Microbiol.* 103, 2580–2592. doi: 10.1111/j.1365-2672.2007.03494.x

Darriba, D., Taboada, G. L., Doallo, R., and Posada, D. (2012). jModelTest 2: more models, new heuristics and parallel computing. *Nat. Methods* 9, 772–772. doi: 10.1038/nmeth.2109

Ding, L., and Yokota, A. (2010). *Curvibacter fontana* sp. nov., a microaerobic bacteria isolated from well water. *J. Gen. Appl. Microbiol.* 56, 267–271. doi: 10.2323/jgam.56.267

Du, H., Harata, N., and Li, F. (2018). Responses of riverbed sediment bacteria to heavy metals: integrated evaluation based on bacterial density, activity and community structure under well-controlled sequencing batch incubation conditions. *Water Res.* 130, 115–126. doi: 10.1016/j.watres.2017.10.070

Farias, P., Espírito Santo, C., Branco, R., Francisco, R., Santos, S., Hansen, L., et al. (2015). Natural hot spots for gain of multiple resistances: arsenic and antibiotic resistances in heterotrophic, aerobic bacteria from marine hydrothermal vent fields. *Appl. Environ. Microbiol.* 81, 2534–2543. doi: 10.1128/AEM.03240-14

Farnelid, H. M., Turk-Kubo, K. A., and Zehr, J. P. (2016). Identification of associations between bacterioplankton and photosynthetic picoeukaryotes in coastal waters. *Front. Microbiol.* 7:339. doi: 10.3389/fmicb.2016.00339

First, M. R., Park, N. Y., Berrang, M. E., Meinersmann, R. J., Bernhard, J. M., Gast, R. J., et al. (2012). Ciliate ingestion and digestion: flow cytometric measurements and regrowth of a digestion-resistant *Campylobacter jejuni*. *J. Eukaryot. Microbiol.* 59, 12–19. doi: 10.1111/j.1550-7408.2011.00589.x

Fraune, S., Anton-Erxleben, F., Augustin, R., Franzenburg, S., Knop, M., Schröder, K., et al. (2015). Bacteria-bacteria interactions within the microbiota of the ancestral metazoan *Hydra* contribute to fungal resistance. *ISME J.* 9, 1543–1556. doi: 10.1038/ismej.2014.239

Fu, R., and Gong, J. (2017). Single cell analysis linking ribosomal (r)DNA and rRNA copy numbers to cell size and growth rate provides insights into molecular protistan ecology. *J. Eukaryot. Microbiol.* 64, 885–896. doi: 10.1111/jeu.12425

Galtier, N., Gouy, M., and Gautier, C. (1996). SEAVIEW and PHYLO_WIN: two graphic tools for sequence alignment and molecular phylogeny. *Bioinformatics* 12, 543–548. doi: 10.1093/bioinformatics/12.6.543

Gomiero, A., and Viarengo, A. (2014). Effects of elevated temperature on the toxicity of copper and oxytetracycline in the marine model, *Euplotes crassus*: a climate change perspective. *Environ. Pollut.* 194, 262–271. doi: 10.1016/j.envpol.2014.07.035

Gong, J., Qing, Y., Guo, X., and Warren, A. (2014). "*Candidatus Sonnebornia yantaiensis*", a member of candidate division OD1, as intracellular bacteria of the ciliated protist *Paramecium bursaria* (Ciliophora. Oligohymenophorea). *Syst. Appl. Microbiol.* 37, 35–41. doi: 10.1016/j.syapm.2013.08.007

Gong, J., Qing, Y., Zou, S., Fu, R., Su, L., Zhang, X., et al. (2016). Protist-bacteria associations: gammaproteobacteria and alphaproteobacteria are prevalent as digestion-resistant bacteria in ciliated protozoa. *Front. Microbiol.* 7:498. doi: 10.3389/fmicb.2016.00498

Guindon, S., Delsuc, F., Dufayard, J.-F., and Gascuel, O. (2009). "Estimating maximum likelihood phylogenies with PhyML," in *Bioinformatics for DNA Sequence Analysis. Methods in Molecular Biology*, ed. D. Posada (Totowa, NJ: Humana Press), 113–137. doi: 10.1007/978-1-59745-251-9_6

Han, J.-I., Choi, H.-K., Lee, S.-W., Orwin, P. M., Kim, J., Laroe, S. L., et al. (2011). Complete genome sequence of the metabolically versatile plant growth-promoting endophyte *Variovorax paradoxus* S110. *J. Bacteriol.* 193, 1183–1190. doi: 10.1128/JB.00925-10

Hu, A., Yang, X., Chen, N., Hou, L., Ma, Y., and Yu, C.-P. (2014). Response of bacterial communities to environmental changes in a mesoscale subtropical watershed, Southeast China. *Sci. Total Environ.* 472, 746–756. doi: 10.1016/j.scitotenv.2013.11.097

Huber, T., Faulkner, G., and Hugenholtz, P. (2004). Bellerophon: a program to detect chimeric sequences in multiple sequence alignments. *Bioinformatics* 20, 2317–2319. doi: 10.1093/bioinformatics/bth226

Ibekwe, A. M., Ma, J., and Murinda, S. E. (2016). Bacterial community composition and structure in an urban river impacted by different pollutant sources. *Sci. Total Environ.* 566–567, 1176–1185. doi: 10.1016/j.scitotenv.2016.05.168

Izaguirre, I., Sinistro, R., Schiaffino, M. R., Sánchez, M. L., Unrein, F., and Massana, R. (2012). Grazing rates of protists in wetlands under contrasting light conditions due to floating plants. *Aquat. Microb. Ecol.* 65, 221–232. doi: 10.3354/ame01547

Jiang, B., Li, A., Cui, D., Cai, R., Ma, F., and Wang, Y. (2014). Biodegradation and metabolic pathway of sulfamethoxazole by *Pseudomonas psychrophila* HA-4, a newly isolated cold-adapted sulfamethoxazole-degrading bacterium. *Appl. Microbiol. Biotechnol.* 98, 4671–4681. doi: 10.1007/s00253-013-5488-3

Jousset, A. (2012). Ecological and evolutive implications of bacterial defences against predators. *Environ. Microbiol.* 14, 1830–1843. doi: 10.1111/j.1462-2920.2011.02627.x

Katoh, K., and Standley, D. M. (2013). MAFFT multiple sequence alignment software version 7: improvements in performance and usability. *Mol. Biol. Evol.* 30, 772–780. doi: 10.1093/molbev/mst010

Kim, S.-H., Jung, M.-Y., and Lee, Y.-M. (2011). Effect of heavy metals on the antioxidant enzymes in the marine ciliate *Euplotes crassus*. *Toxicol. Environ. Health Sci.* 3, 213–219. doi: 10.1007/s13530-011-0103-4

Kodama, Y., and Fujishima, M. (2014). Symbiotic *Chlorella variabilis* incubated under constant dark conditions for 24 hours loses the ability to avoid digestion by host lysosomal enzymes in digestive vacuoles of host ciliate *Paramecium bursaria*. *FEMS Microbiol. Ecol.* 90, 946–955. doi: 10.1111/1574-6941.12448

Lane, D. J. (1991). *16S/23S rRNA Sequencing*. New York, NY: John Wiley & Sons Ltd.

Lasica, A. M., Ksiazek, M., Madej, M., and Potempa, J. (2017). The type IX secretion system (T9SS): highlights and recent insights into its structure and function. *Front. Cell. Infect. Microbiol.* 7:215. doi: 10.3389/fcimb.2017.00215

Leng, L., Wei, L., Xiong, Q., Xu, S., Li, W., Lv, S., et al. (2020). Use of microalgae based technology for the removal of antibiotics from wastewater: a review. *Chemosphere* 238:124680. doi: 10.1016/j.chemosphere.2019.124680

Liu, J., Meng, Z., Liu, X., and Zhang, X.-H. (2019). Microbial assembly, interaction, functioning, activity and diversification: a review derived from community compositional data. *Mar. Life Sci. Technol.* 1, 112–128. doi: 10.1007/s42995-019-00004-3

Mahowald, M. A., Rey, F. E., Seedorf, H., Turnbaugh, P. J., Fulton, R. S., Wollam, A., et al. (2009). Characterizing a model human gut microbiota composed of members of its two dominant bacterial phyla. *Proc. Natl. Acad. Sci. U.S.A.* 106, 5859–5864. doi: 10.1073/pnas.0901529106

Martinez-Garcia, M., Brazel, D., Poulton, N. J., Swan, B. K., Gomez, M. L., Masland, D., et al. (2012). Unveiling in situ interactions between marine protists and bacteria through single cell sequencing. *ISME J.* 6, 703–707. doi: 10.1038/ismej.2011.126

Matz, C., and Kjelleberg, S. (2005). Off the hook-how bacteria survive protozoan grazing. *Trends Microbiol.* 13, 302–307. doi: 10.1016/j.tim.2005.05.009

Matz, C., Nouri, B., Mccarter, L., and Martinez-Urtaza, J. (2011). Acquired type III secretion system determines environmental fitness of epidemic *Vibrio*

parahaemolyticus in the interaction with bacterivorous protists. *PLoS One* 6:e20275. doi: 10.1371/journal.pone.0020275

Miranda, C. D., and Zemelman, R. (2002). Bacterial resistance to oxytetracycline in Chilean salmon farming. *Aquaculture* 212, 31–47. doi: 10.1016/S0044-8486(02)00124-2

Montagnes, D. J. S., and Weisse, T. (2000). Fluctuating temperatures affect growth and production rates of planktonic ciliates. *Aquat. Microb. Ecol.* 21, 97–102. doi: 10.3354/ame021097

Moree, W. J., Mcconnell, O. J., Nguyen, D. D., Sanchez, L. M., Yang, Y.-L., Zhao, X., et al. (2014). Microbiota of healthy corals are active against fungi in a light-dependent manner. *ACS Chem. Biol.* 9, 2300–2308. doi: 10.1021/cb500432j

Newton, R. J., Jones, S. E., Eiler, A., Mcmahon, K. D., and Bertilsson, S. (2011). A guide to the natural history of freshwater lake bacteria. *Microbiol. Mol. Biol. Rev.* 75, 14–49. doi: 10.1128/MMBR.00028-10

Nguyen, B.-A. T., Chen, Q.-L., He, J.-Z., and Hu, H.-W. (2020). Microbial regulation of natural antibiotic resistance: understanding the protist-bacteria interactions for evolution of soil resistome. *Sci. Total Environ.* 705:135882. doi: 10.1016/j.scitotenv.2019.135882

Osborn, A. M., Moore, E. R. B., and Timmis, K. N. (2000). An evaluation of terminal-restriction fragment length polymorphism (T-RFLP) analysis for the study of microbial community structure and dynamics. *Environ. Microbiol.* 2, 39–50. doi: 10.1046/j.1462-2920.2000.00081.x

Pernthaler, J. (2005). Predation on prokaryotes in the water column and its ecological implications. *Nat. Rev. Microbiol.* 3, 537–546. doi: 10.1038/nrmicro1180

Persat, A., and Gitai, Z. (2014). Bacterial evolution: rewiring modules to get in shape. *Curr. Biol.* 24, R522–R524. doi: 10.1016/j.cub.2014.04.022

Petroni, G., Spring, S., Schleifer, K.-H., Verni, F., and Rosati, G. (2000). Defensive extrusive ectosymbionts of *Euplotidium* (Ciliophora) that contain microtubule-like structures are bacteria related to Verrucomicrobia. *Proc. Natl. Acad. Sci. U.S.A.* 97, 1813–1817. doi: 10.1073/pnas.030438197

Pucciarelli, S., Devaraj, R. R., Mancini, A., Ballarini, P., Castelli, M., Schrallhammer, M., et al. (2015). Microbial consortium associated with the antarctic marine ciliate *Euplotes focardii*: an investigation from genomic sequences. *Microb. Ecol.* 70, 484–497. doi: 10.1007/s00248-015-0568-9

Purcell, E. B., Siegal-Gaskins, D., Rawling, D. C., Fiebig, A., and Crosson, S. (2007). A photosensory two-component system regulates bacterial cell attachment. *Proc. Natl. Acad. Sci. U.S.A.* 104, 18241–18246. doi: 10.1073/pnas.0705887104

Richards, G. P., Watson, M. A., Needleman, D. S., Uknalis, J., Boyd, E. F., and Fay, J. P. (2017). Mechanisms for *Pseudoalteromonas piscicida*-induced killing of *vibrios* and other bacterial pathogens. *Appl. Environ. Microbiol.* 83:e00175-17. doi: 10.1128/AEM.00175-17

Ronquist, F., and Huelsenbeck, J. P. (2003). MrBayes 3: Bayesian phylogenetic inference under mixed models. *Bioinformatics* 19, 1572–1574. doi: 10.1093/bioinformatics/btg180

Sambles, C., Moore, K., Lux, T. M., Jones, K., Littlejohn, G. R., Gouveia, J. D., et al. (2017). Metagenomic analysis of the complex microbial consortium associated with cultures of the oil-rich alga *Botryococcus braunii*. *MicrobiologyOpen* 6:e00482. doi: 10.1002/mbo3.482

Sarkar, S., and Chakraborty, R. (2008). Quorum sensing in metal tolerance of *Acinetobacter junii* BB1A is associated with biofilm production. *FEMS Microbiol. Lett.* 282, 160–165. doi: 10.1111/j.1574-6968.2008.01080.x

Schloss, P. D., Westcott, S. L., Ryabin, T., Hall, J. R., Hartmann, M., Hollister, E. B., et al. (2009). Introducing mothur: open-source, platform-independent, community-supported software for describing and comparing microbial communities. *Appl. Environ. Microbiol.* 75, 7537–7541. doi: 10.1128/AEM.01541-09

Serra-Maia, R., Bernard, O., Gonçalves, A., Bensalem, S., and Lopes, F. (2016). Influence of temperature on *Chlorella vulgaris* growth and mortality rates in a photobioreactor. *Algal Res.* 18, 352–359. doi: 10.1016/j.algal.2016.06.016

Sherr, B. F., Sherr, E. B., and Rassoulzadegan, F. (1988). Rates of digestion of bacteria by marine phagotrophic protozoa: temperature dependence. *Appl. Environ. Microbiol.* 54, 1091–1095. doi: 10.1128/aem.54.5.1091-1095.1988

Shibata, A., Takahashi, F., Kasahara, M., and Imamura, N. (2016). Induction of maltose release by light in the endosymbiont *Chlorella variabilis* of *Paramecium bursaria*. *Protist* 167, 468–478. doi: 10.1016/j.protis.2016.08.007

Šimek, K., Kasalický, V., Jezbera, J., Horňák, K., Nedoma, J., Hahn, M. W., et al. (2013). Differential freshwater flagellate community response to bacterial food quality with a focus on *Limnohabitans* bacteria. *ISME J.* 7, 1519–1530. doi: 10.1038/ismej.2013.57

Stoecker, D. K., Hansen, P. J., Caron, D. A., and Mitra, A. (2017). Mixotrophy in the marine plankton. *Ann. Rev. Mar. Sci.* 9, 311–335. doi: 10.1146/annurev-marine-010816-060617

Storesund, J. E., Erga, S. R., Ray, J. L., Thingstad, T. F., and Sandaa, R.-A. (2015). Top-down and bottom-up control on bacterial diversity in a western Norwegian deep-silled fjord. *FEMS Microbiol. Ecol.* 91:fiv076. doi: 10.1093/femsec/fiv076

Stürmeyer, H., Overmann, J., Babenzien, H.-D., and Cypionka, H. (1998). Ecophysiological and phylogenetic studies of *Nevskia ramosa* in pure culture. *Appl. Environ. Microbiol.* 64, 1890–1894. doi: 10.1128/aem.64.5.1890-1894.1998

Tang, B.-L., Yang, J., Chen, X.-L., Wang, P., Zhao, H.-L., Su, H.-N., et al. (2020). A predator-prey interaction between a marine *Pseudoalteromonas* sp. and *Gram-positive* bacteria. *Nat. Commun.* 11:285. doi: 10.1038/s41467-019-14133-x

Terry, L. R., Kulp, T. R., Wiatrowski, H., Miller, L. G., and Oremland, R. S. (2015). Microbiological oxidation of antimony (III) with oxygen or nitrate by bacteria isolated from contaminated mine sediments. *Appl. Environ. Microbiol.* 81, 8478–8488. doi: 10.1128/AEM.01970-15

Wang, Q., Garrity, G. M., Tiedje, J. M., and Cole, J. R. (2007). Naïve bayesian classifier for rapid assignment of rRNA sequences into the new bacterial taxonomy. *Appl. Environ. Microbiol.* 73, 5261–5267. doi: 10.1128/AEM.00062-07

Wang, Y., Wang, H., Liu, J., Lai, Q., Shao, Z., Austin, B., et al. (2010). *Aestuariibacter aggregatus* sp. nov., a moderately *Halophilic* bacterium isolated from seawater of the Yellow Sea. *FEMS Microbiol. Lett.* 309, 48–54. doi: 10.1111/j.1574-6968.2010.02011.x

Wertz, J. T., Kim, E., Breznak, J. A., Schmidt, T. M., and Rodrigues, J. L. M. (2012). Genomic and physiological characterization of the Verrucomicrobia isolate *Diplosphaera colitermitum* gen. nov., sp. nov., reveals microaerophily and nitrogen fixation genes. *Appl. Environ. Microbiol.* 78, 1544–1555. doi: 10.1128/AEM.06466-11

Woods, H. A., Makino, W., Cotner, J. B., Hobbie, S. E., Harrison, J. F., Acharya, K., et al. (2003). Temperature and the chemical composition of poikilothermic organisms. *Funct. Ecol.* 17, 237–245. doi: 10.1046/j.1365-2435.2003.00724.x

Xu, Y., Shen, Z., Gentekaki, E., Xu, J., and Yi, Z. (2020). Comparative transcriptome analyses during the vegetative cell cycle in the mono-cellular organism *Pseudokeronopsis erythrina* (Alveolata, Ciliophora). *Microorganisms* 8:108. doi: 10.3390/microorganisms8010108

Yao, S., Lyu, S., An, Y., Lu, J., Gjermansen, C., and Schramm, A. (2019). Microalgae-bacteria symbiosis in microalgal growth and biofuel production: a review. *J. Appl. Microbiol.* 126, 359–368. doi: 10.1111/jam.14095

Yi, H., Bae, K. S., and Chun, J. (2004). *Aestuariibacter salexigens* gen. nov., sp. nov. and *Aestuariibacter halophilus* sp. nov., isolated from tidal flat sediment, and emended description of *Alteromonas macleodii*. *Int. J. Syst. Evol. Microbiol.* 54, 571–576. doi: 10.1099/ijs.0.02798-0

Zou, S., Zhang, Q., and Gong, J. (2020). Comparative transcriptomics reveals distinct gene expressions of a model ciliated protozoan feeding on bacteria-free medium, digestible, and digestion-resistant bacteria. *Microorganisms* 8:559. doi: 10.3390/microorganisms8040559

Conflict of Interest: The authors declare that the research was conducted in the absence of any commercial or financial relationships that could be construed as a potential conflict of interest.

frontiers in Marine Science

ORIGINAL RESEARCH
published: 26 November 2020
doi: 10.3389/fmars.2020.602317

Ontogeny and Phylogeny of a New Hypotrichous Ciliate (Protista, Ciliophora), *Metaurostylopsis alrasheidi* n. sp., With Establishment of a New Genus *Monourostylopsis* n. gen.

Wenya Song[1,2], Yu Qiao[1], Jingyi Dong[1], William A. Bourland[3], Tengteng Zhang[1] and Xiaotian Luo[2]**

[1] Institute of Evolution and Marine Biodiversity, Ocean University of China, Qingdao, China, [2] Key Laboratory of Aquatic Biodiversity and Conservation of Chinese Academy of Sciences, Institute of Hydrobiology, Chinese Academy of Sciences, Wuhan, China, [3] Department of Biological Sciences, Boise State University, Boise, ID, United States

OPEN ACCESS

Edited by:
Hongbo Pan, Shanghai Ocean University, China

Reviewed by:
Lingyun Chen, Northwest Normal University, China
Xiangrui Chen, Ningbo University, China

***Correspondence:**
Tengteng Zhang
tengtzhang@foxmail.com
Xiaotian Luo
luoxiaotian@ihb.ac.cn

Specialty section:
This article was submitted to Marine Evolutionary Biology, Biogeography and Species Diversity, a section of the journal Frontiers in Marine Science

Received: *03 September 2020*
Accepted: *27 October 2020*
Published: *26 November 2020*

Citation:
Song W, Qiao Y, Dong J, Bourland WA, Zhang T and Luo X (2020) Ontogeny and Phylogeny of a New Hypotrichous Ciliate (Protista, Ciliophora), Metaurostylopsis alrasheidi n. sp., With Establishment of a New Genus Monourostylopsis n. gen. Front. Mar. Sci. 7:602317. doi: 10.3389/fmars.2020.602317

In the present study, based on both morphologic and phylogenetic analyses, a new genus, *Monourostylopsis* n. gen., and new species, *Metaurostylopsis alrasheidi* n. sp. as well as a new combination, *Monourostylopsis antarctica* (Jung et al., 2011) n. comb. (original combination: *Metaurostylopsis antarctica* Jung et al., 2011), are suggested. The new genus is diagnosed mainly by having three or more frontoterminal cirri, a midventral complex with midventral pairs and a single midventral row, one right marginal row and two or more left marginal rows. The new genus can be easily separated from the morphologically similar genera mainly by having single right marginal row (vs. two or more right marginal rows). Based on live observation and protargol staining, the morphology and morphogenesis of a new species, *M. alrasheidi* n. sp. isolated from China, were investigated. The new species can be characterized by: two types of cortical granules; about 22 adoral membranelles; three or four frontoterminal, four or five transverse cirri; about eight midventral pairs and a midventral row of three or four unpaired midventral cirri; three or four left and right marginal rows. The main morphogenetic features of *Metaurostylopsis alrasheidi* n. sp. can be summarized as: (1) the entire parental ciliature, including the oral apparatus, is renewed; (2) the oral primordium of the proter probably originates within a pouch; (3) the oral primordium of the opisthe forms *de novo* on the cell surface; (4) the anlagen of marginal rows and dorsal kineties are formed intrakinetally, and (5) the fusion of macronuclear nodules results in an irregular branched mass prior to karyokinesis. In the phylogenetic trees, all the available *Metaurostylopsis* sequences cluster together in a clade with full support (ML/BI: 100/1.00) revealing that the genus is monophyletic within the large group of core urostylids.

Keywords: *Metaurostylopsis*, *Monourostylopsis* n. gen., ontogenesis, 18S rRNA gene, systematics, taxonomy

INTRODUCTION

Hypotrichs have been widely regarded as the most complex and highly differentiated ciliate group (Foissner, 1982, 2016; Tuffrau and Fleury, 1994; Berger, 1999, 2006, 2008, 2011; Song et al., 2009; Li et al., 2018). Recent faunistic studies have revealed numerous new hypotrichous taxa, suggesting that the diversity of this group is still underestimated (Kaur et al., 2019; Luo et al., 2019; Dong et al., 2020; Lu et al., 2020; Ma et al., 2020; Wang et al., 2020a). Furthermore, the extensive studies on morphogenesis and molecular phylogeny of hypotrichs have led to a better understanding of their systematics and evolutionary relationships (Song and Shao, 2017; Lyu et al., 2018; Kim and Min, 2019; Shao et al., 2019; Wang et al., 2020b; Zhang et al., 2020).

Urostylids, with a diversity of more than 200 species, are one of the largest groups in hypotrichs, and are commonly found in marine, soil and freshwater habitats. Morphologically, they are characterized by a midventral complex composed of zigzag-patterned midventral cirral pairs (Berger, 2006; Kumar et al., 2010; Chen et al., 2011; Pan et al., 2016; Kim et al., 2017; Hu et al., 2019; Jung and Berger, 2019). Based mainly on the presence of frontoterminal cirri, the clearly differentiated frontal cirri and several morphogenetic features, Song et al. (2001) transferred *Urostyla marina* Kahl, 1932 to a newly established urostylid genus, *Metaurostylopsis*, with *M. marina* (Kahl, 1932) Song et al., 2001 as the type species. In the following decades, more species of this genus have been identified and described (Song and Wilbert, 2002; Lei et al., 2005; Shao et al., 2008a,b; Chen et al., 2011, 2013; Jung et al., 2011; Lu et al., 2016). Nevertheless, detailed ontogenetic and molecular information has consistently questioned the assignments of some *Metaurostylopsis* species and further revisions of the genus have been made. Based on comprehensive analyses, Song et al. (2011) recognized five species in the genus *Metaurostylopsis* (*M. marina*, *M. rubra* Song and Wilbert, 2002, *M. salina* Lei et al., 2005, *M. struederkypkeae* Shao et al., 2008, and *M. cheni* Chen et al., 2011) and reassigned *M. sinica* Shao et al., 2008 into a new genus *Apourostylopsis*. While *M. flavicans* Wang et al., 2011 and *M. songi* Lei et al., 2005 were treated as incertae sedis. In the same year, a new *Metaurostylopsis* species, *M. antarctica* Jung et al., 2011 was reported. Subsequently, Chen et al. (2013) transferred the two incertae sedis, *M. flavicans* and *M. songi*, into a new genus *Neourostylopsis* and provided improved diagnoses for both the genus *Metaurostylopsis* and *Apourostylopsis*. Most recently, Lu et al. (2016) added a new species, *Metaurostylopsis parastruederkypkeae* to the genus. As of this writing, seven species are included in *Metaurostylopsis*.

In the present work, morphological, ontogenetic, and molecular data for a new urostylid species, *Metaurostylopsis alrasheidi* n. sp., are provided. In addition, morphological, morphogenetic, and phylogenetic analyses comparing *Metaurostylopsis antarctica* and other *Metaurostylopsis* species are carried out, leading to the establishment of a new genus for *Metaurostylopsis antarctica*.

MATERIALS AND METHODS

Sampling, Observation, and Identification

Metaurostylopsis alrasheidi n. sp. was discovered on June 3, 2019 in a freshwater sample from Lake Weishan (34°46′14″N, 117°12′56″E) (**Figures 1A–D**), China. A raw culture was established in Petri dishes with rice grains added to facilitate the growth of bacteria as food source for the ciliates. A single cell was transferred with a micropipette to a mini Petri dish containing mineral water with squeezed rice grains to establish a clonal culture which was maintained for about 1 month at room temperature about 25°C, and from which DNA extraction was done.

Live observation, protargol preparation, and drawings of protargol-impregnated specimens, live cells, and dividers are according to Shao et al. (2019). Classification is mainly according to Jankowski (2007) and terminology is according to Berger (2006).

DNA Extraction, PCR, and Sequencing

A total of five clonal cells were isolated, washed several times with sterilized freshwater. Subsequently, the five cells were picked into three 1.5 ml microfuge tubes with as little water as possible, two tubes with one cell each and three cells in the third tube. Genomic DNA of cells was extracted using the DNeasy Blood & Tissue Kit (Qiagen, Germantown, MD) following the manufacturer's instructions. The PCR primers for 18S rRNA gene amplification were 82SF (5′-GAAACTGCGAATGGCTC-3′) (Jerome et al., 1996) and 5.8SR (5′-TACTGATATGCTTAAGTTCAGCGG-3′) (Gao et al., 2012). Q5®HotStart High-Fidelity 2 × Master Mix DNA Polymerase (NEB, Ipswich, MA) (Wang et al., 2017a) was selected for PCR, with parameters according to Lian et al. (2019). The PCR target product was sent to Tsingke, Biological Technology Company (Qingdao, China) to sequence bidirectionally using primers 82SF, 5.8SR, Pro + B (5′-GGTTAAAAAGCTCGTAGT-3′), 900F (5′-CGATCAGATACCGTCCTAGT-3′), and 900R (5′-ACTAGGACGGTATCTGATCG-3′) (Wang et al., 2017b). Seqman 5.0 (DNAStar) was used to assemble contigs, which included the partial 18S rRNA gene and ITS1-5.8S rRNA-ITS2 sequence. The sequence was aligned using 18SR (5′-TGATCCTTCTGCAGGTTCACCTAC-3′) (Medlin et al., 1988) to remove ITS1-5.8S rRNA-ITS2. The 18S rRNA gene sequence with a length of 1,647 bp was used for phylogenetic analyses.

Phylogenetic Analyses

In this work, 18S rRNA gene sequences of *Metaurostylopsis alrasheidi* n. sp. and 65 other Hypotrichia relatives were selected to perform phylogenetic analyses. According to Chen et al. (2020), *Holosticha diademata* (KF306396), *Holosticha* cf. *heterofoissneri* (KP717081), *Holosticha heterofoissneri* (KP717082), *Uncinata bradburyae* (EF123706), and *Uncinata gigantea* (KP717083) were selected as outgroup species.

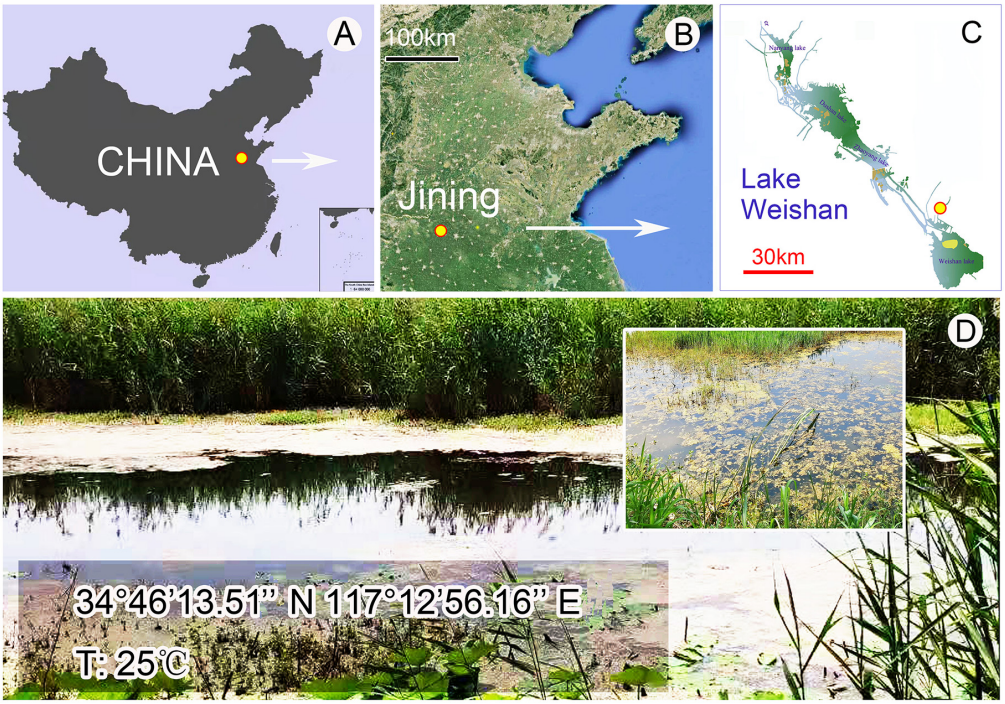

FIGURE 1 | Location of the sampling site. **(A–C)** Map showing the location of the Lake Weishan, China. **(D)** Photographs of the Lake Weishan where *Metaurostylopsis alrasheidi* n. sp. was collected.

The 66 18S rRNA gene sequences were aligned using the MUSCLE algorithm on the webserver GUIDANCE 2[1] (Sela et al., 2015). Both primers were removed using BioEdit 7.0 (Hall, 1999). The final alignment of 1,709 positions was used to construct phylogenetic trees. Maximum likelihood (ML) analysis with 1,000 bootstrap replicates was performed using RAxML-HPC2 on XSEDE 8.2.12 on the online server CIPRES Science Gateway (Stamatakis, 2014), with the GTRGAMMA model as the optimal choice. Bayesian inference (BI) analysis was carried out using MrBayes on XSEDE 3.2.6 (Ronquist et al., 2012) on CIPRES Science Gateway with the GTR + I + G model selected under Akaike Information Criterion (AIC) by jModelTest 2 (Darriba et al., 2012). Four Markov chain Monte Carlo (MCMC) chains were run for 1,000,000 generations, with sampling every 100 generations, the first 2,500 trees as burn-in. SeaView 4.6.1 (Gouy et al., 2010) and MEGA X (Kumar et al., 2018) were used to adjust the tree topologies.

RESULTS

ZooBank Registration

Present work: LSIDurn:lsid:zoobank.org:pub:0085C8A1-6EE5-4E85-A245-D30CF9E18FC2.

Monourostylopsis n. gen.: LSIDurn:lsid:zoobank.org:act:CF7BB200-33C6-4BBE-8998-2299FA70A0E7.

Metaurostylopsis alrasheidi n. sp.: LSIDurn:lsid:zoobank.org:act:077DAC39-8F8B-4BCD-849A-D07BE1C0C790.

Taxonomy and Morphological Description of the New Species

Subclass Hypotrichia Stein, 1859.
Order Urostylida Jankowski, 1979.
Family Urostylidae Bütschli, 1889.
Genus *Metaurostylopsis* Song et al., 2001
Metaurostylopsis alrasheidi n. sp. (**Figures 2–5** and **Table 1**).

Diagnosis

Body 60–115 × 20–60 μm *in vivo*; two types of cortical granules: larger yellow-greenish ones and smaller colorless ones; about 22 adoral membranelles; three frontal, three or four frontoterminal, one buccal, four or five transverse cirri; 5–13 midventral pairs and a midventral row of three or four unpaired ventral cirri; three or four left and right marginal rows respectively; invariably three dorsal kineties; over 40 macronuclear nodules; freshwater habitat.

Type Locality

Lake Weishan (34°46′14″N, 117°12′56″E), Shandong Province, China, a freshwater lake crowded with water plants, algae and decaying plant matter.

Material Deposited

The protargol slide (accession no. SWY2019060301-1) containing the holotype and several paratype slides (accession

[1]http://guidance.tau.ac.il/

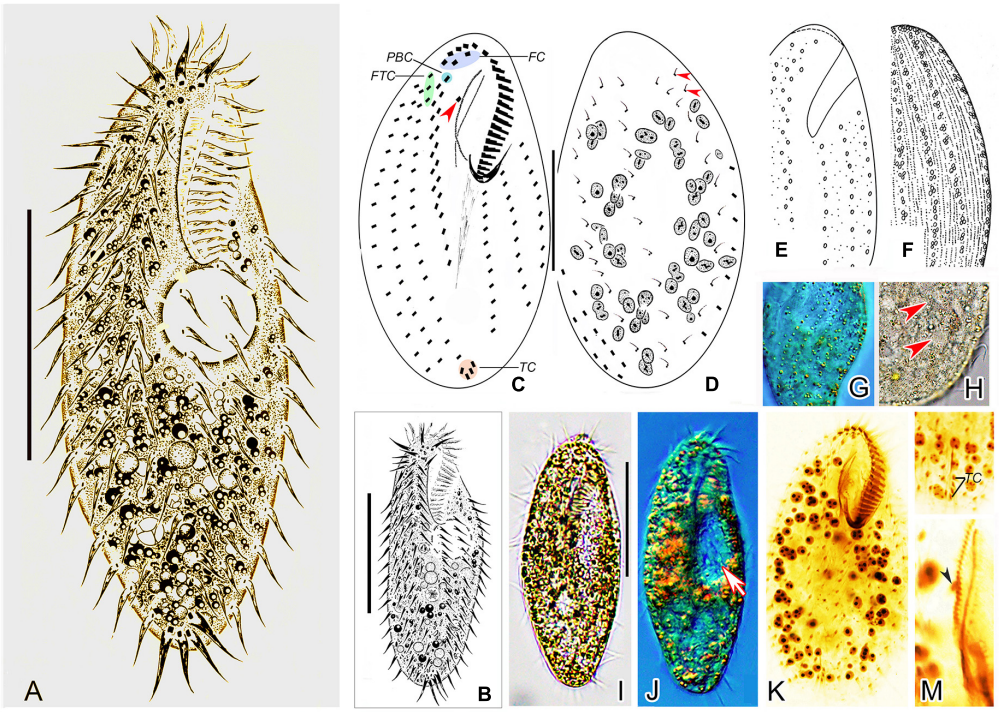

FIGURE 2 | Morphology of *Metaurostylopsis alrasheidi* n. sp. from life (**A,B,E,F,H,I**, bright field; **G,J**, differential interference contrast) and after protargol preparation (**C,D,K–M**). **(A,B)** Ventral views showing representative individuals. **(C,D)** Ventral **(C)** and dorsal **(D)** views, arrowhead in **(C)** indicates the buccal cirrus, arrowheads in **(D)** mark the extra dorsal bristles. **(E–H)** Arrangement of cortical granules on ventral **(E,G)** and dorsal **(F,H)** side, arrowheads in **(H)** indicate small cortical granules. **(I,J)** Ventral views of different individuals, arrow in **(J)** shows the contractile vacuole. **(K)** Ventral view of the holotype specimen to show the ciliature and nuclear apparatus. **(L)** Showing the J-shaped transverse cirri. **(M)** Details of the undulating membranes, arrowhead indicates the buccal cirrus. FC, frontal cirri; FTC, frontoterminal cirri; PBC, parabuccal cirrus; TC, transverse cirri. Scale bars = 40 μm.

no. SWY2019060301-2–9) are deposited in the Laboratory of Protozoology, Ocean University of China.

Dedication

We dedicate this new species to our eminent colleague, Prof. Khaled A.S. Al-Rasheid, King Saud University, Saudi Arabia, in recognition of his contributions to ciliatology.

Description

Cell size about 60–115 × 20–60 μm *in vivo*, with ratio of length to width about 2–3:1, body outline broad to elongated elliptical (**Figures 2A,B,I,J**). Cortex rather flexible, but not contractile. Two types of cortical granules on both ventral and dorsal sides (**Figures 2E–H**): larger ones about 1.0 μm in size, yellow-greenish, wheat-grain shaped along the cirral rows, dorsal kineties and between dorsal dikinetids, giving cells a yellow-greenish appearance; smaller ones colorless, about 0.4–0.5 μm in diameter, relatively densely arranged. Cytoplasm colorless, usually with many tiny lipid droplets (about 0.6–1.0 μm across) and food vacuoles containing algae. Contractile vacuole about 15–18 μm across, located at two-fifth of body length, behind buccal vertex, near left body margin, collecting canals not observed (**Figures 2A,B,J**). On average 67 (46–80) spherical to elliptical macronuclear nodules (**Figure 2K**). Micronuclei not easily distinguished from macronuclear nodules in stained individuals. Locomotion unremarkable, by moderately fast crawling on bottom of Petri dishes and debris.

Adoral zone extending about 38% of body length, with cilia up to 10 μm long *in vivo*, consisting of 19–30 (on average 22) membranelles (**Table 1**), distal end of adoral zone of membranelles (AZM) bending only slightly to the right of the midline in protargol preparations (**Figures 2C,K**). Paroral and endoral of nearly equal length, slightly curved and optically intersect at about posterior quarter of the paroral (**Figures 2C,K,M**). Three clearly differentiated frontal cirri (**Figures 2C,K** and **Table 1**). Single buccal cirrus located at level of anterior one-third of paroral (**Figures 2C,K,M** and **Table 1**). Three or four frontoterminal cirri behind the distal end of adoral zone (**Figures 2C,K** and **Table 1**). Midventral complex extending to about half of cell length, composed of five to thirteen pairs of cirri arranged in typical zigzag pattern and a midventral row of three or four unpaired ventral cirri posteriorly (**Figures 2A–C,K** and **Table 1**). Four or five transverse cirri in J-shaped row (**Figures 2A–C,K,L** and **Table 1**). Both right and left marginal cirri composed of three to four rows (**Figures 2A–C,K** and **Table 1**). Three complete dorsal kineties and two or three dorsal bristles to right of dorsal

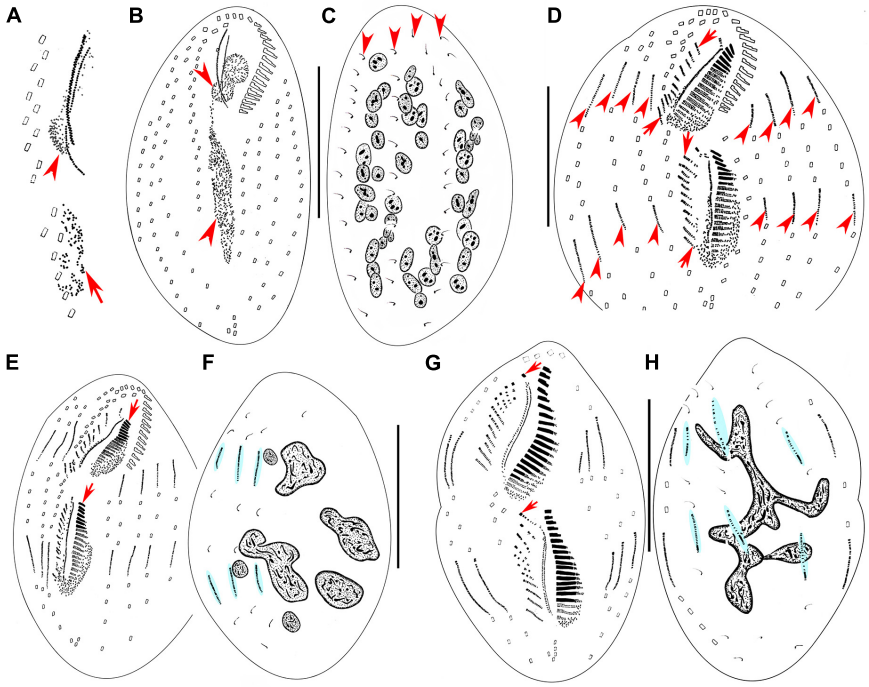

FIGURE 3 | Morphogenesis of *Metaurostylopsis alrasheidi* n. sp. from early to middle stages after protargol impregnation. **(A)** Newly formed oral primordium in proter (arrowhead) and opisthe (arrow) at very early stage. **(B,C)** Ventral **(B)** and dorsal **(C)** views of an early divider to show the development of oral primordia for proter and opisthe (arrowheads), and the unchanged dorsal ciliature (arrowheads). **(D)** Ventral view of an early-middle divider, showing the streak-like frontoventral transverse cirral anlagen (arrows) and the intrakinetally formed marginal anlagen (arrowheads). **(E,F)** Ventral **(E)** and dorsal **(F)** views of the same early-middle divider, to show the newly formed adoral membranelles (arrows), and dorsal kinety anlagen (shaded in light-blue). **(G,H)** Ventral **(G)** and dorsal **(H)** views of a middle divider, showing the leftmost frontal cirrus (arrowheads) forming from the undulating membrane anlagen, dorsal kinety anlagen (shaded in light-blue) and macronuclear nodules fusing into a mass with few branches in **(H)**. Scale bars = 50 μm.

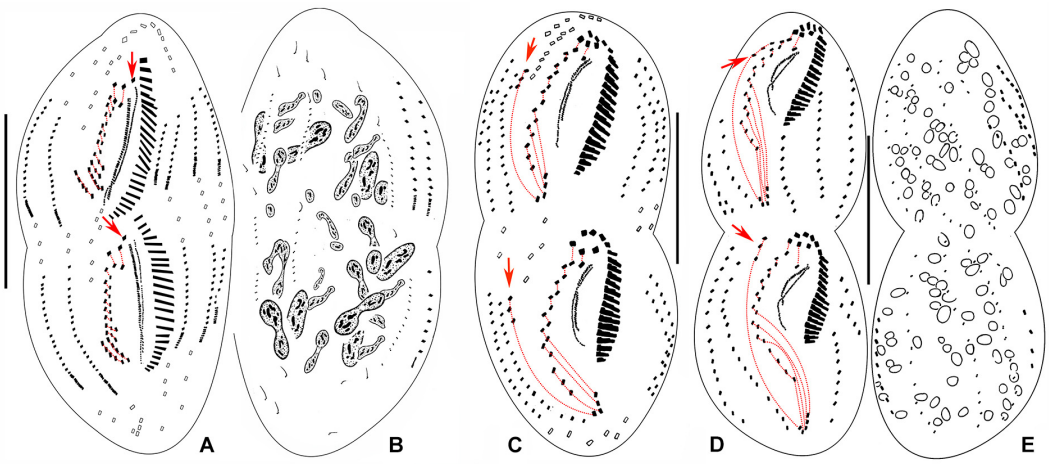

FIGURE 4 | Morphogenesis of *Metaurostylopsis alrasheidi* n. sp. from middle-late to late stages after protargol impregnation, hatched lines show cirri originated from the same cirral anlage. **(A,B)** Ventral **(A)** and dorsal **(B)** views of the same middle-late divider, arrows indicate the leftmost frontal cirrus. **(C)** Ventral view of a divider, arrows show the migration of newly formed frontoterminal cirri. **(D,E)** Ventral **(D)** and dorsal **(E)** views of the same divider, arrows mark the frontoterminal cirri migrating toward their final positions. Scale bars = 50 μm.

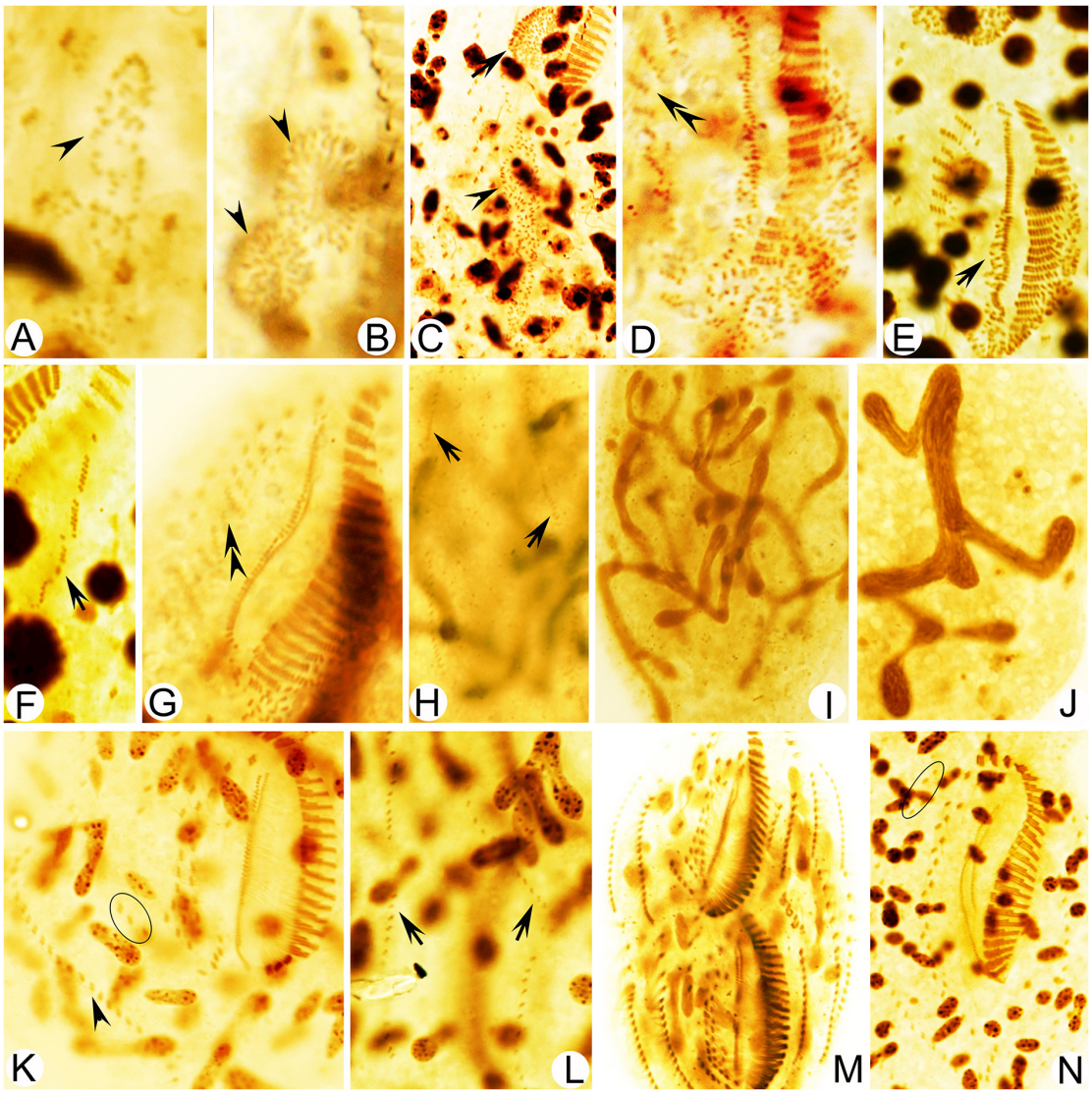

FIGURE 5 | Photomicrographs of *Metaurostylopsis alrasheidi* n. sp. during morphogenesis after protargol impregnation. **(A,B)** Ventral view of a very early divider, arrowheads point to the oral primordium of the opisthe **(A)** and the proter **(B)**. **(C)** The oral primordium continues to grow by further proliferation for proter (arrow) and opisthe (arrowhead) at early stage. **(D,E)** Ventral views, to show the formation of streak-like frontoventral transverse cirral anlagen (double-arrowheads) and newly formed undulating membrane anlagen (arrow) at early-middle stage. **(F,G)** Ventral views of middle dividers, to show the intrakinetally formed left marginal anlagen (arrow) and the newly developed cirri (double-arrowhead) formed from the frontoventral transverse cirral anlagen. **(H)** Dorsal view to show the dorsal kinety anlagen (arrows). **(I,J)** Macronuclear nodules fusing into a branching mass. **(K)** Ventral view of a late divider to show the newly formed right marginal cirri (arrowhead) and frontoterminal cirri (circle). **(L)** Dorsal view to show the new dorsal kineties, no caudal cirri are formed. **(M,N)** Ventral views of very late dividers, to show the immigration of frontoterminal cirri (circle). Scale bars = 50 μm.

kinety 3 anteriorly (**Figure 2D**, arrowheads), with cilia 2–3 μm long.

Divisional Ontogenesis

Stomatogenesis and Development of Frontal-Ventral-Transverse Cirral Anlagen

Stomatogenesis commences with the proliferation of densely arranged basal bodies forming a slender anarchic field, that is, the opisthe's oral primordium, which occurs *de novo* to the left of posterior midventral pairs (**Figures 3A**, **5A**). Simultaneously, a small field of basal bodies, the proter's oral primordium, appears *de novo* in a subsurface pouch beneath the buccal field and near the parental undulating membranes (UM). Subsequently, the opisthe's oral primordium widens and lengthens between the midventral complex and the inner left marginal row during which time the parental structures remain unchanged. At the same time, the proter's oral primordium continues to develop within the pouch, which is clearly outlined (**Figures 3B**, **5B,C**). The oral primordium

TABLE 1 | Morphometric characterization of *Metaurostylopsis alrasheidi* n. sp. based on protargol-stained specimens (measurements in μm).

Character	Min	Max	Mean	M	SD	CV	*n*
Body, length	65	120	91.5	90	11.5	12.6	25
Body, width	34	86	45.2	44	10.5	23.3	25
Adoral zone, length	22	42	32.5	42	4.7	14.2	25
Adoral membranelles, number	19	30	22.1	27	2.5	11.5	25
Frontal cirri, number	3	3	3.0	3	0	0	25
Buccal cirrus, number	1	1	1.0	1	0	0	25
Frontoterminal cirri, number	3	4	3.0	3	0.2	6.4	25
Midventral pairs, number	5	13	8.1	8	2.0	25.0	25
Ventral cirri, number	3	4	3.5	3	0.5	14.4	25
Transverse cirri, number	4	5	4.4	4.0	0.5	11.0	22
Left marginal row, number	3	4	3.0	3	0.7	21.8	25
Right marginal row, number	3	4	3.3	3	0.4	13.7	25
Cirri in left marginal row 1, number	10	19	13.7	14	2.0	14.9	25
Cirri in left marginal row 2, number	11	23	15.0	14	3.0	20.2	25
Cirri in left marginal row 3, number	13	24	16.2	15	3.0	18.6	25
Cirri in left marginal row 4, number	14	24	18.4	18	3.5	19.0	9
Cirri in right marginal row 1, number	13	23	17.7	18	2.4	13.5	25
Cirri in right marginal row 2, number	13	23	18.4	18	2.3	12.5	25
Cirri in right marginal row 3, number	11	21	14.8	14	2.9	19.6	25
Cirri in right marginal row 4, number	8	15	12.3	13.0	2.7	21.9	4
Dorsal kineties, number	3	3	3.0	3	0	0	25
Macronuclear nodules, number	46	80	66.8	67	10.0	14.9	21

CV, coefficient of variation in %; M, median; Max, maximum; Mean, arithmetic mean; Min, minimum; n, number of cells measured; SD, standard deviation.

then differentiates into new adoral membranelles, and the UM anlage appears to the right of the oral primordium in both proter and opisthe (**Figures 3D,E**, **5D–G**). During this time, the parental oral structures remain unchanged, while the frontal-ventral-transverse cirral anlagen (FVTA) appear as several streak-like collections of basal bodies to the right of the UM anlage for both proter and opisthe (**Figures 3D,E**, **5D,E,G**). In the next stage, the differentiation of adoral membranelles is almost complete, forming new structures for both proter and opisthe. The UM anlagen split and give rise to the paroral and endoral membranes and the leftmost frontal cirrus is generated from the anterior end of the UM anlage (=FVTA I) (**Figures 3G**, **5G**). Simultaneously the FVTA begin to break apart and differentiate into new cirri. In the following stages, the new cirri formed from the FVTA and migrate to their final positions as follows: FVTA II produces the middle frontal cirrus and the buccal cirrus; FVTA III provides the rightmost frontal cirrus and the parabuccal cirrus (III/2); FVTA IV to n-2 each develops a midventral pair, with the last two or three streaks forming one transverse cirrus; FVTA n-1 provides a short midventral row composed of three or four cirri and one transverse cirrus; FVTA n, the last anlage, develops three or four frontoterminal cirri and probably the rightmost transverse cirrus (**Figures 4A,C,D**, **5K,M,N**).

Development of Marginal Rows and Dorsal Kineties

At the early-to-middle stages, the marginal anlagen are formed intrakinetally both in proter and opisthe. Subsequently, these anlagen elongate toward both ends and generate new cirri and gradually replace the parental structures (**Figures 3D,E,G**, **4A,C,D**, **5F,K,M,N**). In the same way, the dorsal kineties develop by intrakinetal basal body proliferation. During cell division, no caudal cirri are formed. As some key stages were not observed, the origins of the extra dorsal bristles (usually only two) are not clear (**Figures 3C,F,H**, **4B,E**, **5H,L**).

Division of Nuclear Apparatus

Although macronuclear replication bands were not definitely identified in *M. alrasheidi* n. sp., they have been identified (but seen with some difficulty) in *M. rubra* and *M. marina* which, otherwise, have the same macronuclear morphology as *M. alrasheidi* n. sp. during division and replication bands were very possibly overlooked in the new species (Song et al., 2001; Song and Wilbert, 2002). During the middle stage, all macronuclear nodules fuse into a single somewhat branched complex which then divides into numerous nodules (**Figures 3C,F,H**, **4B,E**, **5I,J,N**). Division of the micronuclei was not observed.

Phylogeny Analyses Based on 18S rRNA Gene Sequence

The partial 18S rRNA gene sequence of *Metaurostylopsis alrasheidi* n. sp. has been submitted into GenBank database (acc. no. MT911525), with 1,643 bp long and G + C content of 44.92%.

According to sequence comparisons of the 18S rRNA gene, the sequence of *Metaurostylopsis alrasheidi* n. sp. differs by 8 bp from an unidentified *Metaurostylopsis* sequence (FJ870098) (from a taxonomic research lab), 13–14 bp from five populations of *M. cheni*, 16 bp from *M. salina*, 34–44 bp from four *M. struederkypkeae* sequences, and 73 bp from *Monourostylopsis antarctica* (Jung et al., 2011) n. comb (**Figure 6**).

The topologies of the ML and BI trees are mostly congruent. As a result, only the ML tree with nodal supports inferred from both algorithms is shown (**Figure 7**). According to our 18S rRNA gene tree, *M. alrasheidi* n. sp. clusters with *Metaurostylopsis* sp. (FJ870098), *M. salina* (EU220229) and five *M. cheni* populations (GU170204, FJ775719, HM623916, MG603611, FJ775720) with full support, forming a sister clade of four *M. struederkypkeae* populations (JQ424832, GU942568, EU220228, JN880477). *Monourostylopsis antarctica* (Jung et al., 2011) n. comb. (JF906730) is sister to all *Metaurostylopsis* species with strong to full support (ML/BI: 97/1.00).

Geographic Distribution

Metaurostylopsis alrasheidi n. sp. was isolated from freshwater habitat. All the other *Metaurostylopsis* species have been reported in marine or brackish water (Song et al., 2001; Lei et al., 2005; Berger, 2006; Shao et al., 2008a,b; Chen et al., 2011; Lu et al., 2016). These studies have shown that *Metaurostylopsis* species can be found in a variety of habitats (**Figure 8**). *Metaurostylopsis marina*, has been reported in Mauritania, Poland, China, Korea, and United States, and is probably a cosmopolitan species. While most of the other *Metaurostylopsis* species have been found in one place only, this likely reflects undersampling.

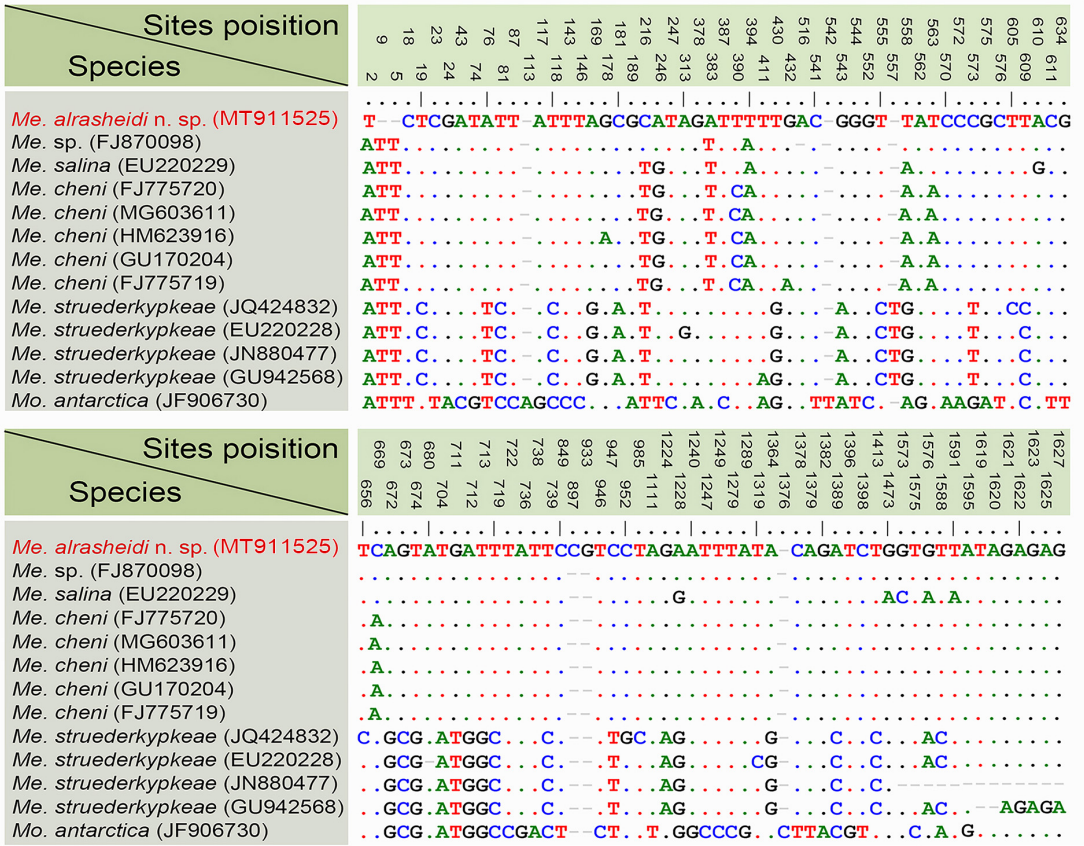

FIGURE 6 | Nucleotide differences among populations of *Metaurostylopsis* species and *Monourostylopsis antarctica* (Jung et al., 2011) n. comb., based on 18S rRNA gene sequences. The vertical numbers indicate the unmatched site positions. The new sequence is in red. Short lines (–) suggest the insertions and deletions. Solid dots represent matched sites.

DISCUSSION

Comparison of *Metaurostylopsis alrasheidi* n. sp. With Closely Related Species (Table 2)

With respect to the ciliature, that is, frontal and transverse cirri clearly differentiated, buccal cirri present, more than two frontoterminal cirri, midventral complex with midventral pairs and a single short midventral row, more than two marginal rows on each body side; pretransverse cirri and caudal cirri absent, the new isolate corresponds well with the diagnosed characteristics of the genus *Metaurostylopsis* (Chen et al., 2013).

Metaurostylopsis alrasheidi n. sp. is most similar to *M. cheni*, especially in body shape, yellow-greenish cell color, two types of cortical granules, and most aspects of the ciliature, but differs from the latter by having a relatively smaller body size *in vivo* 60–115 × 20–60 μm vs. 90–140 × 40–60 μm, a dense distribution pattern of the smaller type of cortical granules on dorsal side (vs. sparse), contractile vacuole located anteriorly (2/5 of body length vs. equatorial region), relatively more midventral pairs (5–13 vs. 5–9) and less transverse cirri (4–5 vs. 5–8) (Chen et al., 2011). The 18S rRNA gene sequence of the newly isolated organism differs from that of *M. cheni* (GU170204) by 13 nucleotides (**Figure 6**), which also reveals these two species are not conspecific.

Metaurostylopsis alrasheidi n. sp. differs from *M. marina* in body shape (broad to elongated elliptical vs. oval), two (vs. one) types of cortical granules, relatively fewer frontoterminal cirri (3–4 vs. 3–6), frontal cirri (3 vs. 4), transverse cirri (4–5 vs. 5–9), and different habitat (freshwater vs. marine) (Song et al., 2001).

Metaurostylopsis parastruederkypkeae is distinguished from *M. alrasheidi* n. sp. by having reddish body (vs. yellow-greenish), reddish cortical granules (vs. yellow-greenish), more frontoterminal cirri (5–7 vs. 3–4), more adoral membranelles (28–47 vs. 19–30), and more cirri in midventral row (5–9 vs. 3–4) (Lu et al., 2016).

Metaurostylopsis rubra can be easily distinguished from *M. alrasheidi* n. sp., by its distinctly larger body size (150–300 × 50–90 vs. 60–115 × 20–60 μm), brick-reddish body color (vs. yellow-greenish), one (vs. two) type of cortical granules, and higher numbers of membranelles (35–46 vs. 19–30) (Song and Wilbert, 2002).

Metaurostylopsis salina differs from *M. alrasheidi* n. sp. mainly in terms of having only one (vs. two) type of cortical granules and relatively more cirri in the midventral row 5–8 (vs. 3–4) (Shao et al., 2008a).

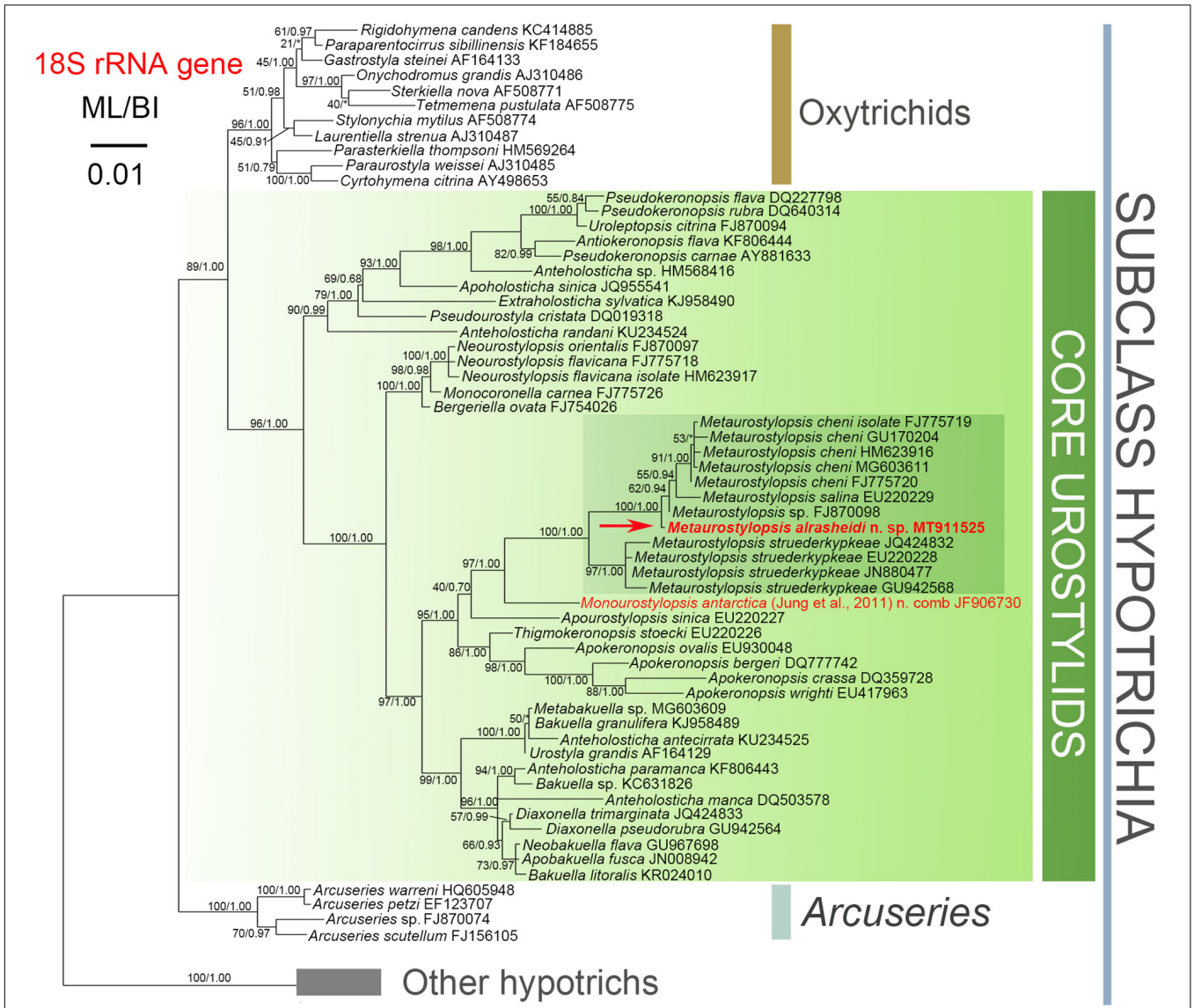

FIGURE 7 | Maximum likelihood (ML) phylogenetic tree with 18S rRNA gene as gene marker. The newly characterized sequence is in red (arrow). Numbers near nodes represent bootstrap values of ML and posterior probability values of Bayesian inference (BI), respectively. Asterisks (*) indicate the disagreement between ML and BI. The scale bar represents 1 substitution for every 100 nucleotides.

Metaurostylopsis struederkypkeae can be easily separated from *M. alrasheidi* n. sp. by its cell coloration (rose-reddish vs. yellow-greenish), the number of frontal cirri (4 vs. 3), frontoterminal cirri (4–6 vs. 3–4), and the distribution of the smaller cortical granules (in irregular rows vs. evenly distributed) (Shao et al., 2008b).

Metaurostylopsis antarctica resembles *M. alrasheidi* n. sp. closely in terms of body size, number of membranelles and types of cortical granules, but can be separated from the new species by having fewer midventral pairs (2–5 vs. 5–13), and fewer left and right marginal rows (2 vs. 3–4, 1 vs. 3–4 respectively) and transverse cirri (2 vs. 4–5) (Jung et al., 2011).

The character of cortical granules, that is, two types of cortical granules, of the new species is distinguishable from some of the congeners with only one type of cortical granules present (**Table 2**). However, it is possible that earlier researchers overlooked the tiny type of cortical granules. Considering the habitat, *Metaurostylopsis alrasheidi* n. sp. can be separated from all the other congeners (freshwater vs. marine or brackish, **Table 2**).

All the *Neourostylopsis* species can be separated from *M. alrasheidi* n. sp. by having fewer frontoterminal cirri (2 vs. 3–4), lack of a midventral row (vs. midventral row present) (Lei et al., 2005; Wang et al., 2011; Chen et al., 2013; Pan et al., 2016; Zhang et al., 2018).

Apourostylopsis sinica (Shao et al., 2008) Song et al., 2011 differs from our new species in its more transverse cirri (5–8 vs. 4–5), pretransverse cirri present (vs. absent), and midventral row absent (vs. present) (Shao et al., 2008a).

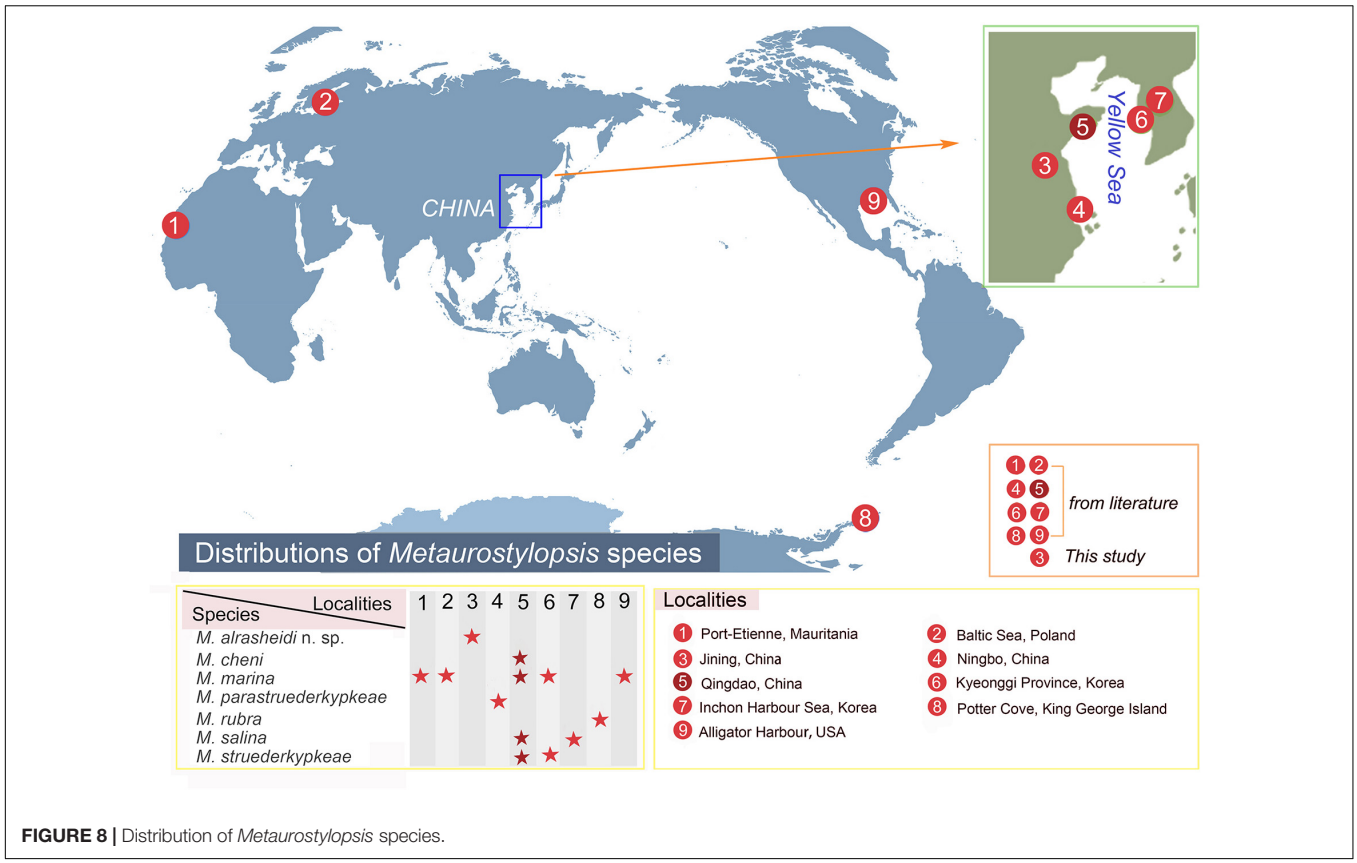

FIGURE 8 | Distribution of *Metaurostylopsis* species.

Emended Diagnosis of Genus *Metaurostylopsis* and Reassignment of the Species, *M. antarctica* Jung et al., 2011

In the most recent revision of the genus *Metaurostylopsis*, Chen et al. (2013) provided an improved diagnosis for the genus *Metaurostylopsis*, which were defined as marine urostylids with characteristics mentioned in the above section. However, the new species in the present study, *Metaurostylopsis alrasheidi* n. sp., which was isolated from a freshwater lake, fits the morphological characteristics of the genus *Metaurostylopsis* very well. Moreover, our new species clusters in a clade together with all the other *Metaurostylopsis* sequences, indicating the close relationship among them and supporting the classification of the new species in the genus *Metaurostylopsis*. Thus, an emended diagnosis including marine, brackish and freshwater habitats is supplied.

As discussed above, the genus *Metaurostylopsis* is characterized by having more than one marginal row on each body side. However, *M. antarctica* was characterized by having only one right marginal row, which does not fit the diagnosis of *Metaurostylopsis*. Also, in the phylogenetic trees, *M. antarctica* is placed as sister to the clade including all the other *Metaurostylopsis* sequences with strong to full support. Therefore, we propose that *M. antarctica* should be excluded from the genus *Metaurostylopsis*. As *M. antarctica* also can be separated from other morphologically similar genera, i.e., *Neourostylopsis* and *Apourostylopsis*, by having only one right marginal row (vs. two or more right marginal rows) (**Table 2**), this suggests that *M. antarctica* represents a new genus. Hence, an emended diagnosis of the genus *Metaurostylopsis* and diagnosis of a new genus, *Monourostylopsis* n. gen., are supplied here.

Metaurostylopsis Song et al., 2001

Improved Diagnosis

Marine, brackish or freshwater urostylids with frontal and transverse cirri clearly differentiated; three or more frontoterminal cirri; midventral complex with midventral pairs extending to the level of the buccal vertex and a single midventral row; buccal and transverse cirri present; pretransverse ventral and caudal cirri absent; more than two marginal rows on each body side.

Type Species

Urostyla marina Kahl, 1932.

Species Assignable

Metaurostylopsis marina (Kahl, 1932) Song et al., 2001 (type species); *Metaurostylopsis rubra* Song and Wilbert, 2002; *Metaurostylopsis salina* Lei et al., 2005; *Metaurostylopsis struederkypkeae* Shao et al., 2008; *Metaurostylopsis cheni* Chen

TABLE 2 | Morphometric comparison of *Metaurostylopsis alrasheidi* n. sp. with closely related species.

Characters	*M. alrasheidi* n. sp.	*M. cheni*	*M. marina*	*M. parastrue derkypkeae*	*M. rubra*	*M. salina*	*M. strueder kypkeae*	*Mo. antarctica*	*N. flava*	*N. flavicana*	*N. flava paraflava*	*N. orientalis*	*N. songi*	*A. sinica*
Body size	60–115 × 20–65	90–140 × 40–60	80–120 × 50–80	165–200 × 45–60	150–300 × 50–90	70–120 × 20–30	90–120 × 20–30	70–110 × 20–30	150–220 × 50–75	130–200 × 30–60	150–220 × 45–80	120–200 × 45–75	90–150 × 20–35	100–120 × 25–35
Cell color	Yellow-greenish	Yellow-greenish	Colorless to grayish	Brown to reddish	Brick-reddish	Colorless to grayish	Rose–reddish	Grayish to colorless	Yellowish	Yellowish	Reddish brown	Slightly yellow–brownish	Colorless	Yellow–brownish
Cortical granules	Type I: yellow-green; type II: colorless	Type I: yellow-green; type II: colorless	Colorless or slightly greenish	Type I: yellow-green; type II: reddish	Colorless	Colorless	Type I: yellow-green; type II: wine reddish	Type I: yellow-green; type II: colorless	Bright yellow to yellow-brownish	Bright-yellow	Bright yellow to yellow-brownish	Yellow–brownish	Colorless	Type I yellow; type II: colorless
AZM/BL (%)	38	33	40	35–40	33	33	30	33	35	35		35	25–33	35
Position of CV	Anterior 2/5	Equatorial level	Above mid-body	Anterior 2/5	Above mid-body	Anterior 2/5	Anterior 2/5	33% of the body length	Anterior 2/5	35% of the body length	Anterior 2/5	Anterior 2/5	Anterior of mid-body	Anterior 2/5
No. AZM	ca. 22 (19–30)	ca. 23 (21–26)	ca. 28 (27–30)	ca. 33 (26–41)	ca. 39 (35–46)	ca. 23 (21–25)	ca. 23 (20–25)	ca. 22 (19–24)	40–55	33–45	33–72	25–31	ca. 34 (28–47)	ca. 27 (25–29)
No. FC	3	3	3	3	3	4	4	4	6–8	4–8	8–15	5	5	4
No. FTC	ca. 3 (3–4)	4	ca. 4 (3–6)	ca. 6 (5–7)	ca. 6 (5–8)	ca. 5 (4–5)	ca. 5 (4–6)	ca. 4 (2–5)	2	2	2	2	ca. 2 (2–3)	2
No. MP	ca. 8 (6–13)	ca. 7 (5–9)	ca. 9 (7–11)	ca. 9 (7–13)	ca. 10 (8–11)	ca. 6 (6–7)	ca. 11 (8–14)	ca. 4 (3–5)	13–20	13–17	17–29	8–10	ca. 11 (9–12)	ca. 13 (11–15)
No. VC	ca. 3 (2–4)	ca. 4 (4–5)	4–7	ca. 7 (5–9)	ca. 10 (8–13)	ca. 6 (5–8)	ca. 5 (4–8)	ca. 12 (10–15)	0	0	0	0	0	0
No. LMR	3–4	ca. 3 (3–4)	ca. 4 (3–5)	ca. 6 (5–7)	ca. 8 (6–9)	ca. 3 (2–4)	ca. 4 (4–5)	2	4–5	4	6–9	3	3	2
No. RMR	3–4	3	ca. 4 (3–5)	ca. 4 (3–5)	ca. 6 (6–7)	3	3	1	4	3	4–6	3	3	3
No. TC	ca. 4 (4–5)	ca. 6 (5–8)	ca. 7 (5–9)	ca. 4 (3–6)	ca. 5 (4–6)	ca. 4 (3–5)	ca. 3 (2–5)	2	7–9	7–10	8–13	5–7	ca. 7 (6–7)	ca. 7 (5–8)
No. Ma	ca. 67 (46–80)	ca. 40 (30–65)	ca. 50	ca. 75 (59–92)	ca. 100	ca. 29 (17–36)	ca. 61 (50–71)	ca. 43 (38–50)	49–98	62–97	110–190	ca. 61 (39–67)	54	Ca. 70
Salinity	0‰	30‰	32‰	24‰	33‰	Saline	31‰	34.9‰	0‰	20‰	6‰	9‰	Saline	30‰
Ref.	Original	Chen et al., 2011	Song et al., 2001	Lu et al., 2016	Song and Wilbert, 2002	Lei et al., 2005	Shao et al., 2008b	Jung et al., 2011	Pan et al., 2016	Wang et al., 2011	Zhang et al., 2018	Chen et al., 2013	Lei et al., 2005	Shao et al., 2008a

AZM, Adoral zone of membranelles; BL, Body length; CV, contractile vacuole; FC, frontal cirri; FTC, frontoterminal cirri; MP, midventral pair; VC, unpaired ventral cirri; LMR, left marginal row; RMR, right marginal row; TC, transverse cirri; Ma, macronuclear nodules; Ref, reference; A, Apourostylopsis; M., Metaurostylopsis; Mo., Monourostylopsis; N, Neourostylopsis.

et al., 2011; *Metaurostylopsis parastruederkypkeae* Lu et al., 2016; *Metaurostylopsis alrasheidi* n. sp.

Monourostylopsis n. gen.

Diagnosis

Urostylids with frontal and transverse cirri clearly differentiated; three or more frontoterminal cirri; midventral complex with midventral pairs extending to the level of the buccal vertex and a single midventral row; buccal and transverse cirri present; pretransverse ventral and caudal cirri absent; one right marginal row and two or more left marginal rows.

Type Species

Monourostylopsis antarctica (Jung et al., 2011) n. comb. (original combination: *Metaurostylopsis antarctica* Jung et al., 2011).

Species Assignable

Monourostylopsis antarctica (Jung et al., 2011) n. comb. (type species).

Etymology

The generic name is a composite of the Greek mono- (single), referring to the single right marginal row, and the posterior part (-urostylopsis) of the genus-group name *Metaurostylopsis*.

Morphogenetic Comparison

As of this writing, the morphogenetic process of four *Metaurostylopsis* species, i.e., *M. alrasheidi* n. sp., *M. cheni*, *M. marina*, and *M. rubra* has been investigated (Wilbert and Song, 2005; Chen et al., 2011; Song et al., 2011). The morphogenetic pattern of the genus *Metaurostylopsis* shows high stability, and shares similar morphogenetic features with *Apourostylopsis*, *Monourostylopsis*, and *Neourostylopsis* as follows: (1) in the proter, the oral primordium (OP) is formed *de novo* in a subcortical pouch beneath (i.e., dorsal to) the buccal field, the new undulating membranes (UM) anlage is generated near the OP, and the parental oral structures are completely replaced; (2) in the opisthe, both the OP and the UM anlage develop apokinetally on the cell surface; (3) the FVT cirral anlagen are formed apokinetally, and none of the old ciliature seems to be involved in the development of the new primordia; (4) marginal anlagen and dorsal anlagen develop intrakinetally; (5) all macronuclear nodules fuse to a single branching mass during the middle divisional stage (Wilbert and Song, 2005; Shao et al., 2008a; Chen et al., 2011; Jung et al., 2011; Song et al., 2011; Zhang et al., 2018).

Ontogenetic features of *Metaurostylopsis* show striking differences when compared with genera *Apourostylopsis* and *Neourostylopsis*, namely: (1) FVTA n-1 forms a row of unpaired ventral cirri which migrates along with the midventral pairs, whereas in *Apourostylopsis* and *Neourostylopsis*, no unpaired ventral cirri are generated; (2) FVTA n formed a transverse cirrus and more than two frontoterminal cirri in *Metaurostylopsis* (i.e., typical *Metaurostylopsis* mode), whereas the FVTA n forms two frontoterminal cirri, a pretransverse and a transverse cirrus in *Apourostylopsis* (i.e., typical urostylid mode), and whether FVTA n forms pretransverse cirrus in *Neourostylopsis* is variable (Wilbert and Song, 2005; Shao et al., 2008a; Chen et al., 2011; Jung et al., 2011; Song et al., 2011; Song and Shao, 2017; Zhang et al., 2018).

Phylogenetic Analyses

Consistent with previous studies (Shao et al., 2008a; Chen et al., 2011; Song et al., 2011; Lu et al., 2016), we confirm the monophyly of genus *Metaurostylopsis* based on the phylogenetic analyses in present work.

In the 18S rRNA gene tree, our new taxon, *Metaurostylopsis alrasheidi* n. sp., clusters with *Metaurostylopsis* species and falls into the monophyletic clade of *Metaurostylopsis*, which can also be supported by the shared morphological features, such as, similar body shape and size, as well as semblable ciliature. Additionally, 8–44 different nucleotides of 18S rRNA gene are discovered between *M. alrasheidi* n. sp. and its congeners, further indicating the validity of our isolate as a distinct species. It is worth noting that the genus *Metaurostylopsis* forms a sister clade to *Monourostylopsis* n. gen., with which it shares some similar characteristics: (1) three or more frontoterminal cirri; (2) midventral complex with midventral pairs and a single midventral row; (3) buccal and transverse cirri present; (4) pretransverse ventral and caudal cirri absent. However, in addition to its molecular phylogenetic position, *Metaurostylopsis* can be clearly separated from *Monourostylopsis* n. gen. morphologically by having more than two marginal rows on each body side (vs. one left marginal row and two right marginal rows) (Jung et al., 2011).

DATA AVAILABILITY STATEMENT

The datasets generated for this study can be found in the online repositories. The names of the repository/repositories and accession number(s) can be found below: NCBI GenBank (accession: MT911525).

AUTHOR CONTRIBUTIONS

XL and TZ conceived the study. WS carried out the live observation, protargol staining, DNA extraction, and data analyses. All authors contributed to the manuscript and approved the final version.

FUNDING

This work was financially supported by the National Natural Science Foundation of China (Nos. 32030015 and 31900319) and the China Postdoctoral Science Foundation Grants (Nos. BX20180348 and 2018M642955).

ACKNOWLEDGMENTS

We would like to express our gratitude to Dr. Xumiao Chen, Institute of Oceanology, Chinese Academy of Sciences, for her kind help and advice on the identification of this species.

REFERENCES

Berger, H. (1999). *Monograph of the Oxytrichidae (Ciliophora, Hypotrichia)*. Vol. 78, Berlin: Springer, 1–1080. Monographiae Biologicae.

Berger, H. (2006). *Monograph of the Urostyloidea (Ciliophora, Hypotricha)*. Vol. 85, Berlin: Springer, 1–1304. Monographiae Biologicae.

Berger, H. (2008). *Monograph of the Amphisiellidae and Trachelostylidae (Ciliophora, Hypotricha)*. Vol. 88, Dordrecht: Springer, 1–737. Monographiae Biologicae.

Berger, H. (2011). *Monograph of the Gonostomatidae and Kahliellidae (Ciliophora, Hypotricha)*. Vol. 90, Dordrecht: Springer, 1–740. Monographiae Biologicae.

Chen, L., Dong, J., Wu, W., Xin, Y., Warren, A., Ning, Y., et al. (2020). Morphology and molecular phylogeny of a new hypotrich ciliate, *Anteholosticha songi* nov. spec., and an American population of *Holosticha pullaster* (Müller, 1773) Foissner et al., 1991 (Ciliophora, Hypotrichia). *Eur. J. Protistol.* 72:125646. doi: 10.1016/j.ejop.2019.125646

Chen, X., Huang, J., and Song, W. (2011). Ontogeny and phylogeny of *Metaurostylopsis cheni* sp. n. (Protozoa, Ciliophora), with estimating the systematic position of *Metaurostylopsis*. *Zool. Scr.* 40, 99–111. doi: 10.1111/j.1463-6409.2010.00451.x

Chen, X., Shao, C., Liu, X., Huang, J., and Al-Rasheid, K. A. S. (2013). Morphology and phylogenies of two hypotrichous brackish-water ciliates from China, *Neourostylopsis orientalis* n. sp. and *Protogastrostyla sterkii* (Wallengren, 1900) n. comb., with establishment of a new genus *Neourostylopsis* n. gen. (Protista, Ciliophora, Hypotrichia). *Int. J. Syst. Evol. Microbiol.* 63, 1197–1209. doi: 10.1099/ijs.0.049403-0

Darriba, D., Taboada, G. L., Doallo, R., and Posada, D. (2012). jModelTest 2: more models, new heuristics and parallel computing. *Nat. Methods* 9:772. doi: 10.1038/nmeth.2109

Dong, J., Li, L., Fan, X., Ma, H., and Warren, A. (2020). Two *Urosoma* species (Ciliophora, Hypotrichia): a multidisciplinary approach provides new insights into their ultrastructure and systematics. *Eur. J. Protistol.* 72:125661. doi: 10.1016/j.ejop.2019.125661

Foissner, W. (1982). Ökologie und taxonomie der hypotrichida (Protozoa: Ciliophora) einiger österreichischer Böden). *Arch. Protistenk.* 126, 19–143. doi: 10.1016/S0003-9365(82)80065-1

Foissner, W. (2016). Terrestrial and semiterrestrial ciliates (Protozoa, Ciliophora) from venezuela and Galápagos. *Denisia* 35:912.

Gao, F., Katz, L. A., and Song, W. (2012). Insights into the phylogenetic and taxonomy of philasterid ciliates (Protozoa, Ciliophora, Scuticociliatia) based on analyses of multiple molecular markers. *Mol. Phylogenet. Evol.* 64, 308–317. doi: 10.1016/j.ympev.2012.04.008

Gouy, M., Guindon, S., and Gascuel, O. (2010). SeaView version 4: a multiplatform graphical user interface for sequence alignment and phylogenetic tree building. *Mol. Biol. Evol.* 27, 221–224. doi: 10.1093/molbev/msp259

Hall, T. A. (1999). BioEdit: a user-friendly biological sequence alignment editor and analyses program for windows 95/98/NT. *Nucleic Acids Symp. Ser.* 41, 95–98.

Hu, X., Lin, X., and Song, W. (2019). *Ciliate Atlas: Species found in the South China Sea*. Beijing: Science Press.

Jankowski, A. V. (2007). "Phylum ciliophora doflein, 1901. Review of taxa," in *Protista: Handbook on Zoology*, Part 2, ed. A. F. Alimov (St. Petersburg: Nauka), 415–993.

Jerome, C. A., Simon, E. M., and Lynn, D. H. (1996). Description of *Tetrahymena empidokyrea* n. sp., a new species in the *Tetrahymena pyriformis* sibling species complex (Ciliophora, Oligohymenophorea), and an assessment of its phylogenetic position using small-subunit rRNA sequences. *Can. J. Zool.* 74, 1898–1906. doi: 10.1139/z96-214

Jung, J. H., Baek, Y. S., Kim, S., Choi, H. G., and Min, G. S. (2011). A new marine ciliate, *Metaurostylopsis antarctica* nov. spec. (Ciliophora, Urostylida) from the Antarctic Ocean. *Acta Protozool.* 50, 289–300. doi: 10.4467/16890027AP.11.026.0063

Jung, J. H., and Berger, H. (2019). Monographic treatment of *Paraholosticha muscicola* (Ciliophora, Keronopsidae), including morphological and molecular biological characterization of a brackish water population from Korea. *Eur. J. Protistol.* 68, 48–67. doi: 10.1016/j.ejop.2018.12.004

Kaur, H., Shashi, L., Negi, R. K., and Kamra, K. (2019). Morphological and molecular characterization of *Neogastrostyla aqua* nov. gen., nov. spec. (Ciliophora, Hypotrichia) from River Yamuna, Delhi; comparison with Gastrostyla-like genera. *Eur. J. Protistol.* 68, 68–79. doi: 10.1016/j.ejop.2019.01.002

Kim, K. S., Jung, J. H., and Min, G. S. (2017). Morphology and molecular phylogeny of two new ciliates, *Holostichides heterotypicus* n. sp. and *Holosticha muuiensis* n. sp. (Ciliophora: Urostylida). *J. Eukaryot. Microbiol.* 64, 873–884. doi: 10.1111/jeu.12421

Kim, K. S., and Min, G. S. (2019). Morphology and molecular phylogeny of *Oxytricha seokmoensis* sp. nov. (Hypotrichia: Oxytrichidae), with notes on its morphogenesis. *Eur. J. Protistol.* 71:125641. doi: 10.1016/j.ejop.2019.125641

Kumar, S., Kamra, K., and Sapra, G. R. (2010). Ciliates of the silent valley National Park, India: *Urostyloid hypotrichs* of the region with a note on the habitat. *Acta Protozool.* 49, 339–364.

Kumar, S., Stecher, G., Li, M., Knyaz, C., and Tamura, K. (2018). MEGA X: molecular evolutionary genetics analysis across computing platforms. *Mol. Biol. Evol.* 35, 1547–1549. doi: 10.1093/molbev/msy096

Lei, Y., Choi, J. K., Xu, K., and Petz, W. (2005). Morphology and infraciliature of three species of *Metaurostylopsis* (Ciliophora, Stichotrichia): *M. songi* n. sp., *M. salina* n. sp., and *M. marina* (Kahl 1932) from sediments, saline ponds, and coastal waters. *J. Eukaryot. Microbiol.* 52, 1–10. doi: 10.1111/j.1550-7408.2005.3294rr.x

Li, F., Li, Y., Luo, D., Miao, M., and Shao, C. (2018). Morphology, morphogenesis, and molecular phylogeny of a new soil ciliate, *Sterkiella multicirrata* sp. nov. (Ciliophora, Hypotrichia) from China. *J. Eukaryot. Microbiol.* 65, 627–636. doi: 10.1111/jeu.12508

Lian, C., Zhang, T., Al-Rasheid, K. A. S., Yu, Y., Jiang, J., and Huang, J. A. (2019). Morphology and SSU rDNA-based phylogeny of two *Euplotes* species from China: *E. wuhanensis* sp. n. and *E. muscicola* Kahl, 1932 (Ciliophora, Euplotida). *Eur. J. Protistol.* 67, 1–14. doi: 10.1016/j.ejop.2018.10.001

Lu, B., Wang, C., Huang, J., Shi, Y., and Chen, X. (2016). Morphology and SSU rDNA sequence analysis of two hypotrichous ciliates (Protozoa, Ciliophora, Hypotrichia) including the new species *Metaurostylopsis parastruederkypkeae* n. sp. *J. Ocean Univ. China* 15, 866–878. doi: 10.1007/s11802-016-3148-9

Lu, X., Wang, Y., Al-Farraj, S. A., El-Serehy, H., Huang, J., and Shao, C. (2020). The insights into the systematic relationship of *Gastrostyla*-affinitive genera, with report on a new saline soil ciliate genus and new species (Protozoa, Ciliophora). *BMC Evol. Biol.* 20:92. doi: 10.1186/s12862-020-01659-8

Luo, X., Huang, J. A., Li, L., Song, W., and Bourland, W. A. (2019). Phylogeny of the ciliate family Psilotrichidae (Protista, Ciliophora), a curious and poorly-known taxon, with notes on two algae-bearing psilotrichids from Guam, USA. *BMC Evol. Biol.* 19:125. doi: 10.1186/s12862-019-1450-z

Lyu, Z., Wang, J., Huang, J., Warren, A., and Shao, C. (2018). Multigene-based phylogeny of *Urostylida* (Ciliophora, Hypotrichia), with establishment of a novel family. *Zool. Scr.* 47, 243–254. doi: 10.1111/zsc.12267

Ma, J., Zhao, Y., Zhang, T., Shao, C., Al-Rasheid, K. A. S., and Song, W. (2020). Cell-division pattern and phylogenetic analyses of a new ciliate genus *Parasincirra* n. g. (Protista, Ciliophora, Hypotrichia), with a report of a new soil species, *P. sinica* n. sp. from northwest China. *BMC Evol. Biol.*

Medlin, L., Elwood, H. J., Stickel, S., and Sogin, M. L. (1988). The characterization of enzymatically amplified eukaryotes 16S-like ribosomal RNA coding regions. *Gene* 71, 491–500. doi: 10.1016/0378-1119(88)90066-2

Pan, X., Fan, Y., Gao, F., Qiu, Z., Al-Farraj, S. A., Warren, A., et al. (2016). Morphology and systematics of two freshwater urostylid ciliates, with description of a new species (Protista, Ciliophora, Hypotrichia). *Eur. J. Protistol.* 52, 73–84. doi: 10.1016/j.ejop.2015.11.003

Ronquist, F., Teslenko, M., Van Der, M., Daniel, La, Darling, A., Hohna, S., et al. (2012). MrBayes 3.2: efficient bayesian phylogenetic inference and model choice across a large Model space. *Syst. Biol.* 61, 539–542. doi: 10.1093/sysbio/sys029

Sela, I., Ashkenazy, H., Katoh, K., and Pupko, T. (2015). GUIDANCE2: accurate detection of unreliable alignment regions accounting for the uncertainty of multiple parameters. *Nucleic Acids Res.* 43, W7–W14. doi: 10.1093/nar/gkv318

Shao, C., Hu, C., Fan, Y., Warren, A., and Lin, X. (2019). Morphology, morphogenesis and molecular phylogeny of a freshwater ciliate, *Monomicrocaryon euglenivorum* euglenivorum (Ciliophora, Oxytrichidae). *Eur. J. Protistol.* 68, 25–36. doi: 10.1016/j.ejop.2019.01.001

Shao, C., Miao, M., Song, W., Warren, A., Al-Rasheid, K. A. S., Al-Quraishy, S. A., et al. (2008a). Studies on two marine *Metaurostylopsis* spp. from China with notes on morphogenesis in *M. sinica* nov. spec. (Ciliophora, Urostylida). *Acta Protozool.* 47, 95–112.

Shao, C., Song, W., Al-Rasheid, K. A. S., Yi, Z., Chen, X., Al-Farraj, S. A., et al. (2008b). Morphology and infraciliature of two new marine urostylid ciliates: *Metaurostylopsis struederkypkeae* n. sp. and *Thigmokeronopsis stoecki* n. sp. (Ciliophora, Hypotrichida) from China. *J. Eukaryot. Microbiol.* 55, 289–296. doi: 10.1111/j.1550-7408.2008.00327.x

Song, W., Petz, W., and Warren, A. (2001). Morphology and morphogenesis of the poorly-known marine urostylid ciliate, *Metaurostylopsis marina* (Kahl, 1932) nov. gen., nov. comb. (Protozoa, Ciliophora, Hypotrichida). *Eur. J. Protistol.* 37, 63–76. doi: 10.1078/0932-4739-00802

Song, W., and Shao, C. (2017). *Ontogenetic Patterns of Hypotrich Ciliates (in Chinese)*. Beijing: Science Press.

Song, W., Warren, A., and Hu, X. (2009). *Free-Living Ciliates in the Bohai and Yellow Seas, China*. Beijing: Science Press.

Song, W., and Wilbert, N. (2002). Faunistic studies on marine ciliates from the Antarctic benthic area, including descriptions of one epizoic form, 6 new species and, 2 new genera (Protozoa: Ciliophora). *Acta Protozool.* 41, 23–61.

Song, W., Wilbert, N., Li, L., and Zhang, Q. (2011). Re-evaluation on the diversity of the polyphyletic genus *Metaurostylopsis* (Ciliophora, Hypotricha): ontogenetic, morphologic, and molecular data suggest the establishment of a new genus *Apourostylopsis* n. g. *J. Eukaryot. Microbiol.* 58, 11–21. doi: 10.1111/j.1550-7408.2010.00518.x

Stamatakis, A. (2014). RAxML version 8: a tool for phylogenetic analysis and post-analysis of large phylogenies. *Bioinformatics* 30, 1312–1313. doi: 10.1093/bioinformatics/btu033

Tuffrau, M., and Fleury, A. (1994). Classe des hypotrichea Stein, 1859. *Trait. Zool.* 2, 83–151.

Wang, C., Zhang, T., Wang, Y., Katz, L. A., Gao, F., and Song, W. (2017a). Disentangling sources of variation in SSU rDNA sequences from single cell analyses of ciliates: impacts of copy number variation and experimental errors. *P. Roy. Soc. B-Biol. Sci.* 284:20170425. doi: 10.1098/rspb.2017.0425

Wang, J., Li, J., and Shao, C. (2020a). Morphology, morphogenesis, and molecular phylogeny of a novel saline soil ciliate, *Heterourosomoida sinica* n. sp. (Ciliophora, Hypotrichia). *Eur. J. Protistol.* 73:125666. doi: 10.1016/j.ejop.2019.125666

Wang, J., Li, L., Warren, A., and Shao, C. (2017b). Morphogenesis and molecular phylogeny of the soil ciliate *Rigidohymena quadrinucleata* (Dragesco and Njine, 1971) Berger, 2011 (Ciliophora, Hypotricha, Oxytrichidae). *Eur. J. Protistol.* 60, 1–12. doi: 10.1016/j.ejop.2017.04.006

Wang, J., Zhao, Y., Lu, X., Lyu, Z., Warren, A., and Shao, C. (2020b). Does the *Gonostomum*-patterned oral apparatus in Hypotrichia carry a phylogenetic signal? Evidence from morphological and molecular data based on extended taxon sampling using three nuclear genes (Ciliophora, Spirotrichea). *Sci. China Life Sci.* 63. doi: 10.1007/s11427-020-1667-3

Wang, Y., Hu, X., Huang, J., Al-Rasheid, K. A. S., and Warren, A. (2011). Characterization of two urostylid ciliates, *Metaurostylopsis flavicana* spec. nov. and *Tunicothrix wilberti* (Lin & Song, 2004) Xu et al., 2006 (Ciliophora, Stichotrichia), from a mangrove nature protection area in China. *Int. J. Syst. Evol. Microbiol.* 61, 1740–1750. doi: 10.1099/ijs.0.024935-0

Wilbert, N., and Song, W. (2005). New contributions to the marine benthic ciliates from the Antarctic area, including description of seven new species (Protozoa, Ciliophora). *J. Nat. Hist.* 39, 935–973. doi: 10.1080/00222930400001509

Zhang, T., Dong, J., Cheng, T., Duan, L., and Shao, C. (2020). Reconsideration of the taxonomy of the marine ciliate *Neobakuella aenigmatica* Moon et al., 2019 (Protozoa, Ciliophora, Hypotrichia). *Mar. Life Sci. Technol.* 2, 97–108. doi: 10.1007/s42995-020-00032-4

Zhang, T., Qi, H., Zhang, T., Sheng, Y., Warren, A., and Shao, C. (2018). Morphology, morphogenesis and molecular phylogeny of a new brackish water subspecies, *Neourostylopsis flava paraflava* nov. subsp. (Ciliophora, Hypotrichia, Urostylidae), with redefinition of the genus *Neourostylopsis*. *Eur. J. Protistol.* 66, 48–62. doi: 10.1016/j.ejop.2018.07.004

Conflict of Interest: The authors declare that the research was conducted in the absence of any commercial or financial relationships that could be construed as a potential conflict of interest.

frontiers in Marine Science

ORIGINAL RESEARCH
published: 01 December 2020
doi: 10.3389/fmars.2020.604704

Taxonomy and Molecular Phylogeny of Three Species of Scuticociliates From China: *Citrithrix smalli* gen. nov., sp. nov., *Homalogastra binucleata* sp. nov. and *Uronema orientalis* Pan et al., 2015 (Protozoa, Ciliophora, Oligohymenophorea), With the Proposal of a New Family, Citrithrixidae fam. nov.

Mingjian Liu[1,2†], Chundi Wang[1,2†], Xiaozhong Hu[1,2], Zhishuai Qu[3], Limin Jiang[1,2], Saleh A. Al-Farraj[4], Hamed A. El-Serehy[4], Alan Warren[5] and Weibo Song[1*]*

[1] Institute of Evolution & Marine Biodiversity, Ocean University of China, Qingdao, China, [2] College of Fisheries and Key Laboratory of Mariculture of the Education Ministry of China, Ocean University of China, Qingdao, China, [3] Ecology Group, Technische Universität Kaiserslautern, Kaiserslautern, Germany, [4] Department of Zoology, College of Science, King Saud University, Riyadh, Saudi Arabia, [5] Department of Life Sciences, Natural History Museum, London, United Kingdom

The morphology and taxonomy of three scuticociliates found in China, viz. *Citrithrix smalli* sp. nov., *Homalogastra binucleata* sp. nov., and *Uronema orientalis* Pan et al., 2015, were investigated. The small subunit ribosomal RNA (SSU rRNA) gene of these species, and the cytochrome *c* oxidase subunit I (*COI*) gene of *Uronema orientalis*, were sequenced and compared with those of related taxa to determine their systematic positions. The new monotypic genus *Citrithrix* gen. nov. is characterized by its lemon-shaped body, posteriorly located cytostome, dominant oral groove, and the compact structure of its multi-rowed membranelles 1 and 2 (M1, M2). Based on both morphological and molecular data, this new genus cannot be assigned to any known family and thus, a new family, Citrithrixidae fam. nov., is proposed within the order Philasterida. *Homalogastra binucleata* sp. nov., a brackish water form (salinity 2‰), differs from all congeners in having two macronuclear nodules. *Uronema orientalis* closely resembles the type population in all respects other than having fewer somatic kineties.
This article is registered in ZooBank under: urn:lsid:zoobank.org:pub:5727F18E-5421-446D-B22C-774783539FE4.

Keywords: biodiversity, ciliated protozoa, ciliature, molecular systematics, new taxa

OPEN ACCESS

Edited by:
Hongbo Pan,
Shanghai Ocean University, China

Reviewed by:
Xuming Pan,
Harbin Normal University, China
Mann Kyoon Shin,
University of Ulsan, South Korea

***Correspondence:**
Xiaozhong Hu
xiaozhonghu@ouc.edu.cn
Weibo Song
wsong@ouc.edu.cn

†These authors have contributed equally to this work

Specialty section:
This article was submitted to Marine Evolutionary Biology, Biogeography and Species Diversity, a section of the journal Frontiers in Marine Science

Received: *10 September 2020*
Accepted: *05 November 2020*
Published: *01 December 2020*

Citation:
Liu M, Wang C, Hu X, Qu Z, Jiang L, Al-Farraj SA, El-Serehy HA, Warren A and Song W (2020) Taxonomy and Molecular Phylogeny of Three Species of Scuticociliates From China: Citrithrix smalli gen. nov., sp. nov., Homalogastra binucleata sp. nov. and Uronema orientalis Pan et al., 2015 (Protozoa, Ciliophora, Oligohymenophorea), With the Proposal of a New Family, Citrithrixidae fam. nov. Front. Mar. Sci. 7:604704. doi: 10.3389/fmars.2020.604704

INTRODUCTION

Ciliates in the subclass Scuticociliatia Small, 1967 are usually small in size, speciose and can be found in various environments such as aquatic as well as terrestrial habitats all over the world (Foissner et al., 1982, 1994; Lynn and Strüder-Kypke, 2005; Jankowski, 2007; Lynn, 2008). However, many scuticociliates lack a detailed description using modern methods resulting in problems of species identification, delineation and systematics (Borror, 1972; Carey, 1992; Jankowski, 2007; Song et al., 2009; Gao et al., 2016).

Recent studies on the ciliate fauna in coastal and freshwater habitats in China have revealed a much higher diversity of scuticocliates than was previously assumed (Song et al., 2009; Gao et al., 2012, 2013, 2014, 2017; Pan H. et al., 2016; Pan X. et al., 2016; Hu et al., 2019; Zhang et al., 2019; Liu et al., 2020; Pan et al., 2020). Among these, the philasterids are generally well-studied in terms of the application of modern silver staining and molecular methods to determine their taxonomy (Song et al., 2009; Liu et al., 2017). Six new genera and 22 new species have been added to the order Philasterida Small, 1967 since the beginning of the Twenty-first century (Aescht, 2001; Gong et al., 2007; Jankowski, 2007; Pan X. et al., 2016; Pan et al., 2020), which implies the diversity of this group may be underestimated.

During recent studies of marine and brackish water ciliates in China, three scuticociliates were investigated. Based on further morphological as well as molecular analyses, one of the species has been assigned to new genus and new family. The molecular phylogeny of all three species was investigated based on sequence data for the small subunit ribosomal RNA (SSU rRNA) gene and, for one species, the cytochrome *c* oxidase 1 (*COI*) gene.

MATERIALS AND METHODS

Collection and Isolation

Citrithrix smalli sp. nov. and *Uronema orientalis* Pan et al., 2015 were both collected from a bathing beach near the Zhanqiao Pier, Qingdao, China (**Figure 1**), the former from marine water on reefs (36°03'43" N; 120°19'12" E) in September 2016, and the latter from the intertidal zone (36°03'42" N; 120°19'25" E) in March 2017. *Homalogastra binucleata* sp. nov. was collected from an inland brackish water sewage ditch in Lanzhou (36°05'37" N; 103°44'58" E), China, in April, 2017 (**Figure 1**). In all three cases the sample comprised water and sediment after gently stirring the water.

Morphological Studies

Observations of specimens *in vivo* and specimens stained with silver were performed to reveal the general morphology and ciliary pattern based on the methods described by Bai et al. (2020). The protargol silver proteinate reagent was made in-house according to Pan et al. (2013). Counts, measurements, and drawings of specimens were made according to Qu et al. (2020). Terminology and systematics followed Lynn (2008).

DNA Extraction, PCR Amplification and Sequencing

Genomic DNA extraction, polymerase chain reaction (PCR), and gene sequencing were conducted, mainly according to Chi et al. (2020). The SSU rRNA gene was amplified using the primers 82F (Jerome et al., 1996) and 18S-R (Medlin et al., 1988). The primers for the *COI* gene amplification were COI-NEW-17-F1 and COI-NEW-812-R2 (Zhang et al., 2019). To minimize the amplification

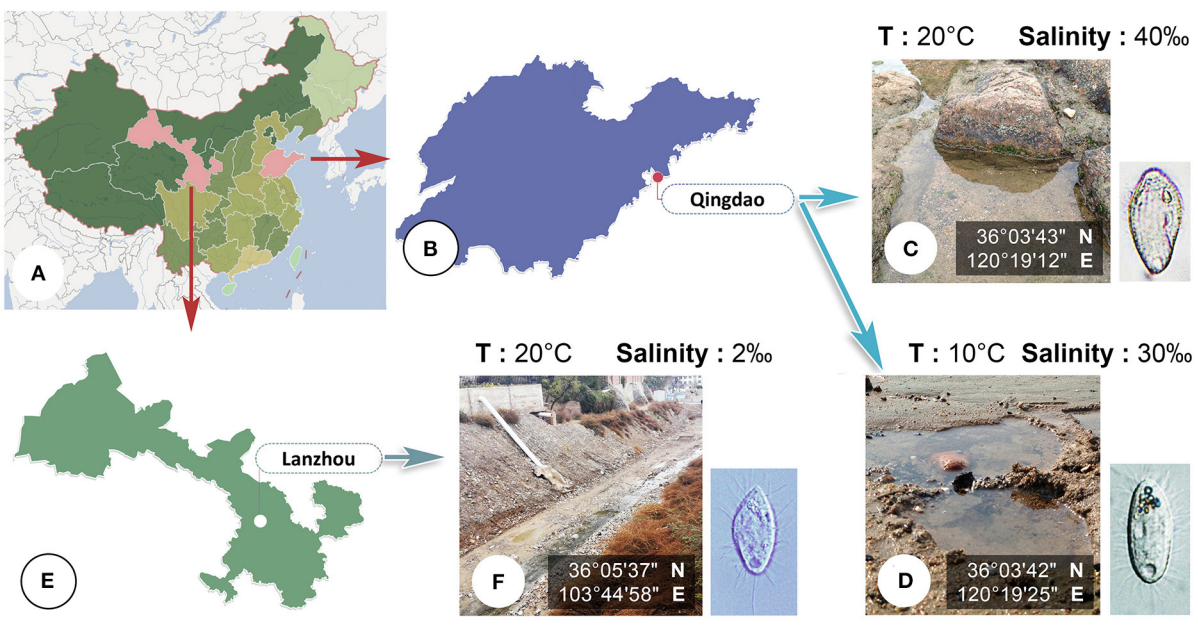

FIGURE 1 | (A–F) Map, sampling sites and habitats. **(A)** Map of China. **(B)** Shandong Province, showing the location of Qingdao. **(C,D)** Photographs of sampling sites in Qingdao where *Citrithrix smalli* sp. nov. (C) and *Uronema orientalis* Pan et al., 2015 **(D)** were collected. **(E)** Gansu Province, showing the location of Lanzhou. **(F)** Photograph of sampling site in Lanzhou where *Homalogastra binucleata* sp. nov. was collected.

errors, Q5 Hot Start High-Fidelity 2× Master Mix (New England BioLabs) was used (Wang et al., 2017). PCR for the SSU rRNA and *COI* genes were performed according to Chi et al. (2020) and Lynn and Strüder-Kypke (2006), respectively.

Phylogenetic Analyses

The SSU rRNA gene sequences of the three newly obtained isolates were aligned with 65 sequences from 50 related taxa, retrieved from GenBank. The accession numbers of these sequences are provided in the phylogenetic trees. Eight sequences of pleuronematids were selected as the outgroup. Alignments were conducted, edited, and trimmed according to Zhang et al. (2020). Comparisons of SSU rRNA gene sequences of *Citrithrix smalli* sp. nov., *Homalogastra binucleata* sp. nov., and *Uronema orientalis* with related sequences were performed, and the number of unmatched nucleotides and sequence identities were calculated, using the program BioEdit version 7.0.5.2 (Hall, 1999). The *COI* gene sequence of the newly isolated population of *Uronema orientalis* was compared with that of *U. orientalis* (MH605553).

Two maximum likelihood (ML) analyses, i.e., RAxML (Stamatakis, 2014) and IQTREE, and one Bayesian inference (BI) analysis, were carried out according to Wang et al. (2019). The IQ-trees were constructed on IQTREE 2.0.6 (Minh et al., 2020) with 10^4 ultrafast bootstrap replicates (Hoang et al., 2018). The best-fit model (GTR + F + R3) was selected based on the Bayesian information criterion (BIC) using the in-built ModelFinder program (Kalyaanamoorthy et al., 2017).

BI analysis was performed with the best-fit model GTR + I + G, selected by the Akaike Information Criterion using MrModeltest 2 (Nylander, 2004). Markov chain Monte Carlo (MCMC) simulations were run with two sets of four chains for 10^7 generations at a sampling frequency of 10^2 and a burn-in of 10^4 trees (10%).

Tree topologies were visualized using SeaView version 4 (Gouy et al., 2010).

RESULTS

Morphological Study

Subclass: Scuticociliatia Small, 1967

Order: Philasterida Small, 1967

Citrithrixidae fam. nov.

ZooBank. urn:lsid:zoobank.org:act:F65C9B97-42EE-47A2-ABA8-DC8B581C289F

Diagnosis. Free-living philasterid with highly developed and compact membranelles 1 and 2; cytostome located in a long and conspicuous buccal grove; somatic ciliature of Uronematidae-type.

Type genus. *Citrithrix* gen. nov.

Citrithrix gen. nov.

ZooBank. urn:lsid:zoobank.org:act:9A7480F9-A487-40B5-9784-815368E5E09B

Diagnosis. Body lemon-shaped to cylindrical in outline; cytostome located in posterior half of cell within a conspicuous, concave oral groove; multi-rowed membranelles 1 and 2 extremely close-set and highly developed; membranelle 3 small; paroral membrane extends anteriorly to level of mid-region of membranelle 2; somatic kineties composed of dikinetids and monokinetids; single caudal cilium.

Etymology. The genus-group name *Citrithrix* is a composite of *citri-* (Latin noun; lemon) and *thrix* (Greek noun; hair∼ciliate s.l.). It alludes to the typical lemon-shaped body. Feminine gender.

Type species. *Citrithrix smalli* sp. nov.

Citrithrix smalli sp. nov.

(**Figures 2A–N**; **Table 1**)

ZooBank. urn:lsid:zoobank.org:act:94C52D9F-DE13-4D33-B40A-4328D9D88FD3

Diagnosis. Cell size about 25–35 × 10–20 μm *in vivo*; 19–22 somatic kineties; single macronucleus; M1 composed of two or three rows; M2 irregular pentagon-shaped; contractile vacuole terminally positioned; marine biotope.

Dedication. We dedicate the new species to Prof. Eugene B. Small, University of Maryland, USA, in recognition of his significant contributions to the taxonomy and classification of ciliates in general and scuticociliates in particular.

Type locality and habitat. Seawater on reefs at a sandy beach in Qingdao (36°03'18" N; 120°20'22" E), northern China. Salinity 40‰, water temperature about 20°C.

Deposition of type slide. One protargol slide containing the holotype specimen and several paratype specimens (registration number: LMJ2016091901) was deposited in the Laboratory of Protozoology, Ocean University of China, Qingdao, China.

SSU rRNA gene sequence. The length is 1640 bp, G + C content 45.00% and GenBank accession number MT982807.

Description. Body about 25–35 × 10–20 μm *in vivo*, lemon- or spindle-shaped, widest part about one-third down length of cell (**Figures 2A,F,G**). Anterior end prominently truncated with apical plate about one-quarter to one-third of maximum body width (**Figures 2A,F**). Buccal field deeply concaved, length one-third to half of cell length; cytostome located in posterior half of cell (**Figures 2A,F,G**). Pellicle conspicuously notched with longitudinal ridges between ciliary rows (**Figures 2A,F–H**). No extrusomes recognizable. Cytoplasm colorless to slightly grayish, usually containing a few bar-shaped crystals in anterior region of cell (**Figures 2A,F,G**). Most cells with single ellipsoidal macronucleus located in mid-body region, 10–15 μm in diameter (**Figures 2D,J,K**); two out of 25 specimens examined with several (six to seven) spherical macronuclear nodules, each about 5–6 μm across (**Figure 2L**). Micronucleus closely associated with macronucleus, ∼3 μm across (**Figures 2D,J,L**). Single contractile vacuole caudally positioned, about 5 μm in diameter during diastole (**Figures 2A,F**), pulsating at intervals of 20–45 s. Somatic cilia about 7 μm long, densely arranged; single caudal cilium ∼15 μm long, emerging from a small depression at posterior end of cell (**Figures 2A,I**).

Locomotion by swimming moderately fast in upper layer of water, with anterior end swinging from side to side and body rotating continuously about longitudinal axis (**Figure 2B**).

Nineteen to 22 somatic kineties (SK), each commencing anteriorly around apical plate and extending almost to posterior end of cell (**Figures 2C,D,J,K**). SK composed of closely arranged

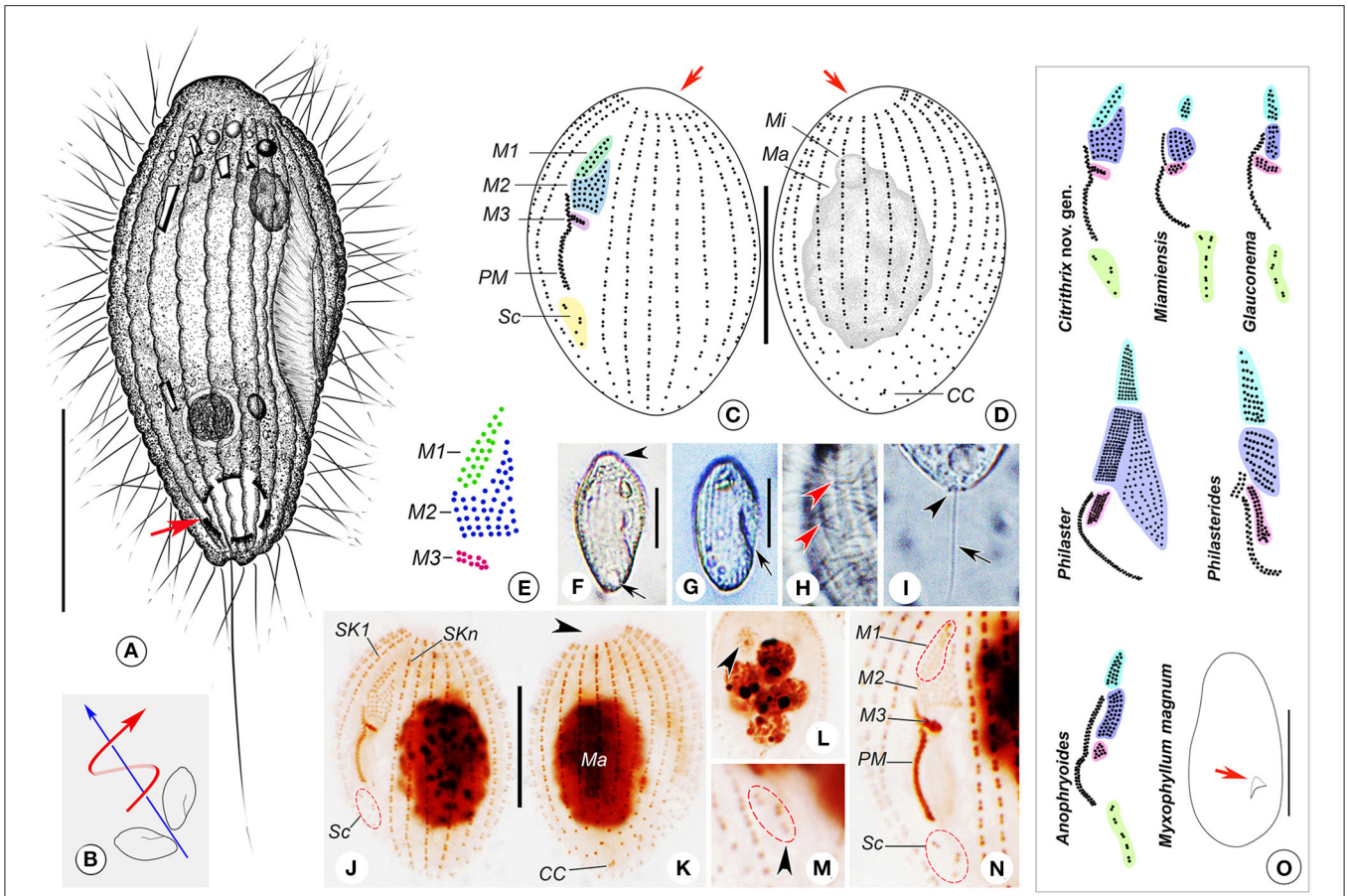

FIGURE 2 | (A–O) *Citrithrix smalli* sp. nov. from life **(A,B,F–I)**, after protargol staining **(C–E,J–N)**, and a comparison with related genera **(O)**. **(A)** Right ventrolateral view of a representative cell, arrow shows the contractile vacuole. **(B)** Swimming trace, red arrow indicates the body rotation, blue arrow shows the swimming direction. **(C,D)** Left ventrolateral **(C)** and right dorsolateral **(D)** views of the holotype specimen, arrows indicate the apical plate. **(E)** Oral structure showing three-rowed membranelle 1. **(F,G)** Right ventrolateral views, showing the variation in body shape, arrow and arrowhead in F point to the apical plate and contractile vacuole, respectively, arrow in G indicates the oral groove. **(H)** Detail of pellicle, arrowheads mark the grooves on the ciliary rows. **(I)** Lateral view of rear end of cell, arrowhead points to the small depression at basal position, arrow indicates the caudal cilium. **(J,K)** Left ventrolateral **(J)** and right dorsolateral **(K)** views of the holotype specimen, arrowhead shows the glabrous apical plate. **(L)** Nuclear apparatus of an individual with several macronuclear nodules, arrowhead indicates the micronucleus. **(M)** Arrowhead marks the scutica. **(N)** Detailed view of oral apparatus. **(O)** An oral structure comparison with related genera and a body size and shape comparison with *Myxophyllum magnum*, all redrawn based on previous studies except for the new genus (Cawthorn et al., 1996; Song, 2000; Song and Wilbert, 2000; Xu and Song, 2000; Ma et al., 2006; Pan et al., 2015b). Arrow in *M. magnum* points to the buccal field. CC, caudal cilium; M1–3, membranelle 1–3; Ma, macronucleus; Mi, micronucleus; PM, paroral membrane; Sc, scutica; SK1, somatic kinety 1; SKn, somatic kinety n. Scale bars: 15 μm **(A,C,D,F,G,J,K)**; 100 μm **(O)**.

dikinetids in anterior four-fifths of kinety and loosely arranged monokinetids in posterior one-fifth (**Figures 2C,D,J,K**). Somatic kinety 1 (SK1, first kinety on right of buccal field) composed of 24–31 kinetids of which 2–6 are monokinetids; mid somatic kinety on dorsal side composed of 18–25 kinetids of which 2–6 are monokinetids; somatic kinety n (SKn, first kinety on left of buccal field) composed of 18–29 kinetids including 0–4 monokinetids. Caudal complex consisting of three argentophilic granules (**Figures 2D,K**).

Oral apparatus consisting of three membranelles (M1–3) and one paroral membrane (PM). Characteristically M1 and M2 closely apposed, gap between them difficult to observe (**Figure 2E**). M1 comprising two or three longitudinal kinety rows that are progressively shortened at anterior ends (five cells of 25 examined having three-rowed M1) (**Figures 2C,E,J,N**). Rightmost row in M1 composed of eight or nine basal bodies, commencing anteriorly about one-sixth down length of cell; second row with seven or eight basal bodies; third row containing five or six basal bodies (**Figures 2C,E,J,N**). M2 irregular pentagon-shaped, usually consisting of two parts: upper left part with basal bodies arranged in triangle shape, and lower part with five or six horizontal kinety rows basically arranged in rectangle shape (**Figures 2C,E,J,N**). M3 slightly distant from M2, horizontally oriented, with six to 10 basal bodies (**Figures 2C,E,J,N**). PM on right side of oral groove, with basal bodies arranged in zig-zag pattern, length about one-quarter to one-third of cell length, anterior end commencing at level of middle portion of lower (rectangular) part of M2, posterior end terminating in mid-region of cell (**Figures 2C,E,J,N**). Scutica (Sc) located below posterior end of PM, usually consisting of three

TABLE 1 | Morphometric data for *Citrithrix smalli* sp. nov. (upper row), *Homalogastra binucleata* sp. nov. (middle row) and *Uronema orientalis* Pan et al., 2015 (lower row).

Character	Min	Max	Mean	Median	SD	SE	CV	*n*
Body length (*in vivo*) (μm)	25	35	30.5	30	4.14	1.69	13.6	6
	20	30	24.5	24	2.54	0.77	10.4	11
	25	40	33.5	35	3.78	1.09	11.3	12
Body width (*in vivo*) (μm)	10	20	15.7	17	3.88	1.58	24.8	6
	10	15	12.0	12	2.00	0.60	16.67	11
	12	20	16.1	15	2.27	0.66	14.1	12
Ratio of body length/body width (*in vivo*)	1.75	2.50	2.01	1.86	0.33	0.13	16.3	6
	1.67	2.40	2.06	2.00	0.22	0.07	10.76	11
	1.94	2.33	2.09	2.04	0.16	0.05	7.7	12
Body length (μm)	25	35	29.4	30	2.99	0.60	10.2	25
	23	28	25.5	25	1.51	0.45	5.9	11
	20	35	28.2	28	4.10	0.58	14.5	50
Body width (μm)	12	25	21.0	22	3.13	0.63	14.9	25
	12	17	15.3	15	1.27	0.38	8.3	11
	10	25	16.5	16.5	4.44	0.63	27.0	50
Buccal field length (μm)	11	16	13.8	14	1.50	0.30	10.9	25
	13	17	15.8	16	1.40	0.42	8.9	11
	9	15	11.7	11	1.32	0.19	11.3	50
Raito of buccal field length/body length	0.39	0.60	0.47	0.47	0.06	0.01	13.5	25
	0.54	0.68	0.62	0.61	0.04	0.01	6.0	11
	0.33	0.50	0.42	0.43	0.05	0.01	11.5	50
Number of SK	19	22	20.5	21	0.87	0.17	4.3	25
	11	11	11.0	11	0	0	0	11
	15	17	16.2	16	0.47	0.04	2.9	115
Number of kinetids in SK1	24	31	26.9	27	1.51	0.30	5.6	25
	18	23	20.3	20	1.42	0.43	7.0	11
	16	22	19.2	19	1.43	0.20	7.5	50
Number of monokinetids in SK1	2	6	4.1	4	1.20	0.24	29.2	25
	9	13	10.6	10	1.12	0.34	10.5	11
	4	13	9.1	9	2.42	0.34	26.6	50
Number of kinetids in middle SK	18	25	21.5	22	1.71	0.34	7.9	25
	14	18	15.0	15	1.18	0.36	7.9	11
	13	21	17.0	17	1.76	0.25	10.3	50
Number of monokinetids in middle SK	2	6	3.2	3	0.96	0.19	29.9	25
	2	4	3.0	3	0.45	0.13	14.9	11
	2	18	10.0	10	3.71	0.52	37.1	50
Number of kinetids in SKn	18	29	23.4	23	2.65	0.53	11.3	25
	13	15	13.8	14	0.83	0.28	6.0	9
	15	19	16.8	17	1.34	0.27	8.0	25
Number of monokinetids in SKn	0	4	2.1	2	1.22	0.24	58.8	25
	3	5	4.0	4	0.71	0.24	17.7	9
	3	11	8.0	9	2.23	0.45	28.0	25
Number of macronuclei	1	7	1.4	1	1.53	0.31	106.2	25
	2	2	2.0	2	0	0	0	46
	1	1	1.0	1	0	0	0	50
Diameter of macronucleus (μm)	5	15	12.0	12	2.71	0.54	22.6	25
	4	9	5.8	5.6	0.73	0.11	12.6	46
	6	12	9.1	9	1.35	0.19	14.9	50
Number of micronuclei	1	1	1.0	1	0	0	0	20
	1	3	1.4	1	0.61	0.15	44.8	17
	1	1	1.0	1	0	0	0	9
Diameter of micronucleus (μm)	2.0	4.0	2.4	2.0	0.59	0.13	25.0	20
	1.0	1.5	1.3	1.4	0.20	0.05	15.0	17
	1.5	3.0	1.9	2.0	0.49	0.16	25.7	9

All data are based on randomly selected protargol-stained specimens except where stated otherwise. CV, coefficient of variation in %; Max, maximum; Mean, arithmetic mean; Min, minimum; n, number of specimens observed; SD, standard deviation; SE, standard error of arithmetic mean; SK, somatic kineties; SK1, first somatic kinety on right of buccal field; SKn, first somatic kinety on left of buccal field.

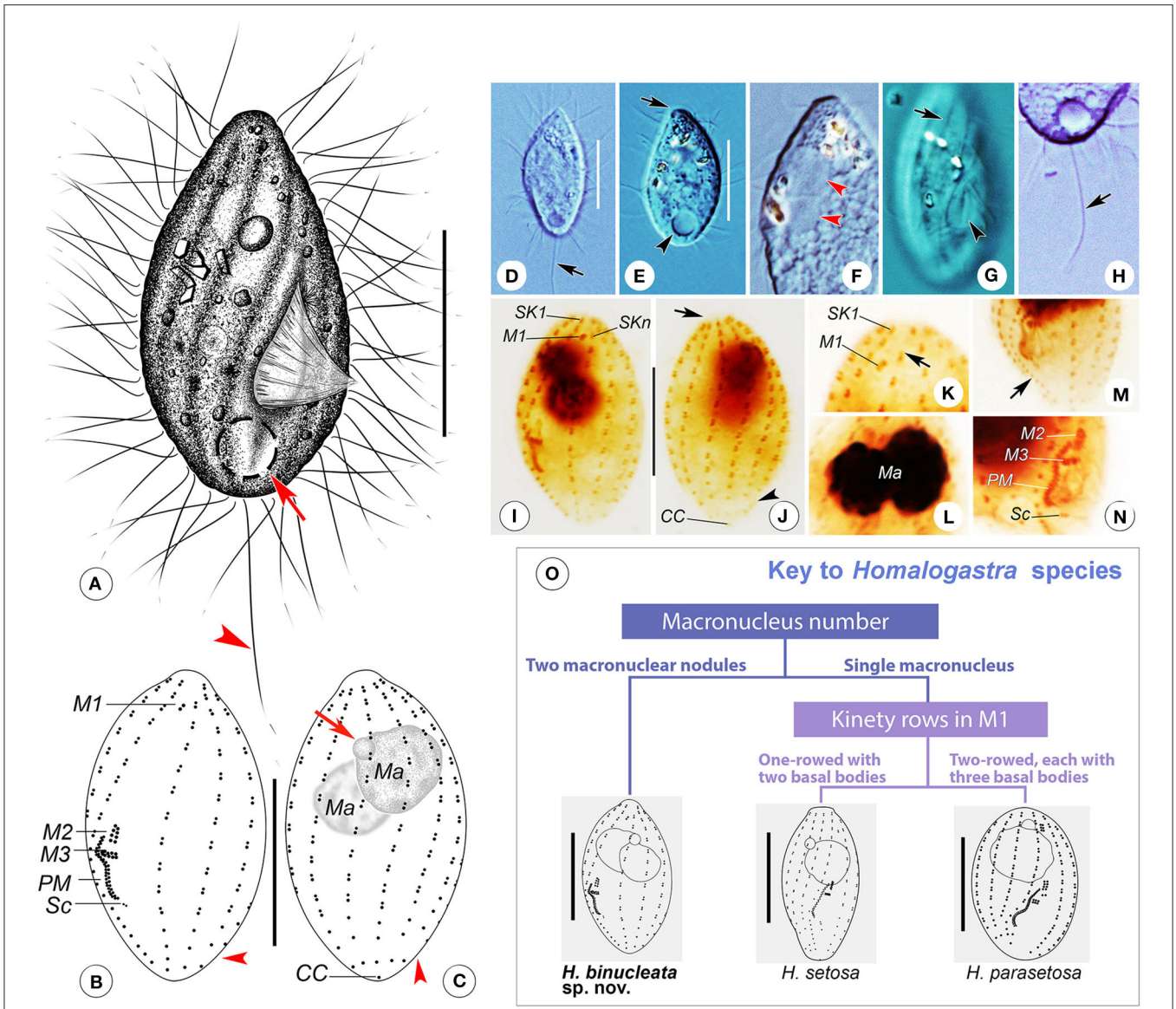

FIGURE 3 | (A–O) *Homalogastra binucleata* sp. nov. from life **(A,D–H)**, after protargol staining **(B,C,I–N)** and key to species of *Homalogastra* **(O)**. **(A)** Right ventrolateral view of a representative individual, arrow shows the contractile vacuole, arrowhead points to the caudal cilium. **(B,C)** Left ventrolateral **(B)** and right dorsolateral **(C)** views of the holotype specimen, arrowheads in B and C indicate the gap between last two basal bodies in somatic kineties, arrow in C points to the micronucleus. **(D,E)** Cells showing the variations in body shape, arrow in D marks the caudal cilium, arrow in E indicates the apical plate, arrowhead shows the contractile vacuole. **(F)** Left lateral view of a compressed cell, arrowheads show the two macronuclear nodules. **(G)** Detail of pellicle, arrow marks the grooves on the ciliary rows, arrowhead points to the buccal field. **(H)** Detailed view, arrow indicates the caudal cilium. **(I,J)** Left ventrolateral **(I)** and right dorsolateral **(J)** views of the holotype specimen, arrow in J shows the apical plate and arrowhead points to the gap between last two basal bodies in somatic kineties. **(K)** Anterior ventral side of protargol-stained cell, arrow indicates the shortened anterior end of SKn. **(L)** Nuclear apparatus, showing the two macronuclear nodules. **(M)** Posterior half of stained cell, arrow points to the densely arranged monokinetids in SK1. **(N)** Oral apparatus except for membranelle 1. **(O)** A species key of *Homalogastra*. Two congeners are redrawn based on previous studies (Foissner et al., 1982; Pomp and Wilbert, 1988). CC, caudal cilium; M1–3, membranelle 1–3; Ma, macronucleus; PM, paroral membrane; Sc, scutica; SK1, somatic kinety 1; SKn, somatic kinety n. Scale bars: 12 μm.

pairs of basal bodies (**Figure 2C**) or two pairs with additional one or two posteriorly located basal bodies (**Figures 2C,E,J,N**).

Genus: *Homalogastra* Kahl, 1926

Homalogastra binucleata sp. nov.

(**Figures 3A–N**; **Table 1**)

ZooBank. urn:lsid:zoobank.org:act:F828E465-8119-4D59-9DD8-6B58C7870678

Diagnosis. Body spindle- or pear-shaped, about 20–30 × 10–15 μm *in vivo*; invariably two spherical macronuclear nodules; 11 somatic kineties; membranelle 1 highly reduced with only

one pair of basal bodies, conspicuously separated from other membranelles; single caudal cilium; contractile vacuole caudally positioned; freshwater or brackish water habitat.

Etymology. The species-group name *binucleata* (having two nuclei) is a composite of the Latin numeral *bi-* (Latin numeral; two) and *nucleatus, -a, -um* [Latin adjective (m; f; n); kernel-like], and indicates the two macronuclear nodules, a diagnostic feature of the species.

Type locality and habitat. A brackish water sewage ditch in Lanzhou (36°05'37" N; 103°44'58" E), China. Salinity 2‰, water, temperature about 20°C.

Deposition of type slides. One protargol slide containing the holotype specimen (registration number: QZS2017043001-1) and one protargol slide with paratype specimens (registration number: QZS2017043001-2) were deposited in the Laboratory of Protozoology, Ocean University of China, Qingdao, China.

SSU rRNA gene sequence. The length is 1643 bp, G + C content 43.64% and GenBank accession number MT982808.

Description. Body about 20–30 × 10–15 μm *in vivo*, spindle-shaped, with oral groove in mid- to posterior region, cytostome located about two-thirds down length of cell (**Figures 3A,D,E,G**). Anterior end conspicuously pointed, with a small apical plate (**Figures 3A,D–F**). Pellicle with twisted shallow grooves along cilia rows (**Figures 3A,G**). No extrusomes detectable. Cytoplasm colorless, usually containing several irregular-shaped crystals in anterior half of cell (**Figures 3D–F**). One contractile vacuole caudally located, about 4–5 μm in diameter during diastole, pulsating at intervals of 35–45 s (**Figures 3A,D,E,H**). Invariably two spherical macronuclear nodules (in 46 individuals examined), closely apposed, each nodule about 5 μm in diameter (**Figures 3C,I,J,L**). Usually one micronucleus, about 1.5 μm in diameter, in anterior half of body. Somatic cilia about 7 μm long; single caudal cilium about 15–20 μm in length (**Figures 3A,H**).

Locomotion by rapid swimming while rotating continuously about longitudinal body axis or by crawling on substrate.

Constantly 11 somatic kineties (**Figures 3B,C,I,J**). Anterior ends commencing below apical plate except for SKn, which shortened anteriorly and commencing slightly above level of M1 (**Figures 3B,I**). SK1 comprising dikinetids in anterior three-fifths of body and densely arranged monokinetids in posterior two-fifths (**Figures 3B,I,M**). Other kineties composed of dikinetids in anterior four-fifths of kinety and loosely arranged monokinetids in posterior one-fifth (**Figures 3B,C,I,J**). Conspicuous gap between last two basal bodies in each somatic kinety with exception of SK1 and SKn (**Figures 3B,C,I,J**). SK1 composed of 18–23 kinetids of which 9–13 are monokinetids; mid somatic kinety on dorsal side composed of 14–18 kinetids including 2–4 monokinetids; SKn composed of 13–15 kinetids including 3–5 monokinetids. Caudal cilium monokinetid.

Oral apparatus typical of genus. M1 with two basal bodies longitudinally arranged, located apically in buccal field and clearly separated from M2 and M3 (**Figures 3B,I,K**). M2 two-rowed, each row with four basal bodies, situated in mid-region of cell (**Figures 3B,I,N**). M3 also two-rowed, each row comprising about eight to 10 basal bodies, horizontally oriented and located close to M2 (**Figures 3B,I,N**). Paroral membrane on right side of oral groove, two-rowed with basal bodies arranged in a zig-zag pattern; anterior end commencing at level of middle portion of M2, terminating posteriorly about two-thirds down length of cell, occupying about one-fifth of body length (**Figures 3B,I,N**). Scutica located below posterior end of paroral membrane, consisting of one pair of basal bodies (**Figures 3B,N**).

Family: Uronematidae Thompson, 1964

Genus: *Uronema* Dujardin, 1841

Uronema orientalis Pan et al., 2015

(**Figures 4A–O**; **Table 1**)

Improved diagnosis. Marine *Uronema* with 15 to 20 somatic kineties, single macronucleus and single micronucleus; body size about 25–55 × 12–30 μm *in vivo*, with narrowed anterior end; cytostome constantly sub-equatorial; membranelle 1 one-rowed or partly two-rowed, occasionally divided into two parts; membranelle 2 two-rowed; contractile vacuole caudally located, contractile vacuole pore positioned at end of the second somatic kinety.

Deposition of voucher slides. Three voucher slides containing protargol-stained specimens (registration numbers: LMJ2017031004, LMJ2017031003-1, LMJ2017031003-2) were deposited in the Laboratory of Protozoology, Ocean University of China, Qingdao, China.

SSU rRNA gene sequence. The length is 1633 bp, G + C content 42.38% and GenBank accession no. MT982806.

***COI* gene sequence.** The length is 764 bp, G + C content 27.75% and GenBank accession no. MT981149.

Description of the Qingdao population. Body about 25–40 × 12–20 μm *in vivo*, basically cylindrical in shape, anterior end truncated, with a glabrous apical plate about one-third of maximum body width, posterior end rounded (**Figures 4A,E,G**). Buccal cavity about one-quarter of body length, cytostome located in mid-body region (**Figures 4A,E,F**). Pellicle thin with inconspicuous notches and, in some individuals, prominent depressions on ventral and dorsal sides (**Figure 4G**). Extrusomes not detected. Cytoplasm colorless to grayish. Several irregular-shaped crystals usually clustered in anterior third of cell, forming a "black spot" when viewed at low magnification (**Figures 4A,E–G**). One spherical macronucleus, 8–12 μm in diameter, located in mid-region of cell; single spherical micronucleus, about 2 μm in diameter, adjacent to macronucleus (**Figures 4C,K**). One caudally located contractile vacuole, about 5 μm in diameter, pulsating at intervals of 20–50 s (**Figures 4A,E**). Somatic cilia about 5–7 μm in length; single caudal cilium about 12–15 μm long (**Figure 4A**).

Locomotion by swimming moderately fast without fixed pattern, or by crawling on substrates; sometimes suspended in water with anterior end moving in circles.

Fifteen to 17 somatic kineties, usually 16 (only two cells with 15 somatic kineties out of 115 cells examined). Each kinety commencing around apical plate and extending almost to rear end of cell (**Figures 4B,C,I–K,O**). SKn extending posteriorly further than other somatic kineties (**Figures 4B,O**). Generally, kineties composed of closely arranged dikinetids in anterior half and loosely arranged monokinetids in posterior half (**Figures 4B,C,I–K**). First dikinetid in SKn closely apposed to that in SK1, leaving a conspicuous space between first two dikinetids in SKn (**Figures 4B,J,O**). SK1 composed of 16–22 kinetids of

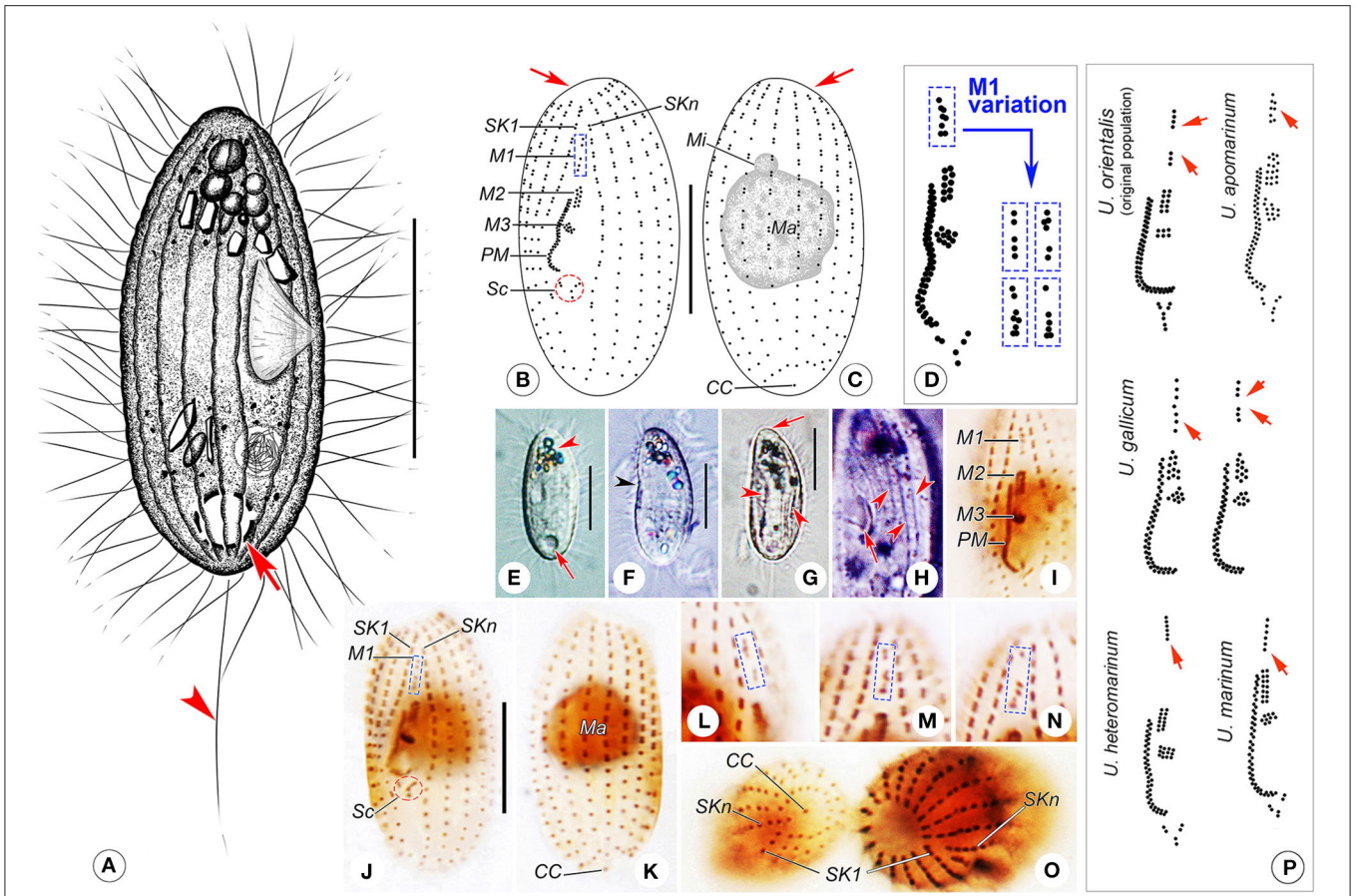

FIGURE 4 | (A–P) *Uronema orientalis* Pan et al., 2015 from life **(A,E–H)**, after protargol staining **(B–D,I–O)**, and comparison of the oral apparatus with that in related population/species **(P)**. **(A)** Right ventrolateral view of a representative cell, arrow shows the contractile vacuole and arrowhead points to the caudal cilium. **(B,C)** Ventral **(B)** and dorsal **(C)** views of a specimen with a gap in the mid-region of M1, arrows indicate the apical plate. **(D)** Oral apparatus of the Qingdao population of *Uronema orientalis*, and the variation of M1 structure. **(E)** Left ventrolateral view, arrow marks the contractile vacuole, arrowhead shows the clustered crystals at anterior of cell. **(F)** Left lateral view, arrowhead indicates the depressed buccal field on ventral side. **(G)** Individual with prominent depressions (arrowheads), arrow shows the apical plate. **(H)** Detail of pellicle, showing the buccal field (arrow) and ridges between ciliary rows (arrowheads). **(I)** Oral apparatus of a protargol-stained cell. **(J,K)** Ventral **(J)** and dorsal **(K)** views of a protargol-stained specimen, showing the ciliature and nuclear apparatus. **(L–N)** Variety of M1 structures that are bipartite. **(O)** Protargol-stained cells, revealing the structures of the posterior end (left cell) and the anterior end (right cell). **(P)** Comparison of oral apparatus with that in related population/species, all redrawn based on previous studies (*Uronema orientalis*, original population: Pan et al., 2015a; *U. apomarinum*: Liu et al., 2020; *U. gallicum*: Pérez-Uz and Song, 1995; *U. heteromarinum*: Pan et al., 2010; *U. marinum*: Song et al., 2009), arrows point to M1. CC, caudal cilium; M1–3, membranelle 1–3; Ma, macronucleus; Mi, micronucleus; PM, paroral membrane; Sc, scutica; SK1, somatic kinety 1; SKn, somatic kinety n. Scale bars: A, E–G: 15 μm; B, C, I–K: 10 μm.

which 4–13 are monokinetids; middle somatic kinety on dorsal side composed of 13–21 kinetids including 2–18 monokinetids; SKn composed of 15–19 kinetids including 3–11 monokinetids. Caudal cilium monokinetid (**Figures 4C,K,O**).

Oral apparatus typical of genus. M1 located about one-fifth down length of cell, about equal to M2 in length; in most cases, M1 partly two-rowed, that is, about eight basal bodies arranged in five transverse rows of which first and fourth rows each has only one basal body (**Figure 4D**). Occasionally (in eight out of 79 individuals examined) with gap in anterior or mid-portion dividing M1 into two parts, five or six transverse rows in total, making M1 slightly longer than M2 (**Figures 4B,D,J,L–N**). M2 located about one-third down length of cell, consisting of two equal-length longitudinal kinety rows (**Figures 4B,D,I,J**). M3 comprising about eight to 10 basal bodies arranged in a small patch below M2 (**Figures 4B,D,I,J**). Paroral membrane on right side of buccal field, comprising two rows of basal bodies arranged in a zig-zag pattern, about one-fifth of body length, commencing anteriorly at level of mid-portion of M2 and terminating posteriorly about two-thirds down length of cell (**Figures 4B,D,I,J**). Scutica located below posterior end of PM, usually consisting of three pairs of basal bodies arranged in Y-shape (**Figures 4B,D,I,J**).

Molecular Phylogenies and Sequence Comparisons

The topologies of the SSU rRNA gene trees constructed by two ML methods (RAxML and IQTREE) and one BI method (MrBayes) are generally congruent. Therefore, only the RAxML

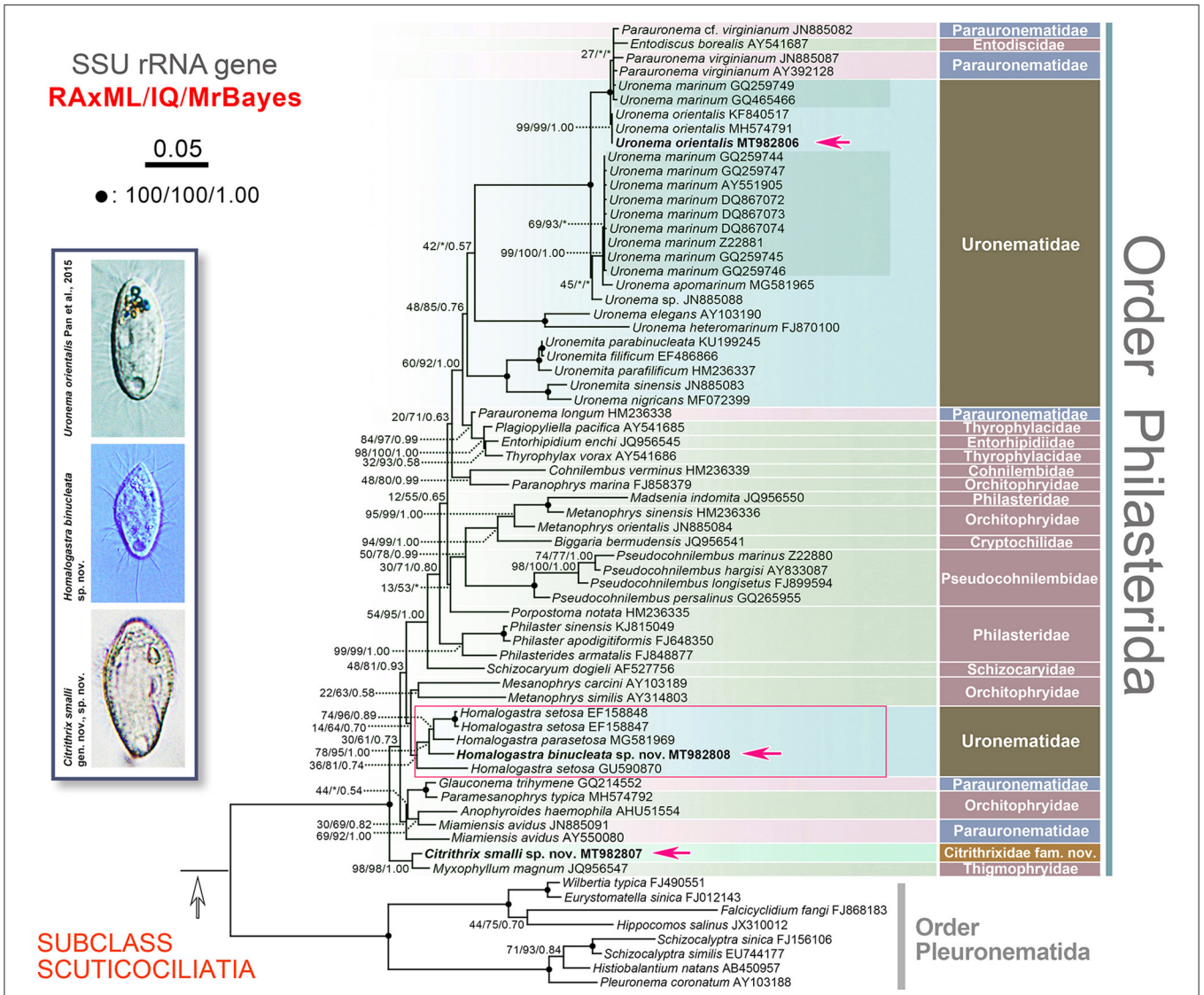

FIGURE 5 | RAxML tree inferred from SSU rRNA gene sequence data, red arrows point out the three newly sequenced populations. Numbers at nodes denote RAxML bootstrap values/IQTREE ultrafast bootstrap values/Bayesian inferences posterior probabilities. Asterisks (*) indicate mismatches of the topologies between RAxML, IQTREE and/or Bayesian inferences conducted in MrBayes. Fully supported (100%/100%/1.00) nodes are marked with black dots. The scale bar corresponds to five substitutions per 100 nucleotide positions. All branches are drawn to scale. The systematic classification mainly follows Lynn (2008).

tree is presented here with support values from all algorithms (**Figure 5**).

Citrithrix smalli sp. nov. MT982807 clusters with *Myxophyllum magnum* JQ956547 with strong to full support (98% RAxML, 98% IQ, 1.00 MrBayes) (**Figure 5**). The clade formed by *C. smalli* and *M. magnum*, a highly specialized parasitic form, then clusters with full support (100% RAxML, 100% IQ, 1.00 MrBayes) with the group containing all other representative sequences of the order Philasterida used in this study (**Figure 5**). Currently, few data are available to infer the evolutionary relationships and taxonomic rank of the *C. smalli* + *M. magnum* clade, but this basal branch very likely represents a lineage at about suborder level.

We compared the sequence identity of the SSU rRNA gene among *C. smalli* sp. nov., *M. magnum*, *Anophyroides haemophila*, *Miamiensis avidus*, *Glauconema trihymene* and *Paramesanophrys typica*, and found that *C. smalli* sp. nov. MT982807 differs in 28–71 nucleotides from the others with a sequence identity ranging from 95.6 to 98.2% (**Figure 6A**).

All five sequences of the genus *Homalogastra* group together forming a clade in the SSU rRNA gene tree (**Figure 5**). *Homalogastra binucleata* sp. nov. falls outside the group formed by *H. setosa* EF158847, *H. setosa* EF158848, and *H. parasetosa* MG581969, with medium to full support (78% RAxML, 95% IQ, 1.00 MrBayes). However, *H. setosa* GU590870 branches separately from these four *Homalogastra* sequences rather

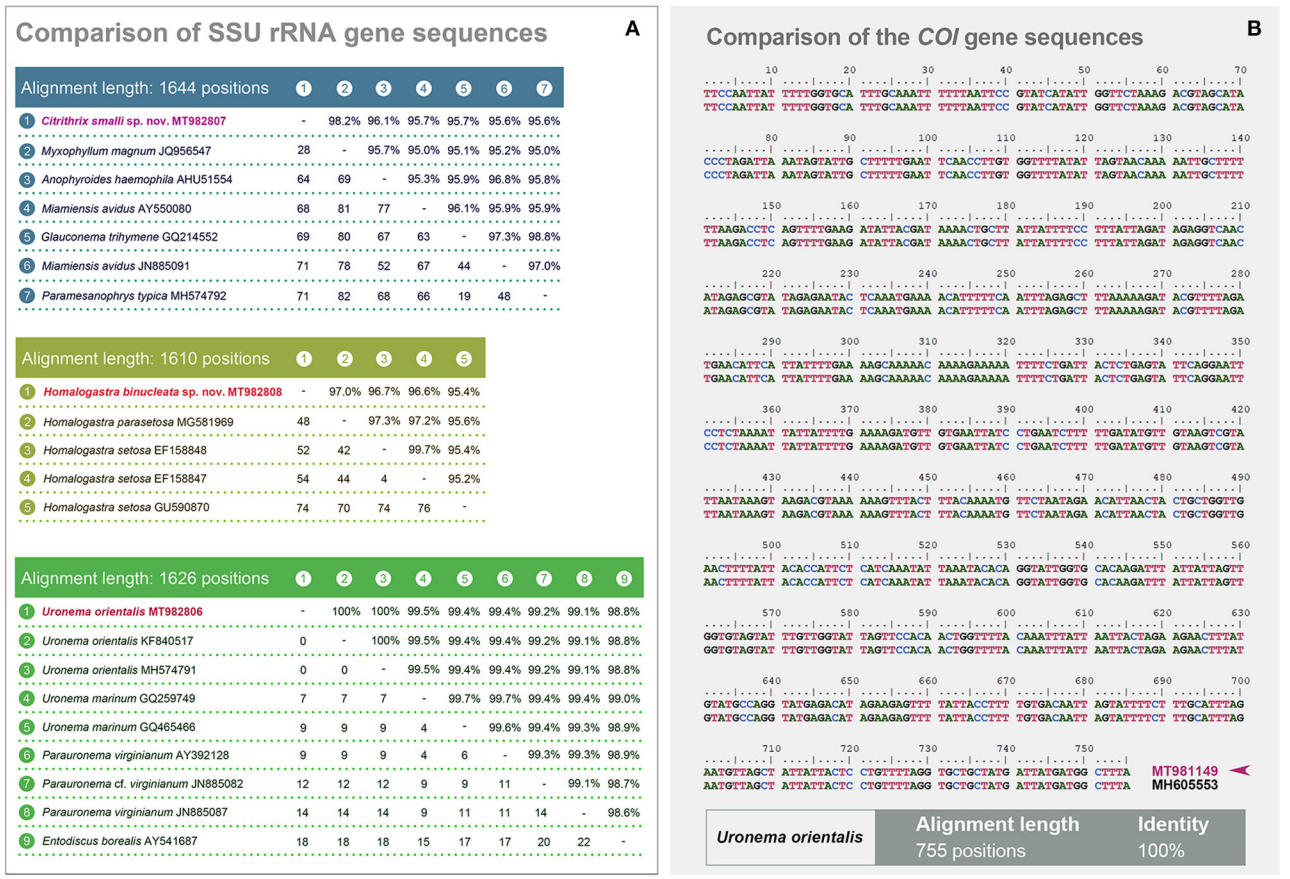

FIGURE 6 | (A, B) Comparisons of SSU rRNA and the *COI* gene sequences. **(A)** Comparisons of the SSU rRNA gene sequences of *Citrithrix smalli* sp. nov. (upper matrix), *Homalogastra binucleata* sp. nov. (middle matrix), and *Uronema orientalis* Pan et al., 2015 (lower matrix), with their related sequences. The lengths of each alignment after trimming both ends are shown. The lower left values in each matrix are numbers of unmatched nucleotides, while the upper right numbers indicate the sequence identity. **(B)** Comparison of the *COI* gene sequences between *Uronema orientalis* MT981149 (from the present study, with arrowhead) and *Uronema orientalis* MH605553 (from the original population). The final alignment length is 755 positions, with a 100% sequence identity.

than clustering with the two strains of *H. setosa*. In the SSU rRNA gene sequence alignment of the five *Homalogastra* species/strains, *H. binucleata* sp. nov. MT982808 differs from the other *Homalogastra* sequences in 48 to 74 nucleotides and has a sequence identity ranging from 95.4 to 97.0% (**Figure 6A**).

Apart from *Homalogastra*, other species/strains of Uronematidae cluster with Parauronematidae and Entodiscidae (48% RAxML, 85% IQ, 0.76 MrBayes). The genus *Uronema* is not monophyletic (**Figure 5**). The newly sequenced *Uronema orientalis* MT982806 clusters with two *U. orientalis* sequences (KF840517, MH574791) from the same population (Pan et al., 2015a) with high or full statistical support (99% RAxML, 99% IQ, 1.00 MrBayes), and then groups with the Parauronematidae + Entodiscidae + *Uronema marinum* (GQ259749; GQ465466) clade (**Figure 5**). Sequence comparison of the SSU rRNA gene shows that there is no difference between *U. orientalis* MT982806 and two previous *U. orientalis* sequences (KF840517, MH574791) (**Figure 6A**). The *COI* gene sequence of the present population of *U. orientalis* (MT981149) is identical to that of the original population (MH605553) after trimming both ends of the alignment, giving 755 nucleotides in the final alignment (**Figure 6B**).

DISCUSSION

Morphological Comparison and Phylogenetic Analyses of *Citrithrix smalli* gen. nov., sp. nov.

Citrithrix smalli gen. nov., sp. nov. has a distinct oral structure (extremely close-set M1 and M2 when compared with morphologically similar genera) which slightly resembles that of parauronematids (**Figure 2O**). However, the new taxon can be distinguished from all four known genera of parauronematids [i.e., *Miamiensis*, *Glauconema*, *Parauronema*, and *Potomacus* (**Table 2**)] by the long, conspicuously deep oral groove (vs. absent or inconspicuous in the latter four genera) and the closely apposed M1 and M2 (vs. M1 and M2 clearly separated in the latter four genera) (Thompson

TABLE 2 | Comparison of *Citrithrix* nov. gen. with related genera.

Genus	*Citrithrix* nov. gen.	*Miamiensis* Thompson & Moewus, 1964	*Glauconema* Thompson, 1966	*Parauronema* Thompson, 1967	*Potomacus* Thompson, 1966	*Paranophrys* Thompson & Berger, 1965	*Anophryoides* de Puytorac & Grolière, 1979	*Paramesanophrys* Pan et al., 2016
Body shape	Lemon-shaped to cylindrical in outline; widest at anterior one third of cell	Plump pyriform	Usually reniform, highly asymmetrical when viewed laterally	Usually oval to elliptical	Basically fusiform	Usually elongated oval or cylindrical	Elongated ovoid	Elongated, spindle-shaped
Anterior end truncated?	Yes	No	Yes	Yes	No	No	NA	No
Buccal field concave?	Yes	No	Yes	Yes	No	No	No	Yes
With basal depression from which caudal cilium emerges?	Yes	No	No	No	NA	No	No	Yes
Number of longitudinal rows in M1	2 or 3	2	2 or 3	2	2 or 3	3	3	2
Rows in M1 equal in length?	No	Yes	No	Yes	Yes	No	No	Yes
Structure of M2	Basal bodies clustered in two parts: upper-left triangle and lower five or six horizontal rowed rectangle	4 or 5 longitudinal rows	2 or 3 longitudinal rows, unequal in length	2 or 3 longitudinal rows, almost equal in length	3 longitudinal rows or more, almost equal in length	3 longitudinal rows, unequal in length	4 longitudinal rows, equal in length, forming a slightly curved rectangle	Irregularly multi-rowed
Length of M2 relative to M1	Longer than M1	Longer than M1	Same length as M1	Slightly longer than M1	Longer than M1	Much shorter than M1	Longer than M1	Longer than M1
Distance between M1 and M2	Extremely short, not well separated	Shorter than length of M1	Shorter than or equal to length of M1	Slightly shorter than length of M1	Shorter than or equal to length of M1	Much shorter than length of M1	Shorter than length of M1	Shorter than length of M1
Structure of PM	Double-rowed in zig-zag pattern	Single-rowed in anterior 1/3 and rest 2/3 double-rowed in zig-zag pattern	Double-rowed in zig-zag pattern	Double-rowed in zig-zag pattern	Double-rowed in zig-zag pattern	Double-rowed in zig-zag pattern	Double-rowed	Double-rowed in zig-zag pattern
Position of anterior end of PM	Mid portion of lower rectangle of M2 on right side	Right front end of M2	About at first 1/3 of M2 on right side	Mid portion of M2 on right side	Mid portion of M2 on right side	Right front end of M2	Right front end of M2	Posterior end of M3
Data source	Present study	Thompson and Moewus (1964) and Song and Wilbert (2000)	Thompson (1966) and Ma et al. (2006)	Thompson (1967), Grolière (1974), Wilbert and Kahan (1981), and Song and Wilbert (2000)	Thompson (1966)	Thompson and Berger (1965), Borror (1972), Czapik and Wilbert (1986), Song and Wilbert (2000), and Song et al. (2002)	Cawthorn et al. (1996)	Pan X. et al. (2016)

M1 and 2, membranelle 1 and 2; NA, not available; PM, paroral membrane.

and Moewus, 1964; Thompson, 1966, 1967; Grolière, 1974; Wilbert and Kahan, 1981; Song and Wilbert, 2000; Ma et al., 2006). In addition, *Citrithrix* gen. nov. is not closely related to the parauronematids in the SSU rRNA gene tree (**Figure 5**).

Three genera in the family Orchitophryidae, namely *Paranophrys*, *Anophryoides*, and *Paramesanophrys*, should be compared with *Citrithrix* gen. nov. since the M1 and M2 of all these genera are multi-rowed (**Table 2**). *Citrithrix* gen. nov. differs from them mainly in the presence of an oral groove, the

TABLE 3 | Comparison of *Homalogastra binucleata* sp. nov. with congeners.

Character	*Homalogastra binucleata* sp. nov.	*Homalogastra setosa* Kahl, 1926	*Homalogastra parasetosa* Liu et al., 2020
Body size *in vivo*	20–30 × 10–15 μm	15–30 × 7–15 μm	20–30 × 10–15 μm
Body size after protargol staining	23–28 × 12–17 μm	20–25 × 9–13 μm	20–35 × 12–25 μm
Body shape	Spindle-shaped in outline	Spindle-shaped in outline	Spindle-shaped to oval in outline
Pellicle	Thin and rough, with twisted shallow grooves along cilia rows	Weakly notched along cilia rows	Basically smooth, with straight shallow grooves along cilia rows
M1 structure	One-rowed, with two basal bodies	One-rowed, with two basal bodies	Two-rowed, each row with three basal bodies
Number of SK	11	12	10–14
Number of macronucleus (or macronuclear nodules)	2	1	1
Habitat	Brackish water	Soil	Brackish water and soil
Data source	Present study	Kahl (1931) and Foissner et al. (1982)	Buitkamp (1977), Pomp and Wilbert (1988), Alekperov (2005), and Liu et al. (2020)

M1, membranelle 1; SK, somatic kineties.

arrangement of M1 and M2, and the position of the anterior end of the PM (Thompson and Berger, 1965; Borror, 1972; Czapik and Wilbert, 1986; Cawthorn et al., 1996; Song and Wilbert, 2000; Song et al., 2002; Pan X. et al., 2016).

These morphological differences are reflected in the molecular analyses in the present study: *Citrithrix smalli* sp. nov. is well-separated from the families Parauronematidae, Orchitophryidae and Philasteridae, which belong to the core part of the order Philasterida, and occupies the basal position within the order suggesting that *Citrithrix* gen. nov. may represent the ancestral group of philasterids (**Figure 5**).

Although *Citrithrix smalli* sp. nov. clusters with *Myxophyllum magnum* JQ956547 and shows a sequence identity of 98.2% (**Figures 5**, **6A**), the former differs significantly from the latter in its morphology and ecology, e.g., the number of somatic kineties, the oral structure, and the free-living (vs. parasitic) life-style (Xu and Song, 2000).

In conclusion, both the morphological and the molecular data indicate that our new taxon cannot be assigned to any extant family. A new family, Citrithrixidae fam. nov., is thus proposed within the order Philasterida.

Morphological Comparison and Phylogenetic Analyses of *Homalogastra binucleata* sp. nov.

Based on its body size and shape, conspicuous oral groove and oral structure, *Homalogastra binucleata* sp. nov. corresponds well with the genus diagnosis of *Homalogastra* (Liu et al., 2020). Hitherto there are only two known congeners, i.e., *H. setosa* (type species) and *H. parasetosa* (**Table 3**).

Homalogastra binucleata sp. nov. can easily be separated from both congeners by having two (vs. one) macronuclear nodules. In addition, it differs from *H. parasetosa* in the structure of its M1 which comprises a pair of basal bodies in *H. binucleata* sp. nov. (and *H. setosa*) vs. M1 two-rowed, each row with three basal bodies, in *H. parasetosa* (**Figure 3O**) (Kahl, 1931; Buitkamp, 1977; Foissner et al., 1982; Pomp and Wilbert, 1988; Alekperov, 2005; Liu et al., 2020).

In the SSU rRNA gene tree, *H. binucleata* sp. nov. nests within the *Homalogastra* clade (**Figure 5**). The SSU rRNA gene sequence of our new species has the highest sequence identity with *H. parasetosa* MG581969 (97%), although there are 48 unmatched nucleotides (**Figure 6A**). Therefore, clarification of the phylogenetic relationships among *Homalogastra* species awaits data from more gene markers and from additional populations and species. Such data might also be helpful to determine how their morphological characteristics reflect their evolutionary relationships.

Morphological Comparison and Phylogenetic Analyses of Qingdao Population of *Uronema orientalis* Pan et al., 2015

Uronema orientalis was established by Pan et al. (2015a) mainly according to its bipartite M1 and its high number of somatic kineties. The Qingdao population resembles the original population in cell size, shape and oral structure, but it differs from the latter by having: fewer somatic kineties, i.e., 15–17, usually 16 (vs. constantly 20 in the type population); each kinety with mono- and dikinetids (vs. each kinety usually comprises monokinetids only in the type population); M1 partly two-rowed that occasionally with a gap (vs. one-rowed and divided by a gap, but the stability of M1 structure is not available in the original report). Besides, the extrusomes in the current population are not detected (vs. bar-shaped extrusomes, 4 μm in length in the original population) (Pan et al., 2015a) (**Figures 4D,J,L–N,P**).

Based on the morphological differences, the current population can be a new subspecies of *Uronema orientalis*. However, the locations of the inhabitation of the current and the original populations are not geographically separate. In addition,

TABLE 4 | Comparison of *Uronema orientalis* Pan et al., 2015 with selected congeners.

Characters	*U. orientalis* Pan et al., 2015	*U. gallicum* Pérez-Uz & Song, 1995	*U. apomarinum* Liu et al., 2020	*U. heteromarinum* Pan et al., 2010	*U. marinum* Dujardin, 1841
Body size *in vivo*	25–55 × 12–30 μm	20–30 × 8–11 μm	25–35 × 10–15 μm	25–50 × 10–25 μm	25–35 × 10–15 μm
Body size after silver staining	25–58 × 12–35 μm	21–28 × 9–14 μm	25–32 × 10–15 μm	30–50 × 20–30 μm	28–39 × 14–20 μm
Body shape	Basically cylindrical in outline	Usually elongated, well-nourished cells often ovoid	Elongate-ovate in outline, anterior end slightly pointed	Usually elliptical to cylindrical	Elongate-elliptical in outline
Pellicle	Thin and inconspicuously notched	Thin and inconspicuously notched	Thin and inconspicuously notched	Notched with conspicuous reticulate ridges	Basically smooth
Extrusomes	Bar-shaped, about 4 μm long	Fine and rod-like, about 2 μm long	Not detected	Bar-shaped, about 2 μm long	Bar-shaped, about 2 μm long
M1 structure	One- or partly two-rowed; occasionally with a gap in anterior or mid-portion	One-rowed, with 6–7 widely spaced kinetosomes in a row that sometimes seems to break in the middle	Partly two-rowed, consisting of ca. 6–8 basal bodies, totally arranged in five transverse rows	One-rowed, consisting of ca. 4–7 basal bodies, well-separated from other membranelles	One-rowed with 5–7 basal bodies
Number of longitudinal kinety rows in M2	2	3	3	2	2
Number of SK	15–20	13–15 (usually 14, *n* = 74)	12–13	15–16	12–14
Habitat	Marine	Marine	Brackish water	Marine	Marine
Data source	Present study; Pan et al. (2015a)	Pérez-Uz and Song (1995)	Liu et al. (2020)	Pan et al. (2010)	Song et al. (2009) and Pan et al. (2010)

M1 and 2, membranelle 1 and 2; n, number of specimens observed; SK, somatic kineties.

the sequence comparisons of the SSU rRNA and *COI* genes of the two populations show that the sequences of each gene are identical (**Figure 6**), strongly supporting the identity of the current population as *U. orientalis*. Therefore, it is reasonable to treat the current population as *U. orientalis* Pan et al., 2015 with some morphological variations.

Morphological Comparison of *Uronema orientalis* Pan et al., 2015 With Closely Related Congeners

Considering the structure of the oral apparatus and the somatic ciliature, four *Uronema* species should be compared with *Uronema orientalis* Pan et al., 2015, namely *U. gallicum* Pérez-Uz and Song, 1995, *U. apomarinum* Liu et al., 2020, *U. heteromarinum* Pan et al., 2010, and *U. marinum* Dujardin, 1841 (**Figure 4P**; **Table 4**).

Uronema orientalis most closely resembles *U. gallicum* in the M1 structure, that is, occasionally bipartite with a gap in the anterior or mid-region of M1 dividing it into two parts (**Figures 4D,J,L–N,P**). However, the latter can be distinguished from the former by its slimmer body shape (body width *in vivo* 8–11 μm vs. 12–30 μm in *U. orientalis*), and in having fewer somatic kineties (13–15 vs. 15–20 in *U. orientalis*) (Pérez-Uz and Song, 1995; Pan et al., 2015a).

Uronema orientalis can be separated from the other three *Uronema* species mainly by the number of somatic kineties and by the structure of M1 and M2 (Song et al., 2009; Pan et al., 2010; Liu et al., 2020) (**Figures 4B–D,P**; **Table 4**).

DATA AVAILABILITY STATEMENT

The datasets generated for this study can be found in online repositories. The names of the repository/repositories and accession number(s) can be found in the article/supplementary material.

AUTHOR CONTRIBUTIONS

XH and WS conceived and designed the paper. ML, ZQ, and LJ carried out the live observation and protargol staining. CW analyzed the data. ML, CW, XH, ZQ, LJ, SA-F, HE-S, AW, and WS wrote the paper. All authors contributed to the article and approved the submitted version.

FUNDING

This work was supported by the Marine S and T Fund of Shandong Province for Pilot National Laboratory for

Marine Science and Technology (Qingdao) (2018SDKJ0406-1), the National Natural Science Foundation of China (project numbers: 41976086, 41706168), and the Researchers Supporting Project Number (RSP-2020/7), King Saud University, Riyadh, Saudi Arabia.

ACKNOWLEDGMENTS

Many thanks are due to Ms. Jiyang Ma (OUC) for providing the samples, and to Dr. Zhe Wang for the advice on the IQTREE 2.0.6 program.

REFERENCES

Aescht, E. (2001). *Catalogue of the Generic Names of Ciliates (Protozoa, Ciliophora)*. Linz: Biologiezentrum des Oberösterreichischen Landesmuseums.

Alekperov, I. (2005). *Atlas Svobodnozhivushchikh Infuzorii (Atlas of Free-living Ciliates)*. Baku: Institute of Zoology NAS of Azerbaijan.

Bai, Y., Wang, R., Song, W., Suzuki, T., and Hu, X. (2020). Redescription of five tintinnine ciliates (Alveolata: Ciliophora: Oligotrichea) from coastal waters of Qingdao, China. *Mar. Life Sci. Technol.* 2, 209–221. doi: 10.1007/s42995-020-00034-2

Borror, A. C. (1972). Tidal marsh ciliates (Protozoa): morphology, ecology, systematics. *Acta Protozool.* 10, 29–71.

Buitkamp, U. (1977). Die Ciliatenfauna der Savanne von Lamto (Elfenbeinküste). *Acta Protozool.* 16, 249–276.

Carey, P. C. (1992). *Marine Interstitial Ciliates: An Illustrated Key*. London: Chapman & Hall

Cawthorn, R. J., Lynn, D. H., Despres, B., MacMillan, R., Maloney, R., Loughlin, M., et al. (1996). Description of Anophryoides haemophila n. sp. (Scuticociliatida: Orchitophryidae), a pathogen of American lobsters Homarus americanus. *Dis. Aquat. Organ.* 24, 143–148. doi: 10.3354/dao024143

Chi, Y., Duan, L., Luo, X., Cheng, T., Warren, A., Huang, J., et al. (2020). A new contribution to the taxonomy and molecular phylogeny of three, well-known freshwater species of the ciliate genus *Spirostomum* (Protozoa: Ciliophora: Heterotrichea). *Zool. J. Linn. Soc.* 189, 158–177. doi: 10.1093/zoolinnean/zlz115

Czapik, A., and Wilbert, N. (1986). Sur une nouvelle espèce de cilié *Paranophrys carnivora* sp. n. (Scuticociliatida). *Acta Protozool.* 25, 427–432.

Foissner, W., Adam, H., and Foissner, I. (1982). Morphologie, infraciliatur und silberliniensystem einiger wenig bekannter Scuticociliatida (Protozoa: Ciliophora). *Zool. Jb. Syst.* 109, 443–468.

Foissner, W., Berger, H., and Kohmann, F. (1994). Taxonomische und ökologische revision der ciliaten des saprobiensystems - Band III: Hymenostomata, Prostomatida, Nassulida. *Informationsber. Bayer. Landesamtes Wasserwirtschaft* 1/94, 1–548.

Gao, F., Gao, S., Wang, P., Katz, L. A., and Song, W. (2014). Phylogenetic analyses of cyclidiids (Protista, Ciliophora, Scuticociliatia) based on multiple genes suggest their close relationship with thigmotrichids. *Mol. Phylogenet. Evol.* 75, 219–226. doi: 10.1016/j.ympev.2014.01.032

Gao, F., Huang, J., Zhao, Y., Li, L., Liu, W., Miao, M., et al. (2017). Systematic studies on ciliates (Alveolata, Ciliophora) in China: progress and achievements based on molecular information. *Eur. J. Protistol.* 61, 409–423. doi: 10.1016/j.ejop.2017.04.009

Gao, F., Katz, L. A., and Song, W. (2012). Insights into the phylogenetic and taxonomy of philasterid ciliates (Protozoa, Ciliophora, Scuticociliatia) based on analyses of multiple molecular markers. *Mol. Phylogenet. Evol.* 64, 308–317. doi: 10.1016/j.ympev.2012.04.008

Gao, F., Katz, L. A., and Song, W. (2013). Multigene-based analyses on evolutionary phylogeny of two controversial ciliate orders: Pleuronematida and Loxocephalida (Protista, Ciliophora, Oligohymenophorea). *Mol. Phylogenet. Evol.* 68, 55–63. doi: 10.1016/j.ympev.2013.03.018

Gao, F., Warren, A., Zhang, Q., Gong, J., Miao, M., Sun, P., et al. (2016). The all-data-based evolutionary hypothesis of ciliated protists with a revised classification of the phylum Ciliophora (Eukaryota, Alveolata). *Sci. Rep.* 6:24874. doi: 10.1038/srep24874

Gong, J., Choi, J. K., Roberts, D. M. L., Kim, S. Y., and Min, G. S. (2007). Morphological descriptions of new and little-known benthic ciliates from Ganghwa tidal flat, Korea. *J. Eukaryot. Microbiol.* 54, 306–316. doi: 10.1111/j.1550-7408.2007.00268.x

Gouy, M., Guindon, S., and Gascuel, O. (2010). SeaView version 4: a multiplatform graphical user interface for sequence alignment and phylogenetic tree building. *Mol. Biol. Evol.* 27, 221–224. doi: 10.1093/molbev/msp259

Grolière, C. A. (1974). Étude comparée de la stomatogenèse chez quelques cilies hymenostomes des genres *Paralembus* Kahl, 1933 *Philaster* Fabre-Domergue, 1885 *Parauronema* Thompson, 1967, *Tetrahymena* Furgasson, 1940. *Protistologica* 10, 319–331.

Hall, T. A. (1999). BioEdit: a user-friendly biological sequence alignment editor and analysis program for Windows 95/98/NT. *Nucleic Acids Symp. Ser.* 41, 95–98.

Hoang, D. T., Chernomor, O., von Haeseler, A., Minh, B. Q., and Vinh, L. S. (2018). UFBoot2: improving the ultrafast bootstrap approximation. *Mol. Biol. Evol.* 35, 518–522. doi: 10.1093/molbev/msx281

Hu, X., Lin, X., and Song, W. (2019). *Ciliate Atlas: Species Found in the South China Sea. Beijing: Science Press*. doi: 10.1007/978-981-13-5901-9

Jankowski, A. V. (2007). "Phylum Ciliophora Doflein, 1901. Review of taxa," in *Protista: Handbook on Zoology*, ed A. F. Alimov (St. *Petersburg: Nauka)*, 415–993.

Jerome, C. A., Simon, E. M., and Lynn, D. H. (1996). Description of Tetrahymena empidokyrea n. *sp., a new species in the Tetrahymena pyriformis sibling species complex (Ciliophora, Oligohymenophorea), and an assessment of its phylogenetic position using small-subunit rRNA sequences. Can. J. Zool.* 74, 1898–1906. doi: 10.1139/z96-214

Kahl, A. (1931). Urtiere oder Protozoa I: wimpertiere oder Ciliata (Infusoria) 2. Holotricha. *Tierwelt Dtl.* 21, 181–398.

Kalyaanamoorthy, S., Minh, B. Q., Wong, T. K. F., von Haeseler, A., and Jermiin, L. S. (2017). ModelFinder: fast model selection for accurate phylogenetic estimates. *Nat. Methods* 14, 587–589. doi: 10.1038/nmeth.4285

Liu, M., Li, L., Zhang, T., Fan, X., Yi, Z., and Lin, X. (2020). Two new scuticociliates from southern China: Uronema apomarinum sp. nov. and Homalogastra parasetosa sp. nov., with improved diagnoses of the genus Homalogastra and its type species Homalogastra setosa (Ciliophora, Oligohymenophorea). *Int. J. Syst. Evol. Microbiol.* 70, 2405–2419. doi: 10.1099/ijsem.0.004046

Liu, W., Jiang, J., Xu, Y., Pan, X., Qu, Z., Luo, X., et al. (2017). Diversity of free-living marine ciliates (Alveolata, Ciliophora): faunal studies in coastal waters of China during the years 2011–2016. *Eur. J. Protistol.* 61, 424–438. doi: 10.1016/j.ejop.2017.04.007

Lynn, D. H. (2008). *The Ciliated Protozoa: Characterization, Classification, and Guide to the Literature. 3rd Edn*. Dordrecht: Springer.

Lynn, D. H., and Strüder-Kypke, M. (2005). Scuticociliate endosymbionts of echinoids (phylum Echinodermata): phylogenetic relationships among species in the genera *Entodiscus*, *Plagiopyliella*, *Thyrophylax*, and *Entorhipidium* (phylum Ciliophora). *J. Parasitol.* 91, 1190–1199. doi: 10.1645/GE-445R.1

Lynn, D. H., and Strüder-Kypke, M. C. (2006). Species of *Tetrahymena* identical by small subunit rRNA gene sequences are discriminated by mitochondrial cytochrome *c* oxidase I gene sequences. *J. Eukaryot. Microbiol.* 53, 385–387. doi: 10.1111/j.1550-7408.2006.00116.x

Ma, H., Song, W., Warren, A., Roberts, D., Gong, J., and Al-Rasheid, K. A. S. (2006). Redescription of the marine scuticociliate *Glauconema trihymene* Thompson, 1966 (Protozoa: Ciliophora): life cycle and stomatogenesis. *Zootaxa* 1296, 1–17. doi: 10.11646/zootaxa.1296.1.1

Medlin, L., Elwood, H. J., Stickel, S., and Sogin, M. L. (1988). The characterization of enzymatically amplified eukaryotic 16S-like rRNA-coding regions. *Gene* 71, 491–499. doi: 10.1016/0378-1119(88)90066-2

Minh, B. Q., Schmidt, H. A., Chernomor, O., Schrempf, D., Woodhams, M. D., von Haeseler, A., et al. (2020). IQ-TREE 2: new models and efficient methods for phylogenetic inference in the genomic era. *Mol. Biol. Evol.* 37, 1530–1534. doi: 10.1093/molbev/msaa015

Nylander, J. A. A. (2004). *MrModeltest*. Uppsala: Evolutionary Biology Centre, Uppsala University.

Pan, H., Hu, J., Jiang, J., Wang, L., and Hu, X. (2016). Morphology and phylogeny of three *Pleuronema* species (Ciliophora, Scuticociliatia) from Hangzhou Bay, China, with description of two new species, P. *binucleatum n. sp. and P. parawiackowskii n. sp. J. Eukaryot. Microbiol.* 63, 287–298. doi: 10.1111/jeu.12277

Pan, H., Huang, J., Hu, X., Fan, X., Al-Rasheid, K. A. S., and Song, W. (2010). Morphology and SSU rRNA gene sequences of three marine ciliates from Yellow Sea, China, including one new species, *Uronema heteromarinum* nov. spec. (Ciliophora, Scuticociliatida). *Acta Protozool.* 49, 45–59.

Pan, M., Chen, Y., Liang, C., and Pan, X. (2020). Taxonomy and molecular phylogeny of three freshwater scuticociliates, with descriptions of one new genus and two new species (Protista, Ciliophora, Oligohymenophorea). *Eur. J. Protistol.* 74:125644. doi: 10.1016/j.ejop.2019.125644

Pan, X., Bourland, W. A., and Song, W. (2013). Protargol synthesis: an in-house protocol. *J. Eukaryot. Microbiol.* 60, 609–614. doi: 10.1111/jeu.12067

Pan, X., Fan, X., Al-Farraj, S. A., Gao, S., and Chen, Y. (2016). Taxonomy and morphology of four "*ophrys*-related" scuticociliates (Protista, Ciliophora, Scuticociliatia), with the description of a new genus, *Paramesanophrys* gen. *nov. Eur. J. Taxon.* 2016, 1–18. doi: 10.5852/ejt.2016.191

Pan, X., Huang, J., Fan, X., Ma, H., Al-Rasheid, K. A. S., Miao, M., et al. (2015a). Morphology and phylogeny of four marine scuticociliates (Protista, Ciliophora), with descriptions of two new species: *Pleuronema elegans* spec. nov. and *Uronema orientalis* spec. nov. *Acta Protozool.* 54, 31–43.

Pan, X., Yi, Z., Li, J., Ma, H., Al-Farraj, S. A., and Al-Rasheid, K. A. S. (2015b). Biodiversity of marine scuticociliates (Protozoa, Ciliophora) from China: description of seven morphotypes including a new species, *Philaster sinensis* spec. *nov. Eur. J. Protistol.* 51, 142–157. doi: 10.1016/j.ejop.2015.02.005

Pérez-Uz, B., and Song, W. (1995). *Uronema gallicum* sp. n. (Protozoa: Ciliophora) a new marine scuticociliate from the coastal area of Calais. *Acta Protozool.* 34, 143–149.

Pomp, R., and Wilbert, N. (1988). Taxonomic and ecological studies of ciliates from Australian saline soils: colpodids and hymenostomate ciliates. *Mar. Freshw. Res.* 39, 479–495. doi: 10.1071/MF9880479

Qu, Z., Weinisch, L., Fan, X., Katzenmeier, S., Stoeck, T., and Filker, S. (2020). Morphological, phylogenetic and ecophysiological characterization of a new ciliate, *Platynematum rosellomorai* (Oligohymenophorea, Scuticociliatia), detected in a hypersaline pond on Mallorca, Spain. *Protist* 171:125751. doi: 10.1016/j.protis.2020.125751

Song, W. (2000). Morphological and taxonomical studies on some marine scuticociliates from China Sea, with description of two new species, *Philasterides armatalis* sp. n. and *Cyclidium varibonneti* sp. n. (Protozoa: Ciliophora: Scuticociliatida). *Acta Protozool.* 39, 295–322.

Song, W., Ma, H., Wang, M., and Zhu, M. (2002). Comparative studies on two closely related species *Uronemella filificum* (Kahl, 1931) and *Uronema elegans* Maupas, 1883 with redescription of *Paranophrys marina* Thompson et Berger, 1965 (Ciliophora: Scuticociliatida) from China seas. *Acta Protozool.* 41, 263–278.

Song, W., Warren, A., and Hu, X. (eds.) (2009). Free-living Ciliates in the Bohai and Yellow Seas, China. Beijing: Science Press.

Song, W., and Wilbert, N. (2000). Redefinition and redescription of some marine scuticociliates from China, with report of a new species, *Metanophrys sinensis* nov. spec. (Ciliophora, Scuticociliatida). *Zool. Anz.* 239, 45–74.

Stamatakis, A. (2014). RAxML version 8: a tool for phylogenetic analysis and post-analysis of large phylogenies. *Bioinformatics* 30, 1312–1313. doi: 10.1093/bioinformatics/btu033

Thompson, J. C. (1966). Glauconema trihymene n. *g., n. sp., a hymenostome ciliate from the Virginia coast. J. Protozool.* 13, 393–395. doi: 10.1111/j.1550-7408.1966.tb01927.x

Thompson, J. C. (1967). Parauronema virginianum n. *g., n. sp., a marine hymenostome ciliate. J. Protozool.* 14, 731–734. doi: 10.1111/j.1550-7408.1967.tb02069.x

Thompson, J. C., and Berger, J. (1965). Paranophrys marina n. *g., n. sp., a new ciliate associated with a hydroid from the northeast Pacific (Ciliata: Hymenostomatida). J. Protozool.* 12, 527–531. doi: 10.1111/j.1550-7408.1965.tb03252.x

Thompson, J. C., and Moewus, L. (1964). Miamiensis avidus n. *g., n. sp., a marine facultative parasite in the ciliate order Hymenostomatida. J. Protozool.* 11, 378–381. doi: 10.1111/j.1550-7408.1964.tb01766.x

Wang, C., Zhang, T., Wang, Y., Katz, L. A., Gao, F., and Song, W. (2017). Disentangling sources of variation in SSU rDNA sequences from single cell analyses of ciliates: impact of copy number variation and experimental error. *Proc. R. Soc. B Biol. Sci.* 284:20170425. doi: 10.1098/rspb.2017.0425

Wang, Y., Wang, C., Jiang, Y., Katz, L. A., Gao, F., and Yan, Y. (2019). Further analyses of variation of ribosome DNA copy number and polymorphism in ciliates provide insights relevant to studies of both molecular ecology and phylogeny. *Sci. China Life Sci.* 62, 203–214. doi: 10.1007/s11427-018-9422-5

Wilbert, N., and Kahan, D. (1981). Ciliates of Solar Lake on the Red Sea shore. *Arch. Protistenkd.* 124, 70–95. doi: 10.1016/S0003-9365(81)80004-8

Xu, K., and Song, W. (2000). Studies on pathogenetic ciliates from marine molluscs II. Philasterine ciliates (Protozoa, Ciliophora, Scuticociliatida). *J. Ocean Univ. Qingdao* 30, 224–229.

Zhang, T., Dong, J., Cheng, T., Duan, L., and Shao, C. (2020). Reconsideration of the taxonomy of the marine ciliate *Neobakuella aenigmatica* Moon et al., 2019 (Protozoa, Ciliophora, Hypotrichia). *Mar. Life Sci. Technol.* 2, 97–108. doi: 10.1007/s42995-020-00032-4

Zhang, T., Fan, X., Gao, F., Al-Farraj, S. A., El-Serehy, H. A., and Song, W. (2019). Further analyses on the phylogeny of the subclass Scuticociliatia (Protozoa, Ciliophora) based on both nuclear and mitochondrial data. *Mol. Phylogenet. Evol.* 139:106565. doi: 10.1016/j.ympev.2019.106565

Conflict of Interest: The authors declare that the research was conducted in the absence of any commercial or financial relationships that could be construed as a potential conflict of interest.

frontiers in Marine Science

ORIGINAL RESEARCH
published: 02 December 2020
doi: 10.3389/fmars.2020.602323

Single-Cell Genomic Sequencing of Three Peritrichs (Protista, Ciliophora) Reveals Less Biased Stop Codon Usage and More Prevalent Programmed Ribosomal Frameshifting Than in Other Ciliates

Xiao Chen[1†], Chundi Wang[1†], Bo Pan[2], Borong Lu[2], Chao Li[2], Zhuo Shen[3,4], Alan Warren[5] and Lifang Li[1]*

[1] Marine College, Shandong University, Weihai, China, [2] Institute of Evolution & Marine Biodiversity, Ocean University of China, Qingdao, China, [3] Institute of Microbial Ecology and Matter Cycle, School of Marine Sciences, Sun Yat-sen University, Zhuhai, China, [4] Southern Marine Science and Engineering Guangdong Laboratory (Zhuhai), Zhuhai, China, [5] Department of Life Sciences, Natural History Museum, London, United Kingdom

OPEN ACCESS

Edited by:
Zhijun Dong,
Yantai Institute of Coastal Zone Research, Chinese Academy of Sciences (CAS), China

Reviewed by:
Carolina Bastidas,
Massachusetts Institute of Technology, United States
Andreas Altenburger,
Arctic University of Norway, Norway

***Correspondence:**
Lifang Li
qd_liliy@sina.com

[†] These authors have contributed equally to this work

Specialty section:
This article was submitted to Marine Evolutionary Biology, Biogeography and Species Diversity, a section of the journal Frontiers in Marine Science

Received: 03 September 2020
Accepted: 04 November 2020
Published: 02 December 2020

Citation:
Chen X, Wang C, Pan B, Lu B, Li C, Shen Z, Warren A and Li L (2020) Single-Cell Genomic Sequencing of Three Peritrichs (Protista, Ciliophora) Reveals Less Biased Stop Codon Usage and More Prevalent Programmed Ribosomal Frameshifting Than in Other Ciliates. Front. Mar. Sci. 7:602323. doi: 10.3389/fmars.2020.602323

Peritrichs are one of the largest groups of ciliates with over 1,000 species described so far. However, their genomic features are largely unknown. By single-cell genomic sequencing, we acquired the genomic data of three sessilid peritrichs (*Cothurnia ceramicola*, *Vaginicola* sp., and *Zoothamnium* sp. 2). Using genomic data from another 53 ciliates including 14 peritrichs, we reconstructed their evolutionary relationships and confirmed genome skimming as an efficient approach for expanding sampling. In addition, we profiled the stop codon usage and programmed ribosomal frameshifting (PRF) events in peritrichs for the first time. Our analysis reveals no evidence of stop codon reassignment for peritrichs, but they have prevalent +1 or -1 PRF events. These genomic features are distinguishable from other ciliates, and our observations suggest a unique evolutionary strategy for peritrichs.

Keywords: ***Cothurnia*, evolution, phylogenomics, *Vaginicola*, *Zoothamnium***

INTRODUCTION

Peritrich ciliates have ubiquitous distribution and occupy a broad array of freshwater, brackish water, marine, and terrestrial ecosystems (Lynn, 2008; Zhuang et al., 2016; Lu et al., 2019, 2020). They are also one of the largest groups within the phylum Ciliophora Doflein, 1901 with over 1,000 nominal species. Historically, the subclass Peritrichia Stein, 1859 was considered to be a well-defined, monophyletic group comprising two orders, the Sessilida Stein, 1859, and the Mobilida Kahl, 1933 (Corliss, 1979; Lynn and Small, 2002; **Figure 1**). In recent years, however, the monophyly of the subclass Peritrichia has been questioned due to discordance between the molecular and morphological evidence (Miao et al., 2001; Utz and Eizirik, 2007; Williams and Clamp, 2007; Zhan et al., 2009; Sun et al., 2013). In particular, analyses based on sequences of ribosomal DNA (rDNA; 18S, 5.8S, and 28S) and alpha-tubulin, either individually or in combination, show that the order Sessilida clusters with the subclass Hymenostomatia rather than with the order Mobilida, rendering

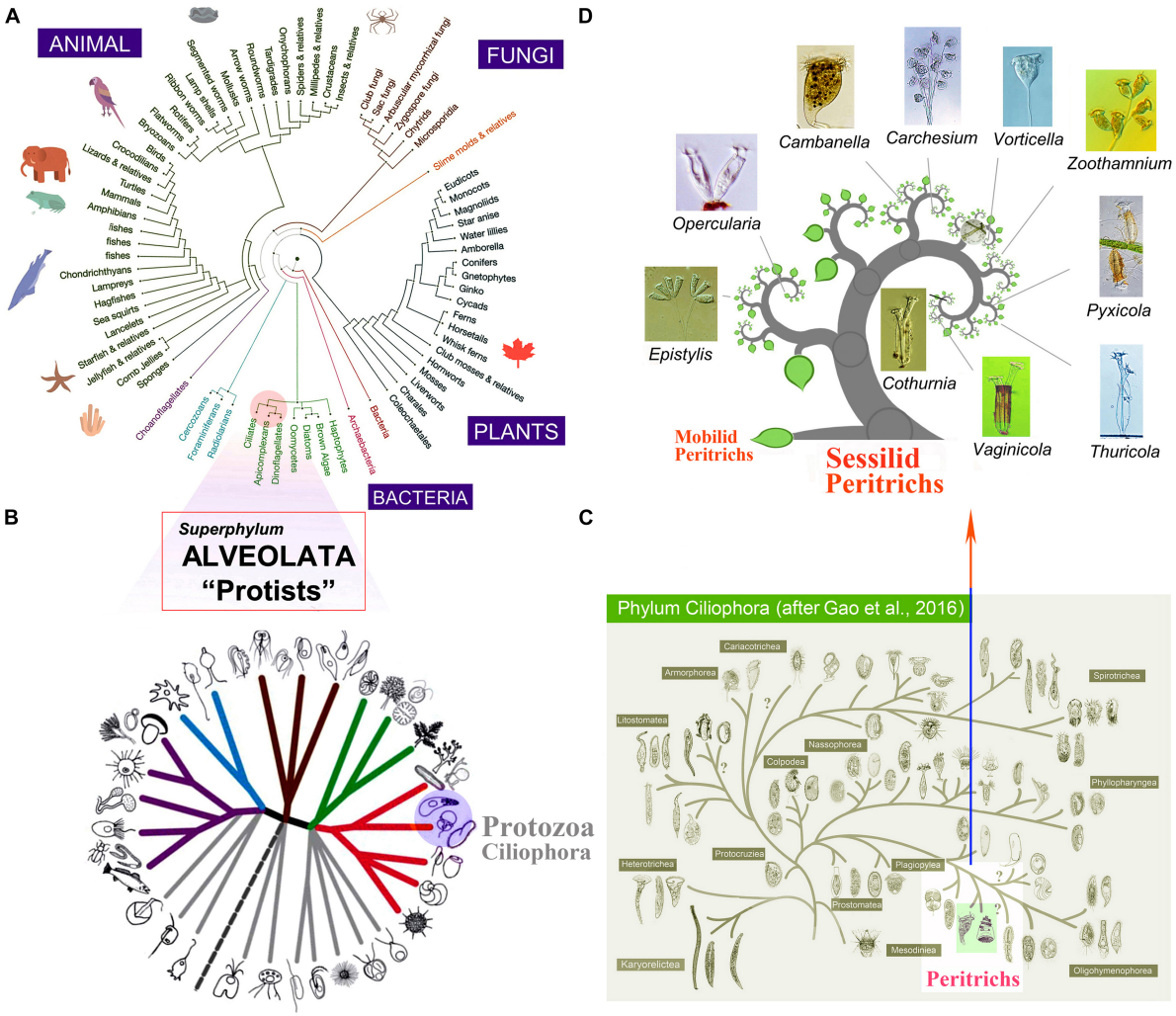

FIGURE 1 | Systematic arrangement of peritrichs in the evolutionary history and current taxonomy of phylum Ciliophora. **(A)** Tree of life, adapted from Pennisi (2003). **(B)** Classification of eukaryotes, adapted from Adl et al. (2019). **(C)** Classification of ciliates, adapted from Gao et al. (2016). **(D)** The phylogeny of peritrichs based on 18S rDNA gene sequences, generated by OneZoom (Rosindell and Harmon, 2012).

the subclass Peritrichia non-monophyletic (Utz and Eizirik, 2007; Zhan et al., 2009; Gao et al., 2016). Following the development of next-generation sequencing techniques, two studies using phylogenomic analysis of sequences from more than 100 genomic loci concluded that the orders Sessilida and Mobilida are sister groups, and the subclass Peritrichia is monophyletic (Gentekaki et al., 2017; Jiang et al., 2019). However, genomic data are available for only about 2% of known peritrich species and are lacking for several families (Jiang et al., 2019), so it is probably too early to draw solid conclusions on high-level peritrich systematics based on phylogenomic analyses.

Previous studies have reported the large flexibility of the nuclear genetic code in ciliates by demonstrating that standard stop codons are reassigned to amino acids (Lozupone et al., 2001; Swart et al., 2016). To address the question of how ambiguous genetic codes enabled species to thrive during their evolutionary history, evolutionary biologists have intensively investigated stop codon preference in both bacteria and eukaryotes (Alff-Steinberger and Epstein, 1994; Belinky et al., 2018). The stop codon reassignment in euplotid ciliates has also been linked to programmed ribosomal frameshifting (PRF) events (Wang et al., 2016; Lobanov et al., 2017; Chen et al., 2019). For peritrichs, such genomic features are still far from clear since many are not culturable and thus cannot satisfy the requirement of sufficient amounts of DNA for whole-genome sequencing.

To access the genomic profiles of unexplored peritrich lineages, we applied the single-cell genomic sequencing technique to three sessilid peritrichs, i.e., the marine species *Cothurnia ceramicola* and *Zoothamnium* sp. 2 and a freshwater species of *Vaginicola*. Based on genomic data of peritrichs and other ciliates, both from the current work and previous studies, we systematically reconstructed their phylogenomic relationships and, for the first time, profiled the stop codon usage and PRF events in peritrich genomes. Understanding the genomic features

of peritrichs may help uncover their evolutionary history and could improve our understanding of their unique advantages for environmental adaptation.

MATERIALS AND METHODS

Single-Cell Sample Preparation

Cothurnia ceramicola and *Zoothamnium* sp. 2 were collected from seawater along the coast of the Yellow Sea at Qingdao (35°56′18″ N, 120°12′44″ E and 36°03′03″ N, 120°21′01″ E, respectively), China. *Vaginicola* sp. was collected from a freshwater pond in Baihuayuan Park at Qingdao (36°03′58″ N, 120°20′24″ E), China. Ciliates were detached from their substrate (aquatic plants) using a glass micropipette under a stereomicroscope (40×). Specimens were observed *in vivo* with differential interference contrast microscopy (40× to 1,000×) and following silver staining, i.e., protargol staining to reveal their infraciliature and wet silver nitrate staining to reveal their silverline system (Song and Wilbert, 1995). They were identified based on morphological characteristics, such as body size, contractile vacuole, spasmoneme, lorica, branching pattern of the stalk patterns of infracilature, and numbers of silverlines using published keys and guides (Song et al., 2009; Lu et al., 2019). *C. ceramicola* is characterized by its cylindroid-shaped and annulated lorica, with a striated stalk, one-fourth to one-third of the body projecting outside the lorica, and marine habitat. *Zoothamnium* sp. 2 has the typical characters of its genus, i.e., colonial, with a continuous spasmoneme that runs throughout the entire colony causing the stalk to contract in a "zig-zag" fashion, and with transverse silverlines. *Vaginicola* sp. has a lorica that adheres directly to the substrate by the posterior end without a stalk. A single cell of each species was washed in phosphate-buffered saline (PBS) buffer (without Mg^{2+} or Ca^{2+}), and genomic DNA amplification was carried out by MALBAC (Lu et al., 2012) using the Single-Cell WGA Kit (Yikon, YK001A) according to the manufacturer's guidelines.

Illumina Sequencing and Genome Assembly

Illumina libraries were prepared from amplified single-cell genomic DNA according to manufacturer's instructions and paired-end sequencing (150 bp read length) was performed using an Illumina HiSeq4000 sequencer. The sequencing adapter was trimmed, and low-quality reads (reads containing more than 10% Ns or 50% bases with Q value < 5) were filtered out. The single-cell genome of each species was assembled using SPAdes v3.7.1 (-k 21,33,55,77; Bankevich et al., 2012; Nurk et al., 2013). *Oxytricha trifallax* mitochondrial genomic peptides and bacterial genomes were downloaded from GenBank as BLAST databases to remove contamination caused by mitochondria or bacteria (BLAST E < 1.0e-5). CD-HIT v4.6.1 (CD-HIT-EST, -c 0.98 -n 8 -r 1) was employed to eliminate the redundancy of contigs (with sequence identity threshold = 98%; Fu et al., 2012). Poorly supported contigs (coverage < 1 or >20 and length < 400 bp) were discarded, considering the inherent characteristics of single-cell genomic sequencing technique (Zong et al., 2012).

Ortholog Detection and Phylogenomic Analysis

Genome-wide gene predictions were performed using AUGUSTUS v3.2.2 (—species = peritrichia, trained by transcriptomic data of the sessilid *Vorticella microstoma*; Stanke et al., 2006). Orthologs were detected from the top hits of homolog sequence alignment between predicted protein sequences and the ciliate protein library from National Center for Biotechnology Information (NCBI) GenBank using BLASTP version 2.3.0 (E value < 1e-5; Camacho et al., 2009). The orthologs detected from predicted protein sequences were aligned with 157 well-defined ciliate proteins from another 53 ciliates and from 13 apicomplexans/dinoflagellates that were used as outgroups taxa. Phylogenomic analysis was carried out using GPSit (relaxed masking mode, **Supplementary Table 1** and **Supplementary Figure 1**; Chen et al., 2018). The gene recovery rate (GRR) of a taxon was equivalent to its coverage of a total of 157 multiple sequence alignments (MSAs) and calculated as previously described (Chen et al., 2018). The concatenated dataset output from GPSit was used for phylogenomic analysis on CIPRES Science Gateway server v3.3 (phylo.org; Miller et al., 2010). RAxML-HPC2 v8.2.9 under LG model of amino acid substitution (Γ distribution + F, four rate categories, 500 bootstrap replicates) was used to perform maximum likelihood (ML) analysis (Stamatakis, 2014). PhyloBayes MPI 1.5a (CAT-GTR model + Γ distribution, four independent chains, 10,000 generations with 10% burn-in, convergence Maxdiff < 0.3) was used to perform Bayesian inference (BI) analysis (Lartillot et al., 2009). The phylogenetic tree was visualized using MEGA v7.0.20 (Kumar et al., 2016).

Stop Codon Usage and PRF Events Detection

Usage of the stop codons (TAA, TGA, and TAG) was measured from the homolog sequence alignment between the predicted gene sequences, or transcripts from each species and the ciliate protein library, using BLASTX version 2.3.0 (E value cutoff = 1e-5) and a Perl script (Camacho et al., 2009; Chen et al., 2019). Stop codon usage bias was examined by the chi-squared test. PRF events were detected from the homolog sequence alignment using the R package FScanR[1]. To identify high-confidence PRF events and avoid false-positive frameshifting introduced by introns, the fidelity of homolog sequence alignments and the distance between two hits with changed frames were strictly controlled with rigorous cutoffs (evalue_cutoff = 1e-10, frameDist_cutoff = 10 nt).

RESULTS AND DISCUSSION

Genomic Profiles of Peritrichs by Single-Cell Sequencing

We collected the genomic data from single cells and assembled the genomes for three peritrich species, *C. ceramicola*,

[1]github.com/seanchen607/FScanR

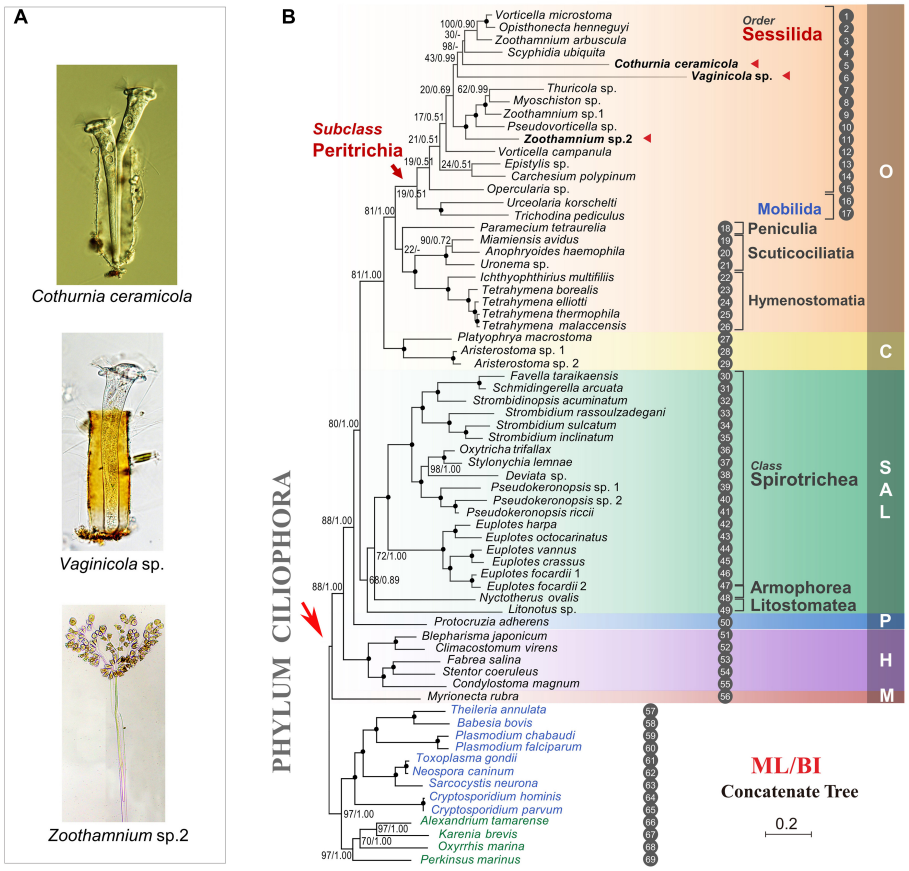

FIGURE 2 | Phylogenomic analysis based on genome-wide homolog protein sequences. **(A)** Photomicrographs of *Cothurnia ceramicola*, *Vaginicola* sp., and *Zoothamnium* sp. 2 **(B)** Phylogenomic trees estimated from a 157-gene concatenated dataset by maximum likelihood (ML) and Bayesian inference (BI). Black dots denote full support (ML 100%/BI 1.0). Hyphens denote topological disagreement between BI and ML analyses. The three sessilid peritrichs sequenced in the current work are in bold and are marked by red triangles. The outgroup taxa, nine apicomplexans, and four dinoflagellates, are in blue and green, respectively. SAL, classes Spirotrichea, Armophorea, and Litostomatea; O, class Oligohymenophorea; C, class Colpodea; P, class Protocruziea; H, class Heterotrichea; and M, class Mesodiniea. Scale bar corresponds to 20 substitutions per 100 nucleotide positions. The numbers in the circles adjacent to species names correspond to those in **Supplementary Table 1** and **Supplementary Figure 1**.

Vaginicola sp., and *Zoothamnium* sp. 2 (**Figure 2A**). The mean size of genome assemblies is 104 Mb (**Table 1**). The large contig numbers (94,558 on average) and small N50 (1,539 on average) indicate that the genome assembly is not integral, probably due to the bias of whole-genome amplification, which is a necessary procedure during the library preparation in single-cell genomic sequencing (Lu et al., 2012). However, genome skimming is a suitable technique for generating data that can be used in several downstream analyses such as ortholog detection and phylogenetic analyses.

After gene annotation and ortholog detection, the GRR, which is equivalent to the coverage of 157 common orthologous genes in each ciliate taxon (Gentekaki et al., 2014; Chen et al., 2018), is 50.3% for *C. ceramicola*, 32.5% for *Vaginicola* sp., and 51.0% for *Zoothamnium* sp. 2. These values are comparable to those for other ciliates from public datasets (**Table 1** and **Supplementary Table 1**). Although the coverage of gene sequences in these datasets is not as high as the bulk genomic or transcriptomic sequencing, single-cell whole-genome sequencing provides the opportunity to expand the phylogenetic

TABLE 1 | Information of single-cell genome assemblies.

	Cothurnia ceramicola	*Vaginicola* sp.	*Zoothamnium* sp. 2
Genome size (Mb)	67.9	227.8	46.3
%GC	42.9	49.5	38.6
# Contig	93,298	153,423	36,954
Contig N50	726	2,075	1,815
Coverage	7.233	4.979	5.110
Predicted genes	75,338	145,990	31,853
Predicted CDSs	93,734	228,202	43,704
Predicted proteins	62,343	135,663	27,174
GRR*	79/157 (50.3%)	51/157 (32.5%)	80/157 (51.0%)

*CDS, coding sequence. *Gene recovery rate (GRR) of a taxon was equivalent to its coverage of 157 multiple sequence alignments (MSAs).*

scope to more peritrich lineages and to those species that are non-culturable.

Expanded Sampling by Single-Cell Sequencing Partially Supports the Monophyly of the Subclass Peritrichia

With expanded sampling and new single-cell genomic sequencing profiles from three sessilid peritrichs, we reconstructed their phylogenomic relationships using both ML and Bayesian inference (BI) methods (**Figure 2B**). The reconstructed phylogenomic trees show that the three species cluster with the 14 other peritrich species from previous studies using bulk genome/transcriptome sequencing. Furthermore, *Zoothamnium* species do not cluster together (see *Zoothamnium* sp. 1 and *Z.* sp. 2 in **Figure 2B**), as reported in previous studies based on either genomic-scale data or single locus sequences (Li et al., 2008; Zhuang et al., 2018; Jiang et al., 2019; Wu et al., 2020). These findings suggest that genome skimming from single cells is an efficient approach for expanding the sampling of genomic data to more ciliate species and resolving their phylogenomic positions. Our analysis supports the monophyly of the subclass Peritrichia, although the support values are low (ML, 19%; BI, 0.51). However, the application of genome skimming from single cells should enable more peritrich lineages to be included in future investigations, thereby facilitating more reliable conclusions to be drawn concerning the systematics of the Peritrichia.

Stop Codons Are Not Reassigned in Peritrichs

A recent study profiling stop codon usage in 33 ciliates across nine classes revealed that all 33 show stop codon reassignment (Pan et al., 2019). Most (30 out of 33) of the species investigated use either TAA or TGA as the biased stop codon and reassign the other two stop codons to code amino acids. In each of the five species representing the class Oligohymenophorea, TAA and TAG were reassigned to code the amino acid glutamine leaving TGA as the only stop codon. In the current study, we depict the stop codon usage in peritrichs for the first time (**Figure 3**). In contrast to other oligohymenophorean species, 10 out of 12 peritrichs show no sign of significant bias in stop codon usage, which suggests a unique evolutionary strategy of peritrichs.

Previous studies in bacteria show that three stop codons are decoded by two release factors (RF1 for UAA and UAG and RF2 for UAA and UGA) and that UGA is used much more frequently than UAG in *Escherichia coli*, as RF2 is consistently more abundant than RF1 (Scolnick et al., 1968; Milman et al., 1969; Scolnick and Caskey, 1969; Korkmaz et al., 2014). This association between the frequency of a stop codon and its decoder concentration has also been documented in eukaryotes

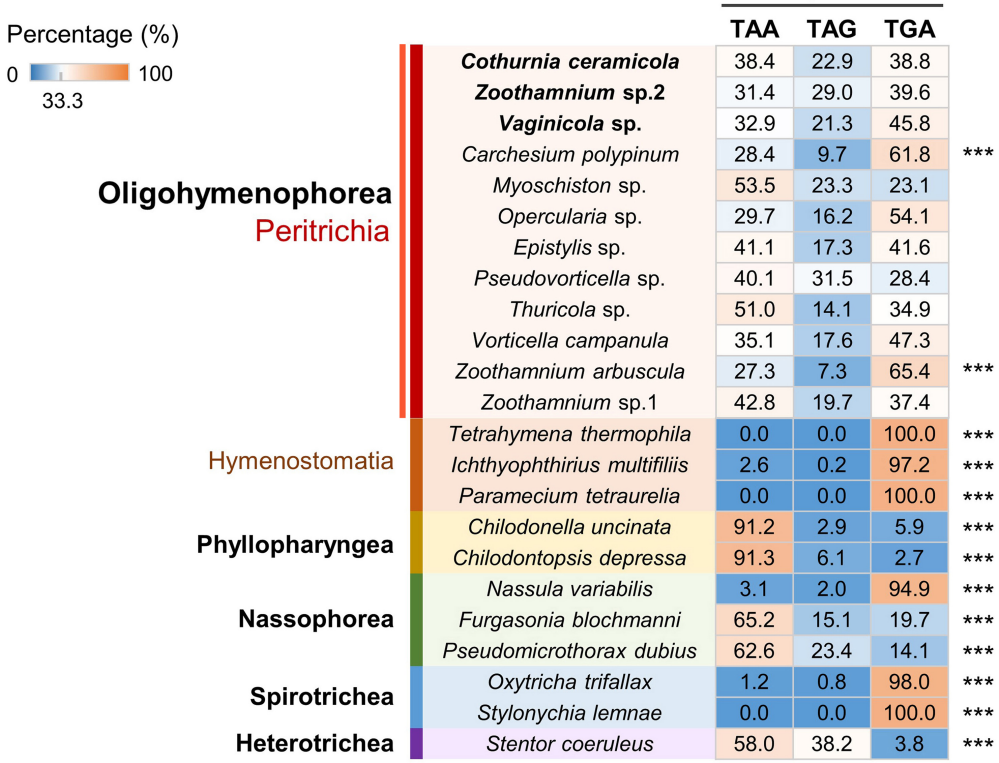

FIGURE 3 | Stop codon usage analysis shows most peritrichs have no significant bias in the usage frequency of three stop codons in their genomes. The color scale denotes the percentage of the usage frequency for each stop codon in each species. ***Significant biased stop codon usage ($p < 0.001$; Fisher's exact test).

(Chavancy et al., 1979). Although a recent study suggests that GC content has a major impact on stop codon frequencies (Belinky et al., 2018), the translation termination mechanism in ciliates remains poorly understood and should be addressed in future studies.

+1 and −1 PRF Events Are Prevalent in Peritrichs

Based on the available ciliate genomic or transcriptomic data, we systematically investigated PRF events in ciliates (**Figure 4**). As the shortest spliceosomal introns currently known are reported in *Stentor* (15–16 nt; Slabodnick et al., 2017), unrecognized tiny introns may cause false-positive PRF events in those species for which transcriptomic data are lacking. To avoid this potential issue and identify high-confidence PRF events from genomic data, we searched for the adjacent homolog sequence alignment between ciliate genomic DNA and ciliate protein sequences with frames changed within a narrow window of 10 nt. PRF events (14 on average) were detected in 93% (42 out of 45) of the species examined. Furthermore, we identified a large number of +1 PRF events (34 on average) in all five species of *Euplotes* included in the analysis. This is consistent with previous studies that indicated that +1 PRF events are highly abundant in *Euplotes* (Wang et al., 2016; Chen et al., 2019). The present study revealed that, of 12 the peritrich species included in the analysis, 11 have prevalent +1 and -1 PRF events (12 and four events on average, respectively) in their genomes, which is not common to many ciliate groups. Our systematic investigation also revealed abundant +1 PRF and -1 PRF events in the genomes of *Paramecium tetraurelia* (58 events) and *Ichthyophthirius multifiliis* (37 events), respectively. The two representatives of the class Colpodea included in this study showed an intermediate frequency of PRF events of all

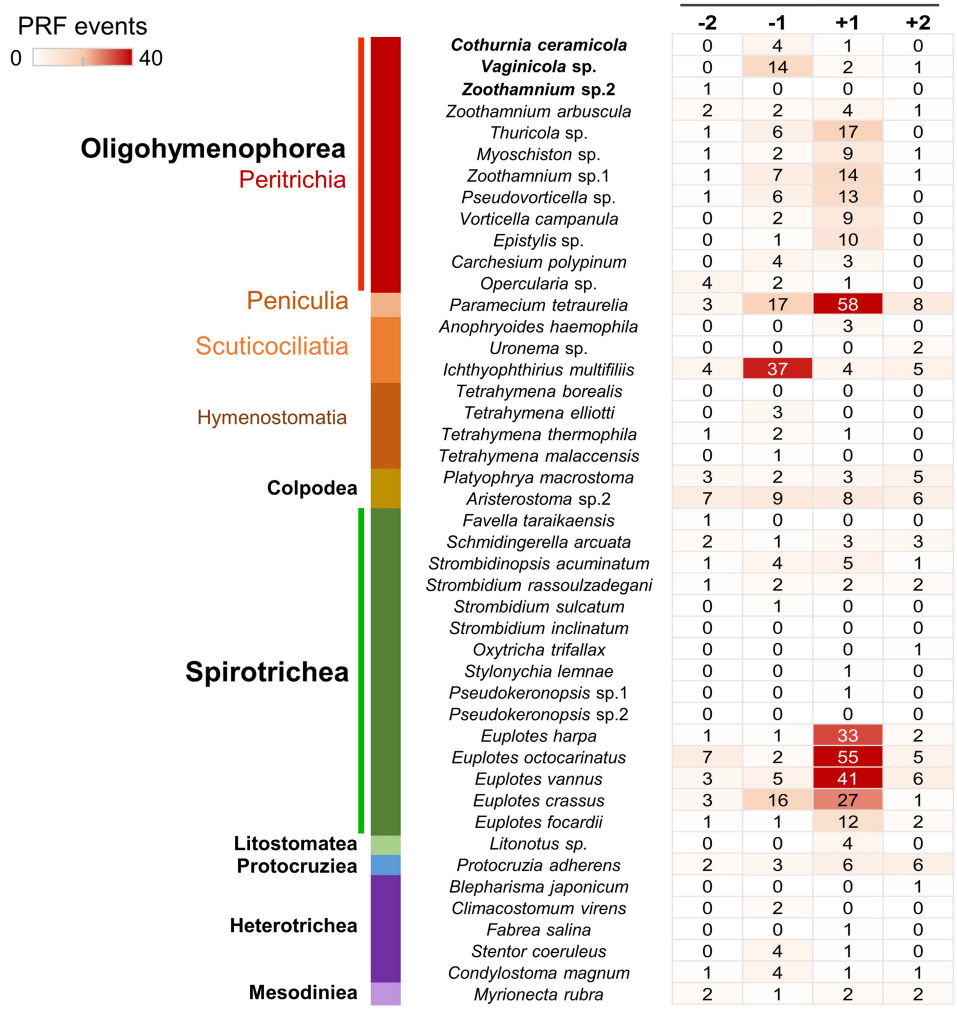

	PRF types			
	-2	-1	+1	+2
Cothurnia ceramicola	0	4	1	0
***Vaginicola* sp.**	0	14	2	1
***Zoothamnium* sp.2**	1	0	0	0
Zoothamnium arbuscula	2	2	4	1
Thuricola sp.	1	6	17	0
Myoschiston sp.	1	2	9	1
Zoothamnium sp.1	1	7	14	1
Pseudovorticella sp.	1	6	13	0
Vorticella campanula	0	2	9	0
Epistylis sp.	0	1	10	0
Carchesium polypinum	0	4	3	0
Opercularia sp.	4	2	1	0
Paramecium tetraurelia	3	17	58	8
Anophryoides haemophila	0	0	3	0
Uronema sp.	0	0	0	2
Ichthyophthirius multifiliis	4	37	4	5
Tetrahymena borealis	0	0	0	0
Tetrahymena elliotti	0	3	0	0
Tetrahymena thermophila	1	2	1	0
Tetrahymena malaccensis	0	1	0	0
Platyophrya macrostoma	3	2	3	5
Aristerostoma sp.2	7	9	8	6
Favella taraikaensis	1	0	0	0
Schmidingerella arcuata	2	1	3	3
Strombidinopsis acuminatum	1	4	5	1
Strombidium rassoulzadegani	1	2	2	2
Strombidium sulcatum	0	1	0	0
Strombidium inclinatum	0	0	0	0
Oxytricha trifallax	0	0	0	1
Stylonychia lemnae	0	0	1	0
Pseudokeronopsis sp.1	0	0	1	0
Pseudokeronopsis sp.2	0	0	0	0
Euplotes harpa	1	1	33	2
Euplotes octocarinatus	7	2	55	5
Euplotes vannus	3	5	41	6
Euplotes crassus	3	16	27	1
Euplotes focardii	1	1	12	2
Litonotus sp.	0	0	4	0
Protocruzia adherens	2	3	6	6
Blepharisma japonicum	0	0	0	1
Climacostomum virens	0	2	0	0
Fabrea salina	0	0	1	0
Stentor coeruleus	0	4	1	0
Condylostoma magnum	1	4	1	1
Myrionecta rubra	2	1	2	2

FIGURE 4 | Systematic investigation of programmed ribosomal frameshifting (PRF) events in ciliate genomes reveals that +1 and -1 PRF events are prevalent in peritrichs. The color scale denotes the number of four types of PRF events in each species. The class names are labeled in bold, and the subclass names are labeled in color.

four types (−2, −1, +1, +2) without an obvious bias toward any one in particular. These observations may help us understand their evolutionary history but need further validation by expanded sampling of more species.

CONCLUDING REMARKS

In the current work, we applied single-cell genomic sequencing to representatives of three well-known sessilid peritrich genera. The results of our phylogenomic analysis partially supports the monophyly of the subclass Peritrichia. We also systematically investigated the stop codon reassignment and PRF events in peritrichs and other ciliates. Our findings reveal that peritrichs have less biased stop codon usage and more prevalent +1 and -1 PRF than other ciliates. Together, these findings suggest that peritrichs have a unique evolutionary strategy among ciliates.

DATA AVAILABILITY STATEMENT

All Illumina sequencing data are deposited in the NCBI Short Read Archive (SRA), under the BioProject PRJNA609448.

AUTHOR CONTRIBUTIONS

XC performed the conceptualization (lead), data curation (lead), formal analysis (lead), investigation (lead), methodology (lead), resources (equal), software (lead), and validation (equal), visualization (lead), and wrote the original draft (lead). CW, BP, BL, and CL performed the data curation (equal), formal analysis (supporting), investigation (equal), and validation (supporting). ZS and AW reviewed and edited the manuscript (equal). LL performed funding acquisition (lead), project administration (lead), resources (equal), and supervision (lead), and reviewed and edited the manuscript (lead). All authors contributed to the article and approved the submitted version.

FUNDING

This work was supported by the National Natural Science Foundation of China (project numbers 31772431, 31801984, 31970486, and 32030015).

ACKNOWLEDGMENTS

The authors would like to thank Dr. Weibo Song (Ocean University of China, China) for his advice during the preparation of the manuscript and Dr. Chao Lu (Columbia University Medical Center, United States) for institutional support.

SUPPLEMENTARY MATERIAL

The Supplementary Material for this article can be found online at: https://www.frontiersin.org/articles/10.3389/fmars.2020.602323/full#supplementary-material

Supplementary Figure 1 | The matrix of updated multiple sequence alignments showing the presence of 157 homologous genes in each species. The numbering of species corresponds to that in **Supplementary Table 1**.

Supplementary Table 1 | The data sets analyzed in the current work, including the information on taxonomy, numbers of homologous genes and genomic data source.

REFERENCES

Adl, S. M., Bass, D., Lane, C. E., Lukeš, J., Schoch, C. L., Smirnov, A., et al. (2019). Revisions to the classification, nomenclature, and diversity of eukaryotes. *J. Eukaryot. Microbiol.* 66, 4–119. doi: 10.1111/jeu.12691

Alff-Steinberger, C., and Epstein, R. (1994). Codon preference in the terminal region of *E. coli* genes and evolution of stop codon usage. *J. Theor. Biol.* 168, 461–463. doi: 10.1006/jtbi.1994.1124

Bankevich, A., Nurk, S., Antipov, D., Gurevich, A. A., Dvorkin, M., Kulikov, A. S., et al. (2012). SPAdes: a new genome assembly algorithm and its applications to single-cell sequencing. *J. Comput. Biol.* 19, 455–477. doi: 10.1089/cmb.2012.0021

Belinky, F., Babenko, V. N., Rogozin, I. B., and Koonin, E. V. (2018). Purifying and positive selection in the evolution of stop codons. *Sci. Rep.* 8, 1–11. doi: 10.1038/s41598-018-27570-3

Camacho, C., Coulouris, G., Avagyan, V., Ma, N., Papadopoulos, J., Bealer, K., et al. (2009). BLAST+: architecture and applications. *BMC Bioinformatics* 10:421. doi: 10.1186/1471-2105-10-421

Chavancy, G., Chevallier, A., Fournier, A., and Garel, J.-P. (1979). Adaptation of iso-tRNA concentration to mRNA codon frequency in the eukaryote cell. *Biochimie* 61, 71–78. doi: 10.1016/S0300-9084(79)80314-4

Chen, X., Jiang, Y., Gao, F., Zheng, W., Krock, T. J., Stover, N. A., et al. (2019). Genome analyses of the new model protist *Euplotes vannus* focusing on genome rearrangement and resistance to environmental stressors. *Mol. Ecol. Res.* 19, 1292–1308. doi: 10.1111/1755-0998.13023

Chen, X., Wang, Y., Sheng, Y., Warren, A., and Gao, S. (2018). GPS it: an automated method for evolutionary analysis of nonculturable ciliated microeukaryotes. *Mol. Ecol. Res.* 18, 700–713. doi: 10.1111/1755-0998.12750

Corliss, J. O. (1979). *The Ciliated Protozoa: Characterization, Classification and Guide to the Literature*. Oxford: Pergamon Press.

Fu, L., Niu, B., Zhu, Z., Wu, S., and Li, W. (2012). CD-HIT: accelerated for clustering the next-generation sequencing data. *Bioinformatics* 28, 3150–3152. doi: 10.1093/bioinformatics/bts565

Gao, F., Warren, A., Zhang, Q., Gong, J., Miao, M., Sun, P., et al. (2016). The all-data-based evolutionary hypothesis of ciliated protists with a revised classification of the phylum Ciliophora (Eukaryota, Alveolata). *Sci. Rep.* 6:24874. doi: 10.1038/srep24874

Gentekaki, E., Kolisko, M., Boscaro, V., Bright, K., Dini, F., Di Giuseppe, G., et al. (2014). Large-scale phylogenomic analysis reveals the phylogenetic position of the problematic taxon *Protocruzia* and unravels the deep phylogenetic affinities of the ciliate lineages. *Mol. Phylogenet. Evol.* 78, 36–42. doi: 10.1016/j.ympev.2014.04.020

Gentekaki, E., Kolisko, M., Gong, Y., and Lynn, D. (2017). Phylogenomics solves a long-standing evolutionary puzzle in the ciliate world: the subclass Peritrichia is monophyletic. *Mol. Phylogenet. Evol.* 106, 1–5. doi: 10.1016/j.ympev.2016.09.016

Jiang, C., Wang, G., Xiong, J., Yang, W., Sun, Z., Feng, J., et al. (2019). Insights into the origin and evolution of Peritrichia (Oligohymenophorea, Ciliophora) based on analyses of morphology and phylogenomics. *Mol. Phylogenet. Evol.* 132, 25–35. doi: 10.1016/j.ympev.2018.11.018

Korkmaz, G., Holm, M., Wiens, T., and Sanyal, S. (2014). Comprehensive analysis of stop codon usage in bacteria and its correlation with release factor abundance. *J. Biol. Chem.* 289, 30334–30342. doi: 10.1074/jbc.M114.606632

Kumar, S., Stecher, G., and Tamura, K. (2016). MEGA7: molecular evolutionary genetics analysis version 7.0 *for bigger datasets*. *Mol. Biol. Evol.* 33, 1870–1874. doi: 10.1093/molbev/msw054

Lartillot, N., Lepage, T., and Blanquart, S. (2009). PhyloBayes 3: a Bayesian software package for phylogenetic reconstruction and molecular dating. *Bioinformatics* 25, 2286–2288. doi: 10.1093/bioinformatics/btp368

Li, L., Song, W., Warren, A., Shin, M. K., Chen, Z., Ji, D., et al. (2008). Reconsideration of the phylogenetic positions of five peritrich genera, *Vorticella, Pseudovorticella, Zoothamnopsis, Zoothamnium*, and *Epicarchesium* (Ciliophora, Peritrichia, Sessilida), based on small subunit rRNA gene sequences. *J. Eukaryot. Microbiol.* 55, 448–456. doi: 10.1111/j.1550-7408.2008.00351.x

Lobanov, A. V., Heaphy, S. M., Turanov, A. A., Gerashchenko, M. V., Pucciarelli, S., Devaraj, R. R., et al. (2017). Position-dependent termination and widespread obligatory frameshifting in *Euplotes* translation. *Nat. Struct. Mol. Biol.* 24:61. doi: 10.1038/nsmb.3330

Lozupone, C. A., Knight, R. D., and Landweber, L. F. (2001). The molecular basis of nuclear genetic code change in ciliates. *Curr. Biol.* 11, 65–74. doi: 10.1016/S0960-9822(01)00028-8

Lu, B., Li, L., Hu, X., Ji, D., Al-Rasheid, K. A., and Song, W. (2019). Novel contributions to the peritrich family Vaginicolidae (Protista: Ciliophora), with morphological and phylogenetic analyses of poorly known species of *Pyxicola, Cothurnia* and *Vaginicola*. *Zool. J. Linn. Soc.* 187, 1–30. doi: 10.1093/zoolinnean/zlz009

Lu, B., Shen, Z., Zhang, Q., Hu, X., Warren, A., and Song, W. (2020). Morphology and molecular analyses of four epibiotic peritrichs on crustacean and polychaete hosts, including descriptions of two new species (Ciliophora, Peritrichia). *Eur. J. Protistol.* 73:125670. doi: 10.1016/j.ejop.2019.125670

Lu, S., Zong, C., Fan, W., Yang, M., Li, J., Chapman, A. R., et al. (2012). Probing meiotic recombination and aneuploidy of single sperm cells by whole-genome sequencing. *Science* 338, 1627–1630. doi: 10.1126/science.1229112

Lynn, D. (2008). *The Ciliated Protozoa: Characterization, Classification, and Guide to the Literature*. Berlin: Springer Science & Business Media.

Lynn, D. H., and Small, E. B. (2002). *An Illustrated Guide to the Protozoa*. Kansas: Allen Press Inc.

Miao, W., Yu, Y., and Shen, Y. (2001). Phylogenetic relationships of the subclass Peritrichia (Oligohymenophorea, Ciliophora) with emphasis on the genus *Epistylis*, inferred from small subunit rRNA gene sequences. *J. Eukaryot. Microbiol.* 48, 583–587. doi: 10.1111/j.1550-7408.2001.tb00194.x

Miller, M. A., Pfeiffer, W., and Schwartz, T. (2010). Creating the CIPRES science gateway for inference of large phylogenetic trees. *Gateway Comput. Environ. Workshop (GCE)* 1, 1–8. doi: 10.1109/GCE.2010.5676129

Milman, G., Goldstein, J., Scolnick, E., and Caskey, T. (1969). Peptide chain termination, III. *Stimulation of in vitro termination*. *Proc. Natl. Acad. Sci. U.S.A.* 63, 183–190. doi: 10.1073/pnas.63.1.183

Nurk, S., Bankevich, A., Antipov, D., Gurevich, A. A., Korobeynikov, A., Lapidus, A., et al. (2013). Assembling single-cell genomes and mini-metagenomes from chimeric MDA products. *J. Comput. Biol.* 20, 714–737. doi: 10.1089/cmb.2013.0084

Pan, B., Chen, X., Hou, L., Zhang, Q., Qu, Z., Warren, A., et al. (2019). Comparative genomics analysis of ciliates provides insights on the evolutionary history within "Nassophorea–Synhymenia–Phyllopharyngea" assemblage. *Front. Microbiol.* 10:2819. doi: 10.3389/fmicb.2019.02819

Pennisi, E. (2003). Modernizing the tree of life. *Science* 300, 1692–1697. doi: 10.1126/science.300.5626.1692

Rosindell, J., and Harmon, L. J. (2012). OneZoom: a fractal explorer for the tree of life. *PLoS Biol.* 10:e1001406. doi: 10.1371/journal.pbio.1001406

Scolnick, E., and Caskey, C. (1969). Peptide chain termination, V. *The role of release factors in mRNA terminator codon recognition*. *Proc. Natl. Acad. Sci. U.S.A.* 64, 1235–1241. doi: 10.1073/pnas.64.4.1235

Scolnick, E., Tompkins, R., Caskey, T., and Nirenberg, M. (1968). Release factors differing in specificity for terminator codons. *Proc. Natl. Acad. Sci. U.S.A.* 61:768. doi: 10.1073/pnas.61.2.768

Slabodnick, M. M., Ruby, J. G., Reiff, S. B., Swart, E. C., Gosai, S., Prabakaran, S., et al. (2017). The macronuclear genome of *Stentor coeruleus* reveals tiny introns in a giant cell. *Curr. Biol.* 27, 569–575. doi: 10.1016/j.cub.2016.12.057

Song, W., Warren, A., and Hu, X. (2009). *Free-living Ciliates in the Bohai and Yellow Seas*. Beijing: Science Press.

Song, W., and Wilbert, N. (1995). "Benthische ciliaten des Süßwassers," in *Praktikum der Protozoologie*, ed. R. Röttger (Stuttgart: Gustav Fischer Verlag), 156–168.

Stamatakis, A. (2014). RAxML version 8: a tool for phylogenetic analysis and post-analysis of large phylogenies. *Bioinformatics* 30, 1312–1313. doi: 10.1093/bioinformatics/btu033

Stanke, M., Tzvetkova, A., and Morgenstern, B. (2006). AUGUSTUS at EGASP: using EST, protein and genomic alignments for improved gene prediction in the human genome. *Genome Biol.* 7:1. doi: 10.1186/gb-2006-7-s1-s11

Sun, P., Clamp, J. C., Xu, D., Huang, B., Shin, M. K., and Turner, F. (2013). An ITS-based phylogenetic framework for the genus Vorticella: finding the molecular and morphological gaps in a taxonomically difficult group. *P. Roy. Soc. Lond. B Bio.* 280:20131177. doi: 10.1098/rspb.2013.1177

Swart, E. C., Serra, V., Petroni, G., and Nowacki, M. (2016). Genetic codes with no dedicated stop codon: context-dependent translation termination. *Cell* 166, 691–702. doi: 10.1016/j.cell.2016.06.020

Utz, L. R., and Eizirik, E. (2007). Molecular phylogenetics of subclass Peritrichia (Ciliophora: Oligohymenophorea) based on expanded analyses of 18S rRNA sequences. *J. Eukaryot. Microbiol.* 54, 303–305. doi: 10.1111/j.1550-7408.2007.00260.x

Wang, R., Xiong, J., Wang, W., Miao, W., and Liang, A. (2016). High frequency of +1 programmed ribosomal frameshifting in *Euplotes octocarinatus*. *Sci. Rep.* 6:21139. doi: 10.1038/srep21139

Williams, D., and Clamp, J. C. (2007). A molecular phylogenetic investigation of *Opisthonecta* and related genera (Ciliophora, Peritrichia, Sessilida). *J. Eukaryot. Microbiol.* 54, 317–323. doi: 10.1111/j.1550-7408.2007.00262.x

Wu, T., Li, Y., Lu, B., Shen, Z., Song, W., and Warren, A. (2020). Morphology, taxonomy and molecular phylogeny of three marine peritrich ciliates, including two new species: *Zoothamnium apoarbuscula* n. *sp. and Z. apohentscheli n. sp.(Protozoa, Ciliophora, Peritrichia)*. *Mar. Life. Sci. Technol.* 2, 334–348. doi: 10.1007/s42995-020-00046-y

Zhan, Z., Xu, K., Warren, A., and Gong, Y. (2009). Reconsideration of phylogenetic relationships of the subclass Peritrichia (Ciliophora, Oligohymenophorea) based on small subunit ribosomal RNA gene sequences, with the establishment of a new subclass Mobilia Kahl, 1933. *J. Eukaryot. Microbiol.* 56, 552–558. doi: 10.1111/j.1550-7408.2009.00435.x

Zhuang, Y., Clamp, J. C., Yi, Z., and Ji, D. (2016). A new peritrich ciliate from a hypersaline habitat in northern China. *Zootaxa* 4169, 179–186. doi: 10.11646/zootaxa.4169.1.10

Zhuang, Y., Clamp, J. C., Yi, Z., and Ji, D. (2018). Phylogeny of the families Zoothamniidae and Epistylididae (Protozoa: Ciliophora: Peritrichia) based on analyses of three rRNA-coding regions. *Mol. Phylogenet. Evol.* 118, 99–107. doi: 10.1016/j.ympev.2017.09.023

Zong, C., Lu, S., Chapman, A. R., and Xie, X. S. (2012). Genome-wide detection of single-nucleotide and copy-number variations of a single human cell. *Science* 338, 1622–1626. doi: 10.1126/science.1229164

Conflict of Interest: The authors declare that the research was conducted in the absence of any commercial or financial relationships that could be construed as a potential conflict of interest.

frontiers in Marine Science

ORIGINAL RESEARCH
published: 08 December 2020
doi: 10.3389/fmars.2020.615413

Novel Contributions to the Taxonomy of the Ciliates Genus *Euplotes* (Ciliophora, Euplotida): Redescription of Two Poorly Known Species, With a Brief Note on the Distributions of This Genus in Coastal Waters of Southern China

Weiwei Liu[1,2], *Jiamei Jiang*[3], *Yehui Tan*[1,2] *and Xiaofeng Lin*[4]*

[1] *Key Laboratory of Tropical Marine Bio-Resources and Ecology, South China Sea Institute of Oceanology, Chinese Academy of Sciences, Guangzhou, China,* [2] *Guangdong Provincial Key Laboratory of Applied Marine Biology, South China Sea Institute of Oceanology, Chinese Academy of Sciences, Guangzhou, China,* [3] *Shanghai Universities Key Laboratory of Marine Animal Taxonomy and Evolution, Shanghai Ocean University, Shanghai, China,* [4] *Key Laboratory of the Ministry of Education for Coastal and Wetland Ecosystem, The Fujian Provincial Key Laboratory for Coastal Ecology and Environmental Studies, College of the Environment and Ecology, Xiamen University, Xiamen, China*

OPEN ACCESS

Edited by:
Xiaoshou Liu,
Ocean University of China, China

Reviewed by:
Yuan Xu,
East China Normal University, China
Yong Jiang,
Ocean University of China, China

***Correspondence:**
Xiaofeng Lin
linxf@xmu.edu.cn

Specialty section:
This article was submitted to Marine Evolutionary Biology, Biogeography and Species Diversity, a section of the journal Frontiers in Marine Science

Received: *09 October 2020*
Accepted: *16 November 2020*
Published: *08 December 2020*

Citation:
Liu W, Jiang J, Tan Y and Lin X (2020) Novel Contributions to the Taxonomy of the Ciliates Genus Euplotes (Ciliophora, Euplotida): Redescription of Two Poorly Known Species, With a Brief Note on the Distributions of This Genus in Coastal Waters of Southern China. Front. Mar. Sci. 7:615413. doi: 10.3389/fmars.2020.615413

As the typical periphytic ciliate, the genus *Euplotes* Ehrenberg, 1830 is highly diversified and commonly observed in marine water. In this study, the living morphology, infraciliature and silverline system of two poorly known *Euplotes* species, *E. neapolitanus* Wichterman, 1964 and *E. antarcticus* Fenchel and Lee, 1972, isolated from coastal water of southern China, were investigated. The original description of these two species were brief, and thus we provided detailed redescription based on our Chinese population. Their diagnoses were improved by adding some morphology characteristics and their detailed illustrations and photomicrographs were first supplied here. Based on the sufficient justification for identification of our population by morphology, their small subunit ribosomal RNA gene sequences which have been reported were linked to the accurate species name. Phylogenetic analyses showed that these two species cluster with their congeners which shared high morphological similarities with them. In addition, the geographic distribution of the genus *Euplotes* in coast of southern China was revealed, and the mangrove was considered as the ideal habitat for them by possessing the higher species richness.

Keywords: ***Euplotes neapolitanus*** **Wichterman, 1964,** ***Euplotes antarcticus*** **Fenchel and Lee, 1972, biogeography, morphology, phylogeny**

INTRODUCTION

The species of the ciliate genus *Euplotes* Ehrenberg, 1830 are frequently observed in marine samples (Lynn, 2008; Song et al., 2009). This genus is typical periphytic microorganism which can colonize the submerged substrates and are usually the most primary components of aufwuchs in high abundance and richness. They often feed on bacteria and microalgae, and play a crucial role in the flow of energy in microbial food webs (Lynn, 2008).

The genus *Euplotes* is highly diverse with over 150 species, which were often distinguished using the characteristics including the body size and shape, the dorsal and ventral ridges, the cirral pattern, the adoral zone of membranelles, the macronucleus shape, the dorsal kineties, and the silverline system pattern (Tuffrau, 1960; Borror, 1972; Carter, 1972; Curds, 1975; Lynn, 2008). Recently many reports on this group integrate aspects of their living morphology, infraciliature and molecular sequences, thus offering a more comprehensive understanding of their taxonomy. Despite of many descriptions of new species and redescriptions of insufficiently known species (Lobban et al., 2005; Fan et al., 2010; Jiang et al., 2010a,b; Pan et al., 2012; Chen et al., 2013; Fotedar et al., 2016; Lian et al., 2018, 2019; Yan et al., 2018; Hu et al., 2019; Gao et al., 2020), some species still require a re-investigation due to lacking detailed morphological description *in vivo* or after protargol preparation, as well as the molecular data (Gao et al., 2017; Liu et al., 2017).

Two poorly known species, namely *E. neapolitanus* Wichterman, 1964 and *E. antarcticus* Fenchel and Lee, 1972, were collected in coastal waters of southern China, which gave us an opportunity to re-recognize them. In previous studies, their SSU rRNA gene sequences have been reported, but no detailed morphological data from specimens are linked with them (Yi et al., 2009; Gao et al., 2017; Zhao et al., 2018). In present paper, the morphology of these two species is thus redescribed based on live observation and protargol-impregnated material. For the first time, their detailed illustrations and photomicrographs were supplied here. In addition, the study on the diversity of *Euplotes* species has been extensively conducted in the coastal waters of southern China in the past decade, and a large number of species have been collected and reported with taxonomy description (Hu et al., 2019; Lian et al., 2020). Based on a compilation of their faunal data, the biogeographical patterns of the genus *Euplotes* in different sites and habitats of southern China coast were reviewed here.

MATERIALS AND METHODS

Collection and Identification

Both species were found near a fishing dock of Daya Bay, Huizhou, China (22°42′N; 114°32′E). *Euplotes neapolitanus* were collected directly using 100 ml bottle from surface water that contained some organic debris on March 31, 2007. The salinity was about 28.6‰, the water temperature 23.1°C and pH 8.2. *Euplotes antarcticus* was collected using 20 μm mesh plankton nets from the upper 0.5 m water on March 31, 2007. The salinity was about 28.7‰, the water temperature 29.7°C and pH 8.4. After isolation, specimens were maintained in Petri dishes in the laboratory at room temperature. Attempts to culture the two species failed; therefore all studies were carried out on freshly isolated specimens.

Cells were observed *in vivo* using a light microscope equipped with differential interference contrast (Zhang et al., 2020). Protargol (Wilbert, 1975), silver nitrate (Foissner, 2014) staining methods were used respectively to reveal the infraciliature and silverline systems. Measurements and counts were made at 1,000 × magnification; drawings of stained cells were performed with the help of a camera and photomicrographs. Terminology is mainly according to Curds (1975).

Phylogenetic Analyses

The SSU rRNA gene sequences of *E. neapolitanus* and *E. antarcticus* have been published in previous studies with accession number FJ998024 and FJ998023, respectively. The two sequence were aligned with the sequences of 127 other ciliates downloaded from GenBank da ase (see **Figure 5** for accession numbers) using the GUIDANCE2 algorithm[1]. Representative species of Discocephalida, Aspidiscidae, Gastrocirrhidae, Uronychiidae were chosen as outgroup taxa. The final alignment used for phylogenetic analyses included 1,506 sites. Maximum likelihood (ML) analysis with 1,000 bootstrap replicates was performed on the CIPRES Science Gateway applying the GTRGAMMA model (Miller et al., 2010) using RAxML-HPC2 on XSEDE 8.2.9 (Stamatakis, 2014). Bayesian inference (BI) analysis was carried out with MrBayes 3.2.6 on XSEDE (Ronquist et al., 2012) on the CIPRES Science Gateway using the model GTR + I + G selected by AIC in MrModeltest 2.2 (Nylander, 2004). Markov chain Monte Carlo (MCMC) simulations were run for 1,000,000 generations with sampling every 100 generations and a burn-in of 1,000 trees (Dong et al., 2020). MEGA 6 (Tamura et al., 2013) was used to visualize the tree topologies.

Biogeographic Distribution

The regional biogeographic patterns of *Euplotes* species are inferred based on a compilation of faunal data from different sources include one monographs (Hu et al., 2019) and all papers on the taxonomy and biodiversity of *Euplotes* in southern China coast. Totally 15 species from six habitats of seven coastal sites were collected as the data set (see **Table 2** for a complete list). Considering that the results in these sources come from the extensive and high-frequency samplings in all sites of southern China coast, the compiled faunal data can generally reflect their distribution characters. Therefore, the presences of each species in these sampling sites and habitats were summarized, based on which the distribution variations of these species among different sites were analyzed and the species richness among habitats were compared.

RESULTS

Euplotes neapolitanus Wichterman, 1964

Improved Diagnosis

Large marine *Euplotes* with eight or nine low dorsal ridges, 120–150 × 70–80 μm *in vivo*, ellipsoidal in outline, anterior more truncated than posterior; adoral zone of membranelles about 3/4 of cell length, abruptly curved to anterior end of cell, composed of 62–73 membranelles; always 10 frontoventral, five transversal, two caudal and two left marginal cirri; mostly 11 dorsal kineties

[1]http://guidance.tau.ac.il/ver2/

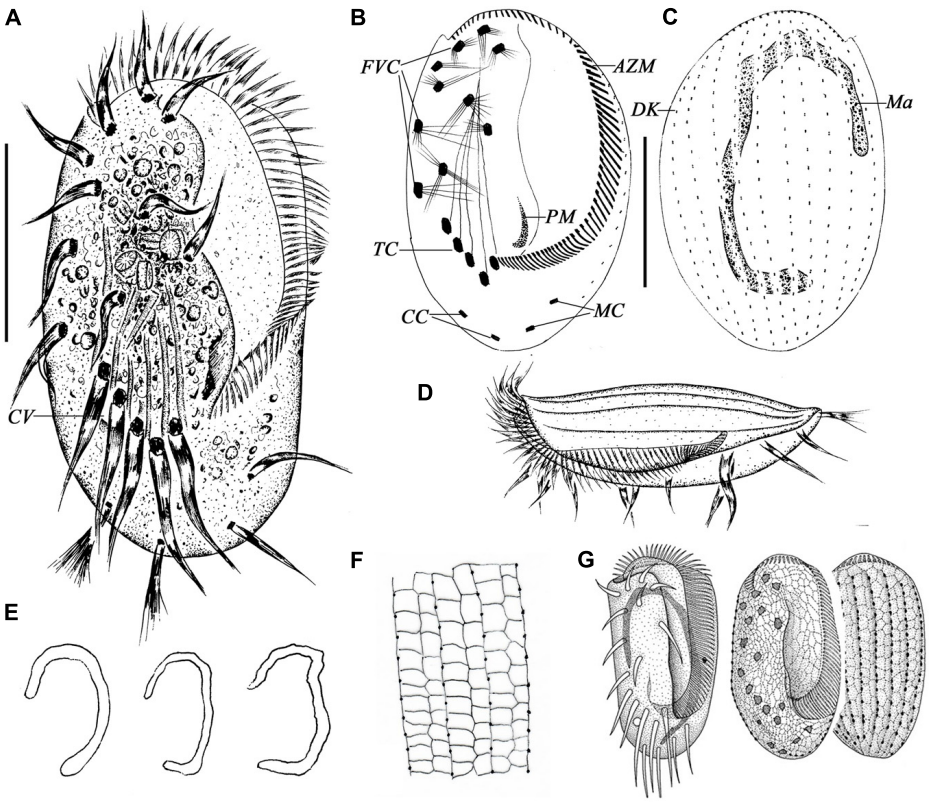

FIGURE 1 | Morphology of *Euplotes neapolitanus* Wichterman, 1964 *in vivo* **(A,D)**, after protargol **(B,C,E)** and silver nitrate impregnation **(F,G)**. **(A)** Ventral view of a representative specimen. **(B,C)** Ventral **(B)** and dorsal **(C)** view of the same specimen showing the ciliary pattern and nuclear apparatus. **(D)** Left lateral view showing the AZM and the dorsal ridges. **(E)** Different shapes of macronucleus. **(F)** Details of the silverline system of dorsal side. **(G)** Silverline system on ventral and dorsal sides, from Wichterman (1964). AZM, adoral zone of membranelles; CC, caudal cirri; CV, contractile vacuole; DK, dorsal kinety; FVC, frontoventral cirri; Ma, macronucleus; MC, marginal cirri; PM, paroral membrane; TC, transverse cirri. Scale bars = 50 μm.

with 17–23 dikinetids in mid-kinety rows; Macronucleus 3- or C-shaped; silverline system double-eurystomus type.

Description

Body shape generally ellipsoidal with truncated anterior end and bluntly round posterior end, left margin slightly curved while right margin straight (**Figures 1A**, **2A,B**). Size range 120–150 × 70–80 μm *in vivo*, dorsoventrally flattened about 3:2 (**Figures 1D**, **2C**), dorsal surface slightly convex with eight or nine low longitudinal ridges extending over entire length of body (**Figures 1D**, **2D,E**); ventral side more or less concave so transverse section slightly arciform (**Figure 2D**), five or six short ventral ridges among transverse cirri (**Figures 1A**, **2G**). At anterior end of ventral side, a hyaline collar-like plasmatic protrusion formed at base of adoral zone (**Figures 1A**, **2F**). Buccal field prominent, extending about 3/4 of cell length, right border located almost in middle axis of body, obviously indented in middle portion, forming a broad buccal open area (**Figures 1A**, **2A–C**).

Cytoplasm colorless, highly transparent at marginal area, but dark brownish in right central part due to many lipid globules (3–5 μm) and food vacuoles (10–12 μm) containing yellow alga (*Coscinodiscus* sp.) (**Figures 1A**, **2A,B,F**). Contractile vacuole posterior to the rightmost transverse cirrus, about 15 μm in diameter (**Figure 1A**, arrow). Macronucleus usually untypical 3-shaped with inconspicuous concave notch which even disappeared in some individuals (**Figures 1E**, **2L,N**). Locomotion typically by fast crawling on substrate, occasionally remaining stationary for short periods.

Infraciliature as shown in **Figures 1B,C**. Paroral membrane easily observed *in vivo* with cilia about 20 μm long, forming an L-shaped kinetosomes area about 20 μm long after staining, with anterior portion thin, and posterior portion thick and slightly curved (**Figures 1B**, **2M**). Adoral zone composed of 62–73 membranelles, which straightly arranged along the left cell margin and abruptly curved to anterior end of cell especially in living cells (**Figures 1A,B**, **2F,H,I,K**). The bases of membranelles up to 10–20 μm long and cilia of membranelles about 15–25 μm long. Consistently 10 frontoventral cirri arranged in normal pattern about 25–30 μm long, and five strong transverse cirri about 40 μm long (**Figures 1B**, **2K**). Usually two, rarely three caudal cirri brush-like, about 30 μm long (**Figures 1B**, **2K**). Two left marginal cirri, positioned below the buccal cavity and close to caudal cirri, the length equal to caudal cirri (**Figures 1B**, **2K**). About 11 or 12 (mostly 11) dorsal kineties almost extending over

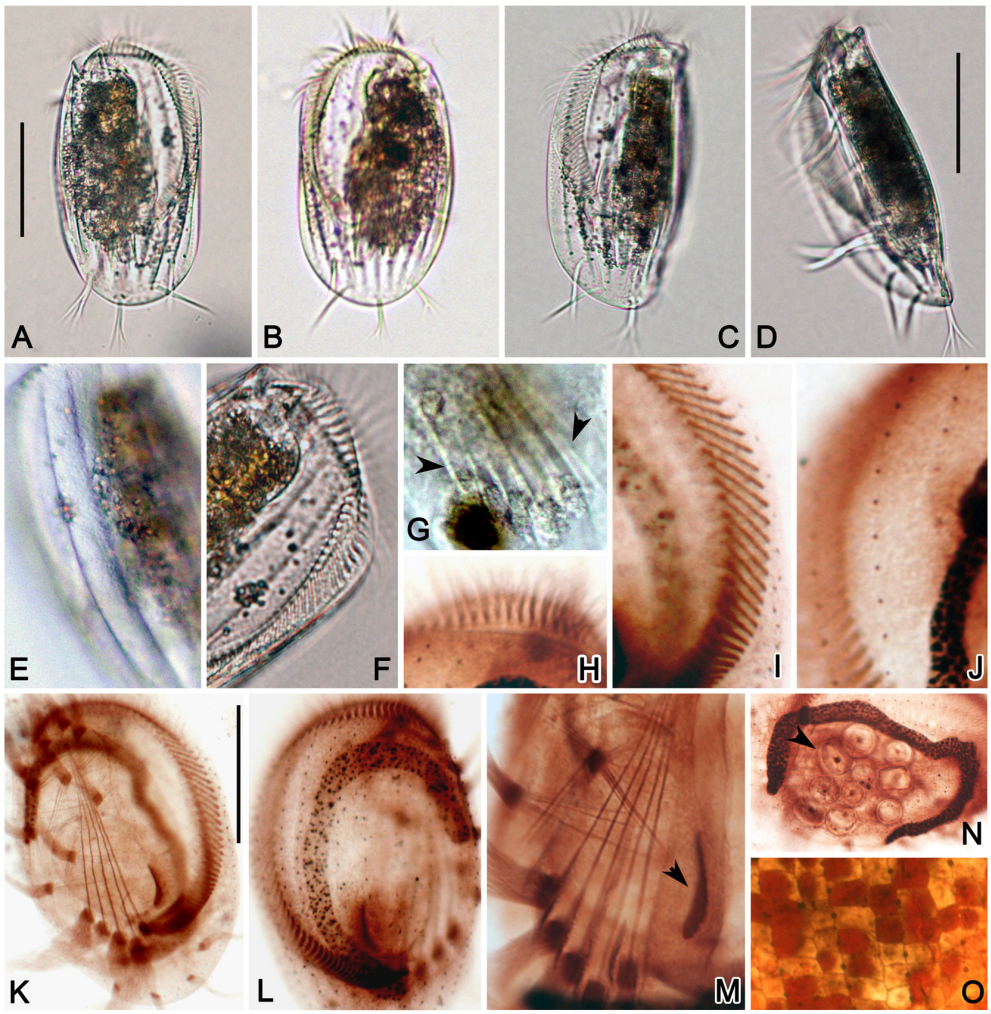

FIGURE 2 | Photomicrographs of *E. neapolitanus in vivo* **(A–G)**, and after protargol **(H–N)** and silver nitrate **(O)** impregnation. **(A,B)** Ventral **(A)** and dorsal **(B)** views of typical specimens. **(C,D)** Left-dorsal **(C)** and lateral **(D)** views. **(E)** Detail of dorsal side to show the ridges. **(F)** Anterior part of ventral side showing the abruptly curved AZM. **(G)** Detail of ventral side, arrowheads show the short ridge between transverse cirri. **(H,I)** Anterior **(H)** and middle **(I)** portions of AZM. **(J)** Detail of dorsal kinety. **(K,L)** Ventral **(K)** and dorsal **(L)** views of infraciliature. **(M)** Center portion of ventral side to show the transverse cirri, paroral membrane (arrowhead) and developed fiber system around the cirri. **(N)** Macronucleus and food (arrowhead) in cell center. **(O)** Detailed dorsal view of silverline system. Scale bars = 50 μm.

entire length of cell with the leftmost one usually positioned near body margin on ventral side; middle row with about 17–23 dikinetids (**Figures 1C**, **2J**). Silverline system on dorsal side double-eurystomus type (**Figures 1F**, **2O**).

Euplotes antarcticus Fenchel and Lee, 1972

Improved Diagnosis

Slender marine *Euplotes*, 50–70 × 25–35 μm *in vivo*, body elongated ellipsoidal shape with anterior end obliquely truncated and right anterior end protruded; left and right margins bended to ventral side; six longitudinal ridges forming three furrows in neighboring pair on dorsal side; buccal filed about 3/4 of cell length with 26–30 membranelles; ventral cirri fine, including 10 frontoventral, five transversal, two caudal and two left marginal cirri; eight dorsal kineties with 13–17 dikinetids in mid-kinety rows and five or six dikinetids in leftmost one; macronucleus C-shaped or inverted J-shaped; silverline system double-patella type.

Description

Cells measuring 50–70 × 25–35 μm *in vivo*. Body slender ellipsoidal shaped, anterior end obliquely truncated with right part conspicuously protruded, and posterior end narrowly round (**Figures 3A,B**, **4A–C,J**). Dorsoventrally flattened about 3:2, with left margin strongly and right margin slightly bended to ventral side, which lead to the left margin significantly higher than right one in transverse section of cell (**Figures 3E,F**, **4D,E**). Dorsal surface slightly convex in posterior 2/5 area with about six longitudinal ridges extending over entire length of body (**Figures 3E,H**, **4D**). These ridges separated into three pairs, in

TABLE 1 | Morphometric characteristics of *Euplotes neapolitanus* (upper rows) and *E. antarcticus* (lower rows) from protargol impregnated specimens.

Characters	Min	Max	Mean	Med	SD	SE	CV	n
Body length	101	142	115.3	115.0	9.06	1.55	7.9	34
	44	56	50.4	51	3.05	0.52	6.1	35
Body width	69	105	81.7	80.0	8.11	1.39	9.9	34
	23	31	26.6	27	2.10	0.36	7.9	35
Length of buccal field	75	96	86.1	85.0	4.57	0.78	5.3	34
	34	44	39.9	40	2.26	0.38	5.7	35
Number of adoral membranelles	62	73	66.6	67	2.49	0.45	3.7	31
	26	30	28.7	29	1.10	0.19	3.8	33
Number of frontoventral cirri	10	10	10.0	10.0	0.00	0.00	0.0	32
	10	11	10.0	10.0	0.18	0.03	1.8	32
Number of transverse cirri	5	5	5.0	5.0	0.00	0.00	0.0	32
	5	5	5.0	5.0	0.00	0.00	0.0	32
Number of left marginal cirri	2	2	2.0	2.0	0.00	0.00	0.0	32
	2	2	2.0	2.0	0.00	0.00	0.0	32
Number of caudal cirri	2	3	2.0	2.0	0.18	0.03	9.0	32
	2	3	2.1	2.0	0.25	0.04	11.9	32
Number of dorsal kineties	11	12	11.0	11.0	0.25	0.04	2.3	32
	8	8	8.0	8.0	0.00	0.00	0.0	32
Number of dikinetids in middle dorsal kinety row	17	23	20.3	21	1.62	0.29	8.0	31
	13	17	14.8	15.0	1.27	0.25	8.6	26

All measurements in μm.
CV, coefficient of variation in%; Max: maximum, Mean: arithmetic mean; Med, median; Min, minimum; N, number of individuals examined; SD, standard deviation; SE, standard error of mean.

each pair two ridges slightly inclined to each other, which thus producing a 2 μm wide groove between the ridge pair on dorsal surface (**Figures 3F**, **4H**). Three conspicuous ridges in ventral center among transverse cirri. The left and right margins of ventral side uplift, forming the ventral bending (**Figures 3A**, **4G**).

Cytoplasm colorless, several lipid droplets (2–4 μm across) and food vacuoles (3–6 μm across) scattered in cell, rendering cells brown in color at low magnification (**Figures 3A**, **4B,C**). Contractile vacuole located right posterior 1/4 and below the last two ventral cirri, about 8 μm in diameter (**Figures 3A**, **4B,K**). Macronucleus usually open C-shaped and the posterior curve not conspicuous in some individuals which presents an inverted J-shape of macronucleus (**Figures 3G**, **4L,Q,R**). Locomotion untypical, cells usually keep swimming slowly by rotation around the main axis, and occasionally crawls on the substrate.

Buccal field extending to 3/4 of body length, right border slightly indented in lower half, forming a buccal open area accounting for left 40% of body width (**Figures 3A**, **4A,F**). Adoral zone composed of 26–30 membranelles, proximal portion slightly curved and anterior portion obliquely extend along the left cell shoulder to the dorsal anterior end of cell (**Figures 3A,C**, **4A,L**). The bases of membranelles up to 5–9 μm long and cilia of membranelles about 8–12 μm long. Paroral membrane composed of many irregularly arranged kinetosomes which forming a clavate shape about 7 μm long (**Figures 3C**, **4N**).

The ventral cirri generally fine. Invariably 10 frontoventral cirri, about 12 μm long; five transverse cirri about 21 μm long, and two caudal cirri about 15 μm long (**Figures 3A,C**, **4F,G,L**). Two marginal cirri obliquely arranged below the proximal end of adoral membranelles, bearing thicker cilia and larger basal plaque than caudal cirri but equal to the latter in length (**Figures 3C**, **4P**). Eight dorsal kineties with the leftmost and rightmost one usually positioned on ventral side. Most dorsal kineties extending over the entire length of the cell, except for the leftmost one which is shortest and positioned below the proximal end of adoral membranelles. The mid-kinety kinety with 13–17 dikinetids, while the rightmost one with only five or six dikinetids (**Figures 3D**, **4M**). The dorsal silverline system double-patella type while in groove area the polygons slightly shrunk due to the inclination of ridges and seem to be double-eurystoma type (**Figures 3I**, **4O**).

Phylogenetic Position of *E. neapolitanus* and *E. antarcticus* Based on SSU rRNA Gene Sequence Data

In phylogeny trees, *E. neapolitanus* clusters with another population from Korea, which, however, was weakly supported (53ML/0.76BI), and then forms a clade with *E. harpa* and *E. platystoma* (**Figure 5**). *E. antarcticus* groups together with *E. trisulcatus* with high support value (1.00BI/100ML), which then form a sister branch with the clade consisting of *E. euryhalinus*, *E.* sp. 6 and *E. magnicirratus* (**Figure 5**).

Geographic Distribution of the *Euplotes* Species in Coast of Southern China

Totally 15 *Euplotes* species have been found and reported with taxonomy description in seven sites of coast of southern China (**Figure 6** and **Table 2**). Among these species, *E. charon* has a most extensive distribution and was detected in three sites, followed by *E. balteatus*, *E. encysticus*, *E. parawoodruffi*, *E. platystoma*, *E. rariseta*, and *E. vannus* which were detected in two sites

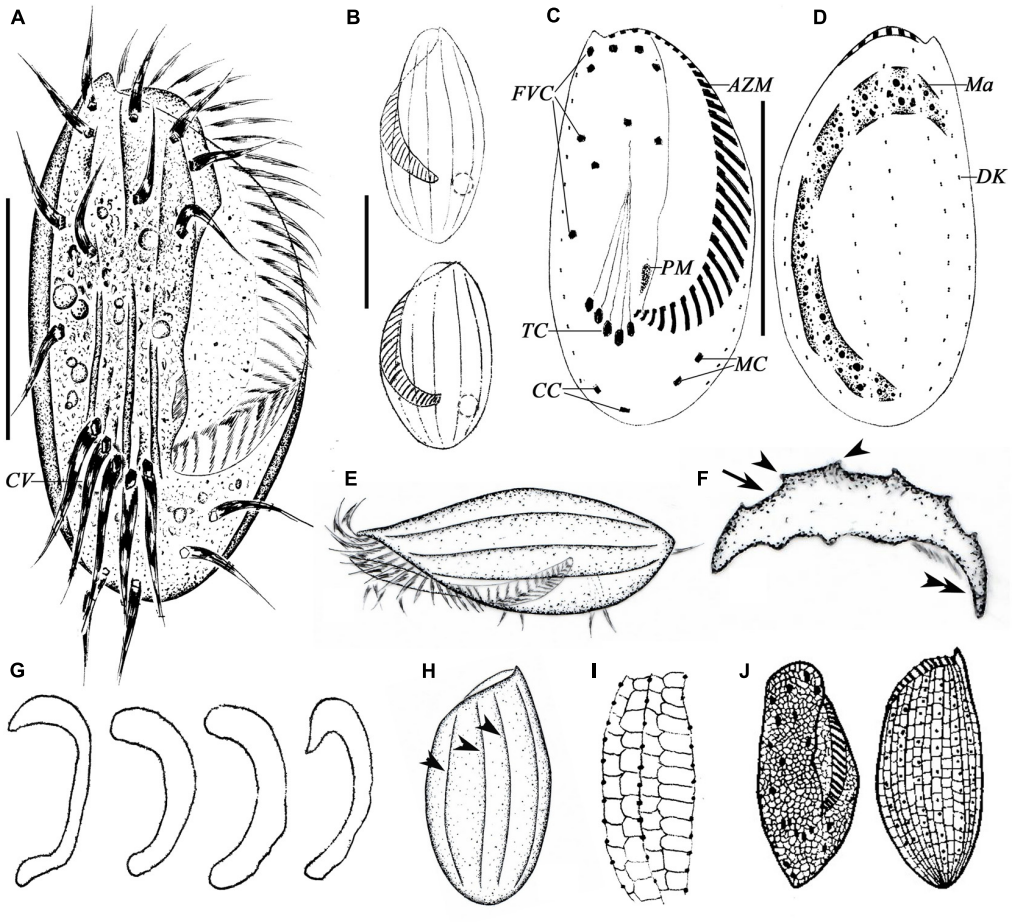

FIGURE 3 | Morphology of *E. antarcticus* Fenchel and Lee, 1972 *in vivo* **(A,B,E,F,H)**, after protargol **(C,D,G)** and silver nitrate **(I,J)** impregnation. **(A)** Ventral view of a representative specimen. **(B)** Dorsal views of different body shapes. **(C,D)** Ventral **(C)** and dorsal **(D)** views of the same specimen showing the ciliary pattern and nuclear apparatus. **(E)** Left lateral view showing the AZM and the dorsal ridges. **(F)** Cross section view to show bended left and right margins (double-arrowhead), note the furrows (arrow) and ridges (arrowheads) on dorsal side. **(G)** Different shapes of macronucleus. **(H)** Dorsal view to show the ridges (arrowheads). **(I)** Details of the silverline system of dorsal side. **(J)** Ventral and dorsal views, from Curds (1975). AZM, adoral zone of membranelles; CC, caudal cirri; CV, contractile vacuole; DK, dorsal kinety; FVC, frontoventral cirri; Ma, macronucleus; MC, marginal cirri; PM, paroral membrane; TC, transverse cirri. Scale bars = 30μm.

(**Figure 7**). The rest eight species were only found in one site. The species richness of *Euplotes* is variable among these sites. The highest species richness (13 species) was occurred in Huizhou and the lowest one was occurred in Donghai Island, Zhuhai and Shenzhen with only one species collected there (**Figure 7**). In addition, regarding the distributions among the six habitat types, the *Euplotes* has highest species number in both mangrove and offshore waters and lowest one in estuary habitat (**Figure 7**).

DISCUSSION

Comparison of *Euplotes neapolitanus* With Related Congeners

Euplotes neapolitanus was first found in Bay of Naples in Mediterranean and described briefly by Wichterman (1964). There was no other record or redescription of this species until present work. The organism we collected corresponds well with the original description referring to the large cell size, ellipsoidal body shape with wider and truncated anterior end, conspicuous buccal field with adoral zone of membranelles abruptly curved in anterior end, as well as the basic infraciliature.

In terms of the large size (more than 100 μm), the double-eurystomus type silverline system, 10 frontoventral, two caudal and two marginal cirri, *E. neapolitanus* is similar with five congerens: *E. platystoma* Dragesco and Dragesco-Kernéis, 1986, *E. harpa* Stein, 1859, *E. shanghaiensis* Song et al., 1998, *E. focardii* Valbonesi and Luporini, 1990.

Besides with above aspects, *E. harpa* is similar to *E. neapolitanus* in having dorsal ridges. However, *E. harpa* differs from *E. neapolitanus* by the larger body size (150–160 vs. 130–150 μm), more dorsal kineties (13 vs. 11), and more dikinetids in mid-kinety rows (40–45 vs. 17–23) (Kahl, 1932).

Although most of the morphometric data of *E. platystoma* overlap with *E. neapolitanus*, *E. neapolitanus* can be separated

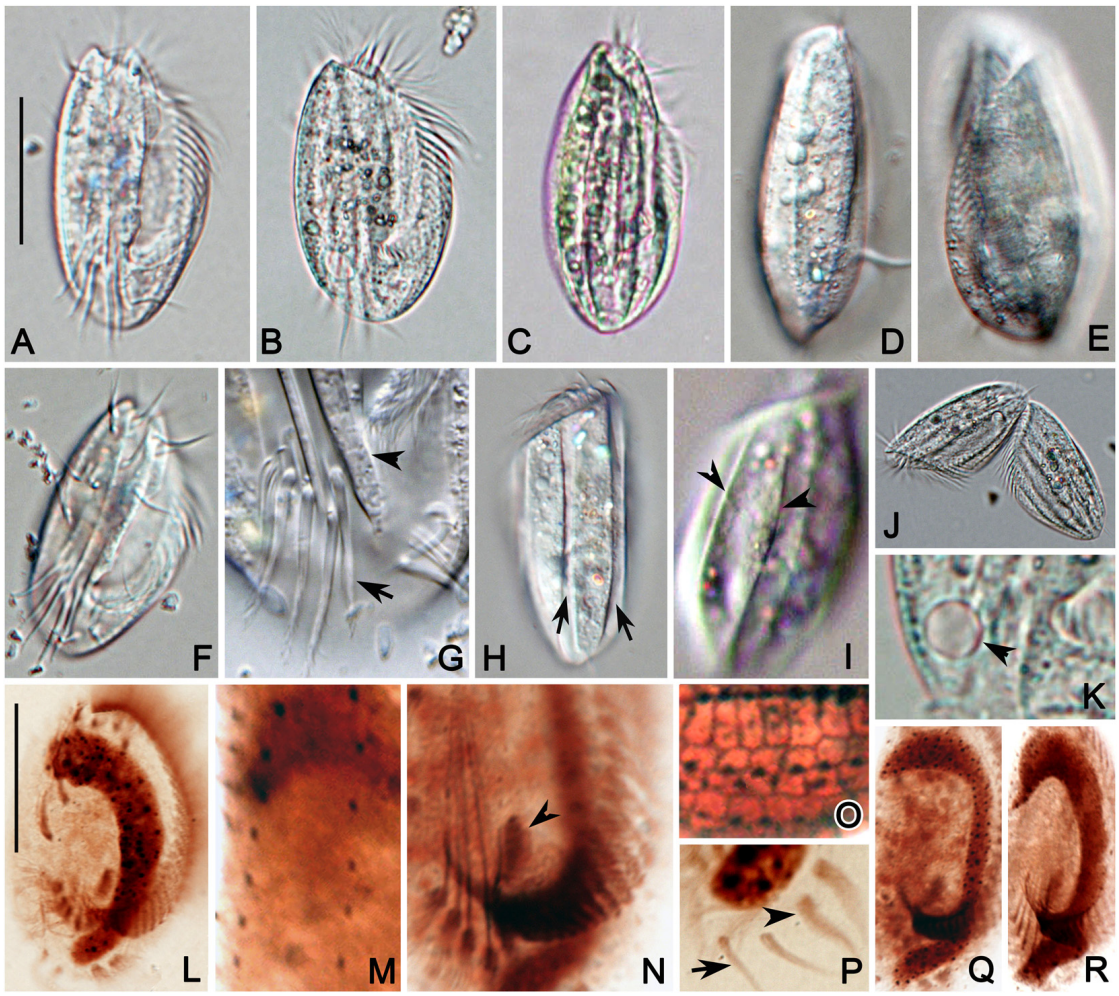

FIGURE 4 | Photomicrographs of *E. antarcticus in vivo* **(A–K)**, and after protargol **(L–N,P–R)** and silver nitrate **(O)** impregnation. **(A)** A representative specimen. **(B,C)** Cells of different shapes. **(D,E)** Right **(D)** and left **(E)** views showing the slightly convex dorsal side. **(F)** Ventral view showing the cirri. **(G)** Detail of posterior portion of ventral side to show the transverse cirri (arrow) and ridges (arrowhead). **(H,I)** Dorsal views to show the grooves (arrow) formed by inclined ridges (arrowhead). **(J)** A late divider. **(K)** Detail of contractile vacuole (arrowhead). **(L)** Ventral view of infraciliature. **(M)** Detail of dorsal kineties. **(N)** Center portion of ventral side to show the transverse cirri, paroral membrane (arrowhead) and posterior end of AZM. **(O)** Detail of dorsal view of silverline system. **(P)** Posterior portion of ventral side showing the marginal (arrowhead) and caudal (arrow) cirri. **(Q,R)** Macronucleus of different shapes. Scale bars = 30 μm.

from former by the truncated anterior end of cell (vs. rounded), the anterior adoral zone abruptly curved to dorsal side (vs. evenly curved), and the present of dorsal ridges (vs. absent) (Yan et al., 2018).

Euplotes shanghaiensis can be distinguished from *E. neapolitanus* by the smaller body size (80–120 × 30–35 vs. 130–150 × 70–75μm *in vivo*), fewer adoral membranelles (53–58 vs. 62–73), more dorsal kineties (12–13 vs. 11), and freshwater habitat (vs. marine) (Song et al., 1998).

Euplotes focardii differs from *E. neapolitanus* by the smaller body size (38–110 × 30–92 vs. 130–150 × 70–75 μm *in vivo*), fewer dorsal kineties (10 vs. 11), and the absent of dorsal ridges (vs. present) (Valbonesi and Luporini, 1990).

Beside, *E. damammensis* Chen et al., 2013 is also a large *Euplotes* with 10 frontoventral, two caudal and two marginal cirri as well as 11 dorsal kineties, although its silverline system was not revealed yet. It can be separated from *E. neapolitanus* by fewer adoral membranelles (44–51 vs. 62–73), and the shape of the macronucleus (sigmoidal vs. C-shaped) (Chen et al., 2013).

In phylogeny trees, *E. neapolitanus* clusters with *E. harpa* and *E. platystoma*, which agrees with their high morphologic similarities. There is another available SSU rRNA gene sequence under the species name *E. neapolitanus* [Korean isolation; GenBank accession number: HM635774; submitted by Khan et al., unpublished] in the GenBank, which, however, display a significant difference with our population in 55 nucleotides and 5% dissimilarity but a high similarity to *E. platystoma* with only a difference of four nucleotides. Considering the sufficient justification for identification of our population by morphology, the SSU rRNA gene sequence under the name *E.*

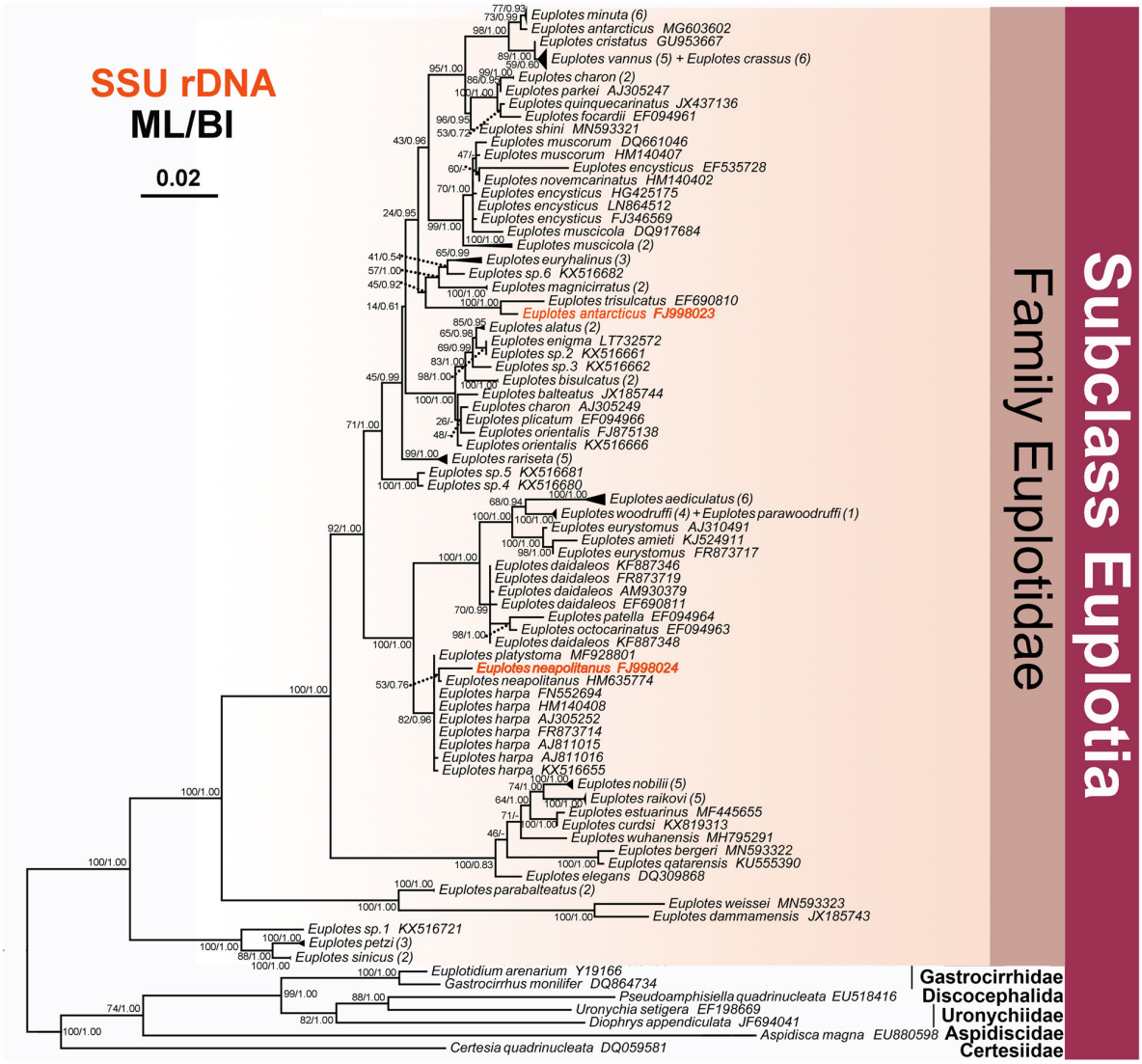

FIGURE 5 | The Maximum likelihood (ML) tree inferred from 18S rRNA gene sequences, showing the position of *E. neapolitanus* and *E. antarcticus*. Numbers in the brackets mark the number of populations for each species. Numbers at nodes represent the bootstrap values of the ML analysis and the posterior probability of the Bayesian inference (BI) analysis. "–" indicates topologies that differ between the ML and BI phylogenies. Scale bar corresponds to five substitutions per 100 nucleotide positions.

neapolitanus should be undoubtedly linked to our population. Any conclusion about the taxonomy identification of the Korean isolations shouldn't be made until its morphological data are available.

Comparison of *Euplotes antarcticus* With Related Congeners

Euplotes antarcticus was initially reported by Fenchel and Lee (1972) with some brief description by emphasizing its oblong body outline. The specimens studied here corresponds well with the original reports regarding its body shape, six dorsal ridges and basic infraciliature such as the numbers of adoral membranelles, ventral cirri, and especially the eight dorsal kineties of which six were on the dorsal surface. Some slight differences could be observed between these two populations, in terms of the cell size *in vivo* (50–70 × 25–35 μm in our specimens vs. 85–90 × 30–35 μm), and the sampling location (subtropic water in our specimens vs. Antarctica). In addition, the dorsal furrows observed in our specimens were not mentioned in previous descriptions, which was probably because that the dorsal ridges didn't incline to forming the obvious groove in original population and suggest that the furrows are population-dependent characteristics for this species. Curds (1975) reviewed the original study and supplied some detailed characteristics such as rectangular outline with pointed posterior end, and a cleft presented in the right peristomial margin, which were not prominent or

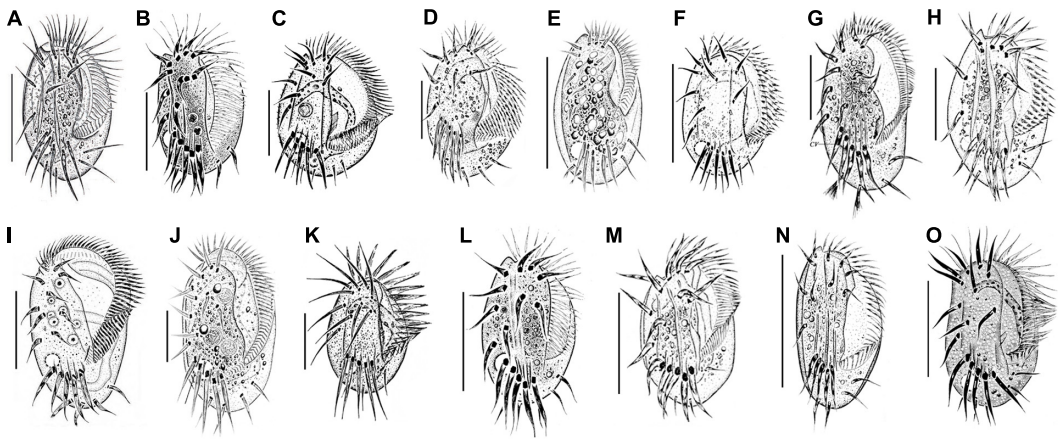

FIGURE 6 | *Euplotes* species collected in the coastal waters of southern China. **(A)** *E. balteatus* (Dujardin, 1841) Kahl, 1932 (from Chen et al., 2013); **(B)** *E. bergeri* Lian et al., 2020 (from Lian et al., 2020); **(C)** *E. charon* (Müller, 1773) Ehrenberg, 1830 (from Song and Packroff, 1997); **(D)** *E. encysticus* Yonezawa, 1985 (from Fan et al., 2010); **(E)** *E. estuarinus* Yan et al., 2018 (from Yan et al., 2018); **(F)** *E. minuta* (Yocum, 1930) Borror and Hill, 1995 (from Song and Wilbert, 1997); **(G)** *E. neapolitanus* Wichterman, 1964 (present work); **(H)** *E. orientalis* Jiang et al., 2010 (from Jiang et al., 2010b); **(I)** *E. parawoodruffi* Song and Bradbury, 1997 (from Shen et al., 2008); **(J)** *E. platystoma* Dragesco and Dragesco-Kernéis, 1986 (from Yan et al., 2018); **(K)** *E. rariseta* Curds et al., 1974 (from Song and Packroff, 1997); **(L)** *E. shini* Lian et al., 2020 (from Lian et al., 2020); **(M)** *E. sinicus* Jiang et al., 2010 (from Jiang et al., 2010a); **(N)** *E. antarcticus* (present work); **(O)** *E. vannus* (Müller, 1786) Borror and Hill, 1995 (from Song and Packroff, 1997). Scale bars: 50 μm **(A–G,I,J,L–O)**; 20 μm **(H,K)**.

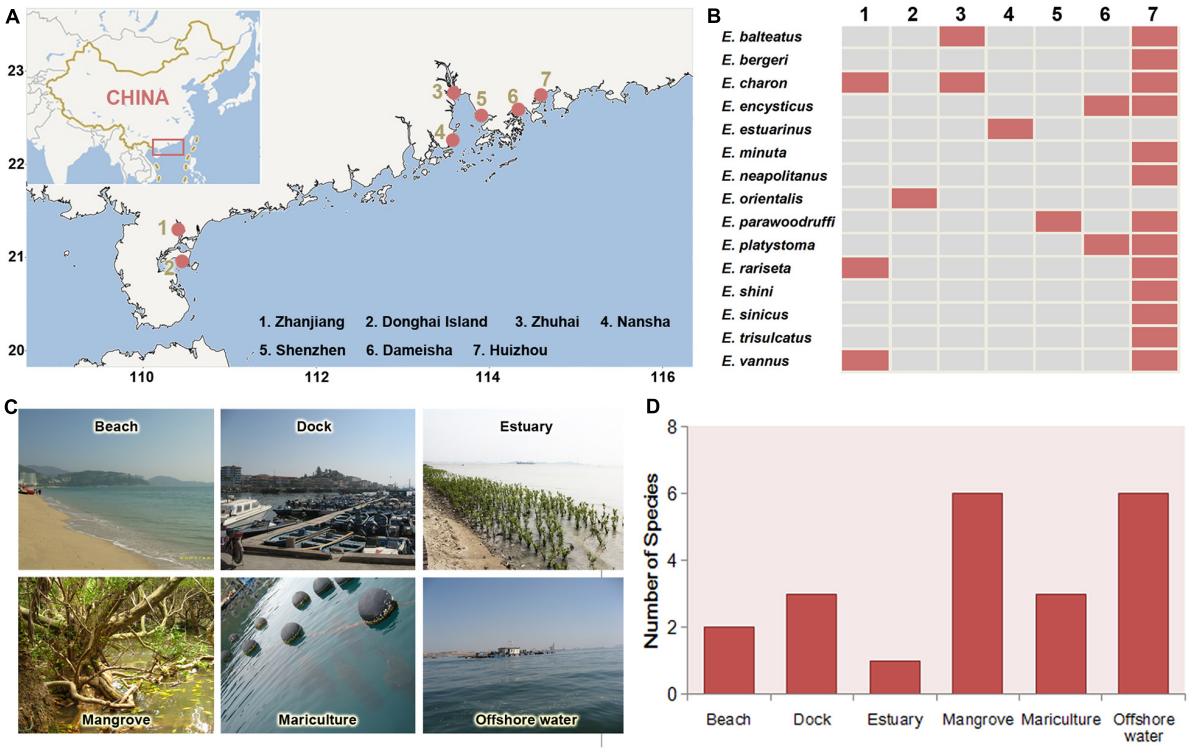

FIGURE 7 | Geographic distribution of the *Euplotes* species in coastal waters of southern China. **(A)** Locations (red spots) where the species were collected. **(B)** Distributions of each species in the seven sites. **(C)** Main habitat types. **(D)** Species richness in each habitat types.

lacked in our specimens. Considering that these supplementary characters were obtained based on the observation on the original figures, those may be over-interpreted and cannot represent the general characters for this species. Moreover, the dargyrome also displayed dissimilarity between them (double-patella type in our specimens vs. double-eurystomus type in Curds's description). Given that the inclined ridges were observed *in vivo* in our specimens, the size of each argyrome grid close to

TABLE 2 | *Euplotes* species collected in the coastal waters of southern China and their morphological comparison.

Species	Body size (μm)	No. adoral membranelles	No. dorsal kinety	Silverline system	Location	Habitat	References
E. balteatus	70–100 × 50–75	31–39	7	Double-eurystomus	Huizhou, Zhuhai	Mangrove, Mariculture	Hu et al., 2019
E. bergeri	70–80 × 45–50	43–57	12–14	Double-eurystomus	Huizhou	Offshore water	Lian et al., 2020
E. charon	70–100 × 65–90	51–60	9–10	Double-eurystomus	Huizhou, Zhanjiang, Zhuhai	Mangrove, Mariculture	Hu et al., 2019
E. encysticus	80–90 × 50–65	50–80	7	Complex	Huizhou, Dameisha	Beach	Fan et al., 2010; Hu et al., 2019
E. estuarinus	50–75 × 30–50	25–33	7	Double-eurystomus	Nansha	Estuary	Yan et al., 2018
E. minuta	50–70 × 40–55	33–41	7–9	Single-vannus	Huizhou	Offshore water	Hu et al., 2019
E. neapolitanus	120–150 × 70–80	62–73	11	Double-eurystomus	Huizhou	Dock	Present work
E. orientalis	35–45 × 20–30	18–25	6–7	Double-patella	Donghai Island	Mariculture	Hu et al., 2019
E. parawoodruffi	90–140 × 60–90	60–70	9	Double-eurystomus	Shenzhen, Huizhou	Mangrove, Offshore water	Shen et al., 2008; Hu et al., 2019
E. platystoma	100–150 × 50–80	46–54	10–11	Double-eurystomus	Huizhou, Dameisha	Beach, Mangrove	Lian et al., 2018; Yan et al., 2018
E. rariseta	30–50 × 20–40	17–22	7	Double-patella	Zhanjiang, Huizhou	Mangrove, Offshore water	Hu et al., 2019
E. sinicus	60–95 × 35–65	38–46	7	Double-patella	Huizhou	Offshore water	Hu et al., 2019
E. shini	65–75 × 35–45	37–46	9	Single-vannus	Huizhou	Offshore water	Lian et al., 2020
E. antarcticus	50–70 × 25–35	26–30	8	Double-patella	Huizhou	Dock	Present work
E. vannus	90–140	60	9–10	Single-vannus	Huizhou, Zhanjiang	Mangrove, Dock	Hu et al., 2019

the ridge would be shrunk in the appearance in this case and thus double-patella might visually shift to double-eurystomus. Similar result was proposed in the study of Foissner et al. (1991).

Petz et al. (1995) described a *Euplotes* species under the name of *E. antarcticus*. However, it is clearly different from the original description *E. antarcticus* in terms of the cell size *in vivo* (90–145 × 30–80 vs. 85–90 × 30–35 μm), the numbers of adoral membranelles (38–70 vs. about 30 in original description), dorsal kineties (9–14 vs. 8 in original description), dorsal ridges (7–10 vs. 6 in original description), and caudal cirri (three or two vs. two in original description). Therefore, it was probably a misidentification.

Several congeners with elongated ellipsoidal body shape and double-type silverline system should be compared with *E. antarcticus*, namely *E. affinis* (Dujardin, 1841) Kahl, 1932, *E. trisulcatus* Kahl, 1932, *E. dogieli* Agamaliev, 1967, *E. poljanskyi* Agamaliev, 1966 and *E. zenkewitchi* Burkovsky, 1970.

Euplotes trisulcatus is most similar to *E. antarcticus* in the body shape and having dorsal ridges and furrows. However, *E. antarcticus* has a larger body size (50–90 × 25–35 vs. 35–50 × 25–40 μm *in vivo*), more dorsal kineties (eight vs. seven), and more dikinetids in the middle row (13–17 vs. 11) (Tuffrau, 1960; Carter, 1972). Therefore, it can be clearly separated from *E. trisulcatus*.

Both *E. dogieli* and *E. poljanskyi* can be easily distinguished from *E. antarcticus* by the absent of dorsal ridges (vs. present), the number of adoral membranelles (35–38 in *E. dogieli* and 36–40 in *E. poljanskyi* vs. 26–30 in *E. antarcticus*), dorsal kineties (seven in *E. dogieli* and *E. poljanskyi* vs. eight in *E. antarcticus*) frontoventral (nine in *E. dogieli* and eight in *E. poljanskyi* vs. 10 in *E. antarcticus*) and marginal cirri (one in *E. dogieli* and *E. poljanskyi* vs. two in *E. antarcticus*) (Agamaliev, 1966, 1967).

Euplotes zenkewitchi differs from *E. antarcticus* in having more adoral membranelles (50–55 vs. 26–30), more dorsal kineties (ten vs. eight), fewer frontoventral cirri (nine vs. ten), and distinctively curved macronucleus (vs. slightly curved with angular posterior end) (Burkovsky, 1970).

Euplotes affinis is a small organism and resembles *E. antarcticus* with prominent dorsal ridge. It differs from the latter, however, by the feature of freshwater habitat (vs. marine), 3-shaped macronucleus (vs. C-shaped), having fewer adoral membranelles (18–20 vs. 26–30), and fewer frontoventral cirri (nine vs. ten) (Kahl, 1932).

Besides, *E. aberrans* Dragesco, 1960 is also similar to *E. antarcticus* in the body shape although its silverline system was not revealed yet. It can be separated from *E. antarcticus* by the feature of macronucleus shape (horseshoe shaped with ends almost meet one another vs. obviously opened C-shape), having more adoral membranelles (about 50 vs. 26–30), fewer dorsal ridges (four vs. six) and fewer frontoventral cirri (eight vs. ten) (Dragesco, 1960).

In previous phylogeny studies, the gene sequences of our population of *E. antarcticus* have been published under the name *E.* cf. *antarcticus*. There is another available SSU rRNA gene sequence under the species name *E. antarcticus* [Korean isolation; accession number: MG603602; submitted by Park et al. (2019)]

in the GenBank, which, however, display a significant difference with our population in 94 nucleotides and 5.2% dissimilarity. Considering the sufficient justification for identification of our population by morphology, we suggest to link the SSU rRNA gene sequence of *E. antarcticus* with our population. Detailed morphological description of the Korean specimen (EF690810) is necessary to reconsider the identification. In phylogeny trees, our population of *E. antarcticus* clusters with *E. trisulcatus*, which is consistent with their high morphologic similarities.

Remarks on the Distribution of Genus *Euplotes*

According to the compilation of faunal data, 15 *Euplotes* species have been found in southern China coast, which is significantly more than eight species reported in northern China coast such as Bohai and Yellow seas (Song et al., 2009). Moreover, six species, i.e., *E. vannus, E. charon, E. minuta, E. rariseta, E. sinicus, E. parawoodruffi* were found in both southern and northern China coasts (Song et al., 2009), suggesting their widely distibution in China.

Our results revealed that the highest species richness was occurred in Huizhou, which probably attributes to the diverse habitats there being suitable for different species (**Table 2**). In addition, mangrove wetlands possess the highest species richness of *Euplotes* species among the habitats in coast of southern China. The high diversity in mangrove has also been reported for other ciliate groups such as oligotrichs and stichotrichs (Zhang et al., 2018; Liang et al., 2019; Liu et al., 2019; Song et al., 2019), which suggest mangrove is an ideal habitat for ciliates. There are several reasons supporting the large ciliate species diversity in mangrove (Langenheder et al., 2010). First, the water in mangrove is normally eutrophic with high productivity due to the litter decomposition of plants, which supplies sufficient food source for ciliates. Second, the intricate root network of mangrove plant can dissipate the waves and conserve water and soil, which produces a stable habitat for ciliates especially for periphytons. Moreover, the dominant plants and terrain features of the mangroves are spatially varied, which leads to extensive environmental difference among the mangroves and thus supplies a wide range of niches for ciliates.

DATA AVAILABILITY STATEMENT

All data generated or used during the study appear in the article.

AUTHOR CONTRIBUTIONS

WL and XL conceived the research. WL wrote the manuscript. JJ and YT critically reviewed the findings and improved the manuscript. All authors contributed to the article and approved the submitted version.

FUNDING

This work was supported by the Guangdong MEPP Fund [No. GDOE (2019) A23], the Natureal Science Foundation of China (Nos. 31761133001 and 32070517), Science and Technology Planning Project of Guangdong Province, China (No. 2017B030314052), Science and Technology Basic Resources Investigation Program of China (No. 2017FY201404), and the Science and Technology Planning Project of Guangzhou (No. 202002030489).

REFERENCES

Agamaliev, F. G. (1966). New species of psammobiotic ciliates of the western part of the Caspian Sea. *Acta Protozool.* 4, 169–183.

Agamaliev, F. G. (1967). Faune des ciliés mésopsammiques de la côte ouest de la. *Mer Caspienne. Cahiers de Biol. Mar.* 8, 359–402.

Borror, A. C. (1972). Revision of the order Hypotrichida (Ciliophora. Protozoa). *J. Protozool.* 19, 1–23. doi: 10.1111/j.1550-7408.1972.tb03407.x

Burkovsky, I. V. (1970). The ciliates of the mesopsammon of the Kandalaksha Gulf (White Sea). *Acta Protozool.* 7, 475–489.

Carter, H. P. (1972). Infraciliature of eleven species of the genus *Euplotes*. *Trans. Am. Microsc. Soc.* 91, 466–492. doi: 10.2307/3225477

Chen, X. R., Zhao, Y., Al-Farraj, S. A., Al-Quraishy, S. A., El-Serehy, H. A., Shao, C., et al. (2013). Taxonomic descriptions of two marine ciliates, *Euplotes dammamensis* n. sp. and *Euplotes balteatus* (Dujardin, 1841) Kahl, 1932 (Ciliophora, Spirotrichea, Euplotida), collected from the Arabian Gulf, Saudi Arabia. *Acta Protozool.* 52, 73–89.

Curds, C. R. (1975). A guide to the species of the genus *Euplotes* (Hypotrichida, Ciliatea). *Bull. Br. Mus. Nat. Hist.* 28, 3–61.

Dong, J. Y., Li, L. F., Fan, X. P., Ma, H. G., and Warren, A. (2020). Two *Urosoma* species (Ciliophora, Hypotrichia): A multidisciplinary approach provides new insights into their ultrastructure and systematics. *Eur. J. Protistol.* 72:125991.

Dragesco, J. (1960). Ciliés mésopsammiques littoraux. Systématiquemorphologie, écologie. *Trav. Stn. Biol. Roscoff* 12, 1–356.

Fan, X. P., Huang, J., Lin, X. F., Li, J. Q., Al-Rasheid, K. A. S., and Hu, X. Z. (2010). Morphological and molecular characterization of *Euplotes encysticus* (Protozoa: Ciliophora: Euplotida). *J. Mar.Biol. Assoc. UK* 90, 1411–1416. doi: 10.1017/s002531541000038x

Fenchel, T., and Lee, C. C. (1972). Studies on ciliates associated with the sea ice from Antarctica. I. The nature of the fauna. *Arch. Protistenk.* 114, 231–236.

Foissner, W. (2014). An update of basic light and scanning electron microscopic methods for taxonomic studies of ciliated protozoa. *Int. J. Syst. Evol. Microbiol.* 64, 271–292. doi: 10.1099/ijs.0.057893-0

Foissner, W., Berger, H., Blatterer, H., and Kohmann, F. (1991). Taxonomische und ökologische Revision der Ciliaten des Saprobiensystems. Informationsberichte des Bayer. *Landesamtes für Wasserwirtschaft* 1991, 1–471.

Fotedar, R., Stoeck, T., Filker, S., Fell, J. W., Agatha, S., Marri, M. A., et al. (2016). Description of the halophile *Euplotes qatarensis* nov. spec. (Ciliophora Spirotrichea, Euplotida) isolated fromthe hypersaline Khor Al-Adaid lagoon in Qatar. *J. Eukaryot. Microbiol.* 63, 578–590. doi: 10.1111/jeu.12305

Gao, F., Huang, J., Zhao, Y., Li, L. F., Liu, W. W., Miao, M., et al. (2017). Systematic studies on ciliates (Alveolata, Ciliophora) in China: progress and achievements based on molecular information. *Eur. J. Protistol.* 61, 409–423. doi: 10.1016/j.ejop.2017.04.009

Gao, Y. Y., Gong, R. T., Jiang, Y. H., Pan, B., Li, Y., Warren, A., et al. (2020). Morphogenetic characters of the model ciliate *Euplotes vannus* (Ciliophora, Spirotrichea): Notes on cortical pattern formation during conjugational and postconjugational reorganization. *Eur. J. Protistol.* 73:125675. doi: 10.1016/j.ejop.2020.125675

Hu, X. Z., Lin, X. F., and Song, W. B. (2019). *Ciliate atlas: species found in the South China Sea*. Beijing: Science Press.

Jiang, J. M., Zhang, Q. Q., Hu, X. Z., Shao, C., Al-Rasheid, K. A. S., and Song, W. B. (2010a). Two new marine ciliates, *Euplotes sinicus* sp. nov. and *Euplotes parabalteatus* sp. nov., and a new small subunit rRNA gene sequence of *Euplotes rariseta* (Ciliophora, Spirotrichea, Euplotida). *Int. J. Syst. Evol. Microbiol.* 60, 1241–1251. doi: 10.1099/ijs.0.012120-0

Jiang, J. M., Zhang, Q. Q., Warren, A., Al-Rasheid, K. A. S., and Song, W. B. (2010b). Morphology and SSU rRNA gene-based phylogeny of two marine *Euplotes* species, *E. orientalis* spec. nov. and E. raikovi Agamaliev, 1966 (Ciliophora, Euplotida). *Eur. J. Protistol.* 46, 121–132. doi: 10.1016/j.ejop.2009.11.003

Kahl, A. (1932). Urtiere oder Protozoa. I: Wimpertiere oder Ciliata (Infusoria) 3. Spirotricha. *Tierwelt Dtl.* 25, 399–650.

Langenheder, S., Bulling, M. T., Solan, M., and Prosser, J. I. (2010). Bacterial biodiversity-ecosystem functioning relations are modified by environmental complexity. *Plos One.* 5:e10834. doi: 10.1371/journal.pone.0010834 doi: 10.1371/journal.pone.0010834

Lian, C. Y., Luo, X. T., Fan, X. P., Huang, J., Yu, Y. H., Bourland, W., et al. (2018). Morphological and molecular redefinition of *Euplotes platystoma* Dragesco & Dragesco Kernéis, 1986 and *Aspidisca lynceus* (Müller,1773) Ehrenberg, 1859, with reconsideration of a "well-known"*Euplotes* ciliate, *Euplotes harpa* Stein, 1859 (Ciliophora, Euplotida). *J. Eukaryot. Microbiol.* 65, 531–543. doi: 10.1111/jeu.12499

Lian, C. Y., Wang, Y. R., Li, L. F., Al-Rasheid, K. A. S., Jiang, J. M., and Song, W. B. (2020). Taxonomy and SSU rDNA-based phylogeny of three new *Euplotes* species (Protozoa, Ciliophora) from China seas. *J. King. Saud. Univ. Sci.* 32, 1286–1292. doi: 10.1016/j.jksus.2019.11.013

Lian, C. Y., Zhang, T. T., Al-Rasheid, K. A. S., Yu, Y. H., Jiang, J. M., and Huang, J. (2019). Morphology and SSU rDNA-based phylogeny of two *Euplotes* species from China: *E. wuhanensis* sp. n. and *E. muscicola* Kahl, 1932 (Ciliophora, Euplotida). *Eur. J. Protistol.* 67, 1–14. doi: 10.1016/j.ejop.2018.10.001

Liang, Z., Shen, Z., Zhang, Y., Ji, D. D., Li, J. Q., Warren, A., et al. (2019). Morphology and phylogeny of four new *Vorticella* species (Ciliophora: Peritrichia) from coastal waters of southern China. *J. Eukaryot. Microbiol.* 66, 267–280. doi: 10.1111/jeu.12668

Liu, W. W., Jiang, J. M., Xu, Y., Pan, X. M., Qu, Z. S., Luo, X. T., et al. (2017). Diversity of free-living marine ciliates (Alveolata, Ciliophora): faunal studies in coastal waters of China during the years 2011-2016. *Eur. J. Protistol.* 61, 424–438. doi: 10.1016/j.ejop.2017.04.007

Liu, W. W., Zhang, K. X., Chen, C. Z., Li, J. Q., Tan, Y. H., Warren, A., et al. (2019). Overview of the biodiversity and geographic distribution of aloricate oligotrich ciliates (Protozoa, Ciliophora, Spirotrichea) in coastal waters of southern China. *Syst. Biodivers.* 17, 787–800. doi: 10.1080/14772000.2019.1691081

Lobban, C., Modeo, L., Verni, F., and Rosati, G. (2005). *Euplotes uncinatus* (Ciliophora, Hypotrichia), a new species with zooxanthelae. *Mar. Biol.* 147, 1055–1061. doi: 10.1007/s00227-005-0024-3

Lynn, D. H. (2008). *The ciliated protozoa: characterization, classification, and guide to the literature*, 3rd Edn. Dordrecht: Springer.

Miller, M., Pfeiffer, W., and Schwartz, T. (2010). "Creating the CIPRES Science Gateway for inference of large phylogenetic trees," in *Proceedings of the Gateway Computing Environments Workshop (GCE)*, (New Orleans, LA), 1–8.

Nylander, J. A. (2004). *MrModeltest*. Uppsala: Evolutionary Biology Centre, Uppsala University.

Pan, Y., Li, L. Q., Shao, C., Hu, X. Z., Ma, H. G., Al-Rasheid, K. A., et al. (2012). Morphology and ontogenesis of a marine ciliate, *Euplotes balteatus* (Dujardin, 1841) Kahl, 1932 (Ciliophora, Euplotida) and definition of *Euplotes wilberti* nov. spec. *Acta Protozool.* 51, 29–38.

Park, M., Jung, J., Jo, E., Park, K., Baek, Y., Kim, S., et al. (2019). Utility of mitochondrial CO1 sequences for species discrimination of Spirotrichea ciliates (Protozoa, Ciliophora). *Mitochondrial DNA A.* 30, 148–155. doi: 10.1080/24701394.2018.1464563

Petz, W., Song, W. B., and Wilbert, N. (1995). Taxonomy and ecology of the ciliate fauna (Protozoa, Ciliophora) in the Endopagial and Pelagial of the Weddell Sea, Antarcitica. *Stapfia.* 40, 1–223.

Ronquist, F., Teslenko, M., Van der Mark, P., Ayres, D. L., Darling, A., Höhna, S., et al. (2012). MrBayes 3.2: efficient Bayesian phylogenetic inference and model choice across a large model space. *Syst. Biol.* 61, 539–542. doi: 10.1093/sysbio/sys029

Shen, Z., Lin, X. F., and Li, J. Q. (2008). Morphological redescription of a rare marine Euplotids, *Euplotes parawoodruffi* (Protozoa, Ciliophora, Euplotida). *Acta. Zootaxon. Sin.* 33, 335–339.

Song, W. B., and Packroff, G. (1997). Taxonomische Untersuchungen an marinen Ciliaten aus China mit Beschreibungen von zwei neuen Arten, *Strombidium globosaneum* nov. spec. und S. platum nov. spec. (Protozoa, Ciliophora). *Arch. Protistenkd.* 147, 331–360. doi: 10.1016/S0003-9365(97)80059-0

Song, W. B., and Wilbert, N. (1997). Morphological investigations on some free living ciliates (Protozoa, Ciliophora) from China Sea with description of a new hypotrichous genus, Hemigastrostyla nov.gen. *Arch. Protistenkd.* 148, 413–444. doi: 10.1016/S0003-9365(97)80020-6

Song, W. B., Warren, A., and Hill, B. F. (1998). Description of a new fresh-water ciliate, *Euplotes shanghaiensis* nov. spec. from China(Ciliophora, Euplotidae). *Eur. J. Protistol.* 34, 104–110. doi: 10.1016/s0932-4739(98)80019-9

Song, W. B., Warren, A., and Hu, X. Z. (2009). *Free-living ciliates in the Bohai and Yellow Seas, China* (Eds.). Beijing: Science Press.

Song, W., Xu, D. P., Zhang, Q. Q., Liu, W. W., Warren, A., and Song, W. B. (2019). Taxonomy and phylogeny of two poorly studied genera of marine oligotrich ciliates including descriptions of two new species: *Cyrtostrombidium paraboreale* sp. n. and *Apostrombidium orientale* sp. n. (Ciliophora: Spirotrichea). *Eur. J. Protistol.* 70, 1–16. doi: 10.1016/j.ejop.2019.05.001

Stamatakis, A. (2014). RaxML version 8: a tool for phylogenetic analysis and post-analysis of large phylogenies. *Bioinformatics.* 30, 1312–1313. doi: 10.1093/bioinformatics/btu033

Tamura, K., Stecher, G., Peterson, D., Filipski, A., and Kumar, S. (2013). MEGA6: molecular evolutionary genetics analysis version 6.0. *Mol. Biol. Evol.* 30, 2725–2729. doi: 10.1093/molbev/mst197

Tuffrau, M. (1960). Révision du genre *Euplotes*, fondée sur la comparaison des structures superficielles. *Hydrobiologia.* 15, 1–77. doi: 10.1007/bf00048080

Valbonesi, A., and Luporini, P. (1990). Description of two new species of *Euplotes* and *Euplotes rariseta* from Antarctica. *Polar Biol.* 11, 47–53.

Wichterman, R. (1964). Description and life cycle of *Euplotes neapolitanus* sp. nov. (Protozoa, Ciliophora, Hypotrichida)from the Gulf of Naples. *Trans. Am. Microsc. Soc.* 83, 362–370. doi: 10.2307/3224748

Wilbert, N. (1975). Eine verbesserte Technik der Protargolimprägnation für Ciliaten. *Mikrokosmos*. 64, 171–179.

Yan, Y., Fan, Y. B., Luo, X. T., El-Serehy, H. A., Bourland, W., and Chen, X. R. (2018). New contribution to the species-rich genus *Euplotes*: morphology, ontogeny and systematic position of two species (Ciliophora; Euplotia). *Eur. J. Protistol.* 64, 20–39. doi: 10.1016/j.ejop.2018.03.003

Yi, Z. Z., Song, W. B., Clamp, J., Chen, Z. G., Gao, S., and Zhang, Q. Q. (2009). Reconsideration of systematic relationships within the order Euplotida (Protista, Ciliophora) using new sequences of the gene coding for small-subunit rRNA and testing the use of combined data sets to construct phylogenies of the *Diophrys*-like species. *Mol. Phylogen. Evol.* 50, 599–607. doi: 10.1016/j.ympev.2008.12.006

Zhang, T. Y., Dong, J. Y., Cheng, T., Duan, L. L., and Shao, C. (2020). Reconsideration on taxonomy of the marine ciliate *Neobakuella aenigmatica* Moon et al., 2019 (Protozoa, Ciliophora, Hypotrichia). *Mar. Life. Sci. Technol.* 2, 97–108. doi: 10.1007/s42995-020-00032-4

Zhang, T. Y., Qi, H. L., Zhang, T. T., Sheng, Y. L., Warren, A., and Shao, C. (2018). Morphology, morphogenesis and molecular phylogeny of a new brackish water subspecies, *Neourostylopsis flava paraflava* nov. subsp. (Ciliophora, Hypotrichia, Urostylidae), with redefinition of the genus *Neourostylopsis*. *Eur. J. Protistol.* 66, 48–62. doi: 10.1016/j.ejop.2018.07.004

Zhao, Y., Yi, Z., Warren, A., and Song, W. B. (2018). Species delimitation for the molecular taxonomy and ecology of the widely distributed microbial eukaryote genus *Euplotes* (Alveolata, Ciliophora). *Proc. R. Soc. B.* 285:20172159. doi: 10.1098/rspb.2017.2159

Conflict of Interest: The authors declare that the research was conducted in the absence of any commercial or financial relationships that could be construed as a potential conflict of interest.

frontiers in Marine Science

ORIGINAL RESEARCH
published: 08 December 2020
doi: 10.3389/fmars.2020.610886

Systematics and Multi-Gene Phylogeny of the Subfamily Nothoholostichinae (Ciliophora, Hypotrichia), With Integrative Description of a New Marine Species *Nothoholosticha luporinii* n. sp.

Tengyue Zhang[1,2,3†], Yurui Wang[1,2†], Ting Cheng[2,4†], Jiyang Ma[1,2], Peter Vd'ačný[3], Weibo Song[1,2] and Chen Shao[1]*

[1] Laboratory of Protozoological Biodiversity and Evolution in Wetland, College of Life Sciences, Shanxi Normal University, Xi'an, China, [2] Institute of Evolution and Marine Biodiversity, Ocean University of China, Qingdao, China, [3] Department of Zoology, Comenius University in Bratislava, Bratislava, Slovakia, [4] College of Marine Life Sciences, Ocean University of China, Qingdao, China

OPEN ACCESS

Edited by:
Hongbo Pan, Shanghai Ocean University, China

Reviewed by:
Santosh Kumar, Zoological Survey of India, India
Barbara Nascimento Borges, Federal University of Pará, Brazil

***Correspondence:**
Chen Shao
shaochen@snnu.edu.cn

† These authors have contributed equally to this work

Specialty section:
This article was submitted to Marine Evolutionary Biology, Biogeography and Species Diversity, a section of the journal Frontiers in Marine Science

Received: *27 September 2020*
Accepted: *11 November 2020*
Published: *08 December 2020*

Citation:
Zhang T, Wang Y, Cheng T, Ma J, Vd'ačný P, Song W and Shao C (2020) Systematics and Multi-Gene Phylogeny of the Subfamily Nothoholostichinae (Ciliophora, Hypotrichia), With Integrative Description of a New Marine Species Nothoholosticha luporinii n. sp. Front. Mar. Sci. 7:610886. doi: 10.3389/fmars.2020.610886

Morphogenesis of ciliated protists attracts a lot of attention, because their huge morphological diversity is related to formation of ciliary structures during cell division. In the present work, the morphology and morphogenesis as well as the phylogenetic position of a new, marine hypotrich ciliate, *Nothoholosticha luporinii* n. sp., were investigated. The new species is characterized by having a combination of the following features: a bicorona whose anterior row contains four frontal cirri and posterior row includes only two cirri, a single buccal cirrus, midventral complex composed of about 30 cirral pairs, one pretransverse cirrus, 3–6 transverse cirri, one left and one right marginal cirral row; three bipolar dorsal kineties; contractile vacuole located in about 2/3 of the body length, two types of cortical granules, and many macronuclear nodules scattered throughout the cytoplasm. The morphogenesis of *N. luporinii* follows the ontogenetic mode of *Pseudokeronopsis*, a well-known and closely related genus except that the macronucleus fuses into a single mass in the middle fission stage. Phylogenetic analyses based on the rDNA operon classify *Nothoholosticha* in the family Pseudokeronopsidae and support the distinctness of the new taxon as well as the monophyletic origin of the subfamily Nothoholostichinae.

Keywords: ciliated protists, ontogenesis, phylogeny, rDNA operon, integrative taxonomy

INTRODUCTION

Ciliates (phylum Ciliophora Doflein, 1901), a highly diverse and ubiquitously distributed group of unicellular microbial eukaryotes, play substantial roles in various ecosystems. A lot of attention has been therefore paid to their diversity, function and evolution (e.g., Bharti et al., 2019; Hu et al., 2019; Jung and Berger, 2019; Kaur et al., 2019; Luo et al., 2019; Wang et al., 2019;

Yan et al., 2019; Gong et al., 2020; Shao et al., 2020; Sheng et al., 2020; Wang Y. R. et al., 2020; Zhang et al., 2020). Hypotrichs (subclass Hypotrichia Stein, 1859) are not only among the most differentiated ciliate groups, but also among the most confused ones in terms of their systematics and phylogeny (for reviews, see Berger, 1999, 2006, 2008, 2011; Luo et al., 2017; Song and Shao, 2017; Luo et al., 2018; Lyu et al., 2018; Kim and Min, 2019; Chen et al., 2020; Dong et al., 2020; Paiva, 2020; Park et al., 2020; Wang J. et al., 2020; Xu et al., 2020). In the present study, we focus on the hypotrich family Pseudokeronopsidae, which was established by Borror and Wicklow (1983). Hitherto, this family includes the following genera: *Antiokeronopsis* Fan et al., 2014b, *Apoholosticha* Fan et al., 2014a, *Heterokeronopsis* Pan et al., 2013, *Nothoholosticha* Li et al., 2009, *Pseudokeronopsis* Borror and Wicklow, 1983 (type genus), *Tetrakeronopsis* Paiva et al., 2014, and *Uroleptopsis* Kahl, 1932 (Li et al., 2009, 2016; Pan et al., 2013; Fan et al., 2014a,b; Paiva et al., 2014; Hu et al., 2015). Rather recently, the family Pseudokeronopsidae was divided into two subfamilies by Paiva et al. (2014): Nothoholostichinae Paiva et al., 2014, with an atypical bicorona whose anterior portion is formed by four frontal cirri, and Pseudokeronopsinae Borror and Wicklow, 1983, with a typical bicorona whose anterior portion is formed by more than four frontal cirri. As a result, *Apoholosticha*, *Heterokeronopsis*, *Nothoholosticha*, and *Tetrakeronopsis* were classified within the Nothoholostichinae, and only the three remaining genera, *Antiokeronopsis*, *Pseudokeronopsis,* and *Uroleptopsis*, were assigned to the Pseudokeronopsinae. The monophylies of both subfamilies are supported not only by the cirral pattern of the bicorona, but also by molecular analyses (Fan et al., 2014a; Huang et al., 2014; Paiva et al., 2014; Hu et al., 2015; Li et al., 2016).

So far, only two species have been assigned to the genus *Nothoholosticha*, namely, *N. fasciola* (Kahl, 1932) Li et al., 2009 (type species) and *N. flava* Li et al., 2016. In this study, a new species, *Nothoholosticha luporinii* n. sp., has been discovered in the intertidal sediment of Chizhou Island near the city of Shenzhen in the southern China. Its morphology, ontogenesis, and complete ribosomal operon (SSU rDNA, the ITS1-5.8S-ITS2 region, and LSU rDNA) have been studied to further extended our knowledge about the diversity and phylogeny of pseudokeronopsids.

MATERIALS AND METHODS

Sampling and Cultivation

Samples including sea water and sediment were collected from the intertidal zone in the Daya Bay, Chizhou Island, near the city of Shenzhen, southern China (22°38′11″N, 114°38′32″E) on 1st April 2018, when the water temperature was 26°C and salinity was 32‰. The original sample was divided into aliquots that were used to establish raw cultures in Petri dishes. Single specimens of *Nothoholosticha luporinii* n. sp. were isolated from the raw cultures and used to set up clonal cultures in filtered *in situ* sea water at room temperature (25°C). Some rice grains were added to stimulate the growth of bacteria, which served as prey organisms for ciliates.

Taxonomic Methods and Terminology

Nothoholosticha luporinii n. sp. was investigated using a combination of detailed *in vivo* observation and protargol impregnation. Living cells were observed under a microscope Olympus BX 53 (Olympus Corporation, Tokyo, Japan) using bright field illumination and differential interference contrast optics at a magnification of 100–1,000×. Protargol impregnation followed the Wilbert's method and served to reveal the nuclear apparatus and ciliary pattern of the new species (Wilbert, 1975). Also, the morphogenetic processes were rebuilt from the protargol-impregnated preparations. Stained cells were investigated mostly at high magnification (1,000×).

In vivo measurements were made from microphotographs of freely swimming specimens, while measurements on protargol-impregnated specimens were conducted using an ocular micrometer. Illustrations of living cells were based on free-hand sketches and photographs, while those of impregnated specimens were made at 1,000× magnification with the help of a drawing device. All illustrations were finally processed in Adobe PhotoShop CS5. To distinguish parental and daughter structures during the morphogenetic processes, new (daughter) structures are painted solid, while old ciliary structures are depicted by contour. General terminology and systematics mostly follow Berger (2006) and Lynn (2008).

DNA Extraction, PCR Amplification, and Sequencing

Single cells were picked, carefully washed five times in filtered *in situ* marine water, and lysed in 45 μl of Cell Lysis Buffer (DNeasy Blood and Tissue Kit, Qiagen, Hilden, Germany). To confirm the sequencing results, altogether three different types of samples were prepared: the first contained just one cell, the second comprised two cells, and finally the third included three cells. Genomic DNA was extracted with the DNeasy Blood and Tissue Kit, but only 1/4 of the suggested volume for all reagents was used as suggested by Lu et al. (2020). Amplification of SSU rDNA was achieved with the primers 82-F (5′-GAA ACT GCG AAT GGC TC-3′) (Jerome et al., 1996) and 18S-R (5′-TGA TCC TTC TGC AGG TTC ACC TAC-3′) (Medlin et al., 1988). Fragments containing ITS-5.8S rDNA and LSU rDNA were amplified with the primers ITS-F (5′-GTA GGT GAA CCT GCG GAA GGA TCA TTA-3′) (Miao et al., 2008) and 28S-R2 (5′-AAC CTT GGA GAC CTG AT-3′) (Moreira et al., 2007), using the same thermo cycler program as described by Huang et al. (2014). PCR products were purified using the *EasyPure*® Quick Gel Extraction Kit (TransGen Biotech Co., Ltd., Beijing, China) and subsequently cloned using the *pEASY*® -Blunt Cloning Kit (TransGen Biotech Co., Ltd., Beijing, China). Recombinant plasmids were sequenced in both directions on an ABI-PRISM 3730 automatic sequencer (Applied Biosystems, Tsingke Biological Technology Company, Qingdao, China) with the PCR primers. To obtain high quality sequences, two internal sequencing primers were used for SSU rDNA: 900F (5′-CGA TCA GAT ACC GTC CTA GT-3′) and 900R (5′-ACT AGG ACG GTA TCT GAT CG-3′), and also two internal primers for LSU rDNA: F2 (5′-GGA GTG TGT AAC AAC TCA CCT GC-3′) and

R3 (5′-CAT TCG GCA GGT GAG TTG TTA CAC-3′) (Zhao et al., 2014). Subsequently, the newly obtained sequences were carefully inspected, trimmed, and assembled into contigs using SeqMan Pro ver. 7.1.0 (Anson and Myers, 1997). Sequences obtained from all samples were identical and therefore only those derived from the single-cell sample were included into the subsequent phylogenetic analyses.

Molecular Phylogeny

The newly obtained sequences were blasted against the nucleotide NCBI database[1]. The BLASTn algorithm revealed that the new species belongs to the core urostylids (subclass Hypotrichia). Sequences of all related urostylids, except for those without associated publication information, were included into the phylogenetic analyses. The taxon sampling in the single-gene dataset (SSU rDNA) and in the concatenated, multi-gene dataset (SSU rDNA + ITS1-5.8S-ITS2 + LSU rDNA) mostly followed Huang et al. (2014) and Zhao et al. (2014). SeaView ver. 4 was used to prepare the concatenated dataset (Galtier et al., 1996; Gouy et al., 2010). *Oxytricha granulifera* (accession no. AF508762), *Stylonychia lemnae* (accession no. AF508773), *Stylonychia mytilus* (accession no. AF508774), *Sterkiella nova* (accession no. AF508771), and *Sterkiella histriomuscorum* (accession no. FJ545743) were used as outgroup taxa. GenBank accession numbers are provided in **Supplementary Tables S1, S2**. Sequences were aligned online using the MAFFT algorithm on the GUIDANCE2 server[2] with the following parameters: the 6mer pairwise method, the maximum number of 100 iterations, and 100 bootstrap repeats (Landan and Graur, 2008; Sela et al., 2015). The 5′ and 3′ ends of the resulting alignments were trimmed manually in the program BioEdit ver. 7.0 (Hall, 1999). The number of unmatched nucleotides and the pairwise SSU rDNA sequence identities within the subfamily Nothoholostichinae were calculated in the program BioEdit, using the "sequence difference count matrix" and "sequence identity matrix" options, respectively. The single-gene alignment contained 1,530 nucleotide positions, while the multi-gene alignment comprised 3,078 positions.

Maximum likelihood (ML) analyses were performed in RAxML-HPC2 ver. 8.2.10 on XSEDE (Stamatakis, 2014) on the CIPRES Science Gateway,[3] using the GTR + gamma evolutionary model and 1,000 bootstrap replicates. Bayesian inference (BI) was carried out in MrBayes ver. 3.2.6 on XSEDE (Ronquist et al., 2012) with the GTR + I + G evolutionary model selected by MrModeltest ver. 2.2 via the Akaike information criterion (Nylander, 2004). Markov chain Monte Carlo simulations were run for six million generations with a sampling frequency of 100 and a burn-in of 6,000 trees (10%). Remaining trees were used to calculate the 50%-majority rule consensus trees and their posterior probabilities. ML and BI trees were computed as unrooted and were rooted using the outgroup taxa in FigTree ver. 1.2.3[4].

[1]https://www.ncbi.nlm.nih.gov/

[2]http://guidance.tau.ac.il/ver2/

[3]http://www.phylo.org

[4]http://tree.bio.ed.ac.uk/software/figtree/

RESULTS

Systematics

Subclass Hypotrichia Stein, 1859
Family Pseudokeronopsidae Borror and Wicklow, 1983
Subfamily Nothoholostichinae Paiva et al., 2014
Genus *Nothoholosticha* Li et al., 2009

Nothoholosticha luporinii n. sp.

Zoobank registration number of work.

urn:lsid:zoobank.org:pub:8E7FD944-5497-4AF0-9FC4-0B8280B07F41

Zoobank registration number of new species.

urn:lsid:zoobank.org:act:AB581D7E-CB84-42C0-8528-1836369B3185

Diagnosis

Size *in vivo* 130–280 × 25–60 μm. Many macronuclear nodules. One contractile vacuole located near left body margin in about 2/3 of body length. Two types of cortical granules: big ones colourless, 1.5–2.0 μm in length, irregularly ellipsoid or slightly blood-cell shaped, and densely distributed throughout cortex; small ones bright brown-reddish in color, spherical, clustered in groups around dorsal bristles or sparsely arranged along cirral rows. Six frontal cirri arranged in two rows (four cirri in anterior row and two cirri in posterior row), 3–6 frontoterminal cirri, one buccal cirrus, one pretransverse cirrus, 3–6 transverse cirri, midventral complex composed of 17–43 cirral pairs, 38–84 left and 43–91 right marginal cirri. Three dorsal kineties. Adoral zone bipartite, composed of 7–13 crown and 23–39 lapel membranelles.

Type Locality

Sediment from the intertidal zone of Daya Bay, Chizhou Island, Shenzhen, southern China (22°38′11″N, 114°38′32″E).

Type Material

The protargol slide (no. ZTY2018040101_1) with the holotype specimen (**Figures 1K,L, 2I**) marked with an ink circle, and eight paratype slides (no. ZTY2018040101_2–9), are deposited in the Laboratory of Protozoology, Ocean University of China, Qingdao, China.

Gene Sequences

The nuclear SSU rDNA, ITS1-5.8S-ITS2 and LSU rDNA sequences have been deposited in GenBank under the following accession nos. MW035040, MW035039, and MW035042.

Dedication

We dedicate this species to Prof. Dr. Pierangelo Luporini (University of Camerino, Italy) in recognition of his great contributions to ciliatology.

Morphological Description of *Nothoholosticha luporinii* n. sp.

Size of specimens from fresh raw cultures about 130–280 × 25–60 μm, usually 200 × 35 μm *in vivo*. Body elongate ellipsoidal

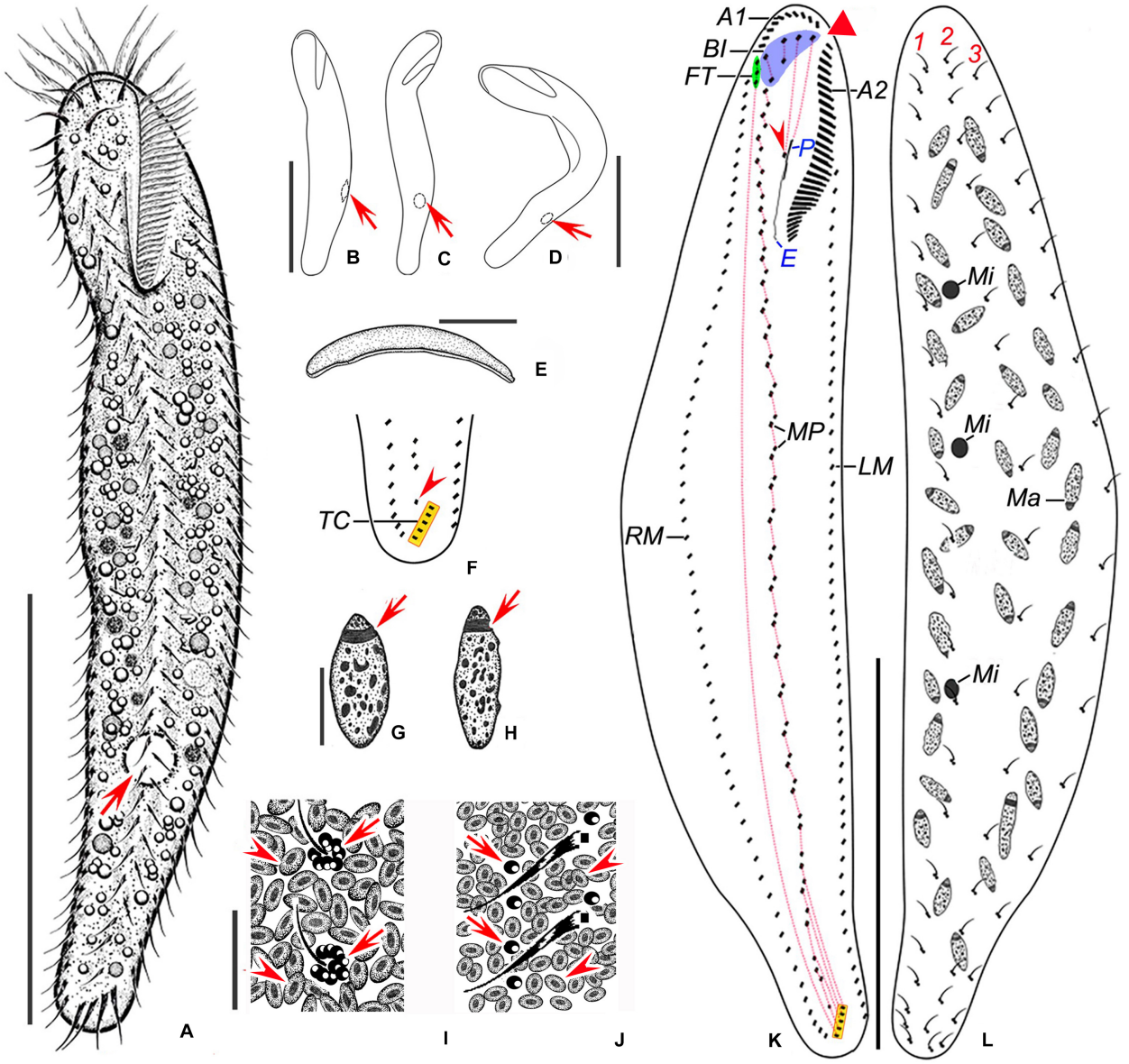

FIGURE 1 | *Nothoholosticha luporinii* n. sp. from life **(A–E,I,J)** and after protargol impregnation **(F–H,K,L)**. **(A)** Ventral view of a representative individual, arrow marks the contractile vacuole. **(B–D)** Overviews, showing the body flexibility, arrows mark contractile vacuoles. **(E)** Lateral overview. **(F)** Detail of the posterior body region, showing the single pretransverse cirrus (arrowhead) and transverse cirri (yellow rectangle). **(G,H)** Macronuclear nodules, arrows indicate replication bands. **(I,J)** Dorsal **(I)** and ventral **(J)** surface views, showing the arrangement of cortical granules, arrowheads denote the larger cortical granules, arrows point the smaller ones. **(K,L)** Ventral **(K)** and dorsal **(L)** views of the holotype specimen, showing the ciliary pattern and the nuclear apparatus. Red triangle in **(K)** marks the conspicuous gap between two parts of the adoral zone of membranelles, arrowhead marks the buccal cirrus, yellow rectangle delimits transverse cirri. Frontal-ventral-transverse cirri originating from the same anlagen are connected by dotted lines. A1 and A2, crown and lapel adoral membranelles; BI, bicorona; E, endoral membrane; FT, frontoterminal cirri; LM, left marginal cirral row; Ma, macronuclear nodules; Mi, micronuclei; MP, midventral cirral pairs; P, paroral membrane; RM, right marginal cirral row; TC, transverse cirri; 1–3, dorsal kineties. Scale bars = 5 μm **(G–J)** and 100 μm **(A–E,K,L)**.

with conspicuous longitudinal groove along midventral cirral complex (**Figure 2F**, arrowhead), anterior end broadly rounded and wider than posterior one; dorsoventrally flattened from about 2:1 to 3:2; rather flexible but not contractile (**Figures 1A–E**, **2A–E**). About 34–80 ellipsoidal macronuclear nodules scattered throughout cytoplasm, individual nodules approximately 3–5 × 6–11 μm in size after protargol impregnation; 1–3 globular micronuclei but exact number difficult to determine because hardly distinguishable from similar-sized and impregnated cytoplasmic inclusions (**Figures 1G,H,L**, **2I,J,N**). Contractile vacuole approximately 15 μm across during diastole, located in posterior two thirds of body length near left body margin (**Figures 1A–D**, **2A–C**, arrows). Cytoplasm colourless, transparent at high magnifications,

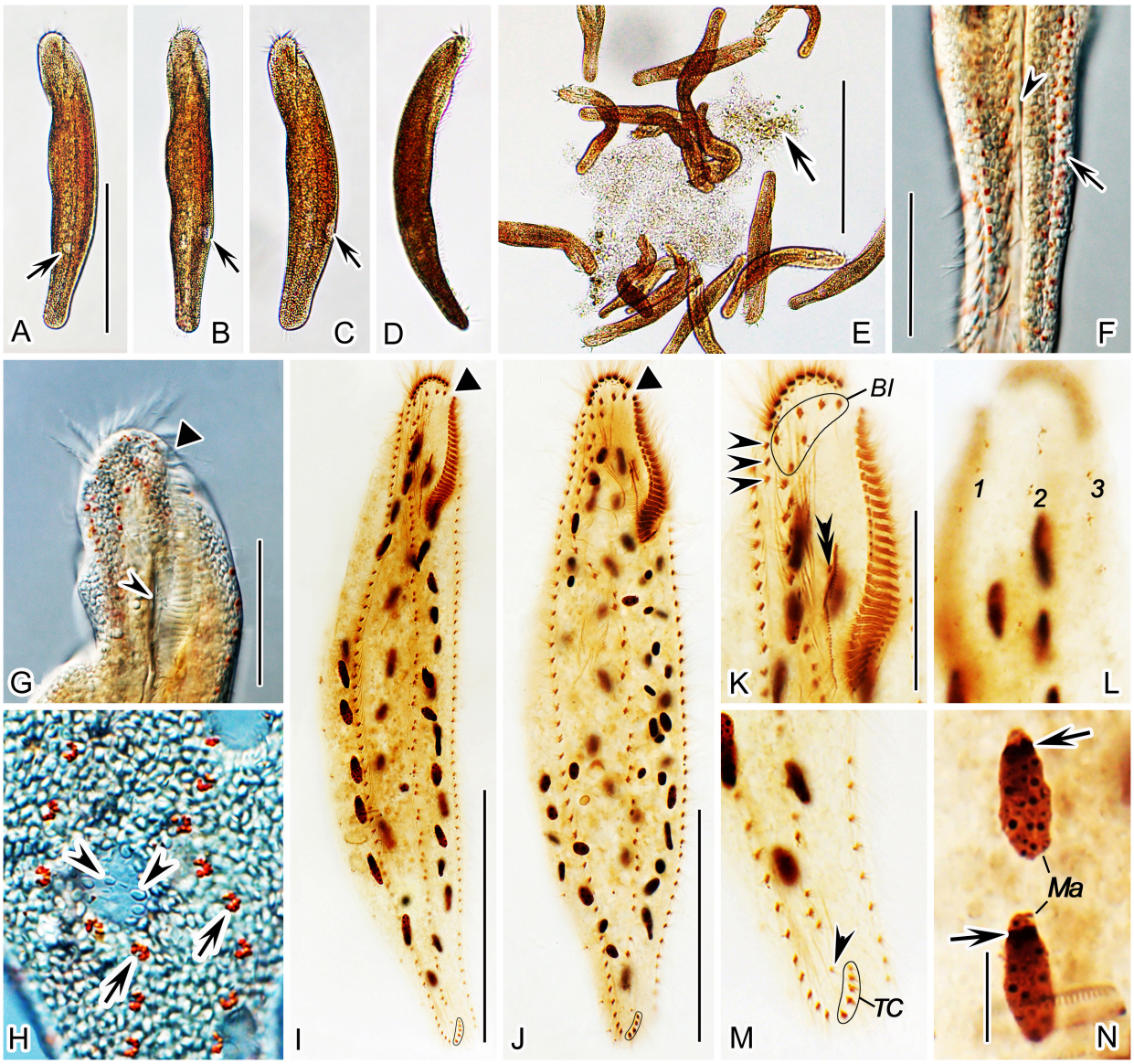

FIGURE 2 | *Nothoholosticha luporinii* n. sp. from life **(A–H)** and after protargol impregnation **(I–N)**. **(A–D)** Ventral **(A–C)** and lateral **(D)** overviews of different individuals, showing the body shape and the localization of the contractile vacuole (arrows in **A–C**). **(E)** Free-foraging individuals, arrow indicates a mass of microalgae. **(F)** Ventral view of the posterior body portion, showing the red cortical granules (arrow) and the longitudinal groove along the midventral cirral complex (arrowhead). **(G)** Ventral view of the anterior body portion, showing the gap between the two parts of the adoral zone (triangle) and the buccal cavity (arrowhead). **(H)** Dorsal surface view, showing the arrangement of colourless (arrowheads) and bright red (arrows) cortical granules. **(I,J)** Ventral view of the holotype **(I)** and the paratype **(J)** specimen, showing the ciliary pattern and the nuclear apparatus. Triangles mark the gap between the two parts of the adoral zone of membranelles. **(K,L)** Ventral **(K)** and dorsal **(L)** views of the anterior body portion of the same specimen. Arrowheads in **(K)** indicate the frontoterminal cirri, double-arrowhead shows the buccal cirrus. **(M)** Ventral view of the posterior body portion, arrowhead denotes the single pretransverse cirrus. **(N)** Details of the macronuclear nodules, arrows mark replication bands. BI, bicorona; Ma, macronuclear nodules; TC, transverse cirri; 1–3, dorsal kineties. Scale bars = 5 μm **(N)**, 35 μm **(G,K–M)**, 100 μm **(A–D,I,J)**, and 200 μm **(E)**.

packed with macronuclear nodules, lipid droplets, and food vacuoles. Cortex flexible, contains two types of granules: type I bigger, i.e., 1.5–2.0 μm in diameter, irregularly ellipsoidal or slightly blood cell-shaped, colourless, narrowly arranged underneath cortex, possibly mitochondria (**Figures 1I,J**, **2F–H**, arrowheads); type II smaller, i.e., about 0.5 μm in diameter, bright brown-reddish, clustered in a flower-like pattern around dorsal bristles or sparsely arranged along cirral rows (**Figures 1I,J**, **2F,H**, arrows), provides cells with a reddish-brown appearance under low magnifications (40×, 100× and 200×; **Figures 2A–E**) and with a yellowish appearance under moderate magnification (400×) (**Figures 2F,G**). Crawls moderately slowly on debris particles, sometimes swims by rotation about main body axis.

TABLE 1 | Morphometric characterization of *Nothoholosticha luporinii* n. sp.

Character	Min	Max	Mean	M	SD	CV	N
Body, length	190.0	315.0	253.5	255.0	31.5	12.4	20
Body, width	35.0	100.0	70.8	67.5	19.3	27.3	20
Body length:width, ratio	2.5	7.3	3.9	3.7	1.2	31.5	20
Anterior body end to buccal cirrus, distance	27.0	44.0	35.1	35.0	4.2	12.0	20
Anterior body end to paroral membrane, distance	24.0	39.0	30.7	30.0	3.8	12.3	20
Anterior body end to endoral membrane, distance	25.0	40.0	32.2	32.0	3.7	11.3	20
Macronuclear nodules, number	34.0	80.0	58.2	56.5	11.7	20.1	20
Frontal cirri, number	6.0	6.0	6.0	6.0	0.0	0.0	20
Buccal cirri, number	1.0	1.0	1.0	1.0	0.0	0.0	20
Frontoterminal cirri, number	3.0	6.0	3.7	3.5	0.8	22.3	20
Midventral cirral pairs, number	17.0	43.0	30.7	30.5	6.8	22.1	20
Left marginal cirri, number	38.0	84.0	62.0	62.5	11.6	18.6	20
Right marginal cirri, number	43.0	91.0	69.0	71.5	11.9	17.2	20
Pretransverse cirrus, number	1.0	1.0	1.0	1.0	0.0	0.0	20
Transverse cirri, number	3.0	6.0	4.7	5.0	0.7	15.6	20
Adoral zone of membranelles, length	45.0	75.0	62.8	62.5	8.0	12.8	20
Adoral zone of membranelles, % of body length	21.0	30.6	24.9	25.0	2.7	10.7	20
Adoral membranelles, total number	31.0	50.0	41.3	41.0	5.9	14.3	20
Crown membranelles, number	7.0	13.0	10.0	10.0	1.7	17.5	20
Lapel membranelles, number	23.0	39.0	31.3	31.5	4.7	15.0	20
Paroral membrane, length	6.0	15.0	11.1	11.5	3.2	28.5	20
Endoral membrane, length	18.0	35.0	27.2	27.5	4.9	18.1	20
Dorsal kineties, number	3.0	3.0	3.0	3.0	0.0	0.0	20
Bristles in dorsal kinety 1, number	19.0	45.0	32.7	31.0	7.7	23.6	20
Bristles in dorsal kinety 2, number	16.0	37.0	26.9	26.0	6.1	22.7	20
Bristles in dorsal kinety 3, number	16.0	42.0	27.8	28.5	7.1	25.5	20

All data based on protargol-impregnated specimens.
Measurements in μm. Min, minimum; Max, maximum; Mean, arithmetic mean; SD, standard deviation; M, median; CV, coefficient of variation in %; N, number of cells investigated.

Cirri about 10–15 μm long *in vivo*; number of frontal, buccal, and pretransverse cirri invariable, while number of frontoterminal cirri, midventral cirral pairs, transverse, and marginal cirri rather highly variable (CV = 15.6–22.3%) (**Table 1**). Frontal cirri approximately 13 μm long *in vivo*, arranged in an atypical bicorona, invariably four cirri in anterior coronal row and constantly two cirri in posterior coronal row (**Figure 1K**, blue area, **Figure 2K**). Buccal cirrus about 10 μm long *in vivo*, situated right of mid-portion of paroral membrane (**Figure 1K**, red arrowhead, **Figure 2K**, black double arrowhead). Three to six frontoterminal cirri, about 10 μm long *in vivo*, located posterior to distal end of crown adoral membranelles (**Figure 1K**, green area, **Figure 2K**, black arrowheads). Midventral complex consists of 17–43 cirral pairs arranged in a zigzag pattern, left cirrus of midventral pairs slightly longer than right one, i.e., about 10 vs. 9 μm (**Figures 1K**, **2I,J**); posterior most cirrus of midventral complex, labeled as a pretransverse cirrus, distinctly shifted toward transverse cirri and hence more or less separated from midventral complex (**Figures 1F**, **2M**, arrowhead). Three to six transverse cirri, about 13–15 μm long *in vivo*, arranged in an oblique row (**Figures 1F,K**, yellow rectangle, **Figures 2I,J,M**). One left and one right marginal cirral row, composed of 38–84 and 43–91 cirri, respectively, individual cirri about 11 μm long *in vivo* (**Figures 1K**, **2I,J**).

Dorsal bristles about 4 μm long *in vivo*, arranged in three bipolar rows. All three dorsal kineties begin subapically and extend to posterior body end (**Figures 1L**, **2L**). Dorsal kinety 1 composed of 19–45 dikinetids, kinety 2 of 16–37, and kinety 3 of 16–42 (**Table 1**). Caudal cirri absent.

Adoral zone of membranelles occupies 20–30% of body length; bipartite, i.e., divided into crown and lapel region separated by a conspicuous gap (**Figures 1A,K**, **2I–K** and **Table 1**). Crown region composed of 7–13 membranelles arranged in an arch-shaped pattern along anterior cell pole, length of membranellar cilia 18–22 μm. Lapel region composed of 23–39 membranelles forming a *Gonostomum*-like pattern, i.e., extends along left body margin to one fifth or third of body length, where it bends rather abruptly rightwards to run almost in parallel with undulating membranes, length of membranellar cilia up to 17 μm. Undulating membranes arranged in a *Pseudokeronopsis*-like pattern, i.e., paroral and endoral almost straight, extend in parallel and only partially overlap. Endoral membrane commences posterior to buccal cirrus and runs to buccal vertex, 18–35 μm long after protargol impregnation. Paroral membrane begins anterior to endoral, remarkably shorter than endoral, i.e., only 6–15 μm long in protargol preparations (**Figures 1K**, **2I–K**).

Morphogenesis of *Nothoholosticha luporinii* n. sp.

Oral Primordium and Cirral Streaks

Morphogenesis commences with *de novo* formation of small groups of basal bodies adjacent to left cirri of the midventral complex about in the mid-body (**Figure 6A**). Groups of proliferating basal bodies join to form a longitudinal field, i.e., the oral primordium of the opisthe. Simultaneously, the proter's oral primordium develops as a single anarchic field of closely spaced basal bodies in the region of the buccal vertex (**Figures 3A**, **6B,C**). New adoral membranelles differentiate within the oral primordium of both the proter and the opisthe in a posteriad direction (**Figures 3B,C**, **6D–F**). The undulating membranes (UM) anlage (streak I) forms to the right of and possibly from the oral primordium both in the proter and the opisthe (**Figures 3C**, **4A**, **6F**, arrowheads). The anterior portion of the UM anlage splits a single cirrus that migrates anteriorly to become the leftmost frontal cirrus in the anterior row of the bicorona (**Figures 4C**, **6J,K**, arrowheads). Then, the UM anlage divides longitudinally to give rise to the paroral membrane and the endoral membrane (**Figures 4C**, **6J–N**, arrowheads). Meanwhile, multiple frontal-midventral-transverse (FVT) cirral anlagen develop as series of oblique streaks to the right of the oral primordia (**Figures 3C**, **4A,C**, **6F,J,K**, arrows). Streak II (FVT

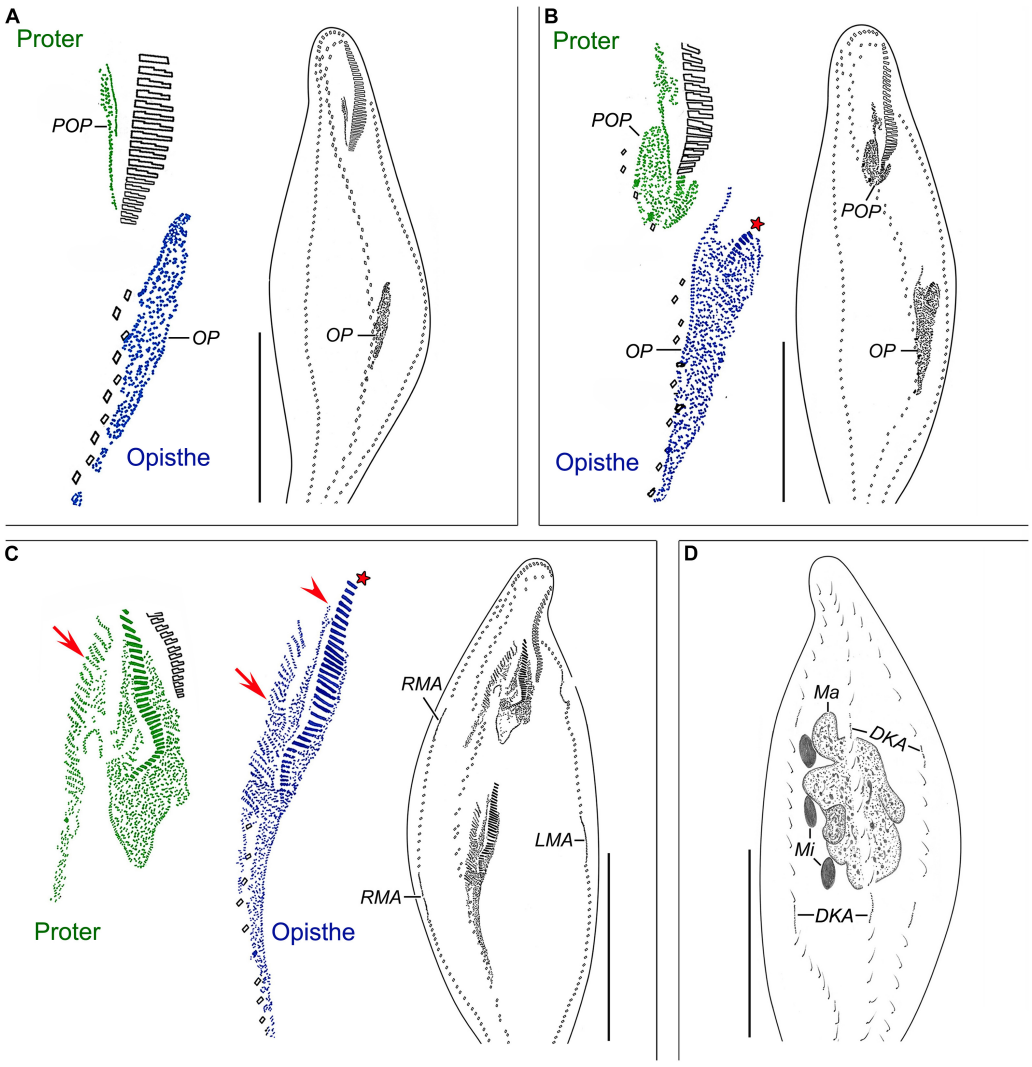

FIGURE 3 | *Nothoholosticha luporinii* n. sp., early dividers **(A,B)** and a mid-divider **(C,D)** after protargol impregnation. Magnified details of the proter's ciliature are in green colour, while those of the opisthe's ciliature are in blue colour. **(A)** Ventral view of an early divider, showing the formation of oral primordia in the proter and the opisthe. **(B)** Ventral view of another early divider, whose opisthe's oral primordium begins to differentiate into adoral membranelles (red asterisk). **(C,D)** Ventral **(C)** and dorsal **(D)** views of the same early mid-divider. Arrows indicate formation of frontal-ventral–transverse cirral anlagen, arrowhead marks the undulating membranes anlage, asterisk denotes the newly formed adoral membranelles from the opisthe's oral primordium. DKA, dorsal kineties anlagen; LMA, left marginal cirral row anlagen; Ma, macronuclear mass; Mi, micronuclei; OP, opisthe's oral primordium; POP, proter's oral primordium; RMA, right marginal cirral row anlagen. Scale bars = 120 μm.

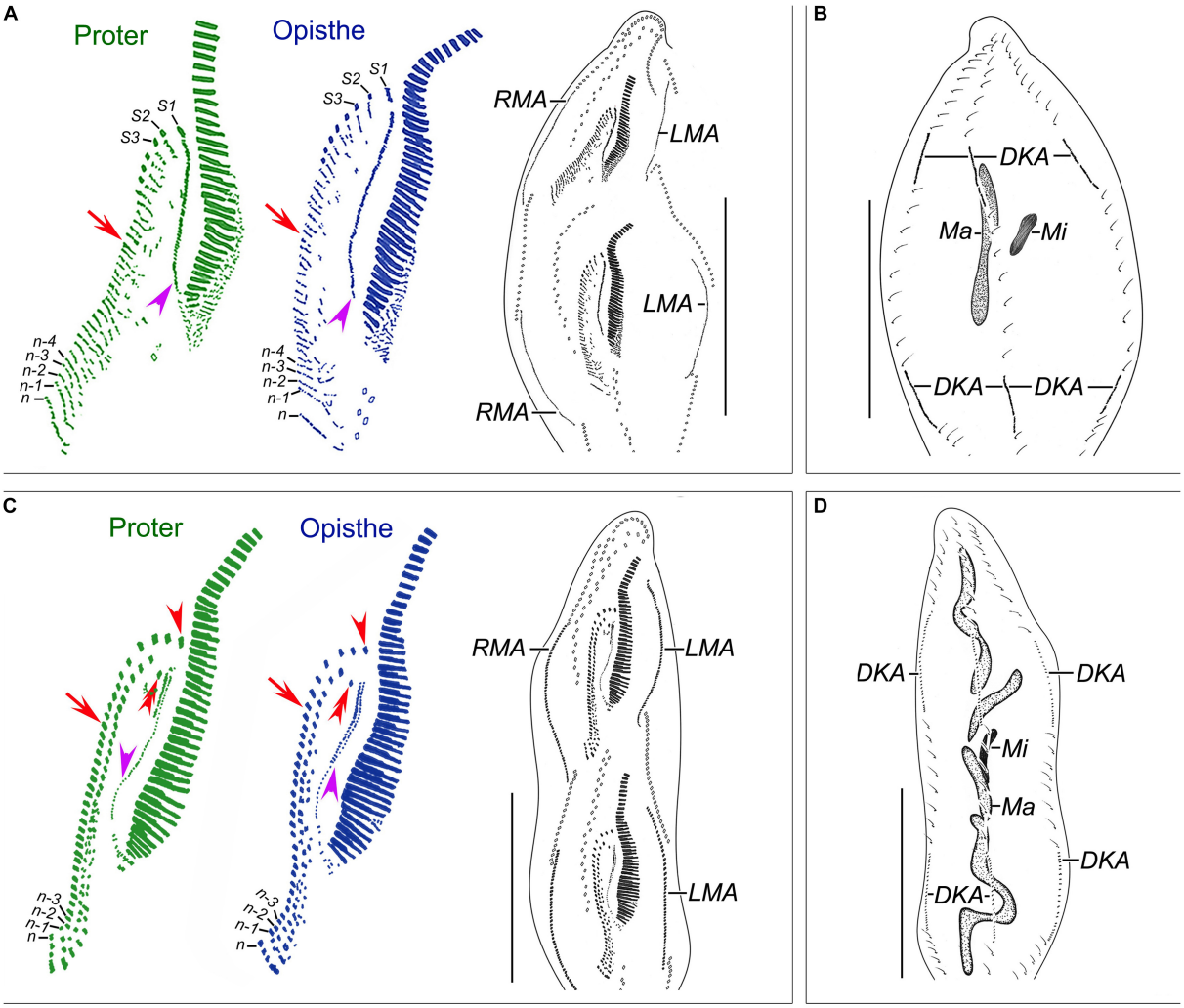

FIGURE 4 | *Nothoholosticha luporinii* n. sp., a late mid-divider **(A,B)** and a late divider **(C,D)** after protargol impregnation. Magnified details of the proter's ciliature are in green colour, while those of the opisthe's ciliature are in blue colour. **(A,B)** Ventral **(A)** and dorsal **(B)** views of a late mid-divider, showing the undulating membrane anlagen (purple arrowheads), frontal-midventral-transverse cirral anlagen (red arrows), the anlagen for marginal cirral rows and dorsal kineties, and the dividing macronuclear mass. **(C,D)** Ventral **(C)** and dorsal **(D)** views of a late divider, showing the buccal cirri (red double-arrowheads), frontal cirri (red arrowheads), undulating membranes (purple arrowheads), frontal-midventral-transverse cirral anlagen differentiating into cirri (red arrows), and dividing macronucleus. DKA, dorsal kinety anlagen; LMA, left marginal cirral row anlagen; Ma, macronucleus; Mi, micronuclei; *n*, last frontal-midventral-transverse cirral anlage; *n–1*, *n–2*, *n–3*, *n–4*, second, third, fourth, and fifth rearmost frontal-midventral-transverse cirral anlagen; RMA, right marginal cirral row anlagen; S1–3, first, second, and third streaks. Scale bars = 140 μm.

anlage I) generates the second frontal cirrus of the anterior row of the bicorona as well as the buccal cirrus, which migrates toward the newly formed paroral membrane in mid-dividers; streak III (FVT anlage II) splits the third frontal cirrus of the anterior row of the bicorona as well as the left frontal cirrus of the posterior row of the bicorona; streak IV (FVT anlage III) produces the rightmost frontal cirrus of the anterior row of the bicorona as well as the right frontal cirrus of the posterior row of the bicorona; the rearmost (rightmost) streak develops the rightmost transverse cirrus and the 3–6 frontoterminal cirri, which migrate anteriorly to their species-specific position during the late division stages; streak $n-1$ (n represents the last FVT cirral anlage) provides the rearmost midventral cirral pair, a single pretransverse cirrus and one transverse cirrus. Streaks $n-2$ to $n-5$ (deduced from morphometric data) contribute one midventral cirral pair and a single transverse cirrus each (**Figures 4C**, **5A,B**, **6L,N–Q**). The remaining streaks (FVT anlagen) provide one midventral cirral pair each (**Figures 5A,B**). When the formation of the new oral apparatus is almost completed in each daughter cell, new cirri migrate to their final positions.

Marginal and Dorsal Anlagen

The proter's left and right marginal cirral row anlagen form within the parental marginal cirral rows, very likely by dissociation of some cirri, about at level of the growing

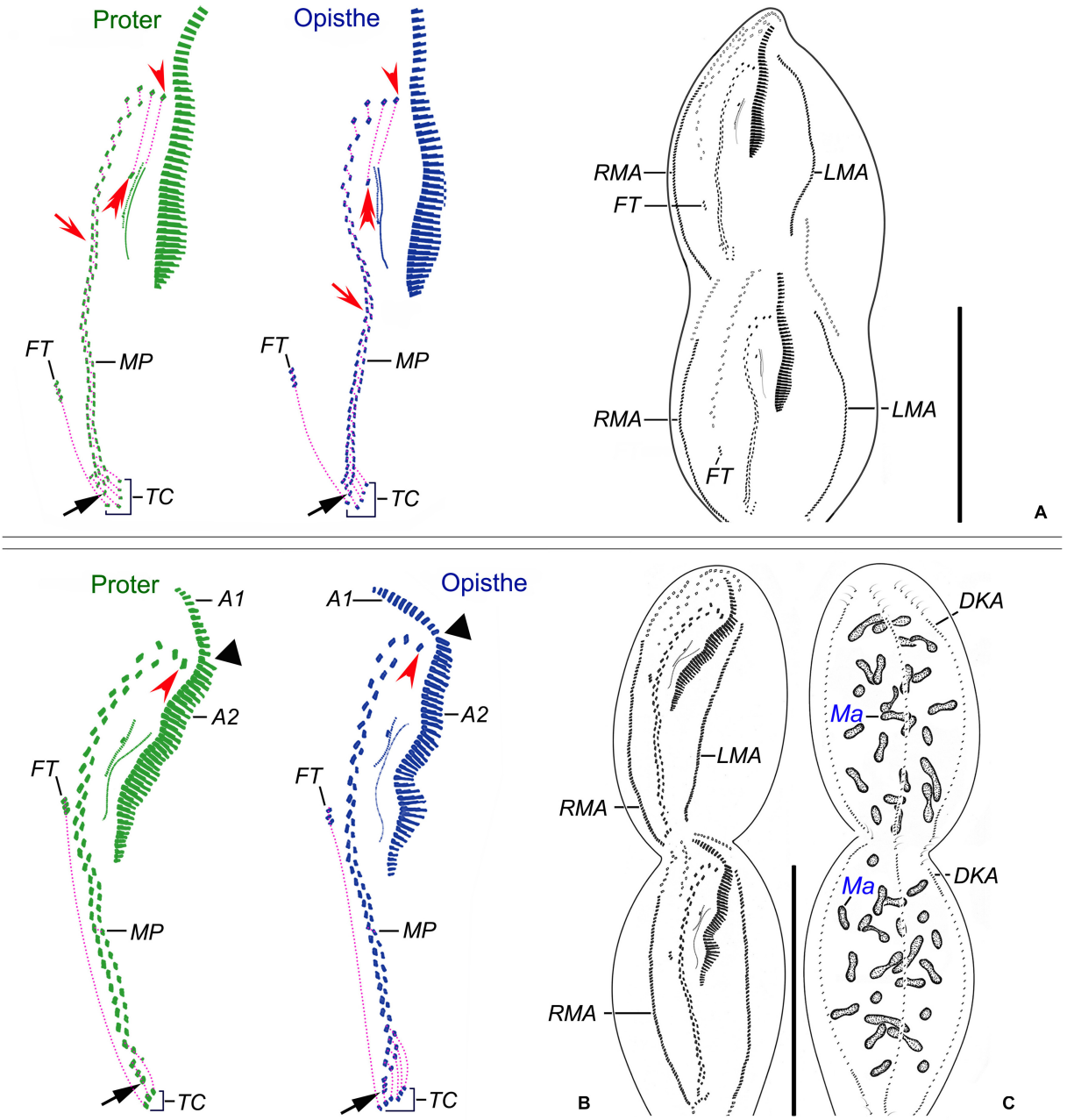

FIGURE 5 | *Nothoholosticha luporinii* n. sp., a late **(A)** and a very late **(B,C)** divider after protargol impregnation. Magnified details of the proter's ciliature are in green colour, while those of the opisthe's ciliature are in blue colour. Frontal-ventral-transverse cirri originating from the same anlagen are connected by dotted lines. **(A)** Ventral view of a late divider, showing the buccal cirri (red double-arrowheads), the leftmost frontal cirri (red arrowheads), the single pretransverse cirri (black arrows), and the migrating frontoterminal cirri. **(B,C)** Ventral **(B)** and dorsal **(C)** views of a very late divider, showing the formation of a gap in the adoral zone of membranelles (black triangles) as well as the formation of the anlagen for marginal cirral rows and dorsal kineties. The leftmost frontal cirri are marked by red arrowheads, the pretransverse cirri by black arrows. A1 and A2, crown and lapel adoral membranelles; DKA, dorsal kinety anlagen; FT, frontoterminal cirri; LMA, left marginal cirral row anlagen; Ma, macronuclear nodules; MP, midventral cirral pairs; RMA, right marginal cirral row anlagen; TC, transverse cirri. Scale bars = 140 μm.

proter's oral primordium. Similarly, the opisthe's left and right marginal cirral row anlagen develop within the parental marginal cirral rows about at level of the opisthe's oral primordium (**Figures 3C**, **6I**). The marginal row anlagen extend posteriorly, gradually producing new cirri already in early mid-dividers and stretch toward both ends of the dividing cell to form new ones for each daughter cell (**Figures 4A,C**, **5A,B**). The morphogenesis of the dorsal side ciliature begins in mid-dividers (**Figure 3D**). Specifically, within-row primordia appear in the parental dorsal kineties at two sites, viz., anterior and posterior to

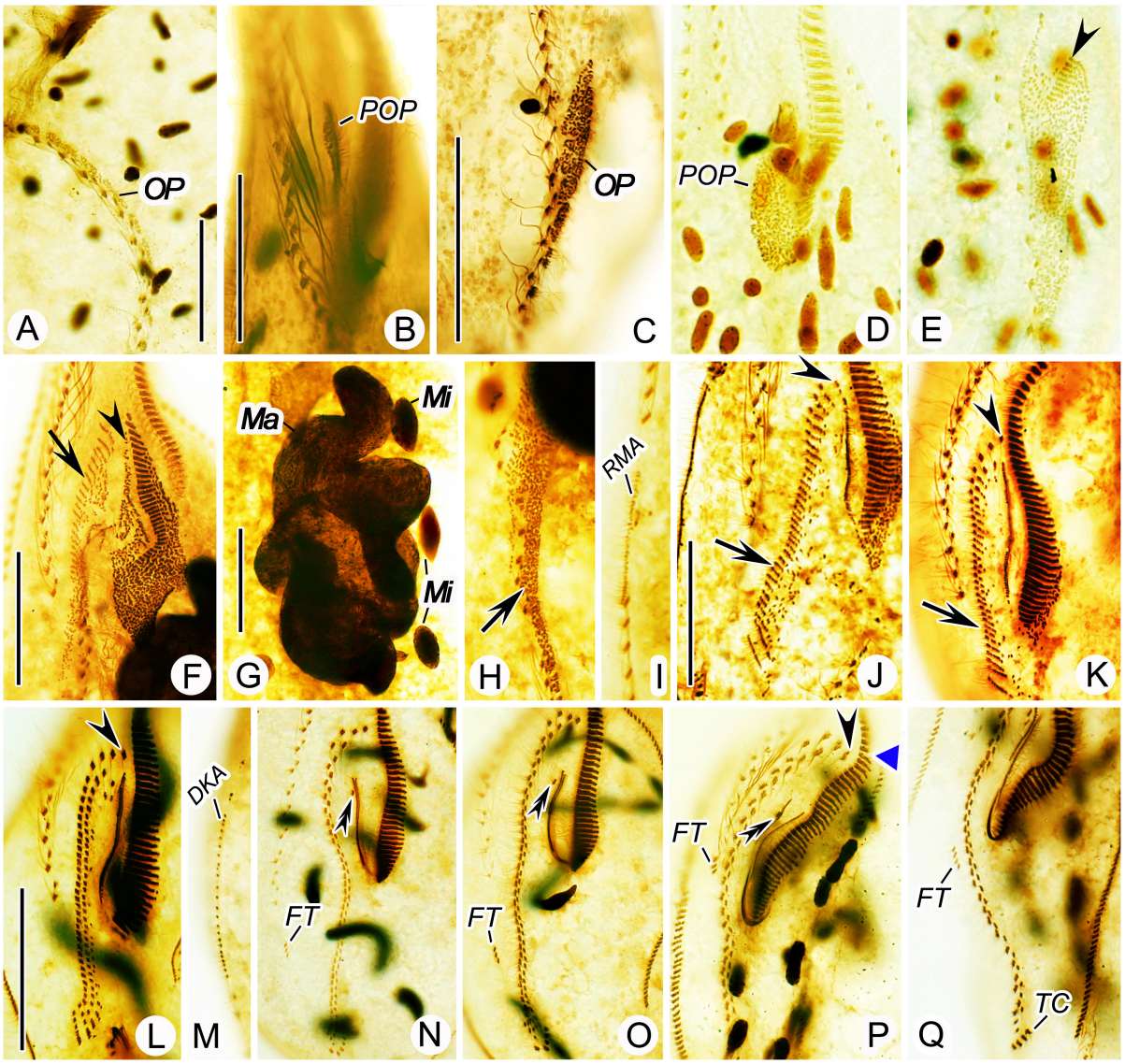

FIGURE 6 | *Nothoholosticha luporinii* n. sp., various division stages after protargol impregnation. **(A)** Ventral view of an early divider, showing the opisthe's oral primordium. **(B,C)** Ventral view of an early divider, showing the oral primordium in the proter **(B)** and the opisthe **(C)**. **(D,E)** Ventral view of another early divider, arrow marks the proter's oral primordium **(D)** and arrowhead denotes the differentiating adoral membranelles from the opisthe's oral primordium **(E)**. **(F–I)** Ventral view of an early mid-divider, showing the undulating membranes anlage (arrowheads) and the frontal-midventral-transverse cirral anlagen (arrows) in **(F,H)**, the fusing macronuclear nodules and dividing fusiform micronuclei in **(G)**, the right marginal cirral row anlage in **(I)**. **(J,K)** Ventral view of a mid-divider, showing the leftmost frontal cirrus originating from the undulating membranes anlage (arrowheads) and the frontal-midventral-transverse cirral anlagen (arrows) in the proter **(J)** and the opisthe **(K)**. **(L–Q)** Details of different late dividers, showing the leftmost frontal cirrus (arrowheads) in **(L,P)**, the buccal cirrus (double-arrowheads) in **(N–P)**, the forming gap in the adoral zone of membranelles (blue triangle) in **(P)**, the migrating frontoterminal cirri in **(N–Q)**, the transverse cirri in **(Q)**, and the dorsal kinety anlage in **(M)**. DKA, dorsal kinety anlage; FT, frontoterminal cirri; Ma, macronuclear nodules; Mi, micronuclei; OP, opisthe's oral primordium; POP, proter's oral primordium; RMA, right marginal cirral row anlage; TC, transverse cirri. Scale bars = 30 μm **(F–K)**, 40 μm **(A–E)**, and 60 μm **(L–Q)**.

the prospective fission area (**Figure 4B**). The new dorsal kineties elongate and obtain their characteristic positions in late dividers (**Figures 4D**, **5C**, **6M**).

Nuclear Division

The macronuclear nodules fuse in mid-dividers to a branched mass (**Figures 3D**, **6G**), becoming oblong before and during the cell fission (**Figure 4B**). The elongate macronucleus divides into two pieces in late mid-dividers (**Figure 4D**). Each piece develops into a tree-dimensional macronuclear reticulum that gradually fragments into individual ellipsoidal nodules in very late dividers (**Figure 5C**). Micronuclei divide only once during the middle stages of binary fission (**Figures 3D**, **4B,D, 6G**). More specifically, the micronuclei become spindle-shaped when the macronuclear nodules are fused into a branched mass (**Figures 3D**, **6G**). Then, the micronuclei assume a dumbbell-shaped morphology

as the macronuclear mass elongates into an oblong structure constricted in the middle (**Figure 4B**). Finally, the daughter micronuclei are connected by an internal fiber bundle that conspicuously elongates in late dividers. During the post-divisional patterning, the micronuclei move to the scattered macronuclear nodules (**Figure 5C**).

Phylogenetic Analyses

Both maximum likelihood (ML) and Bayesian (BI) trees were constructed to determine the phylogenetic position of *N. luporinii* n. sp. (**Figures 7**, **8**). Although the taxon sampling slightly differed between the single- and multi-gene datasets, *N. luporinii* was consistently assigned to the order Urostylida with very strong or full statistical support. All members of the family Pseudokeronopsidae, including *N. luporinii*, always clustered together with *Anteholosticha pulchra* with full statistical support. Monophylies of the Pseudokeronopsinae and Nothoholostichinae were strongly to fully statistically supported in phylogenetic analyses of both single- and multi-gene datasets. The Pseudokeronopsinae clustered with the Nothoholostichinae in the multi-gene trees, but with very weak support (50% ML, 0.79 BI). On the other hand, their sister-group relationship was not recognized in the single-gene trees, as the Pseudokeronopsinae grouped with *A. pulchra*, but with very weak support (63% ML, 0.62 BI).

According to the single-gene and multi-gene trees, *N. luporinii* clustered with full statistical support in the monophyletic subfamily Nothoholostichinae, which encompasses *N. fasciola*, *N. flava*, *Heterokeronopsis pulchra* Pan et al., 2013, and *Apoholosticha sinica* Fan et al., 2014a. Within this subfamily,

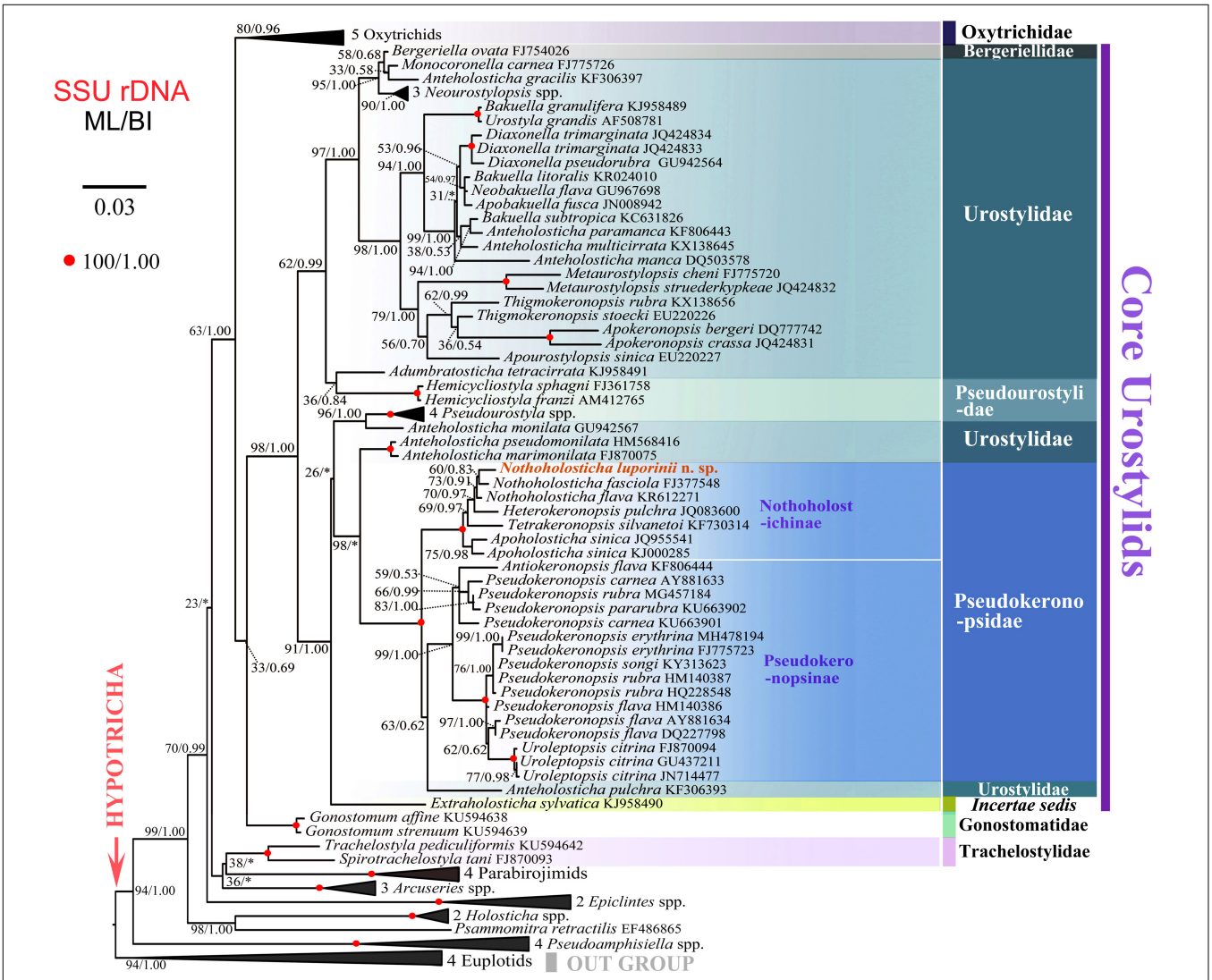

FIGURE 7 | Maximum likelihood tree inferred from SSU rDNA sequences, showing the systematic position of *Nothoholosticha luporinii* n. sp. (indicated in red). Numbers near branches denote bootstrap values for maximum likelihood (ML) and posterior probabilities for Bayesian inference (BI). Asterisk indicates the disagreement between ML and BI trees. GenBank accession numbers are provided after species names. For taxon sampling and GenBank accession numbers in the collapsed clades, see **Supplementary Table S1**. Scale bar corresponds to three substitutions per 100 nucleotide positions.

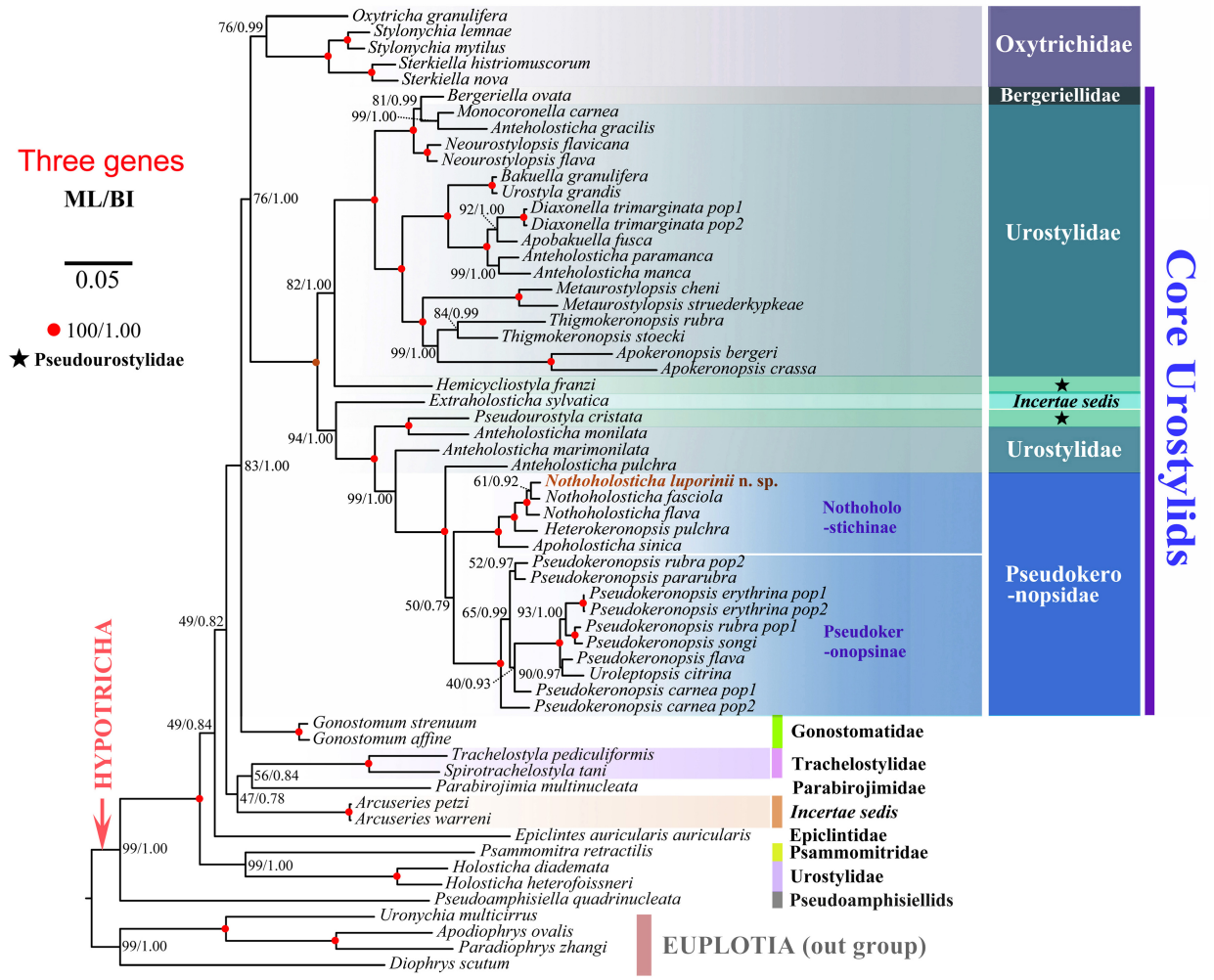

FIGURE 8 | Maximum likelihood tree inferred from SSU rDNA, ITS region and LSU rDNA sequences, showing the systematic position of *Nothoholosticha luporinii* n. sp. (indicated in red). Numbers near branches denote bootstrap values for maximum likelihood (ML) and posterior probabilities for Bayesian inference (BI). GenBank accession numbers are provided in **Supplementary Table S2**. Scale bar corresponds to five substitutions per 100 nucleotide positions.

the genus *Nothoholosticha* was depicted as monophyletic with very weak support in the single-gene analyses (73% ML, 0.91 BI), but with full statistical support in the multi-gene analyses. *Nothoholosticha luporinii* was shown to be most closely related to *N. fasciola*, but this relationship was very poorly statistically supported in all analyses. According to the multi-gene analyses, *Nothoholosticha* was sister to the monotypic genus *Heterokeronopsis*. And, finally, *Apoholosticha* was placed in a sister position to the *Nothoholosticha-Heterokeronopsis* cluster in the multi-gene trees.

The number of unmatched nucleotide positions and the pairwise SSU rDNA sequence similarities among members of the subfamily Nothoholostichinae are summarized in **Table 2**. *Nothoholosticha luporinii* differs from *N. flava* by 13 nucleotide positions (99.1% sequence identity), from *N. fasciola* by 14 nucleotides (99.1% identity), from *H. pulchra* by 21 nucleotides (98.6% identity), from *T. silvanetoi* by 26 nucleotides (98.3% identity, the 121 Ns positions in the *T. silvanetoi* sequence were coded according to other related species as this region was fully conserved), from *A. sinica* population 1 by 26 nucleotides (98.3% identity), and from *A. sinica* population 2 by 25 nucleotides (98.4% identity).

DISCUSSION

The New Species *Nothoholosticha luporinii*

Nothoholosticha luporinii n. sp. can be easily separated from members of the genera *Anteholosticha*, *Antiokeronopsis*, *Pseudokeronopsis*, and *Uroleptopsis* by having an atypical bicorona composed of four anterior and two posterior frontal cirri (vs. only three frontal cirri in *Anteholosticha* and more than four anterior coronal cirri in the three latter genera); from members of the genus *Apoholosticha* by possessing (vs. lacking) buccal cirri; and from *Heterokeronopsis* by exhibiting

TABLE 2 | Numbers of unmatched nucleotides (above diagonal) and pairwise similarities (below diagonal) of SSU rDNA sequences among members of the subfamily Nothoholostichinae.

Species	1	2	3	4	5	6	7
1 *Nothoholosticha luporinii* n. sp. (accession number: MW035040)		13	14	21	26	26	25
2 *Nothoholosticha flava* (accession number: KR612271)	0.991		7	15	20	19	16
3 *Nothoholosticha fasciola* (accession number: FJ377548)	0.991	0.995		18	24	22	19
4 *Heterokeronopsis pulchra* (accession number: JQ083600)	0.986	0.990	0.998		28	22	23
5 *Tetrakeronopsis silvanetoi* (accession number: KF730314)	0.983	0.909	0.987	0.982		24	27
6 *Apoholosticha sinica* pop. 1 (accession number: JQ955541)	0.983	0.987	0.985	0.985	0.984		11
7 *Apoholosticha sinica* pop. 2 (accession number: KJ000285)	0.984	0.989	0.987	0.985	0.982	0.992	

(vs. lacking) frontoterminal and transverse cirri. On the other hand, the new species highly resembles taxa assigned to the genera *Nothoholosticha* and *Tetrakeronopsis* (**Figure 9**). Hitherto, *Nothoholosticha* comprises two species, *N. fasciola* and *N. flava*, while *Tetrakeronopsis* is monotypic and includes only *T. silvanetoi*.

Our newly discovered species cannot be confused with *N. fasciola*, the type species of *Nothoholosticha*, because it lacks frontoterminal cirri (Li et al., 2009). On the other hand, *N. luporinii* highly resembles *N. flava* in the body shape and size as well as in the number and arrangement of the macronuclear nodules and cirri (Li et al., 2016). Morphologically, *N. luporinii* can be distinguished from *N. flava* only by the lower number of crown (7–13 vs. 13–18) and lapel (23–39 vs. 36–47) adoral membranelles. However, the proper identification requires molecular data, because both differentiating characters partially overlap. The SSU rDNA sequences of *N. luporinii* and *N. flava* differ in 13 nucleotide positions (**Table 2**), which undoubtedly supports the distinctness of both taxa.

Because of the high morphological similarity, it might be speculated whether *N. luporinii* should not be classified as a subspecies of *N. flava*. However, the 13 different nucleotide positions in the SSU rDNA stand strongly against this suggestion. This is, indeed, a very pronounced genetic difference as the SSU rRNA gene is highly conservative with a rate of only 1.24–3.96 $\times$ 10^{-4} substitutions per site per one million years (Wright and Lynn, 1997; Vďačný, 2015; Vďačný et al., 2019). Kumar et al. (2017) showed that one base pair difference in SSU rDNA is sufficient to separate two closely related hypotrich taxa. Although *Bistichella variabilis* (HQ699895), *Uroleptoides magnigranulosus* (AM412774), and *Orthoamphisiella breviseries* (AY498654) are classified in different genera on the basis of morphological data, they differ only by 5–9 nucleotide positions (99.5–99.7% identity) in their SSU rDNA sequences (He and Xu, 2011). In this light, we find the species status of *N. luporinii* proposed in the present study to be justified.

Finally, *N. luporinii* can be distinguished from *T. silvanetoi* by the higher number of frontoterminal cirri (3–6 vs. invariably 2), the lower number of pretransverse cirri (1 vs. 2), the lower number of crown (7–13 vs. 12–17) and lapel (23–39 vs. 40–52) adoral membranelles as well as by the arrangement of the smaller type of bright brown–reddish cortical granules (clustered in a flower-like pattern around dorsal bristles vs. loosely scattered throughout the cortex). The morphological differences are supported also by the genetic differences in SSU rDNA sequences. Thus, there are 21 unmatched nucleotides between *N. luporinii* and *T. silvanetoi* (**Table 2**).

Generic Classification of *Nothoholosticha luporinii*

Generic classification of hypotrichs is traditionally based on the cirral and oral patterns as well as on the morphogenesis of the ventral and the dorsal ciliature (for reviews, see Berger, 1999, 2006, 2008, 2011). The generic classification of *N. luporinii* is a difficult matter, because its cirral pattern is a mixture of features found in the type species of *Nothoholosticha* (an "extra" cirrus between the midventral complex and transverse cirri) and the monotypic genus *Tetrakeronopsis* (multiple frontoterminal cirri). More specifically, *N. fasciola*, the type species of *Nothoholosticha*, lacks frontoterminal cirri (Li et al., 2009), which are present not only in two further *Nothoholosticha* species, *N. flava* and *N. luporinii*, but also in *T. silvanetoi* (Paiva et al., 2014; Li et al., 2016; present study). The extra cirrus, situated between the midventral complex and transverse cirri, is interpreted as the last cirrus of the midventral complex in *N. fasciola* and *N. flava* (Li et al., 2009, 2016), while as a pretransverse cirrus in *N. luporinii*. Regardless of the terminology, it is very likely the same cirrus, which is derived from the second rearmost frontal-midventral-transverse cirral streak $n-1$ (**Figures 4C**, **5A,B**). *Tetrakeronopsis* exhibits even two cirri between the midventral complex and transverse cirri. Because these two extra cirri are situated ahead of the rightmost transverse cirri, they also might be designated as pretransverse cirri. The right pretransverse cirrus is derived from the rearmost streak n and the left pretransverse cirrus from the second rearmost streak $n-1$ (Paiva et al., 2014). In this light, all *Nothoholosticha* species have retained only the left pretransverse cirrus and *N. fasciola* further lost the frontoterminal cirri, which are derived from the rearmost streak n in *N. luporinii* and *Tetrakeronopsis* (**Figure 9**). Because *N. luporinii* is more closely related to *N. fasciola* than to *T. silvanetoi* in SSU DNA phylogenies (**Figure 7**), we classify our new species in the genus *Nothoholosticha*. However, the results of the present phylogenetic analyses question the generic diagnostic value of the loss of frontoterminal and pretransverse cirri in *N. fasciola*, which are derived from the two rearmost frontal-midventral-transverse cirral anlagen. Nevertheless, we prefer to await discovery

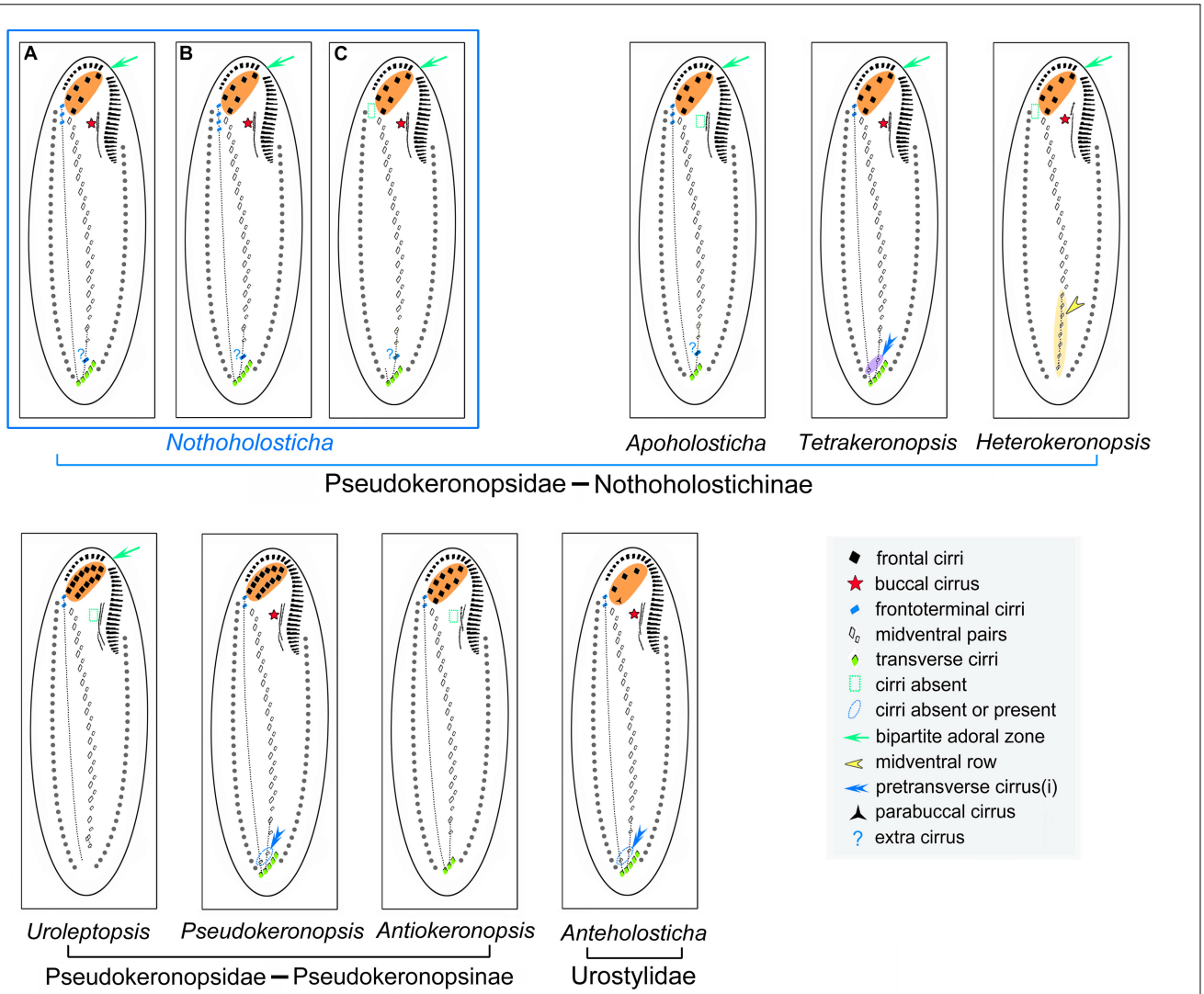

FIGURE 9 | Comparison of cirral patterns of some related urostylid genera. Cirri originating from the two rightmost (rearmost) frontal-midventral-transverse anlagen are connected by a dotted line. **(A)** *N. luporinii* n. sp. **(B)** *N. flava*. **(C)** *N. fasciola*. Note that the "extra" cirrus is regarded as a pretransverse cirrus in *N. luporinii* **(A)**, while as a midventral cirrus in the two remaining *Nothoholosticha* species **(B,C)**.

of further species to improve the diagnosis of the genus *Nothoholosticha*.

Classification Framework of the Subfamily Nothoholostichinae

The structure of the bicorona represents an important subfamily-level character that was used to divide the family Pseudokeronopsidae into two subfamilies by Paiva et al. (2014): the Nothoholostichinae, with an atypical bicorona whose anterior portion is formed by four frontal cirri, and the Pseudokeronopsinae, with a typical bicorona whose anterior portion is formed by more than four frontal cirri. The present phylogenetical analyses corroborate this subdivision as well as the monophyletic origin of the Nothoholostichinae (**Figures 7**, **8**). Interestingly, there are as many as three monotypic genera within the subfamily Nothoholostichinae. However, they can be easily distinguished from each other either by the loss or by the retention of some cirri, with respect to the type genus *Nothoholosticha*. Thus, *Apoholosticha* lost the buccal cirrus, *Heterokeronopsis* lost the frontoterminal and transverse cirri, while *Tetrakeronopsis* maintained both the left and the right pretransverse cirrus (Pan et al., 2013; Fan et al., 2014a; Paiva et al., 2014; Hu et al., 2015; **Figure 9**), which seems to be the plesiomorphic condition in the family Pseudokeronopsidae. Remarkably, frontoterminal cirri were lost in *Heterokeronopsis* and *N. fasciola*, but not in any other *Nothoholosticha* species. Homoplastic nature of this character thus questions its taxonomic significance at genus level. On the other hand, the loss of the buccal cirrus in *Heterokeronopsis* and of the right pretransverse cirrus in *Nothoholosticha* might serve as good generic characters at the present state of knowledge. Likewise,

the long midventral row found in *Heterokeronopsis*, seems to be another good generic diagnostic feature for separation of genera within the subfamily Nothoholostichinae.

Multi-Gene Phylogenetic Analyses of the Family Pseudokeronopsidae

The SSU rRNA gene is very conservative and it is generally known that it bears mainly information for deeper nodes of phylogenetic trees. Therefore, manifold studies pursued to improve the knowledge about phylogenetic interrelationships within the subclass Hypotrichia using mostly sequences of that gene (e.g., Luo et al., 2017, 2018; Song and Shao, 2017; Lyu et al., 2018; Kim and Min, 2019; Chen et al., 2020; Dong et al., 2020; Paiva, 2020; Park et al., 2020; Wang J. et al., 2020; Xu et al., 2020). On the other hand, the ITS1-5.8S-ITS2 region as well as the LSU rRNA gene are much faster evolving parts of the rDNA operon and hence bear phylogenetic signal also for more recent divergences (Abraham et al., 2019). Therefore, the concatenation of SSU rDNA, ITS1-5.8S-ITS2 region and LSU rDNA might lead to better resolved phylogenetic trees, as also evidenced in the present study (**Figures 7**, **8**). For instance, *Anteholosticha pulchra*, a typical urostylid, clustered in a sister position to the subfamily Pseudokeronopsinae in the SSU rDNA tree, causing non-monophyly of the family Pseudokeronopsidae (**Figure 7**), as defined by Paiva et al. (2014). On the other hand, *A. pulchra* was placed outside the Pseudokeronopsidae in the multi-gene trees although the statistical support remained poor (**Figure 8**). This position is, however, much more consistent with morphological classifications, because *A. pulchra* possesses three enlarged frontal cirri while pseudokeronopsids have a bicorona. The internal branching pattern within the subfamilies Pseudokeronopsinae and Nothoholostichinae as well as the placement of the new species within the genus *Nothoholosticha* were also much better statistically supported in multi-gene than in the single-gene analyses (**Figures 7**, **8**). Likewise, the sister-group relationship of *Uroleptopsis citrina* and *Pseudokeronopsis flava* within the Pseudokeronopsinae obtained much better support in the multi-gene trees. Thus, the whole rDNA operon strongly suggests that the genus *Pseudokeronopsis* is non-monophyletic and might be split into multiple genera in future. *Pseudokeronopsis* species are, however, highly similar in terms of their nuclear apparatus and cirral patterns (for details, see Li et al., 2017). This was the main reason why multiple species were synonymized, misidentified, or their species status was questioned. Nevertheless, the distinctness of most *Pseudokeronopsis* species was corroborated by analyses of SSU rDNA sequences along with ITS-5.8S rDNA sequences (Li et al., 2017). To summarize, the combination of the traditionally used SSU rDNA sequences with ITS region and LSU rDNA sequences improves phylogenetic inferences and classifications of pseudokeronopsids in specific and of ciliates in general.

DATA AVAILABILITY STATEMENT

GenBank accession numbers of sequences used in phylogenetic analyses can be found in the **Supplementary Material**.

AUTHOR CONTRIBUTIONS

WS and CS conceptualized the project. TZ and TC performed the laboratory work. TZ, YW, and JM prepared the data sets and conducted analyses. TZ and PV wrote the first draft of the article. YW, CS, and WS revised the manuscript. All authors approved the final version of the manuscript.

FUNDING

This work was supported by the National Natural Science Foundation of China (Project numbers: 32070428 and 32030015) and by the Slovak Research and Development Agency (grant number APVV-19-0076) and by the Grant Agency of the Ministry of Education, Science, Research and Sport of the Slovak Republic and Slovak Academy of Sciences (grant number VEGA 1/0041/17).

SUPPLEMENTARY MATERIAL

The Supplementary Material for this article can be found online at: https://www.frontiersin.org/articles/10.3389/fmars.2020.610886/full#supplementary-material

REFERENCES

Abraham, J. S., Sripoorna, S., Maurya, S., Makhija, S., Gupta, R., and Toteja, R. (2019). Techniques and tools for species identification in ciliates: a review. *Int. J. Syst. Evol. Microbiol.* 69, 877–894. doi: 10.1099/ijsem.0.003176

Anson, E. L., and Myers, E. W. (1997). ReAligner: a program for refining DNA sequence multi-alignments. *J. Comput. Biol.* 4, 369–383. doi: 10.1089/cmb.1997.4.369

Berger, H. (1999). Monograph of the Oxytrichidae (Ciliophora, Hypotrichia). *Monogr. Biol.* 78, 1–1080. doi: 10.1007/978-94-011-4637-1

Berger, H. (2006). Monograph of the Urostyloidea (Ciliophora, Hypotricha). *Monogr. Biol.* 85, 1–1304. doi: 10.1007/1-4020-5273-1_1

Berger, H. (2008). Monograph of the Amphisiellidae and Trachelostylidae (Ciliophora, Hypotricha). *Monogr. Biol.* 88, 1–737. doi: 10.1007/978-1-4020-8917-6

Berger, H. (2011). Monograph of the Gonostomatidae and Kahliellidae (Ciliophora, Hypotricha). *Monogr. Biol.* 90, 1–741. doi: 10.1007/978-94-007-0455-8

Bharti, D., Kumar, S., Terza, A. L., and Chandra, K. (2019). Morphology and ontogeny of *Tetmemena pustulata indica* nov. subspec. (Ciliophora, Hypotricha), from the Thane Creek, Mumbai, India. *Eur. J. Protistol.* 71:125629. doi: 10.1016/j.ejop.2019.125629

Borror, A., and Wicklow, B. (1983). The suborder Urostylina Jankowski (Ciliophora, Hypotrichida): morphology, systematics and identification of species. *Acta Protozool.* 22, 97–126.

Chen, L., Dong, J., Xin, Y., Warren, A., Ning, Y., and Zhao, Y. (2020). Morphology and molecular phylogeny of a new hypotrich ciliate, *Anteholosticha songi* nov. spec., and an American population of *Holosticha pullaster* (Muller, 1773) Foissner et al., 1991 (Ciliophora, Hypotricha). *Eur. J. Protisotol.* 72:125646. doi: 10.1016/j.ejop.2019.125646

Dong, J., Li, L., Fan, X., Ma, H., and Warren, A. (2020). Two *Urosoma* species (Ciliophora, Hypotrichia): a multidisciplinary approach provides new insights into their ultrastructure and systematics. *Eur. J. Protistol.* 72:125661. doi: 10.1016/j.ejop.2019.125661

Fan, Y., Chen, X., Hu, X., Shao, C., Al-Rasheid, K. A. S., Al-Farraj, S. A., et al. (2014a). Morphology and morphogenesis of *Apoholosticha sinica* n.g., n. sp. (Ciliophora, Hypotrichia), with consideration of its systematic position among urostylids. *Eur. J. Protistol.* 50, 78–88. doi: 10.1016/j.ejop.2013.06.003

Fan, Y., Pan, Y., Huang, J., Lin, X., Hu, X., and Warren, A. (2014b). Molecular phylogeny and taxonomy of two novel brackish water hypotrich ciliates, with the establishment of a new genus, *Antiokeronopsis* gen. n. (Ciliophora, Hypotrichia). *J. Eukaryot. Microbiol.* 61, 449–462. doi: 10.1111/jeu.12125

Galtier, N., Gouy, M., and Gautier, C. (1996). SEAVIEW and PHYLO_WIN: two graphic tools for sequence alignment and molecular phylogeny. *Comput. Appl. Biosci.* 12, 543–548. doi: 10.1093/bioinformatics/12.6.543

Gong, R., Jiang, Y., Vallesi, A., Gao, Y., and Gao, F. (2020). Conjugation in Euplotes raikovi (Protista, Ciliophora): new insights into nuclear events and macronuclear development from micronucleate and amicronucleate cells. *Microorganisms*, 8:162. doi: 10.3390/microorganisms8020162

Gouy, M., Guindon, S., and Gascuel, O. (2010). SeaView version 4: a multiplatform graphical user interface for sequence alignment and phylogenetic tree building. *Mol. Biol. Evol.* 27, 221–224. doi: 10.1093/molbev/msp259

Hall, T. A. (1999). BioEdit: a user-friendly biological sequence alignment editor and analysis program for Windows 95/98/NT. *Nucleic Acids Symp. Ser.* 41, 95–98. doi: 10.1021/bk-1999-0734.ch008

He, Y., and Xu, K. (2011). Morphology and small subunit rDNA phylogeny of a new soil ciliate, *Bistichella variabilis* n. sp. (Ciliophora, Stichotrichia). *J. Eukaryot. Microbiol.* 58, 332–338. doi: 10.1111/j.1550-7408.2011.00554.x

Hu, X., Fan, Y., and Warren, A. (2015). New record of *Apoholosticha sinica* (Ciliophora, Urostylida) from the UK: morphology, 18S rRNA gene phylogeny and notes on morphogenesis. *Int. J. Syst. Evol. Microbiol.* 40, 78–92. doi: 10.1016/j.ejop.2016.09.005

Hu, X., Lin, X., and Song, W. (2019). *Ciliate atlas: Species Found in the South China Sea*. Beijing: Science Press. doi: 10.1007/978-981-13-5901-9

Huang, J., Chen, Z., Song, W., and Berger, H. (2014). Three-gene based phylogeny of the Urostyloidea (Protista, Ciliophora, Hypotricha), with notes on classification of some core taxa. *Mol. Phylogenet. Evol.* 70, 337–347. doi: 10.1016/j.ympev.2013.10.005

Jerome, C. A., Lynn, D. H., and Simon, E. M. (1996). Description of *Tetrahymena empidokyrea* n. sp., a new species in the *Tetrahymena pyriformis* sibling species complex (Ciliophora, Oligohymenophorea), and an assessment of its phylogenetic position using small-subunit rRNA sequences. *Can. J. Zool.* 74, 1898–1906. doi: 10.1139/z96-214

Jung, J. H., and Berger, H. (2019). Monographic treatment of *Paraholosticha muscicola* (Ciliophora, Keronopsidae), including morphological and molecular biological characterization of a brackish water population from Korea. *Eur. J. Protistol.* 68, 48–67. doi: 10.1016/j.ejop.2018.12.004

Kaur, H., Negi, S. R. K., and Kamra, K. (2019). Morphological and molecular characterization of *Neogastrostyla aqua* nov. gen., nov. spec. (Ciliophora, Hypotrichia) from River Yamuna, Delhi; comparison with *Gastrostyla*-like genera. *Eur. J. Protistol.* 68, 68–79. doi: 10.1016/j.ejop.2019.01.002

Kim, K. S., and Min, G. S. (2019). Morphology and molecular phylogeny of *Oxytricha seokmoensis* sp. nov. (Hypotrichia: Oxytrichidae), with notes on its morphogenesis. *Eur. J. Protistol.* 71:125641. doi: 10.1016/j.ejop.2019.125641

Kumar, S., Bharti, D., Shazib, S. U. A., and Shin, M. K. (2017). Discovery of a new hypotrich ciliate from petroleum contaminated soil. *PLoS One* 12:e0178657. doi: 10.1371/journal.pone.0178657

Landan, G., and Graur, D. (2008). Local reliability measures from sets of co-optimal multiple sequence alignments. *Pacific Symp. Biocomput.* 13, 15–24. doi: 10.1142/9789812776136_0003

Li, J., Chen, X., and Xu, K. (2016). Morphology and small subunit rDNA phylogeny of two new marine urostylid ciliates, *Caudiholosticha marina* sp. nov. and *Nothoholosticha flava* sp. nov. (Ciliophora, Hypotrichia). *J. Eukaryot. Microbiol.* 63, 460–470. doi: 10.1111/jeu.12290

Li, J., Zhan, Z., and Xu, K. (2017). Systematics and molecular phylogeny of the ciliate genus *Pseudokeronopsis* (Ciliophora, Hypotrichia). *J. Eukaryot. Microbiol.* 64, 850–872. doi: 10.1111/jeu.12420

Li, L., Zhang, Q., Hu, X., Warren, A., Al-Rasheid, K. A. S., Al-Khedheiry, A. A., et al. (2009). A redescription of the marine hypotrichous ciliate, *Nothoholosticha fasciola* (Kahl, 1932) nov. gen., nov. comb. (Ciliophora: Urostylida) with brief notes on its cellular reorganization and SSU rRNA gene sequence. *Eur. J. Protistol.* 45, 237–248. doi: 10.1016/j.ejop.2009.01.004

Lu, X., Wang, Y., Al-Farraj, S. A., El-Serehy, H., Huang, J., and Shao, C. (2020). The insights into the systematic relationship of *Gastrostyla*-affinitive genera, with report on a new saline soil ciliate genus and new species (Protozoa, Ciliophora). *BMC Evol. Biol.* 20:92. doi: 10.1186/s12862-020-01659-8

Luo, X., Gao, F., Yi, Z., Pan, Y., Al-Farraj, S. A., and Warren, A. (2017). Taxonomy and molecular phylogeny of two new brackish hypotrichous ciliates, with the establishment of a new genus (Protozoa, Ciliophora). *Zool. J. Linn. Soc.* 179, 475–491. doi: 10.1111/zoj.12451

Luo, X., Huang, J., Li, L., Song, W., and Bourland, W. A. (2019). Phylogeny of the ciliate family Psilotrichidae (Protista, Ciliophora), a curious and poorly-known taxon, with notes on two algae-bearing psilotrichids from Guam, USA. *BMC Evol. Biol.* 19:125. doi: 10.1186/s12862-019-1450-z

Luo, X., Yan, Y., Shao, C., Al-Farraj, S. A., Bourland, W. A., and Song, W. (2018). Morphological, ontogenetic and molecular data support strongylidiids as being closely related to Dorsomarginalia (Protozoa, Ciliophora) and reactivation of the family Strongylidiidae Fauré-Fremiet, 1961. *Zool. J. Linn. Soc.* 184, 237–254. doi: 10.1093/zoolinnean/zly001

Lynn, D. H. (2008). *The ciliated Protozoa: Characterization, Classification, and Guide to the Literature*. Dordrecht: Springer.

Lyu, Z., Wang, J., Huang, J., Warren, A., and Shao, C. (2018). Multigene-based phylogeny of Urostylida (Ciliophora, Hypotrichia), with establishment of a novel family. *Zool. Scr.* 47, 243–254. doi: 10.1111/zsc.12267

Medlin, L., Elwood, H. J., Stickel, S., and Sogin, M. L. (1988). The characterization of enzymatically amplified eukaryotic 16S-like rRNA-coding regions. *Gene* 71, 491–499. doi: 10.1016/0378-1119(88)90066-2

Miao, M., Warren, A., Song, W., Wang, S., Shang, H., and Chen, Z. (2008). Analysis of the internal transcribed spacer 2 (ITS2) region of scuticociliates and related taxa (Ciliophora, Oligohymenophorea) to infer their evolution and phylogeny. *Protist* 159, 519–533. doi: 10.1016/j.protis.2008.05.002

Moreira, D., von der Heyden, S., Bass, D., López-García, P., Chao, E., et al. (2007). Global eukaryote phylogeny: combined small- and large-subunit ribosomal DNA trees support monophyly of Rhizaria, Retaria and Excavata. *Mol. Phylogenet. Evol.* 44, 255–266. doi: 10.1016/j.ympev.2006.11.001

Nylander, J. (2004). *MrModeltest, v.2. Uppsala: Evolutionary Biology Centre*. Sweden: Uppsala University.

Paiva, T. D. (2020). Systematic redefinition of the Hypotricha (Alveolata, Ciliophora) based on combined analyses of morphological and molecular characters. *Protist* 171:125755. doi: 10.1016/j.protis.2020.125755

Paiva, T. D., de Albuquerque, A. F., Borges, B. N., and Harada, M. L. (2014). Description and phylogeny of *Tetrakeronopsis silvanetoi* gen. nov., sp. nov. (Hypotricha, Pseudokeronopsidae), a new benthic marine ciliate from Brazil. *PLoS One* 9:e88954. doi: 10.1371/journal.pone.0088954

Pan, Y., Li, J., Li, L., Hu, X., Al-Rasheid, K. A. S., and Warren, A. (2013). Ontogeny and molecular phylogeny of a new marine ciliate genus, *Heterokeronopsis* g. n. (Protozoa, Ciliophora, Hypotricha), with description of a new species. *Eur. J. Protistol.* 49, 298–311. doi: 10.1016/j.ejop.2012.08.008

Park, K. M., Jung, J. H., Kim, J. H., Min, G. S., and Kim, S. (2020). Morphology, morphogenesis, and molecular phylogeny of a new freshwater ciliate, *Gonostomum jangbogoensis* n. sp. (Ciliophora, Hypotricha), from Victoria Land, Antarctica. *Eur. J. Protistol.* 73:125669. doi: 10.1016/j.ejop.2019.125669

Ronquist, F., Teslenko, M., van der Mark, P., Ayres, D. L., Darling, A., Höhna, S., et al. (2012). MrBayes 3.2: efficient Bayesian phylogenetic inference and model choice across a large model space. *Syst. Biol.* 61, 539–542. doi: 10.1093/sysbio/sys029

Sela, I., Ashkenazy, H., Katoh, K., and Pupko, T. (2015). GUIDANCE2: accurate detection of unreliable alignment regions accounting for the uncertainty of multiple parameters. *Nucleic Acids Res.* 43, W7–W14. doi: 10.1093/nar/gkv318

Shao, C., Chen, X., and Jiang, J. (2020). *Hypotrichous ciliates in China*. Beijing: Science Press.

Sheng, Y., Duan, L., Cheng, T., Qiao, Y., Stover, N. A., and Gao, S. (2020). The completed macronuclear genome of a model ciliate Tetrahymena thermophila and its application in genome scrambling and copy number analyses. *Sci. China Life Sci.* 63, 1534–1542. doi: 10.1007/s11427-020-1689-4

Song, W., and Shao, C. (2017). *Ontogenetic Patterns of Hypotrich Ciliates*. Beijing: Science Press.

Stamatakis, A. (2014). RAxML v.8: a tool for phylogenetic analysis and post-analysis of large phylogenies. *Bioinformatics* 30, 1312–1313. doi: 10.1093/bioinformatics/btu033

Vďačný, P. (2015). Estimation of divergence times in litostomatean ciliates (Ciliophora: Intramacronucleata), with Bayesian relaxed clock and 18S rRNA gene. *Eur. J. Protistol.* 51, 321–334. doi: 10.1016/j.ejop.2015.06.008

Vďačný, P., Rajter, Ľ, Stoeck, T., and Foissner, W. (2019). A proposed timescale for the evolution of armophorean ciliates: clevelandellids diversify more rapidly than metopids. *J. Eukaryot. Microbiol.* 66, 167–181. doi: 10.1111/jeu.12641

Wang, J., Zhao, Y., Lu, X., Lyu, Z., Warren, A., and Shao, C. (2020). Does the *Gonostomum*-patterned oral apparatus in Hypotrichia carry a phylogenetic signal? Evidence from morphological and molecular data based on extended taxon sampling using three nuclear genes (Ciliophora, Spirotrichea). *Sci. China Life Sci.* 63. doi: 10.1007/s11427-020-1667-3

Wang, Y. R., Jiang, Y., Liu, Y., Li, Y., Katz, L. A., Gao, F., et al. (2020). Comparative studies on the polymorphism and copy number variation of mtSSU rDNA in ciliates (Protista, Ciliophora): implications for pylogenetic, environmental, and ecological research. *Microorganisms* 8:316. doi: 10.3390/microorganisms8030316

Wang, Y. Y., Sheng, Y., Liu, Y., Zhang, W., Cheng, T., Duan, L., et al. (2019). A distinct class of eukaryotic MT-A70 methyltransferases maintain symmetric DNA N6-adenine methylation at the ApT dinucleotides as an epigenetic mark associated with transcription. *Nucleic Acids Res.* 47, 11771–11789. doi: 10.1093/nar/gkz1053

Wilbert, N. (1975). Eine verbesserte Technik der Protargolimprägnation für Ciliaten. *Mikrokosmos* 64, 171–179.

Wright, A. D. G., and Lynn, D. H. (1997). Maximum ages of ciliate lineages estimated using a small subunit rRNA molecular clock: crown eukaryotes date back to the Paleoproterozoic. *Arch. Protistenkd.* 148, 329–341. doi: 10.1016/s0003-9365(97)80013-9

Xu, W., Wang, Y., Cheng, T., Yu, Y., El-Serehy, H., Al-Farraj, S. A., et al. (2020). Reevaluation of the 'well-known' *Paraurostyla weissei* complex, with notes on the ontogenesis of a new *Paraurostyla* species (Ciliophora, Hypotrichia). *Eur. J. Protistol.* 73:125672. doi: 10.1016/j.ejop.2020.125672

Yan, Y., Maurer-Alcalá, X. X., Knight, R., Pond, S. L. K., and Katz, L. A. (2019). Single-cell transcriptomics reveal a correlation between genome architecture and gene family evolution in ciliates. *mBio* 10, e2524–e2519. doi: 10.1128/mBio.02524-19

Zhang, T., Dong, J., Cheng, T., Duan, L., and Shao, C. (2020). Reconsideration on taxonomy of the marine ciliate *Neobakuella aenigmatica* Moon et al., 2019 (Protozoa, Ciliophora, Hypotrichia). *Mar. Life Sci. Technol.* 2, 97–108. doi: 10.1007/s42995-020-00032-4

Zhao, X., Gao, S., Fan, Y., Strueder-Kypke, M., and Huang, J. (2014). Phylogenetic framework of the systematically confused *Anteholosticha-Holosticha* complex (Ciliophora, Hypotrichia) based on multigene analysis. *Mol. Phylogenet. Evol.* 91, 238–247. doi: 10.1016/j.ympev.2015.05.021

Conflict of Interest: The authors declare that the research was conducted in the absence of any commercial or financial relationships that could be construed as a potential conflict of interest.

frontiers in Marine Science

ORIGINAL RESEARCH
published: 10 December 2020
doi: 10.3389/fmars.2020.604487

Ultrastructural Features of an Abundant and Ubiquitous Marine Ciliate, *Uronychia binucleata* (Protista, Ciliophora, Euplotida)

Jingyi Dong[1,2], Xinpeng Fan[3], Tengyue Zhang[1,4], Saleh A. Al-Farraj[5], Thorsten Stoeck[2], Honggang Ma[1] and Lifang Li[6]**

[1] Institute of Evolution & Marine Biodiversity, and College of Fisheries, Ocean University of China, Qingdao, China, [2] Ecology Group, University of Kaiserslautern, Kaiserslautern, Germany, [3] School of Life Sciences, East China Normal University, Shanghai, China, [4] Department of Zoology, Comenius University in Bratislava, Bratislava, Slovakia, [5] Zoology Department, College of Science, King Saud University, Riyadh, Saudi Arabia, [6] Marine College, Shandong University, Weihai, China

OPEN ACCESS

Edited by:
Thomas Wilke, University of Giessen, Germany

Reviewed by:
Gabriela Küppers, Consejo Nacional de Investigaciones Científicas y Técnicas (CONICET), Argentina
Carolina Bastidas, Massachusetts Institute of Technology, United States

***Correspondence:**
Lifang Li
qd_liliy@sina.com
Honggang Ma
mahg@ouc.edu.cn

Specialty section:
This article was submitted to Marine Evolutionary Biology, Biogeography and Species Diversity, a section of the journal Frontiers in Marine Science

Received: *09 September 2020*
Accepted: *20 November 2020*
Published: *10 December 2020*

Citation:
Dong J, Fan X, Zhang T, Al-Farraj SA, Stoeck T, Ma H and Li L (2020) Ultrastructural Features of an Abundant and Ubiquitous Marine Ciliate, Uronychia binucleata (Protista, Ciliophora, Euplotida). Front. Mar. Sci. 7:604487. doi: 10.3389/fmars.2020.604487

The ciliate genus *Uronychia* is a marine group with extremely differentiated cortical and ciliary structures. These structures define its unique evolutionary position in the whole subclass Euplotia. However, to date, few data about the ultrastructure of this genus and related taxa is available. In the present work, a dominant species, *Uronychia binucleata*, was investigated using scanning electron microscopy and transmission electron microscopy. The findings are as follows: (i) this species lacks the typical alveolar plate in its cortex, whereas the abundant electron-lucent vesicular structures occurred densely; (ii) the subpellicular microtubules form a triad configuration in the dorsal side, while appearing in a single configuration in the ventral side; (iii) the cortical granules are extrusomes, which represent a kind of mucocyst instead of ampules; (iv) two kinetosomes in different rows of one cirrus are linked by the single longitudinal connection; (v) the undulating membrane is highly developed and their insides and outsides are partially covered by the cortical flap; (vi) the single-membrane-bound pharyngeal disks interposed with microtubular sheets, and are distributed in three distinct zones. This first detailed report about the ultrastructural features of the genus *Uronychia* will be a key to improve the diagnosis and systematics of this widely distributed and ecologically important genus and its family Uronychiidae.

Keywords: ciliates, euplotids, Protista, ultrastructure, *Uronychia*

INTRODUCTION

Ciliated protists (Ciliophora), a large assemblage of unicellular eukaryotes occupying various ecological niches, play different roles of importance in microbial food webs. This makes them valuable organisms on a long list of research fields related to biodiversity, biocomplexity, genetic evolution, and environmental conservation (Hausmann and Bradbury, 1996; Lynn, 2008;

Kchaou et al., 2009; Song et al., 2009; El-Serehy et al., 2012; Wang et al., 2017; Chen et al., 2018; Huang et al., 2018; Hu et al., 2019; Wang et al., 2019; Yan et al., 2019; Gupta et al., 2020; Li et al., 2020; Sheng et al., 2020; Wu et al., 2020). As one of the highly cosmopolitan and diverse groups within ciliated protists, euplotid ciliates have been attracting great interest among ciliate researchers. However, the indications suggest that they have indeterminate biodiversity (Song, 1997; Küppers, 2020; Lian et al., 2020; Mendez-Sanchez et al., 2020). As research is developed and extended, more detailed macroscopic and microscopic characteristics are crucial for improving the identification and documentation of euplotid ciliates (Warren et al., 2017). The accumulation of such knowledge can also improve biodiversity estimations and support robust systematics (Schmidt et al., 2007; Foissner et al., 2014; Vďačný and Rajter, 2015; Gao et al., 2016, 2017; Song and Shao, 2017; Sheng et al., 2018; Chen et al., 2019).

The genus *Uronychia* Stein, 1859 is known as a cosmopolitan group, and most species live in a marine habitat (Foissner, 1984; Valbonesi and Luporini, 1990; Song, 1997; Shen et al., 2009; Kim and Min, 2011; Ma et al., 2019). Within the order Euplotida, *Uronychia* is clearly different from other genera as it has a conspicuously hypertrophied undulating membrane that appears horseshoe-like over the oral region, thick and stiffened cirri at the rear end of the body, left marginal cirri and enlarged transverse inserting at concavities of the cell cortex, and enormous sickle-shaped caudal cirri (Song, 1997; Lynn, 2008; Song et al., 2009). However, ultrastructural information about *Uronychia* is still lacking and so far has only been available in *U. transfuga* (Morelli et al., 1996).

In this study, a more complete and detailed ultrastructural study of *U. binucleata* is presented for the first time.

MATERIALS AND METHODS

Sampling, Collection, and Identification

Uronychia binucleata cells were collected from an indoor artificial seawater tank (300 × 80 × 50 cm) in the Laboratory of Protozoology, Ocean University of China, Qingdao, China on September 19, 2018. The seawater tank was constructed in September 2016 by simulating a natural, shallow coastal marine ecosystem during autumn near Jiaozhou Bay (120°20′29′N; 36°03′26′E), Qingdao, China. All components in the tank (i.e., bottom sediment, marine water and marine organisms) were sampled from coastal waters near Jiaozhou Bay and transferred to the seawater tank within two hours. After one month of cultivation, the seawater-tank ecosystem was stable, and the water temperature and salinity were maintained at 25°C and 30‰, respectively. Samples containing bottom sediment and water were collected from the seawater tank. Aliquots were then examined and specimens were isolated using a stereomicroscope. A raw culture was established at room temperature (25°C) and several wheats were added as carbon sources. Specimens used for all subsequent studies were obtain from this raw culture, which was maintained for a year until the study was finished.

Isolated specimens were observed using bright field and differential interference contrast microscopy (Olympus BX 51, Japan). Protargol impregnation was used to reveal the infraciliature and nuclear apparatus according to Wilbert's protocol (Wilbert, 1975). The voucher slide (registration number: ZTY2018091901) with protargol-stained specimens was deposited in the Laboratory of Protozoology (OUC). Identification and general terminology mainly followed Curds and Wu (1983) and Song et al. (2004).

Electron Microscopy

Scanning Electron Microscopy (SEM)

The SEM method was mainly used according to Gu and Ni (1993) and Dong et al. (2020a). The specimens with approximately 1.5 ml of culture medium were transferred into a 1:6 mixture of 1% OsO_4 (diluted from 4% OsO_4 by 30‰ salinity filtering artificial marine water) and saturated solution of $HgCl_2$ for 10 min at room temperature (25°C). Then, the fixed specimens were rinsed with cacodylate buffer and dehydrated in a graded series of ethanol. After that, they were processed sequentially: dried in a critical point dryer (Leica EM CPD300, Leica Microsystems, Wetzlar, Germany), coated with platinum by a sputter coater (Leica EM ACE600, Leica Microsystems, Wetzlar, Germany), and studied with a Hitachi S-4800 (Hitachi, Tokyo, Japan) with an accelerating voltage of 10 kV.

Transmission Electron Microscopy (TEM)

The TEM method mainly followed the procedure of Gu and Ni (1995) and Gu et al. (2002). The first-fix solution contained 200 μl of 2% OsO_4 (diluted from 4% OsO_4 by 30‰ salinity filtering artificial brackish water) and 600 μl of 2.5% glutaraldehyde, and the post-fixed solution contained 2% OsO_4. After being rinsed with cacodylate buffer, the specimens were dehydrated in a graded acetone series and then embedded with Eponate 12 resin. The uranyl acetate and lead citrate were used to stain the ultrathin sections (approximately 70 nm). Finally, a Hitachi HT7700 (Hitachi, Tokyo, Japan) was used to investigate the stained ultrathin sections at an accelerating voltage of 80 kV.

RESULTS

General Morphology of Qingdao Population of *Uronychia binucleata*

The morphology of the population revealed by optical microscopy matched the original description of *Uronychia binucleata* in Song and Wilbert (1997). Thus, only a brief outline is provided to detail the general morphology of the subject we studied: the body size was approximately 75–100 × 60–70 μm, oval to slightly rectangular body shape (**Figures 1A–C**); four frontal, two ventral, and five transverse cirri; three left marginal and three caudal cirri; six dorsal kineties; pattern of buccal apparatus genus-typical (**Figures 1A–H**).

In SEM preparations, an enormous oval buccal field extended over 60% of the ventral region. It was covered by a large undulating membrane (UM, also called paroral membrane) consisting of left and right components. The undulating membrane followed the left and right border of the peristome and were externally sheltered at the base by a prominent cortical

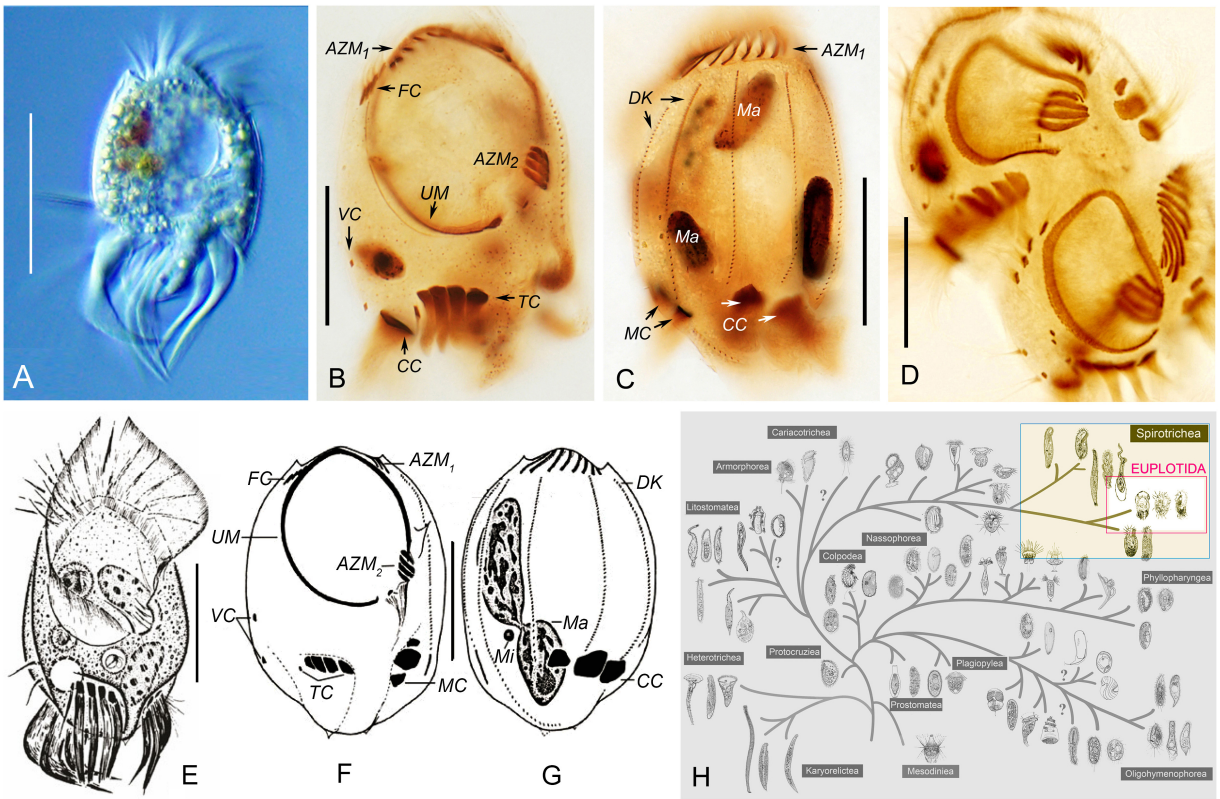

FIGURE 1 | Morphology, infraciliature and taxonomic position of *Uronychia binucleata in vivo* **(A,E)** and after protargol staining **(B–D,F,G)**. **(A,E)** Ventral views of representative individuals. **(B,C,F,G)** Ventral **(B,F)** and dorsal **(C,G)** views, showing nuclear apparatus and infraciliature. **(E–G)** were modified from Song et al. (2009). **(D)** Ventral view of a mid-stage divider. **(H)** Taxonomic positions of *Uronychia binucleata* and related taxa in the hypothetical evolutionary tree of ciliated protozoa according to Gao et al. (2016). Euplotida is highlighted. $AZM_{1,2}$, adoral zone of membranelles 1, 2; CC, caudal cirri; DK, dorsal kineties; FC, frontal cirri; Ma, macronucleus; MC, marginal cirri; TC, transverse cirri; UM, undulating membrane; VC, ventral cirri. Scale bars = 50 μm.

flap (**Figures 2A,C,D,I**). The two components of the undulating membrane were able to close the peristomial cavity, and the right component was always partially covered by the left component in the front (**Figure 2A**). A column of basal bodies that were barren of cilia were arranged along the right side of the right component of the undulating membrane (loss of cilia during preparation cannot be excluded) and could only be observed when the cortical flap was broken (**Figure 2I**). There were two deep concavities on the ventral posterior portion of the body occupied by transverse and left marginal cirri, respectively (**Figures 2A,C,D**). One or two basal body row(s) of transverse and left marginal cirri sometimes lacked cilia (**Figures 2K,L**). Six dorsal kineties were densely inserted in the conspicuous cortical furrows, whose left side was a lifting of the cortex: dorsal kineties 1 and 2 were dorsolaterally located, dorsal kinety 3 was bipolar, and the other three dorsal kineties extended to a deep concavity where caudal cirri emerged (**Figures 2B–D**).

Both ends of the cells were sculpted into spines: (1) Four spines protruded from the anterior end and pointed forward. The rightmost (first) and leftmost (fourth) spine delimited the portion of the anterior part of the adoral zone (AZM_1); the first spine was located on the front left of dorsal kinety 1 and near the margin of the cell; the second and third spines were present in the front of dorsal kineties 2 and 3, respectively, the fourth spine, which was the longest one at approximately 4 μm long, was located between dorsal kineties 3 and 4 (**Figures 2B,C,E,H**). (2) A large spine (approximately 7 μm long) was obvious and situated near the left side of dorsal kinety 1, with the tip oriented toward the cell anterior (**Figures 2C,H**). (3) Two spines usually protruded from the posterior end and pointed backward. One was located under the caudal cirri and on the right side of dorsal kinety 3, and the other was situated under the left marginal cirri and could be observed from the ventral view (**Figures 2B,C,F**).

Ultrastructure of *Uronychia binucleata*

Pellicle

The pellicle was comprised of the typical plasmalemma, which covered the whole cell surface and was subtended by cortical alveoli (**Figures 3B,F,I**). The alveoli were easily distinguished and very electron-lucent; their outer membranes were usually associated with plasmalemma (**Figures 3F,I**). Microtubules were present beneath the inner alveolar membrane and were oriented longitudinally. They were arranged as a single layer in the ventral side and as two layers (showed as triads in a cross section) in the dorsum (**Figures 3B,C**). Densely arranged

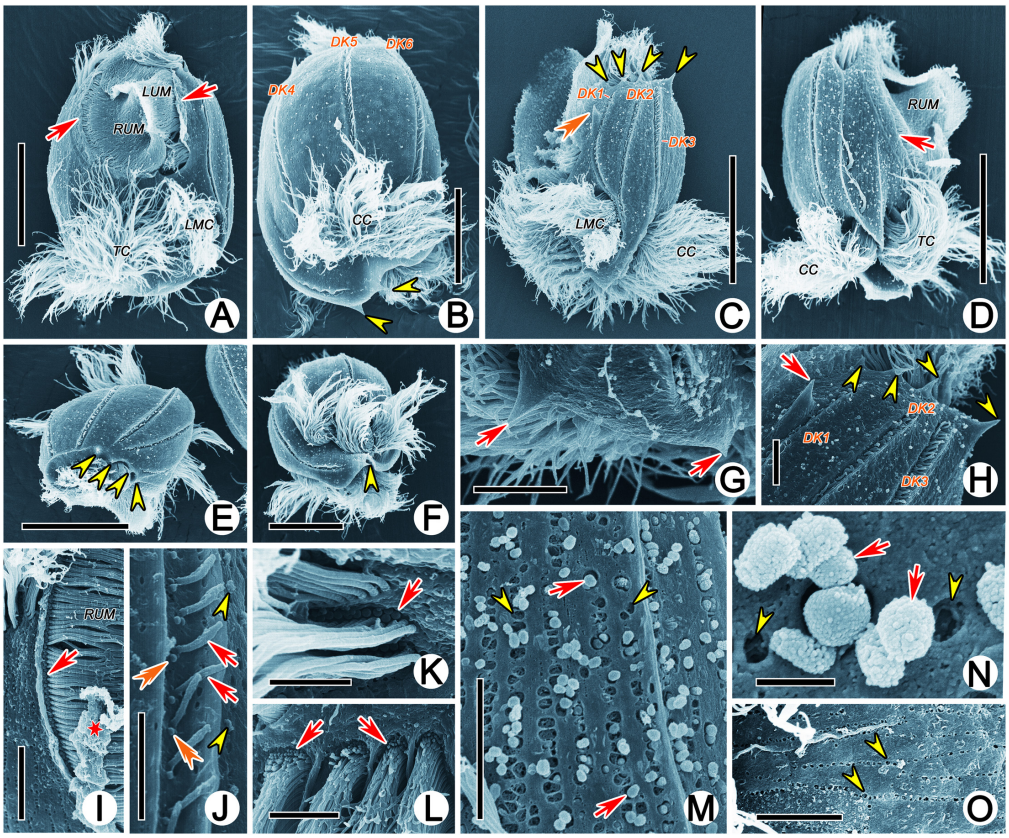

FIGURE 2 | Scanning electron micrographs of *Uronychia binucleata*. **(A–F)** Ventral **(A)**, dorsal **(B)**, left lateral **(C)**, right lateral **(D)**, top **(E)** and bottom **(F)** views of representative individuals. Arrows indicate the cortical flap upon right and left components of the undulating membrane, arrowheads point to the protruding spines of both ends of the cell, double-arrowhead shows the large spine near the left dorsal kinety 1. **(G)** Posterior end of cell to show the two spines (arrows) pointed backward. **(H)** Anterior end of cell showing the four spines (arrowheads) protruding from anterior end and the large spine (arrow) near the left of dorsal kinety 1. **(I)** Proximal of right component of the undulating membrane to show the basal bodies without cilia (arrow). Asterisk indicates the broken cortical flap. **(J)** Cortical groove with dorsal kineties (arrows), showing the two basal bodies, one of which was barren of cilia (double-arrowhead). Arrowheads mark extrusomes. **(K,L)** Basal bodies are barren of cilia (arrows) in left marginal **(K)** and transverse **(L)** cirri. **(M)** Extruding or extruded extrusomes (arrows) arranged in short rows. Arrowheads point to residual "pits." **(N)** Apical view of extruded extrusomes (arrows) sticking together. Arrowheads show residual "pits." **(O)** Residual "pit" (arrowhead) after extrusome has been extruded, arranged in short rows. CC, caudal cirri; DK1–6, dorsal kineties 1–6; LMC, left marginal cirri; LUM, left component of the undulating membrane; TC, transverse cirri; RUM, right component of the undulating membrane. Scale bars = 30 μm **(A,C–E)**, 20 μm **(B,F)**, 5 μm **(G–I,L,M,O)**, 3 μm **(J)**, 2 μm **(K)**, 0.5 μm **(N)**.

vesicular structures were located beneath the subpellicular microtubules and were usually accompanied by extrusomes, especially in the dorsal cortex (**Figures 3A,E–G,I**). They were bounded by unit membranes and had low electron density. Vesicular structures and extrusomes were always restricted by numerous microtubules, thus appearing as rectangle-like instead of spherical (**Figures 3D–H**). In some longitudinal sections of cortical lifting near the dorsal kineties, the subpellicular microtubule layer and extrusomes occurred as two closely associated distinct layers (i.e., microtubules and extrusomes distributed at intervals beneath the inner alveolar membrane; **Figure 3D**). No perilemma or epiplasm were observed.

Cortical Granules (Extrusomes)

Cortical granules were not observed *in vivo*; however, numerous spherical or ovoidal, rough-surfaced, extruded granules (approximately 0.5 μm in diameter) were present on the dorsal and ventral surfaces and even in the cortical grooves occupied by dorsal kineties in SEM preparations (**Figures 2A–D,J**). They were arranged longitudinally in short (including 10 granules at most) or long rows (including more than 50 granules) (**Figures 2M,N**). Residual "pits" could be observed (**Figure 2O**). In TEM preparations, the cortical granules were mostly located in the cortex in long or short longitudinal rows that were distinguishable with SEM (**Figure 3A**), while they were densely clustered in the buccal field (**Figure 4B**) and near cirri (**Figure 4C**). They appeared as ovoidal or even rectangle-like because of the restriction of microtubules, and each was bounded by a unit membrane with content of varying electron density (**Figures 3D–H, 4A–D**). Some granules with lower electron density content were more diffuse, possibly reflecting various stages of extrusion (**Figures 4D–H**).

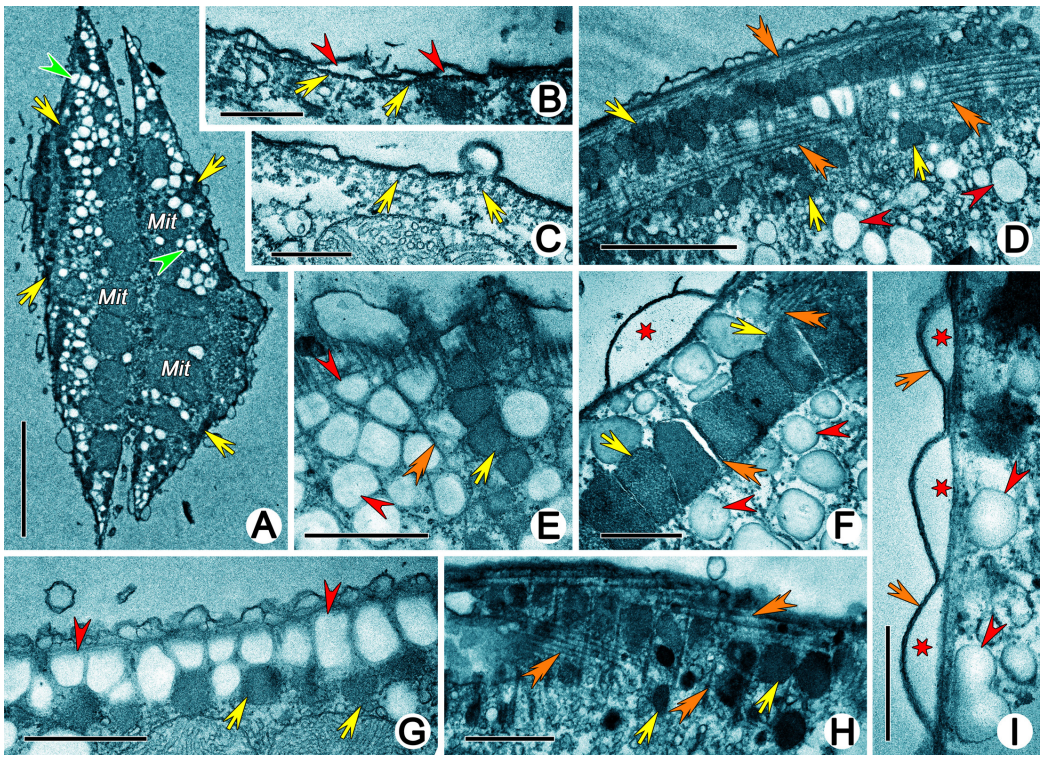

FIGURE 3 | Transmission electron micrographs of cortex of *Uronychia binucleata*. **(A)** Longitudinal section of cell near dorsal surface, showing the arrangement of extrusomes (arrows), vesicular structures (arrowheads) and mitochondria (Mit). **(B,C)** Subpellicular microtubules (arrows) arrange singularly in venter **(B)** and as triads in dorsum **(C)**. Arrowheads mark alveoli. **(D)** Subpellicular microtubules (double-arrowheads) and extrusomes (arrows) distribute at intervals, which might be the longitudinal section of cortical grooves occupied by dorsal kineties. Arrowheads point to vesicular structures. **(E–G)** Vesicular structures (arrowheads) and extrusomes (arrows) are restricted by numerous microtubules (double-arrowheads) and showed as rectangle-like. Asterisk indicates alveolus. **(H)** Extrusomes (arrows) distribute among microtubules (double-arrowheads). **(I)** Cortex region, showing plasmalemma (arrows), alveoli (asterisks) and vesicular structures (arrowheads). Mit, mitochondria. Scale bars = 5 μm **(A)**, 0.5 μm **(B,C,F,I)**, 2 μm **(D)**, 1 μm **(E,G,H)**.

Somatic Ciliature

The fine structure of some fibrillar structures of ciliature (i.e., dikinetids and polykinetids) were revealed as follows by TEM. (1) The dorsal bristle units were in a dikinetid pattern: two kinetosomes were linked by an electron-dense inter-kinetosomal connective; a tangential transverse ribbon was located in front of the anterior kinetosome; and a kinetodesmal connection was associated with posterior kinetosome (**Figure 5B**). (2) The caudal cirri and transverse cirri were polykinetids. Their connective fibers were similar: the kinetosomes were linked to each other in the same row by electron-dense double linkages containing anterior and posterior connections (AC and PC) and were attached to the anterior and posterior kinetosomes in the next row at triplet position by diagonal connections (DC, also called oblique fibrils/connections or diagonal fibrils) and transverse connections (TC, also called transverse fibril or zig-zag fibril) (**Figures 5E,K**, **8A**).

Structures in Buccal Field

The adoral zone of membranelles (AZM) were bipartite and distributed in two distinct zones (i.e., the anterior (AZM_1) and posterior (AZM_2) parts of the adoral zone membranelles; **Figure 1B**). Each membranelle in AZM_2 consisted of three rows of kinetosomes (**Figure 5G**). The diagonal connection interconnected the diagonal row and, upon reaching the most posterior row, extended to contact the electron-dense material called the radial ribbon of microtubules (**Figures 5H**, **8B**). The double linkages (containing anterior and posterior connections) that were parallel to the long rows linked two kinetosomes in the same row (**Figures 5H**, **8B**). The terminal fiber emerged from the right side of each row of kinetosomes (**Figures 5H**, **8B**).

The details of the undulating membrane (including right and left components) were revealed as follows: (1) The undulating membrane contained more than five rows of kinetosomes (**Figures 5F–J**). In a cross section, the connections between kinetosomes of undulating membrane were similar to other cirri, which showed as a polykinetid pattern: the diagonal and longitudinal connection (LC, also called longitudinal fibril) linked the two diagonal kinetosomes in different rows, and double linkages (containing anterior and posterior connections) that were parallel to the long rows connected kinetosomes in the same row (**Figures 5F–J**, **8C**). The interconnecting diagonal connection formed a series of crescent-like structures at the longitudinal innermost part (**Figure 5D**). (2) A series of continuous fibrous layers with condensation knobs beneath the kinetosomes connected the kinetosomes in the right and left

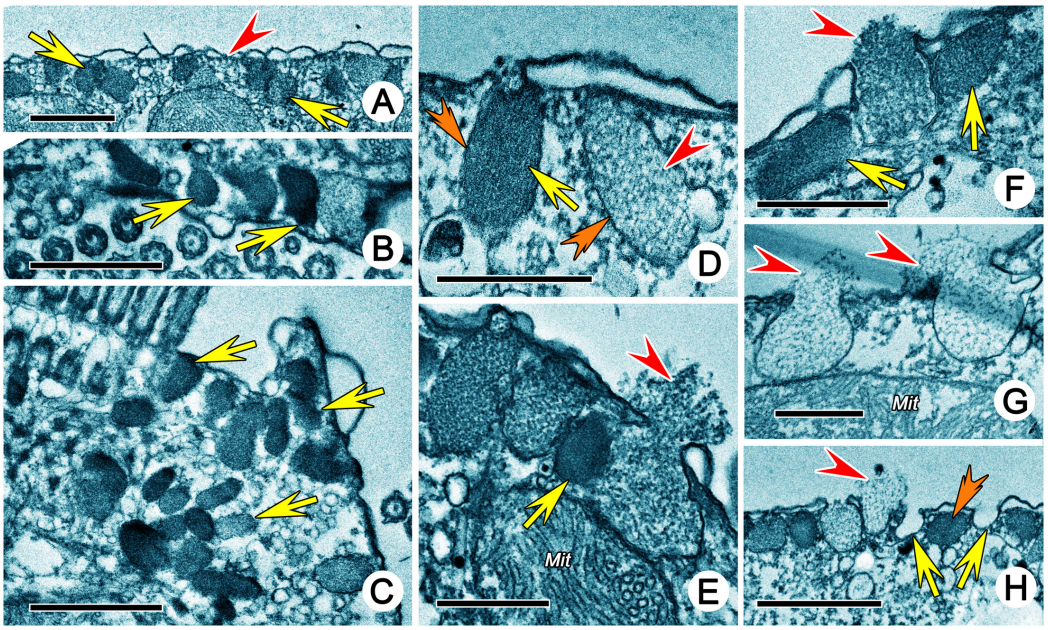

FIGURE 4 | Extrusomes of *Uronychia binucleata* in the transmission electron micrographs. **(A)** Extrusomes (arrows) under pellicle. Arrowhead marks microtubule. **(B,C)** Sections near the buccal region **(B)** and cirri **(C)**, showing the arrangement of extrusomes (arrows) in buccal region **(B)** and around cirri **(C)**. **(D)** Extrusomes with different electron density, arrow points to the electron-dense extrusome, while arrowhead points to the electron-lucent extrusome. Double-arrowheads indicate the unit membrane around extrusomes. **(E–G)** Longitudinal section of extrusomes, showing the fusion of extrusome membrane with pellicle and extruding of diffuse content (arrowheads). Arrows point to extrusomes which are not extruding. **(H)** Section perpendicular to pellicle showing extrusomes with different stages of extrusion: resting (double-arrowhead), extruding (arrowhead) and extruded (arrows show the membrane of extrusome which remains in place after extrusion). Mit, mitochondria. Scale bars = 1 μm **(A–C,H)**, 0.5 μm **(D–G)**.

components of the undulating membrane at the anterior part (**Figure 5C**). (3) Four membrane structures contained cytoplasm, small vesicles, microtubules and extrusomes arranged in a single layer bounded by unit plasmalemma (**Figures 5A**, **6C–G**). The membrane structures located outside the right and left components of the undulating membrane originated from plasmalemma, while those located inside the two components of the undulating membrane extended from plasmalemma of the dorsal wall of the buccal cavity (**Figures 5A**, **6C–E**). In some sections, one or two layer(s) of rootless membrane structures were present beneath the left component (**Figures 6A,D,E**). The membrane structures situated outside the undulating membrane might be the cortical flap observed in SEM.

A large complicated cytopharyngeal apparatus was observed in TEM which extended into cytoplasm as a narrow L-shaped cavity and might be opened at the base of the left component of the undulating membrane (**Figures 6A,B**). The cortex composition of the buccal area was similar, with a pellicle, containing plasmalemma, alveoli, and subpellicular microtubules (**Figure 6J**). Numerous electron-lucent flattened pharyngeal disks were present, interposed with microtubular sheets, located in three parts: (1) beneath the dorsal wall of the buccal cavity (**Figures 6A,H**); (2) at the innermost end of the cytopharyngeal apparatus (**Figures 6B,L**); and (3) at the bottom corner and arm of the cytopharyngeal apparatus (**Figures 6A,K**). A microtubules sheet was present beneath the cytopharyngeal apparatus (**Figures 6B,I**).

Cytoplasm, Cytoplasmic Organelles and Nuclear Apparatus

The cytoplasm was an electron-lucent colloidal matrix containing numerous granules, electron-lucent vesicles, cytoplasmic organelles, and various cytoplasmic inclusions such as lithosomes (**Figures 7E,G**). The lithosomes were globule concentric concretions with multiple lamellae (**Figure 7G**). Some irregularly shaped concentric concretions might also be lithosomes (**Figure 7E**). The mitochondria were approximately 3 μm long, ellipsoidal with tubular cristae and mainly distributed beneath the pellicle (**Figures 7A,F**). Food vacuoles were approximately 5 μm in diameter and contained large amounts of food debris, possibly of bacterial origin (**Figure 7H**). Macronuclear nodules were surrounded by a karyotheca and contained irregular chromatin bodies that were more or less homogenous and several spherical nucleoli that contained scattered, punctate, electron-dense particles (**Figures 7B–D**). A replication band (RB), which consisted of two zones of chromatin reorganization (reticular zone, RZ and diffuse zone, DZ), was present in the macronuclear nodules when numerous chromatin bodies with homogenous electron density were embedded in the macronuclear nodules (**Figures 7B,D**). The movement direction of the RB through the nucleus was observed from DZ to RZ, whereby dense chromatin bodies in the front RB were organized as RZ and the reticular chromatin were then organized as DZ, which contributed to the reconstitution of dense chromatin bodies behind the RB (**Figures 7B,D**).

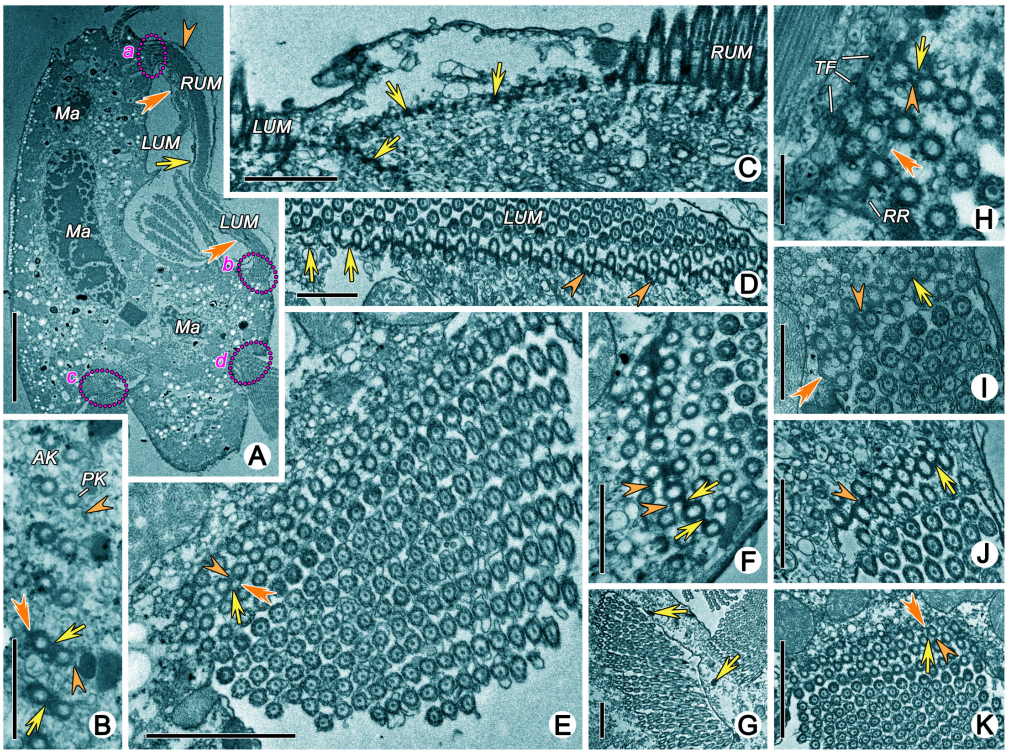

FIGURE 5 | Transmission electron micrographs of ciliature of *Uronychia binucleata*. **(A)** Longitudinal section of cell from right lateral view, to show the membrane structure located outside of right component of the undulating membrane (arrowhead), inside of right component of undulating membrane (arrows), and inside of left component of the undulating membrane (double-arrowhead). Areas marked "a" "b" "c" and "d" are enlarged in **(J,F,E,K)**, respectively. **(B)** Oblique section of dorsal kineties, showing the connections between the anterior (AK) and posterior (PK) kinetosomes. Arrows mark the inter-kinetosomal connective, arrowheads point to kinetodeamal fiber, double-arrowhead indicates the tangential transverse ribbon. **(C)** Section of anterior part of cell showing continuous fibrous layer (arrows) connects the kinetosomes in left and right components of the undulating membrane. **(D)** Cross section of left component of the undulating membrane, to show the show the diagonal connections (arrowheads), some of which forms a series of crescent-like structures (arrows). **(E)** Cross section of caudal cirri, showing the connections among kinetosomes. Arrowhead marks the double linkages between kinetosomes in the same row, arrow points to the diagonal connection, and double-arrowhead indicates the transverse connection. **(F,I,J)** Cross section of left **(F,J)** and right **(I)** components of the undulating membrane showing the kinetosomes linked by double linkages (arrows) and diagonal connections (arrowheads). Double-arrowhead marks a crescent-like structure in left component of the undulating membrane. **(G)** Cross section of adoral zone of membranelles 2 consisting of three rows in each membrane. Arrows point to the extrusomes. **(H)** Detailed magnification of a membrane from adoral zone of membranelles 2, to show the diagonal connection (double-arrowhead) interconnects posterior row and extends out to form radial ribbon of microtubules (RR). Arrow points to anterior connection, arrowhead marks the posterior connections. **(K)** Cross section of transverse cirri. Arrowhead marks electron-dense double linkages linked kinetosomes in the same row, arrow points to the diagonal connection, double-arrowhead indicates the transverse connection. AK, anterior kinetosome; LUM, left component of the undulating membrane; Ma, Macronuclear nodule; PL, posterior kinetosomes; RUM, right component of the undulating membrane; RR, radial ribbon of microtubules; TF, terminal fiber. Scale bars = 10 μm **(A)**, 1 μm **(B–D,F,I,J)**, 2 μm **(E,G,K)**.

The micronuclei contained numerous chromatin bodies of homogenous electron density (**Figure 7C**).

Conclusion

A summary of the present research regarding *Uronychia binucleata* is as follows.

(i) Visual general morphology was observed by SEM, including obvious spines and left and right components of the undulating membrane.

(ii) Details concerning the complicated cortex were elaborated upon. In short: numerous electron-lucent vesicular structures that are usually accompanied by cortical granules (extrusomes) always showed as rectangle-like because of the restriction of microtubules. The cortical granules were not observed *in vivo*; however, they showed as 0.5 μm in diameter, spherical or ovoidal in shape, rough-surfaced, arranged in longitudinal rows in SEM, with varying electron density in TEM.

(iii) The undulating membrane was highly developed, including right and left components, flanked by a prominent cortical flap. Four membrane structures were situated inside and outside of the right and left components of the undulating membrane, respectively.

DISCUSSION

Ultrastructural Features of Pellicle

The organization of a typical ciliate pellicle is generally composed of a continuous plasmalemma, alveoli that are subtended by a

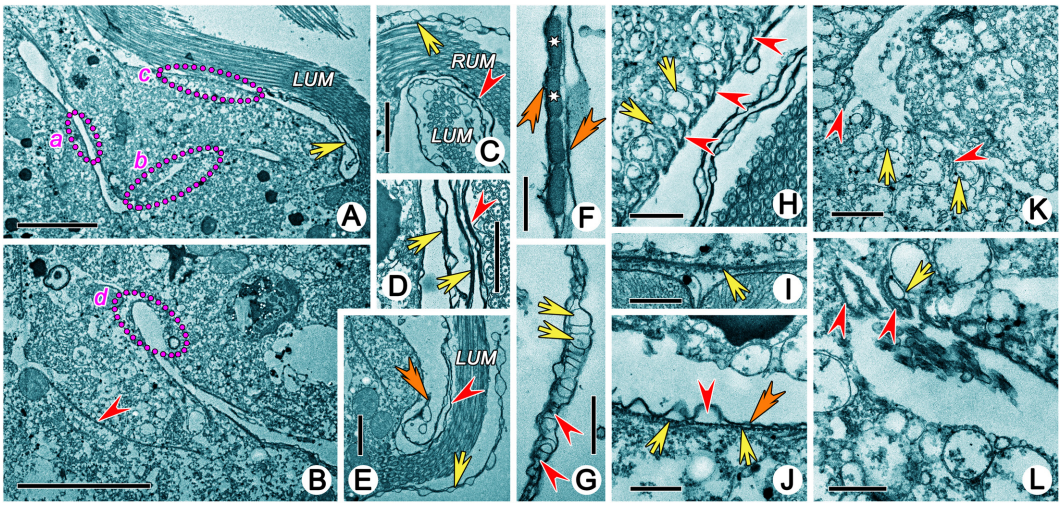

FIGURE 6 | Transmission electron micrographs showing structures in buccal field of *Uronychia binucleata*. **(A,B)** Longitudinal section of buccal field, showing the large cytopharyngeal apparatus which extended into cytoplasm as a narrow L-shaped cavity. Areas marked "a" "b" "c" and "d" are enlarged in **(J,K,H,L)**, respectively. Arrow marks the rootless membrane structure beneath the left component of the undulating membrane, arrowhead points to the microtubules sheet beneath the cytopharyngeal apparatus. **(C,E)** Base of right **(C)** and left **(E)** components of the undulating membrane, to show the membrane structures around it extending from plasmalemma of dorsal wall (arrowhead) and cell surface (arrow). Double-arrowhead points to the rootless membrane structure. **(D)** Longitudinal section of membrane structures. Arrowhead indicates membrane structure inside of left component of the undulating membrane, arrows point the rootless membrane structures. **(F,G)** The membrane structure contains numerous small cytoplasmic vesicles (arrows), microtubules (arrowheads) and extrusomes (asterisk) and is bounded by the plasmalemma (double-arrowheads). Flattened pharyngeal disks (arrows) situated in the dorsal wall of the buccal cavity **(H)**, at the innermost end **(K)** and bottom corner of cytopharyngeal apparatus **(L)**. Arrowheads point to the microtubular sheets interposed between them. **(I)** Microtubules sheet (arrow) located beneath the cytopharyngeal apparatus. **(J)** Cytopharyngeal apparatus contains plasmalemma (double-arrowhead), alveoli (arrowhead) and subpellicular microtubules (arrow) without pharyngeal disks. LUM, left component of the undulating membrane; RUM, right component of the undulating membrane. Scale bars = 5 μm **(A,B)**, 2 μm **(C,E)**, 1 μm **(D,H,K)**, 0.5 μm **(F,G,I,L)**.

membrane, and underlying fibrous epiplasm (Pitelka, 1965; Lynn, 2008). In euplotids, such as in *Aspidisca* (Rosati et al., 1987), *Certesia* (Wicklow, 1983), *Euplotes* (Ruffolo, 1976; Foissner, 1978; Hausmann and Kaiser, 1979) and *Euplotidium* (Lenzi and Rosati, 1993), the alveolar plates were filled with electron-dense material, mainly composed of protein, thus also called platein (Kloetzel, 1991). The alveolar plates appeared to lend form and rigidity to the cell cortex, replacing the epiplasm of other ciliates (Kloetzel, 1991). However, neither the alveolar plates nor the epiplasm could be observed in *Uronychia transfuga* by Morelli et al. (1996), which was the only ultrastructural research on the genus *Uronychia* before our present work. The same result occurred in *U. binucleata* in our research.

The subpellicular microtubules, which are essential parts of the cortex, extend longitudinally beneath the pellicle (Lynn, 2008). Grim (1967) gives a detailed description of the organization and orientation of subpellicular microtubules in *Euplotes*: a series of closely associated longitudinal tubules form a triad configuration (called microtubular triads) in the dorsal, while appearing in a single configuration in the ventral (Ruffolo, 1976; Foissner, 1978; Grim et al., 1980; Fukang and Lingmei, 1996; Schwarz et al., 2007). In this research, the similar arrangement of subpellicular microtubules described by Grim (1967) was also present in *U. binucleata*. However, only a sheet of subpellicular microtubules was described in *U. transfuga* (Morelli et al., 1996), which could mean that the triad configuration in the dorsal was ignored. These kinds of subpellicular microtubules were rarely reported until now, which have only been observed in some euplotids (Rosati, 1970; Wicklow, 1983; Rosati et al., 1987; Gong et al., 2018) and some cyrtophorids (Hofmann and Bardele, 1987; Kurth and Bardele, 2001), thus, we speculate that the arrangement of the subpellicular microtubules might be one of characteristics of the order Euplotida. The function of these kind of arrangements of subpellicular microtubules is still ambiguous, they may be used for support or remarkable rigidity (Sandborn et al., 1964; Gliddon, 1966), sensory conduction or coordination (Randall and Jackson, 1958; Jerka-Dziadosz et al., 1987; Arregui et al., 1994), and fluid conduction (Sandborn et al., 1964).

In addition, numerous electron-lucent sac-like vesicular structures, arranged densely below the subpellicular microtubules could be seen clearly in TEM. These structures have never been reported in other euplotids or hypotrichs until now, and their function is still ambiguous. Thus, further investigations on these vesicular structures are needed in order to fully characterize them and determine their function.

Cortical Granules of *Uronychia binucleata* Are Not Ampules

The cortical granules of *Uronychia binucleata* are membrane-bound organelles that can be extruded and expel their contents to the outside of the cell, which conforms with the definition of extrusomes given by Hausmann (1978).

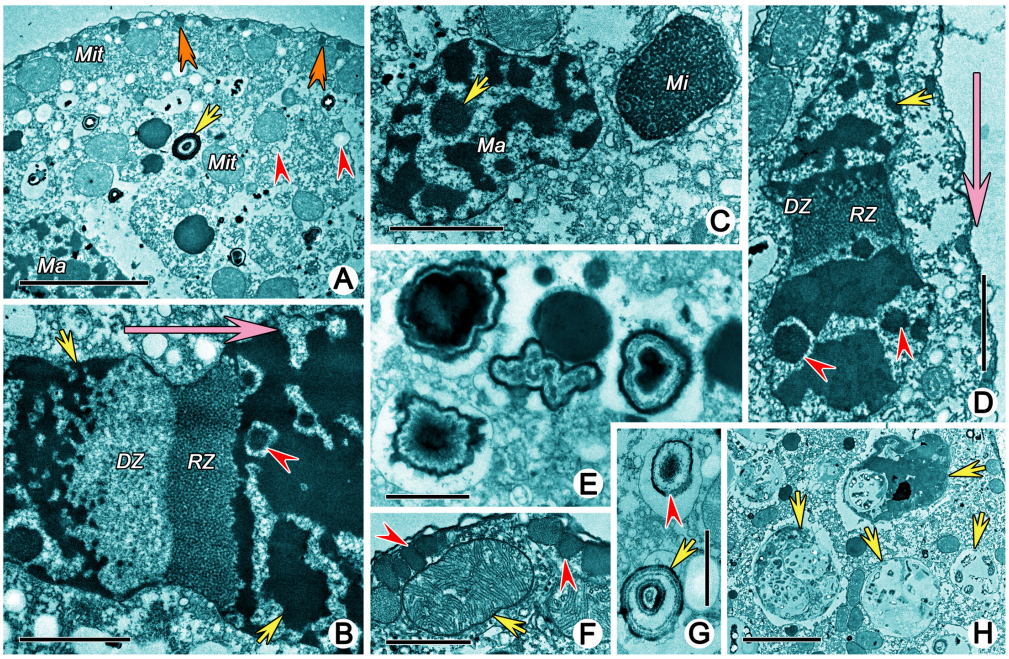

FIGURE 7 | Transmission electron micrographs showing structures in cytoplasm of *Uronychia binucleata*. **(A)** Cytoplasm and cytoplasmic organelles. Arrow marks the lithosome, arrowheads point to vesicles, double-arrowheads indicate the extrusomes. **(B,D)** Replication band is composed of a reticular zone (RZ) and a diffuse zone (DZ). Arrowheads point to nucleoli, arrows mark chromatin bodies, big arrows indicate the movement direction of the replication band. **(C)** Macronuclear nodule and micronucleus. Arrow marks the nucleolus. **(E)**Various shaped concentric concretions which might be lithosomes. **(F)** Section perpendicular to pellicle showing the micronucleus (arrow) and extrusomes (arrowheads). **(G)** Lithosome (arrow) and concentric concretions (arrowhead). **(H)** Food vacuoles containing bacteria. Ma, Macronuclear nodule; Mi, micronucleus; Mit, mitochondria. Scale bars = 5 μm **(A,H)**, 2 μm **(B–D)**, 1 μm **(E,F)**, 0.5 μm **(G)**.

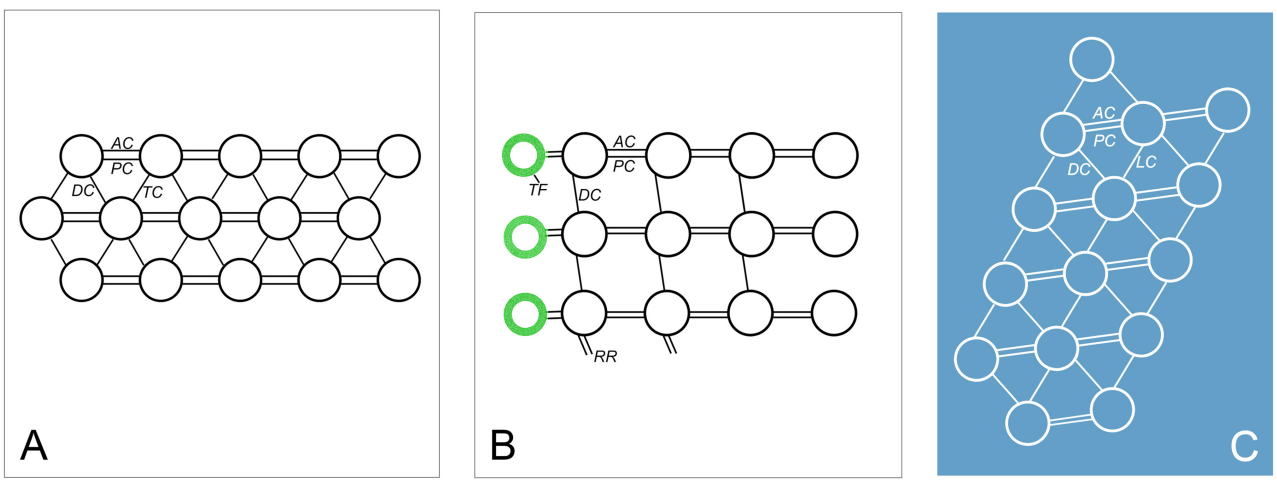

FIGURE 8 | Diagrammatic drawings of the connections of oral and somatic ciliature in *Uronychia binucleata*. **(A)** Scheme of caudal cirri and transverse cirri showing the anterior (AC) and posterior connections (PC) link kinetosomes in the same row, diagonals (DC) and transverse connections (TC) link kinetosomes in the next row. **(B,C)** Scheme representation of cross section of posterior part of adoral zone membranelles **(B)** and undulating membrane **(C)**. AC, anterior connection; DC, diagonals connection; LC, longitudinal connection; PC, posterior connection; RR, radial ribbon of microtubules; TF, terminal fiber.

As a special type of mucocyst, the ampules are defined by Ruffolo (1976) as membrane-bound organelles in association with both dorsal bristles and compound ciliary organelles of the ventral surface (i.e., arranged around the dorsal bristles or ciliary insertion as a "rosette" or "spokes" (Fauré-Fremiet and André, 1968; Ruffolo, 1976). Moreover, this is often considered one of the characteristics of euplotids (Lynn, 2008), as reported in *Euplotes* (Verni et al., 1978; Dallai and Luporini, 1981; Görtz, 1982; Rosati and Modeo, 2003; Lobban et al., 2005), *Diophrys* (Rosati, 1970; Gong et al., 2018), *Certesia* (called muciferous-like bodies;

Wicklow, 1983) and *Aspidisca* (called cytoplasmic vesicles; Rosati et al., 1987). However, the characteristic extrusomes of *Uronychia* can be easily differentiated from these ampules as follows: (1) they are not observed *in vivo* vs. being distinctive *in vivo*; (2) they are arranged in longitudinally oriented rows vs. around the dorsal bristles or ciliary insertion as a "rosette"; (3) most notably, they can be extruded vs. no extrusion process being observed (Fauré-Fremiet and André, 1968; Rosati, 1970; Ruffolo, 1976; Görtz, 1982; Wicklow, 1983; Rosati et al., 1987; Gong et al., 2018). That is to say, in *Uronychia*, as a notable member of Euplotida, the ampules may not exist. However, this is still waiting to be confirmed by further research on other species of *Uronychia*.

Fibrillar Structures of Cirri

As the basis of ciliature, research on the component structures of the ciliate kinetids has a long history. Lynn (1976) defined the monokinetids, dikinetids and polykinetids as kinetids composed of one, two and more than two kinetosomes, respectively, to avoid the confusion implicit in ciliary apparatus, such as a cirrus, a membranelle, or any complex assemblage. Three patterns of polykinetids were classified by Lynn (1981): (1) *Phacodinium* pattern: eight or nine kinetosomes arranged as longitudinal rows and linked by two tangentially oriented transverse ribbons (Didier and Dragescjo, 1979); (2) *Plagiotoma* pattern: two and nine kinetosomes linked by dense material (Albaret and Grain, 1973); and (3) hypotrich pattern: a number of kinetosomes arranged hexagonally and linked in a complex manner, for example, in *Gastrostyla steinii*, *Oxytricha fallax*, *Stylonychia mytilus* and *Euplotes eurystomus* (Gliddon, 1966; Grim, 1972; Grimes, 1972; de Puytorac et al., 1976). The first two types mainly exist in groups of lower forms of ciliates, while the third type is present in hypotrichous and euplotid ciliates. However, in Euplotida two types of kinetosome connections have been reported to date: (1) a single longitudinal connection linking the two kinetosomes in different rows is observed in Uronychiidae and Aspidiscidae, represented by *U. binucleata* (the count of longitudinal connection in *U. transfuga* is not mentioned) and *Aspidisca* sp., respectively (Rosati et al., 1987; Morelli et al., 1996); (2) a double longitudinal connection between kinetosomes in different rows, which is present in the species of Euplotidae (represented by *E. eurystomus*) and Certesiidae (represented by *Certesia quadrinucleata*) (Gliddon, 1966; Wicklow, 1983). *U. binucleata* belongs to the hypotrich pattern with a single longitudinal connection. It is worth mentioning that in the subclass Hypotrichia, the single longitudinal connection is present in Urostylida (e.g., *Paraurostyla weissei*, *Pseudokeronopsis carnea,* and *Pseudourostyla cristata*) while the double longitudinal connection is observed in Sporadotrichida (e.g., *Gastrostyla steinii, Oxytricha fallax,* and *Stylonychia mytilus*) (Gliddon, 1966; Grimes, 1972; de Puytorac et al., 1976; Grimes and L'hernault, 1978; Wirnsberger and Hausmann, 1988; Jerka-Dziadosz and Wiernicka, 1992; Sun et al., 2018). Unfortunately, the data about component structures of the ciliate kinetids is too limited. Furthermore, a TEM-based integrative approach is needed in order to improve the characterization of the structures for research systematics. In conclusion, the variations of component structures of ciliate kinetids revealed that some degree of evolutionary divergence might have occurred in the modifications of a common structural theme. How this divergence is assigned to different higher-level taxonomic groupings remains a challenge in ciliate systematics (Rosati et al., 1987).

Ultrastructural Features in Buccal Field

The conspicuousness and the peculiar organization of the oral membrane distinguishes the *Uronychia* from the members of the Euplotida (Foissner, 1984; Valbonesi and Luporini, 1990; Song, 1997; Shen et al., 2009; Kim and Min, 2011; Ma et al., 2019). As an important characteristic of the genus *Uronychia*, this structure has been described in most species at the light optical level (Borror, 1979; Wilbert and Kahan, 1981; Hill, 1990; Song and Wilbert, 1997; Shen et al., 2009; Kim and Min, 2011; Shi et al., 2017; Ma et al., 2019) and some with SEM (Hill, 1990; Valbonesi and Luporini, 1990; Leonildi et al., 1998), though not in detail. Morelli et al. (1996) provided the ultrastructure based on *U. transfuga*, detailing the organization of cilia and its feeding behavior, called upstream filtration. However, the special membrane structure around the undulating membrane was not mentioned. In the present study, four membrane structures are inside and outside the right and left components of the undulating membrane, respectively, which suggests that the undulating membrane is bounded by a cortical flap. It is worth noting that one or two layer(s) of rootless membrane structures are sometimes present beneath the right component of the undulating membrane, which might be caused by two circumstances: (1) the cortical flap curves and cuts twice; or (2) it is the buccal seal (Foissner and Al-Rasheid, 2006; Berger, 2008; Dong et al., 2020a).

The pharyngeal disks in the oral region are the precursors that rapidly form food vacuole membranes (Kloetzel, 1974; Lynn, 2008). They have been classified into two types by Dong et al. (2020b): (1) Single-membrane-bound pharyngeal disks with low electron density (for example, in *Climacostomum virens*, *Euplotidium itoi*, *Parabistichella variabilis* and *Uronychia transfuga*) and (2) myeloid pharyngeal disks with high electron density (for example, in *Euplotes eurystomus*, *Certesia quadrinucleata*, *Diophrys oligothrix* and *D. scutum*) (Fauré-Fremiet and André, 1968; Kloetzel, 1974; Fischer-Defoy and Hausmann, 1981; Wicklow, 1983; Rosati et al., 1987; Lenzi and Rosati, 1993; Morelli et al., 1996; Verni and Gualtieri, 1997; Gong et al., 2018). The single-membrane-bound pharyngeal disks are present in *U. binucleata*, interposed with microtubular sheets as reported in *U. transfuga* (Morelli et al., 1996). Thus, it could be the typical module of pharyngeal disks in *Uronychia*. It is noteworthy that the pharyngeal disks of *U. binucleata* are divided into three parts, which has not been noted either in *U. transfuga* or other ciliates (Morelli et al., 1996).

CONCLUSION

The major findings of our study can be summarized as follows:

(i) The pellicle of *U. binucleata* not only has typical euplotid features, such as plasmalemma, alveoli and highly

organized subpellicular microtubules, but in addition has unique distinctive characteristics. These are a lack of alveolar plates and of an epiplasm, as well as abundant electron-lucent sac-like vesicular structures arranged densely below the subpellicular microtubules.

(ii) The cortical granules (extrusomes) of *U. binucleata* are mucocyst-like instead of the typical ampules.

(iii) The component structures of the ciliate kinetids of *U. binucleata* belong to the hypotrich pattern with a single longitudinal connection.

(iv) The special membrane structures are inside and outside the right and left components of the undulating membrane, respectively, suggests that the undulating membrane is bound by a cortical flap.

(v) The pharyngeal disks of *U. binucleata* are of a single-membrane-bound type.

These features clearly distinguish the Uronychita from other members of the Euplotida, and will improve the diagnosis of this evolutionary lineage. This finding is relevant not only for advancing systematics, but also for reconstructing the evolutionary history of ciliated protists, and for assessing community composition in ecological studies.

DATA AVAILABILITY STATEMENT

The original contributions presented in the study are included in the article/supplementary material, further inquiries can be directed to the corresponding author/s.

AUTHOR CONTRIBUTIONS

HM and XF conceptualized the project. JD carried out the research. TZ carried out the identification by live observation and protargol staining. JD, LL, XF, TZ, and TS helped data interpretation, wrote and revised the manuscript. All authors approved the final version of the manuscript.

FUNDING

This work was supported by the Marine S&T Fund of Shandong Province for Pilot National Laboratory for Marine Science and Technology (Qingdao) (2018SDKJ0406-1), the National Nature Science Foundation of China (Project Nos: 31772431 to LL; 41876151 to XF; 32070432 to HM and M. Miao), and Researchers Supporting Project Number (RSP-2020/7) of King Saud University, Riyadh, Saudi Arabia.

ACKNOWLEDGMENTS

We thank Prof. Weibo Song (Ocean University of China, China) for his generous help and advice on preparing the manuscript and Dr. Bing Ni (East China Normal University, China) for his helpful guidance in SEM and TEM.

REFERENCES

Albaret, J., and Grain, J. (1973). L'ultrastructure de *Plagiotoma lumbrici* Dujardin (Cilié Hétérotriche). *Protistologica* 9, 221–234.

Arregui, L., Serrano, S., and Guinea, A. (1994). Microtubular elements of the marine antarctic ciliate *Euplotes focardii* (Ciliophora, Hypotrichia). *Arch. Protistenk.* 144, 357–364. doi: 10.1016/S0003-9365(11)80238-1

Berger, H. (2008). Monograph of the amphisiellidae and trachelostylidae (Ciliophora, Hypotricha). *Monogr. Biol.* 88, 1–737. doi: 10.1007/978-1-4020-8917-6_1

Borror, A. C. (1979). Redefinition of the urostylidae (Ciliophora, Hypotrichida) on the basis of morphogenetic characters. *J. Protozool.* 26, 544–550. doi: 10.1111/j.1550-7408.1979.tb04192.x

Chen, X., Jiang, Y., Gao, F., Zheng, W., Krock, T. J., Stover, N. A., et al. (2019). Genome analyses of the new model protist *Euplotes vannus* focusing on genome rearrangement and resistance to environmental stressors. *Mol. Ecol. Resour.* 19, 1292–1308. doi: 10.1111/1755-0998.13023

Chen, X., Wang, Y., Sheng, Y., Warren, A., and Gao, S. (2018). GPS it: an automated method for evolutionary analysis of nonculturable ciliated microeukaryotes. *Mol. Ecol. Resour.* 18, 700–713. doi: 10.1111/1755-0998.12750

Curds, C. R., and Wu, I. C. H. (1983). A review of the Euplotidae (Hypotrichida, Ciliophora). *Bull. Br. Mus. Nat. Hist. (Zool.)* 44, 191–247.

Dallai, R., and Luporini, P. (1981). Membrane specializations in the ciliate *Euplotes crassus* at the site of interaction of the ampules with the plasma membrane. *Eur. J. Cell Biol.* 23, 280–285.

de Puytorac, P., Grain, J., and Rodrigues de Santa Rosa, M. (1976). A propos de l'ultrastructure corticale du cilié hypotriche *Stylonychia mytilus* Ehrbg., 1838: les caracteristiques du cortex buccal adoral et paroral des Polyhymenophora Jankowski, 1967. *Trans. Am. Microsc. Soc.* 95, 327–345. doi: 10.2307/3225124

Didier, P., and Dragescjo, J. (1979). Organisation ultrastructurale du cortex de *Phaconidium metchnicoffi* (Cilié Hétérotriche). *Protistologica* 15, 33–42.

Dong, J., Chen, X., Liu, Y., Ni, B., Fan, X., and Li, L. (2020a). An integrative investigation of *Parabistichella variabilis* (Protista, Ciliophora, Hypotrichia) including its general morphology, ultrastructure, ontogenesis, and molecular phylogeny. *J. Eukaryot. Microbiol.* 0, 1–17. doi: 10.1111/jeu.12809

Dong, J., Li, L., Fan, X., Ma, H., and Warren, A. (2020b). Two *Urosoma* species (Ciliophora, Hypotrichia): a multidisciplinary approach provides new insights into their ultrastructure and taxonomy. *Eur. J. Protistol.* 72:125661. doi: 10.1016/j.ejop.2019.125661

El-Serehy, H. A., Aboulela, H., Al-Misned, F., Kaiser, M., Al-Rasheid, K., and El-Din, H. E. (2012). Heavy metals contamination of a Mediterranean coastal ecosystem, eastern Nile Delta, Egypt. *Turk. J. Fish. Aquat. Sci.* 12, 751–760. doi: 10.4194/1303-2712-v12_4_03

Fauré-Fremiet, E., and André, J. (1968). Fine structure of *Euplotes eurystomus* (Wrz). *Arch. Anat. Microsc. Morphol. Exp.* 57, 53–78.

Fischer-Defoy, D., and Hausmann, K. (1981). Microtubules, microfilaments, and membranes in phagocytosis: structure and function of the oral apparatus of the ciliate *Climacostomum virens*. *Differentiation* 20, 141–151. doi: 10.1111/j.1432-0436.1981.tb01168.x

Foissner, W. (1978). *Euplotes moebiusi* f. *quadricirratus* (Ciliophora, Hypotrichida) I. Die feinstruktur des cortex und der argyrophilen strukturen. Arch. Protistenk. 120, 86–117. doi: 10.1016/S0003-9365(78)80014-1

Foissner, W. (1984). Taxonomie und ökologie einiger ciliaten (Protozoa, Ciliophora) des saprobiensystems. I: genera litonotus, amphileptus, opisthodon. *Hydrobiologia* 119, 193–208. doi: 10.1007/BF00015210

Foissner, W., and Al-Rasheid, K. (2006). A unified organization of the stichotrichine oral apparatus, including a description of the buccal seal (Ciliophora: Spirotrichea). *Acta Protozool.* 45, 1–16. doi: 10.11646/zootaxa.504.1.1

Foissner, W., Jung, J. H., Filker, S., Rudolph, J., and Stoeck, T. (2014). Morphology, ontogenesis and molecular phylogeny of *Platynematum salinarum* nov. spec., a new scuticociliate (Ciliophora, Scuticociliatia) from a solar saltern. *Eur. J. Protistol.* 50, 174–184. doi: 10.1016/j.ejop.2013.10.001

Fukang, G., and Lingmei, J. (1996). An ultrastructural study on cortex and macronucleus of *Euplotes encysticus*. *Zool. Res.* 17, 16–22. (in Chinese with English summary).

Gao, F., Huang, J., Zhao, Y., Li, L., Liu, W., Miao, M., et al. (2017). Systematic studies on ciliates (Alveolata, Ciliophora) in China: progress and achievements based on molecular information. *Eur. J. Protistol.* 61, 409–423. doi: 10.1016/j.ejop.2017.04.009

Gao, F., Warren, A., Zhang, Q., Gong, J., Miao, M., Sun, P., et al. (2016). The all-data-based evolutionary hypothesis of ciliated protists with a revised classification of the phylum Ciliophora (Eukaryota, Alveolata). *Sci. Rep.* 6:24874. doi: 10.1038/srep24874

Gliddon, R. (1966). Ciliary organelles and associated fibre systems in *Euplotes eurystomus* (Ciliata, Hypotrichida): I. Fine structure. *J. Cell Sci.* 1, 439–448.

Gong, Z., Fan, X., Ma, R., and Ni, B. (2018). Ultrastructure of vegetative cells and resting cysts, and live observations of the encystation and excystation processes in *Diophrys oligothrix* Borror, 1965 (Protista, Ciliophora). *J. Morphol.* 279, 1397–1407. doi: 10.1002/jmor.20851

Görtz, H. D. (1982). Discharge of cortical ampules in *Euplotes aediculatus* Pierson, 1943 (Ciliophora, Hypotrichida). *Arch. Protistenk.* 125, 31–40. doi: 10.1016/s0003-9365(82)80003-1

Grim, J. N. (1967). Ultrastructure of pellicular and ciliary structures of *Euplotes eurystomus*. *J. Protozool.* 14, 625–633. doi: 10.1111/j.1550-7408.1967.tb02052.x

Grim, J. N. (1972). Fine structure of the surface and infraciliature of *Gastrostyla steinii*. *J. Eukaryot. Microbiol.* 19, 113–126. doi: 10.1111/j.1550-7408.1972.tb03424.x

Grim, J. N., Halcrow, K. R., and Harshbarger, R. D. (1980). Microtubules beneath the pellicles of two ciliate protozoa as seen with the SEM. *J. Protozool.* 27, 308–310. doi: 10.1111/j.1550-7408.1980.tb04262.x

Grimes, G. W. (1972). Cortical structure in nondividing and cortical morphogenesis in dividing *Oxytricha fallax*. *J. Protozool.* 19, 428–445. doi: 10.1111/j.1550-7408.1972.tb03498.x

Grimes, G. W., and L'hernault, S. W. (1978). The structure and morphogenesis of the ventral ciliature in *Paraurostyla hymenophora*. *J. Protozool.* 25, 65–74. doi: 10.1111/j.1550-7408.1978.tb03869.x

Gu, F., Chen, L., Ni, B., and Zhang, X. (2002). A comparative study on the electron microscopic enzymo-cytochemistry of *Paramecium bursaria* from light and dark cultures. *Eur. J. Protistol.* 38, 267–278. doi: 10.1078/0932-4739-00875

Gu, F., and Ni, B. (1993). The exploration of preparing protozoan specimen for scanning electron microscopy. *J. Chin. Electron Microsc. Soc.* 12, 525–529.

Gu, F., and Ni, B. (1995). An ultrastructural study on resting cyst of *Euplotes encysticus*. *Acta Biol. Exp. Sin.* 28, 163–171.

Gupta, R., Abraham, J. S., Sripoorna, S., Maurya, S., Toteja, R., Makhija, S., et al. (2020). Description of a new species of *Tetmemena* (Ciliophora, Oxytrichidae) using classical and molecular markers. *J. King Saud Univ. Sci.* 32, 2316–2328. doi: 10.1016/j.jksus.2020.03.009

Hausmann, K. (1978). Extrusive organelles in protists. *Int. Rev. Cytol.* 52, 197–276. doi: 10.1016/s0074-7696(08)60757-3

Hausmann, K., and Bradbury, P. C. (1996). *Ciliates: Cells as Organisms*. Heidelberg: Spektrum Akademischer Verlag.

Hausmann, K., and Kaiser, J. (1979). Arrangement and structure of plates in the cortical alveoli of the hypotrich ciliate, *Euplotes vannus*. *J. Ultrastruct. Res.* 67, 15–22. doi: 10.1016/S0022-5320(79)80013-1

Hill, B. F. (1990). *Uronychia transfuga* (O. F. Müller, 1786) Stein, 1859 (Ciliophora, Hypotrichia, Uronychiidae): cortical structure and morphogenesis during division. *J. Protozool.* 37, 99–107. doi: 10.1111/j.1550-7408.1990.tb05877.x

Hofmann, A. H., and Bardele, C. F. (1987). Stomatogenesis in cyrtophorid ciliates: *Trithigmostoma steini* (Blochmann, 1895): from somatic Kkineties to Oral Kineties. *Eur. J. Protistol.* 23, 2–17. doi: 10.1016/s0932-4739(87)80003-2

Hu, X., Lin, X., and Song, W. (2019). *Ciliate Atlas: Species Found in the South China Sea*. Beijing: Science Press.

Huang, J. B., Zhang, T., Zhang, Q., Li, Y., Warren, A., Pan, H., et al. (2018). Further insights into the highly derived haptorids (Ciliophora, Litostomatea): Phylogeny based on multigene data. *Zool. Scr.* 47, 231–242. doi: 10.1111/zsc.12269

Jerka-Dziadosz, M., Dosche, C., Kuhlmann, H. W., and Heckmann, K. (1987). Signal-induced reorganization of the microtubular cytoskeleton in the ciliated protozoon *Euplotes octocarinatus*. *J. Cell Sci.* 87, 555–564.

Jerka-Dziadosz, M., and Wiernicka, L. (1992). Ultrastructural studies on the development of cortical structures in the ciliary pattern mutants of the hypotrich ciliate *Paraurostyla weissei*. *Eur. J. Protistol.* 28, 258–272. doi: 10.1016/s0932-4739(11)80232-4

Kchaou, N., Elloumi, J., Drira, Z., Hamza, A., Ayadi, H., Bouain, A., et al. (2009). Distribution of ciliates in relation to environmental factors along the coastline of the Gulf of Gabes, Tunisia. *Estuarine Coastal Shelf Sci.* 83, 414–424. doi: 10.1016/j.ecss.2009.04.019

Kim, S. J., and Min, G. S. (2011). First record of three *Uronychia* species (Ciliophora: Spirotrichea: Euplotida) from Korea. *Korean J. Syst. Zool.* 27, 25–33. doi: 10.5635/kjsz.2011.27.1.025

Kloetzel, J. A. (1974). Feeding in ciliated protozoa: i. Pharyngeal disks in Euplotes: a source of membrane for food vacuole formation. *J. Cell Sci.* 15, 379–401.

Kloetzel, J. A. (1991). Identification and properties of plateins, major proteins in the cortical alveolar plates of Euplotes. *J. Protozool.* 38, 392–401. doi: 10.1111/j.1550-7408.1991.tb01376.x

Küppers, G. C. (2020). A new species of *Uronychia* (Spirotrichea: Euplotida) from Argentina. *Eur. J. Protistol.* 75:125706. doi: 10.1016/j.ejop.2020.125706

Kurth, T., and Bardele, C. F. (2001). Fine structure of the cyrtophorid ciliate *Chlamydodon mnemosyne* Ehrenberg, 1837. *Acta Protozool.* 40, 33–48. doi: 10.1016/S0378-1097(00)00560-7

Lenzi, P., and Rosati, G. (1993). Ultrastructural study of *Euplotidium itoi* (Ciliata Hypotrichida). *Eur. J. Protistol.* 29, 453–461. doi: 10.1016/S0932-4739(11)80408-6

Leonildi, A., Erra, F., Banchetti, R., and Ricci, N. (1998). The ethograms of *Uronychia transfuga* and *Uronychia setigera* (Ciliata, Hypotrichida): a comparative approach for new insights into the behaviour of protozoa. *Eur. J. Protistol.* 34, 426–435. doi: 10.1016/s0932-4739(98)80011-4

Li, Y., Chen, X., Wu, K., Pan, J., Long, H., and Yan, Y. (2020). Characterization of simple sequence repeats (SSRs) in ciliated protists inferred by comparative genomics. *Microorganisms* 8:662. doi: 10.3390/microorganisms8050662

Lian, C., Luo, X., Warren, A., Zhao, Y., and Jiang, J. (2020). Morphology and phylogeny of four marine or brackish water spirotrich ciliates (Protozoa, Ciliophora) from China, with descriptions of two new species. *Eur. J. Protistol.* 72:125663. doi: 10.1016/j.ejop.2019.125663

Lobban, C. S., Modeo, L., Verni, F., and Rosati, G. (2005). *Euplotes uncinatus* (Ciliophora, Hypotrichia), a new species with zooxanthellae. *Mar. Biol.* 147, 1055–1061. doi: 10.1007/s00227-005-0024-3

Lynn, D. H. (1976). Comparative ultrastructure and systematics of the Colpodida. Structural conservatism hypothesis and a description of Colpoda steinii Maupas. *J. Protozool.* 23, 302–314. doi: 10.1111/j.1550-7408.1976.tb03776.x

Lynn, D. H. (1981). The organization and evolution of microtubular organelles in ciliated protozoa. *Biol. Rev.* 56, 243–292. doi: 10.1111/j.1469-185X.1981.tb00350.x

Lynn, D. H. (2008). *The Ciliated Protozoa: Characterization, Classification, and Guide to the Literature*. Dordrecht: Springer.

Ma, H., Li, J., Warren, A., Ba, S., and Lu, X. (2019). Morphogenesis of the Euplotid ciliate *Uronychia binucleata* Young, 1922 (Ciliophora, Hypotrichia). *J. Ocean Univ. China* 18, 467–473. doi: 10.1007/s11802-019-3956-9

Mendez-Sanchez, D., Mayen-Estrada, R., and Hu, X. (2020). Euplotes octocarinatus Carter, 1972 (Ciliophora, Spirotrichea, Euplotidae): considerations on its morphology, phylogeny, and biogeography. *Eur. J. Protistol.* 74:125667. doi: 10.1016/j.ejop.2019.125667

Morelli, A., Giambelluca, A., Lenzi, P., Rosati, G., and Verni, F. (1996). Ultrastructural features of the peculiar filter-feeding hypotrich ciliate *Uronychia transfuga*. *Micron* 27, 399–406. doi: 10.1016/s0968-4328(96)00027-3

Pitelka, D. R. (1965). New observations on cortical ultrastructure in *Paramecium*. *J. Microsc. (Paris)* 4, 373–394.

Randall, J. T., and Jackson, S. F. (1958). Fine structure and function in *Stentor polymorphus*. *J. Cell Biol.* 4, 807–830. doi: 10.1083/jcb.4.6.807

Rosati, G., and Modeo, L. (2003). Extrusomes in ciliates: diversification, distribution, and phylogenetic implications. *J. Eukaryot. Microbiol.* 50, 383–402. doi: 10.1111/j.1550-7408.2003.tb00260.x

Rosati, G., Verni, F., Bracchi, P., and Dini, F. (1987). An ultrastructural analysis of the ciliated protozoon *Aspidisca* sp. *Trans. Am. Microsc. Soc.* 106, 31–52. doi: 10.2307/3226282

Rosati, R. G. (1970). Fine structure of *Diophrys scutum* (Dujardin). *Arch. Anat. Microsc. Morphol. Exp.* 59, 221–234.

Ruffolo, J. J. (1976). Fine structure of the dorsal bristle complex and pellicle of *Euplotes*. *J. Morphol.* 148, 469–487. doi: 10.1002/jmor.1051480405

Sandborn, E., Koen, P. F., McNabb, J. D., and Moore, G. (1964). Cytoplasmic microtubules in mammalian cells. *J. Ultrastruct. Res.* 11, 123–138. doi: 10.1016/S0022-5320(64)80097-6

Schmidt, S. L., Foissner, W., Schlegel, M., and Bernhard, D. (2007). Molecular phylogeny of the Heterotrichea (Ciliophora, Postciliodesmatophora) based on small subunit rRNA gene sequences. *J. Eukaryot. Microbiol.* 54, 358–363. doi: 10.1111/j.1550-7408.2007.00269.x

Schwarz, M. V. J., Zuendorf, A., and Stoeck, T. (2007). Morphology, ultrastructure, molecular phylogeny, and autecology of *Euplotes elegans* Kahl, 1932 (Hypotrichida; Euplotidae) isolated from the anoxic Mariager Fjord, Denmark. *J. Eukaryot. Microbiol.* 54, 125–136. doi: 10.1111/j.1550-7408.2007.00243.x

Shen, Z., Shao, C., Gao, S., Lin, X., Li, J., Hu, X., et al. (2009). Description of the rare marine ciliate, *Uronychia multicirrus* song, 1997 (Ciliophora; Euplotida) based on morphology, morphogenesis and SS rRNA gene sequence. *J. Eukaryot. Microbiol.* 56, 296–304. doi: 10.1111/j.1550-7408.2009.00409.x

Sheng, Y., Duan, L., Cheng, T., Qiao, Y., Stover, N. A., and Gao, S. (2020). The completed macronuclear genome of a model ciliate *Tetrahymena thermophila* and its application in genome scrambling and copy number analyses. *Sci. China: Life Sci.* 63, 1534–1542. doi: 10.1007/s11427-020-1689-4

Sheng, Y., He, M., Zhao, F., Shao, C., and Miao, M. (2018). Phylogenetic relationship analyses of complicated class Spirotrichea based on transcriptomes from three diverse microbial eukaryotes: *Uroleptopsis citrina*, *Euplotes vannus* and *Protocruzia tuzeti*. *Mol. Phylogenet. Evol.* 129, 338–345. doi: 10.1016/j.ympev.2018.06.025

Shi, X., Liu, G., Wang, C., and Hu, X. (2017). Description of a new brackish water ciliate, *Uronychia xinjiangensis* n. sp. (Ciliophora, Euplotida) based on morphology, morphogenesis and molecular phylogeny. *Acta Protozool.* 56, 303–315. doi: 10.4467/16890027AP.17.026.7828

Song, W. (1997). On the morphology and infraciliature of a new marine hypotrichous ciliate, *Uronychia multicirrus* sp. n. (Ciliophora: Hypotrichida). *Acta Protozool.* 4, 279–285.

Song, W., and Shao, C. (2017). *Ontogenetic Patterns of Hypotrich Ciliates*. Beijing: Science Press.

Song, W., Warren, A., and Hu, X. (2009). *Free-Living Ciliates in the Bohai and Yellow Seas, China*. Beijing: Science Press.

Song, W., and Wilbert, N. (1997). Morphological investigations on some free living ciliates (Protozoa, Ciliophora) from China sea with description of a new hypotrichous genus, *Hemigastrostyla* nov. gen. *Arch. Protistenk.* 148, 413–444. doi: 10.1016/s0003-9365(97)80020-6

Song, W., Wilbert, N., Chen, Z., and Shi, X. (2004). Considerations on the systematic position of *Uronychia* and related euplotids based on the data of ontogeny and 18S rRNA gene sequence analyses, with morphogenetic redescription of *Uronychia setigera* Calkins, 1902 (Cilio-phora: Euplotida). *Acta Protozool.* 43, 313–328.

Sun, J. J., Ren, Z. H., Fan, X., Ni, B., and Gu, F. (2018). Ultrastructural study on the kinetosomes and associated microtubules of adoral membranelles and marginal cirri of *Pseudourostyla cristata*. *J. Chin. Electron Microsc. Soc.* 37, 289–297. doi: 10.3969/j.issn.1000-6281.2018.03.014

Valbonesi, A., and Luporini, P. (1990). A new species of *Uronychia* (Ciliophora, Hypotrichida) from Antarctica: *Uronychia antarctica*. *Boll. Zool.* 57, 365–368. doi: 10.1080/11250009009355721

Vďačný, P., and Rajter, L. (2015). Reconciling morphological and molecular classification of predatory ciliates: evolutionary taxonomy of dileptids (Ciliophora, Litostomatea, Rhynchostomatia). *Mol. Phylogenet. Evol.* 90, 112–128. doi: 10.1016/j.ympev.2015.04.023

Verni, F., and Gualtieri, P. (1997). Feeding behaviour in ciliated protists. *Micron* 28, 487–504. doi: 10.1016/s0968-4328(97)00028-0

Verni, F., Rosati, G., and Luporini, P. (1978). Preconjugant cell-cell interaction in the ciliate *Euplotes crassus*: a possible role of the ciliary ampules. *J. Exp. Zool.* 204, 171–179. doi: 10.1002/jez.1402040205

Wang, C., Zhang, T., Wang, Y., Katz, L. A., Gao, F., and Song, W. (2017). Disentangling sources of variation in SSU rDNA sequences from single cell analyses of ciliates: impact of copy number variation and experimental error. *Proc. R. Soc. B.* 284:20170425. doi: 10.1098/rspb.2017.0425

Wang, Y., Wang, C., Jiang, Y., Katz, L. A., Gao, F., and Yan, Y. (2019). Further analyses of variation of ribosome DNA copy number and polymorphism in ciliates provide insights relevant to studies of both molecular ecology and phylogeny. *Sci. China Life Sci.* 62, 203–214. doi: 10.1007/s11427-018-9422-5

Warren, A., Patterson, D. J., Dunthorn, M., Clamp, J. C., Achilles-Day, U. E. M., Aescht, E., et al. (2017). Beyond the "Code": a guide to the description and documentation of biodiversity in ciliated protists (Alveolata, Ciliophora). *J. Eukaryot. Microbiol.* 64, 539–554. doi: 10.1111/jeu.12391

Wicklow, B. J. (1983). Ultrastructure and cortical morphogenesis in the euplotine hypotrich *Certesia quadrinucleata* Fabre-Domergue, 1885 (Ciliophora, Protozoa). *J. Eukaryot. Microbiol.* 30, 256–266. doi: 10.1111/j.1550-7408.1983.tb02912.x

Wilbert, N. (1975). Eine verbesserte Technik der Protargolimprägnation für Ciliaten. *Mikrokosmos* 64, 171–179.

Wilbert, N., and Kahan, D. (1981). Ciliates of solar lake on the red sea shore. *Arch. Protistenk.* 124, 70–95. doi: 10.1016/s0003-9365(81)80004-8

Wirnsberger, E., and Hausmann, K. (1988). Fine structure of *Pseudokeronopsis carnea* (Ciliophora, Hypotrichida). *J. Eukaryot. Microbiol.* 35, 182–189. doi: 10.1111/j.1550-7408.1988.tb04321.x

Wu, T., Li, Y., Lu, B., Shen, Z., Song, W., and Warren, A. (2020). Morphology, taxonomy and molecular phylogeny of three marine peritrich ciliates, including two new species: *Zoothamnium apoarbuscula* n. sp. and *Z. apohentscheli* n. sp. (Protozoa, Ciliophora, Peritrichia). *Mar. Life Sci. Technol.* 2, 334–348. doi: 10.1007/s42995-020-00046-y

Yan, Y., Maurer-Alcalá, X. X., Knight, R., Pond, S. L. K., and Katz, L. A. (2019). Single-cell transcriptomics reveal a correlation between genome architecture and gene family evolution in ciliates. *Mbio* 10: e002524-19.

Conflict of Interest: The authors declare that the research was conducted in the absence of any commercial or financial relationships that could be construed as a potential conflict of interest.

frontiers in Marine Science

ORIGINAL RESEARCH
published: 05 January 2021
doi: 10.3389/fmars.2020.615377

Morphogenesis of the Ciliature During Sexual Process of Conjugation in the Ciliated Protist *Euplotes raikovi*

Usman Asghar[1,2†], Yong Chi[1,2†], Yunyi Gao[1,2], Borong Lu[1,2], Yaohan Jiang[1,2], Ruitao Gong[1,2], Honggang Ma[1,2], Khaled A. S. Al-Rasheid[3] and Feng Gao[1,2]*

[1] Institute of Evolution and Marine Biodiversity, Ocean University of China, Qingdao, China, [2] Key Laboratory of Mariculture (Ocean University of China), Ministry of Education, Qingdao, China, [3] Zoology Department, College of Sciences, King Saud University, Riyadh, Saudi Arabia

Morphogenesis is an important process that widely occurs in almost all the organisms, including the ciliated protists. Ciliates are a large group of single-celled eukaryotes that can reproduce asexually (e.g., binary fission) and perform sexual process (e.g., conjugation). Morphogenesis happens in both asexual reproduction and sexual process in ciliates and the reorganization during conjugation is more complex. However, studies of morphogenesis focusing on conjugation are very limited. Here we studied the morphogenetic process during conjugation in the marine species *Euplotes raikovi* Agamaliev, 1966. The results indicate that: (1) the ciliature in the ventral side reorganizes twice during sexual process, i.e., conjugational and postconjugational reorganization; (2) the adoral zone of membranelles (AZM) is generated *de novo* in a pouch beneath the cortex during both reorganizations, with the anterior part generated during the first reorganization, while the posterior part formed during the second reorganization; (3) the frontoventral-transverse (FVT) cirri anlagen are formed *de novo* in both processes with the fragmentation pattern of 2:2:3:3:2; (4) one left marginal cirrus is generated *de novo* during both reorganizations; and (5) the dorsal ciliature remains intact during the whole process, except that the two caudal cirri originate from the end of the right-most two dorsal kineties during both reorganizations. Comparisons of the morphogenetic process during conjugation demonstrate a considerably stable pattern within *Euplotes* while the patterns vary dramatically among different ciliate groups.

Keywords: ciliate, *Euplotes raikovi*, conjugation, morphogenesis, exconjugant

OPEN ACCESS

Edited by:
Hongbo Pan,
Shanghai Ocean University, China

Reviewed by:
Pierangelo Luporini,
University of Camerino, Italy
Xumiao Chen,
Institute of Oceanology (CAS), China

***Correspondence:**
Feng Gao
gaof@ouc.edu.cn

† These authors have contributed equally to this work

Specialty section:
This article was submitted to Marine Evolutionary Biology, Biogeography and Species Diversity, a section of the journal Frontiers in Marine Science

Received: *09 October 2020*
Accepted: *07 December 2020*
Published: *05 January 2021*

Citation:
Asghar U, Chi Y, Gao Y, Lu B, Jiang Y, Gong R, Ma H, Al-Rasheid KAS and Gao F (2021) Morphogenesis of the Ciliature During Sexual Process of Conjugation in the Ciliated Protist Euplotes raikovi. Front. Mar. Sci. 7:615377. doi: 10.3389/fmars.2020.615377

INTRODUCTION

Morphogenesis and pattern formation are important processes that occur in the organisms from unicellular to multicellular. It is driven by various cellular and developmental processes including cell proliferation, differentiation, apoptosis, cell migration, and cell adhesion (Jernvall and Newman, 2003). The morphogenesis process is mostly investigated in multicellular organisms, such as embryonic cells differentiating into various functional cell types, tissues, organs, and eventually forming a complex organism (Thomson et al., 1998; Reubinoff et al., 2000). Unicellular

organisms have a high morphological diversity, which require more complex morphogenetic patterns. However, compared to the developmental biology in larger multicellular organisms, the morphogenesis in unicellular organisms is largely unknown (Shulman and Daniel, 1999; Kirschner et al., 2000).

Ciliated protozoans are a morphologically diverse and highly differentiated group among single-celled microorganisms (Song et al., 2009; Li et al., 2019; Wang et al., 2019; Yan et al., 2019; Sheng et al., 2020). The main characters of this group are dimorphic nuclei (both germline and somatic nuclei within one cell) and special sexual process of conjugation, during which there is a reciprocal exchange of haploid gametic nuclei between the two temporarily (most widespread) or totally (as in all peritrichs and chonotrichs) fused mating partners, although some ciliates can also perform autogamy, a process of self-fertilization undertaken by a single cell (Lynn, 2008). The morphogenesis in ciliates mainly includes the formation and regeneration of cortical structures and nuclei, which occurs in both asexual and sexual stages. Compared to that in asexual reproduction, the process is more complex during sexual stages (Diller, 1966; Jin et al., 1985; Zou and Ng, 1991; Ota and Taniguchi, 2003; Xu and Foissner, 2004; Gao et al., 2020).

As the most differentiated group within ciliates, species in the genus *Euplotes* Ehrenberg, 1830 are easy to collect, cultivate, and induce conjugation in the laboratory, which are ideal model organisms for investigating morphogenesis (Song and Shao, 2017; Chen et al., 2019; Jiang et al., 2019). Many investigations have been performed on the morphogenesis during binary fission of *Euplotes* species (Washburn and Borror, 1972; Ruffolo, 1976; Voss, 1989; Jiang et al., 2010; Shao et al., 2010; Song and Shao, 2017), while limited studies focus on the morphogenetic process during conjugation (Diller, 1966; Gao et al., 2020). *Euplotes raikovi* Agamaliev, 1966 is a widely distributed marine species that has been used in research on pheromone signaling and mating behaviors (Luporini et al., 2016). Morphology of *E. raikovi* has been redescribed in detail by Jiang et al. (2010): the adoral zone composed of 22–29 membranelles; invariably seven frontoventral, basal plaque V/2 composed of a single dikinetid, single marginal, two caudal, and five transverse cirri; seven to eight dorsal kineties (three to five dikinetids in leftmost kinety on ventral side), silverline system of double-patella-I type (**Figure 1**). The morphogenesis during binary fission and nuclear development during conjugation of *E. raikovi* have been well investigated (Washburn and Borror, 1972; Voss, 1989; Gong et al., 2020). In the present study, we investigate the morphogenesis of ciliature during conjugation and postconjugation of *E. raikovi* using living observation and protargol staining methods, which revealed two rounds of reorganization. The differences of the morphogenetic process between binary fission and conjugation within and among ciliate species are also compared and discussed.

MATERIALS AND METHODS

Two *E. raikovi* strains of different mating types (I and XIII) used extensively in previous research (Ricci et al., 2019) were selected in the present study. Cell culturing and conjugation induction were according to Gong et al. (2020). The mixed cells began to form mass mating pairs within 2 h and the ratio of conjugation was about 70%. Mating pairs and the ex-conjugant cells were collected every hour and stained using protargol staining method (Gao et al., 2020). Drawings of stained specimens were performed with the help of a drawing device (Lu et al., 2020). Phylogenetic analyses were following Lian et al. (2019).

RESULTS

The whole process of conjugation lasts about 50 h, including three prezygotic micronuclear divisions and two postzygotic synkaryon divisions (**Figure 1H**) (Gong et al., 2020). The ciliary structures in the ventral side reorganize twice during sexual stage. The first reorganization happens after the cells getting paired, here referred as conjugational reorganization, which lasts approximately 11–13 h. About 25 h after the completion of the first reorganization, the second reorganization occurs during the late stage of macronuclear development, which is referred as postconjugational reorganization. The process is synchronized in each partner of a conjugating pair, so description based on one partner is as follows.

Conjugational Reorganization

Stomatogenesis

About 3–5 h after cell–cell union, the old adoral zone of membranelles (AZM) and the paroral membrane of each partner in a conjugating pair were degraded gradually from posterior to anterior, and only a few apical membranelles were left (**Figures 2A**, **3A**). Thereupon, the process of stomatogenesis was commenced in the form of a small patch of kinetosomes (**Figures 2B**, **3B**), which appeared within a pouch beneath the cortex on the ventral side ahead of the marginal cirri. When this pouch started to enlarge, more and more kinetosomes aligned into new membranelles from the anterior to the posterior part to form the new oral primordium (OP). The newly reformed AZM gradually extended, bent, and migrated toward the anterior (**Figures 2C–H**, **3C–I**). They finally reached half the length of the old AZM and replaced the remaining old AZM after the separation of conjugants (**Figures 2I**, **3J**). The old apical membranes were completely resorbed and no paroral membrane was present during the conjugational morphogenesis.

Development of Cirral Anlagen

As the oral primordium extended, a number of basal bodies appeared as frontoventral-transverse (FVT) cirral anlagen, which were generated *de novo* to the anterior side of the old transverse cirri and right of the new oral primordium, and eventually developed into five distinct streaks (**Figures 2E**, **3E,F**). These streaks extended to both directions by the proliferation of kinetosomes, and then broadened and broke apart in a 2:2:3:3:2 pattern, with each part developing into a new cirrus (**Figures 2F,G**, **3G,H**), designated as the second generation cirri. Among them, the posterior one of each streak gradually moved posteriorly to be the five transverse cirri, and the

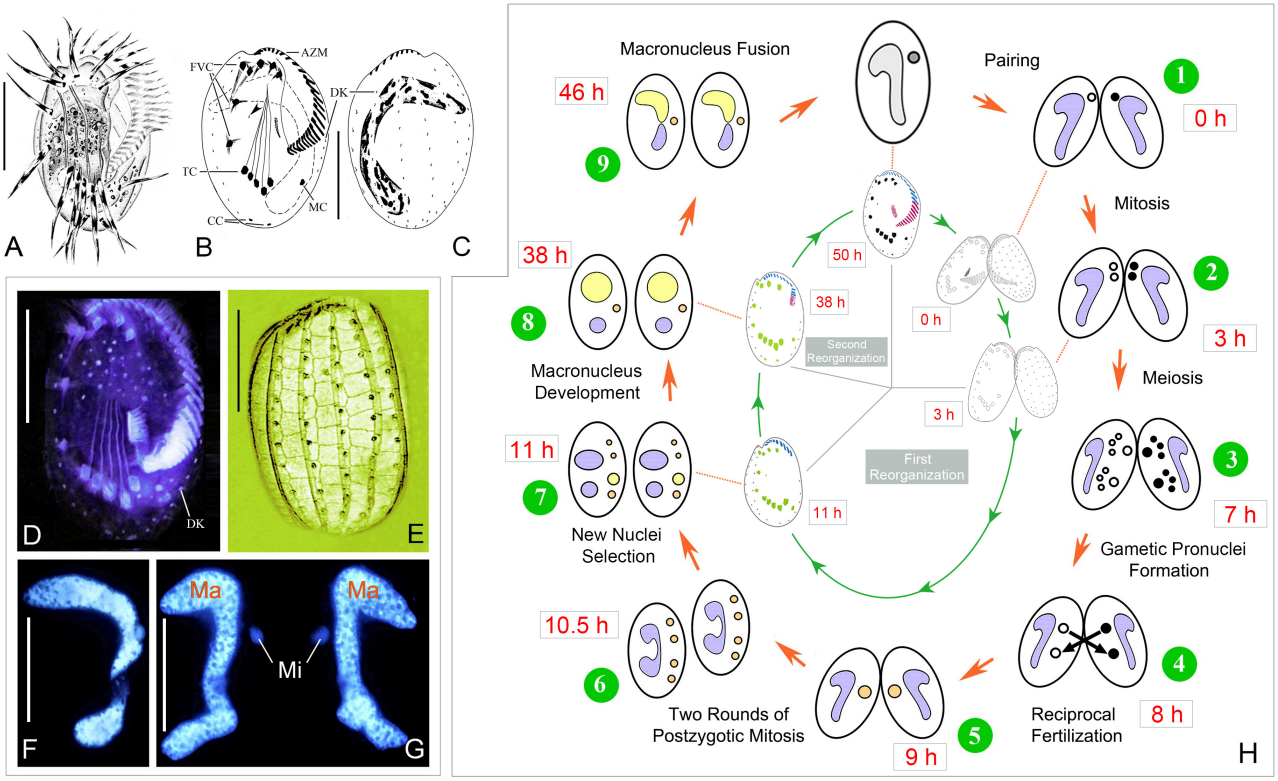

FIGURE 1 | Morphology and life cycle of *Euplotes raikovi*. **(A–E)** *Euplotes raikovi in vivo* **(A)**, after protargol **(B–D)** and silver nitrate **(E)** staining, among which B, C, and E were from Jiang et al. (2010). **(F,G)** Hoechst 33342 staining to show the micronucleus and macronucleus in a vegetative cell **(F)** and a conjugating pair **(G)**. **(H)** Nuclear events according to Gong et al. (2020) (outer) and morphogenesis during conjugation (inner). AZM, adoral zone of membranelles; CC, caudal cirri; DK, dorsal kineties; FVC, frontoventral cirri; Ma, macronucleus; MC, marginal cirrus; Mi, micronucleus; TC, transverse cirri; Scale bars = 30 μm.

others become fronto-ventral cirri with the middle one of the fourth streak gradually degenerating into a single dikinetid (**Figures 2H,I**, **3I,J**).

A short row of kinetosomes appeared *de novo* near the old marginal cirrus, and assembled into the marginal cirral anlage (**Figures 2G**, **3H**). This anlage finally developed into the second generation marginal cirrus, which migrated and replaced the old one (**Figures 2H,I**, **3I,J**).

One cirrus anlage originated at the posterior end of each of the rightmost two dorsal kineties, which later proliferated and developed into two new caudal cirri (**Figures 2G**, **3H**).

Postconjugational Reorganization

Stomatogenesis

After the first round of reorganization, the posterior part of the AZM, the paroral membrane, and the leftmost frontal cirrus were still missing (**Figures 2I**, **3J**). The exconjugants then initiated the second round of morphogenesis at about 36–38 h after cells union. Some kinetosomes started aggregating at the posterior termination of the incomplete AZM (**Figure 2J**), which then assembled into new adoral membranelles from anterior to posterior directions and finally form the complete AZM (**Figures 2K–M**, **3L–N**). The paroral membrane primordium appeared within a subcortical pouch near the posterior end of the oral primordium (**Figures 2L,M**, **3M,N**). This paroral membrane primordium elongated and broadened and eventually developed into the paroral membrane.

Development of Cirral Anlagen

Similar to the conjugational reorganization, the anlagen of the FVT cirri appeared *de novo* almost at the same location as in the first round of reorganization (**Figures 2K**, **3K**). These anlagen broadened and broke apart into five streaks in a 2:2:3:3:2 pattern, which then developed into distinct cirri (**Figures 2L,M**, **3L,M**). At the same time, another anlage (**Figure 2K**) appeared to the left of streaks near the new AZM, then developed into the left-most frontal cirrus (**Figures 2L,M**, **3L,M**). All the cirri migrated to their final positions after differentiation and eventually replaced the old ones (**Figures 2N**, **3N**).

Similarly, one anlage of the marginal cirrus appeared *de novo*, near the distal end of the newly formed oral primordium (**Figures 2L**, **3L**). Kinetosomes continuously aggregated and developed into the new marginal cirrus (**Figures 2M**, **3M**), which moved to its final position and replaced the second generation marginal cirrus.

Same as in the conjugational reorganization, short rows of basal bodies assembled into anlagen at the posterior end of each of the rightmost two dorsal kineties (**Figures 2L,M**, **3M**).

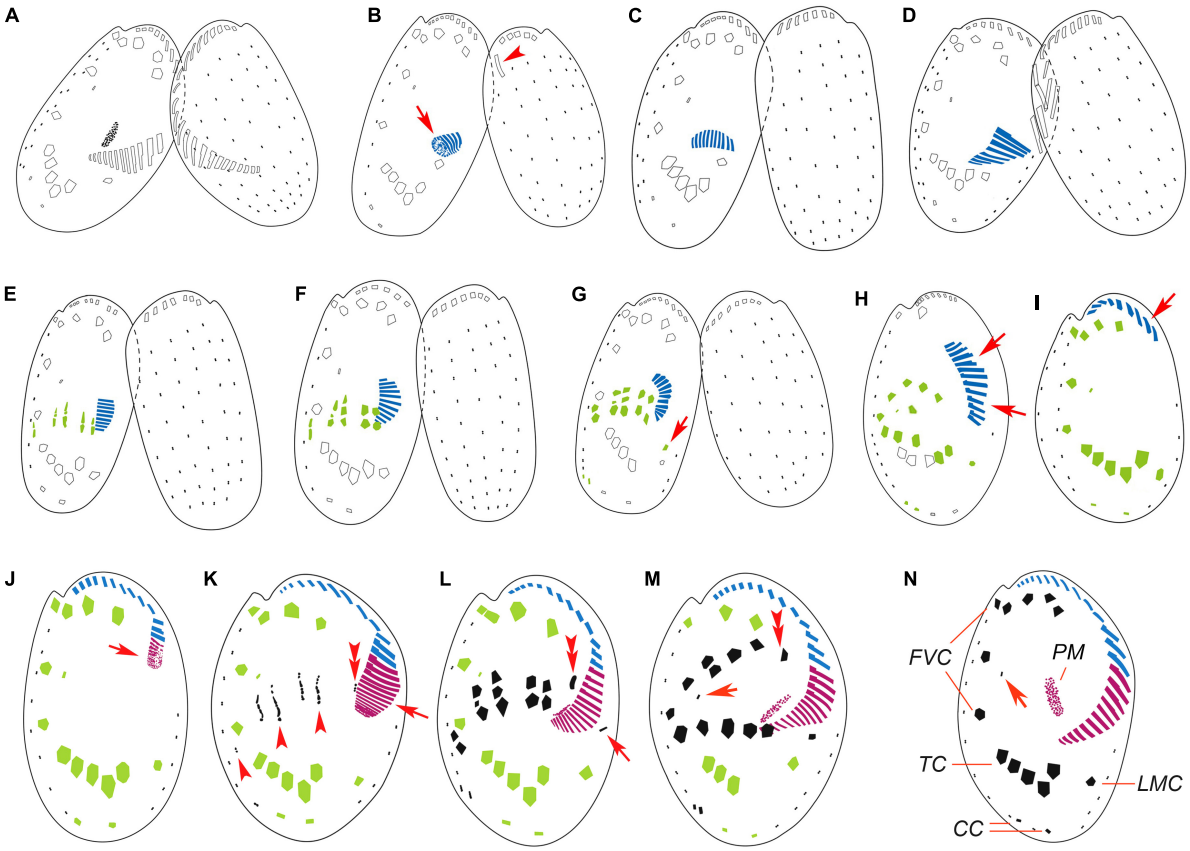

FIGURE 2 | Illustrations of the morphogenesis in conjugants **(A–G)** and exconjugants **(H–M)** after protargol staining. **(A)** Initiation of conjugation showing fusion of old adoral zone of membranelles (AZM) among the two partners. **(B–D)** Start of conjugational morphogenesis showing the formation of new oral primordium (arrow) and the disintegration of the parental one (arrowhead). **(E–G)** Late stages of conjugants showing formation of new adoral membranelles, frontoventral-transverse (FVT) cirri anlagen, marginal cirral anlagen (arrow in **G**), and caudal cirral anlagen. **(H,I)** Early exconjugants showing the migration of the incomplete AZM (arrows) and ventral cirri to their respective positions. **(J)** Start of postconjugational morphogenesis showing the formation of the new oral primordium (arrow). **(K)** Late stage exconjugant showing the formation of new membranelles in AZM (arrow), FVT cirri anlagen (arrowheads), and leftmost frontal cirrus anlage (double arrowheads). **(L–N)** Series of late exconjugants showing completion of AZM, development of FVT cirri, marginal cirrus (arrow in **L**), the leftmost frontal cirrus (double arrowheads in **L** and **M**), and the reduced cirrus (arrows in **M** and **N**). CC, caudal cirri; FVC, frontoventral cirri; LMC, left marginal cirrus; TC, transverse cirri; PM, paroral membrane.

Eventually, two new caudal cirri were formed, which migrated and replaced the second generation caudal cirri.

DISCUSSION

Comparison of the Conjugational and Postconjugational Reorganization in *E. raikovi*

The ciliature in the ventral side goes through two rounds of morphogenetic process during sexual stage in *E. raikovi*. The morphogenetic events during conjugational and postconjugational reorganization are similar in that: (1) the FVT cirral anlagen originate *de novo* in a 2:2:3:3:2 pattern; (2) the marginal cirral anlage is generated *de novo*; (3) the dorsal kineties remain unchanged during both reorganization, except that the two caudal cirri are regenerated at the posterior ends of the rightmost two dorsal kineties.

There are also some significant differences between the two processes. First, although the oral primordium is generated *de novo* in a pouch beneath the cortex during both reorganizations, only the anterior part of the AZM is generated during the conjugational reorganization while the posterior part is formed during the postconjugational reorganization. Second, the parental paroral membrane degrades immediately after the pair formation, but no new one forms during conjugational reorganization. The new paroral membrane develops *de novo* during postconjugational reorganization. Third, the leftmost frontal cirrus is absent during the conjugational morphogenesis while it is formed *de novo* during the postconjugational reorganization only.

It seems that the first round of reorganization is a waste of energy, which is redundant. Maybe the first round of reorganization is simply triggered by the degradation of the peristome, which have to be destroyed temporally for the pairs to fusion. The other explanation is that the morphogenesis may be coupled with the nuclear division, which is similar to that

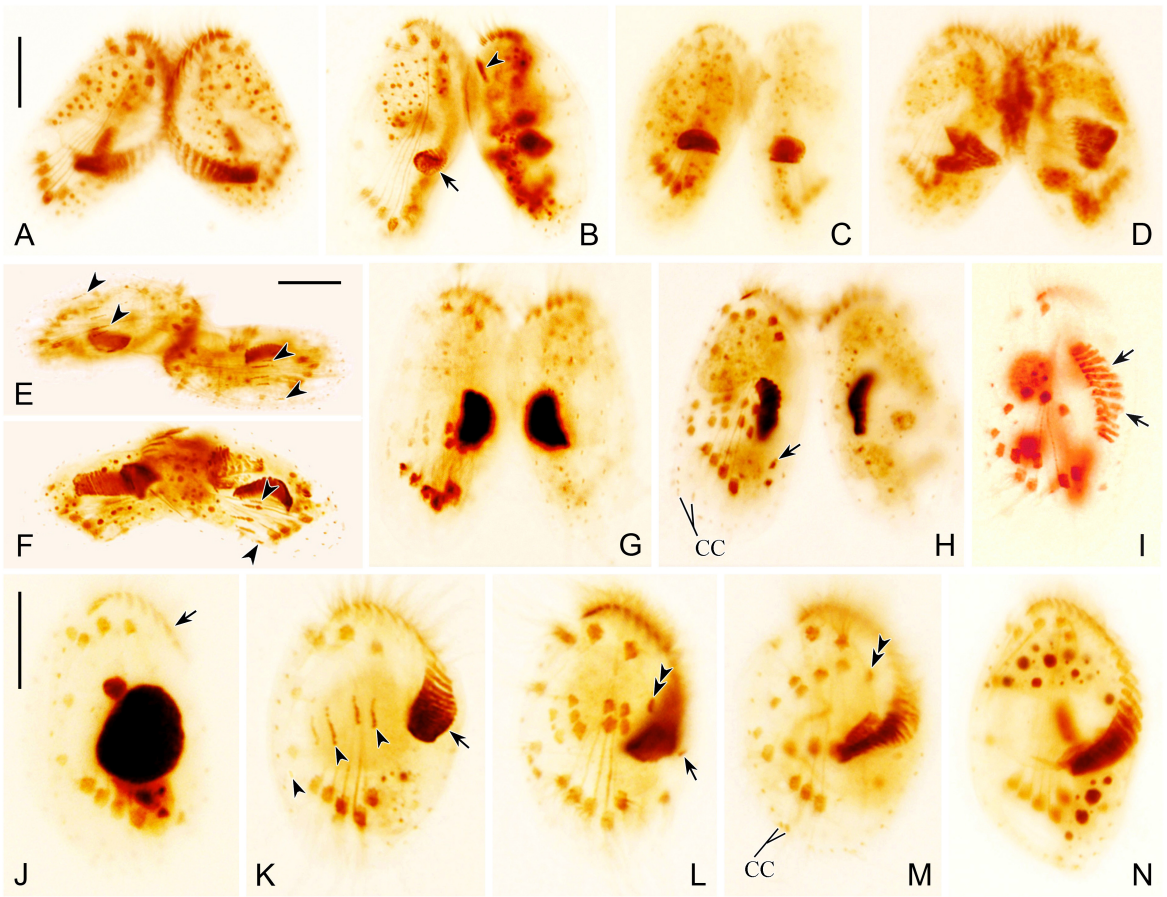

FIGURE 3 | Photomicrographs of morphogenesis of conjugants **(A–H)** and exconjugants **(I–N)** after protargol staining. **(A)** Very early conjugant showing formation of conjugational junction. **(B)** Early stage conjugant showing the origination of oral primordium in a subcortical pouch (arrow) and the disintegration of the parental one (arrowhead). **(C,D)** Conjugants showing formation of new adoral membranelles in the newly developed adoral zone of membranelles (AZM). **(E,F)** Conjugants showing frontoventral-transverse (FVT) cirri anlagen (arrowheads). **(G,H)** Late stage conjugants showing FVT cirri anlagen, broaden and break apart into definite cirri, one marginal cirrus (arrow in **H**) originates near distal end of newly formed AZM. **(I,J)** Early exconjugants showing migration of the anterior part of AZM (arrows) and FVT cirri. **(K)** Exconjugant showing the initiation of postconjugational morphogenesis, formation of new AZM (arrow), and FVT cirri anlagen (arrowheads). **(L)** Exconjugant showing proliferation and differentiation of FVT cirri, the leftmost frontal cirrus (double arrowheads), and the marginal cirrus anlage (arrow). **(M,N)** Series of late exconjugants showing the completed AZM, development of FVT cirri, two caudal cirri (CC in **M**), and the leftmost frontal cirrus (double arrowheads in **M**). Scale bars = 20 μm.

during cell division (Washburn and Borror, 1972; Voss, 1989). There is one prezygotic micronuclear mitosis and two successive postzygotic synkaryon divisions during conjugation (Gong et al., 2020), which may be related to the two rounds of reorganization.

Comparison of Morphogenesis During Asexual and Sexual Stages in *E. raikovi*

Regeneration of cortical structures occurs in both asexual (Washburn and Borror, 1972; Voss, 1989), and sexual stages in *E. raikovi*. The morphogenetic patterns during conjugation and cell division are similar in the origin and segmentation of the FVT cirral anlagen, the absence/presence of reduced cirrus, and the developmental pattern of the caudal and marginal cirri. The differences of morphogenetic observations between conjugation and cell division are as follows: (1) two rounds of reorganization occur during the conjugation of *E. raikovi*, while only one morphogenesis happens during cell division; (2) the new AZM develops *de novo* from two separate and successive oral primordia during conjugation, while the proter's AZM is inherited from the parental AZM and the opisthe's is generated *de novo* from a single oral primordium during cell division; (3) there is one set of the FVT cirral anlagen in each reorganization during conjugation while there are two sets during cell division, which are assigned respectively to the opisthe and proter; and (4) the dorsal kineties remain unchanged during conjugation, while they are renewed during cell division.

Comparison of Morphogenesis Among *Euplotes* Species

Euplotes is a very diverse genus of ciliate group, over 100 species and sub-species have been discovered and assigned to the genus *Euplotes* (Berger, 2001; Lian et al., 2020). The

morphogenesis during cell division have been investigated in detail in ∼20 *Euplotes* species, which demonstrate a considerably stable pattern of cell development (Tuffrau et al., 1976; Voss, 1989; Foissner, 1996; Song and Shao, 2017). Comparatively, morphogenesis during conjugation have been studied in only eight species, *E. vannus* (Tuffrau et al., 1976; Gao et al., 2020), *E. affinis* (Qeng et al., 1992), *E. eurystomus* (Katashima, 1959), *E. aediculatus* (Fleury, 1991), *E. woodruffi* (Wang and Shi, 1989), *E. patella* (Turner, 1930; Hammond and Kofoid, 1937), an indeterminate *Euplotes* species (Diller, 1966), and *E. raikovi* in the present study, which reveal similar patterns. They all go through two rounds of morphogenetic process during conjugation. The first reorganization generates an incomplete ventral infraciliature, lacking the posterior part of AZM, the leftmost frontal cirrus and paroral membrane, which will be completed by the second reorganization. One exception is *E. eurystomus*, which was reported to have only one reorganization during conjugation (Katashima, 1959). Considering the highly conservative pattern among *Euplotes* species, it is very likely that the author missed the first reorganization. It is noteworthy that reorganization of the dorsal kineties is not observed during conjugation in *E. raikovi*, which is consistent with that in other *Euplotes* species except for *E. affinis*. Qeng et al. (1992) investigated the conjugation in *E. affinis* based on protargol staining. They observed the regeneration of dorsal kineties during the postconjugational reorganization (Qeng et al., 1992).

The morphogenetic patterns during conjugation among *Euplotes* species vary slightly mainly in the development of the FVT and caudal cirri, which is similar to those during binary fission (Shao et al., 2010). Based on the origin and number of the FVT, the segmentation of the FVT cirral anlagen, the absence/presence of reduced cirrus, and the migration of the FVT cirri, at least five types are defined, including the affinis-type, the eurystomus-type, the charon-type, the raikovi-type, and the orientalis-type (Shao et al., 2010). *E. raikovi* is obviously the raikovi-type of 2:2:3:2 (+1):2 (7 frontoventral, 1 reduced cirrus, and 5 transverse cirri). *E. vannus* belongs to the charon-type of 3:3:3:2:2 (10 frontoventral and 5 transverse cirri) (Tuffrau et al., 1976; Gong et al., 2020). *E. eurystomus*, *E. aediculatus*, *E. woodruffi*, and *E. patella* belong to the eurystomus-type of 3:3:3:2:2 (nine frontoventral and five transverse cirri, cirrus V/2 clearly medial of cirrus VI/2) (Turner, 1930; Hammond and Kofoid, 1937; Katashima, 1959; Wang and Shi, 1989; Fleury, 1991). *E. affinis* is the affinis-type of 3:3:3:2:2 (nine frontoventral and five transverse cirri, cirrus V/2 directly anterior to cirrus VI/2) (Qeng et al., 1992).

We mapped the characters (the number of the FVT cirri and the segmentation of the FVT cirral anlagen) of the available *Euplotes* species into the phylogenetic trees based on SSU rDNA, which divides the *Euplotes* species into five clades (**Figure 4**). Based on the present data, species in clades 1, 4, and 5 possess 10 frontoventral cirri and 5 transverse cirri with the segmentation pattern of 3:3:3:3:2, which might be plesiomorphy in *Euplotes*, though two frontoventral cirri are reduced in *E. orientalis*. Comparatively, species in clade 2 lose one frontoventral cirrus, with nine frontoventral cirri and five transverse cirri and the segmentation pattern of 3:3:3:2:2. Species in clade 3 lose two frontoventral cirri, with eight frontoventral cirri and five transverse cirri and 2:2:3:3:2 pattern. In general, *Euplotes* species tend to lose their frontoventral cirri, which may occur independently among different subgroups (Zhao et al., 2018).

Morphogenesis During Sexual Stages in Other Ciliates

Limited studies reveal that the patterns of morphogenesis during conjugation vary dramatically among ciliates. For example, there is no obvious reorganization during conjugation in *Protospathidium serpens*, which unite obliquely with the oral bulge (Xu and Foissner, 2004). Only oral structures are reorganized during the conjugation in some species such as *Paramecium tetraurelia* (Ng and Newman, 1984), *Urocentrum turbo* (Serrano et al., 1987), *Caenomorpha medusula* (Martin-Gonzalez et al., 1988), *Nyctotherus cordiformis* (Wichterman, 1937), and *Bursaria truncatella* (Poljansky, 1934), although this reorganization of oral structures may occur at different developmental stages during conjugation, which is taxa specific. It has been indicated that ciliates go through a similar nuclear and cortical reorganization during autogamy as in conjugation (Xu and Shi, 1987). As research focusing on morphogenesis during autogamy is very limited, we only discuss the morphogenetic process during conjugation.

The most complex reorganization of the ciliature, including reorganization of both the buccal organelles and somatic ciliature, occurs in conjugating spirotrichs, which has conspicuous oral ciliature and highly differentiated somatic ciliature (Xu et al., 2020; Zhang et al., 2020). The ciliary reorganization during conjugation may occur only once as reported in *Pelagostrobilidium* sp. (Ota and Taniguchi, 2003) and *Halteria grandinella* (Agatha and Foissner, 2009), twice as in *Euplotes* (present study) and *Aspidisca* (Diller, 1975), and even three times as in *Oxytricha fallax* (Gregory, 1923), *Stylonychia mytilus* (Shi, 1976), and *Pseudourostyla cristata* (Zhang et al., 1985). Despite being a close relative to *E. raikovi* and two rounds of reorganizations occur during conjugation in both species, *Aspidisca costata* showed a different developmental behavior. In *Aspidisca*, the old AZM disintegrate but the new AZM is not developed until in late exconjugants during the second reorganization, so that the exconjugants remained astomatous for a long time (Diller, 1975; Rosati et al., 1998). However, *Aspidisca* species develop an anterior ciliary organelles (ACO) during the first reorganization, which corresponds to the anterior part of *Euplotes* AZM. Moreover, in both genera, the left most frontal cirrus develops only once. In *Aspidisca*, it originates during the first reorganization while in *Euplotes* during the second reorganization (Rosati et al., 1998). Therefore, a full number of cirri is developed after the first reorganization in *Aspidisca* while it is still incomplete in *Euplotes*. As mentioned above, it is obvious that many cytoplasmic organelles generally undergo profound reorganization during conjugation, which display a very high diversity of the morphogenetic patterns among ciliates. The

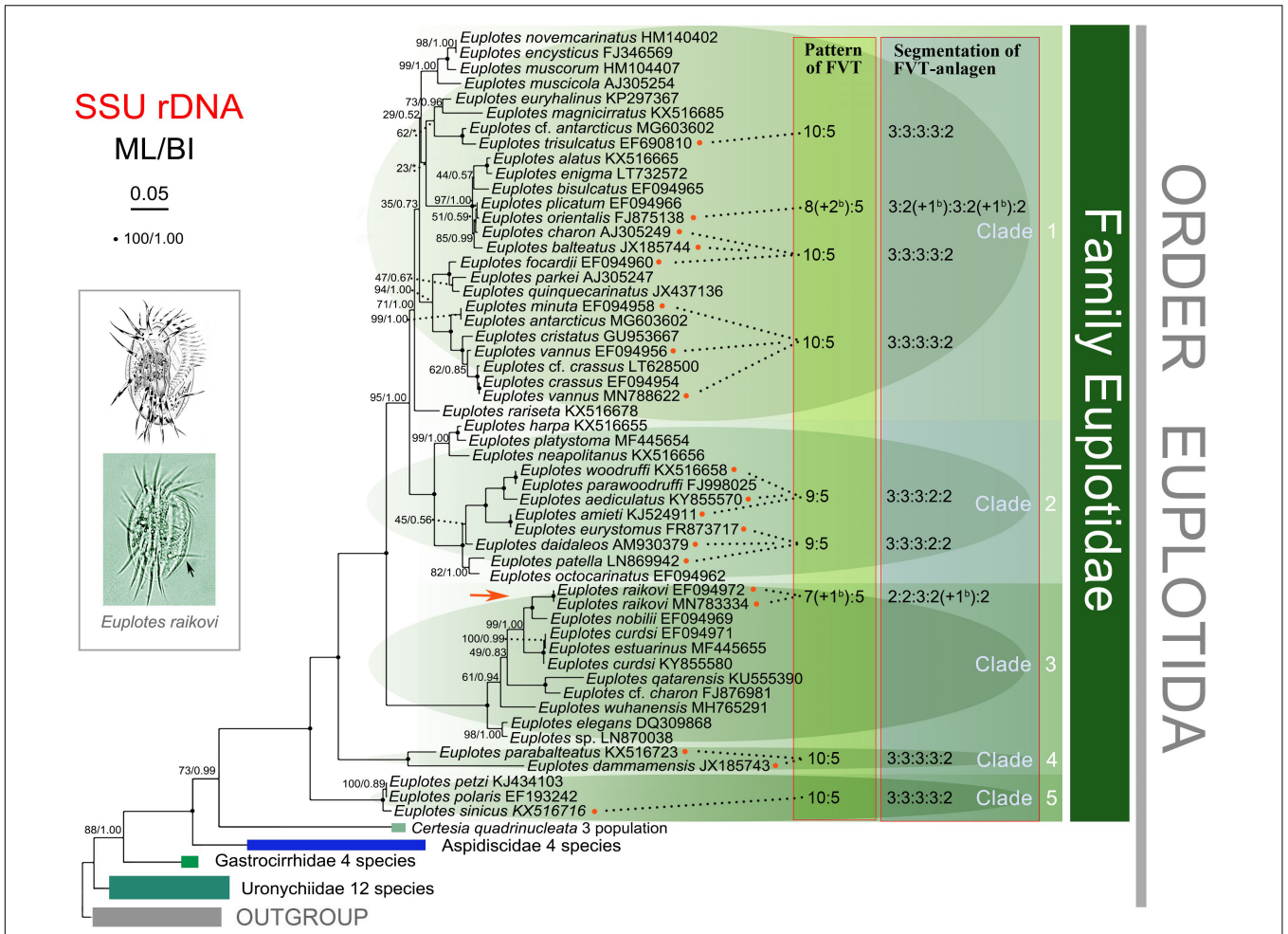

FIGURE 4 | Maximum likelihood (ML) tree based on SSU rDNA sequences showing the evolutionary relationships among *Euplotes* species. The pattern and the segmentation of the frontoventral-transverse (FVT) cirri of the available species are indicated in the tree. The FVT pattern represents the number of frontoventral cirri: transverse cirri. The segmentation of the FVT cirri shows the number of the fragmented anlagen from the first streak to the fifth streak, and the number of additional barren cirri/anlagen is shown in brackets. Numbers near the branches represent bootstrap values of ML analyses and posterior probability of Bayesian analyses (BI). "*" indicates topologies that differ between the ML and BI phylogenies. Fully supported (100/1.00) branches are marked with solid circles. All branches are drawn to scale. The scale bar corresponds to 5 substitutions per 100 nucleotide positions.

deep molecular mechanisms related to this complex process are waiting for further investigations.

DATA AVAILABILITY STATEMENT

The original contributions presented in the study are included in the article/supplementary material, further inquiries can be directed to the corresponding author/s.

AUTHOR CONTRIBUTIONS

FG performed conceptualization, supervision, and funding acquisition. RG performing cell culturing and conjugation induction. UA and YC performing protargol staining. BL performing drawings. YG performing phylogenetic analyses. YJ performing **Figure 1** preparation. UA, YC, YG, BL, YJ, RG, HM, KA, and FG performing original draft, review, and editing. All authors contributed to the article and approved the submitted version.

FUNDING

This work was supported by the National Natural Science Foundation of China (Project Nos. 31922013, 31772428, and 32030015) and Research Supporting Project (RSP-2020/10), King Saud University, Saudi Arabia.

ACKNOWLEDGMENTS

We thank Prof. Weibo Song (OUC) and the two reviewers for their kind help in revising the manuscript.

REFERENCES

Agatha, S., and Foissner, W. (2009). Conjugation in the spirotrich ciliate *Halteria grandinella* (Müller, 1773) Dujardin, 1841 (Protozoa, Ciliophora) and its phylogenetic implications. *Eur. J. Protistol.* 45, 51–63. doi: 10.1016/j.ejop.2008.07.004

Berger, H. (2001). *Catalogue of ciliate names: 1. Hypotrichs*. Salzburg: Verlag Helmut Berger.

Chen, X., Jiang, Y. H., Gao, F., Zheng, W. B., Krock, T. J., Stover, N. A., et al. (2019). Genome analyses of the new model protist *Euplotes vannus* focusing on genome rearrangement and resistance to environmental stressors. *Mol. Ecol. Resour.* 19, 1292–1308. doi: 10.1111/1755-0998.13023

Diller, W. F. (1966). Correlation of ciliary and nuclear development in the life cycle of *Euplotes*. *J. Protozool.* 13, 43–54. doi: 10.1111/j.1550-7408.1966.tb01868.x

Diller, W. F. (1975). Nuclear behavior and morphogenetic changes in fission and conjugation of *Aspidisca costata* (Dujardin). *J. Protozool.* 22, 221–229. doi: 10.1111/j.1550-7408.1975.tb05855.x

Fleury, A. (1991). Dynamics of the cytoskeleton during morphogenesis in the ciliate *Euplotes*. *Eur. J. Protistol.* 27, 220–237. doi: 10.1016/S0932-4739(11)80060-X

Foissner, W. (1996). *Ontogenesis in ciliate*d protozoa with emphasis on stomatogenesis. Hausmann Stuttgart: Gustav Fisher Verlag.

Gao, Y., Gong, R., Jiang, Y., Pan, B., Li, Y., Warren, A., et al. (2020). Morphogenetic characters of the model ciliate *Euplotes vannus* (Ciliophora, Spirotrichea): Notes on cortical pattern formation during conjugational and postconjugational reorganization. *Eur. J. Protistol.* 73:125675. doi: 10.1016/j.ejop.2020.125675

Gong, R., Jiang, Y., Vallesi, A., Gao, Y., and Gao, F. (2020). Conjugation in *Euplotes raikovi* (Protista, ciliophora): New insights into nuclear events and macronuclear development from micronucleate and amicronucleate cells. *Microorganisms* 8:162. doi: 10.3390/microorganisms8020162

Gregory, L. H. (1923). The conjugation of *Oxytricha fallax*. *J. Morphol.* 37, 555–581. doi: 10.1002/jmor.1050370305

Hammond, D. M., and Kofoid, C. A. (1937). The continuity of structure and function in the neuromotor system of *Euplotes patella* during its life cycle. *Proc. Am. Philos. Soc.* 77, 207–218.

Jernvall, J., and Newman, S. (2003). Mechanisms of pattern formation in development and evolution. *Development* 130, 2027–2037. doi: 10.1242/dev.00425

Jiang, J., Zhang, Q., Warren, A., Al-Rasheid, K. A. S., and Song, W. (2010). Morphology and SSU rRNA gene-based phylogeny of two marine *Euplotes* species, *E. orientalis* spec. nov. and *E. raikovi* Agamaliev, 1966 (Ciliophora, Euplotida). *Eur. J. Protistol.* 46, 121–132. doi: 10.1016/j.ejop.2009.11.003

Jiang, Y., Zhang, T., Vallesi, A., Yang, X., and Gao, F. (2019). Time-course analysis of nuclear events during conjugation in the marine ciliate *Euplotes vannus* and comparison with other ciliates (Protozoa, Ciliophora). *Cell Cycle* 18, 288–298. doi: 10.1080/15384101.2018.1558871

Jin, L. P., Zhuang, H., and Tsorun, T. (1985). Studies on conjugation in *Pseudourostyla cristata* â .Nucleogenesis. *Zool. Res.* 6, 159–167.

Katashima, R. (1959). A correlation between morphogenesis and old macronucleus during sexual reproduction in *Euplotes eurystomus*. *J. Sci. Hiroshima Univ. Ser. B* 19, 99–107.

Kirschner, M., Gerhart, J., and Mitchison, T. (2000). Molecular "vitalism.". *Cell* 100, 79–88. doi: 10.1016/s0092-8674(00)81685-2

Li, X., Huang, J., Filker, S., Stoeck, T., Bi, Y., Yu, Y., et al. (2019). Spatio-temporal patterns of zooplankton in a main-stem dam affected tributary: a case study in the Xiangxi River of the Three Gorges Reservoir, China. *Sci. China Life Sci.* 62, 1058–1069. doi: 10.1007/s11427-018-9523-0

Lian, C., Wang, Y., Li, L., Al-Rasheid, K., Jiang, J., and Song, W. (2020). Taxonomy and SSU rDNA-based phylogeny of three new *Euplotes* species (Protozoa, Ciliophora) from China seas. *J. King Saud Univ.* 32, 1286–1292. doi: 10.1016/j.jksus.2019.11.013

Lian, C., Zhang, T., Al-Rasheid, K. A. S., Yu, Y., Jiang, J., and Huang, J. (2019). Morphology and SSU rDNA-based phylogeny of two *Euplotes* species from China: *E. wuhanensis* sp. n. and *E. muscicola* Kahl, 1932 (Ciliophora, Euplotida). *Eur. J. Protistol.* 67, 1–14. doi: 10.1016/j.ejop.2018.10.001

Lu, B., Shen, Z., Zhang, Q., Hu, X., Warren, A., and Song, W. (2020). Morphology and molecular analyses of four epibiotic peritrichs on crustacean and polychaete hosts, including descriptions of two new species (Ciliophora, Peritrichia). *Eur. J. Protistol.* 73:125670. doi: 10.1016/j.ejop.2019.125670

Luporini, P., Pedrini, B., Alimenti, C., and Vallesi, A. (2016). Revisiting fifty years of research on pheromone signaling in ciliates. *Eur. J. Protistol.* 55, 26–38. doi: 10.1016/j.ejop.2016.04.006

Lynn, D. H. (2008). *The ciliated protozoa: Characterization, classification, and guide to the literature*, 3rd Edn. Dordrecht: Springer Press, doi: 10.1007/978-1-4020-8239-9

Martin-Gonzalez, A., Serrano, S., and Fernández-Galiano, D. (1988). Cortical morphogenesis and conjugation process in *Caenomorpha medusula* (Ciliophora, Heterotrichida). *Eur. J. Protistol.* 23, 111–121. doi: 10.1016/S0932-4739(88)80054-3

Ng, S. F., and Newman, A. (1984). The role of the micronucleus in stomatogenesis in sexual reproduction of *Paramecium tetraurelia*: micronuclear and stomatogenic events. *Protistol.* 20, 43–64. doi: 10.1016/s0932-4739(87)80006-8

Ota, T., and Taniguchi, A. (2003). Conjugation in the marine aloricate oligotrich *Pelagostrobilidium* (Ciliophora: Oligotrichia). *Eur. J. Protistol.* 39, 149–160. doi: 10.1078/0932-4739-00878

Poljansky, G. (1934). Geschlechtsprozesse bei Bursaria truncatella O.F. *Mull. Arch. Protistenk.* 81, 420–456.

Qeng, Y., Zou, S., and Tchang, T. (1992). The morphological changes in conjugation of *Euplote affiniss*. *J. East China Norm. Univ. Nat. Sci.* 2, 81–89.

Reubinoff, B. E., Pera, M. F., Fong, C. Y., Trounson, A., and Bongso, A. (2000). Embryonic stem cell lines from human blastocysts: Somatic differentiation in vitro. *Nat. Biotechnol.* 18, 399–404. doi: 10.1038/74447

Ricci, F., Candelori, A., Brandi, A., Alimenti, C., Luporini, P., and Vallesi, A. (2019). The sub-chromosomic macronuclear pheromone genes of the ciliate *Euplotes raikovi*: comparative structural analysis and insights into the mechanism of expression. *J. Eukaryot. Microbiol.* 66, 376–384. doi: 10.1111/jeu.12677

Rosati, G., Verni, F., and Dini, F. (1998). Mating by conjugation in two species of the genus *Aspidisca* (Ciliata, Hypotrichida): an electron microscopic study. *Zoomorphology* 118, 1–12. doi: 10.1007/s004350050051

Ruffolo, J. J. (1976). Cortical morphogenesis during the cell division cycle in *Euplotes*: An integrated study using light optical, scanning electron and transnlission electron microscopy. *J. Morphol.* 148, 489–527. doi: 10.1002/jmor.1051480406

Serrano, S., Martin-Gonzalez, A., and Fernandez-Galiano, D. (1987). Nuclear phenomena and oral reorganization during the conjugation of *Urocentrum turbo* OFM (Ciliata). *Arch. für Protistenkd.* 133, 257–268. doi: 10.1016/S0003-9365(87)80058-1

Shao, C., Ma, H., Gao, S., Khaled, A. R. A., and Song, W. (2010). Reevaluation of cortical developmental patterns in *Euplotes* (s. l.), including a morphogenetic redescription of *E. charon* (Protozoa. Ciliophora, Euplotida). *Chinese J. Oceanol. Limnol.* 28, 593–602. doi: 10.1007/s00343-010-9128-9

Sheng, Y., Duan, L., Cheng, T., Qiao, Y., Stover, N. A., and Gao, S. (2020). The completed macronuclear genome of a model ciliate *Tetrahymena thermophila* and its application in genome scrambling and copy number analyses. *Sci. China Life Sci.* 63, 1534–1542. doi: 10.1007/s11427-020-1689-4

Shi, X. (1976). Studies on conjugation in Stylonychyia mytilus II. Morphogenesis of argentophilic system. *Acta Zool. Sin.* 22, 71–83.

Shulman, J. M., and Daniel, S. J. (1999). Pattern formation in single cells. *Trends Biochem. Sci.* 24, 60–64. doi: 10.1016/S0968-0004(99)01490-5

Song, W., and Shao, C. (2017). *Ontogenetic patterns of hypotrich ciliates*. Beijing: Science Press.

Song, W., Warren, A., and Hu, X. (2009). *Free-living ciliates in the Bohai and Yellow Seas, China*. Beijing: Science Press.

Thomson, J. A., Itskovitz-Eldor, J., Shapiro, S. S., Waknitz, M. A., Swiergiel, J. J., Marshall, V. S., et al. (1998). Embryonic stem cell lines derived from human blastocysts. *Science* 282, 1145–1147. doi: 10.1126/science.282.5391.1145

Tuffrau, M., Tuffrau, H., and Genermont, J. (1976). La réorganisation infraciliaire au cours de la conjugaison et l'origine du primordium buccal dans le genre *Euplotes*. *J. Protozool.* 23, 517–523. doi: 10.1111/j.1550-7408.1976.tb03830.x

Turner, J. P. (1930). Division and conjugation in *Euplotes patella* Ehrenberg with special reference to the nuclear phenomena. *Univ. Calif. Publ. Zool.* 33, 193–258.

Voss, H. (1989). Morphogenetic comparison of 13 species of the genus *Euplotes* (ciliophora, hypotrichida). *Arch. für Protist.* 137, 331–344. doi: 10.1016/s0003-9365(89)80016-8

Wang, H., and Shi, X. (1989). Studies on morphogenesis accompanying binary fission and conjugation in *Euplotes woodruffi* (Ciliata, Protozoa). *Acta Zool. Sin.* 35, 353–359.

Wang, Y., Sheng, Y., Liu, Y., Zhang, W., Cheng, T., Duan, L., et al. (2019). A distinct class of eukaryotic MT-A70 methyltransferases maintain symmetric DNA N^6-adenine methylation at the ApT dinucleotides as an epigenetic mark associated with transcription. *Nucleic. Acids Res.* 47, 11771–11789. doi: 10.1093/nar/gkz1053

Washburn, E. S., and Borror, A. C. (1972). *Euplotes raikovi* Agamaliev, 1966 (Ciliophora, Hypotrichida) from new hampshire: description and morphogenesis. *J. Protozool.* 19, 604–608. doi: 10.1111/j.1550-7408.1972.tb03541.x

Wichterman, R. (1937). Division and conjugation in *Nyctotherus cordiformis* (EHr.) Stein (Protozoa, Ciliata) with special reference to the nuclear phenomena. *J. Morphol.* 60, 563–611. doi: 10.1002/jmor.1050600212

Xu, K., and Foissner, W. (2004). Body, nuclear, and ciliary changes during conjugation of *Protospathidium serpens* (Ciliophora, Haptoria). *J. Eukaryot. Microbiol.* 51, 605–617. doi: 10.1111/j.1550-7408.2004.tb00594.x

Xu, W., Wang, Y., Cheng, T., Yu, Y., El-Serehy, H., Al-Farraj, S. A., et al. (2020). Reevaluation of the 'well-known' *Paraurostyla weissei* complex, with notes on the ontogenesis of a new *Paraurostyla* species (Ciliophora, Hypotrichia). *Eur. J. Protistol.* 73:125672. doi: 10.1016/j.ejop.2020.125672

Xu, Z., and Shi, X. (1987). Research on initiation of sexual reproduction and induced autogamy in *Stylonychia mythus*. *Acta Zool. Sin.* 33, 353–361.

Yan, Y., Maurer-Alcalá, X. X., Kosakovsky Pond, S. L., Knight, R., and Katz, L. A. (2019). Single-cell transcriptomics reveal a correlation between genome architecture and gene family evolution in ciliates. *mBio*. 10:e02524-19. doi: 10.1128/mBio.02524-19

Zhang, T., Dong, J., Cheng, T., Duan, L., and Shao, C. (2020). Reconsideration of the taxonomy of the marine ciliate *Neobakuella aenigmatica* Moon et al., 2019 (Protozoa, Ciliophora, Hypotrichia). *Mar. Life Sci. Technol.* 2, 97–108. doi: 10.1007/s42995-020-00032-4

Zhang, Z., Zhuang, H., and Jin, L. P. (1985). Studies on Conjugation in *Pseudourostyla cristata* II. Morphogenesis of Cortical Structures. *Zool. Res.* 6, 79–92.

Zhao, Y., Yi, Z., Warren, A., and Song, W. (2018). Species delimitation for the molecular taxonomy and ecology of the widely distributed microbial eukaryote genus *Euplotes* (Alveolata, Ciliophora). *Proc. R. Soc. B Biol. Sci.* 285:20172159. doi: 10.1098/rspb.2017.2159

Zou, S. F., and Ng, S. F. (1991). Commitment to the first cortical reorganization during conjugation in *Stylonychia mytilus*: An argument for homology with cortical development during binary fission. *J. Protozool.* 38, 192–200. doi: 10.1111/j.1550-7408.1991.tb04428.x

Conflict of Interest: The authors declare that the research was conducted in the absence of any commercial or financial relationships that could be construed as a potential conflict of interest.

frontiers in Marine Science

ORIGINAL RESEARCH
published: 13 January 2021
doi: 10.3389/fmars.2020.615903

Morphology and Molecular Phylogeny of Four Trachelocercid Ciliates (Protozoa, Ciliophora, Karyorelictea) Found in Marine Coastal Habitats of Northern China, With Description of a New Genus, Two New Species and a New Combination

Mingzhen Ma[1†], Yuqing Li[1†], Honggang Ma[1], Khaled A. S. Al-Rasheid[2], Alan Warren[3], Yurui Wang[1] and Ying Yan[1*]*

[1] Laboratory of Protozoology, Institute of Evolution and Marine Biodiversity, Ocean University of China, Qingdao, China, [2] Zoology Department, College of Science, King Saud University, Riyadh, Saudi Arabia, [3] Department of Life Sciences, Natural History Museum, London, United Kingdom

The morphology of four trachelocercid ciliates, *Foissnerella typica* gen. nov., spec. nov., *Trachelolophos monocaryon* (Dragesco, 1965) comb. nov. (original combination: *Tracheloraphis monocaryon* Dragesco, 1965), *Tracheloraphis katzae* spec. nov., and *Tracheloraphis colubis* (Kahl, 1933) Xu et al., 2011 were studied in live and protargol-stained specimens. All samples were isolated from the intertidal zone of sandy beaches at Qingdao, China. The new genus *Foissnerella* can be distinguished from other trachelocercid genera mainly by the three circumoral kineties each composed of a row of dikinetids and the absence of a brosse or ciliary tuft in the oral cavity. The detailed investigation on the poorly described *Tracheloraphis monocaryon* (Dragesco, 1965) reveals that its oral infraciliature includes one uninterrupted circumoral kinety and a conspicuous ciliary tuft in the center of the oral cavity, which is consistent with the genus *Trachelolophos* rather than *Tracheloraphis*. Therefore, this species is transferred to *Trachelolophos* as *Trachelolophos monocaryon* (Dragesco, 1965) comb. nov. *Tracheloraphis katzae* spec. nov. can be recognized by the combination of its minute brownish cortical granules and 9–15 somatic kineties. The small subunit (SSU) rDNA of each species was sequenced for the first time. Phylogenetic analyses of the SSU rDNA show that *Foissnerella typica* gen. nov., spec. nov. clusters with *Apotrachelocerca arenicola* (Kahl, 1933) Xu et al., 2011 in a group that is sister to all other trachelocercids.

Keywords: infraciliature, SSU rDNA, ciliates, Karyorelictea, Trachelocercidae

OPEN ACCESS

Edited by:
Hongbo Pan,
Shanghai Ocean University, China

Reviewed by:
Xumiao Chen,
Institute of Oceanology (CAS), China
Jun Gong,
Sun Yat-sen University, China

***Correspondence:**
Yurui Wang
wangyurui2011@163.com
Ying Yan
yanying@ouc.edu.cn

† These authors have contributed equally to this work

Specialty section:
This article was submitted to Marine Evolutionary Biology, Biogeography and Species Diversity, a section of the journal Frontiers in Marine Science

Received: *10 October 2020*
Accepted: *03 December 2020*
Published: *13 January 2021*

Citation:
Ma M, Li Y, Ma H, Al-Rasheid KAS, Warren A, Wang Y and Yan Y (2021) Morphology and Molecular Phylogeny of Four Trachelocercid Ciliates (Protozoa, Ciliophora, Karyorelictea) Found in Marine Coastal Habitats of Northern China, With Description of a New Genus, Two New Species and a New Combination. Front. Mar. Sci. 7:615903. doi: 10.3389/fmars.2020.615903

INTRODUCTION

The family Trachelocercidae Kent, 1881 is the largest family within the class Karyorelictea Corliss, 1974 and all its members inhabit marine sandy sediments in intertidal zones (Al-Rasheid, 1996, 1997, 1998, 2001; Foissner and Dragesco, 1996a; Al-Rasheid and Foissner, 1999; Song et al., 2009; Hu et al., 2019). Since the first species was described over 200 years ago, about 80 nominal species of trachelocercids have been reported (Carey, 1992; Xu et al., 2011a, 2014; Yan et al., 2015, 2016). However, only a limited number of detailed studies of trachelocercids have been carried out using modern methods such as protargol staining, scanning electron microscopy and phylogeny analyses (Foissner and Dragesco, 1996a,b; Dragesco, 1997, 1999; Foissner, 1997; Xu et al., 2012; Yan et al., 2019) and most species are known only from live observations (Dragesco, 1960; Raikov et al., 1975; Wilbert, 1986; Carey, 1992). Moreover, the molecular data of trachelocercids remain scarce.

In the present study, the morphological data of four trachelocercids isolated from marine coastal habitats at Qingdao, China, are documented based on observations of specimens *in vivo* and following protargol staining. In addition, the SSU rDNA sequence of each species is provided and phylogenetic analyses are performed to assess their evolutionary relationships. *Foissnerella* gen. nov. is assigned to the family Trachelocercidae based on both morphological and molecular information.

MATERIALS AND METHODS

Sample Collection, Observation, and Identification

Foissnerella typica gen. nov., spec. nov. and *Tracheloraphis colubis* (Kahl, 1933) Xu et al., 2011 were collected from the intertidal zone of Silver Beach, Qingdao (35°55′09″N, 120°11′55″E) on March 11, 2013 and May 27, 2019, respectively. The water temperature on each day of sampling was 11 and 23°C, respectively, and the salinity was about 27‰. *Trachelolophos monocaryon* (Dragesco, 1965) comb. nov. and *Tracheloraphis katzae* spec. nov. were both collected on June 24, 2019, from the intertidal zone of the No. 1 Bathing beach, Qingdao (36°03′24″N, 120°20′32″E) where the water temperature was 26°C and the salinity was about 30‰ (**Figure 1**). For each sample, the top 5 cm of sand or sediment along with seawater from the site was collected. Ciliates were extracted from the sediment using the method from Uhlig (1968). In brief, the sand or sediment was placed in a plastic tube (4.5 cm diameter and 10 cm long, at one end of which was a tightly fitting nylon gauze (mesh size 80–90 μm)). The depth of the sediment in the tube was 5 cm. Finely crushed ice was added to fill the remainder of the tube. A glass culture dish containing about 20 ml filtered seawater was placed under the tube so that the nylon gauze was barely in contact with the seawater surface. Ciliates in the sand/sediment sample migrating downwards to escape the advancing front of meltwater were collected in the culture dish.

Cells were isolated and observed *in vivo* using bright field and differential interference contrast (DIC) microscopy (Olympus BX 53). The infraciliature was revealed using the protargol staining method (Wilbert, 1975). Counts, measurements, and drawings of stained specimens were performed at 1,000 × magnification. Terminology and systematics mainly follow Foissner (1996) and Lynn (2008), respectively.

DNA Extraction, PCR Amplification, and Gene Sequencing

DNA extraction, PCR amplification, and SSU rDNA sequencing of the four species were performed according to Wang et al. (2020). For each species, we extracted total genomic DNA from single cells using the DNeasy Blood and Tissue Kit (Qiagen, Hilden, Germany). The primers 82F (5′-GAA ACT GCG AAT GGC TC-3′) (Jerome et al., 1996), 18S-F (5′-AAC CTG GTT GAT CCT GCC AGT-3′), and 18S-R (5′-TGA TCC TTC TGC AGG TTC ACC TAC-3′) were used to amplify the SSU rDNA (Medlin et al., 1988). PCR amplification was carried out according to Wang et al. (2019, 2020) and PCR products were then sequenced bidirectionally by the Tsingke Biological Technology Company (Beijing, China).

Phylogenetic Analyses

Using MAFFT implemented in GUIDANCE[1] with default parameters (Penn et al., 2010), the newly generated SSU rDNA sequences of the four species were aligned with 54 other sequences of karyorelictean and heterotrich (outgroup) species downloaded from NCBI GenBank. The resulting alignments were manually refined by trimming both ends with Bioedit v.7.0.5 (Hall, 1999) and the final alignments were 1,802 bp.

Maximum likelihood (ML) and Bayesian inference (BI) analyses were both carried out using the CIPRES Science Gateway v.3.3[2] (Stamatakis, 2014). ML bootstrapping analysis was performed online with 1,000 replicates using RAxML-HPC2 on XSEDE v.8.2.12 (Stamatakis et al., 2008) and the GTRGAMMA model. BI analysis was performed with MrBayes on XSEDE v.3.2.7a (Ronquist et al., 2012) using the GTR + I + G model selected by MrModeltest v.2.2 (Nylander, 2004). The chain length for our analysis was 1,000,000 generations with trees sampled every 100 generations, the first 25% of which were discarded as burn-in. MEGA v.5.0 (Tamura et al., 2011) was used to visualize the phylogenetic tree topology.

Topology Testing

The phylogenetic relationships among different taxa within Karyorelictea were assessed using the approximately unbiased (AU) test (Shimodaira, 2002). Two constrained ML trees were generated by RAxML v8.2.10 (Stamatakis, 2014) with the enforced constraints (**Table 1**) and their topologies were compared with those of the best unconstrained ML trees implemented in CONSEL (Shimodaira and Hasegawa, 2001).

[1] http://guidance.tau.ac.il/ver2/

[2] http://www.phylo.org/portal2

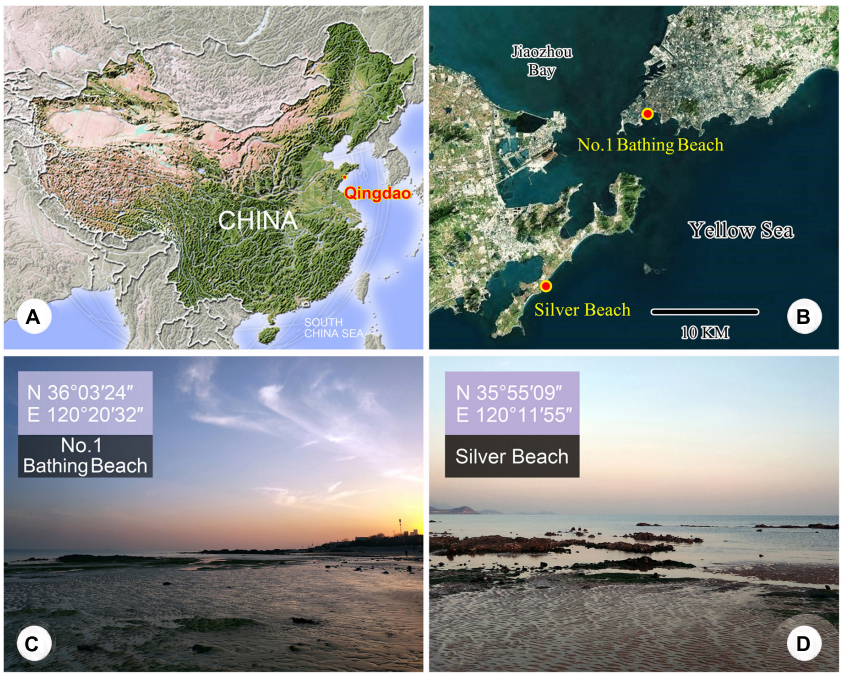

FIGURE 1 | (A–D) Maps and photographs of the sample sites. **(A)** Location of Qingdao. **(B)** The dots indicates the locations of the two sample sites. **(C)** The intertidal zone of the No. 1 Bathing Beach. **(D)** The intertidal zone of Silver Beach.

TABLE 1 | Approximately Unbiased test results based on the SSU rDNA data.

Topology constraints	Log-likelihood (-lnL)	AU test
Unconstrained	−13786.067660	0.935
Tracheloraphis	−13954.259391	7.00E-14
Trachelocerca	−13802.664146	0.065

The topology constraints column refers to proposed taxonomic groups that were tested for monophyly through the approximately unbiased test (AU). Rejected monophyly ($p < 0.05$) is highlighted in gray.

Internal relationships in the constrained group and among the remaining taxa were unspecified.

ZooBank Registration

ZooBank registration number of present work: urn:lsid:zoobank.org:pub:913C263C-56A7-40AC-9885-E06DC530A6D8.

RESULTS AND DISCUSSION

Class Karyorelictea Corliss, 1974
Order Protostomatida Small & Lynn, 1985
Family Trachelocercidae Kent, 1881
Genus *Foissnerella* gen. nov.

Diagnosis

Trachelocercidae with three circumoral kineties each composed of a row of dikinetids. No brosse or ciliary tuft in oral cavity. Marine habitat.

Etymology

The new genus name is dedicated to the eminent ciliatologist, Prof. Wilhelm Foissner, Universität Salzburg, Austria, in recognition of his significant contributions to the study of ciliates.

Type Species

Foissnerella typica spec. nov.

Discussion

Foissnerella gen. nov. possesses all the diagnostic characters of trachelocercids, i.e., elongate body shape with distinct "head" and "neck" and somatic ciliature covering the body apart from longitudinal glabrous zone that is bordered by a "bristle-like" kinety. Therefore, *Foissnerella* gen. nov. undoubtedly belongs to the family Trachelocercidae. The shape and structure of the oral ciliature is the main character for generic classification (Foissner and Dragesco, 1996a,b; Foissner and Al-Rasheid, 1999). *Foissnerella* gen. nov. possesses three circumoral kineties each composed of a row of dikinetids. Consequently, it can be easily separated from its most closely related genera such as *Apotrachelocerca* Xu et al., 2011, which has two rows of uninterrupted circumoral kineties, *Trachelocerca* Ehrenberg, 1840, which has a single uninterrupted circumoral kinety composed of dikinetids, and *Prototrachelocerca* Foissner, 1996 has two rows of circumoral kineties interrupted by short brosse kineties (**Table 2**). It is noteworthy that no anterior or posterior secant system is present in *Foissnerella typica* gen. nov. spec. nov., which is similar to *Apotrachelocerca arenicola* (Kahl, 1933) Xu et al., 2011. However, the presence/absence of the anterior

TABLE 2 | Distinction among genera in trachelocercid karyorelictids.

	Character				
Genus	**Brosse**	**Ciliary tuft in oral cavity**	**Circumoral kinety**	**Secant system**	**Source**
***Foissnerella* gen. nov.**	–	–	**Three rows and uninterrupted**	**Left**	**This study**
Trachelolophos	–	**Present**	**One row and uninterrupted**	**Left**	**Foissner and Dragesco (1996a)**
Tracheloraphis	**Present**	–	**One row and interrupted**	**Left**	**Dragesco (1960)**
Prototrachelocerca	Present	–	Two rows and interrupted	Left	Foissner (1996)
Kovalevaia	Present	–	One row and uninterrupted	Left	Foissner (1997)
Sultanophrys	Present	–	One row and interrupted	Right	Foissner and Al-Rasheid (1999)
Apotrachelocerca	–	–	Two rows and uninterrupted	Left	Xu et al. (2011b)
Trachelocerca	–	–	One row and uninterrupted	Left	Ehrenberg (1840)

–, Absent.
The genera in bold are described in present study.

or posterior secant system is not considered as a genus-level character for trachelocercid classification.

***Foissnerella typica* spec. nov.** (**Figures 2**, **3** and **Table 3**)

Diagnosis

Extended cells *in vivo* about 400–800 μm × 15–25 μm; body ribbon-like and flattened; head dominant and black in color, distinguished from trunk; usually 13–24 macronuclei; 7 ciliary rows on right side of cell; left side unciliated except for bristle kinety; glabrous stripe as wide as trunk; no anterior or posterior secant system on either side of glabrous stripe; cortical granules minute and colorless.

Type Locality

The intertidal zone of Silver Beach, Qingdao (35°55′09″N, 120°11′55″E), China (**Figure 1**).

Type Specimens

A protargol-stained slide containing the holotype specimen marked with an ink circle is deposited in the Laboratory

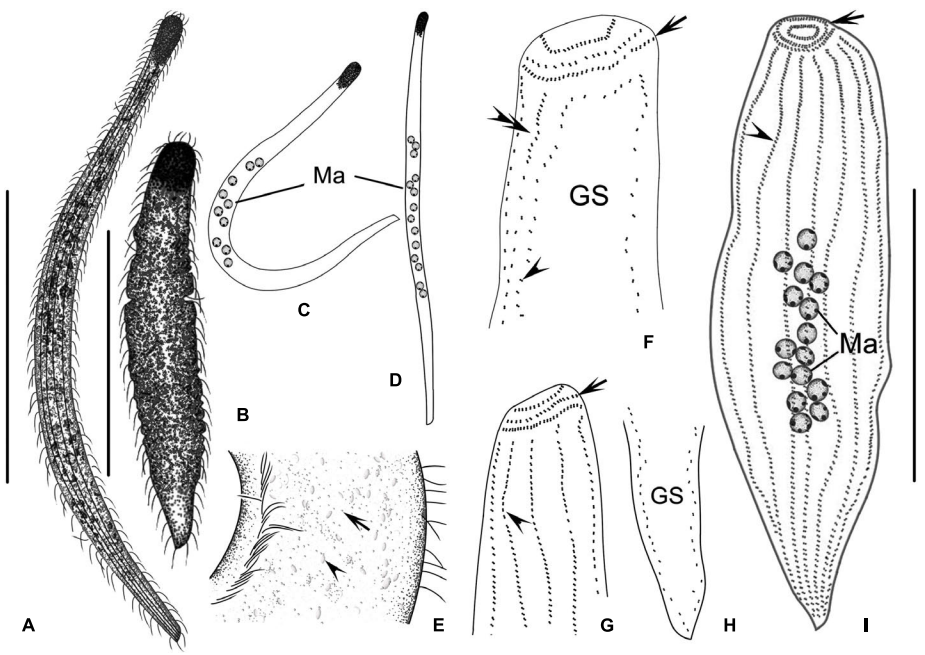

FIGURE 2 | (A–I) *Foissnerella typica* gen. nov., spec. nov. *in vivo* **(A–E)** and after protargol staining **(F–I)**. **(A)** Typical individual. **(B)** An extremely contracted cell. **(C–D)** Different body shapes. **(E)** Distribution of cortical granules in glabrous stripe (arrow). Arrowhead points to the granules. **(F,G)** Detailed ciliature of left **(F)** and right **(G)** side of anterior body region, showing three circumoral kineties each composed of a row of dikinetids (arrow), glabrous stripe, somatic kineties (double arrowheads in **F** and arrowhead in **G**) and bristle kinety (arrowhead in **F**). **(H)** Ciliary pattern of tail region showing glabrous stripe. **(I)** Overview showing ciliary pattern and multiple macronuclei of holotype specimen, three circumoral kineties each composed of a row of dikinetids (arrow) and somatic kineties (arrowhead). GS, glabrous stripe; Ma, macronuclei. Scale bars = 300 μm **(A,B)**; 80 μm **(I)**.

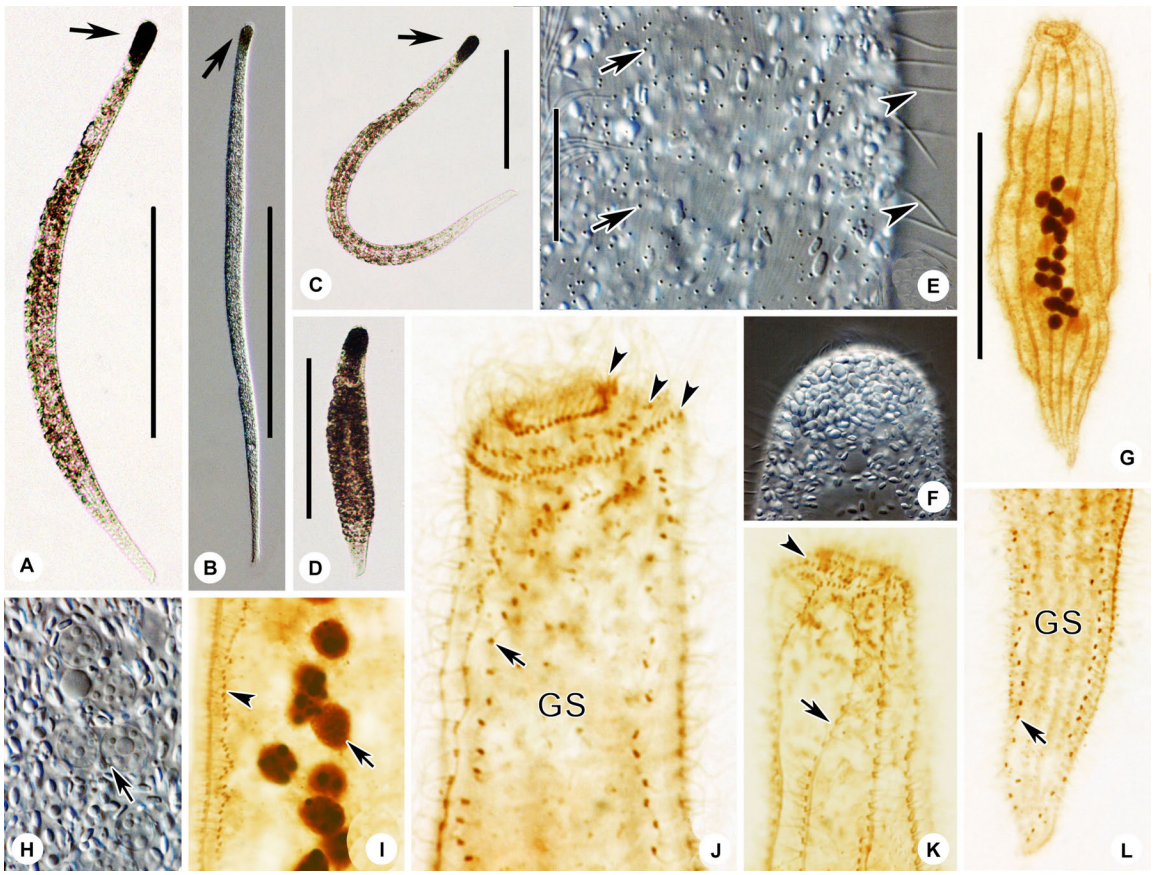

FIGURE 3 | (A–I) *Foissnerella typica* gen. nov., spec. nov. *in vivo* **(A–F,H)** and after protargol staining **(G,I–L)**. **(A–C)** Typical individuals. Arrow showing the head of the cell. **(D)** An extremely contracted cell. **(E)** Distribution of cortical granules in glabrous stripe (arrows) and spine-like bristle cilia (arrowheads). **(F)** Showing head of cell packed with ellipsoidal granules. **(G)** Right side view of the holotype specimen showing the ciliary pattern and multiple macronuclei. **(H)** Showing globular macronuclei. **(I)** Left margin of mid-body showing macronucleus (arrow) and bristle kinety (arrowhead). **(J,K)** Detailed ciliature of left **(J)** and right **(K)** side of anterior body region, three circumoral kineties each composed of a row of dikinetids (arrowheads), glabrous stripe, somatic kineties (arrow in **K**), and bristle kinety (arrow in **J**). **(L)** Ciliary pattern of tail region showing glabrous stripe and bristle kinety (arrow). GS, glabrous stripe. Scale bars = 300 μm **(A–D)**; 30 μm **(E)**; 80 μm **(G)**.

of Protozoology, Ocean University of China, Qingdao, China (No. YY2013031107).

Etymology

This species-group name *typica* means that it is the representative species of this genus.

Morphological Description

Cells *in vivo* 400–800 μm × 15–25 μm, flexible and contractile (**Figures 2A,B**, **3A–D**); ribbon-like flattened (up to 3:1) including oral area (**Figures 2A,C,D**, **3A–C**). Width almost constant throughout anterior three-quarters of cell; head region dominant; no distinct neck; posterior quarter of body narrowed (**Figures 2A,C,D**, **3A–C**). At low magnification, anterior of cell often dark grayish due to multiple inclusions (**Figure 3F**). Cortical granules colorless, about 0.5 μm in diameter, sparsely scattered between ciliary rows and in glabrous stripe (**Figures 2E**, **3E**). Thirteen to 26 macronuclei, 6–9 μm in diameter, arranged in a longitudinally oriented group in mid-body region (**Figures 2C,D**, **3G** and **Table 3**). Macronuclei containing many large chromatin aggregates, possibly nucleoli (**Figures 2I**, **3H,I**).

Locomotion by gliding sluggishly along bottom of Petri dish.

Infraciliature consists of dikinetids (**Figure 2F–I**). Only right side ciliated with seven somatic kineties. Left side occupied by glabrous stripe. Cilia about 8 μm long (**Figure 3G**). No anterior or posterior secant system on either side of glabrous stripe (**Figures 2F,H**, **3I,J,L**). Glabrous stripe bordered by a bristle kinety composed of one row of dikinetids (**Figures 2F,H**, **3I,J,L**). Three circumoral kineties each composed of an uninterrupted row of obliquely oriented and narrowly spaced dikinetids (**Figures 2F,G**, **3J,K**).

Genus *Trachelolophos* Foissner & Dragesco, 1996

Trachelolophos monocaryon (Dragesco, 1965) **comb. nov.** (**Figures 4**, **5** and **Table 3**)

(original combination: *Tracheloraphis monocaryon* Dragesco, 1965**)**

Dragesco (1965) described this species under the name of *Tracheloraphis monocaryon,* based solely on live observations. Thus, this form remained largely unknown for over half a

TABLE 3 | Morphometric data for *Foissnerella typica* gen. nov., spec. nov. (first line), *Trachelolophos monocaryon* (Dragesco, 1965) comb. nov. (second line), *Tracheloraphis katzae* spec. nov. (third line), and *Tracheloraphis colubis* (fourth line).

Characters	Min	Max	Mean	SD	CV	n
Body length in μm	142	329	198.9	53.1	26.7	24
	135	430	279.6	85.0	30.4	25
	104	255	168.5	39.5	23.4	25
	120	308	174.0	38.3	22.0	25
Body width in μm	20	78	46.4	14.2	30.5	24
	42	150	78.6	28.7	36.5	25
	20	53	30.1	8.3	76.5	25
	30	105	62.4	20.5	32.9	25
Somatic kineties, number	7	7	7.0	0	0	21
	30	44	36.7	3.7	10.2	25
	9	15	11.8	1.4	11.8	25
	17	27	21.8	2.6	11.7	23
Macronuclei in single nuclear group, number	–	–	–	–	–	–
	4	4	4.0	0	0	25
	4	4	4.0	0	0	25
	4	4	4.0	0	0	25
Macronuclei in strand, number	13	26	17.0	3.2	19.1	22
	–	–	–	–	–	–
	–	–	–	–	–	–
	–	–	–	–	–	–
Micronuclei in single nuclear group, number	–	–	–	–	–	–
	2	2	2.0	0	0	25
	2	2	2.0	0	0	25
	2	2	2.0	0	0	25
Nuclear group length	–	–	–	–	–	–
	19	33	25.4	4.1	16.3	25
	9	14	10.8	1.4	12.6	25
	9	17	11.4	2.2	18.9	25

All data are based on protargol-stained specimens and morphometric data of Trachelolophos monocaryon (Dragesco, 1965) comb. nov. and Tracheloraphis katzae spec. nov. are based on Qingdao population. CV, coefficient of variation (%); Mean, arithmetic mean; n, number of examined specimens. "–" indicates data unavailable or not applicable.

century due to the lack of knowledge of the infraciliature. Observations of both live and silver-stained specimens of the present isolate indicates that this taxon should be assigned to the genus *Trachelolophos*. Therefore, a new combination is suggested and a redescription and improved diagnosis are supplied.

Improved Diagnosis

Extended cells 500–1,000 μm × 40–70 μm *in vivo* with inconspicuous dark head and a rounded posterior end. Thirty to 44 somatic kineties. Glabrous stripe narrow, about the width occupied by 2–3 somatic kineties. Four macronuclei and two micronuclei in a single group. Cortical granules grayish and ellipsoidal, ca. 0.5 μm × 0.8 μm, densely distributed.

Deposition of Voucher Materials

A voucher slide with protargol-stained specimens has been deposited in the Laboratory of Protozoology, Ocean University of China, Qingdao, China (registration number: MMZ2019062406).

Redescription

Extended cells 500–1,000 μm × 40–70 μm *in vivo*; body cylindrical or rod-like, flexible and contractile (**Figures 4A–C**, **5A–D**); 30–44 somatic kineties; neck and tail indistinctly separated from trunk, head triangular, posterior end of tail rounded (**Figures 4A–C,H**, **5A–D** and **Table 3**). Cortical granules ellipsoidal, ca. 0.5 μm × 0.8 μm, grayish in bright field at high magnifications; densely packed (but non-grouped) between somatic kineties and in glabrous stripe (**Figures 4D**, **5E**). Cytoplasm colorless and transparent, packed with cytoplasmic granules, ellipsoidal, 1–3 μm long and colorless (**Figures 5F,G**).

Locomotion by gliding on substrate, winding between sand grains and organic debris.

Entire infraciliature consisting of dikinetids (**Figures 4H**, **5K**). Cilia about 10 μm long *in vivo* and arranged in longitudinal rows. Oral infraciliature consists of a single uninterrupted circumoral kinety and a conspicuous ciliary tuft located in center of oral cavity (**Figures 4F–H**, **5I,L**). Glabrous stripe very narrow, width about equal to the gap between two adjacent somatic kineties, bordered by irregularly spaced bristle kinety (**Figures 4H**, **5J**). Anterior and posterior secant systems formed on left side of glabrous stripe and some kineties also abut to bristle kinety (**Figures 4H**, **5J**). Four macronuclei (in which crystals are sometimes present) and two micronuclei in a single group (**Figures 4E**, **5H,M**).

Discussion

This organism was first reported by Dragesco (1965) under the name *Tracheloraphis monocaryon* and the original description was based solely on a rather schematic figure and a short description of the cell *in vivo*. The Qingdao population corresponds closely with the original population in several key characters such as the narrow glabrous stripe, the single nuclear group composed of four macronuclei and two micronuclei and the possession of about 40 somatic kineties. Therefore, we consider them to be conspecific. Before transferring this species to *Trachelolophos*, we compare the Qingdao isolate to all four species of *Trachelolophos*.

The four congeners can all be clearly distinguished from the new isolate by body shape, body length, the number of somatic kineties and the number of nuclei or nuclear groups. *Trachelolophos filum* (Dragesco & Dragesco-Kernéis, 1986) Foissner & Dragesco, 1996 differs from the new isolate in having fewer somatic kineties on the trunk (26–35 vs. 30–44) and 4–16 nuclear groups, each with usually two macronuclei and a micronucleus, whereas the Qingdao isolate has only one nuclear group consisting of four macronuclei and two micronuclei (Dragesco and Dragesco-Kernéis, 1986; Foissner and Dragesco, 1996a). *Trachelolophos gigas* Foissner & Dragesco, 1996 differs from *T. monocaryon* in possessing a much longer body (2,000 μm vs. 500–1,000 μm), more somatic kineties on the trunk (52–71 vs. 30–44), and in the number and arrangement of its macronuclei (17–33 forming a strand vs. four in one nuclear group) (Foissner and Dragesco, 1996a). *Trachelolophos binucleatus* Yan et al., 2016 differs from *T. monocaryon* in having fewer somatic kineties

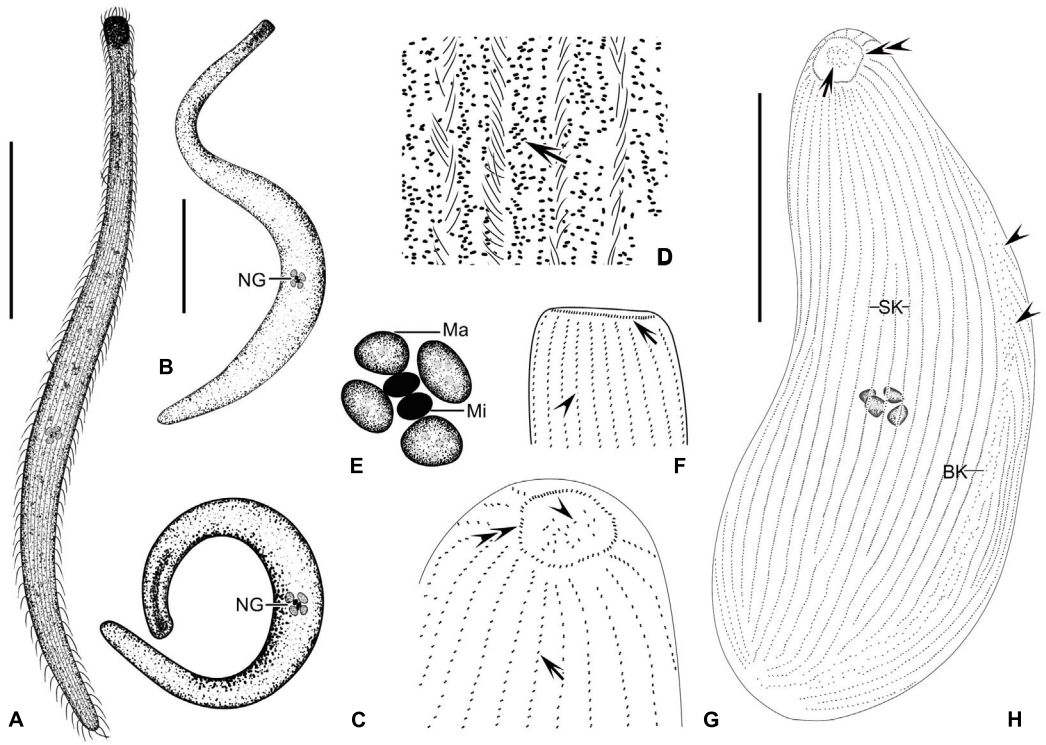

FIGURE 4 | (A–H) *Trachelolophos monocaryon* (Dragesco, 1965) comb. nov. *in vivo* **(A–D)** and after protargol staining **(E–H)**. **(A,B)** Typical individual. **(C)** An extremely curved cell. **(D)** Distribution of cortical granules (arrow) between somatic kineties. **(E)** Nuclear group. **(F)** Lateral view of head showing circumoral kinety (arrow) and somatic kineties (arrowhead). **(G)** Apical view of head, showing the ciliary tuft (arrowhead), somatic kineties (arrow), and circumoral kinety (double arrowheads). **(H)** Overview showing the multiple macronuclei, ciliary tuft (arrow), circumoral kinety (double arrowheads), and secant system (arrowheads). BK, bristle kinety; Ma, macronuclei; Mi, micronuclei; NG, nuclear group; SK, somatic kineties. Scale bars = 200 μm **(A,B)**; 80 μm **(H)**.

on the trunk (17–26 vs. 30–44) and fewer macronuclei (2 vs. 4) (Foissner and Dragesco, 1996a). *Trachelolophos quadrinucleatus* Yan et al., 2016 differs from *T. monocaryon* in possessing a longer body (1,100–1,400 μm vs. 500–1,000 μm) and a wedge-shaped (vs. rounded) posterior body end (Yan et al., 2016). Given these distinctions, the validity of *T. monokaryon* as a distinct species within the genus *Trachelolophos* is strongly supported.

Genus *Tracheloraphis* Dragesco, 1960
***Tracheloraphis katzae* spec. nov.** (**Figures 6**, **7** and **Table 3**)

Diagnosis

Size *in vivo* 400–800 μm × 20–30 μm; 9–15 somatic kineties on trunk; head dark and conspicuous, trunk widened, tail narrowed; single nuclear group composed of four macronuclei and two micronuclei; glabrous stripe as wide as trunk; cortical granules brownish, ellipsoidal, about 0.5 μm × 0.2 μm, densely distributed.

Type Locality

The intertidal zone of the No. 1 Bathing beach, Qingdao (36°03′24″N, 120°20′32″E), China, where the water temperature was 26°C and the salinity was about 30‰ (**Figure 1**).

Type Specimens

A protargol slide containing the holotype specimen marked with an ink circle is deposited in the Laboratory of Protozoology, Ocean University of China, Qingdao, China (No. MMZ2019062407).

Etymology

We dedicate this new species to our eminent colleague, Prof. Laura Katz, Smith College, United States, in recognition of her great contributions to ciliate research.

Description

Fully extended cells about 600 μm × 25 μm *in vivo*; body flexible and flattened, ribbon-like, with claviform head and pointed tail, trunk region conspicuously widened (**Figures 6A–C**, **7A–C**). Trunk dark at low magnification, neck and tail portions transparent due to lack of inclusions (**Figures 6A–C**, **7A**). Globular granules clustering in mid-body region (**Figure 7F**). Single nuclear group located in center of trunk, containing four macronuclei, 5–7 μm in diameter, in which there are some crystals (**Figure 7G**), and two micronuclei, 2–3 μm in diameter (**Figures 6F**, **7G,L**). Brownish cortical granules, ellipsoidal, ca. 0.2 μm × 0.5 μm, densely distributed between ciliary rows and in glabrous stripe (**Figures 6E**, **7D,E**).

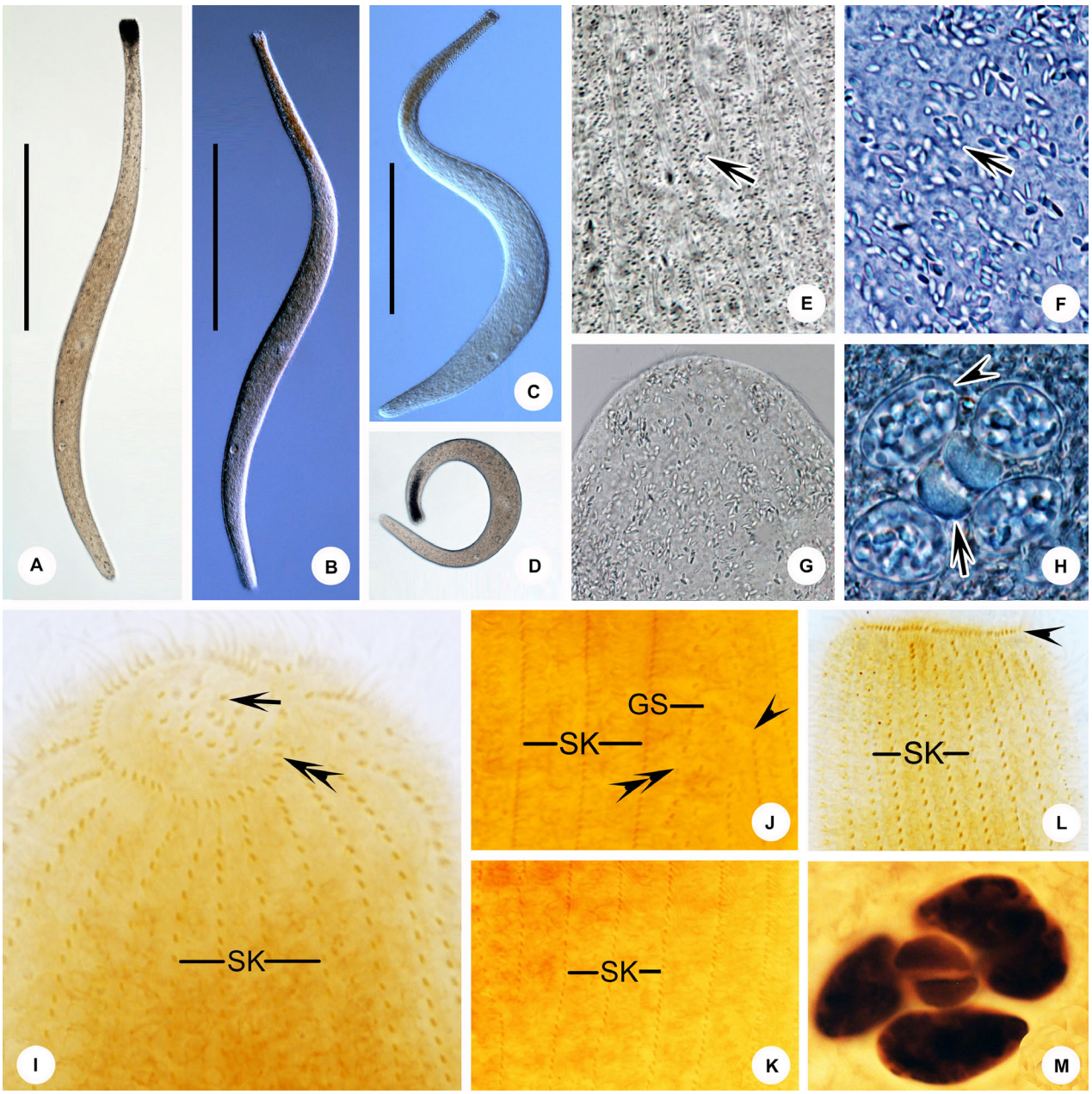

FIGURE 5 | (A–M) *Trachelolophos monocaryon* (Dragesco, 1965) comb. nov. *in vivo* **(A–H)** and after protargol staining **(I–M)**. **(A–C)** Typical individual. **(D)** An extremely curved cell. **(E)** Distribution of cortical granules (arrow) between somatic kineties. **(F)** Showing ellipsoidal granules (arrow). **(G)** Showing the head full of ellipsoidal granules. **(H)** Nuclear group, arrow showing micronuclei, arrowhead showing crystals in the macronuclei. **(I)** Anterior region of cell showing the ciliary tuft (arrow) and circumoral kinety (double arrowheads). **(J)** Detail of trunk showing the glabrous stripe with secant system on left side (arrowheads), bristle kinety (double arrowheads), and somatic kineties. **(K)** Showing the somatic kineties. **(L)** Anterior of cell. arrowhead shows circumoral kinety. **(M)** Nuclear group. GS, glabrous stripe; SK, somatic kineties. Scale bars = 300 μm **(A–C)**.

Locomotion by gliding between sand grains and organic debris. Cells surface densely ciliated (**Figures 6I**, **7H**). Glabrous stripe about as wide as trunk (**Figures 6H**, **7I**). Entire infraciliature consisting of dikinetids with cilia ca. 10 μm long (**Figures 6A,E,I**). Five to ten somatic kinetics on head, 9–15 on trunk. Anterior and posterior secant systems on left side of glabrous stripe, some kineties abut to bristle kinety (**Figures 6D,H**, **7I,K,M**). Oral ciliature composed of single-rowed circumoral kinety, interrupted by two inserted brosses (**Figures 6G,H**, **7I,J**).

Discussion

As shown in **Figure 8** and **Table 4**, the current new species should be compared with its most similar congeners (**Figure 8**

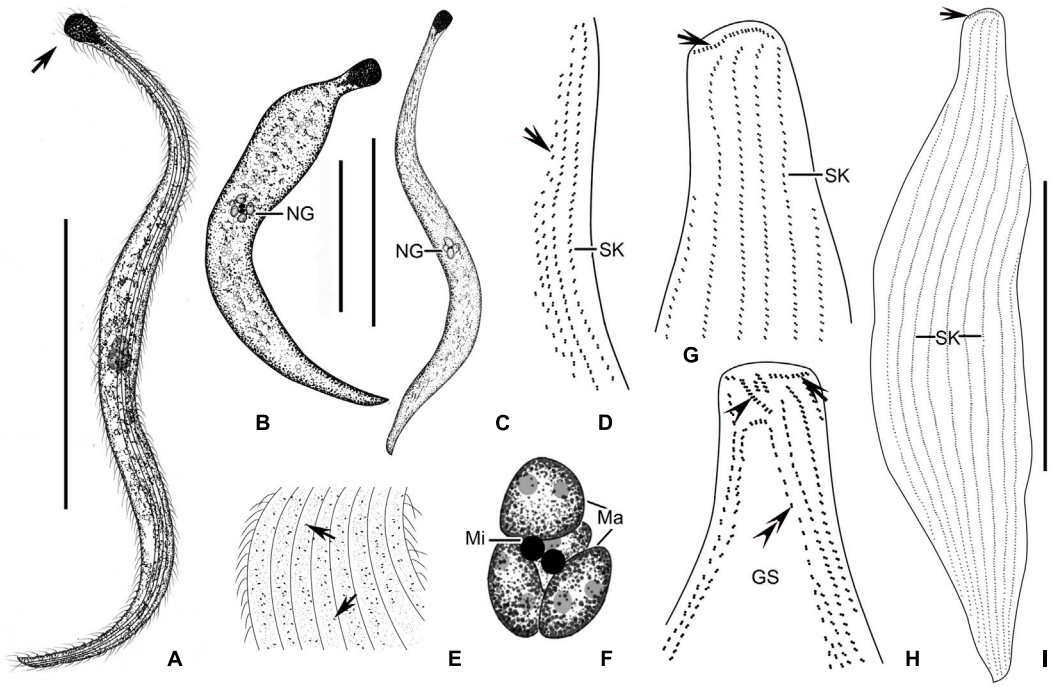

FIGURE 6 | (A–I) *Tracheloraphis katzae* spec. nov. *in vivo* **(A–C,E)** and after protargol staining **(D,F–I)**. **(A–C)** Typical individual. Arrow showing the head of the cell. **(D)** Ciliary pattern of bristle kinety (arrow) and somatic kinety. **(E)** Distribution of cortical granules (arrows) between somatic kineties. **(F)** Nuclear group. **(G,H)** Detailed ciliature of left **(H)** and right **(G)** side of anterior body region. Arrowhead in **(H)** showing brosse, arrow showing circumoral kinety, double arrowheads showing bristle kinety. Arrowhead in **(G)** showing circumoral kinety. **(I)** Right view of the holotype specimen showing the ciliary pattern, arrow depicts circumoral kinety. GS, glabrous stripe; SK, somatic kineties. Scale bars = 200 μm **(A–C)**; 70 μm **(I)**.

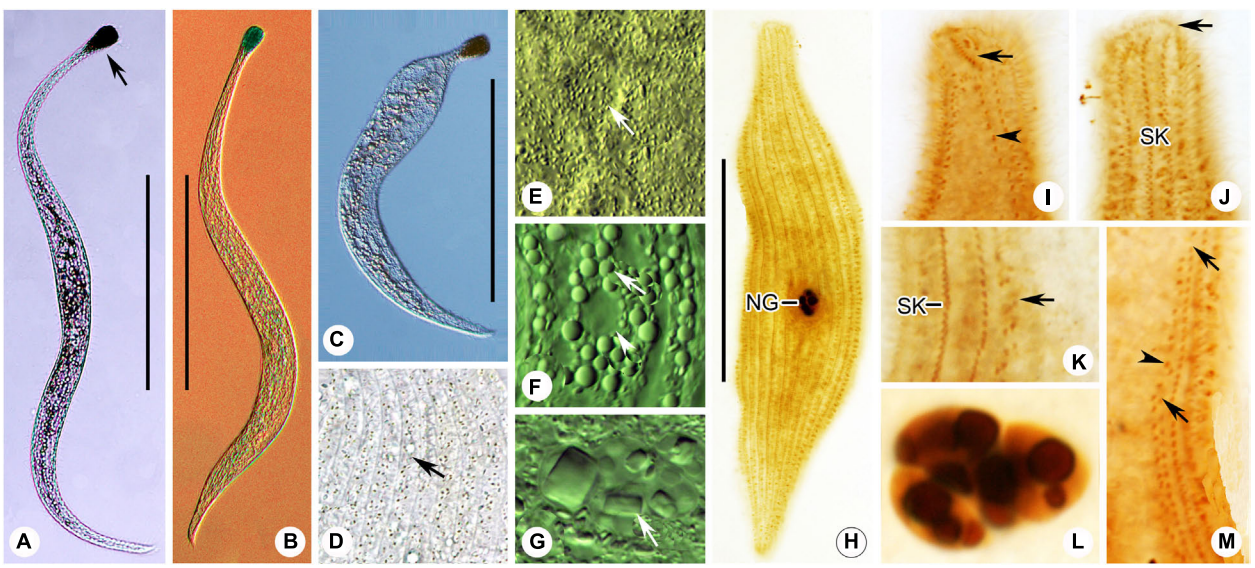

FIGURE 7 | (A–M) *Tracheloraphis katzae* spec. nov. *in vivo* **(A–G)** and after protargol staining **(H–M)**. **(A–C)** Typical individual. Arrow showing the head of the cell. **(D)** Distribution of cortical granules (arrow) between somatic kineties. **(E)** Distribution of cortical granules in glabrous stripe (arrow). **(F)** Arrow showing globular granules in cell. Arrowhead showing a vacuole. **(G)** Nuclear group. Arrow showing crystals in the macronuclei. **(H)** Right view of the holotype specimen showing the ciliary pattern and multiple macronuclei. **(I,J)** Detailed ciliature of left **(I)** and right **(J)** side of anterior body region. Arrow in **I** shows brosse, arrowhead showing bristle kinety. Arrow in **(J)** showing circumoral kinety. **(K)** Arrow showing somatic kineties. **(L)** Nuclear group. **(M)** Arrows showing secant system on left side of glabrous stripe. Arrowhead showing bristle kinety. NG, nuclear group; SK, somatic kineties. Scale bars = 200 μm **(A–C)**; 70 μm **(H)**.

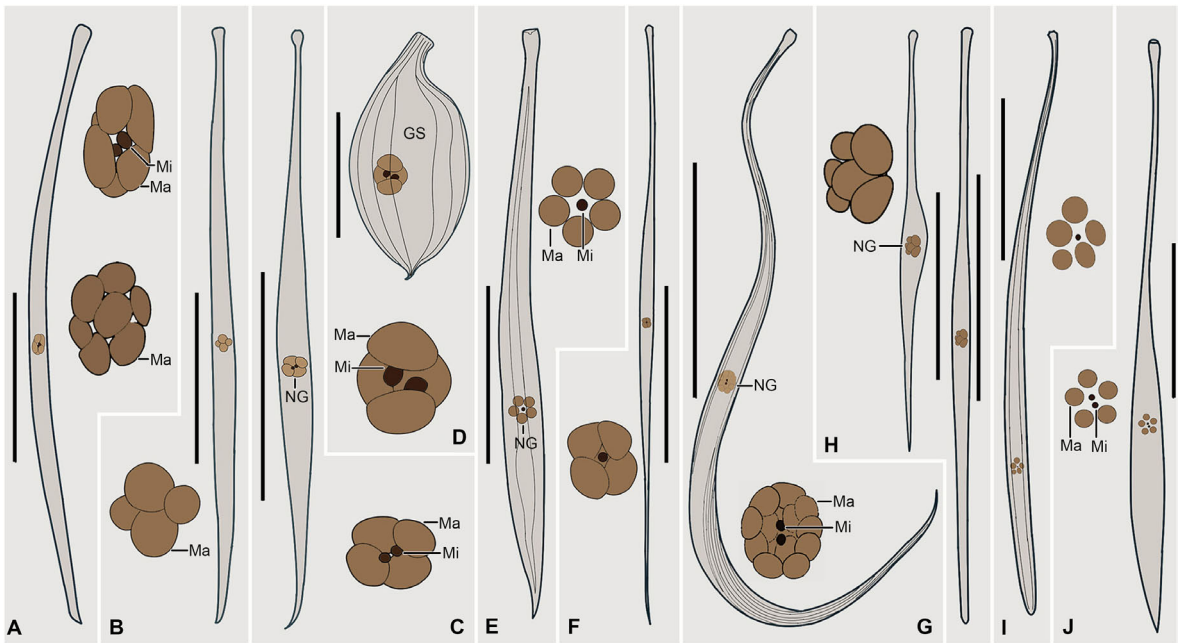

FIGURE 8 | (A–J) Selected *Traceloraphis* species that are morphologically similar to *T. katzae* spec. nov. A. *Tracheloraphis prenanti* (after Ma et al., 2020). B. *T. dragescoi* (after Xu et al., 2014). C. *T. africanus* (after Dragesco and Dragesco-Kernéis, 1986). D. *T. striatus* (after Raikov, 1962). E. *T. remanei* (after Dragesco, 1960). F. *Trachelocerca schulzei* (after Dragesco, 1960). G. *T. phoenicopterus* (after Foissner and Dragesco, 1996b). H. *T. hamatus* (after Dragesco, 2002). I. *T. gracilis* (after Dragesco, 1960). J. *T. enigmaticus* (after Dragesco, 1960). GS, glabrous stripe; Ma, macronuclei; Mi, micronuclei; NG, nuclear group. Scale bars = 200 μm **(A–C,E–J)**; 60 μm **(D)**.

TABLE 4 | Comparison of *Tracheloraphis katzae* spec. nov. (in bold) with morphologically similar congeners.

Species	Body length (μm)	SK (n)	Ma (n)	Source
***Tracheloraphis katzae* spec. nov.**	**400–800**	**9–15**	**4**	**This study**
Tracheloraphis phoenicopterus	1,000–1,500	23–27 19–21	6–12	Foissner and Dragesco (1996b)
Tracheloraphis prenanti	400–2,000	14–26	4–10	Ma et al. (2020)
Tracheloraphis dragescoi	600–1,000	14–22	4	Xu et al. (2014)
Tracheloraphis hamatus	500–900	10–14	3–6	Dragesco (2002)
Tracheloraphis africanus	700	17 or 18	4	Dragesco and Dragesco-Kernéis (1986)
Tracheloraphis gracilis	400–800	12 or 13	4–6	Dragesco (1960)
Tracheloraphis enigmaticus	600	–	5	Dragesco (1960)
Tracheloraphis striatus	500–700	12–14	4	Raikov (1962)
Tracheloraphis remanei	1,000	–	5 or 6	Dragesco (1960)
Trachelocerca schulzei	650	12 or 13	4	Dragesco (1960)

Ma, number of macronuclei; SK, number of somatic kineties; –, no data available.

and **Table 4**). *Tracheloraphis prenanti* Dragesco, 1960 and *T. phoenicopterus* (Cohn, 1866) Dragesco, 1960 resemble *T. katzae* spec. nov. in body shape and the width of the glabrous stripe. They can be distinguished from the latter, however, by their greater number of somatic kineties (14–26, 19–27, vs. 9–15) and macronuclei in the nuclear group (6–12, 4–10, vs. 4). Features of cortical granules can further separate three species. Cortical granules of *T. prenanti* are colorless, globular and about 0.5 μm in diameter, and in *T. phoenicopterus* they are ellipsoidal, yellowish, and 0.6 μm × 1.2 μm, whereas, in *T. katzae* spec. nov. they are ellipsoidal, brownish, and 0.2 μm × 0.5 μm (**Figures 8A,G**; Foissner and Dragesco, 1996b; Ma et al., 2020).

Tracheloraphis dragescoi Xu et al., 2014 has a similar body size and number of macronuclei as *T. katzae* spec. nov., but it can be separated from the latter by its oval cortical granules (colorless, about 0.2 μm × 1 μm vs. brownish, about 0.2 μm × 0.5 μm) and in having 14–22 (vs. 9–15) somatic kineties (**Figure 8B**; Xu et al., 2014).

Tracheloraphis hamatus Wright, 1982 resembles the novel form in body size, width of the glabrous stripe and the number of macronuclei. It can be distinguished from the latter, however, by having a different type of cortical granules (globular, less than 0.5 μm in diameter vs. ellipsoidal, about 0.2 μm × 0.5 μm) (**Figure 8H**).

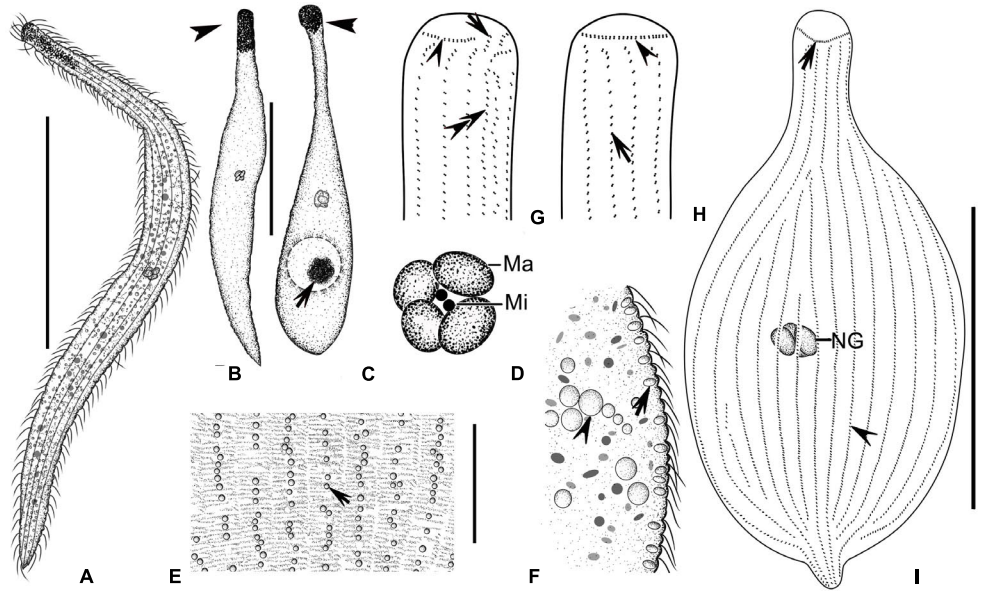

FIGURE 9 | (A–I) *Tracheloraphis colubis in vivo* **(A–F)** and after protargol staining **(G–I)**. **(A,B)** Typical individuals. Arrowhead showing the head of cell. **(C)** An extremely contracted cell, arrow showing algae in the food vacuole, arrowhead showing the head of cell. **(D)** Nuclear group. **(E)** Distribution of cortical granules between somatic kineties (arrow). **(F)** Lateral view, showing the elliptical cortical granules at the cell margin (arrow). Arrowhead showing the spherical inclusions. **(G,H)**. Detailed ciliature of left **(G)** and right **(H)** side of anterior body region. Arrowhead in **(G)** showing circumoral kinety, arrow showing brosse, double arrowheads showing bristle kinety. Arrowhead in **(H)** showing circumoral kinety, arrow showing somatic kinety. **(I)** Overview showing ciliary pattern. Arrow showing circumoral kinety, arrowhead showing somatic kinety. Ma, macronuclei; Mi, micronuclei; NG, nuclear group. Scale bars = 300 μm **(A)**; 200 μm **(B,C)**; 60 μm **(E)**; 100 μm **(I)**.

Tracheloraphis africanus Dragesco, 1965 resembles *T. katzae* spec. nov. in body size and the number of macronuclei. However, it differs from the latter by the absence (vs. presence) of cortical granules although according to Dragesco (1965) the 3 μm long rod-shaped "granules" scattered in the superficial cytoplasm may be bacteria (**Figure 8C**).

Tracheloraphis gracilis Dragesco, 1960 has a similar number of macronuclei compared to *Tracheloraphis katzae* spec. nov. and both species have oval cortical granules, but it can be separated from the latter by its tail which has a rounded (vs. wedge-shaped) end (**Figure 8I**; Dragesco, 1960).

Based on the original illustration, the nuclear apparatus of *Tracheloraphis enigmaticus* Dragesco, 1960 consists of five macronuclei and two micronuclei, but these are not clustered in a nuclear group as they are in *T. katzae* spec. nov. Furthermore, the figure of *T. enigmaticus* shows that it has short subuliform tail, whereas the new species has a narrow tail with a wedge-shaped end (**Figure 8J**; Dragesco, 1965).

The original descriptions of *Tracheloraphis striatus* Raikov, 1962 and *T. remanei* Dragesco, 1960 are based solely on stained specimens, and no information on their live morphology is available. Nevertheless, both can be separated from *T. katzae* spec. nov. by having a narrower glabrous stripe (about double distance between two adjacent somatic kineties, and one-third of the body width, respectively vs. about as wide as the body) (**Figures 8D,E**; Dragesco, 1960; Raikov, 1962).

Although no information on the infraciliature of *Trachelocerca schulzei* Dragesco, 1960 is available, based on the original illustration, it can be separated from *T. katzae* spec. nov. by its larger ratio of body length to body width (about 35:1 vs. about 20:1) in fully extended cells (**Figure 8F**; Dragesco, 1960).

Tracheloraphis colubis (Kahl, 1933) Xu et al., 2011; **Figures 9**, **10** and **Table 3**)

This species was originally reported by Kahl (1933) and redescribed in detail by Xu et al. (2011a). Our population matches both descriptions very well, therefore redescription and an improved diagnosis based on the present and previous populations are provided here.

Improved Diagnosis

Extended cells 250–1,000 μm × 20–50 μm *in vivo*; claviform tail. Seventeen to thirty-one somatic kineties. Glabrous stripe narrow, width about equal to gap between two adjacent somatic kineties. Four macronuclei in a single group. Cortical granules circular in outline when viewed from above, elliptical in lateral view 1.5–2 μm × 2.5 μm, colorless.

Redescription Based on Qingdao Population

Extended cells 250–600 μm × 30–50 μm *in vivo*; body flattened about 3:1, flexible and contractile (**Figures 9A–C**, **10A–C**); neck and tail indistinctly separated from trunk, head triangular and conspicuous, tail claviform (**Figures 9A–C**, **10A–C**). Cortical granules ellipsoidal, 1.5–2 μm × 2.5 μm, colorless in bright field

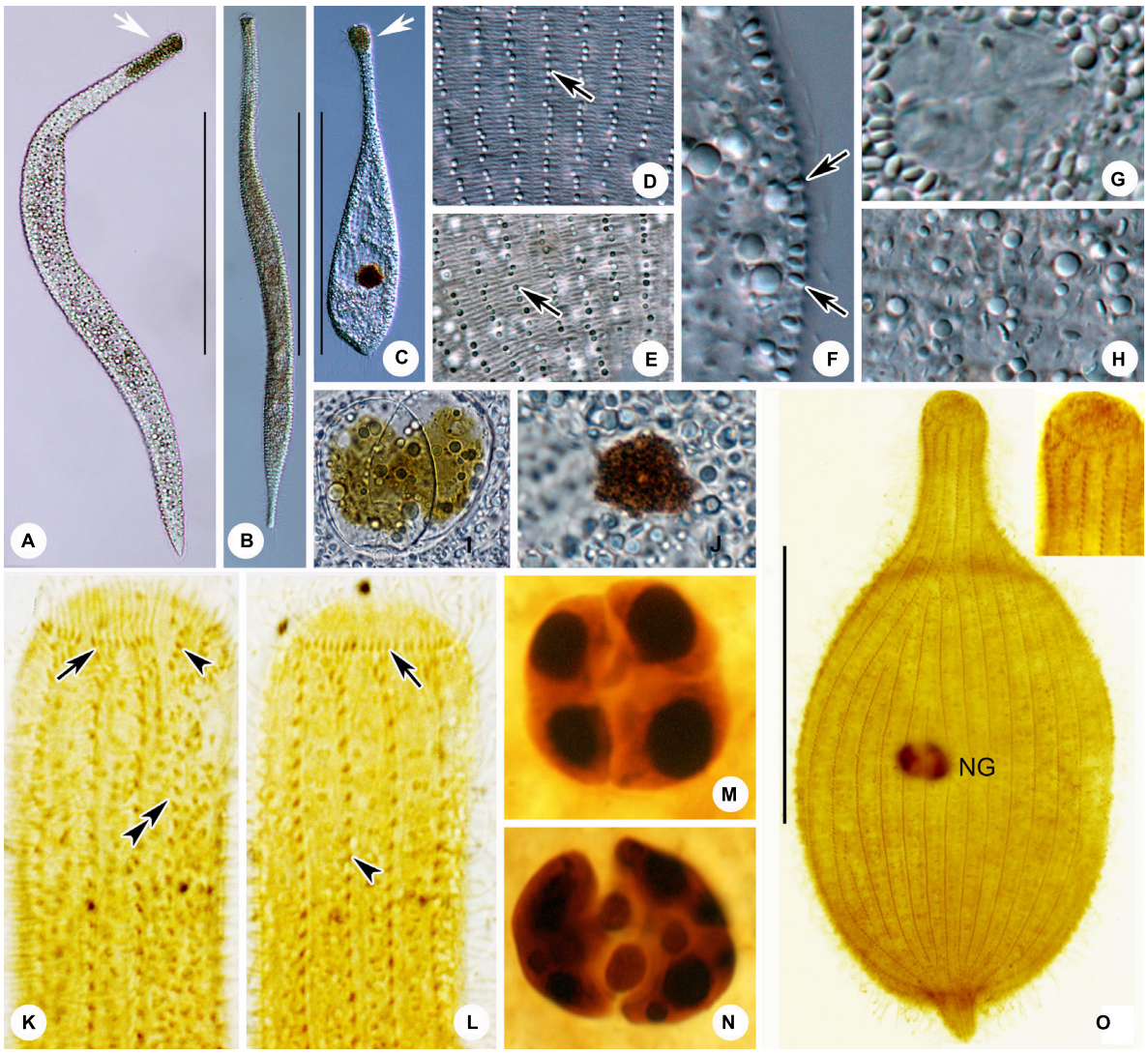

FIGURE 10 | (A–O) *Tracheloraphis colubis in vivo* **(A–J)** and after protargol staining **(K–O)**. **(A,B)** Typical individuals. Arrowhead showing the head of cell. **(C)** An extremely contracted cell. Arrowhead showing the head of cell. **(D,E)** Distribution of cortical granules between somatic kineties (arrow). **(F)** Lateral view, showing the elliptical cortical granules at the cell margin (arrows). **(G)** Nuclear group. **(H)** Showing granules in cell. **(I,J)** Showing algae in the food vacuole. **(K,L)** Detailed ciliature of left **(K)** and right **(L)** side of anterior body region. Arrow in **(K)** showing circumoral kinety, arrowhead showing brosse, double arrowheads showing bristle kinety. Arrow in **(L)** showing circumoral kinety, arrowhead showing somatic kinety. **(M,N)** Nuclear group. **(O)** Overview showing ciliary pattern. NG, nuclear group. Scale bars = 300 μm **(A–C)**; 100 μm **(O)**.

at high magnification; round when viewed from above, elliptical in lateral view; arranged in rows between somatic kineties and sparsely distributed in glabrous stripe (**Figures 9E,F**, **10D–F**). Cytoplasm colorless and transparent, packed with cytoplasmic granules, ellipsoidal, 1–3 μm long and colorless (**Figure 10H**). Some food vacuoles containing algae (**Figures 9C**, **10C,I,J**).

Locomotion by gliding, winding between sand grains and organic debris.

Entire infraciliature consisting of dikinetids (**Figures 9I**, **10O**). Somatic cilia about 10 μm long *in vivo* and arranged in longitudinal rows. Usually one brosse kinety (**Figures 9G,H**, **10K,L**). Glabrous stripe very narrow, width about equal to gap between two adjacent somatic kineties, and bordered by irregularly spaced bristle kinety (**Figures 9G**, **10K**). Seventeen to 27 somatic kineties. Anterior and posterior of secant system formed on left side of glabrous stripe, some kineties abut to bristle kinety (**Figures 9G**, **10K**). Four macronuclei and two micronuclei in a single group (**Figures 9D**, **10G,M,N**).

Discussion

There have been several redescriptions of *Tracheloraphis colubis* since it was first reported (Kahl, 1933; Raikov, 1963; Xu et al., 2011a). Kahl (1933) and Raikov (1963) both assigned this species to the genus *Trachelocerca* due to its curved posterior end and narrow glabrous stripe. However, the shape and structure of the oral ciliature are the most important

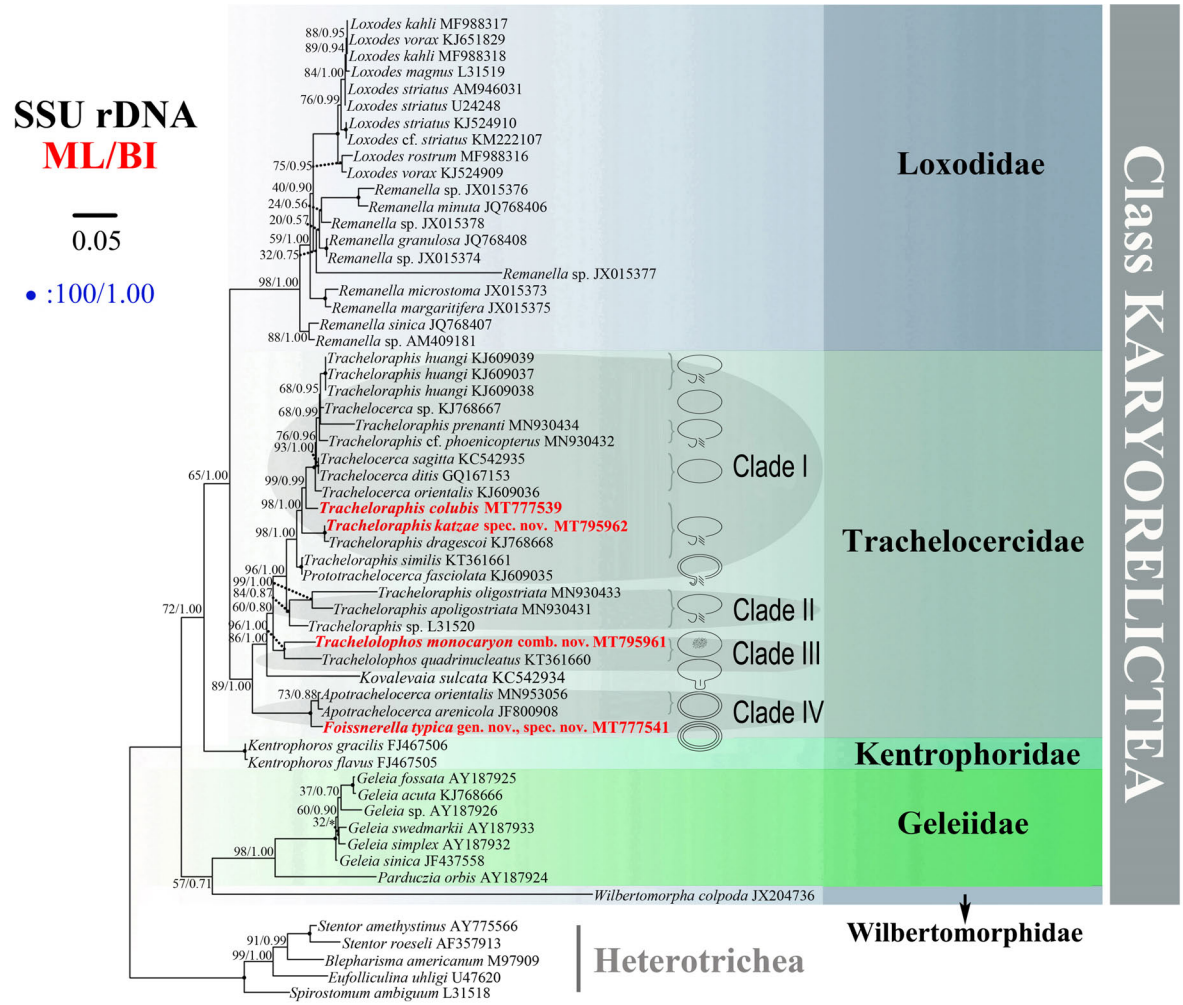

FIGURE 11 | Maximum likelihood (ML) tree inferred from the small subunit rDNA sequences showing the positions of the four newly sequenced Trachelocercidae isolates (in red bold). Nodal support for branches in the ML and BI trees marked in order. Black circles indicate full support in both analyses. Clades with a different topology between the two analyses are shown by an asterisk. Heterotrichous species are the outgroup. The line diagrams show the oral structure of different genera in Trachelocercidae. All branches are drawn to scale. The scale bar corresponds to five substitutions per 100 nucleotides positions.

characters for generic classification (Foissner and Dragesco, 1996a,b; Foissner and Al-Rasheid, 1999). Therefore, Xu et al. (2011a) assigned this species to the genus *Tracheloraphis*. The present population matches the population described by Xu et al. (2011a), so we have no doubt that these two populations are conspecific.

Molecular Phylogeny Based on SSU rDNA Sequence Data (Figure 11)

The length (bp), GC content and Genbank accession numbers of the new SSU rDNA sequences of the four isolates are as follows: *Foissnerella typica* gen. nov., spec. nov.—1,557, 48.62%, MT777541; *Trachelolophos monocaryon* (Dragesco, 1965) comb. nov.—1,473, 48.47%, MT795961; *Tracheloraphis katzae* spec. nov.—1,520, 47.89%, MT795962; *Tracheloraphis colubis*—1,597, 47.65%, MT777539.

The ML and BI trees have similar topologies, therefore only the ML tree is presented (**Figure 11**). The family Trachelocercidae is a well-supported monophyletic group (89% ML, 1.00 BI) that is sister to the family Loxodidae (65% ML, 1.00 BI). Within Trachelocercidae there are four main clades (Clades I, II, III, and IV). *Tracheloraphis colubis* is sister to several *Tracheloraphis* and *Trachelocerca* species. *Tracheloraphis katzae* spec. nov. groups with *T. dragescoi* within Clade I. *Prototrachelocerca fasciolata* shows a close relationship with *Tracheloraphis similis* which together occupy the basal position within Clade I. *Tracheloraphis* species interdigitate with those of *Trachelocerca* resulting in the non-monophyly of both genera, which is consistent with previous studies (Xu et al., 2014; Yan et al., 2016). Clade II consists of three *Tracheloraphis* species. Two *Trachelolophos* species group together forming a sister branch to Clades I and II. Clade III comprises *Trachelolophos monokaryon* and *T. quadrinucleatus*. *Kovalevaia sulcata* is sister group to the assemblage of Clades

I–III. Clade IV comprises *Foissnerella typica* and two species of *Apotrachelocerca*.

Based on the combination of morphological features and molecular evidence, Yan et al. (2016) suggested that *Apotrachelocerca*, which possesses two uninterrupted rows of circumoral kineties, is the closest relative to the common ancestor of trachelocercids, followed by *Kovalevaia*, *Trachelolophos* and *Prototrachelocerca* and that *Trachelocerca*, *Tracheloraphis* and possibly *Sultanophrys* derived from *Prototrachelocerca*. Our results mainly support this hypothesis except that *Kovalevaia* forms a sister branch with Clades I–III (of which Clade III comprises two *Trachelolophos* species) rather than grouping directly with *Trachelolophos* (**Figure 11**). In addition, the early branching of *Foissnerella* gen. nov. within Clade IV provides further evidence that multiple rows of uninterrupted circumoral kineties is probably an ancestral feature.

DATA AVAILABILITY STATEMENT

The datasets generated for this study can be found in the online repositories. The names of the repository/repositories and accession number(s) are as follows: https://www.ncbi.nlm.nih.gov/genbank/, MT777541; http://zoobank.org/, urn:lsid:zoobank.org:pub:913C263C-56A7-40AC-9885-E06DC530A6D8; https://www.ncbi.nlm.nih.gov/genbank/, MT795961; https://www.ncbi.nlm.nih.gov/genbank/, MT795962; https://www.ncbi.nlm.nih.gov/genbank/, MT777539.

AUTHOR CONTRIBUTIONS

YY and YW conceived to the study. MM, YL, and YY carried out the live observation, protargol staining, DNA extraction, and data analyses. All authors contributed to the writing of the manuscript. YY, MM, and AW contributed to the revision and all authors approved the final version.

FUNDING

The work was financially supported by the National Natural Science Foundation of China (Project Nos. 32030015 and 31801984) and the Researchers Supporting Project (RSP-2020/10) of the King Saud University, Saudi Arabia.

ACKNOWLEDGMENTS

Many thanks are given to Weibo Song (OUC) for kind suggestions during drafting the manuscript.

REFERENCES

Al-Rasheid, K. A. S. (1996). Records of free-living ciliates in Saudi Arabia. I. Marine interstitial ciliates of the Arabian Gulf islands of Al-Bātinah and Abū Ali. *Arab Gulf J. Sci. Res.* 14, 747–765.

Al-Rasheid, K. A. S. (1997). Records of free-living ciliates in Saudi Arabia. III. Marine interstitial ciliates of the Arabian Gulf island of Tarut. *Arab Gulf J. Sci. Res.* 15, 733–766.

Al-Rasheid, K. A. S. (1998). Records of marine interstitial karyorelictid ciliates from Jubail Marine Wildlife Sanctuary in the Gulf-shore of Saudi Arabia. *Arab Gulf J. Sci. Res.* 16, 595–610.

Al-Rasheid, K. A. S. (2001). New records of interstitial ciliates (Protozoa Ciliophora) from the Saudi coasts of the Red Sea. *Trop. Zool.* 14, 133–156. doi: 10.1080/03946975.2001.10531148

Al-Rasheid, K. A. S., and Foissner, W. (1999). Apical feeding in the karyorelictids (Protozoa, Ciliophora) *Sultanophrys arabica* and *Tracheloraphis* sp. *J. Eukaryot. Microbiol.* 46, 458–463. doi: 10.1111/j.1550-7408.1999.tb06061.x

Carey, P. G. (1992). *Marine Interstitial Ciliates: An Illustrated Key*. London: Chapman & Hall.

Dragesco, J. (1960). Ciliés mésopsammiques littoraux. Systématique, morphologie, écologie. *Trav. Stn. Biol. Roscoff.* 12, 1–356.

Dragesco, J. (1965). Ciliés mésopsammiques d' afrique noire. *Cah. Biol. Mar.* 6, 357–399.

Dragesco, J. (1997). Infraciliature et morphométrie des cinq espèces deciliés mésopsammiques méditerranéens. *Cah. Biol. Mar.* 37, 261–293.

Dragesco, J. (1999). Revision des Geléiides (Ciliophora, Karyorelictea). *Stapfia* 66, 1–91. doi: 10.1016/s0003-4339(99)80006-9

Dragesco, J. (2002). Infraciliature de quinze especes de cilies mesopsammiques marins comprenant *Trachelocerca stephani* comb. nova, *T. bodiani* comb. nova, *Tracheloraphis filiformis* spec. nova, *T. exilis* spec. nova, et *Sathrophilus arenicolus* spec. nova. *Linz. Biol. Beitr.* 34, 1545–1626.

Dragesco, J., and Dragesco-Kernéis, A. (1986). *Ciliés Libres de l' Afrique Intertropicale Faune Tropicale*, Vol. 26. Paris: Édition de l' ORSTOM. doi: 10.1016/S0932-4739(88)80062-2

Ehrenberg, C. G. (1840). Das grössere Infusorienwerk (Diagnosen von 274 neuen Infusorien). *Ber. Verh. K. Preuss. Akad. Wiss. Berl.* 1840, 197–219.

Foissner, W. (1996). Updating the trachelocercids (Ciliophora, Karyorelictea). II. *Prototrachelocerca* nov. gen. (Prototrachelocercidae nov. fam.), with a redescription of *P. fasciolata* (Sauerbrey, 1928) nov. comb. and *P. caudata* (Dragesco & Raikov, 1966) nov. comb. *Eur. J. Protistol.* 32, 336–355. doi: 10.1016/s0932-4739(96)80058-7

Foissner, W. (1997). Updating the trachelocercids (Ciliophora, Karyorelictea). V. Redescription of *Kovalevaia sulcata* (Kovaleva, 1966) gen. n., comb. n. and *Trachelocerca incaudata* Kahl, 1933. *Acta Protozool.* 36, 197–219.

Foissner, W., and Al-Rasheid, K. A. S. (1999). Updating the trachelocercids (Ciliophora, Karyorelictea). VI. A detailed description of *Sultanophrys arabica* nov. gen., nov. spec. (Sultanophryideae nov. fam.). *Eur. J. Protistol.* 35, 146–160. doi: 10.1016/s0932-4739(99)80032-7

Foissner, W., and Dragesco, J. (1996a). Updating the trachelocercids (Ciliophora, Karyorelictea). I. A detailed description of the infraciliature of *Trachelolophos gigas* n. g., n. sp. and *T. filum* (Dragesco and Dragesco-Kernéis, 1986) n. comb. *J. Eukaryot. Microbiol.* 43, 12–25. doi: 10.1111/j.1550-7408.1996.tb02467.x

Foissner, W., and Dragesco, J. (1996b). Updating the trachelocercids (Ciliophora, Karyorelictea). III. Redefinition of the genera *Trachelocerca* Ehrenberg and *Tracheloraphis* Dragesco, and evolution in trachelocercid ciliates. *Arch. Protistenkd.* 147, 43–91. doi: 10.1016/s0003-9365(96)80007-8

Hall, T. A. (1999). BioEdit: a user-friendly biological sequence alignment editor and analysis program for Windows 95/98/NT. *Nucl. Acids Symp. Ser.* 41, 95–98. doi: 10.1021/bk-1999-0734.ch008

Hu, X. Z., Lin, X. F., and Song, W. (2019). *Ciliate Atlas: Species Found in the South China Sea*. Beijing: Science Press, doi: 10.1007/978-981-13-5901-9

Jerome, C. A., Lynn, D. H., and Simon, E. M. (1996). Description of *Tetrahymena empidokyrea* n. sp., a new species in the *Tetrahymena pyriformis* sibling species complex (Ciliophora, Oligohymenophorea), and an assessment of its phylogenetic position using small-subunit rRNA sequences. *Can. J. Zool.* 74, 1898–1906. doi: 10.1139/z96-214

Kahl, A. (1933). "Ciliata Libera et Ectocommensalia," *Die Tierwelt der Nord-und Ostsee, Leipzig*, eds G. Grimpe and E. Wagler Lief. 23 (Teil II, c3), 29–146.

Lynn, D. H. (2008). *The Ciliated Protozoa: Characterization, Classification, and Guide to the Literature*. Berlin: Springer.

Ma, M. Z., Xu, Y., Yan, Y., Li, Y. Q., Warren, A., and Song, W. B. (2020). Taxonomy and molecular phylogeny of four karyorelictid species belonging to the genera *Apotrachelocerca* and *Tracheloraphis* (Protozoa: Ciliophora), with descriptions of two new species. *Zool. J. Linn. Soc.* 64 (Accepted).

Medlin, L., Elwood, H. J., Stickel, S., and Sogin, M. L. (1988). The characterization of enzymatically amplified eukaryotic 16S-like rRNA-coding regions. *Gene* 71, 491–499. doi: 10.1016/0378-1119(88)90066-2

Nylander, J. (2004). *MrModeltest v2*. Uppsala: Evolutionary Biology Centre, Uppsala University.

Penn, O., Privman, E., Ashkenazy, H., Landan, G., Graur, D., and Pupko, T. (2010). GUIDANCE: a web server for assessing alignment confidence scores. *Nucl. Acids Res.* 38(Suppl. 2), W23–W28. doi: 10.1093/nar/gkq443

Raikov, I. B. (1962). Les cilié mésopsammiques du littoral de la Mer Blanche (U.R.S.S.) avec une description de quelques espèces nouvellesou peu connues. *Cah. Biol. Mar.* 3, 325–361.

Raikov, I. B. (1963). Ciliates of the mesopsammon of the Ussuri Gulf (Japan Sea). *Zool. Zh.* 42, 1753–1767.

Raikov, I. B., Gerassimova-Matvejeva, Z. P., and de Puytorac, P. (1975). Cytoplasmic fine structure of the marine psammobiotic ciliate *Tracheloraphis dogieli* Raikov. I. Somatic infraciliature and cortical organelles. *Acta Protozool.* 14, 17–42.

Ronquist, F., Teslenko, M., Van Der Mark, P., Ayres, D. L., Darling, A., Höhna, S., et al. (2012). MrBayes 3.2: efficient Bayesian phylogenetic inference and model choice across a large model space. *Syst. Biol.* 61, 539–542. doi: 10.1093/sysbio/sys029

Shimodaira, H. (2002). An approximately unbiased test of phylogenetic tree selection. *Syst. Biol.* 51, 492–508. doi: 10.1080/10635150290069913

Shimodaira, H., and Hasegawa, M. (2001). Consel: for assessing the confidence of phylogenetic tree selection. *Bioinformatics* 17, 1246–1247. doi: 10.1093/bioinformatics/17.12.1246

Song, W. B., Warren, A., and Hu, X. Z. (2009). *Free-living Ciliates in the Bohai and Yellow Seas*. Beijing: Science Press.

Stamatakis, A. (2014). RAxML version 8: a tool for phylogenetic analysis and post-analysis of large phylogenies. *Bioinformatics* 30, 1312–1313. doi: 10.1093/bioinformatics/btu033

Stamatakis, A., Hoover, P., and Rougemont, J. (2008). A rapid bootstrap algorithm for the RAxML web-servers. *Systematic Biol.* 75, 758–771. doi: 10.1080/10635150802429642

Tamura, K., Peterson, D., Peterson, N., Stecher, G., Nei, M., and Kumar, S. (2011). MEGA5: molecular evolutionary genetics analysis using maximum likelihood, evolutionary distance, and maximum parsimony methods. *Mol. Biol. Evol.* 28, 2731–2739. doi: 10.1093/molbev/msr121

Uhlig, G. (1968). Quantitative methods in the study of interstitial fauna. *Trans. Am. Microsc. Soc.* 87, 226–232. doi: 10.2307/3224446

Wang, Y. R., Jiang, Y. H., Liu, Y. Q., Li, Y., Katz, L. A., Gao, F., et al. (2020). Comparative studies on the polymorphism and copy number variation of mtSSU rDNA in ciliates (Protista, Ciliophora): implications for phylogenetic, environmental, and ecological research. *Microorganisms* 8:316. doi: 10.3390/microorganisms8030316

Wang, Y. R., Wang, C. D., Jiang, Y. H., Katz, L. A., Gao, F., and Yan, Y. (2019). Further analyses of variation of ribosome DNA copy number and polymorphism in ciliates provide insights relevant to studies of both molecular ecology and phylogeny. *Sci. China Life Sci.* 62, 203–214. doi: 10.1007/s11427-018-9422-5

Wilbert, N. (1975). Eine verbesserte Technik der Protargolimprägnation für Ciliaten. *Mikrokosmos* 64, 171–179.

Wilbert, N. (1986). Die orale infraciliature von *Tracheloraphis dogieli* Raikov, 1957 (Ciliophora, Gymnostomata, Karyorelictida). *Arch. Protistenkd.* 132, 191–195. doi: 10.1016/S0003-9365(86)80020-3

Xu, Y., Esaulov, A., Lin, X., Mazei, Y., Hu, X., Al-Rasheid, K. A. S., et al. (2011a). Morphological studies on five trachelocercids from the Yellow Sea coast of China, with a description of *Tracheloraphis huangi* spec. nov. (Ciliophora, Karyorelictea). *Acta Protozool* 50, 205–218. doi: 10.1016/j.proenv.2011.10.118

Xu, Y., Li, J., Gao, F., Hu, X., and Al-Rasheid, K. A. S. (2011b). *Apotrachelocerca arenicola* (Kahl, 1933) n. g., comb. n. (Protozoa, Ciliophora, Trachelocercidae): morphology and phylogeny. *J. Eukaryot. Microbiol.* 58, 504–510. doi: 10.1111/j.1550-7408.2011.00578.x

Xu, Y., Miao, M., Warren, A., and Song, W. (2012). Diversity of the karyorelictid ciliates: *Remanella* (Protozoa, Ciliophora, Karyorelictida) inhabiting intertidal areas of Qingdao, China, with descriptions of three species. *Syst. Biodivers.* 10, 207–219. doi: 10.1080/14772000.2012.681713

Xu, Y., Yan, Y., Li, L., Al-Rasheid, K. A. S., Al-Farraj, S. A., and Song, W. (2014). Morphology and phylogeny of three karyorelictean ciliates (Protista, Ciliophora), including two novel species, *Trachelocerca chinensis* sp. nov. and *Tracheloraphis dragescoi* sp. nov. *Int. J. Syst. Evol. Microbiol.* 64, 4084–4097. doi: 10.1099/ijs.0.068783-0

Yan, Y., Gao, F., Xu, Y., Al-Rasheid, K. A. S., and Song, W. (2015). Morphology and phylogeny of three trachelocercid ciliates, with description of a new species, *Trachelocerca orientalis* spec. nov. (Ciliophora, Karyorelictea). *J. Eukaryot. Microbiol.* 62, 157–166. doi: 10.1111/jeu.12154

Yan, Y., Maurer-Alcalá, X. X., Knight, R., Pond, S. L. K., and Katz, L. A. (2019). Single cell transcriptomics reveal a correlation between genome architecture and gene family evolution in ciliates. *mBio* 10:e2524-19. doi: 10.1128/mBio.02524-19

Yan, Y., Xu, Y., Al-Farraj, S. A., Al-Rasheid, K. A. S., and Song, W. (2016). Morphology and phylogeny of three trachelocercids (Protozoa, Ciliophora, Karyorelictea), with description of two new species and insight into the evolution of the family Trachelocercidae. *Zool. J. Linn. Soc.* 177, 306–319. doi: 10.1111/zoj.12364

Conflict of Interest: The authors declare that the research was conducted in the absence of any commercial or financial relationships that could be construed as a potential conflict of interest.

frontiers in Marine Science

ORIGINAL RESEARCH
published: 27 January 2021
doi: 10.3389/fmars.2020.623436

Taxonomy of Three Oxytrichids (Protozoa, Ciliophora, Hypotrichia), With Establishment of the New Species *Rubrioxytricha guangzhouensis* spec. nov.

Xiaotian Luo[1], Jie Huang[1], William A. Bourland[2], Hamed A. El-Serehy[3], Saleh A. Al-Farraj[3], Xumiao Chen[4] and Weibo Song[5,6]**

[1] Key Laboratory of Aquatic Biodiversity and Conservation of Chinese Academy of Sciences, Institute of Hydrobiology, Chinese Academy of Sciences, Wuhan, China, [2] Department of Biological Sciences, Boise State University, Boise, ID, United States, [3] Zoology Department, College of Science, King Saud University, Riyadh, Saudi Arabia, [4] Department of Marine Organism Taxonomy & Phylogeny, Institute of Oceanology, Chinese Academy of Sciences, Qingdao, China, [5] Institute of Evolution and Marine Biodiversity, and College of Fisheries, Ocean University of China (OUC), Qingdao, China, [6] Laboratory for Marine Biology and Biotechnology, Qingdao National Laboratory for Marine Science and Technology, Qingdao, China

OPEN ACCESS

Edited by:
Hongbo Pan,
Shanghai Ocean University, China

Reviewed by:
Rosaura Mayén-Estrada,
Universidad Nacional Autonoma de Mexico, Mexico
Fengchao Li,
Hebei University, China
Helmut Berger,
Consulting Engineering Office for Ecology, Austria

***Correspondence:**
Xumiao Chen
xchen@qdio.ac.cn
Weibo Song
wsong@ouc.edu.cn

Specialty section:
This article was submitted to Marine Evolutionary Biology, Biogeography and Species Diversity, a section of the journal Frontiers in Marine Science

Received: *30 October 2020*
Accepted: *21 December 2020*
Published: *27 January 2021*

Citation:
Luo X, Huang J, Bourland WA, El-Serehy HA, Al-Farraj SA, Chen X and Song W (2021) Taxonomy of Three Oxytrichids (Protozoa, Ciliophora, Hypotrichia), With Establishment of the New Species Rubrioxytricha guangzhouensis spec. nov. Front. Mar. Sci. 7:623436. doi: 10.3389/fmars.2020.623436

Two oxytrichid ciliates collected from China, *Oxytricha lithofera* Foissner, 2016 and *Rubrioxytricha haematoplasma* (Blatterer and Foissner, 1990) Berger, 1999 were investigated based on living observations, protargol preparations, and molecular analyses. The Chinese population of *O. lithofera* shares highly distinctive features with the type population, e.g., lithosomes, abutting macronuclear nodules, straight undulating membranes, and long dorsal bristles. The morphology and morphogenesis of our new isolate of *R. haematoplasma* corresponds well with the type population. The 18S rRNA gene sequences of both species were obtained, and the molecular phylogeny of the genera *Oxytricha* Bory de Saint-Vincent in Lamouroux et al., 1824 and *Rubrioxytricha* Berger, 1999 was analyzed. In addition, we found that the Guangzhou population of *R. haematoplasma* described by Chen et al. (2015) can be distinguished from the type population and our isolate by the reddish-brown cortical granules (vs. lemon yellowish to greenish) and mitochondria-like granules present (vs. absent), as well as the slightly red cytoplasm (vs. slightly orange) and the marine or brackish water habitat (vs. freshwater). In addition, a 20-bp divergence in their 18S rRNA gene sequences indicates that they are not conspecific. Thus, we establish a new species, *Rubrioxytricha guangzhouensis*, for *R. haematoplasma* sensu Chen et al. (2015).

Keywords: hypotrich, morphology, morphogenesis, *Oxytricha*, phylogeny

INTRODUCTION

The family Oxytrichidae Ehrenberg, 1830, including more than 200 valid species, is one of the most morphologically and morphogenetically diverse hypotrichid ciliate groups (Berger, 1999, 2008; Foissner et al., 2002; Shao et al., 2011; Foissner, 2016; Hu et al., 2019; Kim et al., 2019; Dong et al., 2020; Wang et al., 2020a). The genus *Oxytricha* Bory de Saint-Vincent in Lamouroux et al., 1824, the type and time-honored genus of the family Oxytrichidae, comprises almost 40 nominal species isolated from various

habitats worldwide and has been a melting pot for flexible 18-cirri hypotrichs with caudal cirri for over one century (Berger, 1999; Shao et al., 2011, 2014; Weisse et al., 2013; Foissner, 2016; Kim and Min, 2019). Even though many studies have been carried out to delimit the genus more clearly (Berger, 1999; Shao et al., 2011, 2015; Foissner, 2016), it is still a polyphyletic genus with species irregularly distributed across the molecular tree (Schmidt et al., 2007; Paiva et al., 2009; Shao et al., 2014). The incongruence between morphology and molecular information suggests that this taxon is a genus with high genetic divergence (Berger, 1999; Foissner, 2016). *Oxytricha lithofera*, a highly distinctive species with a combination of features absent in any other described congeners (*s. l.*), was originally described by Foissner (2016) based on a population collected from moss on stones and soil from an old coral cave in the Golfete de Cuare del Indio, Venezuela. Here, we provide not only a description of the first Chinese population of *O. lithofera* but also the first analysis of the 18S rRNA gene sequence for this species.

In a revision of oxytrichids, Berger (1999) transferred two *Oxytricha* species, viz., *Oxytricha haematoplasma* Blatterer and Foissner, 1990 and *Oxytricha ferruginea* Stein, 1859, to the newly established genus *Rubrioxytricha* Berger, 1999, with the former as the type species. *Rubrioxytricha* was mainly characterized by the homogeneously colored cytoplasm (slightly orange to reddish in *R. haematoplasma* and rusty brown in *R. ferruginea*), the presence of one or two caudal cirri, and four to five dorsal kineties. Three more *Rubrioxytricha* species have since been reported, namely *R. indica* Naqvi et al., 2006, *R. tsinlingensis* Chen et al., 2017, and *R. guamensis* Kumar et al., 2018 (Naqvi et al., 2006; Chen et al., 2017; Kumar et al., 2018). Recently, Chen et al. (2015) reported a brackish/marine population collected from Guangzhou, China, under the name *R. haematoplasma*. Herein, we describe a freshwater population of *R. haematoplasma* based on a detailed investigation of morphology and morphogenesis. A comprehensive comparison between *R. haematoplasma* populations as well as congeners is provided, and a new species is established. Updated phylogenetic analyses based on 18S rRNA gene sequences were also performed, and the non-monophyly of the genera *Oxytricha* and *Rubrioxytricha* are discussed.

MATERIALS AND METHODS

Sample Collection, Observation, and Terminology

A brackish water sample containing *Oxytricha lithofera* was collected from a sandy beach near Zhuhai Fishing Girl Statue (22°15′41″N; 113°35′16″E; **Figures 1A,B**) in Zhuhai, southern China, on 26 May 2014, when the water temperature was about 21°C and the salinity was about 3‰. The sample was maintained at about 22°C in Petri dishes with rice grains to enrich bacteria as a food source for the ciliates. *Oxytricha lithofera* was identified in this sample on 6 June 2014, when the salinity of the sample reached 6‰, and the population collapsed over the next 3 days. Investigations for *O. lithofera* were made with specimens from raw cultures rather than from cloned individuals. However, *O. lithofera* is easily distinguished by its long dorsal bristles and no other *Oxytricha*-like morphotypes were present in the protargol preparations, indicating that our morphological and molecular studies deal with the same species.

Rubrioxytricha haematoplasma was collected on 8 and 11 April 2016 from a freshwater lake in Wuhan Botanical Garden, Chinese Academy of Sciences (30°32′57″N; 114°25′51″E; **Figures 1A,C**), Wuhan, China, when the water temperature was about 21°C. Sponge cubes, with the length about 10 cm, submerged at a depth of about 1 m for about 2 weeks, were used as artificial substrates to allow colonization by ciliates. Samples were collected according to Luo et al. (2018). Cells were selected and cultivated in Petri dishes at about 22°C with Volvic mineral water and rice grains. Although attempts to establish clonal cultures were unsuccessful, no other hypotrichid morphotypes were present in the protargol preparations, indicating that our morphological, morphogenetic, and molecular studies deal with the same species.

Live cells were isolated with micropipettes and then observed and measured with bright field and differential interference contrast microscopy at 40–1,000 × magnification using a Zeiss Axioplan 2 imaging microscope equipped with a Zeiss AxioCam HRc camera. The protargol staining method of Wilbert (1975) was used to reveal the nuclear apparatus and the ciliature. Counts, measurements, and photographs for protargol-stained specimens were made at a magnification of 1,000 × using an Olympus BX53 compound microscope (Tokyo, Japan) equipped with a Pixelink M5DC-SE-CYL camera (Ottawa, Canada). Drawings were made at a magnification of 1,000 × or 1,250 × with the aid of a drawing attachment or photomicrographs as templates. In the drawings of the morphogenetic stages, parental structures are shown as outlines, whereas new ones are shaded in black. Terminology is according to Berger (1999) and Foissner (2016).

DNA Extraction and Gene Sequencing

One to four randomly isolated cells were washed five times with filtered (0.22 μm) habitat water or Volvic mineral water and then transferred to a 1.5-ml microfuge tube as described by Zhang et al. (2020). Total genomic DNA was extracted using the DNeasy Blood and Tissue Kit (Qiagen, Hilden, Germany) according to the manufacturer's instructions with modification according to Lu et al. (2018). The 18S rRNA gene was amplified using the primers 18S-F (5′-AACCTGGTTGATCCTGCCAGT-3′) and 18S-R (5′-TGATCCTTCTGCAGGTTCACCTAC-3′) (Medlin et al., 1988). Cycling parameters of touchdown PCR were as follows: one cycle of initial denaturation at 94°C for 5 min, followed by 18 cycles of amplification (94°C, 30 s; 66–49°C touch down, 40 s; 72°C, 2 min) and another 18 cycles (94°C, 30 s; 48°C, 40 s; 72°C, 2 min), with a final extension of 72°C for 7 min. The purified PCR product of *O. lithofera* of the appropriate size was inserted into the pEASY-T1 Cloning Vector (pEASY-T1 Cloning Kit, TransGen Biotech, Beijing, China) and sequenced using primers M13F (5′-CGCCAGGGTTTTCCCAGTCACGAC-3′) and M13R (5′-AGCGGATAACAATTTCACACAGGA-3′) and two internal primers at Sunny Biotechnology (Shanghai, China) (Zhang et al., 2019). For *R. haematoplasma*, cloning and sequencing in both directions were performed at Icongene

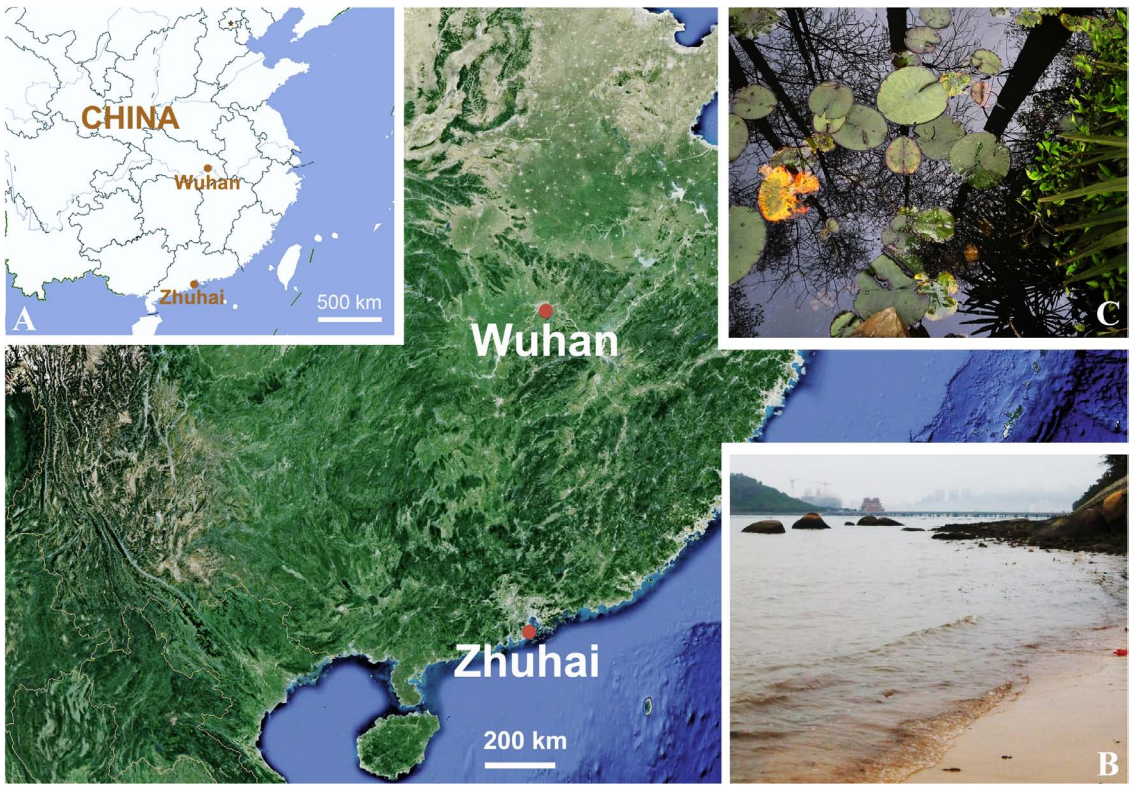

FIGURE 1 | (A–C) Locations and photographs of the sampling sites. **(A)** Locations of the sampling sites, marked with red dots. **(B)** Sandy beach near Zhuhai Fishing Girl Statue (22°15′41″N; 113°35′16″E). **(C)** Freshwater pond in Wuhan Botanical Garden, Chinese Academy of Sciences (30°32′57″N; 114°25′51″E).

(Wuhan, China) using primers M13F and M13R and four internal primers E528F (5′-CGGTAATTCCAGCTCC-3′), E1146F (5′-TGCATGGCCGTTCTTAG-3′), RevD (5′-GGA GCTGGAATTACCG-3′), and RevE (5′-CTAAGAACGG CCATGC-3′). Contigs were assembled using Seqman V. 7.1.0 (DNAStar).

Phylogenetic Analyses

The 18S rRNA gene sequences of 70 hypotrichids and four oligotrichous ciliates, i.e., *Strombidinopsis acuminate* (FJ790209), *Strombidium apolatum* (DQ662848), *Novistrombidium orientale* (FJ422988), and *Parastrombidinopsis minima* (DQ393786), selected as outgroup taxa, were downloaded from the National Center for Biotechnology Information (NCBI) Database[1]. The following stylonychines were selected: *Gastrostyla steinii* (AF508758), *Histriculus histrio* (FM209294), *Laurentiella strenua* (JX893368), *Onychodromus grandis* (AJ310486), *Paraparentocirrus sibillinensis* (KF184655), *Parentocirrus* sp. (KR063273), *Pattersoniella vitiphila* (JX885704), *Pleurotricha lanceolata* (AF508768), *Rigidohymena candens* (KC414885), *Steinia sphagnicola* (JX946276), *Sterkiella cavicola* (GU942565), *Sterkiella histriomuscorum* (FJ545743), *Sterkiella nova* (AF508771), *Stylonychia ammermanni* (FM209295), *Stylonychia lemnae* (AF508773), *Stylonychia mytilus* (AF508774), *Stylonychia notophora* (FM209297), *Styxophrya quadricornuta* (X53485), *Tetmemena bifaria* (FM209296), and *Tetmemena pustulata* (AF508775). The sequence alignment was performed on the GUIDANCE web server[2] with the MUSCLE algorithm (Sela et al., 2015). The MUSCLE alignment score is 0.997502 and unreliable columns below confidence score 0.987 (97% of columns remain) were removed. The program BioEdit 7.2.5 (Hall, 1999) was used to remove the primers from the aligned sequences. The final alignment used for phylogenetic tree construction included 76 taxa with 1,703 positions. The GTR model of nucleotide substitution was selected as the best model by the program MrModeltest v.2.2 (Nylander, 2004) and was then used for Bayesian inference (BI) analysis. BI analysis was performed with MrBayes 3.2.7 on XSEDE (Ronquist et al., 2012) on the CIPRES Science Gateway[3], with 2,000,000 generations, a sampling frequency of every 100th generation, and a burn-in of 5,000 trees. The remaining trees were used to calculate the posterior probabilities with a majority rule consensus. Maximum likelihood (ML) analysis was carried out using RAxML-HPC2 on XSEDE v 8.2.12 in CIPRES Science Gateway with the GTRGAMMA model (Miller et al., 2010; Stamatakis, 2014). The reliability of the internal branches was assessed by a non-parametric bootstrap method using 1,000 resamplings.

[1]https://www.ncbi.nlm.nih.gov/

[2]http://guidance.tau.ac.il/

[3]https://www.phylo.org

Tree topologies were displayed with SeaView v 4.6.1 (Gouy et al., 2010) and MEGA 7.0.26 (Tamura et al., 2013). The systematic classification follows Lynn (2008).

The statistical probability of the monophyletic hypothesis of the genus *Rubrioxytricha* was evaluated using AU tests (Shimodaira, 2002) in the CONSEL package (Shimodaira and Hasegawa, 2001).

RESULTS

ZooBank Registration

Present work: urn:lsid:zoobank.org:pub:C09DE513-8C3A-422C-8953-2AFBF5581313.

Oxytricha lithofera Foissner, 2016

Deposition of Voucher Specimens

Two voucher slides with protargol-stained specimens were deposited in the Laboratory of Protozoology, OUC, China, with registration numbers LXT2014052601-01∼02.

Morphology Based on the Zhuhai Population (Figures 2A–P, 3A–J and Table 1)

Cells 80–115 × 25–40 μm *in vivo*, ellipsoid in outline with both ends rounded, left margin more or less convex, right margin usually more or less straight (**Figures 2A,B**, **3A–E**). Dorsoventrally flattened 2–3:1. Body flexible, not contractile. One contractile vacuole slightly above mid-body at left cell margin, about 8 μm in diameter in diastole (**Figures 2A**,

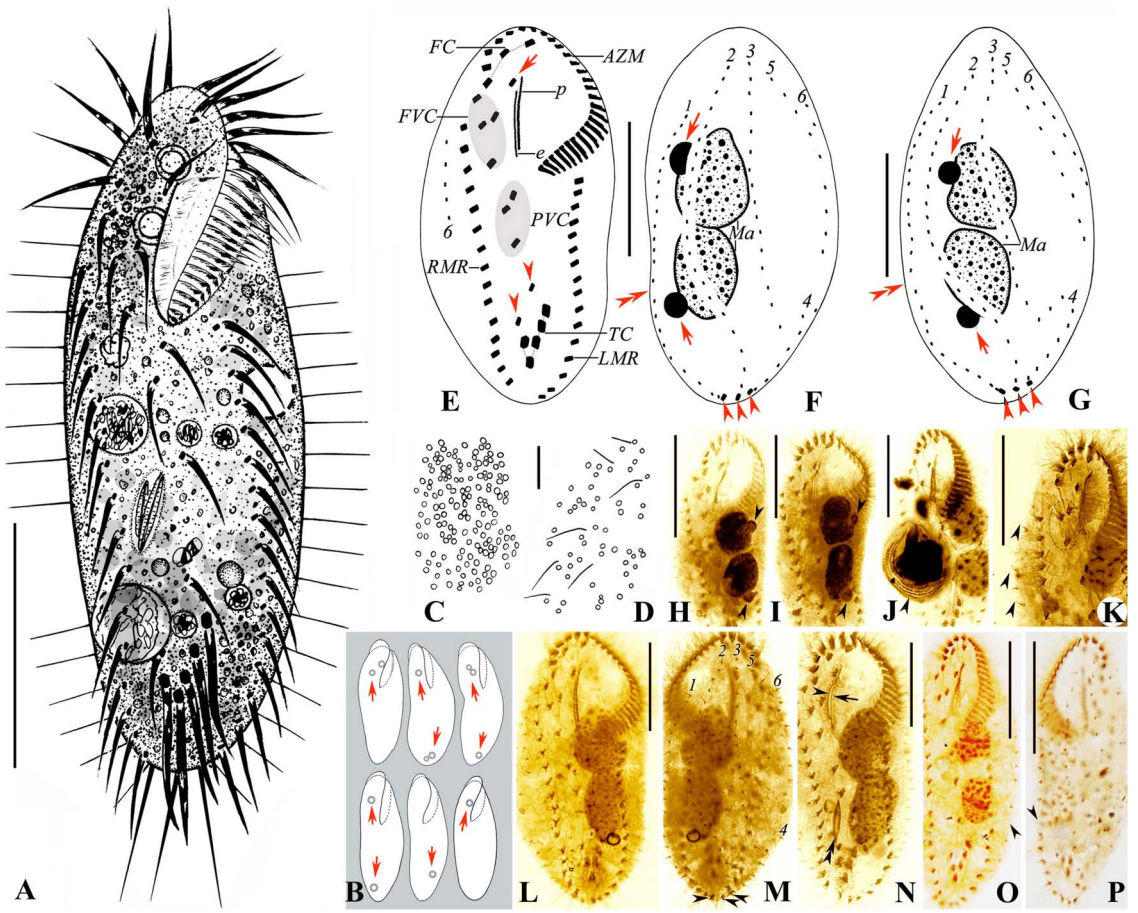

FIGURE 2 | (A–P) Morphology and ciliature of the Zhuhai population of *Oxytricha lithofera* from life **(A–D)** and after protargol impregnation **(E–P)**. **(A)** Ventral view of a representative individual. **(B)** Ventral views, showing body shape and lithosomes (arrows). **(C,D)** Distribution of cortical granules on the ventral **(C)** and dorsal **(D)** side. **(E–G)** Ventral **(E)** and dorsal **(F,G)** views of representative specimens, showing ciliature and nuclear apparatus; arrowheads in **(E)** mark pretransverse ventral cirri; arrow in (**E**) indicates buccal cirrus; arrowheads in **(F,G)** mark caudal cirri; arrows in **(F,G)** indicate micronuclei; double arrowheads in **(F,G)** mark the indeed very indistinct gap in dorsal kinety 1. **(H,I)** Ventral views showing the abutting macronuclear nodules and the large micronuclei (arrowheads) attached to the macronuclear nodules. **(J)** Ventral view, showing a specimen with an ingested ciliate (arrowhead). **(K)** Ventral view of a specimen with three frontoventral cirri; arrowheads indicate the long dorsal bristles of dorsal kinety 6. **(L,M)** Ventral **(L)** and dorsal **(M)** views of a representative specimen, the same one as **(E,F)**; arrowheads mark caudal cirri. **(N)** Ventral view, showing ciliature, the abutting macronuclear nodules, and an ingested diatom (double arrowheads); arrowhead indicates paroral membrane; arrow marks endoral membrane. **(O,P)** Show the slightly conspicuous one-bristle-wide gap in dorsal kinety 1. AZM, adoral zone of membranelles; e, endoral membrane; FC, frontal cirri; FVC, frontoventral cirri; LMR, left marginal row; Ma, macronuclear nodules; p, paroral membrane; PVC, postoral ventral cirri; RMR, right marginal row; TC, transverse cirri; 1–6, dorsal kineties. Scale bars = 30 μm **(A,E–P)** and 10 μm **(C,D)**.

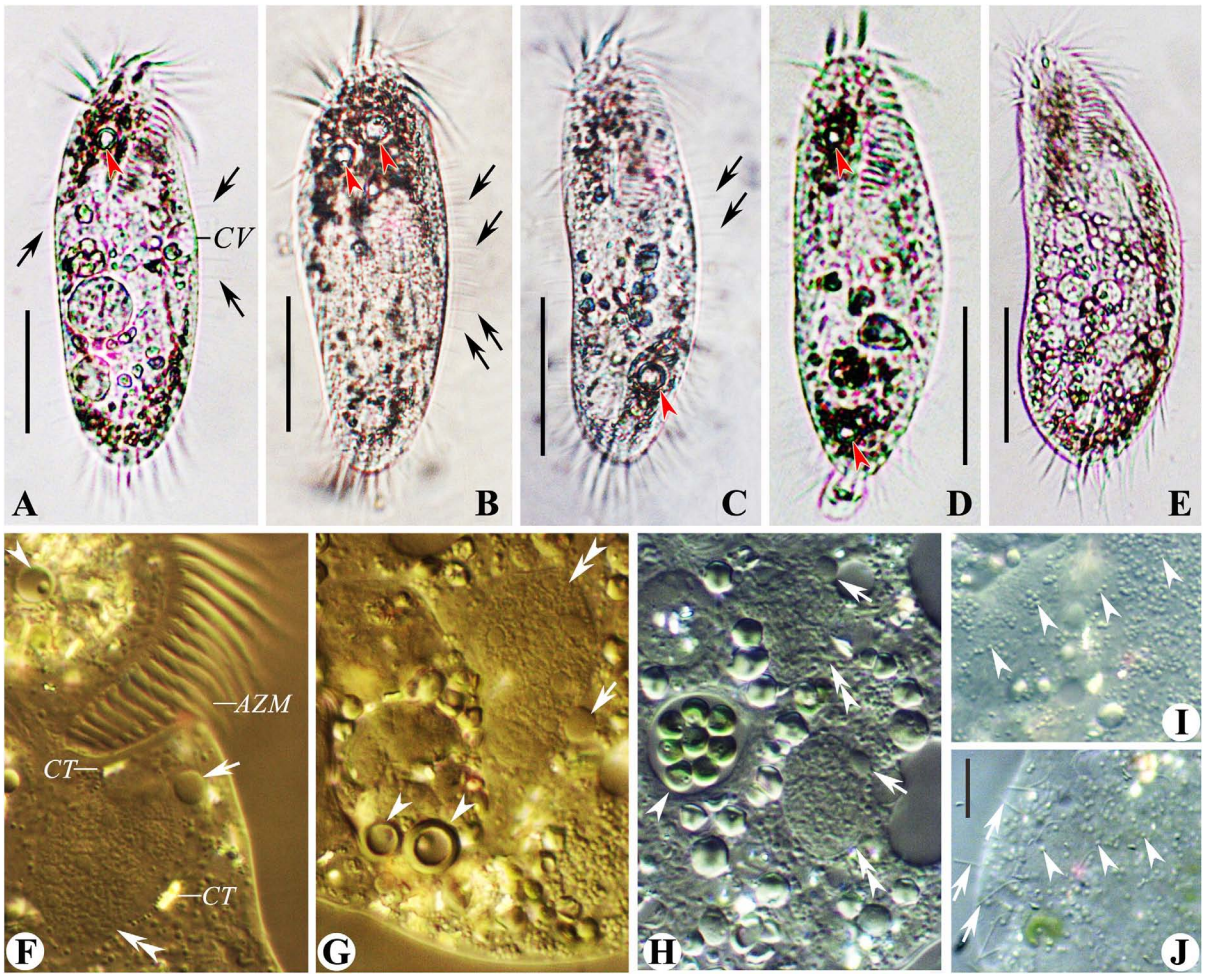

FIGURE 3 | (A–J) Morphology of the Zhuhai population of *Oxytricha lithofera* from life (**A–E**, bright field; **F–J**, differential interference contrast). **(A–E)** Ventral views of representative individuals, showing body shape, flexibility, contractile vacuole, lithosomes (arrowheads), and the long dorsal bristles (arrows). **(F,G)** Anterior **(F)** and posterior **(G)** part of the same specimen, showing three lithosomes (arrowheads), two macronuclear nodules (double arrowheads), two large-sized micronuclei (arrows), and crystals. **(H)** Ventral view, showing macronuclear nodules (double arrowheads), micronuclei (arrows), food vacuole (arrowhead), and inclusions. **(I,J)** Mitochondria-like cortical granules (arrowheads) on ventral **(I)** and dorsal **(J)** side; arrows in **(J)** indicate the long dorsal bristles. AZM, adoral zone of membranelles; CT, crystals; CV, contractile vacuole. Scale bars = 30 μm **(A–E)** and 10 μm **(J)**.

3A). Mitochondria-like cortical granules present, globular, about 1.0–1.5 μm across, irregularly distributed on the ventral and dorsal sides (**Figures 2C,D**, **3I,J**). Cytoplasm colorless, usually packed with numerous irregularly shaped shining granules (3–5 μm-sized), minute crystals (**Figure 3F**), and some food vacuoles, containing ciliates (**Figure 2J**, arrowhead), diatoms (**Figure 2N**, double arrowheads), and green algae (**Figure 3H**, arrowhead). One, two, or three ring-shaped lithosomes, 4–7 μm in diameter, with wall 1.0–1.5 μm thick, located subapically and/or subterminally (**Figures 2B**, **3A–D,F,G**). Two abutting macronuclear nodules, positioned in mid-body and left of midline, broadly to elongate ellipsoid, on average 21 × 15 μm in protargol preparations, with anterior one extending slightly anterior to the buccal vertex (**Figures 2F–I**). Consistently two globular micronuclei about 4 μm across, each one attached to one macronuclear nodule, usually on the left side (**Figures 2F–I**, **3F–H**). Locomotion by moderately fast crawling on the substrate, occasionally swimming.

Adoral zone extending 35–51% of body length (average 42%) in protargol preparations, composed of 21–29 membranelles (**Table 1**), with cilia 13–15 μm long *in vivo*. Paroral and endoral membrane almost equal in length, more or less straight, optically side by side, or superimposed, with paroral extending slightly more anteriorly than endoral (**Figures 2E,L,N**).

Ventral cirral pattern as shown in **Figures 2E,K,L,N**. Three frontal cirri with the right one located behind the distal end of the adoral zone, easily misinterpreted as an adoral membranelle. One buccal cirrus, located anterior to the endoral membrane and right of the anterior end of the paroral membrane. Usually four frontoventral cirri (only one out of 20 cells observed with three, **Figure 2K**) arranged in V shape, three of them (IV/3, VI/3, VI/4) arranged in a line, cirrus III/2 slightly above the level of cirrus

TABLE 1 | Morphometric data of the Chinese populations of *Oxytricha lithofera* (*Ol*) and *Rubrioxytricha haematoplasma* (*Rh*) based on protargol-stained specimens.

Character	Species	Min	Max	Mean	*M*	SD	CV	*n*
Body, length (μm)	*Ol*	60	105	88.6	90	11.5	12.9	19
	Rh	122	175	151.1	154	15	10	17
Body, width (μm)	*Ol*	29	51	41.7	42	6.2	14.9	19
	Rh	45	74	62.1	63	7.9	12.7	17
Body width: length, percentage	*Ol*	40	60	47.3	45.7	5.4	11.5	19
	Rh	31	47	41.2	41.4	4	9.8	17
Adoral zone length (μm)	*Ol*	27	46	37	37	5.7	15.3	19
	Rh	47	62	53.4	53	3.7	7	17
Adoral zone length: body length, percentage	*Ol*	35	51	41.8	41	4.4	10.4	19
	Rh	29	41	35.6	35.1	2.8	8	17
Adoral membranelles, number	*Ol*	21	29	25.8	27	2.7	10.5	19
	Rh	34	41	37.6	38	2	5.4	17
Frontal cirri, number	*Ol*	3	3	3	3	0	0	19
	Rh	3	3	3	3	0	0	17
Buccal cirrus, number	*Ol*	1	1	1	1	0	0	19
	Rh	1	1	1	1	0	0	17
Frontoventral cirri, number	*Ol*	3	4	4	4	0.2	5.7	20
	Rh	4	4	4	4	0	0	17
Postoral ventral cirri, number	*Ol*	3	3	3	3	0	0	19
	Rh	3	3	3	3	0	0	13
Pretransverse ventral cirri, number	*Ol*	2	2	2	2	0	0	19
	Rh	2	2	2	2	0	0	16
Transverse cirri, number	*Ol*	5	5	5	5	0	0	19
	Rh	4	6	5	5	0.4	7.1	17
Left marginal cirri, number	*Ol*	14	18	15.4	15	1	6.6	19
	Rh	29	40	35.2	36	2.7	7.7	17
Right marginal cirri, number	*Ol*	13	16	14.9	15	0.8	5.4	19
	Rh	29	40	34.9	35	3	8.5	17
Caudal cirri, number	*Ol*	3	3	3	3	0	0	19
	Rh	1	1	1	1	0	0	17
Dorsal kineties, number	*Ol*	6	6	6	6	0	0	18
	Rh	4	4	4	4	0	0	17
Dikinetids in dorsal kinety 1, number	*Ol*	13	26	21.7	23	3.9	18.2	18
	Rh	18	27	23.6	24	2.3	9.9	17
Dikinetids in dorsal kinety 2, number	*Ol*	11	25	18.6	20	3.7	19.7	17
	Rh	19	30	22.8	23	2.7	11.6	17
Dikinetids in dorsal kinety 3, number	*Ol*	10	21	14.4	13.5	3.2	22	16
	Rh	19	28	22.6	23	2.4	10.6	17
Dikinetids in dorsal kinety 4, number	*Ol*	3	8	5.4	5	1.5	27.8	18
	Rh	14	26	19.1	19	3.1	16.1	16
Dikinetids in dorsal kinety 5, number	*Ol*	5	18	9.1	9	2.8	30.9	18
Dikinetids in dorsal kinety 6, number	*Ol*	4	9	6.4	6	1.5	22.9	17
Macronuclear nodules, number	*Ol*	2	2	2	2	0	0	19
	Rh	2	2	2	2	0	0	15
Anterior macronuclear nodule, length (μm)	*Ol*	14	26	21.2	22.5	4	19.1	18
	Rh	18	33	24.8	25	4.8	19.4	15
Anterior macronuclear nodule, width (μm)	*Ol*	9	20	15	15.5	3.5	23.5	18
	Rh	8	13	10.1	10	1.8	17.4	15
Posterior macronuclear nodule, length (μm)	*Ol*	14	30	22.2	22.5	4.6	20.8	18
	Rh	19	30	25	25	3.4	13.8	15
Posterior macronuclear nodule, width (μm)	*Ol*	10	18	13.4	14	2.6	19.6	18
	Rh	7	12	9.7	10	1.7	17.3	15

(Continued)

TABLE 1 | Continued

Character	Species	Min	Max	Mean	*M*	SD	CV	*n*
Micronuclei, number	*Ol*	2	2	2	2	0	0	9
	Rh	2	3	2.1	2	0.3	12.9	14
Micronucleus, length (μm)	*Ol*	3	5	4.1	4	0.5	13.2	11
	Rh	5	8	6.5	6.5	0.7	11.5	28
Micronucleus, width (μm)	*Ol*	3	5	3.8	4	0.6	15.1	12
	Rh	3	5	4.2	4	0.5	11.8	28

Abbreviations: CV, coefficient of variation in%; M, median; Max, maximum; Mean, arithmetic mean; Min, minimum; n, number of cells measured; SD, standard deviation.

VI/3. Three postoral ventral cirri arranged in a triangular pattern. Two pretransverse ventral cirri, with the posterior one almost at the same level as transverse cirrus III/1. Five enlarged transverse cirri, arranged in a check-mark shape, with cilia 18–20 μm long *in vivo*, conspicuously protruding beyond the posterior end of the cell (**Figures 2A**, **3A–E**). Single marginal row on either body side, separated by a distinct gap, left one with 14–18 cirri, right one with 13–16 cirri, with cilia about 13 μm in length.

Invariably six dorsal kineties (DK): DK1, the leftmost kinety, strongly shortened anteriorly, reaches the posterior end, with an indeed very indistinct gap in most specimens (**Figures 2F,G**, double arrowheads), only six out of 25 cells observed with a slightly conspicuous gap (**Figures 2O,P**, arrowhead); DK2 almost extending the entire body length; DK3 extends to the anterior body end and splits to form a short row of DK4 (on an average of five dikinetids) at the subterminal end, usually one or two dikinetids between DK3 and DK4; DK5 and DK6, the dorsomarginal kineties, shortened anteriorly, with DK5 reaching the mid-body, DK6 extends slightly above the mid-body (**Figures 2F,G,M**). Bristles conspicuous *in vivo*, even at low magnification (**Figures 3A–C,J**, arrows), anterior bristles of DK1–3 about 5 μm long, gradually increase to 9 μm posteriorly; bristles of DK4 usually 8–9 μm long, bristles of DK5 and DK6 usually 5–7 μm long. Three long caudal cirri, with cilia 18–20 μm long, one each at end of DK1, 2, and 4, optically positioned in gap between ends of marginal rows (**Figures 2F,G,M**).

Rubrioxytricha haematoplasma (Blatterer and Foissner, 1990) Berger, 1999

Deposition of Voucher Specimens

Voucher slides with protargol-stained specimens were deposited in the Laboratory of Protozoology, OUC, China, with registration numbers LXT2016040802-01∼03 and LXT2016041102-01∼02.

Morphology Based on the Wuhan Population (Figures 4A–N and Table 1)

Cells 125–160 × 40–60 μm *in vivo*. Body soft, flexible and not contractile. Body long ellipsoid in shape, both anterior and posterior ends rounded, some with broad ends, some with narrower ends, right and left margins more or less convex (**Figures 4A,D,G–I**). Dorsoventrally flattened about 2:1. Single contractile vacuole slightly behind the buccal vertex and ahead of the mid-body, about 45% of body length, at the left cell margin, approximately 12 μm in diameter in diastole, two longitudinally oriented collecting canals present (**Figures 4A,D,G–I**). Cortical granules of single type, spherical, 0.8–1.0 μm across, lemon yellowish to greenish, arranged in lines or small groups then in long lines on both body sides (**Figures 4B,C,J–L**, slightly squeezed cells). Cytoplasm slightly orange (**Figures 4J,L**), usually packed with numerous irregularly shaped granules (2–6 μm-sized) and food vacuoles, containing diatoms, sometimes rendering cells yellow–brown to slightly darkish at low magnification. Consistently two macronuclear nodules, positioned in the mid-body and more or less left of midline, with the anterior one almost at the level of the buccal vertex, each nodule elongate ellipsoidal in shape, on average 25 × 10 μm after protargol preparation. Usually two ellipsoidal micronuclei, 5–8 × 3–5 μm in size, with one attached to or near each macronuclear nodule (**Figures 4F,M,N**). Locomotion by slowly crawling on the substrate, occasionally swimming with cells rotating around the longitudinal axis.

Adoral zone 29–41% of body length (average 36%) in protargol preparations, composed of 34–41 membranelles (**Table 1**). Cilia of membranelles 18–20 μm long *in vivo*, widest base about 10 μm. Undulating membranes in *Australocirrus* pattern (Kumar and Foissner, 2015), that is, paroral moderately to distinctly curved but not recurved distally, paroral extending slightly anteriorly to endoral and almost equal in length, both membranes optically intersecting at middle of paroral (**Figures 4E,M**).

Ventral cirral pattern as shown in **Figures 4E,M**. Three slightly enlarged frontal cirri continuous with frontoventral cirri arranged in a V-shaped pattern, rightmost three (IV/3, VI/3, VI/4) almost arranged in a line, cirrus III/2 slightly ahead level of the posteriormost one (cirrus IV/3) and distant from cirrus VI/3. Single buccal cirrus, almost at the same level with the right frontal cirrus. Three postoral ventral cirri and two pretransverse ventral cirri. On average five slightly enlarged transverse cirri, with cilia 20–22 μm long, extending slightly behind the rear end of the cell, arranged in a check-mark shape, just behind the pretransverse ventral cirri. Single left and right marginal row, more or less confluent at the posterior end.

Invariably four dorsal kineties (DK): three bipolar ones (DK1–3) with about 23 dikinetids each, one slightly shortened dorsomarginal kinety (DK4) comprising about 19 dikinetids. Always one parental dorsal kinety fragment located between DK3 and DK4, with sparsely arranged monokinetids (**Figures 4F,N**, arrowheads). Dorsal bristles 3–4 μm long *in vivo* (**Figure 4L**, arrowheads). Single caudal cirrus located at the end of DK3 (**Figures 4F,M**, arrow).

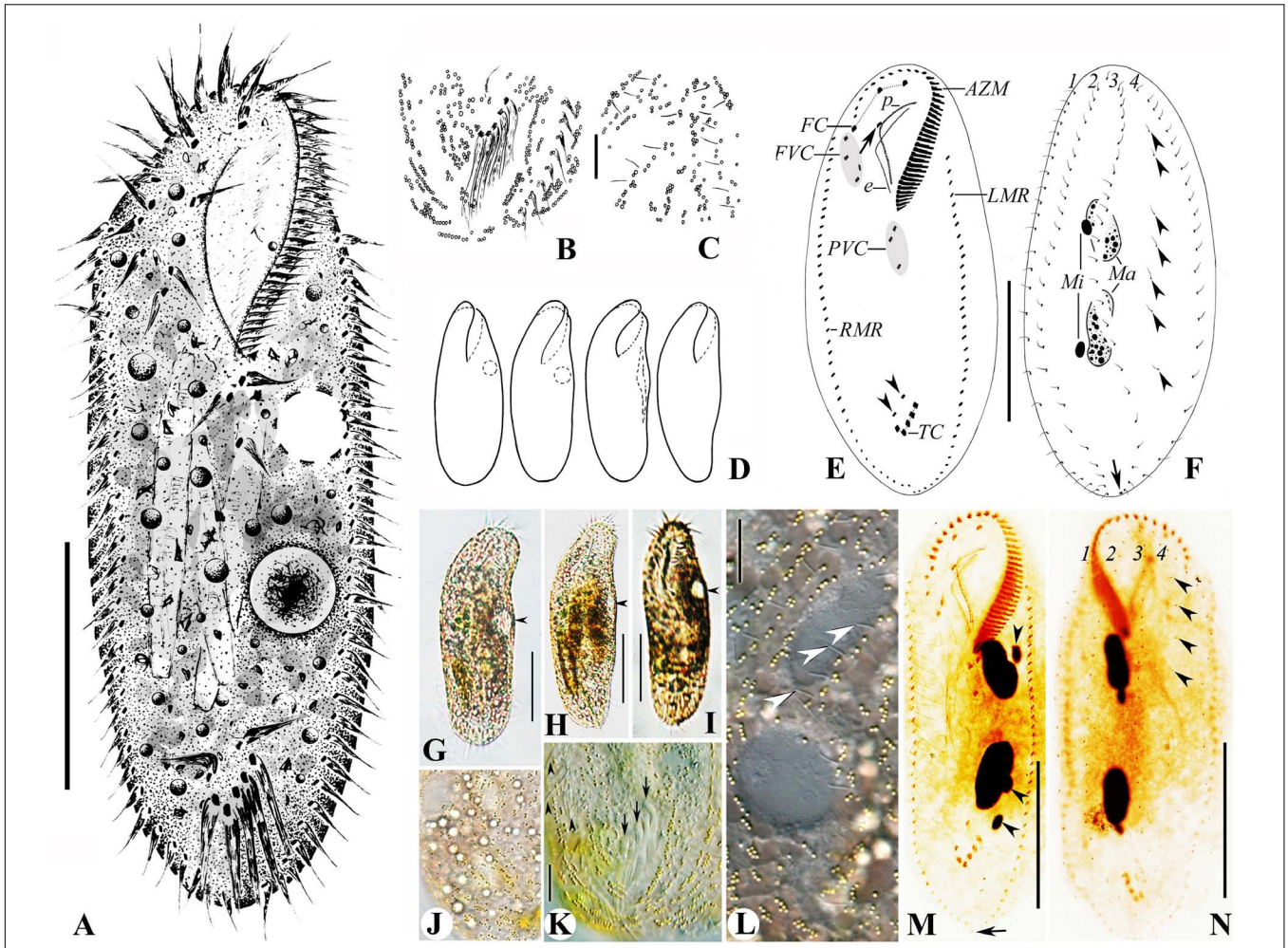

FIGURE 4 | (A–N) Morphology and ciliature of the Wuhan population of *Rubrioxytricha haematoplasma* from life (**A–D**; **G–J**, bright field; **K,L**, differential interference contrast) and after protargol impregnation **(E,F,M,N)**. **(A)** Ventral view of a representative individual. **(B,C)** Distribution of cortical granules on the ventral **(B)** and dorsal **(C)** side. **(D)** Ventral views, showing body shape and contractile vacuole. **(E,F)** Ventral **(E)** and dorsal **(F)** views of a representative specimen, showing ciliature and nuclear apparatus; arrowheads in **(E)** mark pretransverse ventral cirri; arrow in **(E)** indicates buccal cirrus; arrowheads in **(F)** show parental dorsal bristles; arrow in **(F)** marks the single caudal cirrus at end of dorsal kinety 3. **(G–I)** Ventral view of representative individuals, showing body shape, flexibility, and contractile vacuole (arrowhead). **(J)** Dorsal view of a slightly squeezed cell, showing the color of cortical granules and cytoplasm. **(K)** Ventral view of the posterior part of a slightly squeezed cell, showing the distribution of cortical granules; arrowheads indicate right marginal cirri; arrows show the slightly enlarged transverse cirri. **(L)** Dorsal view of a slightly squeezed cell, showing the distribution of cortical granules on the dorsal side; arrowheads indicate dorsal bristles. **(M,N)** Ventral **(M)** and dorsal **(N)** views of representative specimens, showing ciliature and nuclear apparatus; arrowheads in **(M)** show micronuclei; arrow in **(M)** indicates the single caudal cirrus; arrowheads in **(N)** mark parental dorsal bristles. AZM, adoral zone of membranelles; e, endoral membrane; FC, frontal cirri; FVC, frontoventral cirri; LMR, left marginal row; Ma, macronuclear nodules; Mi, micronuclei; p, paroral membrane; PVC, postoral ventral cirri; RMR, right marginal row; TC, transverse cirri; 1–4, dorsal kineties. Scale bars = 50 μm **(A,E,F,G–I,M,N)** and 10 μm **(B,C,K,L)**.

Morphogenesis (Figures 5A–H, 6A–H and Table 1)

In a very early divider (**Figures 5A**, **6A**), stomatogenesis commences with appearance of the oral primordium as groups of basal bodies between the buccal vortex and transverse cirri, including a large group just left to the postoral ventral cirri. At this stage, all parental cirri remain intact and do not contribute to the formation of the oral primordium. Somewhat later (**Figures 5B**, **6B**), the anterior two postoral ventral cirri (IV/2, V/4) dedifferentiate and contribute to the oral primordium. In an early divider (**Figures 5C**, **6C**), the posterior postoral ventral cirrus (V/3) is no longer recognizable and the oral primordium gives rise to new adoral membranelles. Simultaneously, the parental undulating membranes dedifferentiate anteriorly to form the undulating membranes anlage (UMA) (**Figure 5C**, arrow) and the frontal–ventral–transverse cirral anlagen (FVTA) begin to form. In a middle divider (**Figures 5E**, **6D**), two sets of FVTA are formed. Subsequently (**Figures 5G**, **6F**), the UMA forms the new undulating membranes and gives rise to the left frontal cirrus. At the same time, the other streaks differentiate into new cirri in the pattern of 3:3:3:4:4 from left to right. The parental adoral zone, which is inherited by the proter, remains unchanged throughout the whole process (**Figures 5C,E,G**).

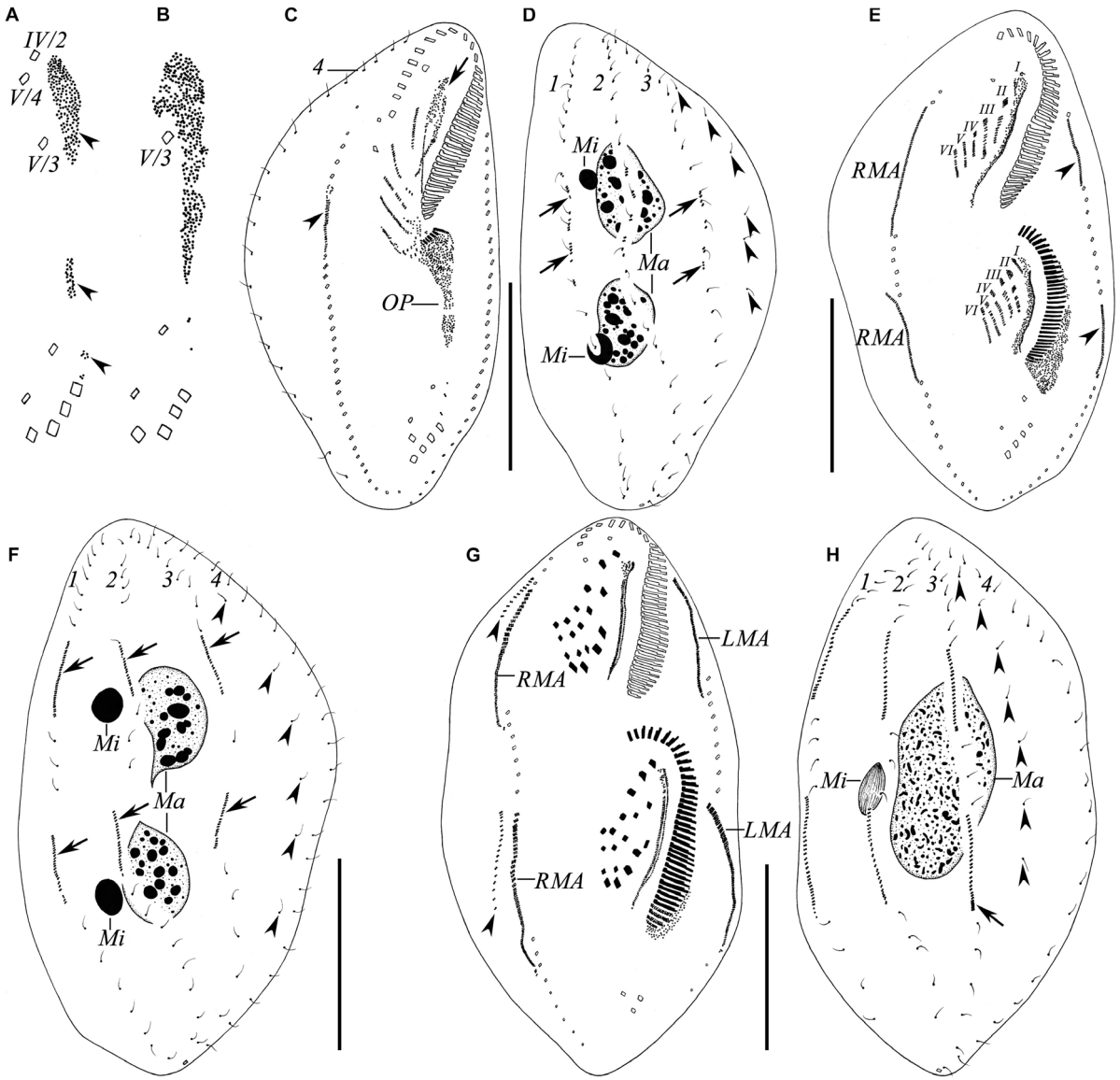

FIGURE 5 | (A–H) Ciliature of the Wuhan population of *Rubrioxytricha haematoplasma* during the ontogenetic process after protargol impregnation. **(A,B)** Ventral views of very early dividers, showing the formation of the oral primordium. **(C,D)** Ventral **(C)** and dorsal **(D)** views of an early divider, showing the formation of frontal–ventral–transverse cirral anlagen; arrow in **(C)** indicates undulating membranes anlage of proter (= anlage I) dedifferentiated from old structure; arrowhead in **(C)** marks right marginal anlage of proter; arrows in **(D)** show newly formed dorsal kinety anlagen; arrowheads in **(D)** indicate grandparental dorsal bristles. **(E,F)** Ventral **(E)** and dorsal **(F)** views of a middle divider, showing two sets of frontal–ventral–transverse cirral anlagen and dorsal kinety anlagen (arrows); arrowheads in **(E)** indicate left marginal anlagen of proter and opisthe; arrowheads in **(F)** indicate grandparental dorsal bristles. **(G,H)** Ventral **(G)** and dorsal **(H)** views of a late divider, showing newly formed frontal–ventral–transverse cirri, fused macronuclear mass and micronucleus; arrowheads in **(G)** mark dorsomarginal kinety anlagen formed near the anterior ends of right marginal anlagen; arrowheads in **(H)** indicate grandparental dorsal bristles; arrow marks new caudal cirrus formed at the end of dorsal kinety 3. LMA, left marginal anlagen; Ma, macronuclear nodules; Mi, micronuclei; OP, oral primordium; RMA, right marginal anlagen; I–VI, frontal–ventral–transverse cirral anlagen; 1–4, parental dorsal kineties. Scale bars = 50 μm.

The marginal anlagen develop by dedifferentiation of the parental structures, and the right marginal anlage of the proter appears earlier than others (**Figures 5C,E**, **6C,D**). Then, all the anlagen extend longitudinally and generate new cirri in both proter and opisthe (**Figures 5G**, **6F**).

Dorsal morphogenesis occurs by two groups of primordia: one group develops by dedifferentiation of the parental structures at the middle stage, that is, each of dorsal kineties 1–3 forms an anlage in both proter and opisthe (**Figures 5F**, **6E**, arrows). Later, all the anlagen lengthen at both ends, and one caudal cirrus is generated at the end of dorsal kinety 3 (**Figures 5H**, **6H**). The second group, that is, the dorsomarginal kinety primordia, develops *de novo* to the anterior right of the right marginal row anlage during the late stage (**Figures 5G**, **6F**, arrowheads).

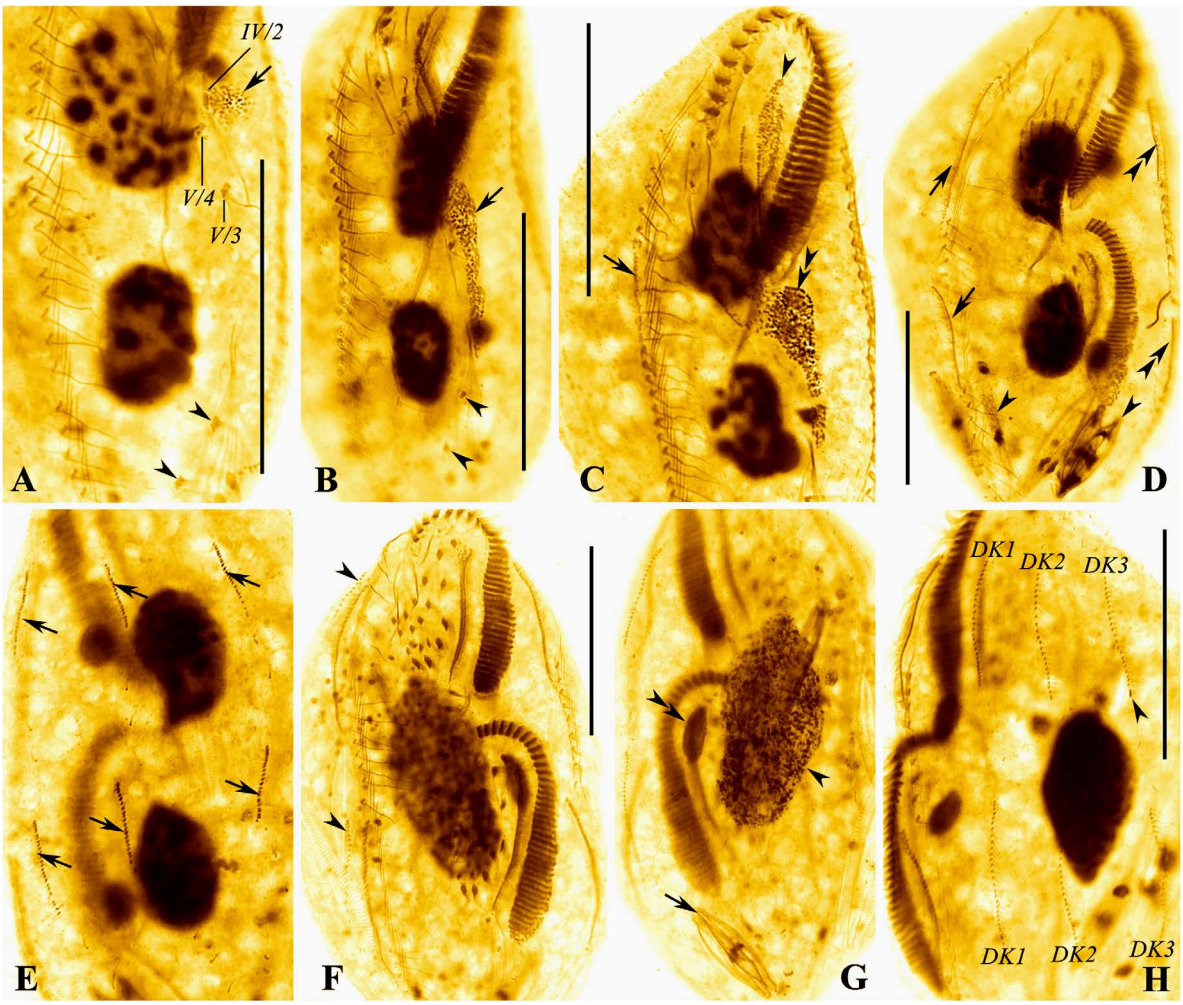

FIGURE 6 | (A–H) Photomicrographs of the Wuhan population of *Rubrioxytricha haematoplasma* during the ontogenetic process after protargol impregnation. **(A,B)** Ventral views of very early dividers, showing the formation of oral primordium (arrows); arrowheads indicate pretransverse ventral cirri. **(C)** Ventral view of an early divider, showing undulating membranes anlage of proter (= anlage I, arrowhead) dedifferentiated from the old structure, right marginal anlage of proter (arrow), and newly formed adoral membranelles of the opisthe (double arrowheads). **(D,E)** Ventral **(D)** and dorsal **(E)** views of a middle divider, showing right marginal anlagen (arrows in **D**), left marginal anlagen (double arrowheads), and dorsal kinety anlagen (arrows in **E**); arrowheads mark diatoms in the cell. **(F,G)** Ventral **(F)** and dorsal **(G)** views of a late divider, showing dorsomarginal kinety anlagen (arrowheads) formed near anterior ends of right marginal anlagen, fused macronuclear mass (arrowhead) and micronucleus (double arrowheads); arrow marks diatoms in the cell. **(H)** Ventral view of a late divider, showing newly formed dorsal kineties and new caudal cirrus (arrowhead) formed at the end of dorsal kinety 3. DK1–3, new dorsal kineties. Scale bars = 50 μm.

During the late stage of the ontogenetic process, the macronuclear nodules fuse with one another and the micronuclei fuse into a single mass as well (**Figures 5H**, **6G**).

18S rRNA Gene Sequences and Phylogenetic Analyses

The 18S rRNA gene sequence of *Oxytricha lithofera* (excluding both primers) has been deposited in GenBank with accession number MT364897. It has a length of 1,726 bp and a G + C content of 45.48%. The closest sequence to *O. lithofera* is *Urosoma salmastra* (KF951419), with the sequence similarity of 98.3% (28 nucleotide difference). The 18S rRNA gene sequence of *Rubrioxytricha haematoplasma* (excluding both primers) has been deposited in GenBank with accession number MT364898. It has a length of 1,724 bp and a G + C content of 45.01%. The 18S rRNA gene sequences of all six *Rubrioxytricha* isolates differ from each other by 0 to 26 nucleotides, with sequence identities from 98.4 to 100% (**Table 2**).

In the phylogenetic trees, *Oxytricha* species are separated into several clades. *Oxytricha lithofera* is sister to *U. salmastra* (KF951419) and distant from the type species of the genus, *O. granulifera* (AF508762), and *O. granulifera chiapasensis* (KX889988) although this relationship is not robust as indicated by the low support in the ML tree (ML/BI, 54%/1.00). All species of *Rubrioxytricha* fall within a well-supported assemblage (ML/BI, 91%/1.00) although this genus

TABLE 2 | Numbers of unmatched nucleotides (upper right) and distribution of percentages of sequence identity (lower left) to all available 18S rRNA gene sequences of *Rubrioxytricha* species.

Species (accession number)	1	2	3	4	5	6
1. *R. haematoplasma* (MT364898)	–	1	1	6	9	20
2. *R. tsinlingensis* (KR817675)	0.999	–	0	5	10	21
3. *Rubrioxytricha* sp. (MG603612)	0.999	1.000	–	5	10	21
4. *R. ferruginea* (AF370027)	0.996	0.996	0.996	–	15	26
5. *R. guamensis* (KY947508)	0.994	0.993	0.993	0.990	–	17
6. *R. guangzhouensis* spec. nov. (KJ645977)	0.987	0.987	0.987	0.984	0.989	–

is not monophyletic as two sequences under the names of *Polystichothrix monilata* (KT192639) and *Pseudogastrostyla flava* (KP266627) nest within it. *Rubrioxytricha guamensis* (KY947508) and *R. guangzhouensis* spec. nov. (KJ645977) branched off first in the large assemblage. The new sequence *R. haematoplasma* (MT364898) is most closely related with a cluster including three congeners, *R. tsinlingensis* (KR817675), *Rubrioxytricha* sp. (MG603612), and *R. ferruginea* (AF370027). However, the sister relationship between the four abovementioned species of *Rubrioxytricha* and the group of *Polystichothrix*–*Pseudogastrostyla* does not receive high support in the ML tree (ML/BI, 59%/1.00). The morphological hypothesis that *Rubrioxytricha* is a monophyletic group was rejected by the AU test (p value = 4×10^{-17}).

DISCUSSION

Identification of the Chinese Population of *Oxytricha lithofera* and Emended Diagnosis of the Species

Based on a population collected from Golfete de Cuare del Indio (salinity 10‰), Venezuela, Foissner (2016) reported a highly distinctive species, *O. lithofera*, with a combination of features not present in any other *Oxytricha* species. Our population, collected from a sandy beach (salinity 3–6‰) of Zhuhai, shares most of the following typical features with the Venezuelan population: (1) cirral pattern; (2) straight and parallel undulating membranes; (3) abutting macronuclear nodules, usually with a globular micronucleus attached to each; (4) large lithosomes present; (5) dorsal bristles increasing in length from the anterior end to the posterior end of dorsal kineties, up to 10 μm long; and (6) mitochondria-like granules present. Compared with the type population, the Zhuhai population has (1) a relatively larger body size *in vivo* (80–115 × 25–40 vs. 60–85 × 23–32 μm) and after protargol impregnation (60–105 × 29–51 vs. 53–75 × 20–28 μm) (shrinkage differed between the two methods); (2) more adoral membranelles (21–29 vs. 19–21); and (3) more marginal cirri (left, 14–18 vs. 12–15; right, 13–16 vs. 9–12). However, all of these differences, most of which overlap with each other, can be considered as population-dependent geographic variations (Berger, 1999; Chen et al., 2020). One difference that cannot be ignored is that there is a one-bristle-wide gap in dorsal kinety 1 of the type population, while the gap in most of the specimens of the Zhuhai population is absent. This may be seen as an intraspecific or intrapopulational difference. Therefore, we consider the Zhuhai population conspecific with the Venezuelan population. Based on the information of the Zhuhai population and the type population, an emended diagnosis is supplied here.

Emended Diagnosis of *Oxytricha lithofera*

Size 60–115 × 23–40 μm *in vivo*; body usually elongate ellipsoid. Mitochondria-like cortical granules present, globular, about 1.0–1.5 μm across. One, two, or three ring-shaped lithosomes, located subapically and/or subterminally. Adoral zone about 39% of body length, with about 23 membranelles. Undulating membranes straight, optically side by side. Eighteen frontoventral, transverse cirri. Six dorsal kineties with two dorsomarginal rows included, dorsal bristles gradually increasing in length from the anterior end to the posterior end. Three conspicuous caudal cirri. Two abutting ellipsoid macronuclear nodules and two globular micronuclei. Brackish habitat.

Identification of the Populations of *Rubrioxytricha haematoplasma*

Hitherto, five *Rubrioxytricha* species have been reported, namely *R. haematoplasma*, *R. ferruginea*, *R. indica*, *R. tsinlingensis*, and *R. guamensis* (Berger, 1999; Naqvi et al., 2006; Chen et al., 2017; Kumar et al., 2018). The type species of the genus, *R. haematoplasma*, was originally reported by Blatterer and Foissner (1990) based on a German population. Subsequently, Shin and Kim (1993) described a Korean population. Recently, Chen et al. (2015) reported a brackish/marine population collected from Guangzhou, China, based on detailed morphological, morphogenetic, and phylogenetic analyses.

The main features of the Wuhan population correspond well with those of the type population of *R. haematoplasma*, e.g., body shape, cirral pattern, dorsal ciliature, especially the color of cortical granules and cytoplasm. There is a tiny difference in terms of the distribution pattern of cortical granules, that is, the cortical granules of the type population are arranged in regular lines as shown in the drawings (Figure 5d in Blatterer and Foissner, 1990), while the cortical granules in the Wuhan population seem more or less irregular, with some in small groups and then in long lines. In addition, the postoral ventral cirri in the type population are distributed in a line, while those in the Wuhan population are in a V pattern.

However, we consider that these differences are not enough to separate them as different species. The Wuhan population of *R. haematoplasma* can be easily distinguished from the other four congeners by the characteristics shown in **Table 3**, while the differences of the 18S rRNA gene sequences of the five *Rubrioxytricha* members ranges from 1 to 20 nucleotides (**Table 2**). It is noteworthy that there is only one nucleotide difference of the 18S rRNA gene between *R. haematoplasma* and *R. tsinlingensis*, while morphologically, they have distinct different dorsal ciliature (four dorsal kineties with only one caudal cirrus vs. six dorsal kineties with three caudal cirri) (**Table 3**). The highly conserved nature of the 18S rRNA gene has been noted in other oxytrichid morphospecies as well (Kumar et al., 2017; Fan et al., 2021). Thus, the Wuhan population can be identified as *R. haematoplasma*.

There was no information about cortical granules or cytoplasm color of the Korean population (Shin and Kim, 1993). The differences in numbers of adoral membranelles and in the dorsal ciliature were considered as geographical variations by Berger (1999) and population differences by Chen et al. (2015). Herein, we tentatively accept these opinions until more information (cortical granules, cytoplasm, molecular data) is available for the Korean population.

Chen et al. (2015) did mention that the paroral and endoral membranes of the Guangzhou population of *R. haematoplasma* are more curved than those of the type population. However, this might be a preparation artifact, because photomicrographs of live specimens do not show a wide and deep buccal cavity as discussed by Kumar et al. (2018), and the undulating membranes of the early dividers (Figures 3a,b in Chen et al., 2015) do not show a strong degree of curvature either. Therefore, there is no distinct difference of the undulating membranes among the populations, all of which are arranged in an *Australocirrus* pattern. Compared with the Guangzhou population described by Chen et al. (2015), the Wuhan population and the type population of *R. haematoplasma* show significant differences in the following aspects: (1) cortical granules (lemon yellowish to greenish in color vs. reddish-brown), (2) mitochondria-like granules (absent vs. present), (3) color of the cytoplasm (slightly orange vs. slightly red), and (4) the habitat (freshwater vs. brackish/marine) (**Table 3**). Hence, we consider the Guangzhou population as a different species from *R. haematoplasma*. Furthermore, the 18S rRNA gene sequences (20 nucleotide difference between the Wuhan and the Guangzhou populations, **Table 2**) indicate that these two populations represent separate species.

In terms of cytoplasm color, cortical granules, cirral pattern, and dorsal ciliature, the Guangzhou population of *R. haematoplasma* should be compared with the other four species of the genus. The Guangzhou population of *R. haematoplasma* can be distinguished from all the others by the color of cortical granules (reddish-brown vs. *R. ferruginea*, brownish; *R. guamensis*, yellowish; *R. indica*, dark green; *R. tsinlingensis*, yellow-green) and the presence of mitochondria-like granules (vs. absent in all the congeners). For more differences among all the species, see **Table 3**. Thus, the Guangzhou population represents a separate species of the genus *Rubrioxytricha*.

Establishment of a New *Rubrioxytricha* Species

Rubrioxytricha guangzhouensis spec. nov. (Figures 7A–J)

2015 *Rubrioxytricha haematoplasma* (Blatterer and Foissner, 1990) Berger, 1999 – Chen et al., Int. J. Syst. Evol. Microbiol., 65, 309–320.

Remarks

As discussed above, a new species should be established for the Guangzhou isolate which was described under the name *R. haematoplasma* by Chen et al. (2015).

Chen et al. (2015) stated "the Chinese population came from two shrimp-farming ponds, one brackish (salinity 8.6‰) and the other marine (34.4‰). However, the brackish water was created artificially by mixing together marine and freshwater, and material was regularly transferred between the two ponds, so it is unclear whether the Chinese population of *R. haematoplasma* was originally from a marine or a freshwater habitat." We think it is possible that the Guangzhou isolate was originally from the marine pond and then transferred to the brackish pond. Therefore, we tentatively treat the marine pond as the type locality.

Diagnosis

Size 90–180 × 30–70 μm *in vivo*; body elongate oval, brown-reddish in color. Cortical granules, approximately 0.8 μm in diameter, reddish-brown, grouped in lines on dorsal; mitochondria-like granules about 3 μm in diameter, colorless and spherical, densely packed. Adoral zone about 30% of body length, with about 37 membranelles. Eighteen frontoventral, transverse cirri. Three bipolar dorsal kineties and one slightly shorter dorsomarginal row; one caudal cirrus at the posterior end of dorsal kinety 3. Two macronuclear nodules and one to three micronuclei. Brackish/marine habitat.

Etymology

The species-group name *guangzhouensis* refers to the geographic locality where the ciliate population was discovered.

Type Locality

Marine shrimp-farming pond (salinity 34‰) at the campus of the South China Normal University, Guangzhou, China (23°08′19″N; 113°21′22″E).

Type Specimens

The protargol-stained slide containing the holotype specimen (**Figures 7C–E**) and 10 paratype slides were deposited in the Laboratory of Protozoology, OUC, China, with registration numbers CXM08112701-01∼11.

ZooBank Registration

Rubrioxytricha guangzhouensis spec. nov. is registered in ZooBank under: urn:lsid:zoobank.org:act:036912E2-4662-40D1-B666-B4091FD50DE1.

TABLE 3 | Morphological and morphometric comparison of *Rubrioxytricha* species.

Character	*Rubrioxytricha haematoplasma*	*Rubrioxytricha haematoplasma*	*Rubrioxytricha haematoplasma*	*Rubrioxytricha guangzhouensis* spec. nov.	*Rubrioxytricha ferruginea*	*Rubrioxytricha guamensis*	*Rubrioxytricha indica*	*Rubrioxytricha tsinlingensis*
BL[a] (μm)	125–160	120–180	100–180	90–180	150–200	85–110	80	100–180
BW[a] (μm)	40–60	40–55	50–90	30–70	/	25–45	30	35–60
BL[b] (μm)	122–175	91–143	112–160	133–195	122–162	74–96	65–74	144–186
BW[b] (μm)	45–74	29–51	42–80	50–95	39–51	20–38	24–32	64–89
AZM, *n*	34–41	30–48	21–30	33–45	35–41	23–32	27–31	36–44
CC, *n*	1	0.8 (0–1)	0.7 (0–1)	1	1.7 (1–2)	1.1 (1–2)	1	3
DK, *n*	4	4	4.1 (4–5)	4	5	4	5	6
DM, *n*	1	1	1	1	/	1	2	/
DKF	Absent	Absent	Absent	Absent	/	Absent	Absent	/
Cortical granules	Lemon yellowish to greenish	Lemon yellowish to greenish	/	Reddish-brown	Brownish	Yellowish	Dark green	Yellow-green
Color of the cytoplasm	Slightly orange	Slightly orange to reddish	/	Slightly red	Rusty	Colorless	More or less colorless	Slightly brown
Color of the cell	Yellow–brown to slightly darkish	Darkish at low magnification	/	Dark-brownish to ashblack	Rusty brown	/	/	Yellow–brown
Habitat	Freshwater pond	Freshwater river	Freshwater river	Brackish/marine	Eutrophic pond	Freshwater pond		Freshwater pond
Data source	Present work	Blatterer and Foissner (1990); Berger (1999)	Shin and Kim (1993)	Chen et al. (2015)	Song and Wilbert (1989); Berger (1999)	Kumar et al., 2018	Naqvi et al. (2006)	Chen et al. (2017)

Characters marked with "/" were not available from the source cited. Abbreviations: AZM, adoral zone of membranelles; BL, body length; BW, body width; CC, caudal cirri; DK, dorsal kineties; DKF, dorsal kinety fragmentation; DM, dorsomarginal kineties; n, number. [a] *Data based on specimens in vivo.* [b] *Data based on specimens after protargol impregnation.*

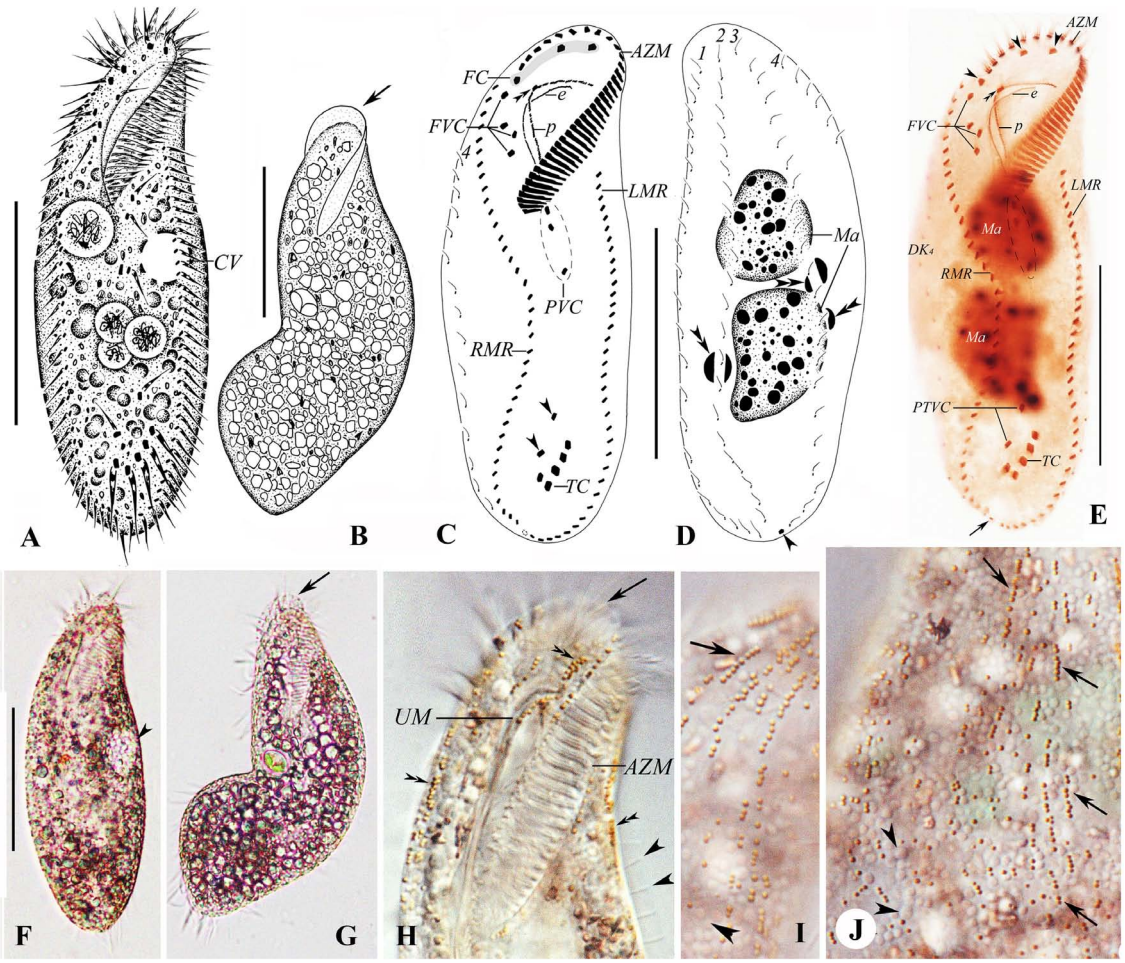

FIGURE 7 | (A–J) Morphology and ciliature of *Rubrioxytricha guangzhouensis* spec. nov. from life (**A,B,F,G**, bright field; **H–J**, differential interference contrast) and after protargol impregnation **(C–E)**. **(A–J)** From Chen et al. (2015). **(A)** Ventral view of a representative individual. **(B)** Ventral view of a bending cell to show the flexibility of the body; arrow marks the frontal scutum. **(C–E)** Ventral **(C,E)** and dorsal **(D)** views of the holotype specimen, showing ciliature and nuclear apparatus; arrowheads in **(C)** mark pretransverse ventral cirri; double arrowheads in **(C,E)** mark buccal cirrus; double arrowheads in **(D)** show micronuclei; arrow in **(D,E)** indicates the single caudal cirrus; arrows in **(E)** show frontal cirri. **(F)** Ventral view of the typical individual; arrowhead marks the contractile vacuole. **(G)** Ventral view of bending cell to show the flexibility of the body; arrow marks the transparent membrane-like structure at the anterior part of the adoral zone. **(H)** Ventral view of anterior cell part; arrow marks the transparent membrane-like structure at the anterior part of the adoral zone; double arrowheads indicate the reddish-brown, spherical, type-I cortical granules; arrowheads indicate the dorsal bristles. **(I,J)** Dorsal views of the anterior **(I)** and middle **(J)** cell parts; arrows indicate the reddish-brown, spherical, type-I cortical granules arranged in lines; arrowheads mark the colorless, densely distributed, mitochondria-like granules. AZM, adoral zone of membranelles; CV, contractile vacuole; e, endoral membrane; FC, frontal cirri; FVC, frontoventral cirri; LMR, left marginal row; Ma, macronuclear nodules; p, paroral membrane; PVC, postoral ventral cirri; RMR, right marginal row; TC, transverse cirri; UM, undulating membranes; 1–4, dorsal kineties. Scale bars = 60 μm.

Morphogenetic Comparison of *Rubrioxytricha* Species

Blatterer and Foissner (1990) gave an incomplete morphogenetic description for the type population of *R. haematoplasma*. In the present study, we supply somewhat more detailed morphogenetic information for *R. haematoplasma* based on the Wuhan population. Chen et al. (2015) provided a detailed morphogenetic description for *R. guangzhouensis* spec. nov. Naqvi et al. (2006) reported the morphogenetic process of *R. indica* and Kumar et al. (2018) provided brief notes on the ontogenesis of *R. guamensis*. All the abovementioned populations share the following morphogenetic features: (1) the parental adoral zone of membranelles is completely inherited, unchanged, by the proter; (2) the undulating membranes anlage of the proter originates by dedifferentiation of the parental structures; (3) parental buccal cirrus (II/2), two frontoventral cirri (III/2, IV/3), and three postoral ventral cirri (IV/2, V/3, V/4) contribute to the formation of the anlagen; (4) the frontal–ventral–transverse (FVT) cirral anlagen are probably formed *via* a primary pattern and the FVT cirri are formed in a typical *Oxytricha* pattern, i.e., in the pattern of 1:3:3:3:4:4 from left to right; (5) marginal anlagen develop intrakinetally within the parental structures; (6) dorsal kineties are formed in the *Urosomoida* pattern, i.e., dorsomarginal row present and without fragmentation of kinety 3; (7) a single caudal cirrus (seldom two caudal cirri

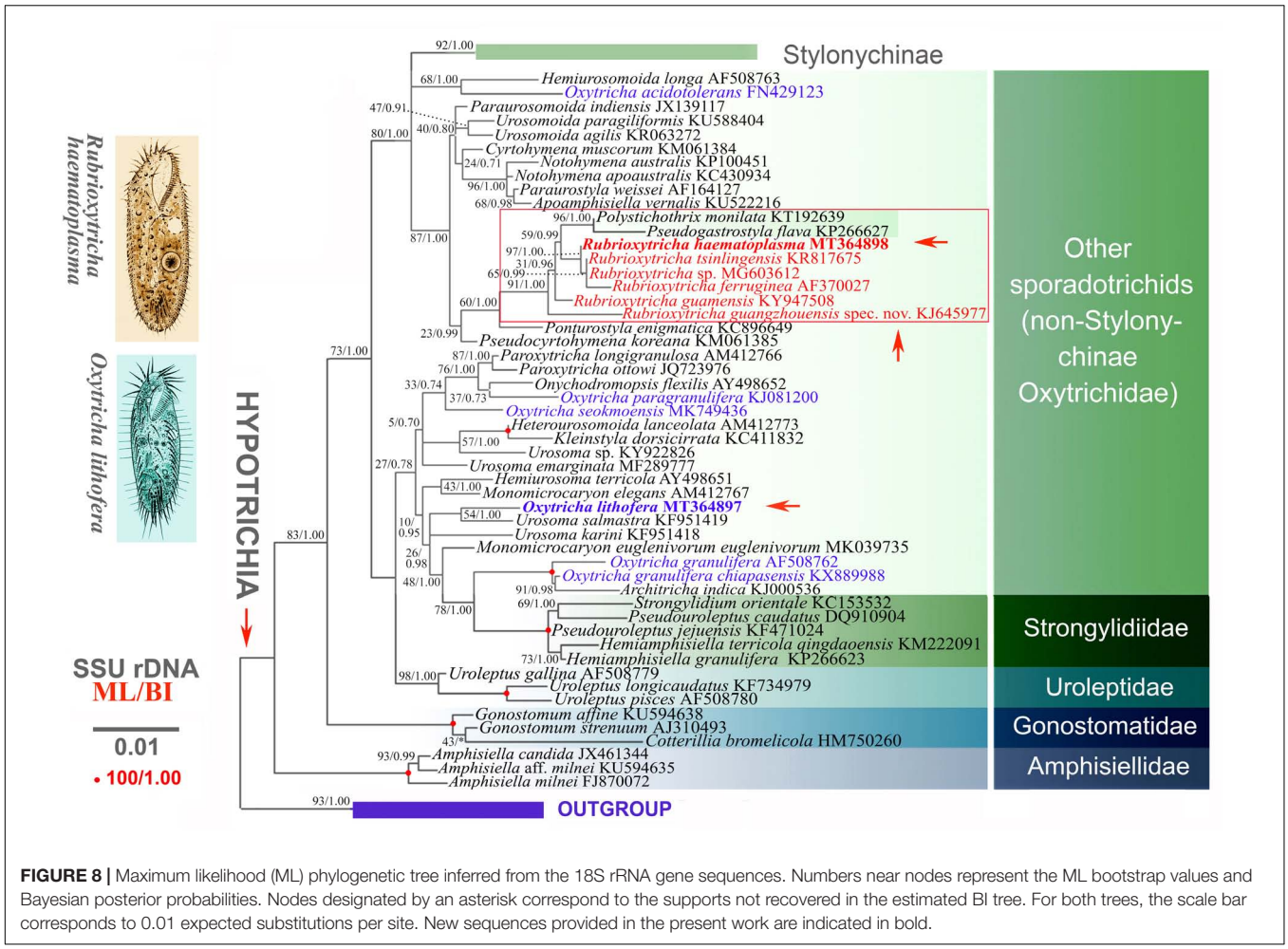

FIGURE 8 | Maximum likelihood (ML) phylogenetic tree inferred from the 18S rRNA gene sequences. Numbers near nodes represent the ML bootstrap values and Bayesian posterior probabilities. Nodes designated by an asterisk correspond to the supports not recovered in the estimated BI tree. For both trees, the scale bar corresponds to 0.01 expected substitutions per site. New sequences provided in the present work are indicated in bold.

in *R. guamensis*) originates at the end of dorsal kinety 3; and (8) two macronuclear nodules fuse into a single mass during the morphogenetic process. This combination of features reveals a highly conservative morphogenetic pattern of the above *Rubrioxytricha* species (Naqvi et al., 2006; Chen et al., 2015; Song and Shao, 2017; Kumar et al., 2018).

Phylogenetic Analyses

As described in previous studies, *Oxytricha* and *Urosoma* species are irregularly distributed over the phylogenetic trees, revealing that both the genus *Oxytricha* and *Urosoma* are non-monophyletic and lack obvious synapomorphies (Schmidt et al., 2007; Paiva et al., 2009; Shao et al., 2014, 2019; Gao et al., 2016; Jung and Berger, 2019; Kaur et al., 2019; Kim and Min, 2019; Dong et al., 2020; Wang et al., 2020b; Xu et al., 2020). In the present phylogenetic trees (**Figure 8**), *O. lithofera* is placed sister to *U. salmastra* (KF951419). Morphologically, they do have the same features as follows: flexible body, single marginal row on each body side, three caudal cirri, two macronuclear nodules, and two micronuclei, which, however, are shared by most of the oxytrichids (Berger, 1999; Wang et al., 2017). Moreover, *O. lithofera* can be easily distinguished from *U. salmastra* by an adoral zone of membranelles more or less in *Stylonychia* pattern (vs. typical *Gonostomum* pattern), having more transverse cirri (five vs. four), and more dorsal kineties (six, kinety fragmentation probably present vs. four, kinety fragmentation absent), which all have been considered as genus-level diagnostic features for the oxytrichids (Berger, 1999; Shao et al., 2015; Wang et al., 2020b). In addition, the grouping of *O. lithofera* and *U. salmastra* is far from stable as this relationship does not receive high support in the ML analysis. The topology may very likely be changed when additional molecular data from more taxa are available.

All species of *Rubrioxytricha* are intermingled with *P. monilata* (KT192639) and *P. flava* (KP266627) in a highly supported assemblage, indicating that *Rubrioxytricha* is paraphyletic. The hypothesis that *Rubrioxytricha* species form a monophyletic group was rejected by the AU test, although the internal relationships are not yet robustly resolved. The close relationship between *Rubrioxytricha* and *Polystichothrix–Pseudogastrostyla* is morphologically supported as they all have a flexible body, one marginal row on each body side, and brightly colored cortical granules. However, *Rubrioxytricha* differs significantly from *Polystichothrix* and *Pseudogastrostyla* in having a typical oxytrichid pattern of 18 FVT cirri (vs. more than 18 FVT cirri in short lines) (Fan et al., 2015; Luo et al., 2017). The phylogenetic placement

of the genera *Polystichothrix* and *Pseudogastrostyla* might be explained by the assumption that those taxa with more than 18 FVT cirri evolved by a secondary increase in the numbers of FVT anlagen and/or additional cirri originated from some of the anlagen (Berger, 1999; Luo et al., 2017). Moreover, the dorsal ciliature pattern, which also carries an informative phylogenetic signal, like the ventral cirral pattern (Berger, 1999; Shao et al., 2011, 2015; Foissner, 2016), shows great variety in the *Rubrioxytricha–Polystichothrix–Pseudogastrostyla* clade: (1) four dorsal kineties in *R. guamensis*, *R. haematoplasma*, *R. indica*, *R. guangzhouensis* spec. nov., and *Pseudogastrostyla*, with one dorsomarginal kinety present, dorsal kinety fragmentation absent, only one caudal cirrus (seldom two caudal cirri in *R. guamensis*) present at the end of dorsal kinety 3; (2) five dorsal kineties in *R. ferruginea* and *Polystichothrix*, very likely including one dorsomarginal kinety and dorsal kinety 4 originated by dorsal kinety 3 fragmentation, one or two caudal cirri present in *R. ferruginea* and caudal cirri lacking in *Polystichothrix*; (3) six dorsal kineties in *R. tsinlingensis*, probably with two dorsomarginal rows included and dorsal kinety 4 originated by dorsal kinety 3 fragmentation, three caudal cirri in total, one each at the posterior end of dorsal kineties 1, 2, and 4 (Berger, 1999; Naqvi et al., 2006; Chen et al., 2015, 2017; Fan et al., 2015; Luo et al., 2017; Kumar et al., 2018).

The incongruence between morphology and molecular data suggests that *Oxytricha* and *Rubrioxytricha* are genera with high genetic divergence, which need to be broken up into multiple new genera. At present, there are over 1,000 nominal hypotrich ciliates (Chen et al., 2017); however, the 18S rRNA gene sequences are only available for about 30% of this group (NCBI database). Thus, molecular data from additional taxa and even phylogenomic data are needed to reveal the natural phylogeny of this group of ciliates.

DATA AVAILABILITY STATEMENT

The original contributions presented in the study are publicly available. This data can be found here: GenBank (https://www.ncbi.nlm.nih.gov/genbank/) with accession numbers MT364897-MT364898.

AUTHOR CONTRIBUTIONS

XL and JH collected the samples. XL carried out the experiments (live observation, protargol impregnation, and DNA amplification) and analyses (morphometrics and phylogenetic analyses). XC and WS supervised the work. All authors wrote the manuscript and approved the final version.

FUNDING

This work was supported by the Natural Science Foundation of China (project numbers 31900319, 31772433, and 32030015), the Natural Science Foundation of Shandong Province (project number: ZR2019QD015), the Deanship of Scientific Research at King Saud University (RSP-2021/7), the Youth Innovation Promotion Association of the CAS (No. 2019333), and the China Postdoctoral Science Foundation Grant (Nos. BX20180348 and 2018M642955).

REFERENCES

Berger, H. (1999). *Monograph of the Oxytrichidae (Ciliophora, Hypotrichia)*. Dordrecht: Springer Netherlands.

Berger, H. (2008). *Monograph of the Amphisiellidae and Trachelostylidae (Ciliophora, Hypotricha)*. Berlin: Springer Science & Business Media.

Blatterer, H., and Foissner, W. (1990). Beiträge zur ciliatenfauna (Protozoa: Ciliophora) der Amper (Bayern, Bundesrepublik Deutschland). *Arch. Protistenkd.* 138, 93–115. doi: 10.1016/s0003-9365(11)80148-x

Chen, L., Dong, J., Wu, W., Xin, Y., Warren, A., Ning, Y., et al. (2020). Morphology and molecular phylogeny of a new hypotrich ciliate, *Anteholosticha songi* nov. spec., and an American population of *Holosticha pullaster* (Müller, 1773) Foissner et al., 1991 (Ciliophora, Hypotrichia). *Eur. J. Protistol.* 72:125646. doi: 10.1016/j.ejop.2019.125646

Chen, L., Zhao, X., Shao, C., Miao, M., and Clamp, J. (2017). Morphology and phylogeny of two new ciliates, *Sterkiella sinica* sp. nov. and *Rubrioxytricha tsinlingensis* sp. nov. (Protozoa, Ciliophora, Hypotrichia) from north-west China. *Syst. Biodivers.* 15, 131–142. doi: 10.1080/14772000.2016.1219426

Chen, W., Chen, X., Li, L., Warren, A., and Lin, X. (2015). Morphology, morphogenesis and molecular phylogeny of an oxytrichid ciliate, *Rubrioxytricha haematoplasma* (Blatterer & Foissner, 1990) Berger, 1999 (Ciliophora, Hypotricha). *Int. J. Syst. Evol. Microbiol.* 65, 309–320. doi: 10.1099/ijs.0.067801-67800

Dong, J., Li, L., Fan, X., Ma, H., and Warren, A. (2020). Two *Urosoma* species (Ciliophora, Hypotrichia): a multidisciplinary approach provides new insights into their ultrastructure and systematics. *Eur. J. Protistol.* 72:125661. doi: 10.1016/j.ejop.2019.125661

Fan, X., Yao, S., Luo, X., Dong, T., Xu, Y., Chen, L., et al. (2021). Some morphologically distinguishable hypotrich ciliates share identical 18S rRNA gene sequences – taxonomic insights from a case study on *Oxytricha* species (Protista, Ciliophora). *Zool. J. Linn. Soc.* doi: 10.1093/zoolinnean/zlaa145 [Epub ahead of print].

Fan, Y., Zhao, X., Hu, X., Miao, M., Warren, A., and Song, W. (2015). Taxonomy and molecular phylogeny of two novel ciliates, with establishment of a new genus, *Pseudogastrostyla* n. g. (Ciliophora, Hypotrichia, Oxytrichidae). *Eur. J. Protistol.* 51, 374–385. doi: 10.1016/j.ejop.2015.06.007

Foissner, W. (2016). Terrestrial and semiterrestrial ciliates (Protozoa, Ciliophora) from Venezuela and Galápagos. *Denisia* 35, 1–912. doi: 10.1007/978-3-319-23534-9_1

Foissner, W., Agatha, S., and Berger, H. (2002). Soil ciliates (Protozoa, Ciliophora) from Namibia (Southwest Africa), with emphasis on two contrasting environments, the Etosha region and the Namib Desert. *Denisia* 5, 1–1459. doi: 10.1007/978-3-319-23534-9_1

Gao, F., Warren, A., Zhang, Q., Gong, J., Miao, M., Sun, P., et al. (2016). The all-data-based evolutionary hypothesis of ciliated protists with a revised classification of the phylum Ciliophora (Eukaryota, Alveolata). *Sci. Rep.* 6:24874. doi: 10.1038/srep24874

Gouy, M., Guindon, S., and Gascuel, O. (2010). SeaView version 4: a multiplatform graphical user interface for sequence alignment and phylogenetic tree building. *Mol. Biol. Evol.* 27, 221–224. doi: 10.1093/molbev/msp259

Hall, T. A. (1999). BioEdit: a user-friendly biological sequence alignment editor and analysis program for windows 95/98/NT. *Nucleic Acids Symp. Ser.* 41, 95–98.

Hu, X., Lin, X., and Song, W. (2019). *Ciliates Atlas: Species Found in the South China Sea*. Beijing: Science Press.

Jung, J. H., and Berger, H. (2019). Monographic treatment of *Paraholosticha muscicola* (Ciliophora, Keronopsidae), including morphological and molecular biological characterization of a brackish water population from Korea. *Eur. J. Protistol.* 68, 48–67. doi: 10.1016/j.ejop.2018.12.004

Kaur, H., Shashi, Negi, R. K., and Kamra, K. (2019). Morphological and molecular characterization of *Neogastrostyla aqua* nov. gen., nov. spec. (Ciliophora,

Hypotrichia) from river Yamuna, Delhi; comparison with *Gastrostyla*-like genera. *Eur. J. Protistol.* 68, 68–79. doi: 10.1016/j.ejop.2019.01.002

Kim, K. S., and Min, G. S. (2019). Morphology and molecular phylogeny of *Oxytricha seokmoensis* sp. nov. (Hypotrichia: Oxytrichidae), with notes on its morphogenesis. *Eur. J. Protistol.* 71:125641. doi: 10.1016/j.ejop.2019.125641

Kim, K. S., Jung, J. H., and Min, G. S. (2019). Morphology and molecular phylogeny of two new terrestrial ciliates, *Australocirrus rubrus* n. sp. and *Notohymena gangwonensis* n. sp. (Ciliophora: Oxytrichidae), from South Korea. *J. Eukaryot. Microbiol.* 66, 740–751. doi: 10.1111/jeu.12718

Kumar, S., and Foissner, W. (2015). Biogeographic specializations of two large hypotrich ciliates: *Australocirrus shii* and *A. australis* and proposed synonymy of *Australocirrus* and *Cyrtohymenides*. *Eur.J. Protistol.* 51, 210–228. doi: 10.1016/j.ejop.2015.02.002

Kumar, S., Bharti, D., Kabir, A. S., Hong, J. S., and Shin, M. K. (2018). *Rubrioxytricha guamensis* nov. spec. (Ciliophora, Spirotricha), a novel hypotrich ciliate from Guam (United States), Micronesia. *J. Eukaryot. Microbiol.* 65, 392–399. doi: 10.1111/jeu.12484

Kumar, S., Bharti, D., Shazib, S. U. A., and Shin, M. K. (2017). Discovery of a new hypotrich ciliate from petroleum contaminated soil. *PLoS One* 12:e0178657. doi: 10.1371/journal.pone.0178657

Lu, X., Huang, J., Shao, C., and Berger, H. (2018). Morphology, cell-division, and phylogeny of *Schmidingerothrix elongata* spec. nov. (Ciliophora, Hypotricha), and brief guide to hypotrichs with *Gonostomum*-like oral apparatus. *Eur. J. Protistol.* 62, 24–42. doi: 10.1016/j.ejop.2017.11.001

Luo, X., Gao, F., Yi, Z., Pan, Y., Al-Farraj, S. A., and Warren, A. (2017). Taxonomy and molecular phylogeny of two new brackish hypotrichous ciliates, with the establishment of a new genus (Ciliophora, Spirotrichea). *Zool. J. Linn. Soc.* 179, 475–491. doi: 10.1111/zoj.12451

Luo, X., Yan, Y., Shao, C., Al-Farraj, S. A., Bourland, W. A., and Song, W. (2018). Morphological, ontogenetic, and molecular data support strongylidiids as being closely related to Dorsomarginalia (Protozoa, Ciliophora) and reactivation of the family Strongylidiidae Fauré-Fremiet, 1961. *Zool. J. Linn. Soc.* 184, 237–254. doi: 10.1093/zoolinnean/zly001

Lynn, D. H. (2008). *The Ciliated Protozoa: Characterization, Classification, and Guide to the Literature*, Third Edn. New York: Springer Press.

Medlin, L., Elwood, H. J., Stickel, S., and Sogin, M. L. (1988). The characterization of enzymatically amplified eukaryotes 16S-like ribosomal RNA coding regions. *Gene* 71, 491–500. doi: 10.1016/0378-1119(88)90066-2

Miller, M. A., Pfeiffer, W., and Schwartz, T. (2010). Creating the CIPRES science gateway for inference of large phylogenetic trees. *Gatew. Comput. Environ. Work* 1–8.

Naqvi, I., Gupta, R., Borgohain, P., and Sapra, G. R. (2006). Morphology and morphogenesis of *Rubrioxytricha indica* n. sp. (Ciliophora: Hypotrichida). *Acta Protozool.* 45, 53–64.

Nylander, J. A. A. (2004). *MrModeltest 2.2. Program Distributed by the Author*. Uppsala: Evolutionary Biology Centre, Uppsala University.

Paiva, T. S., Borges, B. N., Harada, M. L., and Silva-Neto, I. D. (2009). Comparative phylogenetic study on Stichotrichia (Alveolata: Ciliophora: Spirotrichea) based on 18S-rDNA sequences. *Genet. Mol. Res.* 8, 223–246. doi: 10.4238/vol8-1gmr529

Ronquist, F., Teslenko, M., van der Mark, P., Ayres, D. L., Darling, A., Höhna, S., et al. (2012). MrBayes 3.2: efficient Bayesian phylogenetic inference and model choice across a large model space. *Syst. Biol.* 61, 539–542. doi: 10.1093/sysbio/sys029

Schmidt, S. L., Bernhard, D., Schlegel, M., and Foissner, W. (2007). Phylogeny of the Stichotrichia (Ciliophora; Spirotrichea) reconstructed with nuclear small subunit rRNA gene sequences: discrepancies and accordances with morphological data. *J. Eukaryot. Microbiol.* 54, 201–209.

Sela, I., Ashkenazy, H., Katoh, K., and Pupko, T. (2015). GUIDANCE2: accurate detection of unreliable alignment regions accounting for the uncertainty of multiple parameters. *Nucl. Acids Res.* 43, W7–W14.

Shao, C., Hu, C., Fan, Y., Warren, A., and Lin, X. (2019). Morphology, morphogenesis and molecular phylogeny of a freshwater ciliate, *Monomicrocaryon euglenivorum euglenivorum* (Ciliophora, Oxytrichidae). *Eur. J. Protistol.* 68, 25–36. doi: 10.1016/j.ejop.2019.01.001

Shao, C., Lu, X., and Ma, H. (2015). A general overview of the typical 18 frontal-ventral-transverse cirri Oxytrichidae s. l. genera (Ciliophora, Hypotrichia). *J. Ocean Univ. China* 14, 522–532. doi: 10.1007/s11802-015-2482-7

Shao, C., Lv, Z., Pan, Y., Al-Rasheid, K. A. S., and Yi, Z. (2014). Morphology and phylogenetic analysis of two oxytrichid soil ciliates from China, *Oxytricha paragranulifera* n. sp. and *Oxytricha granulifera* Foissner and Adam, 1983 (Protista, Ciliophora, Hypotrichia). *Int. J. Syst. Evol. Microbiol.* 64, 3016–3027. doi: 10.1099/ijs.0.062281-0

Shao, C., Song, W., Al-Rasheid, K. A. S., and Berger, H. (2011). Redefinition and reassignment of the 18-cirri genera *Hemigastrostyla, Oxytricha, Urosomoida*, and actinotricha (Ciliophora, Hypotricha), and description of one new genus and two new species. *Acta Protozool.* 50, 263–287.

Shimodaira, H. (2002). An approximately unbiased test of phylogenetic tree selection. *Syst. Biol.* 51, 492–508. doi: 10.1080/10635150290069913

Shimodaira, H., and Hasegawa, M. (2001). CONSEL: for assessing the confidence of phylogenetic tree selection. *Bioinformatics* 17, 1246–1247. doi: 10.1093/bioinformatics/17.12.1246

Shin, M. K., and Kim, W. (1993). New records of three oxytrichid hypotrichs (Ciliophora: Hypotrichida: Oxytrichidae) from the Han river in Seoul. *Korea. Korean J. Zool.* 36, 223–230.

Song, W., and Shao, C. (2017). *Ontogenetic Patterns of Hypotrich Ciliates*. Beijing: Science Press. (in Chinese).

Song, W., and Wilbert, N. (1989). Taxonomische untersuchungen an aufwuchsciliaten (Protozoa, Ciliophora) im poppelsdorfer weiher, bonn. *Lauterbornia* 3, 2–221.

Stamatakis, A. (2014). RAxML version 8: a tool for phylogenetic analysis and post-analysis of large phylogenies. *Bioinformatics* 30, 1312–1313. doi: 10.1093/bioinformatics/btu033

Tamura, K., Stecher, G., Peterson, D., Filipski, A., Dudley, J., and Kumar, S. (2013). MEGA6: molecular evolutionary genetics analysis version 6.0. *Mol. Biol. Evol.* 30, 2725–2729. doi: 10.1093/molbev/mst197

Wang, J., Li, J., and Shao, C. (2020a). Morphology, morphogenesis, and molecular phylogeny of a novel saline soil ciliate, *Heterourosomoida sinica* n. sp. (Ciliophora, Hypotrichia). *Eur. J. Protistol.* 73:125666. doi: 10.1016/j.ejop.2019.125666

Wang, J., Qi, S., Chen, L., Warren, A., Miao, M., and Shao, C. (2017). Morphogenesis of a saline soil ciliate *Urosoma salmastra* (Dragesco and Dragesco-Kernéis, 1986) Berger, 1999 with notes on the phylogeny of *Urosoma* (Ciliophora, Hypotrichia). *Eur. J. Protistol.* 61, 180–193. doi: 10.1016/j.ejop.2017.08.003

Wang, J., Zhao, Y., Lu, X., Lyu, Z., Warren, A., and Shao, C. (2020b). Does the *Gonostomum*-patterned oral apparatus in Hypotrichia carry a phylogenetic signal? evidence from morphological and molecular data based on extended taxon sampling using three nuclear genes (Ciliophora, Spirotrichea). *Sci. China Life Sci.* doi: 10.1007/s11427-020-1667-1663 [Epub ahead of print].

Weisse, T., Moser, M., Scheffel, U., Stadler, P., Berendonk, T., Weithoff, G., et al. (2013). Systematics and species-specific response to pH of *Oxytricha acidotolerans* sp. nov. and *Urosomoida* sp. (Ciliophora, Hypotrichia) from acid mining lakes. *Eur. J. Protistol.* 49, 255–271. doi: 10.1016/j.ejop.2012.08.001

Wilbert, N. (1975). Eine verbesserte technik der protargolimprägnation für ciliaten. *Mikrokosmos* 64, 171–179.

Xu, W., Zhao, Y., Pan, B., Liu, Y., Li, Y., Bourland, W. A., et al. (2020). Morphology, morphogenesis, and phylogeny of *Urosoma caudata* (Ehrenberg, 1833) Berger, 1999 (Ciliophora, Hypotrichia) based on a Chinese population. *J. Eukaryot. Microbiol.* 67, 76–85. doi: 10.1111/jeu.12756

Zhang, T. T., Fan, X., Gao, F., Al-Farraj, S. A., El-Serehy, H. A., and Song, W. (2019). Further analyses on the phylogeny of the subclass Scuticociliatia (Protozoa, Ciliophora) based on both nuclear and mitochondrial data. *Mol. Phylogenet. Evol.* 139:106565. doi: 10.1016/j.ympev.2019.106565

Zhang, T. Y., Dong, J., Cheng, T., Duan, L., and Shao, C. (2020). Reconsideration on the taxonomy of the marine ciliate *Neobakuella aenigmatica* Moon et al., 2019 (Protozoa, Ciliophora, Hypotrichia). *Mar. Life Sci. Technol.* 2, 97–108. doi: 10.1007/s42995-020-00032-4

Conflict of Interest: The authors declare that the research was conducted in the absence of any commercial or financial relationships that could be construed as a potential conflict of interest.

frontiers in Marine Science

ORIGINAL RESEARCH
published: 04 February 2021
doi: 10.3389/fmars.2021.621349

A New Record of *Oxytricha granulifera granulifera* Foissner and Adam, 1983 (Protozoa, Ciliophora, Oxytrichidae) From a Hot Spring in Iceland, With Notes on Its Abnormal Form During Cultivation

Rong Zhu[1,2], Zhishuai Qu[3], Qi Zhang[1,2], Sabine Filker[4], Thorsten Stoeck[3], Fengchao Li[1,2] and Xiaozhong Hu[5]*

[1] College of Life Science, Hebei University, Baoding, China, [2] Institute of Life Science and Green Development, Hebei University, Baoding, China, [3] Ecology Group, Technische Universität Kaiserslautern, Kaiserslautern, Germany, [4] Department of Molecular Ecology, Technische Universität Kaiserslautern, Kaiserslautern, Germany, [5] Key Laboratory of Mariculture, Ministry of Education, Institute of Evolution and Marine Biodiversity, Ocean University of China, Qingdao, China

OPEN ACCESS

Edited by:
Thomas Wilke, University of Giessen, Germany

Reviewed by:
Xiangrui CHEN, Ningbo University, China
Wenzhe Xu, Tianjin University of Science and Technology, China

***Correspondence:**
Fengchao Li
lifengchao2000@126.com

Specialty section:
This article was submitted to Marine Evolutionary Biology, Biogeography and Species Diversity, a section of the journal Frontiers in Marine Science

Received: *26 October 2020*
Accepted: *14 January 2021*
Published: *04 February 2021*

Citation:
Zhu R, Qu Z, Zhang Q, Filker S, Stoeck T, Li F and Hu X (2021) A New Record of Oxytricha granulifera granulifera Foissner and Adam, 1983 (Protozoa, Ciliophora, Oxytrichidae) From a Hot Spring in Iceland, With Notes on Its Abnormal Form During Cultivation. Front. Mar. Sci. 8:621349. doi: 10.3389/fmars.2021.621349

We isolated a population of *Oxytricha granulifera granulifera* Foissner and Adam (1983) from a hot spring in Iceland. The pure culture of this isolate was established at room temperature in the laboratory. This allowed for a detailed investigation, informed by integrated approaches, of the isolate's morphology and morphogenesis, as well as molecular phylogeny. Results showed that the morphological and morphogenetic characteristics of the Iceland population are consistent with those of other populations. During the 3-year long period of laboratory cultivation, some abnormal individuals appeared repeatedly in the culture system. Interestingly, the morphological characteristics of these abnormal cells were rather stable, and were as follows: 1) body slender and elliptical-shaped; 2) remarkably shortened adoral zone and significantly reduced number of adoral membranelles; and 3) loss of undulating membranes. Resting cysts, binary fission and conjugate reproduction were not found in abnormal specimens. Although the morphology of abnormal individuals changed significantly, the sequences of the SSU rDNA of the normal and abnormal morphotypes were the same. Phylogenetic analyses showed that the two morphotypes clustered in a clade with other populations of *O. granulifera granulifera*.

Keywords: abnormal form, *Oxytricha*, hot spring, Iceland, morphology, phylogeny

INTRODUCTION

Ciliates are a large and diverse group of protozoa, which are distributed in a variety of habitats, including extreme environments (Foissner, 2016; Chen et al., 2019; Li et al., 2019; Luo et al., 2019; Shao et al., 2019, 2020; Bai et al., 2020; Wu et al., 2020). Among ciliates, *Oxytricha* is one of the most diverse and species-rich genera, with approximately 40 nominal species having been reported

so far (Berger, 1999; Song et al., 2009; Shao et al., 2012, 2015; Bai et al., 2018; Kim and Min, 2019; Kaur et al., 2019; Song et al., 2019). *Oxytricha granulifera* Foissner and Adam (1983), type species of the genus, was first discovered from soil in Austria (Foissner and Adam, 1983). Thereafter, more populations were recorded elsewhere, for example in Australia (soil; Blatterer and Foissner, 1988); China (soil; Shao et al., 2014); Costa Rica (bark of *Acacia* trees; Foissner, 1994, 1997); Japan (soil; Berger, 1999); Marion Island (soil; Foissner, 1996); Namibia (soil; Foissner et al., 2002); Peru (soil; Foissner, 1997); and South Korea (freshwater; Kwon and Shin, 2013).

Recently, Méndez-Sánchez et al. (2018) subdivided *Oxytricha granulifera* into three subspecies, namely *Oxytricha granulifera granulifera* (Foissner and Adam, 1983), *O. granulifera quadricirrata* (Blatterer and Foissner, 1988), and *O. granulifera chiapasensis* (Méndez-Sánchez et al., 2018). This subdivision was mainly based on morphological characteristics, i.e., the patterns of undulating membrane, the numbers of dorsal kineties and transverse cirri. Diagnosis of *O. granulifera granulifera* was as follows: cells 70–127 × 28–75 μm *in vivo*; adoral zone with 29–32 membranelles; paroral and endoral membranes in *Oxytricha*-pattern; the right marginal cirri row starting at the same level of the rightmost frontal cirrus; constantly five transverse cirri; rarely a sixth dorsal kinety; confined to terrestrial habitats (Foissner and Adam, 1983; Méndez-Sánchez et al., 2018).

During a protistan fauna investigation, one encysted ciliate was isolated from a geothermal field (hot spring) in Iceland. This isolate was identified as *O. granulifera granulifera* Foissner and Adam (1983). Its pure culture was established at room temperature (20–25°C) in Petri dishes, with rice grains to enrich the bacterial food. During the cultivation, some abnormal individuals appeared repeatedly in the system. Although the abnormal individuals appeared at different times, their morphological characteristics remained consistent, which made it easier to mistakenly deduct that a "new" species had been discovered. *Oxytricha granulifera* has not been recorded from hot springs, especially the abnormal forms in long-term indoor culture system have not been reported, therefore, the morphology and SSU rDNA sequences of the normal and abnormal forms are described in this article, and the morphogenesis of the normal form is also reported.

MATERIALS AND METHODS

Sampling and Cultivation

The sludge sample was collected from a microbial mat in a geothermal field in Iceland near the Hellisheiðarvirkjun geothermal power station (64°01′11.5″N, 21°23′50.5″W), as described in Qu et al. (2018). The temperature was approximately 75°C at the sampling site. The surface sediments were transferred to Petri dishes in water from the sample site and maintained as a raw culture in the laboratory for several days at room temperature (about 25°C). The salinity (0‰) of the hot spring water was measured on site with a portable refractometer. The pH level (7.3) was measured using portable pH sensors. In the laboratory, the pure cultures of *O. granulifera granulifera* were established and maintained using volvic water and sterilized wheat grains. Wheat grains enriched bacteria as a food source for the ciliate. Clonal cultures were obtained by gradually transferring single ciliates from the enrichment culture to artificially distilled freshwater (Qu et al., 2020). One to two wheat grains per 20 mL cell culture were added to support the growth of bacteria. To maintain this population, approximately once every 2 weeks, several cells were picked up and transferred into a new Petri dish containing new water and rice grains to establish a new pure cultivation. The attempt to establish pure cultures using abnormal individuals solely failed, because the abnormal individuals gradually disappeared over the course of about one week. The pH level of the culture systems was 6.0–7.0.

Morphological and Ontogenetic Investigations

Live observations were carried out using a bright field microscope (Olympus BX53) equipped with differential interference contrast (DIC). The protargol silver staining method of Wilbert (1975) was used to reveal the ciliature and the nuclear apparatus. Protargol was synthesized mainly according to Pan et al. (2013). Drawings of stained specimens were conducted at a magnification of 1,000× with the aid of a camera lucida. Measurements were made with an ocular micrometer. To illustrate the changes that occur during ontogenetic processes, ciliary structures of parental cells were depicted by contours, whereas those of the daughter cells were shaded black. The terminology used herein follows Berger (1999) and Song and Shao (2017).

DNA Extraction, PCR Amplification, and Sequencing

Total genomic DNA of the normal and abnormal forms of *O. granulifera granulifera* were extracted from single cells in pure cultures, using the DNeasy Blood and Tissue Kit (Qiagen, Gmbh, Germany) according to the manufacturer's instructions. Each cell was washed three times with distilled water and two times in ultra-pure water in order to remove contaminants and then was immediately transferred to 1.5-mL microfuge tubes with an ATL buffer (Jin et al., 2020). PCR amplifications of SSU rDNA were performed with universal eukaryotic primers 18S-F (5′-AAC CTG GTT GAT CCT GCC AGT-3′) and 18S-R (5′-TGA TCC TTC TGC AGG TTC ACC TAC-3′) (Medlin et al., 1988). The amplification conditions were as follows: a pre-run of 30 s at 98°C followed by 35 cycles consisting of a denaturation at 98°C for 30 s, an annealing at 60°C for 20 s, and an extension at 72°C for 1 min. After 35 cycles, the final extension step was run at 72°C for 2 min. The PCR products were sequenced by Beijing Genomics Institute in Shenzhen, China. Three internal primers, 900S-F (5′-CGA TCA GAT ACC GTC CTA GT-3′), 900S-R (5′-ACT AGG ACG GTA TCT GAT CG-3′) and B (5′-AAY CTG GTT GAT YYT GCC AG-3′) were used in sequencing.

Phylogenetic Analyses

Apart from the newly sequenced SSU rDNA sequences of the normal and abnormal forms of *O. granulifera granulifera* in this article, all of the sequences used in the phylogenetic analyses were obtained from the GenBank database (accession numbers see **Figure 4**). *Novistrombidium orientale*, *Parastrobidinopsis minima*, *Strombidinopsis acuminata*, and *Strombidium apolatum* were selected as outgroups since they were used to construct the phylogenies recently reported by Méndez-Sánchez et al. (2018) and Liao et al. (2020). Sequences were aligned using the MUSCLE package on the European Bioinformatics Institute web page[1]. Both ends of the alignment were then trimmed manually using BioEdit 7.0.9.1, resulting in a final matrix of 1,579 nucleotide positions. A maximum-likelihood (ML) tree was constructed using RAxML-HPC2 on XSEDE v.8.2.10 (Stamatakis, 2014) on the CIPRES Science Gateway (Miller et al., 2010). The model GTR + I + G was used. Support for the best ML tree came from 1,000 bootstrap replicates (Jin et al., 2020). Bayesian inference (BI) analysis was carried out on CIPRES Science Gateway using the MrBayes 3.2.6 on XSEDE (Ronquist and Huelsenbeck, 2003). TreeView v1.6.6 (Page, 1996) and MEGA 7.0 (Kumar et al., 2016) were used to visualize tree topologies.

RESULTS

Morphology of Normal Forms

Size 90–130 × 30–45 μm (average 110 × 35 μm, $n = 10$) *in vivo*, and 79–135 × 28–61 μm (average 102 × 42 μm) in protargol preparations. Body flexible and slightly contractile, elliptical in shape with a ratio of length: width approximately 3.5:1, right margin usually straight and left margin more or less convex. Cell dorsoventrally flattened with a width: thickness ratio of approximately 2:1, ventral side flat and dorsal slightly convex (degree depending of nutrition status). Constantly two globular to ellipsoid macronuclear nodules, on average 16.1 × 9.2 μm in protargol preparations, located in anterior and posterior third of cell. One to four globular micronuclei, on average 2.2 μm across, attached to macronuclear nodules (**Figures 1C**, **3A,B**). Contractile vacuole (about 8 μm across) in mid-body, close to left cell margin; pulsing at intervals of about 8 s (**Figures 1A**, **2B,D**). Cytoplasm colorless, usually containing food vacuoles (about 5 μm), lipid droplets (about 3 μm) and minute crystals (**Figures 1A**, **2A,B**). Colorless cortical granules (about 1 μm across), arranged in longitudinal rows on dorsal side and sparsely arranged in irregular short rows on ventral side (**Figures 2C,D**). Locomotion by swimming in water or crawling on substrate rapidly.

Adoral zone 33–43 μm long after protargol staining, occupying ca. 36% of body length, composed of 26–32 (on average 30) membranelles, with cilia about 12 μm long (**Table 1** and **Figures 1A,B**, **3A,B**). Undulating membranes in *Oxytricha*-pattern (**Figures 1B**, **3A**). Three slightly enlarged frontal cirri arranged at the anterior end of the cell, one buccal cirrus located near anterior end of paroral membrane, invariably four frontoventral cirri positioned between the anterior portion of the right marginal row and the paroral, cirrus III/2 arranged anterior to the level of cirrus VI/3 (**Figure 1B**), three postoral ventral cirri behind the proximal end of the adoral zone, cirrus IV/2 located more anteriorly than V/4 (**Figure 1B**), two pretransverse cirri arranged in front of the transverse cirri, five transverse cirri in a hook-shaped row, inconspicuously projecting above posterior body margin. One right and one left marginal row comprised of 24–36 and 21–34 cirri (cilia about 10 μm long), respectively. Marginal rows not confluent posteriorly (**Figures 1B**, **3A**). All of the cirri about 12 μm long *in vivo*.

Five rows of dorsal bristles in typical *Oxytricha* pattern. Two bipolar rows left of midline of body, each associated with a caudal cirrus at its rear end; row 3 ends at posterior third; row 4 starts below mid-body and also produces a caudal cirrus at its posterior end; row 5 terminates ahead of mid-body (**Figures 1C**, **3B**). Dorsal bristles about 2 μm long *in vivo*.

Resting cyst globular, smooth and colorless, with an average diameter of 35 μm (**Figure 2E**). Abnormal resting cyst usually ellipsoidal, gray, even black, in life about 53 × 36 μm, usually with two hyaline vacuole-like structures (**Figures 2F–H**).

Ontogenesis

The ontogenetic process of *O. granulifera granulifera* is very similar to that of the genus. For further details see **Figures 3F–L**. The main morphogenetic features are: 1) the oral primordium of the opisthe originates *de novo* and the parental adoral zone of membranelles remains unchanged and inherited by the proter; 2) six streaks of frontal-ventral-transverse cirral anlagen are formed; 3) the marginal rows and the nuclear apparatus develop in the usual manner; 4) dorsal kineties 1–3 develop within the parental kineties, dorsal kinety 4 originates from kinety 3 to kinety 5 originates dorsomarginally, that is, from an anlage near the right marginal row (**Figures 3K,L**). Ontogenesis confirms there is only one dorsomarginal kinety.

Detection of Abnormal Forms in Culture System

The present population of *O. granulifera granulifera* was isolated in the summer of 2017 and has been cultured at room temperature in the laboratory since then. However, since November 2018 many abnormal individuals have been found in some cultures. Usually, the course of these abnormal individuals can be described as follows: to begin with, a large number of normal populations bloomed in Petri dishes, and then a lot of abnormal resting cysts (**Figures 2F–H**) were quickly formed, and a certain proportion (about 10–15%) of these cysts then excysted to form abnormal individuals (**Figures 2I–M**). This phenomenon occurred repeatedly in the culture system.

Morphology of Abnormal Forms

Size *in vivo* 115–140 × 20–25 μm, and 96–138 × 23–38 μm in protargol preparations. Body slim with both ends rounded, length: width ratio about 6.5:1, slightly dorsoventrally

[1] http://www.ebi.ac.uk

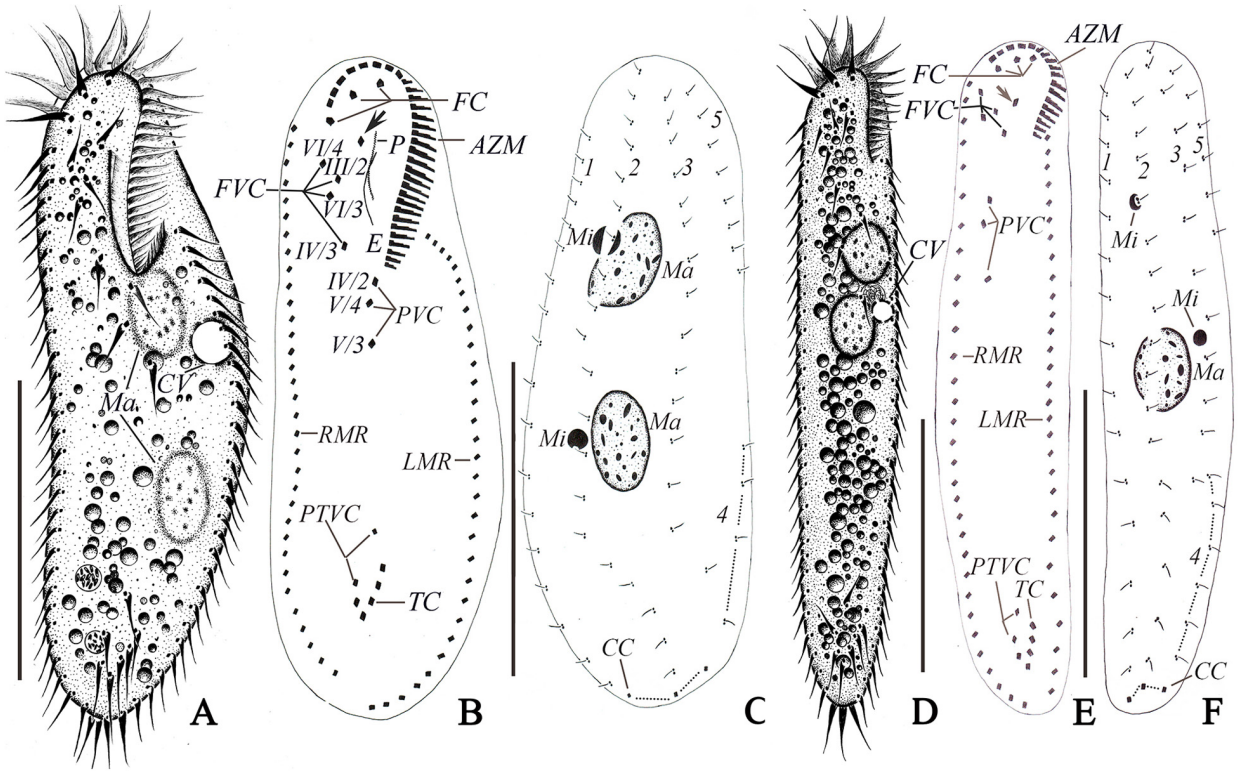

FIGURE 1 | Morphology of normal **(A–C)** and abnormal **(D–F)** forms of *Oxytricha granulifera granulifera in vivo* **(A,D)** and after protargol staining **(B,C,E,F)**. **(A)** Ventral view of a representative normal individual. **(B,C)** Ventral **(B)** and dorsal **(C)** views of a typical specimen to show ciliature and nuclear apparatus, arrow in **(B)** marks the buccal cirrus. **(D)** Ventral view of a representative abnormal cell. **(E,F)** Ventral **(E)** and dorsal **(F)** views of an abnormal cell, arrow in **(F)** marks the buccal cirrus. AZM, adoral zone of membranelles; CC, caudal cirri; CV, contractile vacuole; E, endoral; FC, frontal cirri; LMR, left marginal row; FVC, frontoventral cirri (III/2, IV/3, VI/3, and VI/4); Ma, macronuclear nodules; Mi, micronuclei; P, paroral; PTVC, pretransverse ventral cirri; PVC, postoral ventral cirri (IV/2, V/3, and V/4); RMC, right marginal cirri row; TC, transverse cirri. 1–5, dorsal kineties 1–5. Scale bars = 50 μm.

flattened (**Figures 1D,E**, **2J–M**). Cell highly flexible and slightly contractile. One, two, three or four ellipsoidal macronuclear nodules (percentages are 30, 10, 40, and 20%, respectively), positioned around mid-body, 8–15 × 6–14 μm in size. Two to four micronuclei, size 3–6 × 2–4 μm in protargol preparations (**Figures 3C–E**). Contractile vacuole about 6 μm in diameter located at about 40% of body length near the left body margin (**Figures 1D**, **2K**). Cortical granules colorless, about 1 μm across (**Figure 2M**). Cytoplasm packed with numerous granules (**Figures 1D**, **2J–L**).

Adoral zone occupying about 14% of body length, composed of 11–19 (average 17) membranelles. Buccal cavity short and narrow, undulating membranes absent (**Figures 1E**, **3C,E**). Consistently three frontal, one buccal, and two pretransverse and five transverse cirri; other cirral groups unstable in number, for example three to four frontoventral, two to three postoral ventral cirri (**Figures 1D–F**, **3C,D**). One left and one right marginal row, composed of 24–34 and 17–32 cirri, respectively (**Figures 1E**, **3C**).

Five rows of dorsal bristles, row 1 and row 2 bipolar, composed of 9–16 and 9–17 bristles; row 3, row 4, and row 5 short, composed of 6–13, 3–6, and 4–8 bristles, respectively (**Figures 1F**, **3D**). Three caudal cirri, associated with row 1, row 2, and row 4, respectively. Movement by crawling slowly on the substrate.

Abnormal individuals have never been found to be able to form resting cysts, or carry on dividing and conjugate reproduction. The attempt to cultivate these abnormal individuals failed and the population gradually disappeared within one week.

Sequence Similarity and Phylogenetic Analyses

The partial SSU rDNA sequences of the normal and abnormal forms of *O. granulifera granulifera* were deposited into the GenBank database with the accession numbers MW143562 and MW143561, with a length of 1,677 and 1,631 bp, respectively. The similarity of the common 1,631 bp covered by both forms is 100%.

The topology of ML and BI trees are similar, and, therefore, only the ML tree is shown (**Figure 4**). Subfamily Oxytrichinae was polyphyletic, and five subgroups were recognized (Oxytrichinae-I–V). All strains of *Oxytricha granulifera* except X53486 were exclusively located within Oxytrichinae-IV, while *O. granulifera* X53486 clustered

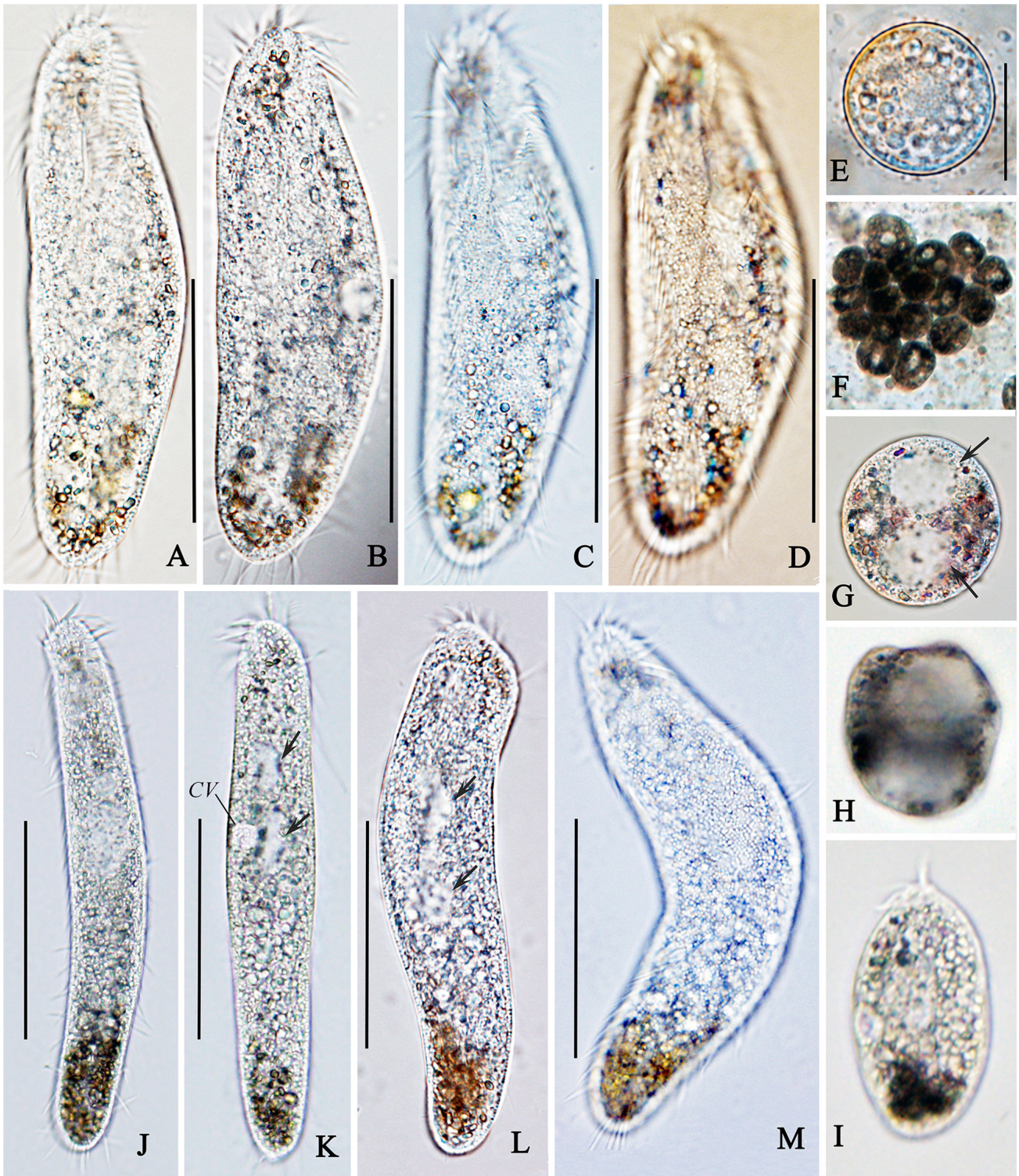

FIGURE 2 | Photomicrographs of normal **(A–E)** and abnormal forms **(F–M)** of *Oxytricha granulifera granulifera in vivo*. **(A–D)** Typical body shapes of the normal cells. **(E)** A normal cyst. **(F–H)** Abnormal cysts; each cyst with two macronuclear nodules (arrows in **G**). **(I)** A newly excysted abnormal cell. **(J–L)** Ventral view of abnormal forms, showing the changes of body shape, arrows in **(K,L)** indicating the macronuclear nodules. **(M)** Cortical granules of an abnormal cell from the dorsal side. CV, contractile vacuole. Scale bars = 50 μm.

TABLE 1 | Morphometric data of normal (upper lines) and abnormal (lower lines) specimens of *Oxytricha granulifera granulifera* in the present work.

Character	Min	Max	Med	Mean	SE	SD	CV	*n*
Body, length (μm)	79.0	135.0	102.0	102.6	2.6	12.6	12.3	25
	96.0	138.0	122.0	119.3	4.8	14.4	12.1	10
Body, width (μm)	28.0	61.0	42.0	42.0	1.7	8.3	19.8	25
	23.0	38.0	29.0	29.7	1.7	5.0	16.8	10
Adoral zone, length (μm)	33.0	43.0	37.0	36.9	0.6	2.8	7.6	25
	11.0	21.0	18.0	17.1	1.0	3.0	17.4	10
Adoral membranelles, number	26.0	32.0	30.0	29.7	0.3	1.5	5.0	25
	11.0	19.0	17.0	16.6	0.8	2.3	14.1	10
Buccal cirri, number	1.0	1.0	1.0	1.0	0.0	0.0	0.0	25
	1.0	1.0	1.0	1.0	0.0	0.0	0.0	10
Frontal cirri, number	3.0	3.0	3.0	3.0	0.0	0.0	0.0	25
	3.0	3.0	3.0	3.0	0.0	0.0	0.0	10
Frontoventral cirri, number	4.0	4.0	4.0	4.0	0.0	0.0	0.0	25
	3.0	4.0	4.0	3.8	0.1	0.4	10.5	10
Postoral ventral cirri, number	3.0	3.0	3.0	3.0	0.0	0.0	0.0	25
	2.0	3.0	3.0	2.6	0.2	0.5	18.8	10
Pretransverse cirri, number	2.0	2.0	2.0	2.0	0.0	0.0	0.0	25
	2.0	2.0	2.0	2.0	0.0	0.0	0.0	10
Transverse cirri, number	5.0	5.0	5.0	5.0	0.0	0.0	0.0	25
	5.0	5.0	5.0	5.0	0.0	0.0	0.0	10
Caudal cirri, number	3.0	3.0	3.0	3.0	0.0	0.0	0.0	25
	3.0	3.0	3.0	3.0	0.0	0.0	0.0	10
Left marginal cirri, number	21.0	34.0	30.0	29.6	0.7	3.3	11.0	25
	24.0	34.0	30.0	29.3	1.0	3.1	10.5	10
Right marginal cirri, number	24.0	36.0	31.0	31.0	0.5	2.6	8.4	25
	17.0	32.0	26.0	26.5	1.5	4.5	16.8	10
Dorsal kineties, number	5.0	6.0	5.0	5.2	0.1	0.4	7.1	25
	5.0	5.0	5.0	5.0	0.0	0.0	0.0	10
Dikinetids in DK1, number	14.0	23.0	18.0	18.1	0.5	2.5	13.9	25
	9.0	16.0	12.0	12.3	0.9	2.6	20.9	10
Dikinetids in DK2, number	12.0	23.0	20.0	19.0	0.5	2.6	13.6	25
	9.0	17.0	12.0	12.2	0.7	2.2	17.9	10
Dikinetids in DK3, number	10.0	21.0	16.0	15.9	0.4	2.2	13.6	25
	6.0	13.0	8.0	8.4	0.6	1.9	22.7	10
Dikinetids in DK4, number	3.0	8.0	5.0	5.0	0.3	1.2	24.7	25
	3.0	6.0	4.0	4.1	0.3	0.9	23.0	10
Dikinetids in DK5, number	7.0	12.0	10.0	9.7	0.3	1.3	13.9	25
	4.0	8.0	6.0	5.8	0.4	1.2	21.5	10
Macronuclear nodules, number	2.0	2.0	2.0	2.0	0.0	0.0	0.0	25
	1.0	4.0	3.0	2.5	0.4	1.1	44.7	10
Micronuclei, number	1.0	4.0	2.0	2.2	0.1	0.7	31.2	25
	2.0	4.0	3.0	2.7	0.3	0.8	28.9	10
Macronuclear nodules, length (μm)	11.0	20.0	16.0	16.1	0.5	2.3	14.5	25
	8.0	15.0	13.0	12.5	0.7	2.0	16.1	10
Macronuclear nodules, width (μm)	7.0	13.0	9.0	9.2	0.3	1.4	15.1	25
	6.0	14.0	10.0	9.9	0.8	2.4	24.5	10
Micronuclei, length (μm)	1.0	4.0	2.0	2.2	0.1	0.6	28.3	25
	3.0	6.0	4.0	4.2	0.3	0.9	20.8	10
Micronuclei, width (μm)	1.0	4.0	2.0	2.2	0.1	0.6	28.3	25
	2.0	4.0	3.0	3.3	0.2	0.6	19.4	10

All data were measured from protargol-stained specimens. CV, coefficient of variation in %; DK, dorsal kinety; Max, maximum; Mean, arithmetic mean; Med, median value; Min, minimum; n, number of cells measured; SD, standard deviation; SE, standard error of arithmetic mean.

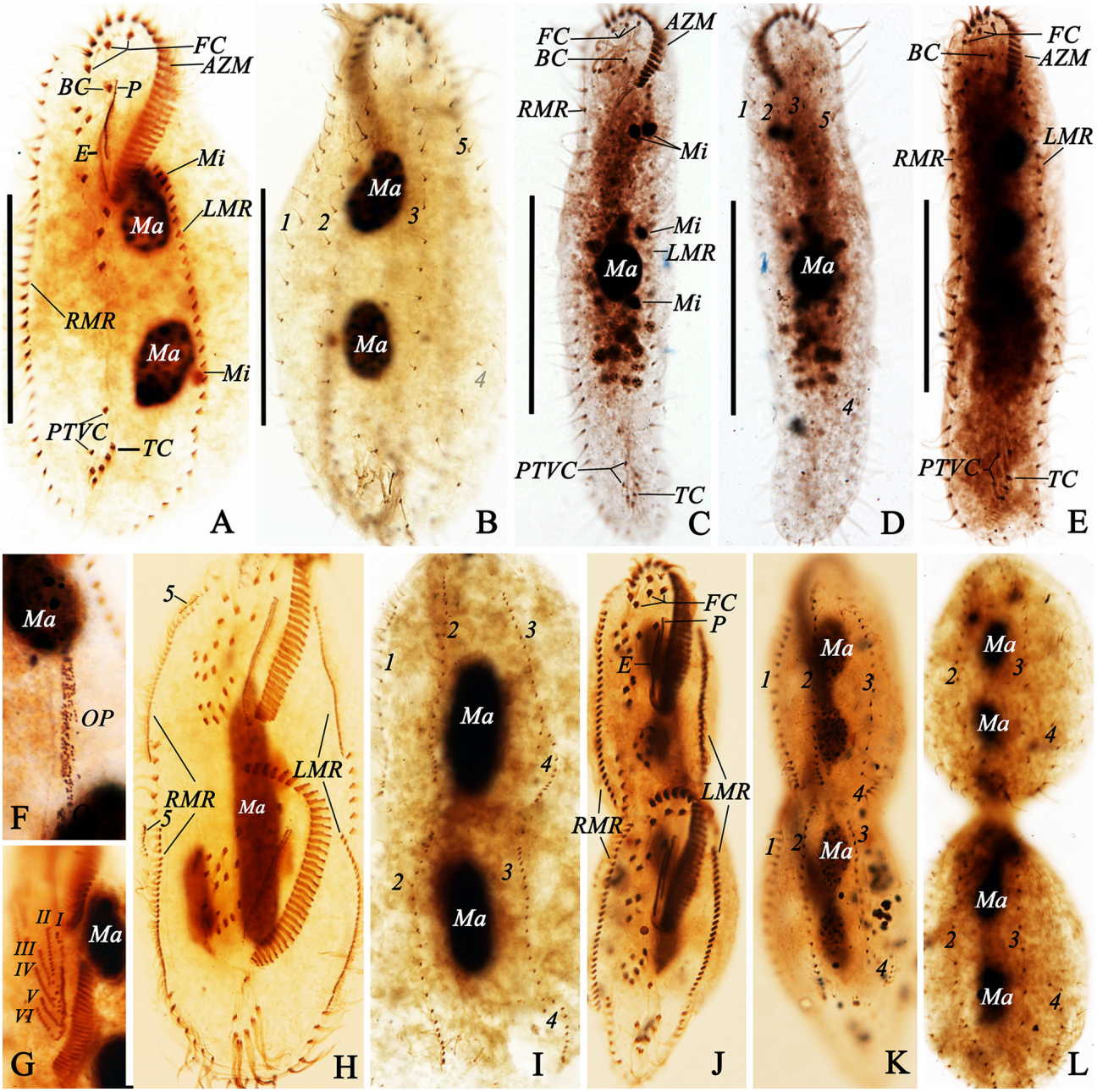

FIGURE 3 | Ciliature of normal **(A,B)** and abnormal **(C–E)** forms, and the morphogenesis **(F–L)** of *Oxytricha granulifera granulifera* after protargol staining. **(A,B)** Ventral and dorsal views of a normal specimen. **(C–E)** Ventral **(C,E)** and dorsal **(D)** views of abnormal specimens. **(F)** Ventral view of a very early stage to show the newly formed oral primordium. **(G)** Partial view of an early divider showing the six streaks (anlagen I–VI) of the opisthe. **(H)** Ventral view of a middle divider, to show the development of marginal cirri anlagen and the fused macronucleus. **(I)** Dorsal view of a divider showing the newly formed dorsal kineties 1–4. **(J,K)** Ventral **(J)** and dorsal views **(K)** of a late divider, to show the newly formed cirri and the origin of dorsal kinety 4. **(L)** Dorsal view of a very late divider which is about to divide. AZM, adoral zone of membranelles; BC, buccal cirri; E, endoral; FC, frontal cirri; LMR, left marginal cirri row; Ma, macronuclear nodules; Mi, micronuclei; OP, oral primordium; P, paroral; PTVC, pretransverse ventral cirri; RMR, right marginal cirri row; TC, transverse cirri. 1–4, dorsal kineties; 5, dorsal marginal kinety. Scale bars = 50 μm.

in Oxytrichinae-III. The normal and abnormal forms of *O. granulifera granulifera* from the present research clustered together without full support (ML/BI, 89, 1.00). These two sequences were close to four other strains of *O. granulifera granulifera* (AM412768, AM412769, AM412771, and AM412772) and a strain of *O. granulifera* (AF164122). This branch then grouped with other *O. granulifera* strains.

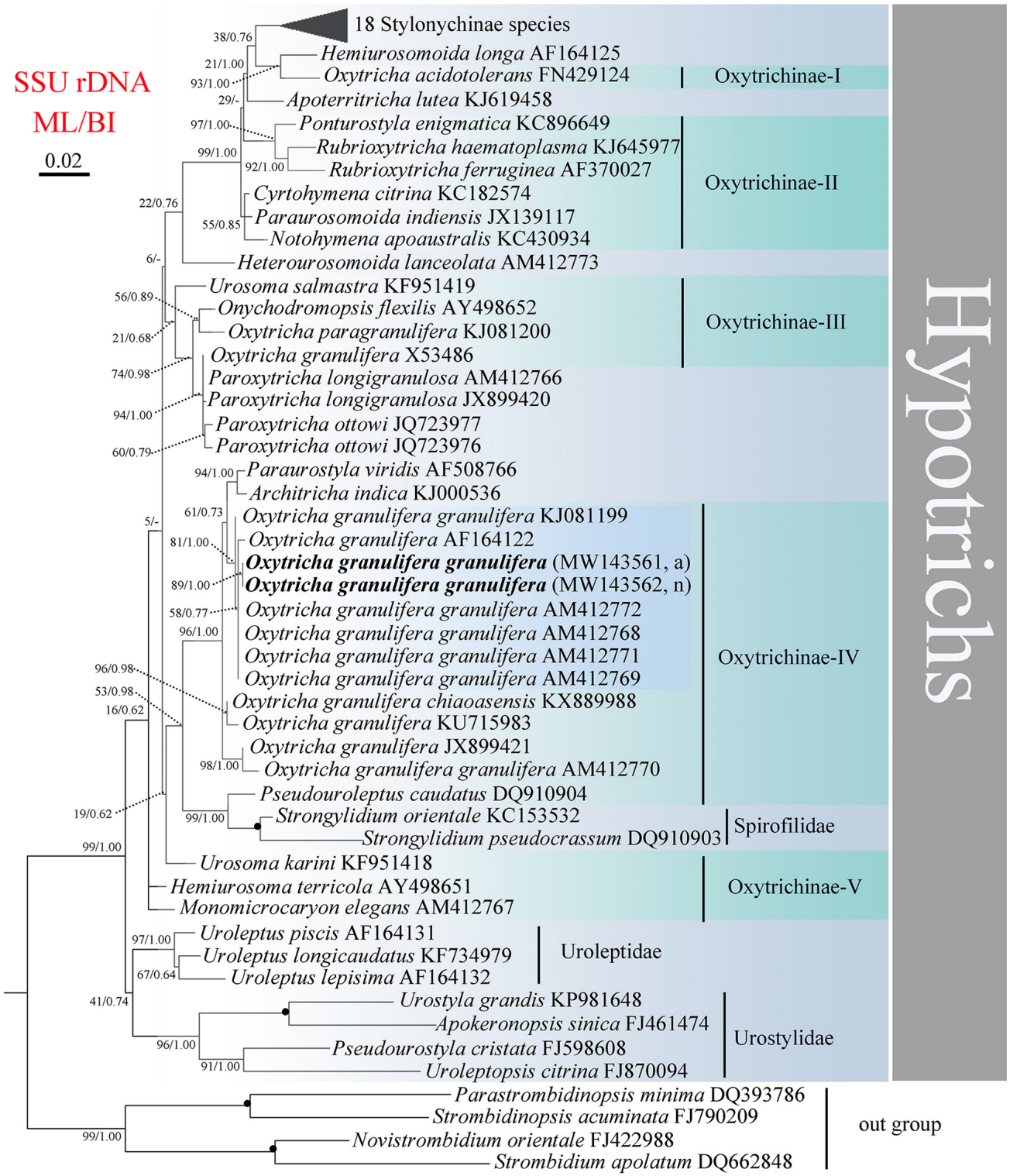

FIGURE 4 | Maximum likelihood (ML) phylogenetic tree inferred from SSU rDNA sequences of 67 hypotrichs. Phylogenetic positions of normal and abnormal forms of *Oxytricha granulifera granulifera* are indicated in bold. Black circles indicate full bootstrap values from both ML and BI (100/1.00). – indicates the topology disagreement between ML and BI, and only the bootstrap values of ML are shown. The scale bar corresponds to two substitutions per 100 nucleotide positions (0.02). a, abnormal form; n, normal form.

DISCUSSION

Identification of Iceland Population as *O. granulifera granulifera*

Oxytricha granulifera was first reported by Foissner and Adam (1983). So far, three subspecies of *Oxytricha granulifera* have been recognized, namely *O. granulifera granulifera* (Foissner and Adam, 1983), *O. granulifera quadricirrata* (Blatterer and Foissner, 1988), and *O. granulifera chiapasensis* (Foissner and Adam, 1983; Blatterer and Foissner, 1988; Méndez-Sánchez et al., 2018). Based on the general morphological features, the Iceland population conforms with the subspecies *O. granulifera granulifera* (**Table 2**). Thus, we identify our isolates as *O. granulifera granulifera*. This classification is also supported by the phylogenetic analyses based on the SSU rDNA sequence (**Figure 4**).

Abnormal Form Could Easily Be Deduced as a "New" Species

The general infraciliature and arrangement of cortical granules of the normal and abnormal individuals are consistent. However, some morphological characteristics of abnormal individuals are quite different from those of normal individuals, and are mainly as follows: 1) the body size: in life 90–128 × 31–43 μm in normal forms vs 115–140 × 21–24 μm in abnormal forms; 2) the body shape: very narrowly elliptical in abnormal forma vs elliptical in normal forms; 3) the length of the adoral zone (14% of the body length in abnormal forms vs 36% of the body length in normal forms) and the number of membranelles (on average in abnormal forms 17 vs on average 30 membranes in normal forms); 4) the undulating membranes (absence in abnormal forms vs presence in normal forms); 5) number of macronuclei (1 to 4 in abnormal forms vs invariably 2 in normal forms); 6) mortality (abnormal individuals slow vs fast in normal individuals). However, because the abnormal individuals appear spontaneously, repeatedly and have stable morphological characteristics in the culture system, it could be easy to regard them as a "new" species without continuous and comprehensive investigation.

Occurrence of Abnormal Resting Cysts and Individuals

The population of *O. granulifera granulifera* Foissner and Adam (1983) was isolated from terrestrial environment, and no abnormal cysts or form were reported. While our population was isolated from sludge in a hot spring, and abnormal cysts and individuals occurred spontaneously in the culture system. Some researchers have reported abnormal cysts from artificial inducing in some ciliate species. Hashimoto (1962, 1964) induced abnormal cysts of *Oxytricha fallax* by embedding cells in agar, exposed to high temperatures, starved, or changing the composition of the culture medium. Another research article reported that abnormal cysts were formed in *Euplotes taylori* due to pressure of the coverslip (Garnjobst, 1928). As for our case, we speculate that the lack of food (necessary nutrients) and space after the outbreak of the high population density from single source of food (wheat grains) might trigger the potential polymorphism, then the abnormal cysts and forms appeared.

TABLE 2 | Morphological comparison of Iceland population of *Oxytricha granulifera granulifera* with other *Oxytricha* populations.

	O. granulifera granulifera	***O. granulifera granulifera***	***O. granulifera quadricirrata***	***O. granulifera***	***O. granulifera***	***O. granulifera chiapasensis***
Body size in life (μm)	90–130 × 30–45	80–130 × 35–50	70–100 × 20–30	90–115 × 25–38	90–130 × 30–50	60–120 × 20–40
Adoral membranelles, number	26–32	29–32	19–21	21–26	28–38	22–29
Left marginal cirri, number	21–34	27–40	13–18	18–25	23–31	21–30
Right marginal cirri, number	24–36	29–41	14–17	20–28	26–32	21–31
Transverse cirri, number	5	5	5	5	5	5
Dorsal kineties, number	5	5	6	6	6	6
Dikinetids in DK 1, number	14–23	16	9	16	20	8–20
Dikinetids in DK 2, number	12–23	18	12	16	20	12–21
Dikinetids in DK 3, number	10–21	16	9	16	-	8–18
Dikinetids in DK 4, number	3–8	4	4	4	-	3–4
Dikinetids in DK 5, number	7–12	8	5	4	-	6–10
Dikinetids in DK 6, number	0	0	1	1–2	2–3	1–3
Habitat	freshwater, hot spring	soil	soil	freshwater	soil	freshwater
References	This study	Foissner and Adam (1983)	Blatterer and Foissner (1988)	Kwon and Shin (2013)	Shao et al. (2014)	Méndez-Sánchez et al. (2018)

DK, dorsal kinety.

The simpler characteristics enabled the abnormal forms to consume less energy than the formal forms which served as a strategy for the ciliate to endure the deteriorative environment. This speculation should be tested by transcriptomics in future work.

CONCLUSION

O. granulifera granulifera was detected in a hot spring in Iceland for the first time. So far, this species has been recorded in all of the main biogeographic regions, indicating its worldwide distribution. Currently, laboratory cultivation is necessary for the study of morphology, ontogenesis and molecular biology of ciliates (Foissner, 1996; Lian et al., 2020; Wang et al., 2020; Zhang et al., 2020). In this study, owing to stable morphological features of abnormal individuals of this species, the possibility that it may be misidentified as a "new" species has been discussed above. Attention to this possibility must be paid in future research. Likewise, the causes of deformities also need to be investigated further.

Protargol Stained Specimens

The protargol slides containing the normal (ZR20181112A–G) and the abnormal specimens (ZR20181129A–F) have been deposited in the Laboratory of Hydrobiology, Hebei University, China.

DATA AVAILABILITY STATEMENT

The datasets presented in this study can be found in online repositories. The names of the repository/repositories and accession number(s) can be found in the article/supplementary material.

AUTHOR CONTRIBUTIONS

SF and TS sampled the material. RZ and QZ conducted indoor culture of ciliate population and silver staining, generated the molecular data, and wrote the manuscript. XH, FL, ZQ, SF, and TS revised and approved the final manuscript. All authors contributed to the article and approved the submitted version.

FUNDING

This work was supported by the Natural Science Foundation of China (Project Numbers: 31872206 and 41976086) and the Scientific Research Foundation of Hebei Province for returned scholars (C201801).

REFERENCES

Bai, Y., Li, S., Li, Y., Miao, M., and Hu, X. (2018). Morphogenesis and molecular characterization of a little known soil ciliate, Oxytricha nauplia Berger et Foissner, 1987 (Ciliophora, Sporadotrichida). *Acta Protozool.* 57, 79–94. doi: 10.4467/16890027AP.18.008.8982

Bai, Y., Wang, R., Song, W., Toshikazu, S., and Hu, X. (2020). Redescription of five tintinnine ciliates (Alveolata: Ciliophora: Oligotrichea) from coastal waters of Qingdao, China. *Mar. Life Sci. Technol.* 2, 209–221. doi: 10.1007/s42995-020-00034-2

Berger, H. (1999). Monograph of the Oxytrichidae (Ciliophora, Hypotrichia). *Monogr. Biol.* 78, 1–1080. doi: 10.1007/978-94-011-4637-1_1

Blatterer, H., and Foissner, W. (1988). Beitrag zur terricolen Ciliatenfauna (Protozoa: Ciliophora) von Australiens und Afrika. *Stapfia* 17, 1–84.

Chen, X., Jiang, Y., Gao, F., Zheng, W., Krock, T. J., Stover, N. A., et al. (2019). Genome analyses of the new model protist *Euplotes vannus* focusing on genome rearrangement and resistance to environmental stressors. *Mol. Ecol. Resour.* 19, 1292–1308. doi: 10.1111/1755-0998.13023

Foissner, W. (1994). *Pentahymena corticicola* nov. gen., nov. spec., a new colpodid ciliate. (Protozoa, Ciliophora) from bark of Acacia trees in Costa Rica. *Arch. Protistenk.* 144, 289–295. doi: 10.1016/s0003-9365(11)80140-5

Foissner, W. (1996). Terrestrial ciliates (protozoa, Ciliophora) from two islands (Gough, Marion) in the southern oceans, with description of two new species, *Arcuospathidium cooperi* and *Oxytricha ollowi*. *Biol. Fertil. Soils* 23, 282–291. doi: 10.1007/bf00335956

Foissner, W. (1997). Soil ciliates (Protozoa: Ciliophora) from evergreen rain forests of Australia, South America and Costa Rica: diversity and description of new species. *Biol. Fertil. Soils* 25, 317–339. doi: 10.1007/s003740050322

Foissner, W. (2016). Terrestrial and semiterrestrial ciliates (Protozoa, Ciliophora) from Venezuela and Galapagos. *Denisia* 35, 1–912.

Foissner, W., Agatha, S., and Berger, H. (2002). Soil ciliates (Protozoa, Ciliophora) from Namibia. (Southwest Africa), with emphasis on two contrasting environments, the Ethosha region and the Namibia desert. *Denisia* 5, 1–1459.

Foissner, W., and Adam, H. (1983). Morphologie und Morphogenese des Bondenciliaten *Oxytricha granulifera* sp. n. (Ciliophora, Oxytrichidae). *Zool. Scr.* 12, 1–11. doi: 10.1111/j.1463-6409.1983.tb00543.x

Garnjobst, L. (1928). Induced encystment and excystment in *Euplotes taylori*, sp. nov. *Physiol. Zool.* 1, 561–575. doi: 10.1086/physzool.1.4.30151345

Hashimoto, K. (1962). Relationships between feeding organelles and encystment in *Oxytricha fallax* Stein. *J. Protozool.* 9, 161–169. doi: 10.1111/j.1550-7408.1962.tb02601.x

Hashimoto, K. (1964). Localization of ciliary primordia in induced abnormal cysts of *Oxytricha fallax*. *J. Protozool.* 11, 75–84. doi: 10.1111/j.1550-7408.1964.tb01722.x

Jin, D., Qu, Z., Wei, B., Montagnes, D. J., Fan, X., and Chen, X. (2020). Two parasitic ciliates (Protozoa: Ciliophora: Phyllopharyngea) isolated from respiratory-mucus of an unhealthy beluga whale: characterization, phylogeny and an assessment of morphological adaptations. *Zool. J. Linn. Soc.* (in press). doi: 10.1093/zoolinnean/zlaa086/5900937

Kaur, H., Negi, S. R. K., and Kamra, K. (2019). Morphological and molecular characterization of. *Neogastrostyla aqua* nov. gen., nov. spec. (Ciliophora, Hypotrichia) from River Yamuna, Delhi; comparison with Gastrostyla-like genera. *Eur. J. Protistol.* 68, 68–79. doi: 10.1016/j.ejop.2019.01.002

Kim, K. S., and Min, G. S. (2019). Morphology and molecular phylogeny of *Oxytricha seokmoensis* sp. nov. (Hypotrichia: Oxytrichidae), with notes on its morphogenesis. *Eur. J. Protistol.* 71, 125–641. doi: 10.1016/j.ejop.2019.125641

Kumar, S., Stecher, G., and Tamura, K. (2016). MEGA7: molecular evolutionary genetics. analysis version 7.0 for bigger datasets. *Mol. Biol. Evol.* 33, 1870–1874. doi: 10.1093/molbev/msw054

Kwon, C. B., and Shin, M. K. (2013). Two oxytrichid ciliates, *Cyrtohymena primicirrata* and *Oxytricha granulifera* (Ciliophora: Sporadotrichida: Oxytrichidae) unknown from Korea. *Anim. Syst. Evol. Divers.* 29, 23–30. doi: 10.5635/ASED.2013.29.1.23

Li, F., Qu, Z., Luo, D., Filker, S., Hu, X., and Stoeck, T. (2019). Morphology, morphogenesis and molecular phylogeny of a new obligate halophile ciliate, *Schmidtiella ultrahalophila* gen. nov., spec. nov. (Ciliophora, Hypotrichia)

isolated from a volcanic crater on Sal (Cape Verde Islands). *J. Eukaryot. Microbiol.* 66, 694–706. doi: 10.1111/jeu.12714

Lian, C., Luo, X., Warren, A., Zhao, Y., and Jiang, J. (2020). Morphology and. phylogeny of four. marine or brackish water spirotrich ciliates from China, with descriptions of two new species. *Eur. J. Protistol.* 72:125663. doi: 10.1016/j.ejop.2019.125663

Liao, W., Gong, Z., Ni, B., Fan, X., and Petroni, G. (2020). Documentation of a new hypotrich species in the family Amphisiellidae, *Lamtostyla gui* n. sp. (Protista, Ciliophora) using a multidisciplinary approach. *Sci. Rep.* 10:3763. doi: 10.1038/s41598-020-60327-5

Luo, X., Huang, J. A., Li, L., Song, W., and Bourland, W. A. (2019). Phylogeny of the ciliate family Psilotrichidae (Protista, Ciliophora), a curious and poorly-known taxon, with notes on two algae-bearing psilotrichids from Guam, USA. *BMC Evol. Biol.* 19:125. doi: 10.1186/s12862-019-1450-z

Medlin, L., Elwood, H. J., Stickel, S., and Sogin, M. L. (1988). The characterization of enzymatically amplified eukaryotic 16S-likerRNA-coding regions. *Gene* 71, 491–499. doi: 10.1016/0378-1119(88)90066-2

Méndez-Sánchez, D., Mayén-Estrada, R., Luo, X., and Hu, X. (2018). A new subspecies of *Oxytricha granulifera* (Hypotrichia: Oxytrichidae) from Mexico, with notes on its morphogenesis and phylogenetic position. *J. Eukaryot. Microbiol.* 65, 357–371. doi: 10.1111/jeu.12479

Miller, M. A., Pfeiffer, W., and Schwartz, T. (2010). "Creating the CIPRES science gateway for inference of large phylogenetic trees," in *Proceedings of the 2010 Gateway Computing Environments Workshop (GCE),* New Orleans, LA. 1–8.

Page, R. D. M. (1996). Tree View: an application to display phylogenetic tree on personal computers. *Comput. Appl. Biosci.* 12, 357–358. doi: 10.1093/bioinformatics/12.4.357

Pan, X., Bourland, W. A., and Song, W. (2013). Protargol synthesis: an in-house protocol. *J. Eukaryot. Microbiol.* 60, 609–614. doi: 10.1111/jeu.12067

Qu, Z., Groben, R., Marteinsson, V., Agatha, S., Filker, S., and Stoeck, T. (2018). Redescription of *Dexiotricha colpidiopsis* (Kahl, 1926) Jankowski, 1964 (Ciliophora, Oligohymenophorea) from a hot spring in Iceland with identification key for *Dexiotricha* species. *Acta Protozool.* 57, 95–106. doi: 10.4467/16890027AP.18.009.8983

Qu, Z., Weinisch, L., Fan, X., Katzenmeiera, S., Stoeck, T., and Filker, S. (2020). Morphological, Phylogenetic and ecophysiological characterization of a new ciliate, *Platynematum rossellomorai* n. sp. (Oligohymenophorea, Scuticociliatia), detected in a hypersaline pond on Mallorca, Spain. *Protist* 171:125751. doi: 10.1016/j.protis.2020.125751

Ronquist, F., and Huelsenbeck, J. (2003). MrBayes 3: Bayesian phylogenetic inference under mixed models. *Bioinformatics* 19, 1572–1574. doi: 10.1093/bioinformatics/btg180

Shao, C., Chen, X., and Jiang, J. (2020). *Hypotrichous Ciliates in China*. Beijing: Science Press.

Shao, C., Hu, C., Fan, Y., Warren, A., and Lin, X. (2019). Morphology, morphogenesis and molecular phylogeny of a freshwater ciliate, *Monomicrocaryon euglenivorum euglenivorum* (Ciliophora, Oxytrichidae). *Eur. J. Protistol.* 68, 25–36. doi: 10.1016/j.ejop.2019.01.001

Shao, C., Lu, X., and Ma, H. (2015). A general overview of the typical 18 frontal-ventral-transverse cirri Oxytrichidae s. l. genera (Ciliophora, Hypotrichia). *J. Ocean Univ. China* 14, 522–532. doi: 10.1007/s11802-015-2482-7

Shao, C., Lv, Z., Pan, Y., Al-Rasheid, K., and Yi, Z. (2014). Morphology and phylogenetic. analysis of two oxytrichid soil ciliates from China, *Oxytricha paragranulifera* n. sp. and *Oxytricha granulifera* Foissner and Adam, 1983 (Protista, Ciliophora, Hypotrichia). *Int. J. Syst. Evol. Microbiol.* 64, 3016–3027. doi: 10.1099/ijs.0.062281-0

Shao, C., Song, W., Al-Rasheid, K. A. S., and Berger, H. (2012). Redefinition and. reassignment of the 18-cirri genera *Hemigastrostyla*, *Oxytricha*, *Urosomoida*, and *Actinotricha* (Ciliophora, Hypotricha), and description of one new genus and two new species. *Acta Protozool.* 50, 263–287. doi: 10.4467/16890027AP.11.025.0062

Song, W., and Shao, C. (2017). *Ontogenetic Patterns of Hyportich Ciliates*. Beijing: Science Press.

Song, W., Warren, A., and Hu, X. (2009). *Free-living Ciliates in the Bohai and Yellow Seas*. Beijing: Science Press.

Song, Y., Liu, Y., Pan, B., Luo, X., Song, W., and Warren, A. (2019). Morphological studies on four brackish water ciliates of the class Spirotrichea (Protista, Ciliophora). *J. Ocean Univ. China* 18, 663–674. doi: 10.1007/s11802-019-4096-y

Stamatakis, A. (2014). RAxML version 8: a tool for phylogenetic analysis and post-analysis. of large phylogenies. *Bioinformatics* 30, 1312–1313. doi: 10.1093/bioinformatics/btu033

Wang, J., Li, J., and Shao, C. (2020). Morphology, morphogenesis, and molecular phylogeny of a novel saline soil ciliate, *Heterourosomoida sinica* n. sp. (Ciliophora, Hypotrichia). *Eur. J. Protistol.* 73:25666. doi: 10.1016/j.ejop.2016.07.005

Wilbert, N. (1975). Eine verbesserte Technik der Protargo-limpragnation für Ciliaten. *Mikrokosmos* 64, 171–179.

Wu, T., Li, Y., Lu, B., Shen, Z., Song, W., and Warren, A. (2020). Morphology, taxonomy and molecular phylogeny of three marine peritrich ciliates, including two new species: *Zoothamnium apoarbuscula* n. sp. and *Z. apohentscheli* n. sp. (Protozoa, Ciliophora, Peritrichia). *Mar. Life Sci. Technol.* 2, 334–348. doi: 10.1007/s42995-020-00046-y

Zhang, T., Dong, J., Cheng, T., Duan, L., and Shao, C. (2020). Reconsideration of the taxonomy of the marine ciliate *Neobakuella aenigmatica* Moon et al., 2019 (Protozoa, Ciliophora, Hypotrichia). *Mar. Life Sci. Technol.* 2, 97–108. doi: 10.1007/s42995-020-00032-4

Conflict of Interest: The authors declare that the research was conducted in the absence of any commercial or financial relationships that could be construed as a potential conflict of interest.

frontiers in Marine Science

ORIGINAL RESEARCH
published: 09 February 2021
doi: 10.3389/fmars.2021.642767

Species Diversity of the Pleurostomatid Ciliate Genus *Amphileptus* (Ciliophora, Haptoria), With Notes on the Taxonomy and Molecular Phylogeny of Three Species

*Lei Wu[1], Jiqiu Li[2], Alan Warren[3] and Xiaofeng Lin[2]**

[1] Guangzhou Key Laboratory of Subtropical Biodiversity and Biomonitoring, Guangdong Provincial Key Laboratory of Healthy and Safe Aquaculture, School of Life Sciences, South China Normal University, Guangzhou, China, [2] The Fujian Provincial Key Laboratory for Coastal Ecology and Environmental Studies, Key Laboratory of the Coastal and Wetland Ecosystems, College of the Environment and Ecology, Xiamen University, Xiamen, China, [3] Department of Life Sciences, Natural History Museum, London, United Kingdom

OPEN ACCESS

Edited by:
Hongbo Pan,
Shanghai Ocean University, China

Reviewed by:
Peter Vd'ačný,
Comenius University, Slovakia
Zhishuai Qu,
University of Kaiserslautern, Germany

***Correspondence:**
Xiaofeng Lin
linxf@xmu.edu.cn

Specialty section:
This article was submitted to Marine Evolutionary Biology, Biogeography, and Species Diversity, a section of the journal Frontiers in Marine Science

Received: *16 December 2020*
Accepted: *11 January 2021*
Published: *09 February 2021*

Citation:
Wu L, Li J, Warren A and Lin X (2021) Species Diversity of the Pleurostomatid Ciliate Genus Amphileptus (Ciliophora, Haptoria), With Notes on the Taxonomy and Molecular Phylogeny of Three Species. Front. Mar. Sci. 8:642767. doi: 10.3389/fmars.2021.642767

Amphileptus is one of the largest genera of pleurostomatid ciliates and its species diversity has been reported in various habitats all over the world. In the present work, we review its biodiversity based on data with reliable morphological records. Our work confirms that there are 50 valid *Amphileptus* species, some of which have a wide range of salinity adaptability and diverse lifestyles. This genus has a high diversity in China but this might be because of the relatively intensive sampling. Phylogenetic analyses based on SSU rDNA sequence data verify the non-monophyly of the genus *Amphileptus*. Furthermore, two new and one poorly known *Amphileptus* species, namely *A. shenzhenensis* sp. n., *A. cocous* sp. n., and *A. multinucleatus* Wang, 1934, from coastal habitats of southern China were investigated using morphological and molecular phylogenetic methods. These three species are highly similar based on their contractile vacuoles and macronuclear nodules. However, they can be discriminated by details of their living morphology and somatic kineties. We also propose two new combinations, *Amphileptus polymicronuclei* (Li, 1990) comb. n. (original combination *Hemiophrys polymicronuclei* Li, 1990) and *Amphileptus salimicus* (Burkovsky, 1970b) comb. n. (original combination *Hemiophrys salimica* Burkovsky, 1970b).

Keywords: biodiversity, *Hemiophrys*, Litostomatea, new species, phylogeny, SSU rDNA

INTRODUCTION

Ciliated protozoa (ciliates) are a highly differentiated and diverse group of eukaryotic unicellular organisms which are common in a wide range of habitats where is sufficient water for their survival (Carey, 1992; Foissner, 1999; Wilbert and Song, 2005; Lynn, 2008; Foissner and Hawksworth, 2009; Song et al., 2009; Vd'ačný and Foissner, 2012; Gao et al., 2016; Liu et al., 2017, 2019, Liu M.J. et al., 2020; Liu W.W. et al., 2020; Qu et al., 2018; Hu et al., 2019; Ma et al., 2019; Fan and Pan, 2020).

Pleurostomatida Schewiakoff, 1896 are a large order within the class Litostomatea Small and Lynn, 1981 and recent studies have revealed that its species diversity is much higher than previously anticipated (Lin et al., 2009; Vďačný et al., 2011, 2014; Vďačný, 2015; Wu et al., 2017; Hu et al., 2019). In the last two decades, investigations in China have demonstrated that pleurostomatids have a high diversity in both marine and brackish habitats (Lin et al., 2005a,b, 2007a,b, 2008, 2009; Pan et al., 2010, 2013, 2014, 2015, 2020; Wu et al., 2013, 2014, 2015a,b, 2017). As a result of these findings, knowledge and understanding of the systematics of the pleurostomatids has greatly improved (Wu et al., 2015a, 2017).

Amphileptus Ehrenberg, 1830 is the oldest genus within the order Pleurostomatida and comprises over 60 nominal species reported from marine (Wang, 1934; Dragesco, 1965; Song, 1991; Carey, 1992; Lin et al., 2005a,b, 2007a), brackish waters (Pan et al., 2014; Wu et al., 2014, 2015b), and freshwater habitats (Wang and Nie, 1933; Wang, 1940; Curds, 1982; Song and Wilbert, 1989; Li, 1990) all over the world. Most are free-living but some live as parasites on the skin and gills of certain freshwater fishes and tadpoles (Wenrich, 1924; Chen, 1955; Mitchell and Smith, 1988; Masoumian et al., 2005). *Amphileptus* is generally defined by the following combination of characters: (1) a single anterior suture formed by the right somatic kineties; (2) the presence of two rows of perioral kineties [three rows were detected in a single species, *A. yuianus*, by Lin et al. (2005b); molecular data are needed to confirm its generic classification]; (3) extrusomes not distributed along the dorsal margin, and (4) the absence of a spoon-shaped apex in the anterior end of the body (Foissner, 1977, 1984; Song and Wilbert, 1989; Foissner and Leipe, 1995; Lin et al., 2007a). Species of *Amphileptus* have a high degree of morphological similarity *in vivo*, and many have not been studied using modern methods such as silver staining. This has resulted in numerous examples of misidentifications and/or synonyms and homonyms within the *Amphileptus-Litonotus-Loxophyllum* complex, especially among the many nominal species described before the 1960s (Kahl, 1931, 1933; Wang and Nie, 1932; Wang, 1934, 1940; Dragesco, 1960; Vuxanovici, 1960, 1961). Since the ciliary pattern as revealed by silver staining is of great importance for species identification, there is an urgent need to redescribe those that are currently known only from *in vivo* observation.

Amphileptus has long been considered to be monophyletic based on morphological information (Fryd-Versavel et al., 1975; Foissner, 1977, 1984; Corliss, 1979; Song and Wilbert, 1989). However, recent studies based on the molecular data have indicated that the molecular and morphological data are not concordant and the molecular data suggest that the genus *Amphileptus* is non-monophyletic (Pan et al., 2014; Wu et al., 2015b). In addition, most congeners within this genus are very similar in terms of their body shape, the number and position of contractile vacuoles, and other aspects of their living morphology. Therefore, more detailed morphological information and molecular data obtained from expanded taxon sampling are necessary.

In this paper we: (1) briefly review previous studies of the species diversity of the genus *Amphileptus*; (2) provide a checklist of valid species including synonyms following analyses of nomenclatural problems, and (3) reconstruct the molecular phylogeny of the family Amphileptidae Ehrenberg, 1830 and the genus *Amphileptus* based on all reliable small subunit (SSU) rDNA sequences from the NCBI/GenBank database. In addition, we investigate three morphologically similar *Amphileptus* species from coastal waters of southern China. After detailed comparisons, they were identified as *Amphileptus multinucleatus* Wang, 1934, *Amphileptus shenzhenensis* sp. n. and *Amphileptus cocous* sp. n.

MATERIALS AND METHODS

Sample Collection, Observation, and Identification

All samples were collected from coastal waters at two sites in southern China using 250 ml wide-mouth bottles after gently stirring the water. *Amphileptus multinucleatus* Wang, 1934 and *A. cocous* sp. n. were collected on 19 December 2011 and 27 October 2011, respectively, from Daya Bay mangrove wetland in Huizhou (22°41′ N, 114°23′ E). *Amphileptus shenzhenensis* sp. n. was isolated on 13 April 2011 from Futian mangrove wetland in Shenzhen (22°38′ N, 114°06′ E). Each species was cultivated at room temperature (∼25°C) in habitat water in Petri dishes with rice grains to enrich the growth of bacteria as a food source for the ciliates.

Observations of living cells were executed with bright field and differential interference contrast microscopy. The number, size and location of contractile vacuoles were recorded based on live observations. The protargol staining method according to Wilbert (1975) was used to reveal the ciliary pattern. Living cells were examined at 100–1,000 × magnifications. Measurements of stained specimens were performed at a magnification of 1,000×. Drawings of stained specimens were conducted with the help of a camera lucida at a magnification of 1,000×. Classification and terminology are according to Vďačný et al. (2015) and Wu et al. (2017).

DNA Extraction, Gene Amplification, and Gene Sequencing

For each species, one or several cells taken from cultures were isolated, repeatedly washed in filtered habitat water and transferred into 45 μl ATL buffer for DNA extraction. Genomic DNA was extracted using DNeasy Blood and Tissue Kit (Qiagen, Shanghai, China) according to the manufacturer's protocol. SSU rDNA amplification and gene sequencing were conducted as described in Wu et al. (2013).

Phylogenetic Analyses

In total, 36 SSU rDNA sequences of the order Pleurostomatida, representing four families and including all available and reliable sequences of the family Amphileptidae, were used to conduct the phylogenetic analyses. Apart from the three new SSU rDNA sequences provided in the present study, all other sequences used in the phylogenetic analyses were obtained from the NCBI/GenBank database (see **Figure 4** for GenBank accession

numbers). Sequences were first aligned with CLUSTAL W and further modified manually using Bioedit v.7.0. The final alignment of 1625 characters and 40 taxa, including four haptorians as outgroup taxa, were used to construct phylogenetic trees using three different methods. Maximum likelihood (ML) analysis was carried out using RaxM-HPC2 v7.2.8 (Stamatakis et al., 2008) on CIPRES Science Gateway[1]. The reliability of internal branches came from a majority rule consensus tree by using a non-parametric bootstrap method with 1,000 replicates. Bayesian inference (BI) analysis was conducted in MrBayes 3.1.2 (Ronquist and Huelsenbeck, 2003) by using the Markov chain Monte Carlo algorithm under the GTR + G + I evolutionary model indicated by MrModeltest v.2 (Nylander, 2004), which was run for 1,500,000 generations with a sample frequency of 100 generations. The first 3,750 generations were discarded as burn-in. Maximum parsimony (MP) analysis was performed with PAUP 4.0b10 (Swofford, 2002) using the tree-bisection-reconnection algorithm and bootstrapping with 1000 replicates.

Statistical Tree Topology Test

The Kishino-Hasegawa (KH) test (Kishino and Hasegawa, 1989) was used to test the hypothesis that the genus *Amphileptus* is monophyletic. The ML tree was generated with a constraint block, enforcing the constraint of focal group monophyly in PAUP 4.0b10 under the GTR + I + G model. The site-wise likelihoods were calculated using PAUP 4.0b10 (Swofford, 2002) for the resulting constrained and non-constrained ML topologies. The scores were then subjected to the KH test as implemented in Consel (Shimodaira and Hasegawa, 2001).

Morphological Diversity Data Collection

The species diversity of the genus *Amphileptus* was studied based on data from the present study and published sources, mainly monographs (Kahl, 1931; Song and Wilbert, 1989; Carey, 1992; Song et al., 2009; Vďačný and Foissner, 2012; Hu et al., 2019) and papers on the taxonomy and biodiversity of *Amphileptus* (see **Tables 1**, **2** for a complete list).

RESULTS

Geographic Distribution of the Genus *Amphileptus*

Amphileptus has been found in a wide variety of habitats worldwide. To date, 50 valid species of this genus have been reported from marine (Carey, 1992; Lin et al., 2005a,b, 2007a,b), brackish (Pan et al., 2010, 2014; Chen et al., 2011), freshwater (Wang and Nie, 1933; Wang, 1940; Song and Wilbert, 1989), and terrestrial (Foissner, 1984) habitats worldwide. In freshwater habitats, species of *Amphileptus* are most commonly reported from lakes (Song and Wilbert, 1989; Li, 1990), rivers (Stokes, 1884), wastewater treatment plants (Foissner, 1984), and as parasites on the body surface and gills of certain freshwater fishes and tadpoles in North America, Asia and Europe (Wenrich, 1924; Chen, 1955; Mitchell and Smith, 1988; Masoumian et al., 2005). In marine and brackish water habitats, species are most commonly reported from mangrove wetlands (Pan et al., 2010, 2013, 2014; Chen et al., 2011; Wu et al., 2013, 2014, 2015a,b, 2017; this study), mariculture ponds (Song, 1991; Lin et al., 2005a,b, 2007a; Song et al., 2009; Pan et al., 2014), the intertidal zones of beaches (Pan et al., 2014), and coastal marine waters (Kahl, 1931; Wang, 1934; Borror, 1963; Dragesco, 1965; Al-Rasheid, 1996). The vast majority of *Amphileptus* species are free-living although a few are reported as parasites on the skin and gills of fish (Chen, 1955; Masoumian et al., 2005), or tadpoles (Wenrich, 1924). Of the known *Amphileptus* species more than one-third have been found in the coastal waters of China (Song et al., 2009; Hu et al., 2019). These include eight species from mariculture ponds in the coastal waters of the Bohai and Yellow seas of northern China and 11 species (12 populations) from coastal waters of the South China Sea, seven of which were isolated from mangrove wetlands. We have listed the references to reliable morphological descriptions of *Amphileptus* in **Table 1**. Species no longer assigned to the genus *Amphileptus*, and species of *Amphileptus* originally assigned to other genera, are listed in **Table 2** along with their current names and taxonomic status.

Morphology and Taxonomy of Three *Amphileptus* Species

Order Pleurostomatida Schewiakoff, 1896
Family Amphileptidae Bütschli, 1889
Genus *Amphileptus* Ehrenberg, 1830

Amphileptus multinucleatus Wang, 1934 (Tables 3, 4 and Figure 1)

Improved Diagnosis

Medium to large *Amphileptus*, 150–450 μm × 40–80 μm *in vivo*; posterior end constantly twisted from left to right in mid-body region; many (40–300) macronuclear nodules; 8–12 left and 29–38 right kineties; based on live observation, several (5–10) contractile vacuoles are located ventrally in posterior 2/3 of cell; extrusomes thick bar-shaped, densely arranged along oral slit; dot-like cortical granules; brackish or marine habitat.

Ecological Features (Daya Bay Population)

Water temperature 19°C, salinity 24.5‰, pH 6.7.

Voucher Material

One voucher slide with protargol-stained specimens is deposited in the Laboratory of Protozoology, OUC, China, with registration number WL2011121901.

SSU rDNA Sequence

The SSU rDNA sequence of *Amphileptus multinucleatus* is deposited in the GenBank database with the accession number, length, and GC content as follows: MT653624, 1560 bp, 43.40%.

Morphological Description Based on Daya Bay Population

Body size highly variable *in vivo*, about 200–450 μm long; body shape fairly stable, generally elongate-pyriform with bluntly pointed; in all individuals ($n > 20$) observed *in vivo*, posterior portion perpetually twisted from left side to right side beginning at mid-dorsal region; conspicuous "neck" region (about 25%

[1]http://www.phylo.org

TABLE 1 | Species list and distribution of *Amphileptus* spp. with reliable morphological description.

Species	LB (μm)[a]	RK/LK[b]	n-CV[c]	P-CV[d]	Ma[i]	Habitat type	Sample location	Data source
A. aeschtae	150–350	29–34/7–10	5–13	V[e]	200–300	Mariculture	Qingdao, China	Lin et al., 2007a
A. affinis	80–130	13–18/5 or 6	1	V	2	Freshwater	Bonn, Germany	Song and Wilbert, 1989
A. agilis	35–65	ca. 10/–	1	V	2	Coastal beach	United Kingdom	Carey, 1992
	30–60	–/–	1	V	2	Freshwater	Bonn, Germany	Song and Wilbert, 1989
A. asetosus	80–160	–/–	6–12	D[f]	2–6	Gulf water	White Sea	Burkovsky, 1970a
A. bellus	250–400	31–35/6 or 7	2–4	V	2–4	Mangrove	Huizhou, China	Wu et al., 2015b
A. bivacuolatus	100–130	ca. 8/–	2	V	2	Freshwater	Germany	Kahl, 1931
*A. branchiarum**	54–70	–/–	–	V, D	2	Freshwater	Philadelphia, United States	Wenrich, 1924
	65–120	–/–	Many	–	–	Freshwater	West Azerbaijan, Iran	Masoumian et al., 2005
A. carchesii	150–160	–/–	–	–	–	Freshwater	Breisach, Germany	Henderson, 1905
	200–360	45/–	–	V	4	Freshwater	–	Canella, 1960
	200–360	45/–	ca. 10	V	4	Freshwater	Europe	Foissner et al., 1995
A. cocous	180–350	27–34/7–10	ca. 10	V	> 200	Mangrove	Huizhou, China	This study
*A. disciformis**	32–46	–	6–8	–	2	Freshwater	China	Chen, 1956
A. dragescoi	90–140	12–15/5	–	T[g]	2	Coastal water	Zhanjiang, China	Pan et al., 2014
A. eigneri	100–200	14–18/6–9	1	V	2	Mariculture	Qingdao, China	Lin et al., 2007a
	190–230	16–19/9 or 10	5–15	V	2	Brackish lake	Gangwon-do, Korea	Kim and Jung, 2017
A. ensiformis	100–200	18–22/5 or 6	Several	V	2	Freshwater	Bonn, Germany	Song and Wilbert, 1989
A. falcatus	25–75	12–17/5 or 6	4–6	S	1	Freshwater	Bonn, Germany	Song and Wilbert, 1989
	–	–	1	–	–	Freshwater	Hron River, Slovakia	Vd'ačný and Rajter, 2014
A. filum	300–500	–/–	–	–	2	Marine	Germany	Kahl, 1931
A. fusidens	40–55	10–14/4 or 5	1	V	2	Freshwater	Bonn, Germany	Song and Wilbert, 1989
	42.2–103.7	10–12/1–4?	1	T?	2	Freshwater	Sulawesi, Indonesia	Fernandez-Leborans and Von Rintelen, 2007
A. fusiformis	45–60	10–14/6	4–7	V, D	2	Freshwater	Bonn, Germany	Song and Wilbert, 1989
	–	–	–	–	–	Freshwater	Zubrovica, Slovakia	Vd'ačný and Rajter, 2014
A. gui	150–300	37–50/7–11	3–7	V	2	Mariculture	Qingdao, China	Lin et al., 2005b
*A. gutta***	215	–/–	1	T	2	Coastal water	Amoy, China	Wang and Nie, 1932
A. houi	100–300	21–27/9–10	2	V	1 or 2	Mariculture	Qingdao, China	Lin et al., 2009
A. incurvatus	53–95	–	–	–	–	–	Germany	Maupas, 1883
A. inquietus	170–200	–/–	4	V	2	Coastal beach	United Kingdom	Carey, 1992
A. litonotiformis	120–220	16–21/7–9	1	V	2	Mariculture	Sheyang, China	Song, 1991
A. loxophylliformis	80–110	–/–	–	–	2	Marine	–	Dragesco, 1960
A. marinus	150–300	13–21/5–8	7	V	2 or 3	Coastal water	Zhanjiang, China	Pan et al., 2014
	135	–/–	5	V	2	Coastal water	Saudi Arabia	Al-Rasheid, 1996
	300	–/–	Many	V, D?	–	Coastal beach	Alligator Harbor, USA	Borror, 1963
	135	–/8	5	V	2	Coastal beach	United Kingdom	Carey, 1992
	150–300	–/–	5	V	2	Coastal water	Sylt, Germany	Kahl, 1931
A. meiianus	150–220	17–23/5 or 6	1	S[h]	2	Freshwater	Bonn, Germany	Song and Wilbert, 1989
A. meleagris	200–300	–/–	ca. 6	V	2	Freshwater	Germany	Kahl, 1931
A. multinucleatus	200–450	29–38/8–12	5–10	V	80–300	Mangrove	Huizhou, China	This study
	150–250	–/–	6–10	V	40–70	Coastal water	Amoy, China	Wang, 1934
A. musicola	ca. 130	–/ca. 8	3 or 4	V	2	Freshwater	Germany	Kahl, 1931
*A. niloticus**	57.5–67.8	10–22	–	–	2	Freshwater	Egypt	El-Tantawy et al., 2016
A. parafusidens	40–90	8–15/4 or 5	1	V	2	Freshwater	Bonn, Germany	Song and Wilbert, 1989
	–	–	–	–	–	Freshwater	Rusovce, Slovakia	Vd'ačný and Rajter, 2014
A. pectinatus	ca. 200	–/ca. 10	ca. 10	V	2	Freshwater	Germany	Kahl, 1931
A. piger	40–80	9–11/4	1	T	2	Freshwater	Austria	Sonntag and Foissner, 2004

(Continued)

TABLE 1 | Continued

Species	LB (μm)[a]	RSK/LSK[b]	n-CV[c]	P-CV[d]	Ma[i]	Habitat type	Sample location	Data source
A. pleurosigma	200–300	25–35/4–6	Several	V, D	1–3	Freshwater	Bierhaum, Austria	Foissner, 1984
	90–380	28–37/6–8	Several	V, D	2	Freshwater	Bonn, Germany	Song and Wilbert, 1989
	150–450	25–35/4–6	6–21	V, D	1–3	Freshwater	Africa; North America	Foissner et al., 1995
	150–450	25–35/4–6	Several	V, D	2	Freshwater	Slovakia	Vd'ačný and Rajter, 2014
*A. polymicronulei***	156.2–338.3	23–25/–	ca. 8–16	V, D	2	Freshwater	Wuhan, China	Li, 1990
A. proceroformis	120–350	14–26/5 or 6	Several	V, D	1 or 2	Freshwater	Bonn, Germany	Song and Wilbert, 1989
A. procerus	600–800	36–47/11–15	Several	V, D	1 or 2	Freshwater	Bonn, Germany	Song and Wilbert, 1989
	200–800	25–40/–	20	V, D	–	Freshwater	Eurasia; North America	Foissner et al., 1995
	–	–	–	–	–	Freshwater	Slovakia	Vd'ačný and Rajter, 2014
A. punctatus	100–150	18–25/4–6	1	S	2 or 3	Lawn	Traun, Austria	Foissner, 1984
	80–150	18–25/4–6	1	S	2 or 3	Freshwater	Eurasia	Foissner et al., 1995
	–	–	–	–	–	Freshwater	Slovakia	Vd'ačný and Rajter, 2014
A. quadrinuleatus	400–650	30–34/ca. 5	Many	V, D	4	Marine	Carmeroun	Dragesco and Njiné, 1971
A. rotundus	160–200	15 or 16/–	5 or 6	V	2	Freshwater	Germany	Kahl, 1931
	–	–	Several	V, S	2	Freshwater	Turiec River, Slovakia	Vd'ačný and Rajter, 2014
A. salignus	180-360	24–29/4	2–7	V, D	2	Mangrove	Shenzhen, China	Chen et al., 2011
	–	–	–	–	–	Mangrove	Hong Kong, China	Chen et al., 2011
*A. salmicus***	70–90	ca. 20–22/–	8–10	D	2	Marine	White Sea	Burkovsky, 1970b
A. shenzhenensis	125–250	22–27/6–8	6–12	V	>200	Mangrove	Shenzhen, China	This study
A. sikorai	90–200	13–18/14–17	2 or 3	D	2	Mariculture	Qingdao, China	Lin et al., 2005a
A. songi	200–450	20–27/10–12	3–7	V	2	Mariculture	Wendeng, China	Pan et al., 2014
A. spiculatus	85–150	11–14/6–8	2 or 3	V	2	Mangrove	Shenzhen, China	Wu et al., 2015b
*A. voracus**	25–45	–/–	–	–	2	Freshwater	Iowa, USA	Davis, 1947
A. wilberti	180–210	15–19/7 or 8	3	V	2	Mangrove	Zhanjiang, China	Pan et al., 2014
A. yuianus	100–200	18–22/4	1	T	2	Mariculture	Qingdao, China	Lin et al., 2005b

[a] *Length of body in living cells.*
[b] *Number of right kineties/number of left kineties.*
[c] *Number of contractile vacuoles.*
[d] *Position of contractile vacuoles.*
[e] *Ventral.*
[f] *Dorsal.*
[g] *Terminal.*
[h] *Subterminal.*
[i] *Number of macronuleus nodules.*
Parasites of certain aquatic animals. **New combination, transferred from Hemiophrys in this study. * Amphileptus gutta sensu Wang and Nie, 1932 non sensu A. gutta (Cohn, 1866). –, N/A.*

of cell length); pointed anterior end always bent toward dorsal side; laterally compressed about 3–4:1 (**Figures 1A,G,H**). Macronuclear nodules numerous (ca. 80–300), ovoid to elliptical in outline, about 3–7 μm × 2–6 μm in size after fixation, and scattered in cytoplasm although most are clustered in mid-region of cell (**Figures 1C,K**). Micronucleus not observed. Often with 5–10 contractile vacuoles, 4–8 μm in diameter, distributed along posterior 2/3 part of ventral margin (**Figures 1A,H**). Extrusomes thick bar-shaped, straight or slightly curved, about 10 μm long, densely arranged along anterior part of buccal area, some scattered in cytoplasm (**Figures 1B,C,I**). Pellicle thin with small (<0.5 μm across), densely spaced, grayish, dot-like cortical granules between ciliary rows on both sides of cell (**Figures 1D,J**). Cytoplasm colorless to pale yellow, often with numerous tiny, refringent globules (1–3 μm across) that render main part of body opaque (**Figures 1G,H**). Locomotion usually by gliding slowly on substrate, or swimming with a slow clockwise rotation about longitudinal axis.

Ciliary pattern as shown in **Figures 1E,F,L,M**. Eight to twelve left kineties (mean 9.9; median 10), including perioral kinety 1 and dorsal brush kinety (DB) which extends to about anterior 2/5 of cell-length and is composed of regularly spaced dikinetids (**Figures 1E,L**). Right side with 29–38 (mean 33.0; median 33) ciliated kineties including perioral kinety 2; intermediate somatic kineties are shortened forming a distinct anterior single-suture on right side (**Figures 1F,M**).

Two perioral kineties located along cytostome. Perioral kinety 1 (PK1) left of oral slit, composed of dikinetids in anterior 1/3 and monokinetids in posterior 2/3 (**Figure 1E**). Perioral kinety 2 (PK2) right of oral slit, consists of widely spaced dikinetids in anterior 1/3 part and continues posteriorly as a row of monokinetids (**Figure 1E**).

Amphileptus shenzhenensis sp. n. (Tables 3, 4 and Figure 2)

Zoobank Registration Number of Work

urn:lsid:zoobank.org:pub:DEE074BB-7B4F-46E7-8CA1-47820074ABBC

ZooBank Registration Number of *A. shenzhenensis* sp. n.

urn:lsid:zoobank.org:act:53746C79-64F6-46D3-9E04-4662951D7CED

Diagnosis

Body 125–250 μm × 40–50 μm *in vivo*; slightly contractile with an inconspicuous beak-like anterior body end; numerous (>200) macronuclear nodules; 6–8 left and 22–27 right kineties; several (6–12) contractile vacuoles along ventral side of posterior 2/3 of cell; extrusomes thick rod-shaped, densely arranged along oral slit; dot-like cortical granules; brackish habitat.

Etymology

Named after Shenzhen, where this species was first isolated.

Type Locality and Ecological Features

Futian mangrove wetland (22°38′N, 114°06′E), Shenzhen, China. Water temperature 26°C, salinity 19.1‰, and pH 7.3.

Type Slides

One protargol slide with the holotype specimen (circled in black ink) and several paratype specimens is deposited in the Laboratory of Protozoology, Ocean University of China (OUC), Qingdao, China, with registration number WL20110413-03.

TABLE 2 | List of species associated with *Amphileptus/Hemiophrys* and their current names and status.

Taxon (basionym)	Current name	Present status	Data resource
Amphileptus anser sensu Ehrenberg, 1833	*Pseudomonilicaryon anser* (Mueller, 1773) Vd'ačný and Foissner, 2012	Synonym	Vd'ačný and Foissner, 2012
Amphileptus cygnus Claparède and Lachmann, 1859	*Pseudomonilicaryon anser* (Mueller, 1773) Vd'ačný and Foissner, 2012	Synonym	Vd'ačný and Foissner, 2012
Amphileptus claparedii Stein, 1867	*Apoamphileptus claparedii* (Stein, 1867) Lin and Song, 2004	Synonym	Lin and Song, 2004
Amphileptus claparedei sensu Bick (1972)	*Apoamphileptus claparedii* (Stein, 1867) Lin and Song, 2004	Synonym	Lin and Song, 2004
Amphileptus claparedei sensu Foissner et al. (1995)	*Apoamphileptus claparedii* (Stein, 1867) Lin and Song, 2004	Synonym	Lin and Song, 2004
Amphileptus flagellatus Rousslett, 1890	*Paradileptus elephantinus* (Švec, 1897) Kahl, 1931	Synonym	Vd'ačný and Foissner, 2012
Amphileptus gigas Claparède and Lachmann, 1859	*Monomacrocaryon gigas* (Claparède and Lachmann, 1859) Vd'ačný et al., 2011	Reliable dileptid*	Vd'ačný and Foissner, 2012
Amphileptus irregularis Maskell, 1887	*Dileptus margaritifer* (Ehrenberg, 1833) Dujardin, 1841	Synonym	Vd'ačný and Foissner, 2012
Amphileptus lacazei Gourret and Roeser, 1886	*Rimaleptus lacazei* (Gourret and Roeser, 1886) Vd'ačný and Foissner, 2012	Reliable dileptid*	Vd'ačný and Foissner, 2012
Amphileptus longicollis Ehrenberg, 1831	*Pseudomonilicaryon anser* (Mueller, 1773) Vd'ačný and Foissner, 2012	Synonym	Vd'ačný and Foissner, 2012
Amphileptus margaritifer Ehrenberg, 1833	*Dileptus margaritifer* (Ehrenberg, 1833) Dujardin, 1841	Reliable dileptid*	Vd'ačný and Foissner, 2012
Amphileptus massiliensis Gourret and Roeser, 1886	–	Identity unclear	Vd'ačný and Foissner, 2012
Amphileptus monilatus Stokes, 1886	*Monilicaryon monilatum* (Stokes, 1886) Jankowski, 1967	Reliable dileptid*	Vd'ačný and Foissner, 2012
Amphileptus moniliger Ehrenberg, 1835	*Paradileptus elephantinus* (Švec, 1897) Kahl, 1931	Synonym	Vd'ačný and Foissner, 2012
Amphileptus ovum sensu Dujardin, 1841	*Trachelius ovum* (Ehrenberg, 1831) Ehrenberg, 1833	Synonym	Vd'ačný and Foissner, 2012
Amphileptus vorax sensu Dujardin, 1841	*Trachelius ovum* (Ehrenberg, 1831) Ehrenberg, 1833	Synonym	Vd'ačný and Foissner, 2012
Amphileptus tracheloides Maskell, 1887	–	Identity unclear	Vd'ačný and Foissner, 2012
Amphileptus viridis Ehrenberg, 1833	*Dileptus viridis* (Ehrenberg, 1833) Foissner, 1987	Reliable dileptid*	Vd'ačný and Foissner, 2012
Amphileptus vareaeus sensu Chen, 1955	*Amphileptus voracus* Davis, 1947	Synonym	Chen, 1955
Hemiophrys macrostoma Chen, 1955	*Pseudoamphileptus macrostoma* (Chen, 1955) Foissner, 1983	Synonym	Small and Lynn, 1981
Hemiophrys lanceolatus Dragesco, 1965	*Amphileptus lanceolatus* (Dragesco, 1965) Lin et al., 2005b	Synonym	Lin et al., 2005b
Hemiophrys polymicronuclei Li, 1990	*Amphileptus polymicronuclei* (Li, 1990) comb. nov.	Synonym	Li, 1990
Hemiophrys salmicus Burkovsky, 1970b	*Amphileptus salmicus* (Burkovsky, 1970b) comb. nov	Synonym	Burkovsky, 1970b

**Considered to be a reliable dileptid.*

SSU rDNA Sequence

The SSU rDNA sequence of *Amphileptus shenzhenensis* is deposited in the GenBank database with the accession number, length, and GC content as follows: MT653621, 1534 bp, 43.22%.

TABLE 3 | Morphological characteristics of *Amphileptus multinucleatus* (1st line), *A. shenzhenensis* sp. n. (2nd line) and *A. cocous* sp. n. (3rd line).

Characters	Min	Max	Mean	SD	CV	n
Body length	200	450	296.7	12.64	4.3	24
	130	250	175.9	5.16	2.9	29
	175	400	284.3	14.70	5.2	20
Body width	60	120	79.0	3.14	4.0	24
	35	85	60.3	2.24	3.7	29
	45	190	93.4	10.80	11.6	20
Number of right	29	38	33.0	0.65	2.0	20
Kineties[a]	22	27	24.0	0.29	1.2	29
	27	34	29.6	0.43	1.5	22
Number of left	8	12	9.9	0.29	2.9	17
Kineties[b]	6	8	6.9	0.13	1.8	29
	7	10	8.6	0.20	2.4	22
Length of	3	7	5.0	0.20	4.0	24
Macronuclear	3	10	5.5	0.32	5.7	29
Nodules	3	10	6.7	0.46	6.9	20
Width of	2	6	4.0	0.25	6.2	24
Macronuclear	3	7	4.2	0.20	4.8	29
Nodules	3	10	5.7	0.48	8.4	20
Length of	8	12	9.1	0.22	2.4	24
Extrusomes	6	10	8.1	0.19	2.3	29
	7	11	9.0	0.20	2.2	22

All measurements in μm. Data based on protargol-stained specimens. CV, coefficient of variation in%; Max, maximum; Mean, arithmetic mean; Min, minimum; n, sample size; SD, standard deviation.
[a]*Perioral kineties 2, 3 included.*
[b]*Perioral kinety 1 and dorsal brush kinety included.*

Morphological Description

Body 125–250 × 40–50 μm *in vivo*, usually 180–200 in length. Laterally compressed about 3:1, not flexible, with an inconspicuous, beak-like anterior end, a bluntly pointed posterior end, and a "neck" region about 1/5 of cell length (**Figures 2A,G,H**). Numerous macronuclear nodules (>200) scattered in cytoplasm but mostly clustered in central region of cell, about 5 μm in diameter *in vivo*, usually discernable in life as slightly transparent areas (**Figures 2F,M–O**). Micronucleus not observed. Six–12 contractile vacuoles, about 5–15 μm in diameter, located near ventral margin in posterior 2/3 of cell (**Figures 2A,G,H,J**). Extrusomes thick rod-shaped, straight to slightly curved, 6–8 μm long, some evenly arranged along oral slit, others scattered in cytoplasm (**Figures 2D,K,N,O**). Pellicle thin with numerous small (< 0.5 μm across), grayish, dot-like cortical granules, densely distributed between ciliary rows on both sides of cell (**Figures 2E,I,L**). Right side densely ciliated with cilia about 8 μm long arranged in rows located within conspicuous longitudinal furrows, and forms a distinct anterior single-suture that is detectable *in vivo* (**Figures 2G,H**). Left somatic cilia generally sparsely distributed, dorsal brush cilia detectable at high magnifications, about 2–3 μm long (**Figure 2I**). Cytoplasm slightly grayish, often with several food vacuoles, about 5–20 μm in diameter (**Figure 2J**). Generally sensitive to disturbance, tending to form a resistant cyst after being placed on glass slide (**Figure 2J**). Locomotion by gliding moderately fast on substrate or by swimming while rotating clockwise about longitudinal axis.

Ciliary pattern as shown in **Figures 2B,C,N–P**. Left side with 6–8 (mean 6.9; median 7) ciliated kineties including perioral kinety 1 (PK1) and dorsal brush kinety (DB) which extends to about 2/5 of cell length and is composed of widely spaced dikinetids (**Figures 2B,N,O**). Twenty-two–27 (mean 24.0; median 24) right kineties including perioral kinety 2 (PK2); intermediate somatic kineties shortened forming a distinct suture in anterior part of body (**Figures 2C,P**).

TABLE 4 | List of all known *Amphileptus* spp. of multiple macronuclear nodules (≥4) and two new species in present study.

Species	LB (μm)[a]	LK/RK[b] (median)	Body shape	S-CG[d]	N and p-CV[e]	Data source
A. multinucleatus	150–250	–/–[c]	Posterior with twist	–	6–10; posterior 2/3 of ventral	Wang, 1934
A. multinucleatus	250–450	8-12 (10)/29–38 (33)	Posterior with twist	Dot-like	5–10; posterior 2/3 of ventral	This study
A. shenzhenensis sp. n	135–200	6–8 (7)/22–27 (24)	Rhombic	Dot-like	6–12; posterior 2/3 of ventral	This study
A. cocous sp. n	180–350	7–10 (9)/27–34 (30)	Elongated blade-shaped	Rice-shaped	6–8; posterior 1/2 of ventral	This study
A. quadrinucleatus	400–650	–/30–34	Broad spindled	Dot-like	Many; both sides of cell	Dragesco and Dragesco-Kernéis, 1986
A. aeschtae	150–350	7–10 (9)/29–34 (31)	Ellipsoid	Dot-like	5–13; posterior 2/3 of ventral	Lin et al., 2007a

[a]*Length of body in vivo.*
[b]*Number of left kineties/number of right kineties.*
[c]*Data not available.*
[d]*Shape of cortical granules.*
[e]*Number and position of contractile vacuoles.*

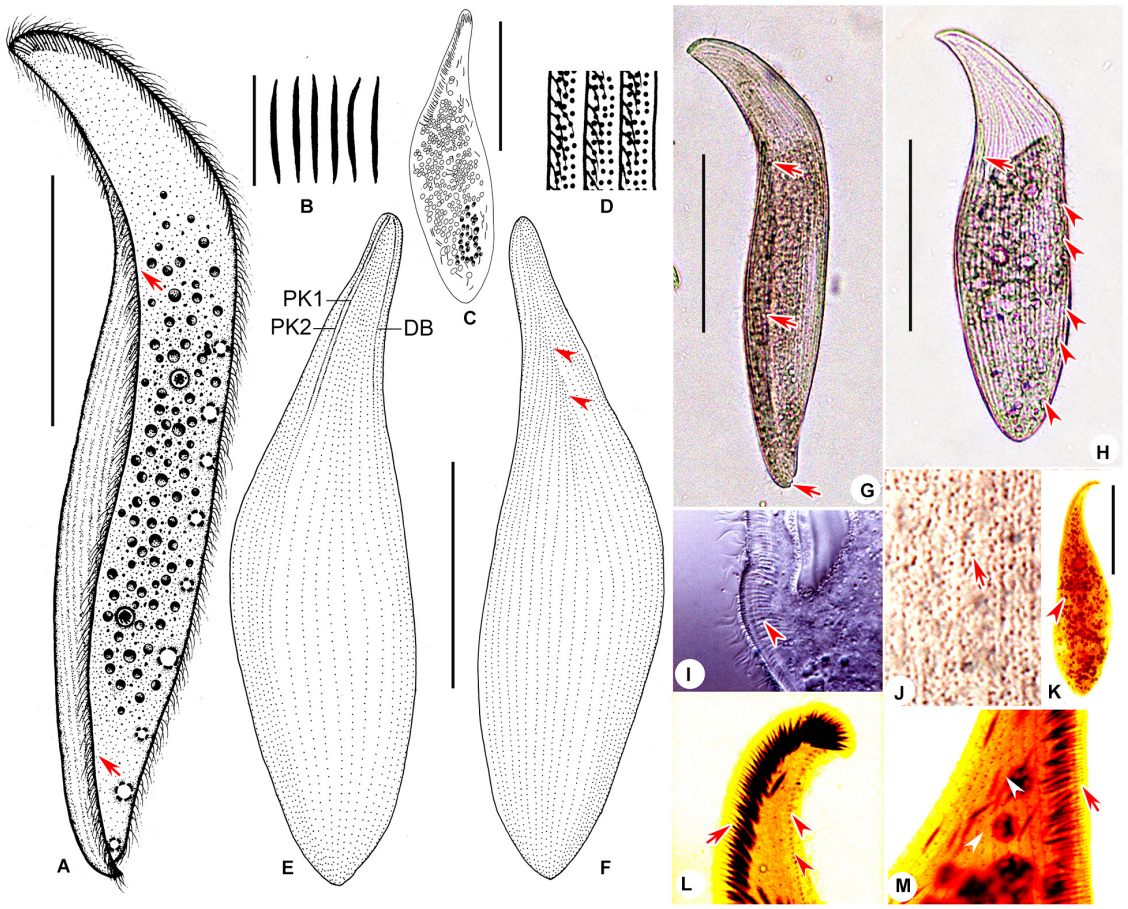

FIGURE 1 | *Amphileptus multinucleatus* Wang, 1934; living individuals **(A,B,D,G–J)** and cells stained with protargol **(C,E,F,K–L)**. **(A)** Right lateral view of a representative cell, arrowheads mark the twisted body. **(B)** Extrusomes. **(C)** Showing the distribution of extrusomes and macronuclear nodules. **(D)** The distribution of cortical granules. **(E,F)** Ciliary patterns of the left **(E)** and right **(F)** side; arrowheads point to the single-suture. **(G,H)** Right view of typical individual, arrows mark the twisted body, arrowheads show the distribution of contractile vacuoles. **(I)** The anterior part of right side, arrowhead shows the extrusomes. **(J)** The mid-region of right side, arrow marks the cortical granules. **(K)** To show the distribution of macronuclear nodules (arrowhead). **(L)** The anterior part of left side, to show perioral kinety 1 (arrow) and brush kinety (arrowheads). **(M)** The anterior part of right side, arrow marks perioral kinety 2, arrowheads show the suture. DB, dorsal brush; PK1, perioral kinety 1; PK2, perioral kinety 2. Scale bars: **(A,G,H)**: 100 μm; **(B)**: 10 μm; **(C,E,F,K)**: 50 μm.

Two perioral kineties along cytostome. Perioral kinety 1 (PK1) left of oral slit, comprises dikinetids in anterior 2/5 and continues posteriorly as a row of monokinetids (**Figures 2B,N,O**). Perioral kinety 2 (PK2) right of oral slit, comprises regularly spaced dikinetids in anterior 1/3 and monokinetids in posterior 2/3 (**Figures 2B,P**).

Amphileptus cocous sp. n. (Tables 3, 4 and Figure 3)

ZooBank Registration Number of *Amphileptus cocous* sp. n.

urn:lsid:zoobank.org:act:96115FDB-E205-4FB0-ADE8-96DFC7767F60

Diagnosis

Medium to large *Amphileptus*, 180–350 × 35–45 μm *in vivo*; body strongly contractile, elongated blade-shaped; numerous (> 200) macronuclear nodules; 7–10 left and 27–34 right kineties; several (6–8) contractile vacuoles along ventral side of posterior half of cell; extrusomes thick bar-shaped, densely arranged along oral slit; rice-shaped cortical granules; brackish habitat.

Etymology

The Latin adjective "*cocous*" (rice-shaped) refers to the shape of cortical granules.

Type Locality and Ecological Features

Daya Bay mangrove wetland (22°41′N, 114°23′E), Huizhou, China. Water temperature 26.8°C, salinity 15.9‰, and pH 7.0.

Type Slides

One protargol slide with the holotype specimen (circled in black ink) and several paratype specimens is deposited in the Laboratory of Protozoology, Ocean University of China (OUC), Qingdao, China, with registration number WL20111027-01.

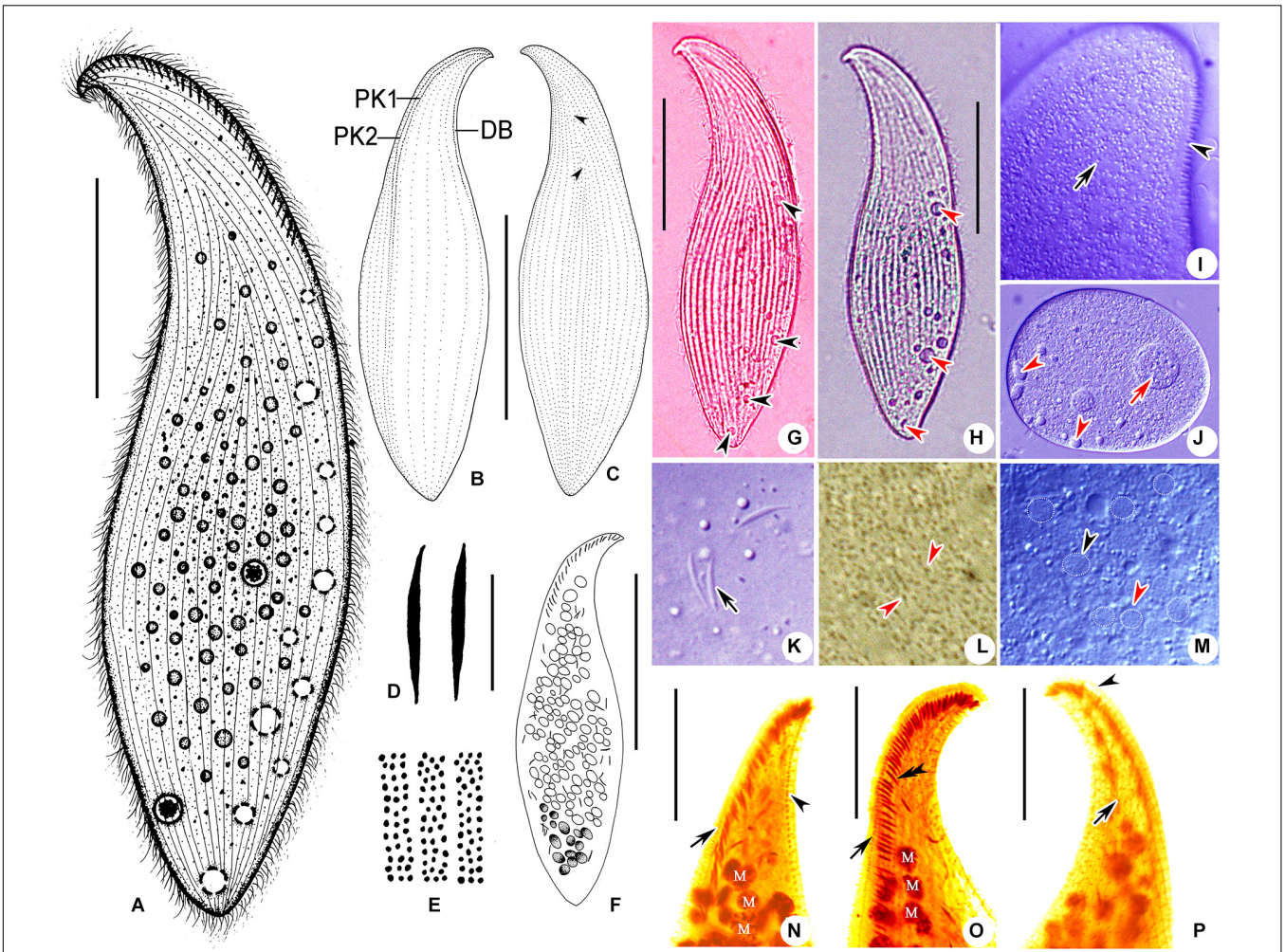

FIGURE 2 | *Amphileptus shenzhenensis* sp. n.; living individuals **(A,D,E,G–M)** and cells stained with protargol **(B,C,F,N–P)**. **(A)** Right lateral view of a representative cell. **(B,C)** Ciliary patterns of left **(B)** and right **(C)** side of the holotype, arrowheads show the suture. **(D)** Extrusomes. **(E)** Cortical granules. **(F)** Distribution of macronuclear nodules. **(G,H)** Right views of typical individuals, arrowheads show the distribution of contractile vacuoles. **(I)** The anterior part of left side, to show the cortical granules (arrow) and dorsal brush kinety (arrowhead). **(J)** A resistant cyst, arrowheads mark the contractile vacuoles, arrowhead shows food vacuole. **(K)** Extrusomes. **(L)** Cortical granules. **(M)** The mid-region of cell, to show the macronuclear nodules (arrowheads). **(N,O)** The anterior part of left side, arrow points to the left perioral kinety, arrowhead marks the dorsal brush kineties and double arrowheads show the extrusomes. **(P)** The anterior part of right side, to show perioral kinety 2 (arrowhead) and the suture (arrow). DB, dorsal brush; PK1, perioral kinety 1; PK2, perioral kinety 2. Scale bars: **(A–C,F–H)** 50 μm; **(D)** 5 μm; **(N–P)** 20 μm.

SSU rDNA Sequence

The SSU rDNA sequence of *Amphileptus cocous* is deposited in the GenBank database with the accession number, length, and GC content as follows: MT653622, 1533 bp, 43.25%.

Morphological Description

Body size highly variable, about 180–350 × 30–45 μm *in vivo*, usually 200–250 μm in length. Elongated blade-shaped, flexible, and strongly contractile, with widely pointed posterior end and an inconspicuous neck region about 15–20% of cell length and usually curved slightly to dorsal side, laterally compressed about 2–3:1 (**Figures 3A,H**). Numerous (>200) macronuclear nodules, ovoid to elliptical in outline, about 5–10 μm × 5–10 μm in size *in vivo*, scattered in cytoplasm, usually discernable in life as slightly transparent areas (**Figure 3L**). Micronucleus not observed. Six–eight contractile vacuoles, about 8–13 μm in diameter, distributed along ventral margin in posterior half of cell (**Figures 3A,D,H,L,K**). Extrusomes spindle-shaped, about 10 μm long, some arranged in oral area, others some scattered in cytoplasm (**Figures 3C,E,J,N,O**). Pellicle thin with numerous short (about 1.0 μm in length), rice-shaped, colorless cortical granules densely packed between ciliary rows on both sides of cell (**Figures 3B,I,M**). Right side flat and densely ciliated, cilia about 8 μm long; left side sparsely ciliated, cilia difficult to detect in life. Cytoplasm colorless to grayish, often with numerous tiny, refringent globules (2–5 μm across) and numerous food vacuoles (3–10 μm across) that render main part of body opaque (**Figures 3H,K**). Locomotion moderately fast, usually gliding

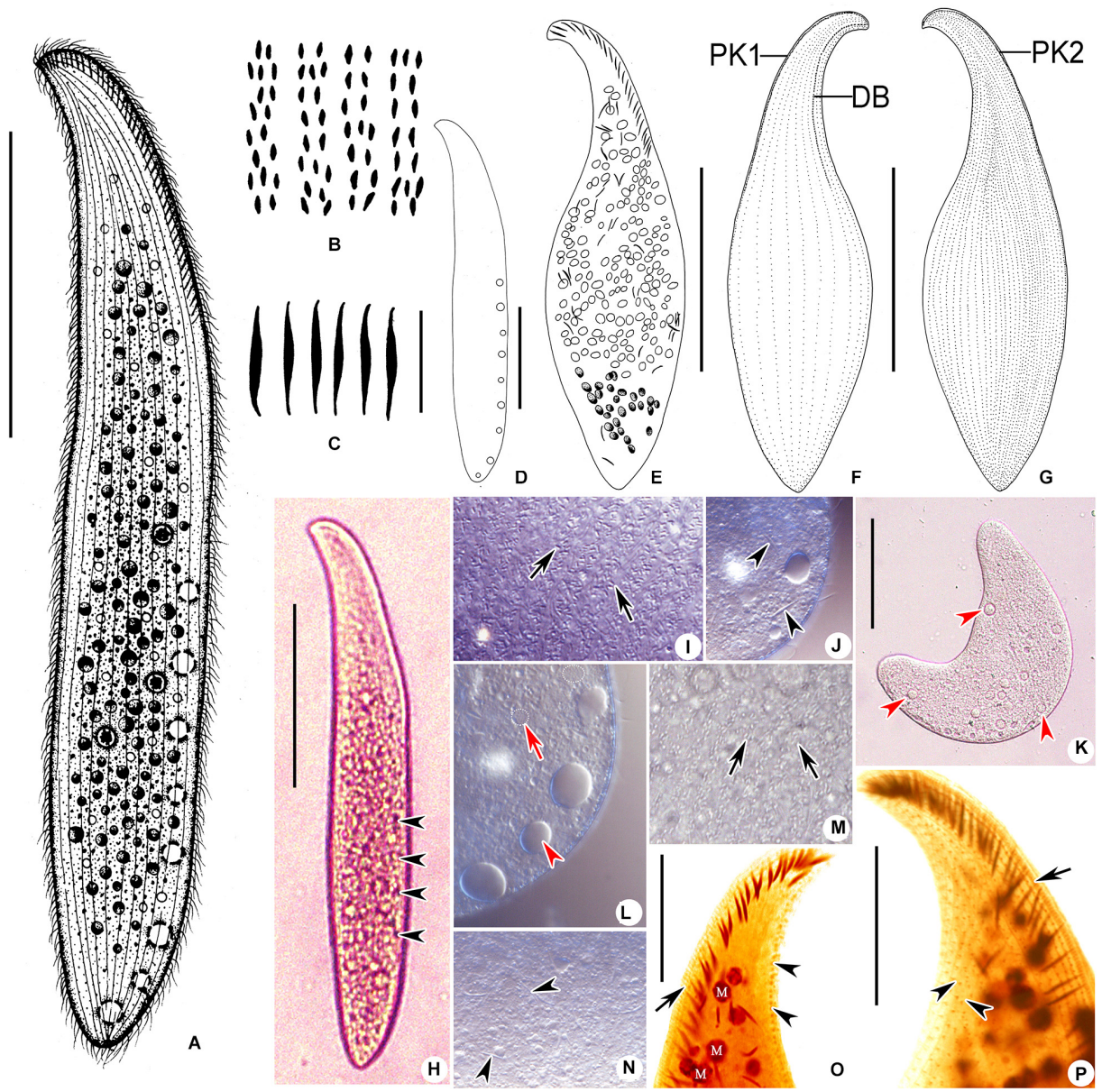

FIGURE 3 | *Amphileptus cocous* sp. n.; living individuals **(A–D,H–N)** and cells stained with protargol **(E–G,O,P)**. **(A,H)** Right lateral view of a representative cell, arrowheads mark the contractile vacuoles. **(B,I,M)** To show the distribution of cortical granules (arrows). **(D)** To show the distribution of contractile vacuoles. **(E)** To show the distribution of macronuclear nodules. **(F,G)** Ciliary patterns of right **(G)** and left **(F)** side of the holotype. **(J)** The ventral part of right side, arrowheads point to extrusomes. **(K)** Contracted individual, arrowheads show the food vacuoles. **(L)** The ventral part of right side, arrow shows a macronuclear nodule, arrowhead shows a contractile vacuole. **(N)** The mid-region of cell, arrowheads show the extrusomes. **(O)** The anterior part of left side of cell, to show perioral kinety 1 (arrow) and dorsal brush kinety (arrowheads). **(P)** The anterior part of right side of cell, arrow marks perioral kinety 2, arrowheads show the suture. DB, dorsal brush; PK1, perioral kinety 1; PK2, perioral kinety 2. Scale bars: **(A,H)** 100 μm; **(C)** 10 μm; **(D–G,K,O,P)** 50 μm.

on substrate or swimming with a slow clockwise rotation about longitudinal axis.

Ciliary pattern as shown in **Figures 3F,G,O,P**. About 7–10 (mean 8.6; median 9) widely spaced left kineties, including perioral kinety 1 (PK1) and dorsal brush (DB) kinety which extends to 2/3 cell-length and is composed of regularly spaced dikinetids (**Figures 3F,O**). Right side densely ciliated, about 27–34 (mean 29.6; median 29) kineties including perioral kinety 2, intermediate somatic kineties shortened anteriorly forming a distinct anterior suture (**Figures 3G,P**).

Two perioral kineties around cytostome: PK1 left of oral slit, composed of closely spaced dikinetids in anterior 2/5 and continues posteriorly as a row of closely spaced monokinetids (**Figures 3F,O**); PK2 right of oral slit, formed of closely spaced dikinetids in anterior 2/5 and continues posteriorly as a row of closely spaced monokinetids (**Figures 3G,P**).

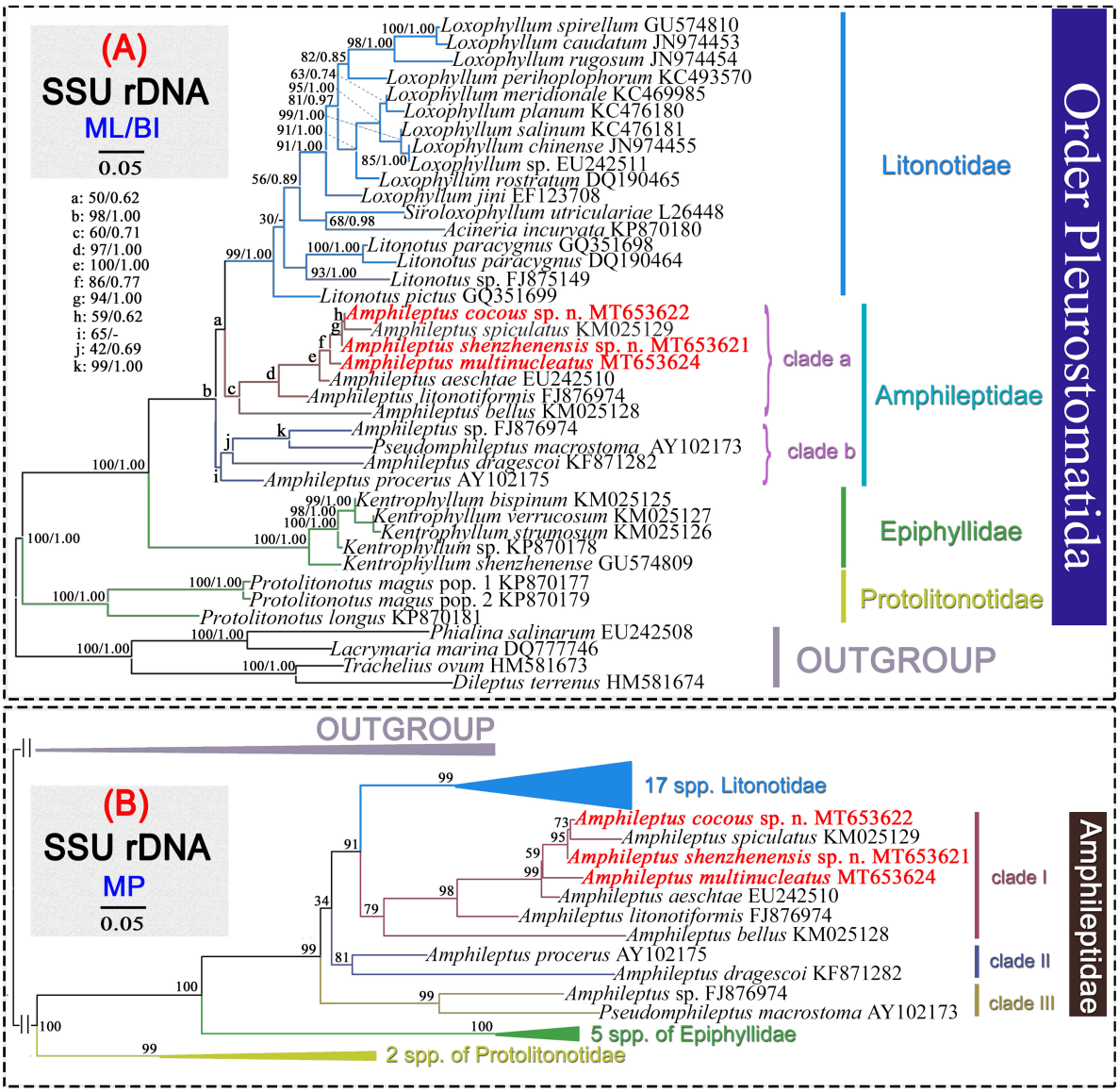

FIGURE 4 | Phylogenetic trees inferred from SSU rDNA sequences performed with maximum likelihood (ML) **(A)** and maximum parsimony (MP) **(B)**. The numbers at the nodes represent the posterior probabilities and the percentage of times the group occurred out of 1,000 trees, respectively. A dash indicates a different topology in the BI tree from ML tree. Newly sequenced species are in bold. GenBank accession numbers are given after the names of species. The scale bar corresponds to 5 substitutions per 100 nucleotide positions.

Molecular Phylogenetic Analysis of *Amphileptus*

Phylogenetic trees conducted using Bayesian inference (BI) and maximum likelihood (ML) had identical topologies so the two trees were combined (**Figure 4A**). The topology of the MP tree differed slightly from that of the ML/BI tree as shown in **Figure 4B**. The genus *Amphileptus* forms a polytomy with two clades in the ML/BI tree and three clades in the MP tree, and the three newly sequenced species form a clade with another four *Amphileptus* spp. (clade a in **Figure 4A**; clade 1 in **Figure 4B**) with poor to moderate support (60% ML, 0.71 BI, 79% MP). Within clade a/clade I, *Amphileptus cocous* groups with *A. spiculatus* which together group with *A. shenzhenensis* with high to maximum support (94% ML, 99% MP, 1.00 BI). These three species cluster with *A. multinucleatus* with poor to moderate support (86% ML, 0.77 BI, 59% MP), and this subclade groups with *A. aeschtae* with high support (100% ML, 1.00 BI, 99% MP), forming a clade that is sister to *A. litonotiformis* with high support (97% ML, 1.00 BI, 98% MP). In the second clade in ML/BI tree (clade b in **Figure 4A**), the remaining three *Amphileptus* spp. (*Amphileptus* sp., *A. dragescoi* and *A. procerus*) group with *Pseudoamphileptus macrostoma* with weak support (0.69 BI, 65% ML). In the MP tree, however, *A. procerus* clusters

with *A. dragescoi* (81% MP) to form the second clade (clade II in **Figure 4B**), and the remaining two species (*Pseudoamphileptus macrostoma* and *Amphileptus* sp.) form the third clade (clade III in **Figure 4B**) with high support (99% MP).

DISCUSSION

A Brief Summary of the Genus *Amphileptus* Ehrenberg, 1830

The genus *Amphileptus* was established by Ehrenberg (1830) and another pleurostomatid genus, *Hemiophrys,* was established by Wrzesniowski (1870). Until the mid-twentieth century, descriptions of *Amphileptus-Hemiophrys* species were exclusively based on observations of live species (Ehrenberg, 1830; Kahl, 1931). Canella (1960) carried out the first detailed investigation of the ciliary pattern of these two genera using silver staining and revealed that the somatic kineties on the right side form a suture in the mid-to-anterior region of the cell in both genera. Furthermore, other morphological differences were regarded as species-level rather than genus-level characters, suggesting that *Hemiophrys* is a junior synonym of *Amphileptus* (Canella, 1960). This recommendation was accepted by Fryd-Versavel et al. (1975). Consequently, the genus *Hemiophrys* was merged into the genus *Amphileptus*, and the diagnosis of genus *Amphileptus* was emended, i.e., the formation of a single suture by the somatic kineties of the right side was considered to be the key diagnostic character. The emended diagnosis of the genus *Amphileptus* and the submersion of *Hemiophrys* were accepted by subsequent investigators (Foissner, 1984; Aescht, 2001; Lynn, 2008).

Species of the genus *Amphileptus* are easily identified by the pattern of right somatic kineties, i.e., the somatic kineties shortened to form a single suture in the median area, and this is the main differentiating feature for certain pleurostomatid genera, e.g., *Amphileptus* and *Apoamphileptus* within the order Pleurostomatida. Therefore, the presence of a single suture is thought to be an important genus-level, and possibly even a family-level character (Lin et al., 2005b; Wu et al., 2017).

The ciliature of *Amphileptus* consists of perioral kineties, right somatic kineties, left somatic kineties and dorsal brush kineties, the number and pattern of which are important for species delimitation. The key characteristics for species determination are: (1) body shape and size; (2) number of right and/or left kineties; (3) number and position of contractile vacuoles; (4) number of macronuclear nodules;, and (5) presence vs. absence and shape of cortical granules (Canella, 1960; Foissner, 1984; Song, 1991; Lin et al., 2007a; Wu et al., 2015b).

The first molecular phylogenetic study of *Amphileptus* was that of Gao et al. (2008) who sequenced the SSU rDNA of *A. procerus* (Penard, 1922) Song and Wilbert, 1989 and *A. aeschtae* Lin et al., 2007a. Pan et al. (2014) added another new sequence and reported the monophyly of the family Amphileptidae and the paraphyly of the genus *Amphileptus* with *Pseudoamphileptus* nested within it. These findings have been both confirmed and rejected in subsequent studies (Wu et al., 2015b, 2017; Pan et al., 2015) (see molecular analyses below). Including the three species described in the present study, there are nine identified and one unidentified SSU rDNA sequences in the NCBI/GenBank database.

Comments on *Amphileptus multinucleatus* Wang, 1934

Amphileptus multinucleatus was originally described by Wang (1934) who gave a good description based on live observations, although the ciliary pattern was not mentioned. It was characterized mainly as follows: body 150–250 μm in length, with 6–10 contractile vacuoles lying in ventral posterior half, numerous (40–70) macronuclear nodules scattered in cytoplasm, and posterior end twisted to one side. In particular, it was noted that "the twisted posterior portion is very constant in all observed individuals and may be considered as one of the specific characteristics" (Wang, 1934). This specific feature was also observed in all observed individuals of the Daya Bay population (n > 20) and has not been recorded in any other species of *Amphileptus*. We conclude that the twisted posterior portion of the body should be considered as a diagnostic character of this species. In addition, our form was identified as *A. multinucleatus* based on the distribution of extrusomes along the oral slit and with some scattered in the cytoplasm. One significant difference between the original description and the Daya Bay population of *A. multinucleatus* is the number of macronuclear nodules, the former having 40–70 and the latter 80–300. It should be noted, however, that the number of macronuclear nodules in the original description was based on observations of specimens fixed in Schaudinn's fluid and stained with iron-alum-hematoxylin which may not show the outline of the macronuclear nodules as clearly as the protargol stain. In addition, the body size of the Daya Bay population is considerably larger than that of the original population (200–400 vs. 150–250 μm in length), which may be another reason for the higher number of macronuclear nodules. We therefore conclude the Daya Bay population is conspecific with the original population of *A. multinucleatus* described by Wang (1934).

Comments on *Amphileptus shenzhenensis* sp. n. and *A. cocous* sp. n.

The most important characters for species identification and circumscription in the genus *Amphileptus* include the number of kineties, the number and positions of contractile vacuoles, the number of macronuclear nodules, the shape and distribution of extrusomes, the presence or absence and the shape of cortical granules, and the body shape *in vivo* (Foissner et al., 1995; Lin and Song, 2004; this study).

Among all the nominal species of *Amphileptus*, only three congeners are reported to have contractile vacuoles arranged along the ventral margin of the cell and four or more macronuclear nodules, i.e., *A. multinucleatus*, *A. quadrinucleatus* and *A. aeschtae* (Wang, 1934; Dragesco and Dragesco-Kernéis, 1986; Lin et al., 2007a; **Table 4**). The two new forms and the three described species strongly resemble each other in body size, position and number of macronuclear nodules, shape of cortical granules, and the number of kineties. However, *A. multinucleatus*

is the only species in this genus with a posterior end constantly twisted to one side (Wang, 1934), therefore it can be clearly distinguished from the other species.

Amphileptus shenzhenensis sp. n. resembles *A. multinucleatus*, *A. quadrinucleatus,* and *A. aeschtae* in having dot-like cortical granules. However, *A. shenzhenensis* sp. n. differs: from *A. multinucleatus* by having fewer kineties on both sides of the cell (6–8 vs. 8–12 on left; 22–27 vs. 29–38 on right), and the posterior portion of the body not twisted (Wang, 1934); from *A. quadrinucleatus* by having fewer right kineties (22–27 vs. 30–34), the distribution of contractile vacuoles (in posterior 2/3 of cell on ventral side vs. down the length of both sides of body) and its significantly smaller body length (135–200 vs. 400–650 μm *in vivo*) (Dragesco and Dragesco-Kernéis, 1986); from *A. aeschtae* by having fewer kineties on both sides of cell, i.e., 6–8, mean 7 vs. 7–10, mean 9 on left; 22–27 vs. 29–34 on right (Lin et al., 2007a; **Table 4**).

Amphileptus cocous sp. n. resembles *A. aeschtae* in having the same number of left kineties (7–9) and almost the same number of right kineties (27–34, mean 30 vs. 29–34, mean 31). However, the former can be separated from the latter by the different shape of cortical granules (rice-shaped vs. dot-like), the distribution of contractile vacuoles (in the posterior half of the body vs. in the posterior 2/3 of the body) and the elongated blade-shaped (vs. ellipsoidal) body (Lin et al., 2007a; **Table 4**).

Amphileptus shenzhenensis sp. n. can be distinguished from *A. cocous* sp. n. by having fewer right kineties (22–27, mean 24 vs. 27–34, mean 30) and dot-like (vs. rice-shaped) cortical granules (**Table 4**).

The phylogenetic analyses based on SSU rDNA sequence data show that *Amphileptus cocous* sp. n. groups with *A. spiculatus* in the core clade. However, the former can be distinguished from the later by the following combination of morphological characters: (1) the different body shape *in vivo* (elongated blade-shaped vs. pyriform); (2) the rice-shaped (vs. dot-like) cortical granules; (3) the number of right kineties (27–34 vs. 11–14); (4) the larger body size (180–350 vs. 85–145 μm long *in vivo*), and (5) having significantly more (>300 vs. 2) macronuclear nodules (Wu et al., 2015b). In addition, the validity of the new species is supported by the SSU rDNA sequence data: *Amphileptus cocous* sp. n. differs in one, two, and five nucleotides from *A. shenzhenensis* sp. n., *A. multinucleatus* and *A. aeschtae*, respectively; and *A. shenzhenensis* sp. n. differs in six and three nucleotides from *A. aeschtae* and *A. multinucleatus*, respectively.

Two New Combinations of the Genus *Amphileptus*

Li (1990) reported a new species from Donghu Lake, Hubei Province, China, under the name *Hemiophrys polymicronuclei*. However, because *Hemiophrys* is a junior synonym of *Amphileptus*, this species should be transferred to the latter (Canella, 1960). Therefore, we propose a new combination, *Amphileptus polymicronuclei* (Li, 1990) comb. n. (original combination *Hemiophrys polymicronuclei* Li, 1990; **Tables 1**, **2**). In addition, another species, *Hemiophrys salimica*, was reported by Burkovsky (1970b) from Kandalaksha Gulf, White Sea, which should be transferred to *Amphileptus* (Canella, 1960; Curds, 1982). Hence, a new combination, *Amphileptus salimicus* (Burkovsky, 1970b) comb. n. (original combination *Hemiophrys salimica* Burkovsky, 1970b), is suggested (**Tables 1**, **2**).

TABLE 5 | Kishino-Hasegawa (KH) test results.

Topology constraints	lnL	KH value (*P*)
Best ML tree (unconstrained)	7582.22678250	0.996
Monophyly of *Amphileptus*	7615.42903834	0.004

P < 0.05 refutes monophyly; P > 0.05 does not refute the possibility of monophyly.

Comments on the Phylogeny of the Genus *Amphileptus*

The family Amphileptidae is characterized by the presence of a single anterior suture on the right side, thereby differentiating it from the other three families within the order Pleurostomatida (Vďačný et al., 2015; Wu et al., 2017). The Amphileptidae, comprises five genera, namely *Amphileptus* (the type genus), *Pseudoamphileptus*, *Amphileptiscus, Apoamphileptus,* and *Opisthodon*, but molecular data are available only the former two genera. Traditionally, the genus *Amphileptus* has been considered to be monophyletic based on morphological (Foissner, 1977, 1983, 1984; Corliss, 1979; Lin et al., 2005a,b, 2007a; Lynn, 2008) and some molecular studies (Pan et al., 2010, 2013; Zhang et al., 2012; Vďačný and Foissner, 2013; Wu et al., 2013, 2015b, 2017; Vďačný, 2015; Vďačný et al., 2015). However, the monophyly of this *Amphileptus* has been questioned by several other molecular phylogenetic studies (Gao et al., 2008; Vďačný et al., 2011, 2015; Pan et al., 2014, 2015; Wu et al., 2014, 2015b). In our SSU rDNA trees (**Figure 4**) which include three new sequences of *Amphileptus*, the non-monophyly of the genus *Amphileptus* was supported, since it was divided into two and three groups in ML/BI and MP tree, respectively. Furthermore, the possibility of the monophyly of *Amphileptus* was also rejected ($p = 0.004 < 0.05$) by the KH test (**Table 5**). Although some previous studies have shown members of the genus *Amphileptus* to group together in phylogenetic trees (Pan et al., 2010, 2013; Zhang et al., 2012; Vďačný and Foissner, 2013; Wu et al., 2013, 2015a, 2017; Vďačný, 2015; Vďačný et al., 2015), these convergent topologies are based on insufficient taxon sampling and have only low nodal support (e.g., 76% ML, 0.65 BI in Pan et al., 2013; 17% ML, 20% MP in Wu et al., 2015a; 50% ML, 0.64 BI, 57% MP in Vďačný et al., 2015; 51% ML, 0.78 BI, 67% MP in Vďačný, 2015). Therefore, the molecular data strongly question the morphology-based relationship of the genus *Amphileptus,* and even the family Amphileptidae, and indicate that this group is paraphyletic. To date, however, only two genera of the family Amphileptidae have molecular data, namely *Amphileptus* and *Pseudoamphileptus*. It is noteworthy that *Pseudoamphileptus* is represented by a single sequence that clusters with sequences of *Amphileptus* (**Figure 4**). Furthermore, no morphological characters can be identified as plesiomorphic or apomorphic, so the question of whether the genus *Amphileptus* and/or the family Amphileptidae is monophyletic will remain unresolved pending

the availability of more morphological and molecular data with expanded taxon sampling.

DATA AVAILABILITY STATEMENT

The datasets presented in this study can be found in online repositories. The names of the repository/repositories and accession number(s) can be found below: NCBI GenBank (accession: MT653621, MT653622, and MT653624).

AUTHOR CONTRIBUTIONS

LW and XL conceived and designed the manuscript. LW carried out the live observation and protargol staining. LW, JL, AW, and XL wrote and revised the manuscript. All authors contributed to the article and approved the submitted version.

FUNDING

This work was supported by the National Natural Science Foundation of China (project numbers: 42076113, 31761133001, and 415761486), Guangdong MEPP Fund [No. GDOE (2019) A23], Guangdong Basic and Applied Basic Research Foundation (project number: 2020A1515111125), and the China Postdoctoral Science Foundation (project number: 2018M640796).

ACKNOWLEDGMENTS

Many thanks to Ms. Wenping Chen, Mr. Chunxu Hu, and Mr. Xudong Cui, the graduates of our laboratory, SCNU, for their help in sampling. We are also grateful to the two reviewers and associate editor HP for their constructive comments and helpful suggestions for improving our manuscript.

REFERENCES

Aescht, E. (2001). Catalogue of the generic names of ciliates (*Protozoa*, *Ciliophora*). *Denisia* 1, 1–350. doi: 10.1007/978-3-319-23534-9_1

Al-Rasheid, K. A. S. (1996). Records of free-living ciliates in Saudi Arabia, II. freshwater benthic ciliates of AI-Hassa Oasis, Eastern region. *Arab. Gulf J. Sci. Res.* 15, 187–205.

Borror, A. (1963). Morphology and ecology of the benthic ciliated protozoa of Alligator harbor, florida. *Arch. Protistenk.* 106, 465–534.

Burkovsky, I. V. (1970a). The ciliates of the mesopsammon of the Kandalaksha Gulf (white sea) I. *Acta Protozool.* 7, 475–489.

Burkovsky, I. V. (1970b). The ciliates of the mesopsammon of the Kandalaksha Gulf (white sea) II. *Acta Protozool.* 7, 47–65.

Canella, M. F. (1960). Contributo ad una revisione dei generi *Amphileptus*, *Hemiophrys* e *Litonotus* (*Ciliata*, *Holotricha*, Gymnostomata). *Ann. Univ. Ferrara* 2, 47–95.

Carey, P. (1992). *Marine Interstitial Ciliates: an Illustrated Key*. London: Chapman & Hall.

Chen, C. L. (1955). The protozoan parasites from four species of Chinese pond fishes: *Ctenopharyngodon idellus*, Mylopharyngodon aethiops, *Aristichthys nobilis* and *Hypophthalmichthys molitrix*. I. the protozoan parasites of *Ctenopharyngodon idellus*. *Acta Hydrobiol. Sinica* 2, 123–164.

Chen, C. L. (1956). The protozoan parasites from four species of Chinese pond fishes: *Ctenopharyngodon idellus*, *Mylopharyngodon aethiops*, *Aristichthys nobilis* and *Hypophthalmichthys molitrix*. III. the protozoan parasites of *Aristichthys nobilis* and *Hypophthalmichthys molitrix*. *Acta Hydrobiol. Sinica* 2, 279–299.

Chen, R., Lin, X., and Warren, A. (2011). A new pleurostomatid ciliate, *Amphileptus salignus* n. sp. (Protozoa, Ciliophora), from mangrove wetlands in southern China. *Zootaxa* 3048, 62–68. doi: 10.11646/zootaxa.3048.1.4

Corliss, J. O. (1979). *The Ciliated Protozoa: Characterization, Classification and Guide to the Literature*. *Second Edition*. New York: Pergamon Press.

Curds, R. C. (1982). *British and Other Freshwater Ciliated Protozoa. Part 1. Ciliophora: Kinetofragminophora*. Cambridge: Cambridge University Press.

Davis, H. S. (1947). Studies of the protozoan parasites of freshwater fishes. *U. S. Fisheries Wildlife Serv. Fishery Bull.* 51, 1–29.

Dragesco, J. (1960). Ciliés mésopsammiques littoraux, systématique,morphologie, écologie. *Trav. Stat. Biol. Roscoff* 12, 1–356.

Dragesco, J. (1965). Ciliés mésopsammiques d'Afrique noire. *Cah. Biol. Mar.* 6, 357–399.

Dragesco, J., and Dragesco-Kernéis, A. (1986). Ciliés libres de l'Afrique intertropicale: introduction à la connaissance et à l'étude des Ciliés. *Faune Trop.* 26, 1–559. doi: 10.2307/j.ctv18phcb3.3

Dragesco, J., and Njiné, T. (1971). Compléments à la connaissance des ciliés libres du Cameroun. *Annls. Fac. Sci. Univ. féd Cameroun* 7– 8, 97–140.

Ehrenberg, C. G. (1830). Beiträge zur Kenntnis der Organisation der Infusorien und ihrer geographischen Verbreitung, besonders in Sibitien. *Abh. dt. Akad. Wiss. Berl.* 1832, 1–88. doi: 10.1159/000404845

El-Tantawy, S. A. M., Abdel-Aziz, A., Ei-Nour, M. F. A., Samn, A., Shaldoum, F., and Rady, I. (2016). Ectoparasitic protozoa scyphidians, amphileptids and tetrahymenid from the Nile perch, *Lates niloticus* (Linnaeus, 1758) in the Dakahlia Province, Egypt. *Egypt. J. Exp. Biol.* 12, 51–61.

Fan, X. P., and Pan, X. M. (2020). *Scuticociliates and Peniculine Ciliates in China*. Beijing: Science Press.

Fernandez-Leborans, G., and Von Rintelen, K. (2007). Epibiontic communities on the freshwater shrimp *Caridina ensifera* (Crustacea, Decapoda, Atyidae) from Lake Poso (Sulawesi, Indonesia). *J. Nat. Hist.* 41, 2891–2917. doi: 10.1080/00222930701787871

Foissner, W. (1977). Taxonomische studien ü ber die ciliaten der GroBglocknergebietes, 2. *Familie Amphileptidae. Ber. Haus. Natur. Salzburg* 8, 87–93.

Foissner, W. (1983). Morphologie und Infraciliatur zweier ectocommensaler Ciliaten (Protozoa: Ciliophora) von *Cyprinus carpio* L. (Pisces: Cypriniformes): Heteropolaria lwoffi (Fauré-Fremiet, 1943) (Peritrichida: Epistylididae) und ihr Predator *Pseudoamphileptus macrostoma* (Chen, 1955) nov. gen. (Pleurostomatida: Amphileptidae). *Zool. Jb. Syst.* 110, 399–418.

Foissner, W. (1984). Taxonomie und Ökologie einiger Ciliaten (*Protozoa*, *Ciliophora*) des Saprobiensystems. I. Genera Litonotus, Amphileptus, Opisthodon. *Hydrobiologia* 119, 193–208. doi: 10.1007/bf00015210

Foissner, W. (1999). Protist diversity: estimates of the near-imponderable. *Protist* 150, 363–368. doi: 10.1016/s1434-4610(99)70037-4

Foissner, W., Berger, H., Blatterer, H. and Kohmann, F. (1995). Taxonomische und ökologische revision der Ciliaten des Saprobiensystems-Band IV: Gymnostomatea, Loxodes, Suctoria. *Landesamtes für Wasserwirtsch.* 1, 1–540.

Foissner, W., and Hawksworth, D. L. (2009). *Protist Diversity and Geographical Distribution*. Dordrecht: Springer.

Foissner, W., and Leipe, D. (1995). Morphology and ecology of *Siroloxophyllum utriculariae* (Penard, 1922) n. g., n. comb. (Ciliphora, Pleurostomatida) and an improved classification of pleurostomatid ciliates. *J. Eukaryot. Microbiol.* 42, 476–490. doi: 10.1111/j.1550-7408.1995.tb05894.x

Fryd-Versavel, G., Lftode, F., and Dragesco, J. (1975). Contribution à la connaissance de quepques ciliés gymnostomes. II. Prostomiens, pleurostomiens: morphologie, stomatogènésc. *Protistologica* 6, 509–530.

Gao, F., Warren, A., Zhang, Q. Q., Gong, J., Miao, M., Sun, P., et al. (2016). The all-data-based evolutionary hypothesis of ciliated protists with a revised classification of the phylum Ciliophora (Eukaryota, Alveolata). *Sci. Rep.* 6:24874.

Gao, S., Song, W. B., Ma, H. W., Clamp, J. C., Yi, Z. Z., Al-Rasheid, K. A. S., et al. (2008). Phylogeny of six genera of the subclass Haptoria (Ciliophora, Litostomatea) inferred from sequences of the gene coding for small subunit ribosomal RNA. *J. Eukaryot. Microbiol.* 55, 562–566. doi: 10.1111/j.1550-7408.2008.00360.x

Henderson, W. D. (1905). "Notes on the infusoria of freiburg in breigau," in *Zoologischer Anzeiger*, ed. E. Korschelt (Leipzig: Wilhelm Engelmann), 1–24.

Hu, X. Z., Lin, X. F., and Song, W. B. (2019). *Ciliates Atlas: Species Found in the South China Sea*. Beijing: Science Press.

Kahl, A. (1931). Urtiere oder protozoa i: wimpertiere oder ciliata (Infusoria) 2. Holotricha außer den im 1. Teil behandelten Prostomata. *Tierwelt Dtl.* 21, 181–398.

Kahl, A. (1933). "Ciliata libera et ectocommensalia," in *Die Tierwelt der Nord-und Ostsee, Lief 23 (Teil P, c3)*, eds G. Grimpe and E. Wagler (Leipzig: Geest & Portig), 29–146.

Kim, J. H., and Jung, J. H. (2017). Brief descriptions of 12 ciliate species previously unrecorded (Protozoa: Ciliophora) in Korea. *J. Species Res.* 6, 15–25.

Kishino, H., and Hasegawa, M. (1989). Evaluation of the maximum likelihood estimate of the evolutionary tree topologies from DNA sequence data, and the branching order in Hominoidea. *J. Mol. Evol.* 29, 170–179. doi: 10.1007/bf02100115

Li, L. X. (1990). A new species of ciliates, *Hemiophrys polymicronuclei* sp. nov. from Donghu lake, Hubei province. *Chin. J. Oceanol. Limnol.* 8, 97–100. doi: 10.1007/bf02846456

Lin, X. F., Li, J. Q., Gong, J., Warren, A., and Song, W. (2008). Taxonomic studies on three marine pleurostomatid ciliates, *Litonotus bergeri* nov. spec., *L. blattereri* nov. spec. and *L. petzi* nov. spec. (Ciliophora, Pleurostomatida) from North China sea. *Eur. J. Protistol.* 44, 91–102. doi: 10.1016/j.ejop.2007.08.005

Lin, X. F., and Song, W. B. (2004). Establishment of a new amphileptid genus, *Apoamphileptus* nov. gen. (Ciliophora, Litostomatea, Pleurostomatida), with description of a new marine species, *Apoamphileptus robertsi* nov. spec. from Qingdao, China. *J. Eukaryot. Microbiol.* 51, 618–625. doi: 10.1111/j.1550-7408.2004.tb00595.x

Lin, X. F., Song, W. B., and Li, J. Q. (2007a). *Amphileptus aeschtae* nov. spec. and *Amphileptus eigneri* nov. spec. (Ciliophora, Pleurostomatida), two new marine pleurostomatid ciliates from China. *Eur. J. Protistol.* 43, 77–86. doi: 10.1016/j.ejop.2006.10.002

Lin, X. F., Song, W., and Li, J. Q. (2007b). Description of two new marine pleurostomatid ciliates, *Loxophyllum choii* nov. spec. and *L. shini* nov. spec. (Ciliophora, Pleurostomatida) from China. *Eur. J. Protistol.* 43, 131–139. doi: 10.1016/j.ejop.2006.12.004

Lin, X. F., Song, W. B., and Warren, A. (2005a). Taxonomic studies on three marine pleurostomatid ciliates: *Kentrophyllum verrucosum* (Stokes, 1893) Petz, Song et Wilbert, 1995, *Epiphyllum soliforme* (Fauré-Frémiet, 1908) gen. n., comb. n. and *Amphileptus sikorai* sp. n., with the establishment of a new genus Epiphyllum (Ciliophora: Pleurostomatida). *Acta Protozool.* 44, 129–145.

Lin, X. F., Song, W. B., and Warren, A. (2005b). Two new marine pleurostomatid ciliates from China, *Amphileptus gui* nov. spec. and *Amphileptus yuianus* nov. spec. (Ciliophora, Pleurostomatida). *Eur. J. Protistol.* 41, 163–173. doi: 10.1016/j.ejop.2005.01.002

Lin, X. F., Song, W. B., and Warren, A. (2009). "Pleurostomatids," in *Free-living Ciliates in the Bohai and Yellow Seas*, eds W. B. Song, X. Z. Hu, and A. Warren (Beijing: Science Press), 93–134.

Liu, M. J., Wang, C. D., Hu, X. Z., Qu, Z. S., Jiang, L. M., Al-Farraj, S. A., et al. (2020). Taxonomy and molecular phylogeny of three species of scuticociliates from China: *Citrithrix smalli* gen. nov., sp. nov., *Homalogastra binucleata* sp. nov. and *Uronema orientalis* Pan et al., 2015 (Protozoa, Ciliophora, Oligohymenophorea), with the proposal of a new family, Citrithrixidae fam. nov. *Front. Mar. Sci.* 7:604704.

Liu, W. W., Jiang, J. M., Tan, Y. H., and Lin, X. F. (2020). Novel contributions to the taxonomy of the ciliates genus *Euplotes* (Ciliophora, Euplotida): redescription of two poorly known species, with a brief note on the distributions of this genus in coastal waters of southern China. *Front. Mar. Sci.* 7:615413.

Liu, W. W., Jiang, J. M., Xu, Y., Pan, X. M., Qu, Z. S., Luo, X. T., et al. (2017). Great diversity in marine ciliates: fauna studies in China seas during the years 2011–2016. *Eur. J. Protistol.* 61, 424–438. doi: 10.1016/j.ejop.2017.04.007

Liu, W. W., Zhang, K. X., Chen, C. Z., Li, J. Q., Tan, Y. H., Warren, A., et al. (2019). Overview of the biodiversity and geographic distribution of aloricate oligotrich ciliates (Protozoa, Ciliophora, Spirotrichea) in coastal waters of southern China. *Syst. Biodivers.* 17, 787–800. doi: 10.1080/14772000.2019.1691081

Lynn, D. (2008). *The Ciliated Protozoa, Characterization, Classification, and Guide to the Literature*. Dordrecht: Springer.

Ma, Z. H., Dong, T. Y., Liao, W. Y., Fan, X. P., Xu, Y., and Gu, F. K. (2019). Ciliates in the marsh wetlands of Chongming island: taxonomy of five species and a species list. *J. Ocean Univ. China* 18, 441–454. doi: 10.1007/s11802-019-3804-y

Masoumian, M., Pazouki, J., Yahyazadeh, M., and Teymornezhad, A. (2005). Protozoan from freshwater fishes from north west of Iran. *Iran. J. Fish. Sci.* 4, 31–42. doi: 10.1201/b18534-6

Maupas, E. (1883). Contribution à l'étude morphologique et anatomique des infusoires ciliés. *Arch. Zool. Exp. 2. Ser. T.* 1, 513–516.

Mitchell, A. J., and Smith, C. E. (1988). *Amphileptus branchiarum* (Protozoa: Amphileptidae) in pond reared fish in Arkansas. *J. Wildl. Dis.* 24, 642–646. doi: 10.7589/0090-3558-24.4.642

Nylander, J. (2004). *MrModeltest version 2. Distributed by the Author*. Uppsala: Evolutionary Biology Centre, Uppsala University.

Pan, H. B., Gao, F., Lin, X. F., Warren, A., and Song, W. B. (2013). Three new *Loxophyllum* species (Ciliophora: Pleurostomatida) from China with a brief review of the marine and brackish *Loxophyllum* species. *J. Eukaryot. Microbiol.* 60, 44–56. doi: 10.1111/jeu.12005

Pan, H. B., Li, L. F., Lin, X. F., Li, J. Q., Al-Farraj, S. A., and Al-Rasheid, K. A. S. (2014). Morphology of three species of *Amphileptus* (Protozoa, Ciliophora, Pleurostomatida) from the South China sea, with note on phylogeny of a. dragescoi sp. n. *J. Eukaryot. Microbiol.* 61, 644–654. doi: 10.1111/jeu.12146

Pan, H. B., Li, L. F., Wu, L., Miao, M., Al-Rasheid, K. A. S., and Song, W. B. (2015). Morphology of three *Litonotus* species (Ciliophora: Pleurostomatida) from China seas, with brief notes on their SSU rDNA-based phylogeny. *Eur. J. Protistol.* 51, 494–506. doi: 10.1016/j.ejop.2015.08.003

Pan, H. B., Zhang, Q. Q., Dong, J. Y., and Jiang, J. M. (2020). Morphology and phylogeny of two novel pleurostomatids (Ciliophora, Litostomatea), establishing a new genus. *J. Eukaryot. Microbiol.* 67, 252–262. doi: 10.1111/jeu.12779

Pan, H., Gao, F., Li, J. Q., Lin, X. F., Al-Farraj, S. A., and Al-Rasheid, K. A. S. (2010). Morphology and phylogeny of two new pleurostomatid ciliates, *Epiphyllum shenzhenense* n. sp. and *Loxophyllum spirellum* n. sp. (*Protozoa*, *Ciliophora*) from a mangrove wetland, south China. *J. Eukaryot. Microbiol.* 57, 421–428. doi: 10.1111/j.1550-7408.2010.00492.x

Qu, Z. S., Li, L. F., Lin, X. F., Stoeck, T., Pan, H. B., Al-Rasheid, K. A. S., et al. (2018). Diversity of the cyrtophorid genus Chlamydodon (Protista, Ciliophora): its systematics and geographic distribution, with taxonomic descriptions of three species. *Syst. Biodivers.* 16, 497–511. doi: 10.1080/14772000.2018.1456493

Ronquist, F., and Huelsenbeck, J. (2003). MrBayes 3: bayesian phylogenetic inference under mixed models. *Bioinformatics* 19, 1572–1574. doi: 10.1093/bioinformatics/btg180

Shimodaira, H., and Hasegawa, M. (2001). CONSEL: for assessing the confidence of phylogenetic tree selection. *Bioinformatics* 17, 1246–1247. doi: 10.1093/bioinformatics/17.12.1246

Small, E. B., and Lynn, D. H. (1981). A new macrosystem for the Phylum Ciliophora Doflein, 1901. *BioSystems* 14, 387–401.

Song, W. B. (1991). A new marine ciliate, *Amphileptus litonotiformis* nov. sp. (Protozoa Ciliophora). *Chin. J. Oceanol. Limnol.* 9, 300–305. doi: 10.1007/bf02850645

Song, W. B., and Wilbert, N. (1989). Taxonomische untersuchungen an aufwuchsciliaten (Protozoa, Ciliophora) im Poppelsdorfer Weiher, Bonn. *Lauterbornia* 3, 2–221.

Song, W. B., Warren, A., and Hu, X. Z. (2009). *Free-living Ciliates in the Bohai and Yellow Seas*. Beijing: Science Press.

Sonntag, B., and Foissner, W. (2004). *Urotricha psenneri* n. sp. and *Amphileptus piger* (Vuxanovici, 1962) n. comb., two planktonic ciliates (*Protozoa*, *Ciliophora*) from an oligotrophic lake in Austria. *J. Eukaryot. Microbiol.* 51, 670–677. doi: 10.1111/j.1550-7408.2004.tb00607.x

Stamatakis, A., Hoover, P., and Rougemont, J. (2008). A fast boostrap algorithm for the RAxML web-servers. *Syst. Biol.* 57, 758–771. doi: 10.1080/10635150802429642

Stokes, A. C. (1884). Notices of new fresh-water infusoria. *Am. Mon. Microsc. J.* 5, 121–125.

Swofford, D. (2002). *PAUP*. Phylogenetic Analysis using Parsimony (*and other Methods). Version 4*. Sunderland, MA: Sinauer Associates.

Vďačný, P., and Rajter, L. (2014). An annotated and revised checklist of pleurostome ciliates (Protista: Ciliophora: Litostomatea) from Slovakia, central Europe. *Zootaxa* 3760, 501–521. doi: 10.11646/zootaxa.3760.4.1

Vďačný, P., Bourland, W. A., Orsi, W., Epstein, S. S., and Foissner, W. (2011). Phylogeny and classification of the Litostomatea (Protista, Ciliophora), with emphasis on free-living taxa and the 18S rRNA gene. *Mol. Phylogenet. Evol.* 59, 510–522. doi: 10.1016/j.ympev.2011.02.016

Vďačný, P., Rajter, L., Shazib, S. U. A., Jang, S. W., Kim, J. H., and Shin, M. K. (2015). Reconstruction of evolutionary history of pleurostomatid ciliates (Ciliophora, Litostomatea, Haptoria): interplay of morphology and molecules. *Acta Protozool.* 54, 9–29.

Vďačný, P. (2015). Estimation of divergence times in litostomatean ciliates (Ciliophora: Intramacronucleata), using Bayesian relaxed clock and 18S rRNA gene. *Eur. J. Protistol.* 51, 321–334. doi: 10.1016/j.ejop.2015.06.008

Vďačný, P., and Foissner, W. (2012). Monograph of the dileptids (Protista, Ciliophora, Rhynchostomatia). *Denisia* 31, 1–529.

Vďačný, P., and Foissner, W. (2013). Synergistic effects of combining morphological and molecular data in resolving the phylogenetic position of Semispathidium (Ciliophora, Haptoria) with description of *Semispathidium breviarmatum* sp. n. from tropical Africa. *Zool. Scr.* 42, 529–549. doi: 10.1111/zsc.12023

Vďačný, P., Breiner, H. W., Yashchenko, V., Dunthorn, M., Stoeck, T., and Foissner, W. (2014). The chaos prevails: molecular phylogeny of the Haptoria (Ciliophora, Litostomatea). *Protist* 165, 93–111. doi: 10.1016/j.protis.2013.11.001

Vuxanovici, A. (1960). Contribitii la studiul grupei subgenurilor litonotus-hemiophrys (Ciliata).*Studii Cerc. Biol.* 12, 125–139.

Vuxanovici, A. (1961). Noi contributii la studiul ciliatelor dulcicole din Republica Polularia Romina (Nota I). *Studii Cerc. Biol.* 12, 353–381.

Wang, C. C. (1934). Notes on the marine infusoria of Amoy. *Rep. Mar. Biol. Assoc. China* 3, 50–70.

Wang, C. C. (1940). Notes on some new fresh-water infusoria. *Sinensia* 11, 11–32.

Wang, C. C., and Nie, D. S. (1932). A survey of the marine protozoa of Amoy. *Contr. Biol. Lab Sci. Soc. China Zoological Series* 8, 285–385.

Wang, C. C., and Nie, D. S. (1933). Report on the rare and new species of fresh-water infusoria, part I. *Contr. Biol. Lab Sci. Soc. China Zoological Series* 10, 1–99.

Wenrich, D. H. (1924). A new protozoan parasite, *Amphileptus branchiarum* n. sp., on the gills of tadpoles. *Trans. Am. Microsc. Soc.* 43, 191–199. doi: 10.2307/3221736

Wilbert, N. (1975). Eine Verbesserte technik der protargolimprägnation für ciliaten. *Mikrokosmos* 64, 171–179.

Wilbert, N., and Song, W. (2005). New contribution to the marine benthic ciliates from the Antarctic area, including description of seven new species (Protozoa, Ciliophora). *J. Nat. Hist.* 39, 935–973. doi: 10.1080/00222930400001509

Wu, L., Chen, R., Yi, Z. Z., Li, J. Q., Warren, A., and Lin, X. F. (2013). Morphology and phylogeny of three new *Loxophyllum* species (Ciliophora, Pleurostomatida) from mangrove wetlands of southern China. *J. Eukaryot. Microbiol.* 60, 267–281. doi: 10.1111/jeu.12032

Wu, L., Chen, R., Yi, Z. Z., Li, J. Q., Warren, A., and Lin, X. F. (2014). The morphology of three *Loxophyllum* species (*Ciliophora*, Pleurostomatida) from southern China, *L. lembum* sp. n., *L. vesiculosum* sp. n. and *L. perihoplophorum* Buddenbrock, 1920, with notes on the molecular phylogeny of *Loxophyllum*. *J. Eukaryot. Microbiol.* 61, 115–125. doi: 10.1111/jeu.12089

Wu, L., Clamp, J. C., Yi, Z. Z., Li, J. Q., and Lin, X. F. (2015a). Phylogenetic and taxonomic revision of an enigmatic group of haptorian ciliates, with establishment of the Kentrophyllidae fam. n. (Protozoa, Ciliophora, Litostomatea, Pleurostomatida). *PloS One* 10:e0123720. doi: 10.1371/journal.pone.0123720

Wu, L., Jiao, X. X., Shen, Z., Yi, Z. Z., Li, J. Q., Warren, A., et al. (2017). New taxa refresh the phylogeny and classification of pleurostomatid ciliates (Ciliophora, Litostomatea). *Zool. Scr.* 46, 245–253. doi: 10.1111/zsc.12193

Wu, L., Yi, Z. Z., Li, J. Q., Warren, A., Xu, H. L., and Lin, X. F. (2015b). Two new brackish ciliates, *Amphileptus spiculatus* sp. n. and *A. bellus* sp. n. from mangrove wetlands in southern China, with notes on the molecular phylogeny of the family Amphileptidae (Protozoa, Ciliophora, Pleurostomatida). *J. Eukaryot. Microbiol.* 62, 662–669. doi: 10.1111/jeu.12225

Zhang, Q. Q., Simpson, A., and Song, W. B. (2012). Insights into the phylogeny of systematically controversial haptorian ciliates (Ciliophora, Litostomatea) based on multigene analyses. *Proc. Royal Soc. B* 279, 2625–2635. doi: 10.1098/rspb.2011.2688

Conflict of Interest: The authors declare that the research was conducted in the absence of any commercial or financial relationships that could be construed as a potential conflict of interest.

frontiers in Marine Science

ORIGINAL RESEARCH
published: 26 February 2021
doi: 10.3389/fmars.2021.625644

Gastronautidae Deroux, 1994 and *Trithigmostoma* Jankowski, 1967: Evolutionary Links Among Cyrtophorian Ciliates (Protista, Ciliophora, and Phyllopharyngea)

*Zhishuai Qu[1,2], Hongbo Pan[3], Congcong Wang[1], Honggang Ma[1], Thorsten Stoeck[2] and Xiaozhong Hu[1]**

[1] *Key Laboratory of Mariculture, Ministry of Education, Institute of Evolution and Marine Biodiversity, Ocean University of China, Qingdao, China,* [2] *Department of Ecology, Technische Universität Kaiserslautern, Kaiserslautern, Germany,* [3] *Shanghai Universities Key Laboratory of Marine Animal Taxonomy and Evolution, Shanghai Ocean University, Shanghai, China*

OPEN ACCESS

Edited by:
Zhijun Dong, Yantai Institute of Coastal Zone Research (CAS), China

Reviewed by:
Jae-Ho Jung, Gangneung–Wonju National University, South Korea
Ming Li, Institute of Hydrobiology (CAS), China

***Correspondence:**
Xiaozhong Hu
xiaozhonghu@ouc.edu.cn

Specialty section:
This article was submitted to Marine Evolutionary Biology, Biogeography and Species Diversity, a section of the journal Frontiers in Marine Science

Received: *03 November 2020*
Accepted: *09 February 2021*
Published: *26 February 2021*

Citation:
Qu Z, Pan H, Wang C, Ma H, Stoeck T and Hu X (2021) Gastronautidae Deroux, 1994 and Trithigmostoma Jankowski, 1967: Evolutionary Links Among Cyrtophorian Ciliates (Protista, Ciliophora, and Phyllopharyngea). Front. Mar. Sci. 8:625644. doi: 10.3389/fmars.2021.625644

Studies on cyrtophorian ciliates (Cyrtophoria) have accumulated much knowledge on morphological taxonomy and molecular phylogeny, and the general classification and phylogenetic relationships of most families have thereby been revealed. However, the phylogenetic position of the family Gastronautidae Deroux, 1994 remains uncertain. This is due to the presence of specialized characteristics (in particular a circumoral kinety in a closed circle), and most importantly, the lack of molecular data of this family. In addition, *Trithigmostoma* Jankowski, 1967 holds a special position among genera in Chilodonellidae Deroux, 1976 due to its divergent characteristics. In the present work, we studied a new gastronautid, *Gastronauta paraloisi* sp. n., and three populations of *Trithigmostoma cucullulus* (Müller, 1786) Jankowski, 1967, using integrative methods. Species identifications were confirmed by morphological research. We also obtained SSU rDNA sequences, which included the first available sequence of Gastronautidae. The following SSU rDNA-inferred phylogenetic analyses showed that the establishment of the family Gastronautidae is necessary, and Gastronautidae and *Trithigmostoma* may represent intermediate evolutionary links in the order Chlamydodontida.

Keywords: ciliate, *Gastronauta*, Gastronautidae, morphology, phylogeny, *Trithigmostoma*

INTRODUCTION

Subclass Cyrtophoria Fauré-Fremiet in Corliss, 1956 is a group of highly specialized and divergent ciliated protistans. Most cyrtophorian ciliates constitute important components of the aquatic periphytic community and can be found in various habitats like freshwater, marine and brackish waters (Kahl, 1931; Deroux, 1976a,b; Foissner et al., 1991; Petz et al., 1995; Jankowski, 2007; Song et al., 2009; Xu et al., 2016; Pan et al., 2017). The morphology-based taxonomy and classification of the cyrtophorians have been studied intensively in the last five decades, and a comprehensive

knowledge has accumulated (e.g., Deroux, 1976a,b, 1994; Gong et al., 2002, 2007; Gong and Song, 2004; Pan et al., 2013, 2016; Qu et al., 2017, 2018a; Chen et al., 2018; Wang et al., 2019). Over the past 20 years, with the employment of phylogenetic analyses inferred from small-subunit ribosome gene (SSU rDNA) sequences, the basic systematic relationship of Cyrtophoria has gradually been revealed. It has generally been in accordance with the morphological classification (Snoeyenbos-West et al., 2004; Lynn, 2008; Gao et al., 2012; Chen et al., 2016; Wang et al., 2017; Qu et al., 2018b; Hu et al., 2019). The relatively well-matching molecular phylogeny and morphological traits make cyrtophorian ciliates potential candidates for evolutionary research. However, only a few studies have looked at the evolutionary relationships among cyrtophorian ciliates based on both molecular phylogeny and morphological data (Gao et al., 2012; Chen et al., 2016). In addition, a lack of data on some key taxa largely restrains the evolutionary resolution and makes many details obscure (Chen et al., 2016).

The main obstacles faced by the cyrtophorian taxonomists are the same as those with other ciliate groups: (1) The sampling is insufficient inferring that a number of species still remain undiscovered, especially from "extreme" environments like hypersaline waters and hot springs. (2) Incomplete and vague descriptions of some known species make the species identification difficult. (3) A lack of molecular data for some intermediate taxa and even some well-known type species largely obstructs the phylogenetic and evolutionary analysis. Therefore, massive sampling along with a combined study tool of morphological observation and gene marker analysis is required to address these issues (Warren et al., 2017).

During a faunal investigation targeting cyrtophorian ciliates in China, we isolated a ciliate belonging to a rarely studied genus, *Gastronauta* Engelmann in Bütschli, 1889, and three populations of *Trithigmostoma cucullulus* (Müller, 1786) Jankowski, 1967. *Gastronauta* is a highly specialized but species-poor cyrtophorid genus. Its most diagnostic characteristic is its elongated oral slit surrounded by a circle of kinetids, which makes it unique among all cyrtophorians (for example, Bütschli, 1889; Kahl, 1931; Nie & Ho, 1943; Wilbert, 1971; Deroux, 1976b; Song and Wilbert, 1989; Foissner et al., 1991; Blatterer & Foissner, 1992; Oberschmidleitner & Aescht, 1996; Xu et al., 2016). The highly specialized oral structure, as well as the combination of several intermediate characteristics, obscures the systematic assignment of *Gastronauta*, but also indicates its potentially special phylogenetic position. Unfortunately, the SSU rDNA sequence of this genus is unavailable yet. Thus, this family has not been included in phylogenetic analyses. In this paper, we describe a new species, *G. paraloisi* sp. n., and *Trithigmostoma cucullulus* morphologically. More importantly, we also provide three SSU rDNA sequences, with a focus on that of Gastronautidae, and analyze their phylogenetic and evolutionary positions. The results indicate that the establishment of the family Gastronautidae by Deroux (1994) is necessary, and Gastronautidae and *Trighigmostoma* present as intermediate groups in evolution, within the order Chlamydodontida.

MATERIALS AND METHODS

Sampling and Cultivation

Gastronauta paraloisi sp. n. and a population of *Trithigmostoma cucullulus* were isolated from a water sample taken from the surface of a freshwater river in Shenzhen, China (22°33′59.57″N, 114°6′52.80″E). The river lays in the inner city and influxes into a sea gulf approximately 10 kilometers away. This river receives household sewage water, and is thus nutrient-rich. The second population of *T. cucullulus* was isolated from an artificial freshwater lake in Qingdao, China (36°3′49.66″N, 120°20′42.86″E). The third population of *T. cucullulus* was found in a puddle near the coast in Zhanjiang, China (21°16′3.80″N, 110°25′31.08″E). The water salinity was about 3‰, and the sample was taken by scratching the substrate that contained diatoms. Immediately after the sampling, the ciliates were maintained by adding rice grains to the originally collected indigenous water in bottles. The attempt to obtain the pure culture with distilled water or Volvic water and rice grains failed. Instead, raw cultures were established by adding rice grains to Petri dishes filled with indigenous water (filtered through 0.65 μm-membranes to maintain indigenous bacteria). The rice grains supported the growth of bacteria as a food source for ciliates.

Morphological Studies

Living cells collected from raw cultures were observed using bright field and differential interference contrast microscopy (Olympus BX53). Wilbert's (1975) protargol-staining method was applied to reveal the ciliature pattern and nuclear apparatus. Morphometric measurement was mainly conducted on specimens after protargol preparation. Illustrations of live specimens were based on photomicrographs and notes, while those of protargol-stained cells were made with the aid of a drawing device and photomicrographs. Terminology mainly follows Foissner (2000), and classification system refers to Lynn (2008).

DNA Extraction, Amplification, and Sequencing

For each of the ciliates, one single cell was picked from the raw culture under a stereomicroscope (SZH-ILLD-200, Olympus, Japan) and washed three times with distilled water in order to remove eukaryotic contaminants. The cell was then immediately transferred into a 1.5 ml-tube with 60 μl ATL buffer (Qiagen, Hilden, Germany). Genomic DNA was then extracted using the DNeasy Tissue Kit (Qiagen, Hilden, Germany) following the manufacturer's instructions for animal tissues. Fifty ng of DNA (measured with a NanoDrop2000, peQLab, Biotechnology GmbH, Germany) from the extract were used for the subsequent amplification of the 18S rDNA. Q5 Hot Start High-Fidelity DNA Polymerase (New England Biolabs Inc., United States) and the primer pair EukA and EukB (Medlin et al., 1988) were used for PCR. Obtained amplicons were purified with the MinElute kit (Qiagen, Germany) and then sent directly for sequencing. Bi-directional Sanger sequencing was done to obtain

a near-complete 18S rDNA sequence (Pan et al., 2019). The NCBI accession numbers of the assembled sequences of *Gastronauta paraloisi* sp. n., as well as the Qingdao and Zhanjiang populations of *Trithigmostoma cucullulus* are MW072507, MW116158, and MW116159, respectively. Sequence similarities were calculated using BioEdit 7.0.9.0.

Phylogenetic Analyses

With the newly obtained 18S rDNA sequences included in the present work, a total of 80 SSU rDNA sequences were used for the phylogenetic analyses (accession numbers shown in **Table 1**). Three Suctoria species, *Acineta compressa*, *Ephelota gemmipara* and *Prodiscophrya* sp., were selected as outgroups, as they are phylogenetically close to Cyrtophoria. Sequences were aligned using the MUSCLE package on the European Bioinformatics Institute website[1]. The resulting alignment was then manually edited by trimming both ends. This resulted in a consensus matrix of 1,721 nucleotide positions. Two phylogenetic tools were used. A maximum-likelihood (ML) analysis was constructed with 1,000 bootstrap replicates using RAxML-HPC2 v. 8.2.12 (Stamatakis, 2014) online (CIPRES Science Gateway; Miller et al., 2010), with the evolutionary model GTR + I + Γ. A Bayesian inference (BI) analysis was run using the MrBayes on XSEDE 3.2.7a package (Ronquist and Huelsenbeck, 2003) on the CIPRES Science Gateway; optional model was GTR + I + Γ, selected using MrModeltest 2.2 with the criterion of Akaike Information Criterion (Nylander, 2004). Markov chain Monte Carlo simulations were run for ten million generations with a sample frequency of every 100th generations; the first 10% of the simulations were discarded as burn-in. The topology of the best ML tree was visualized using MEGA 5.0 (Tamura et al., 2011).

RESULTS

Taxonomy and Morphological Description of the New Species

Phyllopharyngea de Puytorac et al., 1974
Cyrtophoria Fauré-Fremiet in Corliss, 1956
Chlamydodontida Deroux, 1976
Gastronautidae Deroux, 1994
Gastronauta Engelmann in Bütschli, 1889
Gastronauta paraloisi sp. n.
Synonym: *Gastronauta membranaceus* sensu da Silva and da Silva-Neto, 2001

Diagnosis

Cell size 50–120 × 30–80 μm *in vivo*. Body oval to ellipsoid with both ends broadly rounded. Macronucleus positioned at mid-body or slightly below. Two contractile vacuoles in diagonal positions. 18 or 19 kineties on postoral area, including 12 right and six or seven left kineties; two innermost right kineties anteriorly curved leftward, and the anterior ends of innermost right and left kinety almost confluent; outermost left kinety interrupted by oral slit. Three arc kineties above oral slit. Usually three vertical fragments, three or four terminal fragments. Freshwater and saprobic habitat.

Type Locality

The surface layer of a freshwater river in Shenzhen, China (22°33′59.57″N, 114°6′52.80″E), which receives household sewage water.

Type Material

One holotype slide with protargol-stained specimens was deposited in the Laboratory of Protozoology, Ocean University of China, with the accession number QZS2015120202.

Etymology

The species-group name *paraloisi* is a composite of the Greek prefix *par-* (closely related, beside) and the species-group name *aloisi*, indicating that the new species morphologically resembles *Gastronauta aloisi* Oberschmidleitner & Aescht (1996).

ZooBank Accession Number of the New Species

urn:lsid:zoobank.org:act:61698C4E-0FC8-4F45-A4FE-9B26AACFE4B3.

Morphological Description (Figures 1, 2 and Table 2)

Cell size 60–120 × 30–80 μm *in vivo*, and on average 68.4 × 44.9 μm after protargol-staining ($n = 24$). Body oval to ellipsoid with both ends broadly rounded (**Figures 1A,B,D,E**, **2G,H**); dorsoventrally compressed, dorsal side conspicuously humped and ventral side concave. Cell acontractile but flexible. Anterior periphery thin and more transparent. Oral slit about 30 μm in width, slightly obliquely oriented and located in anterior third of cell, extending from approximate left margin to right of midline on ventral side (**Figures 1A,D,E**); oral membrane lamellar *in vivo*; pharyngeal fibers visible after protargol-staining, but individual nematodesmal rods not recognizable. Centrally heteromeric macronucleus about 25 × 15 μm *in vivo* (**Figure 1A**) and about 24 × 13 μm after protargol-staining (**Figures 1I**, **2A–F**), positioned in mid-body or slightly below equator. Micronucleus not detected *in vivo*, but can be seen attached to macronucleus after protargol-staining, about 4 μm across (**Figure 1I**). Two contractile vacuoles in ordinary diagonal positions (**Figures 1A,B,D,E**, **2H**), each approximately 10 μm across, pulsating at an interval of 10–30 s ($n = 2$); excretory pores recognizable after protargol-stating, anterior pore between second and third inner right kineties and posterior pore between fourth and fifth left kineties (**Figure 1I**). Cytoplasm transparent and colorless to grayish, containing many small (about 1–2 μm across) greenish to yellowish algae and colorless food vacuoles. Usually crawling slowly on substrate, and adhering to substrate firmly on concaved ventral side when disturbed; seldom swimming in water.

Ciliary pattern as shown in **Figures 1C,I**, **2A–C**. In total, 18 or 19 (mostly 18) kineties on postoral (below oral slit) area, including 12 right and six or seven left kineties; a conspicuous barren gap (10–20 μm wide) present between right and left kineties. Usually seven outermost right kineties exceeding the level of oral slit and bending leftward anteriorly; remaining five (one out of 24 specimens contains six) right kineties commencing anteriorly below oral slit (postoral right kineties), of which two

[1]http://www.ebi.ac.uk

TABLE 1 | GenBank accessions of SSU rDNA sequences used in the phylogenetic analyses.

Species	Accession number	Species	Accession number
Acineta compressa	FJ865205	*Dysteria paraprocera*	KM103263
Aegyria foissneri	KX364493	*Dysteria pectinata*	FJ870068
Aegyria oliva sp. 1	FJ998029	*Dysteria proraefrons*	KM103261
Aegyria oliva sp. 2	FJ998028	*Dysteria semilunaris*	KX258194
Agnathodysteria littoralis	KC753482	*Dysteria* sp.1	AY331797
Atopochilodon distichum	KT461933	*Dysteria* sp. 2	AY331800
Brooklynella sinensis	KC753483	*Dysteria* sp. 3	FJ868205
Chilodonella acuta	KJ452458	*Dysteria subtropica*	KC753494
Chilodonella parauncinata	KJ509107	*Ephelota gemmipara*	EU600180
Chilodonella uncinata	AF300281	***Gastronauta paraloisi* sp. n.**	**MW072507**
Chlamydodon bourlandi	MG566059	*Hartmannula derouxi*	AY378113
Chlamydodon caudatus	JQ904058	*Hartmannula sinica*	EF623827
Chlamydodon exocellatus	AY331790	*Heterohartmannula fangi*	FJ868204
Chlamydodon mnemosyne	FJ998031	*Lynchella minuta*	KX364494
Chlamydodon obliquus	FJ998030	*Lynchella nordica*	FJ868203
Chlamydodon oligochaetus	KY496620	*Lynchella* sp.	FJ998036
Chlamydodon paramnemosyne	JQ904058	*Microxysma acutum*	FJ870069
Chlamydodon rectus	KT461932	*Mirodysteria decora*	JN86702
Chlamydodon salinus	JQ904057	*Odontochlamys alpestris biciliata*	KC753484
Chlamydodon similis	KY496621	*Paracyrtophoron tropicum*	FJ998035
Chlamydodon triquetrus pop. 1	MG566058	*Phascolodon vorticella*	KX258192
Chlamydodon triquetrus pop. 2	AY331794	*Pithites vorax*	FJ870070
Chlamydodon wilberti	MG566060	*Prodiscophrya* sp.	AY331802
Chlamydonella derouxi	KJ509198	*Pseudochilodonopsis fluviatilis* pop.1	JN867021
Chlamydonella irregularis	KC753486	*Pseudochilodonopsis fluviatilis* pop. 2	KR611083
Chlamydonella pseudochilodon	FJ998032	*Pseudochilodonopsis mutabilis* pop.1	KR611084
Chlamydonellopsis calkinsi	KC753487	*Pseudochilodonopsis mutabilis* pop.2	KC753498
Coeloperix sinica	FJ998034	*Pseudochilodonopsis quadrivacuolata*	KR611082
Coeloperix sleighi	KC753489	*Pseudochilodonopsis* sp.1	KC753495
Dysteria brasiliensis	EU242512	*Pseudochilodonopsis* sp. 2	KC753497
Dysteria compressa	KC753491	*Pseudochilodonopsis* sp.3	KC753496
Dysteria crassipes pop.1	FJ868206	*Spirodysteria kahli*	KC753499
Dysteria crassipes pop.2	KC753492	*Trichopodiella faurei*	EU515792
Dysteria crassipes pop.3	KC753493	***Trithigmostoma cucullulus***	**MW116158**
Dysteria cristata	KC753488	***Trithigmostoma cucullulus***	**MW116159**
Dysteria derouxi	AY378112	*Trithigmostoma cucullulus*	FJ998037
Dysteria lanceolata	KC753490	*Trithigmostoma steini*	X71134
Dysteria nabia pop.1	KM103262	*Trochilia petrani*	JN867016
Dysteria nabia pop.2	KF725634	*Trochilioides recta*	JN867017
Dysteria ovalis	KX258193	*Trochochilodon flavus*	JN867018

The three new sequences in present work are marked in bold.

innermost ones anteriorly curved leftward and the innermost joining the innermost left kinety anteriorly; almost all right kineties bending slightly leftward posteriorly and terminating sub-caudally. Left kineties anteriorly commencing below oral level and posteriorly shortened from right to left; outermost left kinety interrupted by oral slit Three or four terminal fragments (dorsal brush; cilia about 6 μm long) along left anterior margin of cell, each consisting of three to five basal bodies.

Oral ciliature composed of one circumoral kinety, which is closed and surrounds oral slit, as shown in **Figures 1I**, **2A,B**. Three arc kineties shortened from the outside in above oral slit; Usually three short vertical kineties (one of 24 specimens observed contained four) to left anterior of oral slit, extending from anterior ends of fourth to second right kinety to left of circumoral kinety; the innermost one slightly shorter. One short transverse fragment (preoral kinety) in front of vertical kineties, consisting of only three or four basal bodies. Fibers along the cell margins recognizable after protargol-staining (**Figure 1C**).

Morphogenesis

Several stages of morphogenesis were observed in protargol-stained specimens. In an early divider (**Figures 1F**, **2D**), the middle portions of the innermost four left kineties become thickened and curved inward, forming the opisthe's oral primordia; meanwhile, an equatorial fragment occurs to the right of right kineties. In a middle stage (**Figures 1G**, **2E**), equatorial

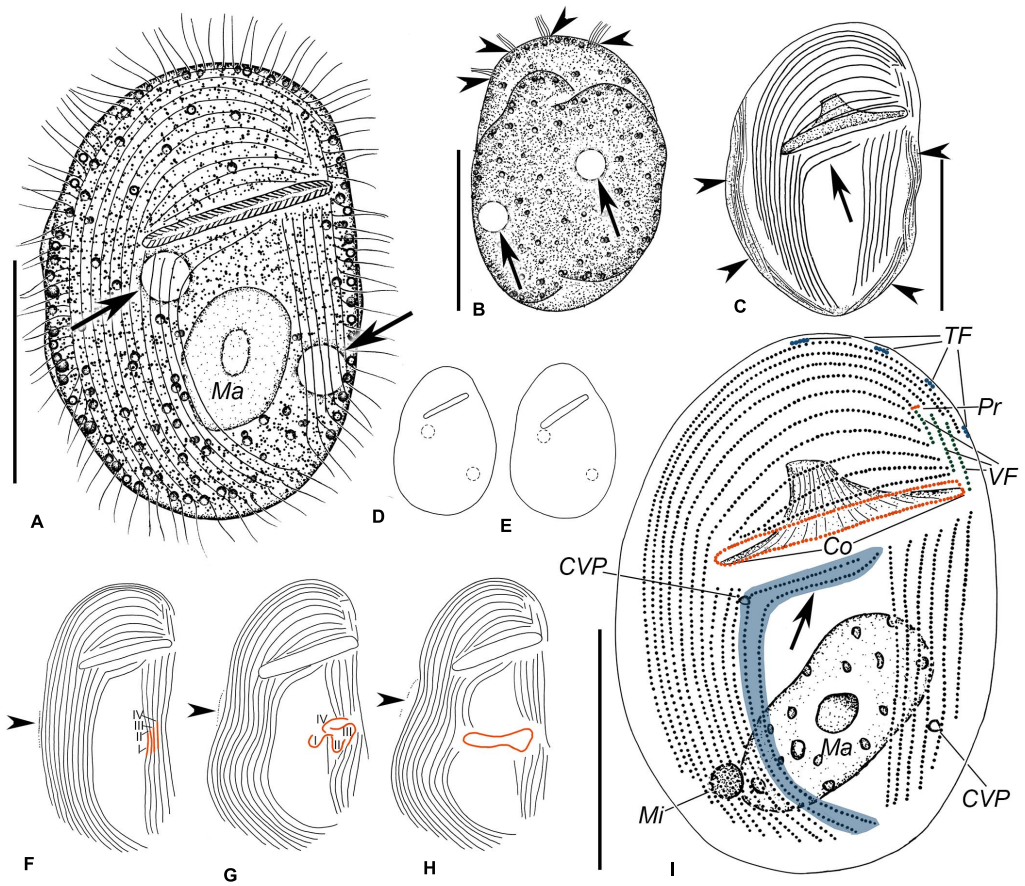

FIGURE 1 | Illustrations of *Gastronauta paraloisi* sp. n. from life **(A,B,D,E)** and after protargol-staining **(C,F–I)**. **(A)** Ventral view of a representative specimen. Arrows mark contractile vacuoles. **(B)** Dorsal view. Arrows indicate contractile vacuoles and arrowheads point to terminal fragments. **(C)** Ventral view of general ciliature; arrowheads denote the fibers along the cell margin after protargol-staining, and arrow shows the two curved postoral right kineties. **(D,E)** Body shape variations. **(F–H)** Several stages of morphogenesis. **(F)** Is an early stage, **(G)** is a middle stage, and **(H)** represents a late stage. Arrowheads indicate the equatorial fragment. I–IV represent anlagen I–IV. **(I)** Ventral overview of the ciliature. Arrow shows the two anteriorly curved right kineties, and special structures of *Gastronauta* are highlighted with different colors. Co, circumoral kinety; CVP, contractile vacuole pore; Ma, macronucleus; Mi, micronucleus; Pr, preoral kinety; TF, terminal fragments; and VF, vertical fragments. Scale bars: 30 μm.

fragment is elongated to form the anlage of opisthe's terminal fragments (dorsal brush). The four oral primordia then dispatch from their original left kineties: anlage IV drifts in an anti-clockwise direction followed by anlagen III, II and I in succession. The fifth left kinety is interrupted in the middle. The middle part of right kineties concave to the left. In a late divider (**Figures 1H**, **2F**), the four parts of the oral primordia merge to form the circumoral kinety of the opisthe. The outermost left kinety and the innermost two right kineties are interrupted in the middle. The anlage of terminal fragments develops into terminal fragments of the opisthe.

Taxonomy and Morphological Description of *Trithigmostoma cucullulus* (Müller, 1786) Jankowski, 1967

Chilodonellidae Deroux, 1970

Trithigmostoma Jankowski, 1967

Trithigmostoma cucullulus (Müller, 1786) Jankowski, 1967

Voucher Slides

Slides of the Qingdao, Zhanjiang and Shenzhen population of *Trithigmostoma cucullulus* were deposited in the Laboratory of Protozoology, Ocean University of China, with accession numbers QZS2015050601, QZS2015040301, and QZS2015120401, respectively.

Morphological Description of Qingdao Population (Figures 3A,B,D–F, 4C–E and Table 3)

Cell size 68–80 × 32–40 μm *in vivo*, and approximately 80 × 35 μm after protargol-staining. Body ellipsoid-shaped, both ends broadly rounded, inconspicuous protrusion located at left anterior end of cell (**Figures 3A,B**, **4E**); dorsoventrally compressed with a width: thickness ratio of about 2:1 (**Figure 3C**). Cell acontractile but flexible. Anterior body end transparent. Cytostome in anterior 1/4 to 1/3, surrounded by 11 to 13 (on average 12) nematodesmal rods (**Figures 3A,B,E**).

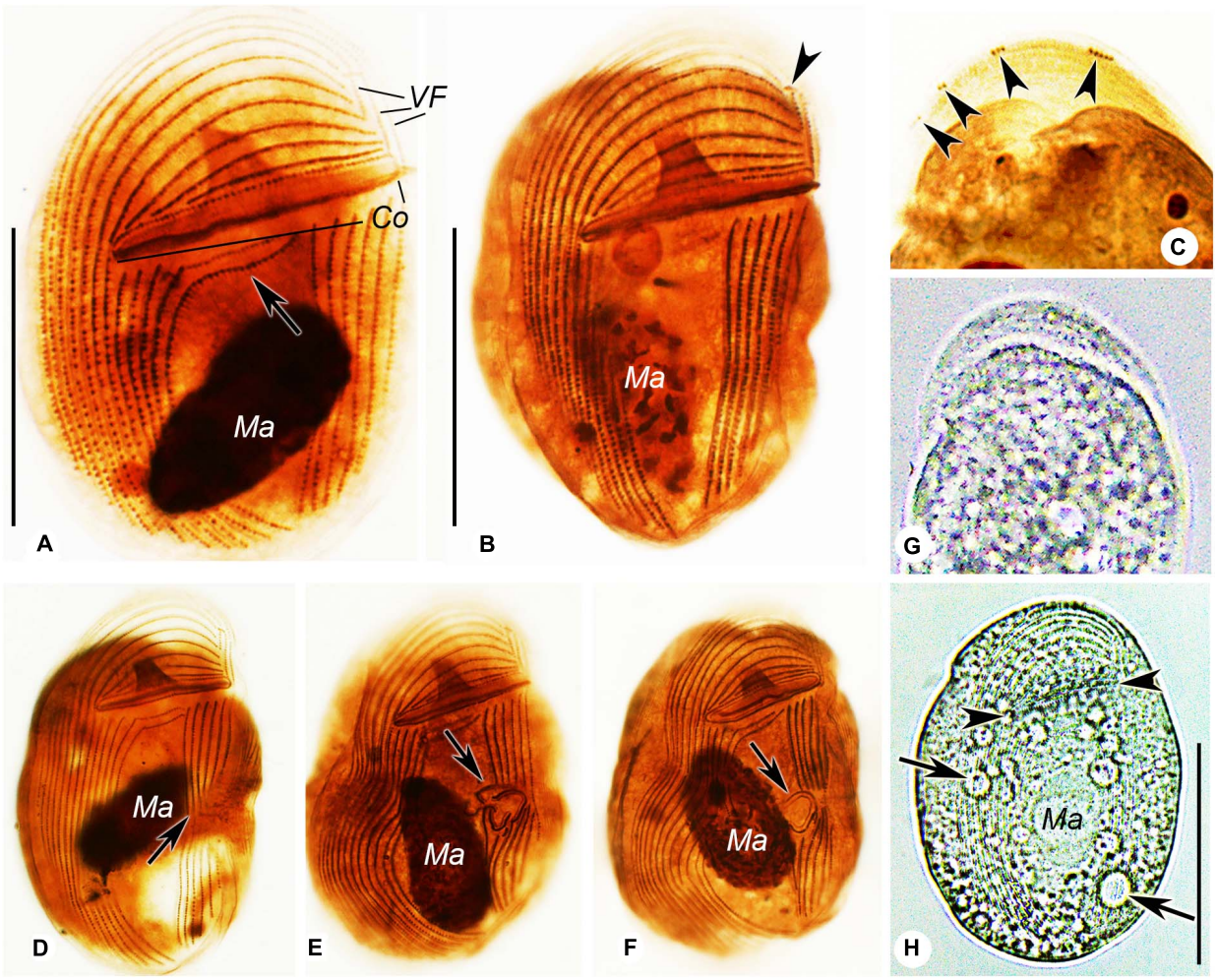

FIGURE 2 | Photomicrographs of *Gastronauta paraloisi* sp. n. after protargol-staining **(A–F)** and from life **(G,H)**. **(A)** Ventral view of general ciliature. Arrow shows the two curved postoral right kineties. **(B)** Ventral view of another individual. Arrowhead marks preoral kinety. **(C)** Dorsal view of anterior cell. Arrowheads point to terminal fragments. **(D–F)** Several stages of morphogenesis. **(D)** is an early stage, **(E)** is a middle stage, and **(F)** is a late stage. Arrows indicate the forming process of oral ciliature (stomatogenesis). **(G)** Dorsal view. **(H)** Ventral view of a slightly compressed individual. Arrows mark contractile vacuoles and arrowheads mark the oral slit. Abbreviations: Co, circumoral kinety; Ma, macronucleus; and VF, vertical fragments. Scale bars: 30 μm.

Approximately eight to 12 contractile vacuoles (diameter about 3 μm) counted from live cells, irregularly distributed on ventral side (**Figure 3A**), pulsating at an interval of 5–10 s; three to eight excretory pores detected in protargol-stained specimens (**Figures 3E,F**, **4C**). Macronucleus in mid-body or slightly below, about 22 × 10 μm *in vivo* and 23 × 10 μm after staining; not (or inconspicuously) centrally heteromeric (**Figures 3A,B,E,F**, **4C**). Cytoplasm usually containing many diatoms (**Figures 3A,D**, **4E,E**). Usually crawling slowly on substrate, occasionally swimming in water; strongly thigmotactic.

Sixteen to 18 somatic kineties composed of three parts: right, postoral, and left kineties (**Figures 3E,F**, **4C**). Constantly eight right kineties, all but the innermost one extending to left anterior cell end; posteriorly extending to rear end of cell. Two postoral kineties, ending at posterior 1/6 of cell, right one usually shortened (**Figures 3E,F**, **4C**). Six to eight left kineties, all but the innermost one commences from preoral kinety, posteriorly shortened from right to left; the innermost left kinety usually starts at the level of cytostome; the outermost left kinety very short, only comprising 20 to 25 basal bodies.

Two circumoral kineties parallel to each other, slightly above cytostome, with the outer one about twice the length of the inner one; preoral kinety obliquely arranged ahead of cytostome and left kinety (**Figures 3E,F**, **4C**). Single and oblique terminal fragment subapically located on dorsal side, comprising 15 to 24 basal bodies (**Figures 3D**, **4D**). Equatorial fragment seldom detected, containing six to 20 basal bodies.

For Shenzhen and Zhanjiang populations, only illustrations, microphotographs and morphometric data are provided (**Figures 3C**, **4A,B,F–H** and **Table 3**).

TABLE 2 | Morphometric data of *Gastronauta paraloisi* sp. n.

Character	Min	Max	Mean	M	SD	CV	*n*
Body, length (μm)	46	95	68.4	69.0	12.23	17.9	24
Body, width (μm)	25	65	44.9	45.0	8.04	17.9	24
Anterior end to Co., distance (μm)	15	25	20.2	20.0	2.89	14.3	24
Anterior end to macronucleus, distance (μm)	20	40	30.9	30.0	6.39	20.7	24
Left and right kineties field, distance (μm)	10	20	13.8	13.5	3.06	22.1	24
Long axis of Co, length (μm)	22	33	28.9	30.0	2.68	9.3	24
Macronucleus, length (μm)	17	32	24.0	25.0	3.80	15.8	24
Macronucleus, width (μm)	9	18	12.6	12.0	2.30	18.3	24
Basal bodies in equatorial fragment, number	6	26	15.4	13.0	7.73	50.1	9
Kineties in right ciliary field, number	12	12	12.0	12.0	0.00	0.0	24
Kineties in left ciliary field, number	6	7	6.2	6.0	0.41	6.7	24
Postoral kineties in right ciliary field, number	5	6	5.0	5.0	0.20	4.0	24
Somatic kineties, number	18	19	18.2	18.0	0.41	2.3	24
Preoral kineties, number	3	4	3.0	3.0	0.20	6.7	24
Vertical kinety fragments, number	3	4	3.0	3.0	0.20	6.7	24
TF groups, number	3	4	3.7	4.0	0.46	12.5	24
Kinetids in TF group 1, number	3	7	5.2	5.0	0.96	18.6	24
Kinetids in TF group 2, number	2	5	3.3	3.0	0.82	24.5	24
Kinetids in TF group 3, number	2	5	3.2	3.0	0.76	24.0	24
Kinetids in TF group 4, number	1	5	2.7	3.0	0.99	36.4	16

Data are based on protargol-stained, mounted and randomly selected specimens from raw culture. CV, coefficient of variation in%; Co., circumoral kinety; M, median; Max, maximum; Mean, arithmetic mean; Min, minimum; n, number of individuals investigated; SD, standard deviation; and TF, terminal fragment.

Sequence Similarity and Molecular Phylogeny

Three SSU rDNA sequences were obtained. The sequence of *Gastronauta paraloisi* sp. n. is highly divergent from available reference sequences in the GenBank database. By pairwise comparison, its closest relative, with a sequence similarity of 92.8%, is *Phascolodon vorticella* KX258192. The two *Trithigmostoma cucullulus* populations in the present work (Qingdao population, *T. cucullulus* QD; Zhanjiang population, *T. cucullulus* ZJ) have a similarity of 99.31%. The result of pairwise comparison of related sequences is shown in **Figure 6F**.

In the phylogenetic trees inferred from SSU rDNA sequences (**Figure 5**), four *Trithigmostoma* sequences form a monophyletic clade with full support. *Gastronauta paraloisis* sp. n. clusters with *Trithigmostoma* species with moderate support values (ML/BI, 80/0.87). This branch is then sister to the clade formed by other Chilodonellidae taxa represented by genera *Chilodonella*, *Odontochlamys*, *Phascolodon,* and *Pseudochilodonopsis*, with full support. The Gatronautidae/Chilodonellidae clade is located within the order Chlamydodontida. As in previous studies (Gao et al., 2012; Chen et al., 2016; Qu et al., 2017; Wang et al., 2017), both Chlamydodontidae and Lynchellidae are monophyletic (arrows in **Figure 5** indicate their monophylies).

DISCUSSION

Brief Review of Family Gastronautidae

The subclass Cyrtophoria contains two orders, Dysteriida and Chlamydodontida, which are mainly characterized by the patterns of flattened body (dorsoventrally or laterally flattened), and the presence or absence of adhesive organelle (podite or secretory organelle) (Lynn, 2008). The dorsoventrally flattened body and the absence of adhesive organelle confirm that *Gastronauta* belongs to the order Chlamydodontida. By this criterion, Kahl (1931) put *Gastronauta* under the family Chlamydodontidae. The range of "Chlamydodontidae" by Kahl equates to order Chlamydodontida in today's classification. While, the special structures, for example, a closed circular circumoral kinety and short vertical fragments in the left anterior body, make *Gastronauta* unique among all families in Chlamydodontida. Corliss (1979) tended to assign it to the family Lynchellidae because they both contain short arc kineties before cytostome (a large portion of kineties interrupted by cytostome). But their differences are also clear: (1) *Gastronauta* has a complete circular oral kinety, whereas Lynchellidae has parallel oral kinety fragments; and (2) *Gastronauta* has a centrally heteromeric macronucleus, while Lynchellidae species possess a parallelly heteromeric macronucleus. Thus, Deroux (1994) established the family Gastronautidae for the genus. Foissner (2000) also briefly discussed the familial assignment of *Gastronauta*, and he agreed with Deroux (1994)'s classification. On top of that, Foissner split the genus into two, based on the presence/absence of the postoral barren gap between right and left kineties: *Gastronauta* has the gap, while *Paragastronauta* does not. Lynn (2008) also adopted Gastronautidae, under subclass Chlamydodontida. *Gastronauta* is currently comprised of six species (including the new species), namely: *G. membranaceus* Engelmann in Bütschli, 1889 (type); *G. fontzoui* Nie & Ho, 1943; *G. derouxi* Blatterer & Foissner, 1992; *G. aloisi* Oberschmidleitner & Aescht, 1996; *G. multistriata* Xu et al., 2016, and *G. paraloisi* sp. n. *Paragastronauta* contains only one species, *P.* (*Gastronauta*) *clatratus* (Deroux, 1976) Foissner, 2000. The key morphometric characteristics of gastronautid species are shown in **Table 4**. A key to the identification of gastronautids based on morphological characteristics is provided below.

1 Barren gap present between right and left kineties	2 *Gastronauta*
1′ Barren gap absent between right and left kineties	*Paragastronauta clatratus*
2 Two curved postoral right kineties	3
2′ One curved postoral right kinety	4
3 Two arc kineties above oral slit	*G. alosi*
3′ Three arc kineties above oral slit	*G. paraloisi* sp. n.
4 No more than 12 right kineties	5
4′ More than 17 right kineties	6
5 Two terminal fragments	*G. membranaceus*
5′ Five to seven terminal fragments	*G. derouxi*
6 Five postoral right kineties	*G. fontzoui*
6′ Ten to twelve postoral right kineties	*G. multistriala*

Morphological Comparison of *Gastronauta paralosisi* sp. n. With Its Congeners

Based on the overall living morphology and the general ciliary pattern, especially the number of kineties and the two leftward curved innermost right kineties, one could be inclined to assign the new ciliate to *Gastronauta aloisi*. However, the new species can be clearly distinguished from the latter by the combination of the following characteristics: (1) body size. Our form is generally larger than *G. aloisi* (60–120 μm *in vivo* and about 68 × 45 μm after staining vs. 50–70 μm *in vivo* and 45 × 35 μm in *G. aloisi*); (2) number of arc kineties above oral slit (three vs. two); (3) number of vertical kinety fragments (three or four vs. two); and (4) the position of the anterior end of the innermost right kinety (almost joining the innermost left kinety vs. slightly left to the middle of the barren gap between right and left kineties) (Oberschmidleitner & Aescht, 1996). Further, the new species can be clearly distinguished from other *Gastronauta* species mainly by the two curved innermost right kineties (morphometric comparison see the identification key above and **Table 4**).

Foissner (2016) synonymized a Brazilian population of *Gastronauta membranaceus* with *G. aloisi* mainly because of the feature of the two curved postoral right kineties. However, this form has three arc kineties and the anterior end of the innermost

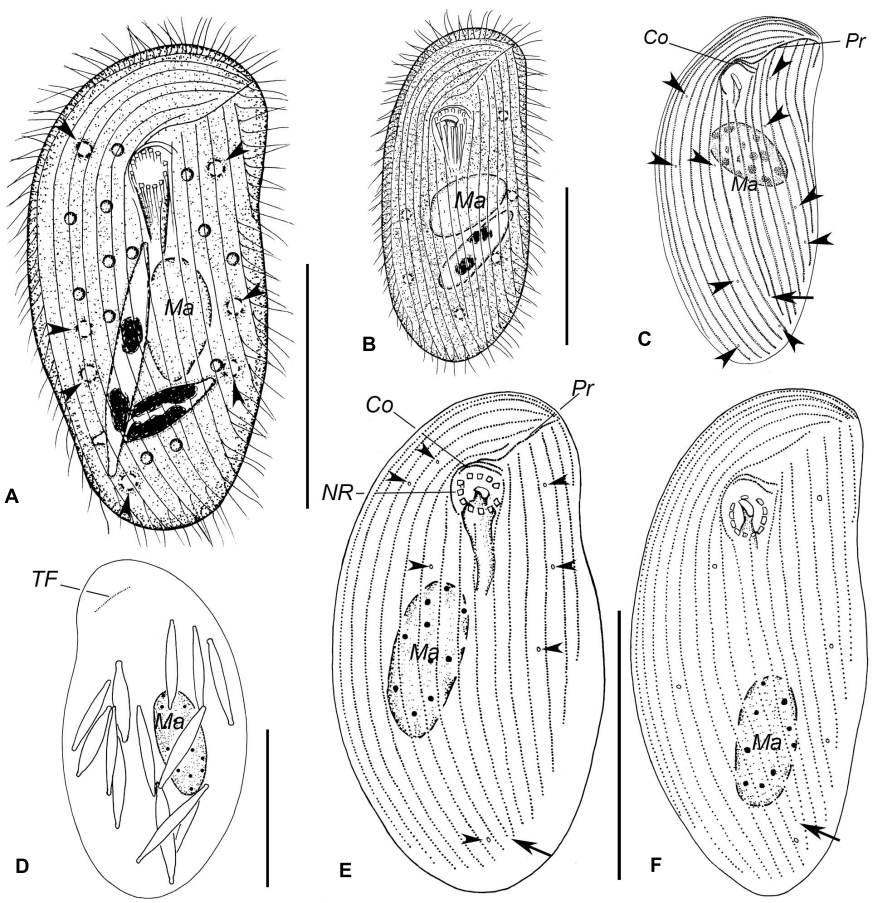

FIGURE 3 | Illustrations of *Trithigmostoma cucullulus*, Qingdao **(A,B,D–F)** and Zhanjiang populations **(C)**. **(A,B)** Ventral view of individuals in different body shapes. Arrowheads denote contractile vacuoles. **(C,E,F)** Ventral ciliature pattern. Arrows point to the end of the right postoral kinety, and arrowheads show the contractile vacuole pores. **(D)** Dorsal side, showing the terminal fragment as well as the food diatoms. Co, circumoral kineties; Ma, macronucleus; NR, nematodesmal rods; Pr, preoral kinety; and TF, terminal fragment. Scale bars: 40 μm.

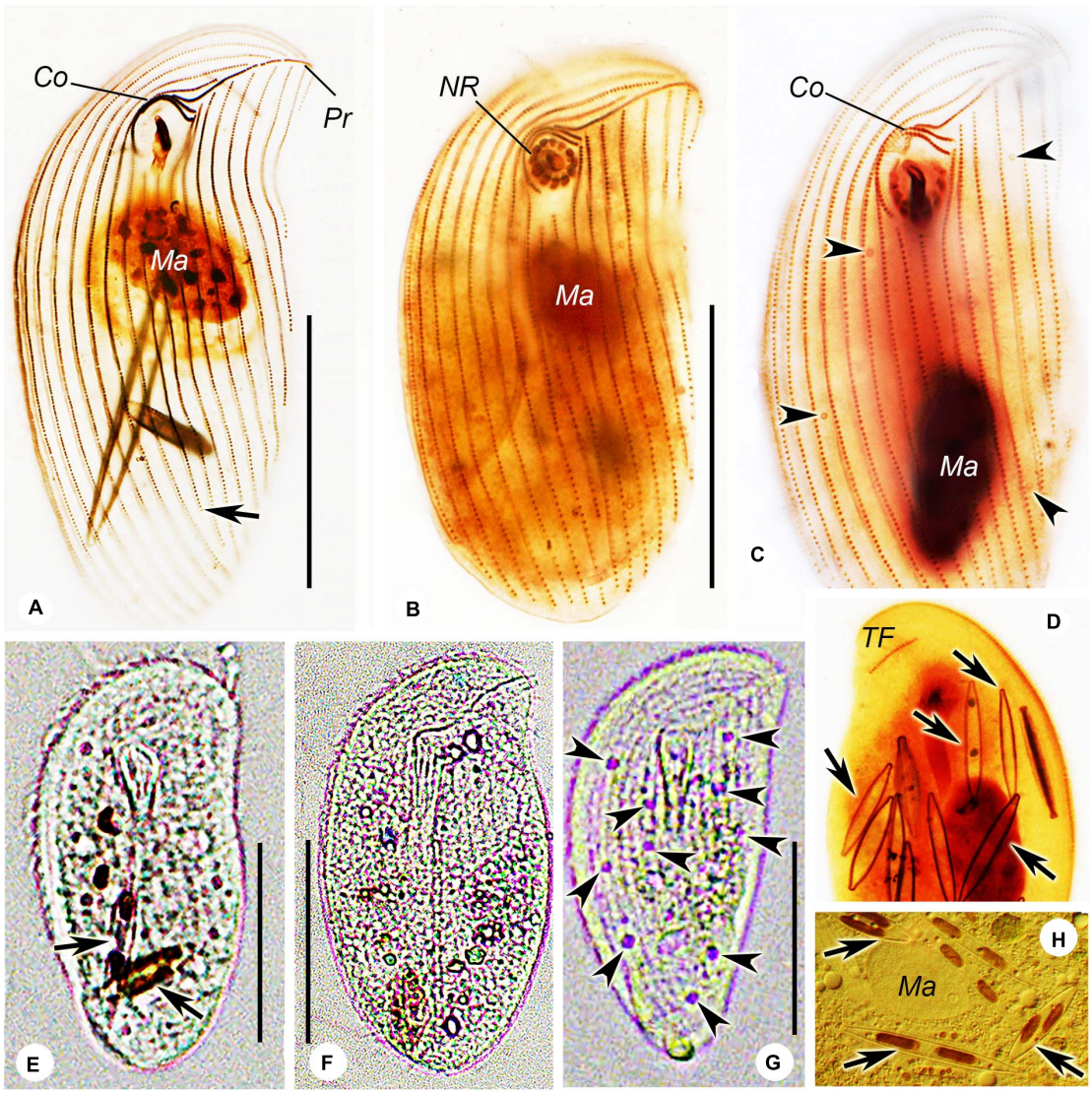

FIGURE 4 | Photomicrographs of *Trithigmostoma cucullulus*, Zhanjiang **(A,F–H)**, Shenzhen **(B)**, and Qingdao populations **(C,D,E)**. **(A–C)** Ventral view of protargol-stained specimens, arrowheads mark contractile vacuole pores, and arrow points to the end of the right postoral kinety. **(D)** Dorsal side of a stained individual, arrows denote the food diatoms. **(E,F)** Ventral view of cells from life. Arrows show food diatoms. **(G)** Ventral view of a starved cell, arrowheads show contractile vacuoles. **(H)** Arrow shows the food diatoms. Co, circumoral kineties; Ma, macronucleus; NR, nematodesmal rods; Pr, preoral kinety; and TF, terminal fragment. Scale bars: 40 μm.

right kinety connects the innermost left kinety (da Silva and da Silva-Neto, 2001), indicating it should be conspecific with the current new form. However, the Brazilian population is slightly different from our form by the position of the macronucleus (in anterior body vs. in mid-body or slightly below) and the number of terminal fragments (5–7 vs. 3–4), which could be considered as intraspecific variations.

Occurrence of *Gastronauta paraloisi* sp. n

da Silva and da Silva-Neto (2001) isolated a population of *Gastronauta paraloisi* sp. n. (see section "Discussion") from an experimental reactor of an activated sludge sewage treatment plant. Although the environmental parameters were not measured in our study, our population was isolated from a similar habitat. The sampling river is part of the sewer system of the inner city, and it seems saprobic, especially in rush hours in the morning and evening. Right after the sampling, the food vacuoles were checked, and many small algae (diameter about 1–2 μm) were found. When the raw culture was established with rice grains added to the indigenous water, *G. paraloisi* sp. n. thrived and cells tended to gather around the grains (bacteria-rich), indicating it is omnivorous (feeding on bacteria and small algae). As demonstrated by Šimek et al. (2019), unselective grazers that feed on a broader size spectrum from bacteria to

TABLE 3 | Morphometric data of *Trithigmostoma cucullulus* from Qingdao (upper rows), Zhanjiang (middle rows), and Shenzhen (lower rows) populations.

Character	Min	Max	Mean	*M*	SD	CV	*n*
Body, length (μm)	65	100	78.8	76.0	8.15	10.3	29
	76	130	99.5	100.0	11.79	11.9	26
	82	123	101.1	100.0	12.32	12.2	13
Body, width (μm)	29	45	35.1	35.0	3.82	10.9	29
	31	57	44.6	45.0	6.30	14.1	26
	45	65	53.3	53.0	5.56	10.4	13
Somatic kineties, number	16	18	17.0	17.0	0.33	1.9	29
	18	20	18.8	19.0	0.65	3.5	26
	18	21	19.6	20.0	1.12	5.7	13
Right kineties, number	8	8	8.0	8.0	0.00	0.0	29
	8	10	8.8	9.0	0.59	6.7	26
	8	9	8.6	9.0	0.51	5.9	13
Postoral kineties, number	2	2	2.0	2.0	0.00	0.0	29
	2	2	2.0	2.0	0.00	0.0	26
	2	2	2.0	2.0	0.00	0.0	13
Left kineties, number	6	8	7.0	7.0	0.33	4.6	29
	7	9	8.0	8.0	0.28	3.5	26
	8	10	9.0	9.0	0.71	7.9	13
Frontocentral kineties, number	7	7	7.0	7.0	0.00	0.0	29
	7	9	8.0	8.0	0.28	3.5	26
	7	8	7.6	8.0	0.51	6.6	13
Nematodesmal rods, number	11	13	12.0	12.0	0.58	4.8	25
	No data						
	10	14	12.4	12.5	1.07	8.7	10
Basal bodies in terminal fragment, number	15	24	19.7	20.0	2.02	10.2	26
	20	36	26.2	27.0	3.30	12.6	26
	16	29	24.3	24.0	3.17	13.1	13
Basal bodies in equatorial fragment, number	6	20	13.4	13.5	5.15	38.5	8
	6	28	18.7	19.5	8.98	48.1	6
	5	38	21.6	22.0	10.85	50.3	7
Contractile vacuole pores, number	3	8	5.6	5.5	1.36	24.4	20
	6	9	7.7	8.0	0.95	12.3	7
	5	14	9.5	9.5	3.34	35.1	8
Macronucleus, length (μm)	19	30	23.0	23.0	2.46	10.7	29
	20	35	24.3	23.0	3.17	13.0	26
	18	40	30.0	32.0	6.96	23.2	13
Macronucleus, width (μm)	6	14	10.3	10.0	1.56	15.1	29
	10	15	11.8	12.0	1.63	13.8	26
	14	20	16.3	16.0	1.89	11.6	13
Micronucleus, diameter (μm)	No data						
	No data						
	4	5	4.2	4.0	0.45	10.6	5
Terminal fragment to anterior cell end, distance (μm)	7	10	8.9	9.0	0.74	8.4	29
	7	13	10.2	10.0	1.74	17.1	26
	8	15	11.9	12.0	1.85	15.5	13

Data are based on protargol-stained, mounted and randomly selected specimens from raw cultures. CV, coefficient of variation in%; CK, circumoral kinety; DB, dorsal brush; M, median; Max, maximum; Mean, arithmetic mean; Min, minimum; n, number of individuals investigated; SD, and standard deviation.

small algae may have a considerable competitive advantage in hypertrophic environments, which explains the occurrence of a high abundance of *G. paraloisi* sp. n. in a saprobic environment. The fact that the attempt to establish the pure culture solely with rice grains and instilled water failed shows that the cultivation of this species may not be monoxenic.

Brief Review of *Trithigmostoma* and Identification of *T. cucullulus*

Jankowski (1967) established the genus *Trithigmostoma* from *Chilodonella*, mainly based on the lack of a barren gap between right and left kineties. The type is *Trithigmostoma cucullulus*. Foissner (1987, 1988) then summarized and made new combinations for some *Chilodonella* species. So far, the genus is comprised of five species, namely: *T. bavariensis* (Kahl, 1931) Foissner, 1987; *T. chattoni* (Mac Dougall, 1936) Foissner, 1988; *T. cucullulus* (Müller, 1786) Jankowski, 1967; *T. srameki* (Sramek-Husek, 1952) Foissner, 1988; and *T. steini* (Blochmann, 1895) Foissner, 1988. Details about the species identification refer to Foissner (1987, 1988) and Blatterer & Foissner (1992). Three other genera, *Odontochlamys* Certes (1891), *Thigmogaster* Deroux, 1976 and *Pseudochilodonopsis* Foissner, 1979 were also separated from *Chilodonella* (Qu et al., 2015), and together with *Trithigmostoma*, are now assigned to the family Chilodonellidae. However, characteristics such as a lack of barren gap between right and left kineties, almost all right kineties reaching posterior cell end, and many irregularly distributed contractile vacuoles, make *Trithigmostoma* very special in Chilodonellidae.

Trithigmostoma cucullulus is one of the earliest identified ciliates. It was originally reported by Müller (1786), using the name *Kolpoda cucullulus* (Aescht, 2001). Because of its wide distribution and relatively high abundance, *Trithigmostoma cucullulus* has been recorded worldwide and its morphology is well studied. Since the original report, the generic assignment of this species (species name) has been changed several times, for example to *Chilodon cucullulus* (Müller, 1786) Klein, 1927, *Chilodonella cucullulus* (Müller, 1786) Kahl, 1931 and *Trithigmostoma cucullus* (Müller, 1786) Foissner (1988) Jankowski, 1967 (spelling mistake was corrected by Foissner, 1988). Foissner et al., 1991 summarized the morphology of the species in detail. Our populations correspond well with the previous populations as well as with a recent estuarine population from China (salinity 4.3‰; Chen et al., 2018). Although reported many times in history, *T. cucullulus* demonstrates very stable morphological features. In addition, considering its worldwide distribution, it might be a cosmopolitan species.

In the present phylogenetic analyses, three sequences of *Trithigmostoma cucullulus* did not form a monophyletic group, but formed a clade within which *T. steini* X71134 (Leipe et al., 1994) nested. In general living morphology, *T. cucullulus* is very similar to *T. steini*. The main differences are the number of somatic kineties (18–22 in *T. cucullulus* vs. 25–33 in *T. steini*) and the number of contractile vacuole pores (2–11 vs. 10–40), which are mainly detectable after staining (Foissner et al., 1991; Chen et al., 2018; and data from the present work). Therefore, it is likely that *T. steini* X71134 (morphological data not available) was misidentified, or that the morphological discrepancy of these two

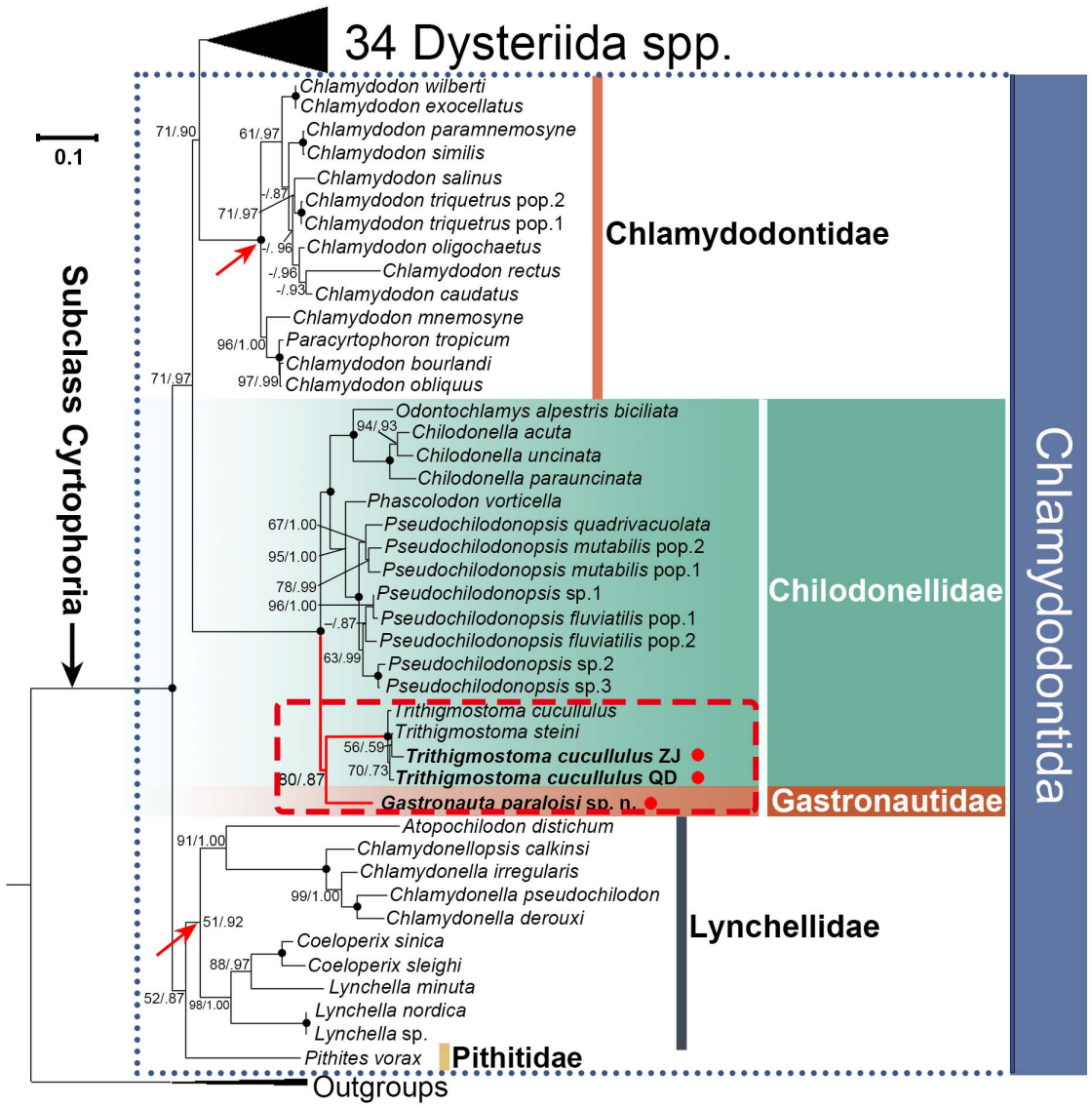

FIGURE 5 | ML tree inferred from SSU rDNA sequences. Support values from ML and posterior probabilities of BI are provided at branching point (ML/BI). Bold dots at branching point mean full support from both analyses. "-" indicates discrepancy between topologies of ML and BI trees, or support values < 50%/0.5 (ML/BI). Red arrows denote the monophyly of Chlamydodontidae and Lynchellidae, and red dots indicate the three sequences from present work. QD and ZJ represent Qingdao and Zhanjiang populations of *Trithigmostoma cucullulus*, respectively. The scale bar represents one substitution per ten nucleotide positions.

species could not be shown by the molecular phylogeny inferred from SSU rDNA sequences.

Intermediate Position of Gastronautidae and *Trithigmostoma*

The special positions of Gastronautidae (*Gastronauta*) and *Trithigmostoma* are also revealed by phylogeny derived from the SSU rDNA sequences. They cluster but also branch away from the core Chilodonellidae genera of the family Chilodonellidae. As mentioned above, *Trithigmostoma* has a special position within Chilodonellidae. The familial assignment to Chilodonellidae is beyond doubt, but its special characteristics also make it close to Chlamydodontidae and Lynchellidae. Chen et al. (2016) briefly discussed the status of this genus using phylogeny from SSU rDNA sequences, and demonstrated that it is a peripheral genus within Chilodonellidae. In another analysis inferred from mitochondrial small subunit ribosome DNA, the genus is also revealed to have an uncertain position in Chilodonellidae (Wang et al., 2017). Chen et al. (2018) concluded that *Trithigmostoma* is a basal genus in Chilodonelliae. Thus, based on previous studies and our own we agree that *Trithigmostoma* represents a basal group in Chilodonellidae, and it may be closely related to the common ancestor (still undiscovered or extinct) of Chilodonellidae, Chlamydodontidae and Lynchellidae.

TABLE 4 | Morphometric comparison of *Gastronauta* and *Paragastronauta* species.

Species	Body length	Numbers of							Data source
		RK	LK	CK	PRK	Arc	TF	VK	
G. paralosisi	46–95 μm	12	6 or 7	2	5 or 6	ca. 3	3 or 4	ca. 3	Present work
G. aloisi	36–53 μm	11–13	5–7	2	3 or 4	ca. 2	3–5	ca. 2	Oberschmidleitner & Aescht, 1996
G. paraloisi	^50–70 μm	–	5–6	2	–	3	5–7	3	da Silva and da Silva-Neto, 2001
G. derouxi	48–77 μm	11	5 or 6	1	5 or 6	4 or 5	5–7	3	Blatterer & Foissner, 1992
G. fontzoui	–	19–21	6 or 7	1	5	6	–	–	Nie & Ho, 1943
*G. membranaceus**	40–62 μm	9 or 10	6	1	5 or 6	4 or 5	2	–	Wilbert, 1972
G. membranaceus	^45–70 μm	9 or 10	6	1	4–6	4–6	2	3	Foissner et al., 1991; Foissner, 2000
G. multistriata	33–98 μm	18–23	5–9	1	10–12	7–10	5–8	2–3	Xu et al., 2016
P. clatratus	47–69 μm	–	–	1	–	8–10	3	3–4	Blatterer & Foissner, 1992; Foissner, 1997

*Data measured from protargol-stained specimens. Arc, arc kineties above cytostome; CK, curved postoral right kineties; LK, kineties in left ciliary field; PRK, postoral right kineties; RK, kineties in right ciliary field; TF, terminal fragments; and VK, vertical fragments. *Original name was G. runcina, but was regarded as a synonym of G. membranaceus (Foissner et al., 1991). ^Measured in vivo.*

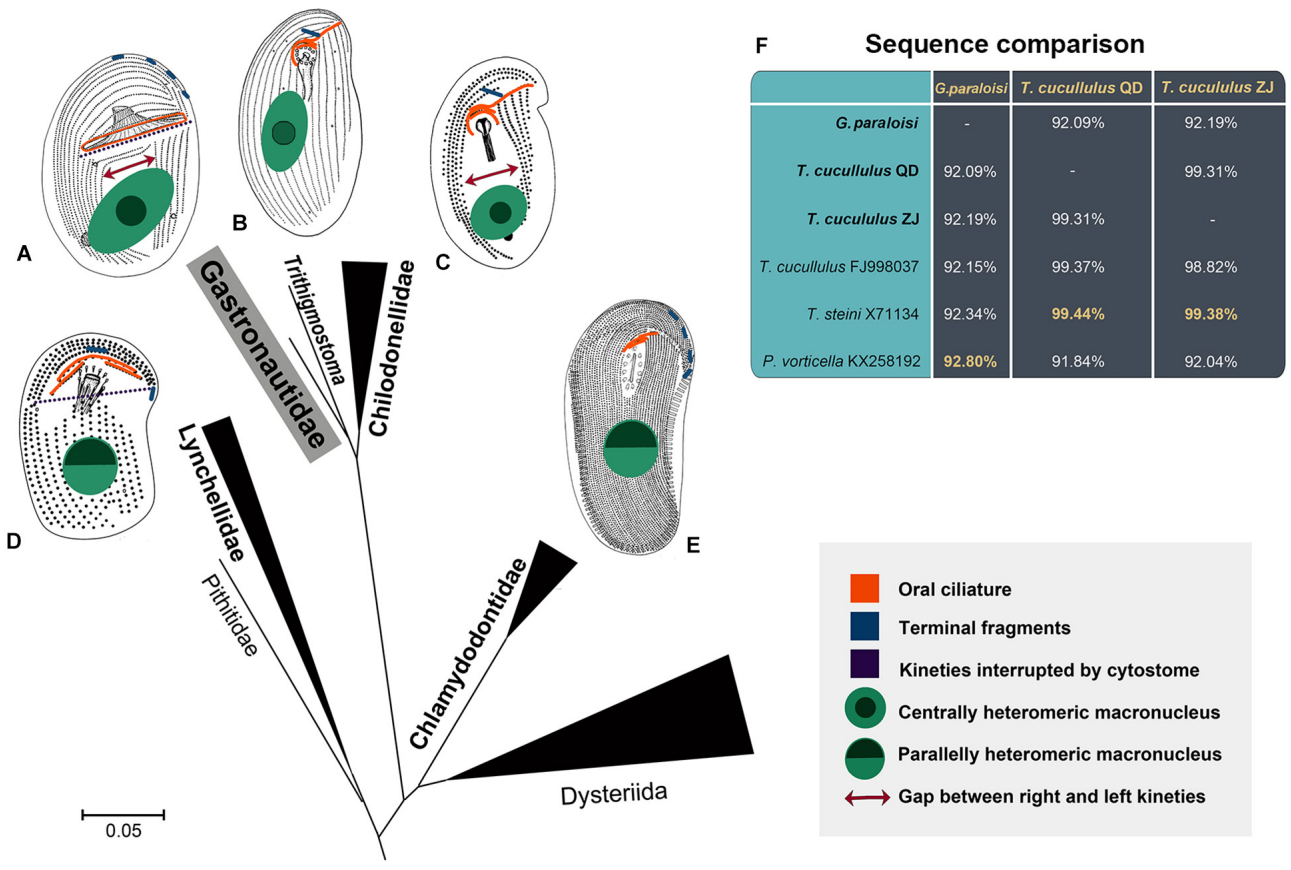

FIGURE 6 | The illustrations display key morphological characteristics (indicated by different colors and shapes) of Chlamydodontida families **(A–E)**. The scale bar represents 5 substitutions per 100 nucleotide positions. **(A)** Gastronautidae (*Gastronauta*). **(B)** *Trithigmostoma*. The heteromeric centralization of the macronucleus is sometimes inconspicuous. **(C)** Chilodonellidae (*Chilodonella*). **(D)** Lynchellidae (*Lynchella*). **(E)** Chlamydodontidae (*Chlamydodon*). **(F)** Comparison of closely related sequences. The greatest similarities to the three sequences in the present work are highlighted.

Gastronautidae has more specialized and intermediate characteristics among the order Chlamydodontida (**Figure 6**). As mentioned above, both Gastronautidae and Lynchellidae have kineties interrupted by cytostome, thus there is no clear suture formed between right and left kineties in the left anterior body (violet dashes in **Figure 6**). Gastronautidae, Lynchellidae and Chilodonellidae usually have two (or sometimes several in Chilodonellidae)

regularly distributed contractile vacuoles (vs. many irregularly distributed in Chlamydodontidae). Gastronautidae and Chilodonellidae have a centrally heteromeric macronucleus (sometimes inconspicuous in *Trithgmostoma*) (marked green in **Figure 6**) and usually well-separated right and left kineties (except for *Trithigmostoma* and *Paragastronauta*) (red double arrows in **Figure 6**), while the other two families have a parallelly heteromeric macronucleus and unseparated right and left kineties (*Atopochilodon* in Lynchellidae has only unobvious separation). In addition, Gastronautidae's multiple terminal fragments make it close to Chlamydodontidae and Lynchellidae but not to Chilodonellidae (blue fragments in **Figure 6**). More importantly, Gastronautidae can be clearly separated from others by its unique, closed circular oral kinety (marked orange in **Figure 6**), which confirms the rationality of the establishment of Gastronautidae. Thus, we assume Gastronautidae represents an evolutionary link among Chlamydodontida ciliates. However, the poor-matching of morphology of *Gastronauta* and *Trithigmostoma*, along with the grouping of these two genera in SSU rDNA phylogeny, indicates that data concerning the key evolutionary link(s) of cyrtophorian ciliates are still missing. But up to date, there is only one sequence of *Gastronauta* available and the molecular representative of the type species, *G. membranaceus*, is still lacking, which largely constrains the phylogenetic resolution. Further study with high phylogenetic resolution needs to be conducted with more morphological and molecular data from Gastronautidae and other related groups.

AUTHOR'S NOTE

This article is registered in ZooBank under:urn:lsid:zoobank.org:pub:384B19A2-DCE5-4CB8-8C5D-379BF9A04EB2.

DATA AVAILABILITY STATEMENT

The datasets presented in this study can be found in online repositories. The names of the repository/repositories and accession number(s) can be found in the article/supplementary material.

AUTHOR CONTRIBUTIONS

ZQ conducted the field and lab work, morphological and molecular analyses, and wrote and revised the draft. HP contributed to the taxonomy and phylogenetic analyses, and revised the draft. CW conducted phylogenetic analyses and figure visualization. HM revised the draft. TS contributed to sections, revised the draft, and improved the language. XH conceived and designed the study, supervised the work, and revised the draft. All authors have read and agreed to be accountable for the content of the work.

FUNDING

This work was financially supported by the National Natural Science Foundation of China (projects numbers: 41976086, 32070432, and 32030015).

ACKNOWLEDGMENTS

The authors gratefully acknowledge Prof. Weibo Song, Ocean University of China, for his valuable comments on drafting the manuscript.

REFERENCES

Aescht, E. (2001). Catalogue of the generic names of ciliates (Protozoa, Ciliophora). *Denisia* 1, 1–350. doi: 10.1007/bf00017483

Blatterer, H., and Foissner, W. (1992). Morphology and infraciliature of some cyrtophorid ciliates (Protozoa, Ciliophora) from freshwater and soil. *Arch. Protistenk.* 142, 101–118. doi: 10.1016/S0003-9365(11)80075-8

Bütschli, O. (1887–1889). "Erster band protozoa. III. Abtheilung. Infusoria und system der radiolaria," in *Klassen und Ordnungen des Thier-Reichs*, Vol. I, ed. H. G. Bronn (Leipzig: Winter'sche Verlagshandlung), 1089–2035.

Chen, X., Li, L., Al-Farraj, S. A., Ma, H., and Pan, H. (2018). Taxonomic studies on *Aegyria apoliva* sp. nov. and *Trithigmostoma cucullulus* (Müller, 1786) Jankowski, 1967 (Ciliophora, Cyrtophoria) with phylogenetic analyses. *Eur. J. Protistol.* 62, 122–134. doi: 10.1016/j.ejop.2017.12.005

Chen, X., Pan, H., Huang, J., Warren, A., Al-Farraj, S. A., and Gao, S. (2016). New considerations on the phylogeny of cyrtophorian ciliates (Protozoa, Ciliophora): expanded sampling to understand their evolutionary relationships. *Zool. Scr.* 45, 334–348. doi: 10.1111/zsc.12150

Corliss, J. O. (1979). *The Ciliated Protozoa. Characterization, Classification, and Guide to the Literature*, 2nd Edn. New York, NY: Pergamon Press

da Silva, S. B. A., and da Silva-Neto, I. D. (2001). Morfologia dos pro-tozoários ciliados presentes em um reator experimental detratamento de esgoto por processo de lodos ativados. *Rev. Bras. Zoociências Juiz de Fora* 3, 203–229.

Deroux, G. (1976a). Le plan cortical des Cyrtophorida unité d'expression et marges de variabilité. I. Le cas des Plesiotrichopidae, fam. nov., dans la nouvelle systématique. *Protistologica* 12, 469–481.

Deroux, G. (1976b). Le plan cortical des Cyrtophorida unité d'expression et marges de variabilité. II. Cyrtophorida a thigmotactisme ventral généralise. *Protistologica* 12, 483–500.

Deroux, G. (1994). "Sous-classe des cyrtophoria fauré-fremiet in Corliss, 1956," in *Traité de Zoologie. Anatomie, Biologie. Infusoires Ciliés, Fasc. 2 Systématique*, Vol. II, ed. P. de Puytorac (Paris: Masson), 401–431.

Foissner, W. (1987). Miscellanea nomenclatorica ciliatea (Protozoa. Ciliophora). *Arch. Protistenk.* 133, 219–235. doi: 10.1016/S0003-9365(87)80054-4

Foissner, W. (1988). Taxonomie und ökologie einiger ciliaten (Protozoa, Ciliophora) des Saprobiensystems. II. Familie Chilodonellidae. *Hydrobiologia* 162, 21–45. doi: 10.1007/BF00014331

Foissner, W. (2000). Revision of the genera *Gastronauta* Engelmann in Bütschli, 1889 and *Paragastronauta* nov. gen. (Ciliophora: Gastronautidae). *Protozool. Monogr.* 1, 63–101.

Foissner, W. (2016). Protists as bioindicators in activated sludge: identification, ecology and future needs. *Eur. J. Protistol.* 55, 75–94. doi: 10.1016/j.ejop.2016.02.004

Foissner, W., Blatterer, H., Berger, H., and Kohmann, F. (1991). Taxonomische und ökologische Revision der Ciliaten des Saprobiensystems. Band I: cyrtophorida, oligotrichida, hypotrichia, colpodea. Informationsberichte des bayer. *Landesamt. Wasserwirtschaft* 1/91, 478.

Gao, S., Huang, J., Li, J., and Song, W. (2012). Molecular phylogeny of the cyrtophorid ciliates (Protozoa, Ciliophora, Phyllopharyngea). *PLoS One* 7:e33198. doi: 10.1371/journal.pone.0033198

Gong, J., and Song, W. (2004). Description of a new marine cyrtophorid ciliate, *Dysteria derouxi* nov. spec., with an updated key to 12 well-investigated *Dysteria* species (Ciliophora, Cyrtophorida). *Eur. J. Protistol.* 40, 13–19. doi: 10.1016/j.ejop.2003.07.002

Gong, J., Song, W., and Warren, A. (2002). Redescriptions of two marine cyrtophorid ciliates, *Dysteria cristata* (Gourret and Roeser, 1888) and *Dysteria monostyla* (Ehrenberg, 1838) Kahl, 1931 (Protozoa, Ciliophora, Cyrtophorida), from China. *Eur. J. Protistol.* 38, 213–222. doi: 10.1078/0932-4739-00862

Gong, J., Song, W., Warren, A., Lin, X., and Roberts, D. M. (2007). Microscopical observations on four marine *Dysteria* species (Ciliophora, Cyrtophorida). *Eur. J. Protistol.* 43, 147–161. doi: 10.1016/j.ejop.2007.01.002

Hu, X., Lin, X., and Song, W. (2019). *Ciliate Atlas: Species Found in the South China Sea*. Beijing: Science Press, doi: 10.1007/978-981-13-5901-9

Jankowski, A. W. (1967). Taxonomy of the genus *Chilodonella* and a new proposed genus *Trithigmostoma* gen. nov. *Zool. Zh.* 46, 1247–1250.

Jankowski, A. W. (2007). "Phylum Ciliophora Doflein, 1901," in *Protista. Part 2. Handbook on Zoology*, ed. A. F. Alimov (St. Petersburg: Russian Academy of Sciences, Zoological Institute), 371–993.

Kahl, A. (1931). Urtiere oder Protozoa I: wimpertiere oder ciliata (Infusoria) 2. *Tierwelt Dtl.* 21, 181–398.

Leipe, D. D., Bernhard, D., Schlegel, M., and Sogin, M. L. (1994). Evolution of 16S-like ribosomal RNA genes in the ciliophoran taxa litostomatea and phyllopharyngea. *Eur. J. Protistol.* 30, 354–361. doi: 10.1016/S0932-4739(11)80083-0

Lynn, D. H. (2008). *The Ciliated Protozoa. Characterization, Classi?cation, and Guide to the Literature*, 3rd Edn. Dordrecht: Springer, doi: 10.1007/978-1-4020-8239-9

Medlin, L., Elwood, H. J., Stickel, S., and Sogin, M. L. (1988). The characterization of enzymatically amplified eukaryotic 16S-like rRNA-coding regions. *Gene* 71, 491–499. doi: 10.1016/0378-1119(88)90066-2

Miller, M. A., Pfeiffer, W., and Schwartz, T. (2010). Creating the CIPRES science gateway for inference of large phylogenetic trees. *Paper presented at the 2010 Gateway Computing Environments Workshop (GCE)*, (New Orleans, LA: IEEE), doi: 10.1109/GCE.2010.5676129

Müller, O. F. (1786). *Animalcula Infusoria Fluviatila et Marina, quae Detexit, Systematice Descripsit et ad Vivum Delineari Curavit*. Hauniae: Typis Nicolai Mölleri.

Nie, D., and Ho, Y. (1943). Notes on some epizoic infusoria from the freshwater shrimp, *Palaemon nipponensis*. *Sinensia* 14, 143–149.

Nylander, J. (2004). *MrModeltest v2.* Program Distributed by the Author. Uppsala: Uppsala University.

Oberschmidleitner, R. A., and Aescht, E. (1996). Taxonomische untersuchungen über einige ciliaten (Ciliophora, Protozoa) aus Belebtschlämmen oberösterreichischer Kläranlagen. *Beitr. Naturk. Oberösterreichs* 4, 3–30.

Pan, B., Chen, X., Hou, L., Zhang, Q., Qu, Z., Warren, A., et al. (2019). Comparative genomics analysis of ciliates provides insights on the evolutionary history within "Nassophorea-Synhymenia-Phyllopharyngea" assemblage. *Front. Microbiol.* 10:2819. doi: 10.3389/fmicb.2019.02819

Pan, H., Jiang, J., Fan, X., Al-Farraj, S. A., and Gao, S. (2017). Phylogeny and taxonomy of five poorly known species of cyrtophorian ciliates (Protozoa, Ciliophora, Phyllopharyngea) from China seas. *Zool. J. Linn. Soc.* 180, 475–492. doi: 10.1093/zoolinnean/zlw006

Pan, H., Li, L., Al-Rasheid, K. A. S., and Song, W. (2013). Morphological and molecular description of three new species of the cyrtophorid genus *Chlamydodon* (Ciliophora, Cyrtophoria). *J. Eukaryot. Microbiol.* 60, 2–12. doi: 10.1111/jeu.12001

Pan, H., Wang, L., Jiang, J., and Stoeck, T. (2016). Morphology of four cyrtophorian ciliates (Protozoa, Ciliophora) from Yangtze Delta, China, with notes on the phylogeny of the genus *Phascolodon*. *Eur. J. Protistol.* 56, 134–146. doi: 10.1016/j.ejop.2016.08.005

Petz, W., Song, W., and Wilbert, N. (1995). Taxonomy and ecology of the ciliate fauna (Protozoa, Ciliophora) in the endopagial and pelagial of the Weddell sea, Antarctica. *Stapfia* 40, 1–223.

Qu, Z., Li, L., Lin, X., Stoeck, T., Pan, H., Al-Rasheid, K. A., et al. (2018a). Diversity of the cyrtophorid genus *Chlamydodon* (Protista, Ciliophora): its systematics and geographic distribution, with taxonomic descriptions of three species. *Syst. Biodivers* 16, 497–511. doi: 10.1080/14772000.2018.1456493

Qu, Z., Ma, H., Al-Farraj, S. A., Lin, X., and Hu, X. (2017). Morphology and molecular phylogeny of *Aegyria foissneri* sp. n. and *Lynchella minuta* sp. n. (Ciliophora, Cyrtophoria) from brackish waters of southern China. *Eur. J. Protistol.* 57, 50–60. doi: 10.1016/j.ejop.2016.10.003

Qu, Z., Pan, H., Hu, X., Li, J., Al-Farraj, S. A., Al-Rasheid, K. A. S., et al. (2015). Morphology and molecular phylogeny of three cyrtophorid ciliates (Protozoa, Ciliophora) from China, including two new species, *Chilodonella parauncinata* sp. n. and *Chlamydonella irregularis* sp. n. *J. Eukaryot. Microbiol.* 62, 267–279. doi: 10.1111/jeu.12175

Qu, Z., Pan, H., Lin, X., Li, L., Aleidan, A. M. A., Al-Farraj, S. A., et al. (2018b). A contribution to the morphology and phylogeny of Chlamydodon, with three new species from China (Ciliophora, Cyrtophoria). *J. Eukaryot. Microbiol.* 65, 236–249. doi: 10.1111/jeu.12472

Ronquist, F., and Huelsenbeck, J. P. (2003). MrBayes 3: bayesian phylogenetic inference under mixed models. *Bioinformatics* 19, 1572–1574. doi: 10.1093/bioinformatics/btg180

Šimek, K., Grujčić, V., Nedoma, J., Jezberová, J., Šorf, M., Matoušů, A., et al. (2019). Microbial food webs in hypertrophic fishponds: omnivorous ciliate taxa are major protistan bacterivores. *Limnol. Oceanogr.* 64, 2295–2309. doi: 10.1002/lno.11260

Snoeyenbos-West, O., Cole, J., Campbell, A., Coats, D. W., and Katz, L. A. (2004). Molecular phylogeny of phyllopharyngean ciliates and their group I introns. *J. Eukaryot. Microbiol.* 51, 441–450. doi: 10.1111/j.1550-7408.2004.tb00392.x

Song, W., Warren, A., and Hu, X. (2009). *Free-living Ciliates in the Bohai and Yellow Seas*. Beijing. Science Press.

Song, W., and Wilbert, N. (1989). Taxonomische untersuchungen an aufwuchsciliaten (Protozoa, Ciliophora) im Poppelsdorfer Weiher, Bonn. *Lauterbornia* 3, 2–221.

Stamatakis, A. (2014). RAxML version 8: a tool for phylogenetic analysis and post-analysis of large phylogenies. *Bioinformatics* 30, 1312–1313. doi: 10.1093/bioinformatics/btu033

Tamura, K., Peterson, D., Peterson, N., Stecher, G., Nei, M., and Kumar, S. (2011). MEGA5: molecular evolutionary genetics analysis using maximum likelihood, evolutionary distance, and maximum parsimony methods. *Mol. Biol. Evol.* 28, 2731–2739. doi: 10.1093/molbev/msr121

Wang, C., Qu, Z., and Hu, X. (2019). Morphology and SSU rDNA sequences of four cyrtophorian ciliates from China, with description of a new species (Protista, Ciliophora, Phyllopharyngea). *Zootaxa* 4664, 206–220. doi: 10.11646/zootaxa.4664.2.3

Wang, P., Wang, Y., Wang, C., Zhang, T., Al-Farraj, S. A., and Gao, F. (2017). Further consideration on the phylogeny of the ciliophora: analyses using both mitochondrial and nuclear data with focus on the extremely confused class phyllopharyngea. *Mol. Phylogenet. Evol.* 112, 96–106. doi: 10.1016/j.ympev.2017.04.018

Warren, A., Patterson, D. J., Dunthorn, M., Clamp, J. C., Achilles-Day, U. E. M., Aescht, E., et al. (2017). Beyond the "code": a guide to the description and documentation of bio-diversity in ciliated protists (Alveolata, Ciliophora). *J. Eukaryot. Microbiol.* 64, 539–554. doi: 10.1111/jeu.12391

Wilbert, N. (1971). Morphologie und Ökologie einiger neuer ciliaten (Holotricha, Cyrtophorina) des Aufwuchses. *Protistologica* 7, 357–363.

Wilbert, N. (1975). Ein verbesserte technik der protargolimprägnation für ciliaten. *Mikrokosmos* 64, 171–179.

Xu, Y., Shao, C., Fan, X., Warren, A., Al-Rasheid, K. A. S., Song, W., et al. (2016). New contributions to the biodiversity of ciliates (Protozoa, Ciliophora) from Antarctica, including a description of *Gastronauta multistriata* n. sp. *Polar Biol.* 39, 1439–1453. doi: 10.1007/s00300-015-1869-7

Conflict of Interest: The authors declare that the research was conducted in the absence of any commercial or financial relationships that could be construed as a potential conflict of interest.

frontiers in Marine Science

ORIGINAL RESEARCH
published: 13 April 2021
doi: 10.3389/fmars.2021.643822

Genetic Diversity in Marine Planktonic Ciliates (Alveolata, Ciliophora) Suggests Distinct Geographical Patterns – Data From Chinese and European Coastal Waters

Maximilian H. Ganser[1], Dominik Forster[2], Weiwei Liu[3], Xiaofeng Lin[4], Thorsten Stoeck[2] and Sabine Agatha[1]*

[1] Department of Biosciences, University of Salzburg, Salzburg, Austria, [2] Ecology Group, Technische Universität Kaiserslautern, Kaiserslautern, Germany, [3] Key Laboratory of Tropical Marine Bio-Resources and Ecology, South China Sea Institute of Oceanology, Chinese Academy of Sciences, Guangzhou, China, [4] Key Laboratory of the Ministry of Education for Coastal and Wetland Ecosystem, The Fujian Provincial Key Laboratory for Coastal Ecology and Environmental Studies, College of the Environment and Ecology, Xiamen University, Xiamen, China

Unraveling geographic distribution patterns of planktonic protists is a central goal in marine microbial ecology. Using a novel combination of recently developed phylogenetic and network analyses on a V4 18S rDNA metabarcoding dataset, we here analyzed the genetic diversity of marine planktonic ciliate communities in Chinese and European coastal waters. Thereby, our approach provided an unprecedented perspective on geographic patterns inferred from ciliate genetic diversity and accomplished a very fine resolution down to single nucleotides within operational taxonomic units (OTUs). While most OTUs (87%) exclusively contained sequences of either Chinese or European origin, those OTUs detected in both regions comprised the vast majority of reads (84%). Phylogenetic analyses of OTUs belonging to the same taxon revealed genetically distinct clades that were geographically restricted to either Chinese or European coastal waters. The detection of signature nucleotides emphasized this genetic distinction of Chinese and European clades. Second-level clustering of OTUs and reference sequences in two selected taxa (the oligotrichid *Spirotontonia* and the tintinnid *Tintinnidium*) revealed the presence of several potentially new species or ones lacking genetic reference data. Geographic patterns were also discovered by network analyses within 700 widespread and abundant OTUs; in 77 of these OTUs, European and Chinese sequences formed significantly assortative groups. These assortative groupings indicated a higher genetic similarity among sequences from the same region than between sequences from different regions. Our results demonstrate that detailed analyses of metabarcoding data down to single nucleotide differences expand our perception of geographical distribution patterns and provide insights into historic and ongoing effective dispersal in protists. The congruent discovery of geographic patterns at different levels of resolution (between and within OTUs) suggests that cosmopolitan distribution in marine planktonic ciliates is less common than previously postulated.

Keywords: distribution, metabarcoding, network analyses, phylogenetic analyses, protists, second-level clustering, Swarm OTU

OPEN ACCESS

Edited by:
Thomas Wilke,
University of Giessen, Germany

Reviewed by:
Xavier Turon,
Consejo Superior de Investigaciones Científicas (CSIC), Spain
Feng Zhao,
Institute of Oceanology (CAS), China

****Correspondence:***
Maximilian H. Ganser
maximilian.ganser@sbg.ac.at

Specialty section:
This article was submitted to Marine Evolutionary Biology, Biogeography and Species Diversity, a section of the journal Frontiers in Marine Science

Received: *18 December 2020*
Accepted: *24 March 2021*
Published: *13 April 2021*

Citation:
Ganser MH, Forster D, Liu W, Lin X, Stoeck T and Agatha S (2021) Genetic Diversity in Marine Planktonic Ciliates (Alveolata, Ciliophora) Suggests Distinct Geographical Patterns – Data From Chinese and European Coastal Waters. Front. Mar. Sci. 8:643822. doi: 10.3389/fmars.2021.643822

INTRODUCTION

Marine planktonic ciliate communities contribute fundamentally to marine food webs by linking different trophic levels (Sherr and Sherr, 1988). This role is especially important in coastal environments that generally harbor a rich biodiversity and additionally host the breeding grounds of many multicellular organisms whose juvenile stages feed on ciliates (Stoecker and Capuzzo, 1990). Despite the importance of ciliates, our understanding of their distribution and speciation patterns is incomplete. Both kinds of patterns are strongly affected by past and ongoing effective dispersal through transport in active or passive state, which includes a subsequent successful establishment of individual organisms (Weisse, 2008). Likewise, dispersal limitations, species sorting caused by the absence of adequate ecological niches, and adaptations to local environmental conditions define a species' geographic distribution.

Communities of marine planktonic ciliates are usually dominated by the oligotrichids and the choreotrichids comprising aloricate (naked) species and the house-forming tintinnids (Pierce and Turner, 1992; McManus and Santoferrara, 2013). Both are assigned to the Oligotrichea Bütschli, 1887 according to morphologic, molecular, and ontogenetic features (Adl et al., 2019). The prevalence of data on the diversity and distribution of the about 1,000 tintinnid morphospecies in the literature (e.g., Merkle, 1909; Laackmann, 1910; Hofker, 1931; Hada, 1938; Zeitzschel, 1966, 1969) is in sharp contrast to the comparatively few taxonomic and ecological papers on the about 140 oligotrichids and 60 aloricate choreotrichids. Moreover, geographic distribution patterns inferred from records of morphospecies are often influenced by investigation methods (e.g., sampling strategy, fixation blurring species-specific features) as well as taxonomic uncertainties caused by phenotypic plasticity and cryptic species (Agatha, 2011). In the latter cases, morphological divergences or convergences are incompletely linked to genetic relationships.

To circumvent the problems regarding species limitations in tintinnids, studies on their global distribution are largely restricted to genus level. Different geographic patterns emerged from the voluminous dataset: cosmopolitan, neritic, warm-temperate, boreal, austral, and tropical Pacific; yet, even in cosmopolitan genera (inhabiting the neritic and oceanic regions from the Arctic through the tropics to the Antarctic), none of its members covers the entire geographic range (Pierce and Turner, 1993). Furthermore, the composition of tintinnid communities also distinctly differs between neritic and oceanic regions (Pierce and Turner, 1993; Dolan and Pierce, 2013). In oligotrichids and aloricate choreotrichids, the records of morphospecies are widely restricted to coastal waters. Keeping the taxonomic impediments in mind, the data demonstrate a wide, possibly cosmopolitan distribution in most genera, while about one third of them seem to be geographically restricted and potentially contain few species with apparently limited distribution (Agatha, 2011).

The stepwise introduction of sequencing technologies into marine planktonic ciliate research complemented morphospecies analyses and allowed for investigating previously untouched aspects of genetic diversity. The first molecular study from coastal sites in the Northwest Atlantic on oligotrichids and choreotrichids used the V3 and V8 regions of the 18S rDNA and applied Sanger sequencing (Doherty et al., 2007). The molecular and morphological data were congruent regarding tintinnids, but revealed a much higher genetic diversity in oligotrichids, especially within the genus *Strombidium* Claparède & Lachmann, 1859 (Doherty et al., 2007, 2010). The comparison of molecular and morphological data on tintinnids by a subsequent study not only confirmed differences in the composition between coastal and adjacent open ocean communities, but also showed the advantages of sequencing studies for detecting less abundant species (Santoferrara et al., 2016b). Global records of 18S rDNA gene sequences also supported biogeographical patterns for tintinnid genera (Santoferrara et al., 2018).

Barcoding approaches, which combine morphological and molecular data, alleviated the limits of taxonomic resolution, and unveiled both phenotypic plasticity and (pseudo-) crypticity in oligotrichean ciliates (McManus et al., 2010; Santoferrara et al., 2015, 2017; Kim et al., 2020). The marker genes employed (e.g., 18S, ITS, and 28S rDNA gene sequences) generally enable to distinguish ciliates down to species rank (Warren et al., 2017). Ideally, a single cell is identified and documented, its marker genes are analyzed, and the sequences are deposited together with metadata in a reference database. Thereby, marker gene sequences are unambiguously linked with corresponding morphospecies (Santoferrara et al., 2016a). Reference databases that cover most of the diversity represent a valuable resource for "meta"-barcoding studies that depend on reliable taxonomic annotations of gene sequences obtained from environmental samples. Yet, species identification using reference sequences is hampered by overlapping interspecific and intraspecific sequence distances, different species divergence times, and arbitrary, *a piori* fixed divergence thresholds (Moritz and Cicero, 2004; Will and Rubinoff, 2004; DeSalle et al., 2005).

Identical marker gene sequences detected in independent samples revealed the occurrence of several marine planktonic ciliate species in different oceanic regions. For example, identical internal transcribed spacer sequences and 18S rDNA gene sequences of some oligotrichids were found to be distributed across the North Atlantic and adjacent sea regions or in the West Atlantic (Agatha et al., 2004; Katz et al., 2005; Doherty et al., 2010). Specimens of the tintinnid *Antetintinnidium mucicola* collected from the Northwest Atlantic are identical in their 18S rDNA sequences to one reference sequence from the Yellow Sea (Ganser and Agatha, 2019). However, even specimens with identical sequences in the rather conserved 18S rDNA might display genetic divergences in other, more variable marker genes (e.g., ITS, 28S, and COI), indicating distinct species (Xu et al., 2012; Santoferrara et al., 2015, 2017; Jung et al., 2018).

While the barcoding of ciliate species continues, metabarcoding studies, which employ high-throughput sequencing (HTS) technologies for rapidly investigating whole ciliate communities, are independent of taxonomic expertise. As outlined above, they make, however, use of the already existing

taxonomic results from barcoding studies in publicly available databases. Despite their exclusive focus on molecular data, metabarcoding studies have considerably contributed to our current perception of geographic distribution patterns in marine planktonic ciliates, as well. The patterns were mainly analyzed via large-scale metabarcoding datasets comprising hyper-variable sequences of either the V4 or the V9 18S rDNA gene regions. Regarding ciliates, the genetic distances of the hyper-variable V4 regions are generally comparable to distances between near full-length 18S rDNA sequences, this applies, however, only to a lesser extent to the hyper-variable V9 region (Dunthorn et al., 2012). The findings of large-scale metabarcoding studies regarding planktonic ciliates in marine habitats suggest that European coastal waters exhibit a high regional genetic diversity and a strong habitat specificity based on V4 sequence data (Forster et al., 2015). By contrast, the global and regionally restricted genetic diversity of planktonic ciliate communities in the open oceans based on V9 sequence data was found to be low (Gimmler et al., 2016).

Moving from whole ciliate communities down to the level of individuals, metabarcoding also contributed to assess the intra- and interspecific genetic diversity (Forster et al., 2019). Whatever the targeted level of investigation, diversity assessments as well as the detection of geographic patterns and their underlying processes strongly depend on the molecular resolution (Hanson et al., 2012). This resolution, in turn, depends on the selected marker gene (Dunthorn et al., 2012) as well as on the approach with which metabarcoding sequences are clustered into operational taxonomic units (OTUs) (Forster et al., 2019). Traditionally, heuristic sequence clustering approaches that rely on global alignment scores (e.g., USEARCH), such as a given percentage of sequence similarity, were used to generate OTUs (Edgar, 2010). While these methods reduce the computational demand for processing a dataset (sequences are only compared with a centroid sequence), several studies have shown that OTUs generated by heuristic approaches lack accuracy and reproducibility (Sun et al., 2012; Bachy et al., 2013; Schmidt et al., 2015). Moreover, heuristically clustered OTUs are designed to assess community structure on the OTU level (e.g., α- and β-diversity), but provide little information about their internal structure and are therefore comparatively coarse in terms of genetic resolution. More recently developed hierarchical sequence clustering approaches that employ all-vs.-all pairwise sequence comparisons allow for a much more fine-grained resolution of diversity. In particular, the algorithm Swarm provides detailed information about the internal structure of its OTUs (Mahé et al., 2015). Swarm OTUs also grow from a centroid 'seed' sequence, but the sequences are linked to each other if their sequence alignment differs by not more than a given number of nucleotides (usually one nucleotide difference, which is likely to arise through biological processes). The internal structure of a Swarm OTU thus represents a network based on the information which sequences are linked to each other, which may be evaluated by means of graph theory (Forster et al., 2020). Evaluating the properties of the internal network structure distinctively increases the resolution of diversity down to single nucleotide differences and, therefore allows unprecedented insights into genetic diversity and geographical distribution patterns. Investigations of intraspecific genetic diversity are especially important within ciliates, which exhibit high copy numbers and sequence variation even within individual specimens (Gong et al., 2013; Wang et al., 2017; Zhao et al., 2019). An additional second-level clustering of Swarm OTUs enables an efficient differentiation of genetically divergent sequences into species-specific network sequence clusters. This strategy thus allows for a closer approximation between morphospecies and OTUs, i.e., a better estimation of the real species diversity from metabarcoding datasets (Forster et al., 2019). Owing to differences in evolutionary rates, however, a refinement of the similarity cut-off values for particular lineages is required (Wang et al., 2019; Zhao et al., 2019).

Current high-throughput sequencing technologies facilitate the rapid assessment of marine planktonic ciliate communities and thus the investigation of distribution patterns on various temporal and spatial scales. The two most common sampling strategies result in (i) a low spatial and high temporal resolution, i.e., the samples are collected several times at locally restricted sites, or (ii) a high spatial and low temporal resolution, i.e., the samples are collected usually only once at sites widely distributed over a coastal or oceanic region. The selection of a strategy depends on the aims of the study. Type 1 studies usually focused on the influence of environmental gradients on the community composition (Santoferrara et al., 2016b; Minicante et al., 2019), the distribution and composition of communities at varying depths (Grattepanche et al., 2015; Sun et al., 2019), or seasonal patterns (Piredda et al., 2017; Giner et al., 2019). However, type 2 studies investigated large-scale diversity and distribution patterns, for example, at a regional scale in European coastal waters (Logares et al., 2014) or at a global scale in the oceans (de Vargas et al., 2015; Logares et al., 2020). Usually, large-scale studies of the marine plankton either analyzed the entire community of eukaryotes or focused on certain size-fractions of protists.

Coastal waters are highly interesting environments for investigating geographic distribution patterns and their evolutionary origin in marine planktonic ciliates, particularly as data covering large spatial scales are lacking. Within these environments, assessments of ciliate diversity and distribution patterns were so far confined to whole communities, genera, morphospecies, or OTUs (Foissner et al., 2008; Doherty et al., 2010; Dolan and Pierce, 2013; Massana et al., 2015; Piredda et al., 2017). In the present study, we apply a novel combination of phylogenetic approaches (Hütter et al., 2020) and network analyses (Forster et al., 2019, 2020) to achieve an unparalleled increase of resolution down to within-OTU level for investigating geographic distribution patterns and their origin in marine planktonic ciliates. Hence, it overcomes the limitations of previous investigations by employing an increased genetic resolution and a unique sampling strategy that links a high spatiotemporal resolution (regional sampling at several sites, at different daytimes, and in different seasons) with a large geographic distance between the regions examined, namely, the

Chinese and European coastal waters. The present analyses aim (i) to detect correlations between phylogenetic relationships and the geographic distribution based on metabarcoding data of the hyper-variable V4 region, (ii) to identify signature nucleotides for geographically restricted OTU clusters (Hütter et al., 2020), (iii) to determine the threshold values that reconcile secondary clusters of Swarm OTUs and morphospecies and allow estimating the diversity of taxa, and (iv) to discover geographic patterns of genetic diversity within Swarm OTUs by means of network analyses.

MATERIALS AND METHODS

Sampling and Filtering Procedure

Following identical protocols, 80 samples were taken from Chinese and European coastal surface waters between October 2017 and November 2018, namely, one day and one night sample per season at each site (**Supplementary Table 1**); the high spatiotemporal sampling aimed to capture as much of the biodiversity of planktonic ciliates as possible. Our sampling sites belong to different Longhurst ecological provinces: the Northeast Atlantic Shelves, the Mediterranean Sea, and the China Seas Coastal provinces (Longhurst, 2007). The Chinese sampling (n = 32) was performed at four sites along the coast of southern China, i.e., in Aotou (coastal town), Donghai Island, Futian (mangrove wetland), and Hailing Island. The European sampling (n = 48) was conducted at the German North Sea coast, i.e., at two sites in Wilhelmshaven, and at two sites in the Baltic Sea, i.e., Warnemünde and Rostock, as well as at two sites in the Mediterranean Sea, i.e., Villefranche-sur-Mer (France) and Trieste (Italy). The spatial distances spanning the shortest sea routes along the coastlines amount to about 150–500 km between the Chinese sites, about 400–6,400 km between the European sites, and about 14,200–18,800 km between the Chinese and European sampling sites.

Surface water samples were collected with a bucket (5 L), and temperature and salinity were immediately measured. The collected water was pre-filtered through a 250 μm-mesh net to remove debris and metazoa and subsequently filtered through a 0.8 μm-pore size polyether sulfone membrane 47 mm across (Pall) in a filtration unit with a manual vacuum pump (Nalgene) until the membrane was clogged or a maximum of about 3.6 L was reached. The membrane filters were immediately placed in Cryo-Vials (Simport) and preserved with LifeGuard® buffer (Qiagen) at 0°C. In the laboratory, they were stored at −80°C until DNA extraction. Using a whole water sample, the entire ciliate community ranging from nano- to microplankton could be collected; plankton nets, which provide usually merely qualitative samples, were exclusively employed in sampling for microscopic inspection.

DNA Extraction, Amplification, and Sequencing

The total DNA from each membrane filter was extracted with the DNeasy® PowerSoil® Kit (Qiagen) with slight modifications of the manufacturer's protocol (**Supplementary Data 1**). The extracted DNA of each sample was amplified and sequenced by Biomarker (Beijing, China). Amplification comprised a nested-PCR approach (**Supplementary Data 1**), using first ciliate-specific primers followed by eukaryotic primers targeting the hyper-variable V4 18S rDNA gene region (Lara et al., 2007; Stoeck et al., 2010). In a single run, paired-end sequencing (2 × 250 bp) of the library with the V4 sequences of all samples was conducted on an Illumina HiSeq 2500 platform. Sequence read data will be made accessible at the NCBI BioProject ID PRJNA714531 (https://www.ncbi.nlm.nih.gov/bioproject/).

Bioinformatic Quality Control and Sequence Clustering

The primer removal from each demultiplexed forward and reverse library was conducted in Cutadapt version 2.8 (Martin, 2011). Primers were clipped from both ends of each read, and only reads without mismatches in the primer regions were retained. Forward and reverse reads were then paired-end assembled by VSEARCH version 2.14.2 (Rognes et al., 2016) with high success rates (≥96.5% merged paired-end reads per sample; mean paired-end fragment lengths ≥344 nucleotides). Paired-end reads with ambiguous bases were discarded and identical reads were dereplicated to amplicons across all samples according to the recommendations for preparing sequence data for OTU clustering[1]. Our terminology follows Mahé et al. (2015) in that we refer to a single sequence obtained from raw HTS data as a 'read,' while an 'amplicon' comprises a set of identical reads obtained via dereplication. The term 'sequence' refers to the sequence of nucleotides of which a read or an amplicon consists.

Amplicons were used as input for OTU clustering by Swarm v. 3.0.0 (Mahé et al., 2015). Swarm is an efficient clustering algorithm for linking only those amplicons into one OTU which differ by a single nucleotide from at least one other amplicon in that OTU. Thereby, the OTUs grow iteratively from a central 'seed' amplicon. In each iteration, the algorithm searches for all amplicons that can be linked to the most recently added amplicon(s). If no more such amplicons can be found, the clustering process stops, the current OTU is closed, and a new OTU is initiated from another central amplicon. In our particular clustering approach, we enabled the options *-d 1*, *-f* (fastidious option), *-i* (output of a structure file), *-j* (output of all pairwise sequence connections into a file), and *-s* (output of a clustering statistics file). Since our goal was to achieve resolutions down to single nucleotide differences, we set the clustering threshold in Swarm accordingly (d = 1). Although not tested here, our methodological workflow allows for adjusting this threshold to the taxonomic group and marker gene under study. For ciliate metabarcoding datasets of the ribosomal V9 and V4 gene regions, a clustering threshold of one nucleotide difference has successfully been applied in previous studies (e.g., Forster et al., 2019). For other taxonomic groups and faster evolving marker genes, such as COI, though, higher clustering thresholds might be necessary for assessing the underlying genetic diversity within and between OTUs (see e.g., Bakker et al., 2019; Siegenthaler et al., 2019; Antich et al., 2020). Swarm uses all sequences in the input

[1]https://github.com/frederic-mahe/swarm/wiki/Fred's-metabarcoding-pipeline

dataset and yields a very fine-scaled resolution of genetic diversity in a sample. The OTU networks generated by Swarm are used for downstream evaluations by means of graph theory.

Chimera detection was conducted after OTU clustering, using VSEARCH's *uchime_denovo* option, an implementation of the UCHIME algorithm (Edgar et al., 2011). After removing chimeras and low-abundant OTUs (i.e., comprising less than three reads), all remaining OTUs were taxonomically annotated, using the PR^2 reference database (Guillou et al., 2013) and the last common ancestor approach in VSEARCH, applying the *sintax* option with default parameters, which is an implementation of the SINTAX algorithm (Edgar, 2016). Those OTUs not assigned to the Ciliophora were removed from the dataset; the final ciliate-specific dataset contained 47,093 Swarm OTUs.

Phylogenetic Analyses

To detect geographic distribution patterns in marine planktonic ciliates, phylogenetic analyses were conducted. Those OTUs with an identical "taxon" annotation were grouped. "Taxon" labels derived from the PR^2 reference database may represent environmental sequences, sequences of species identified to genus level, or reference sequences from known morphospecies (Guillou et al., 2013). All OTUs grouping to a "taxon" label might thus encompass several different but closely related ciliate taxa. Those groups assigned to the Oligotrichea with more than 15 OTUs in one of the two regions and a ratio of OTU numbers from China and Europe higher than 0.15 were chosen to assemble the final dataset. Next, each group was augmented by shared OTUs (i.e., OTUs consisting of amplicons/reads from both geographic regions) that matched the respective "taxon" labels. The final dataset (**Supplementary Table 2**, **Supplementary Data 2**) included 21 "taxon" groups containing in total 2,404 Chinese OTUs (51,369 reads), 2,679 European OTUs (71,085 reads), and 1,124 shared OTUs (1,076,655 reads).

The amplicon sequence of each Swarm OTU with the highest read number (representative Swarm OTU sequence) was chosen for the subsequent alignments, which were calculated for each "taxon" separately with MAFFT v. 7 (Katoh and Standley, 2013), using the *globalpair* command. The phylogenetic tree for each "taxon" was computed with FastTree v. 2.1.11 (Price et al., 2010) under the GTR + CAT model (Tavaré, 1986; Stamatakis, 2006). The trees were edited in FigTree v. 1.4.4[2]. They have a polar tree layout, midpoint rooting, and increasing order of nodes. For displaying the different distribution patterns, the trees represent cladograms (**Figure 4**), whereas the detailed taxon trees show the original branch lengths (**Supplementary Figure 1**). The branches were colored according to the geographic affiliation of the respective OTU, i.e., those from China are marked red, those from Europe are blue, and the shared ones are purple.

Nucleotides characterizing certain tree branches geographically restricted to a large extent were identified with DeSignate (Hütter et al., 2020), using the web-interface[3]. In DeSignate, two sets of aligned sequences chosen by the user (=query and reference groups) are compared and each alignment position is ranked and categorized according to its diagnostic value. Alignment positions with a diagnostic value of 1 are categorized as binary or asymmetric if they are uniform within the query group. The nucleotides at these positions are termed "signature nucleotides" in the context of our study. At binary positions, a nucleotide base (e.g., A) is present in all sequences of the query group and another nucleotide base (e.g., G) is present in all sequences of the reference group. At asymmetric positions, the nucleotide bases in sequences of the reference group do not need to be uniform, but different from the nucleotide base in the query group (e.g., G, C, or T, but not A). These signature nucleotides thus indicate that part of the amplicon diversity of a ciliate taxon can be affiliated to a certain geographic region, namely, China or Europe. Suitable query and reference groups to test for the presence of signature nucleotides in aligned sequences were identified by eye, evaluating branching patterns and branch support values in each of the phylogenetic trees.

Sequence Similarity Networks

For two taxa in which reference sequences can be reliably linked to morphospecies, namely, the oligotrichid *Spirotontonia* and the tintinnid *Tintinnidium*, sequence similarity networks were calculated. The representative sequences of the phylogenetically analyzed Swarm OTUs affiliated to these taxa along with their closest related reference sequences of the PR^2 database and sequences of known morphospecies (updated list of curated reference sequences from Santoferrara et al., 2017) were subjected to a second-level clustering by means of sequence similarity networks (SSNs). The pairwise sequence alignments by VSEARCH yielded similarity values for each "taxon" used for constructing the sequence similarity networks at different thresholds (Forster et al., 2019). The thresholds at which the morphologically distinct species separated into network sequence clusters (NSCs) were determined for elucidating the numbers of connected components that do not include reference sequences; they represent either new species or ones lacking genetic data.

Network Analyses on Geographic Patterns Within Swarm OTUs

The Swarm OTUs were subdivided into two categories: OTUs comprising sequence reads from only Europe or China and shared OTUs comprising sequence reads from both regions. A further subdivision of the European OTUs regarding their affiliation to the two different Longhurst ecological provinces and network analyses considering geographical distances were not performed. A case study on a test dataset of Scandinavian lakes detected no significant patterns on a regional scale (Forster et al., 2020). Therefore, we expanded the spatial scale toward two more distant geographical regions in the current study. For network analyses, only shared OTUs which comprised at least 0.0001% of all reads and included at least three amplicons from both geographic regions (China and Europe) were chosen. These thresholds were set to select those OTUs in which network analyses on the internal structure were feasible, as OTUs poor in reads and amplicons are prone to produce

[2]https://github.com/rambaut/figtree/

[3]https://designate.dbresearch.uni-salzburg.at/home/

statistically insignificant network patterns. The resulting subset consisted of 700 OTUs.

Assortativity is a commonly used metric in graph theory (Newman, 2003). Within a particular OTU, it allows measuring preferential connections between amplicons originating from China or Europe, i.e., the assortativity is high (maximum 1) when amplicons from one region are genetically more similar among each other than to sequences from the other region. The *-i* and *-j* outputs of Swarm served as input for constructing a network which was then subjected to assortativity calculations.

For determining the statistical significance of the assortativity values each OTU network was randomized 1,000 times by shuffling the geographic attributes of the nodes (China or Europe), while the general network structure (i.e., same number of nodes and edges, same node degree) was retained. The assortativity values for the randomized networks were calculated. When the computed assortativity values of the original OTU network exceeded the 95% confidence interval of the 1,000 randomized values, amplicons from the same region were significantly more often connected to each other than expected by chance. The workflow and the bioinformatic commands used have previously been published (Forster et al., 2020) and were run in R Studio v. 3.5.1 (R Core Team, 2018), using the igraph package v. 1.2.2 (Csárdi and Nepusz, 2005).

RESULTS

Geographic Distribution of Swarm OTUs

The following results explicitly focus on the geographic patterns in OTUs from Chinese and European coastal waters representing two spatially distant regions. A detailed comparison of ciliate communities within regions and their variability through seasons and daytime will be the topic of a subsequent publication benefitting from the high spatiotemporal resolution of our sampling strategy. The ciliate-specific dataset shows that only 13% of OTUs consist of reads from both regions (shared OTUs), whereas 43% and 44% of OTUs exclusively consist of reads from China or Europe, respectively (**Figure 1**). On the contrary, most reads (84%) belong to shared OTUs, while the remaining reads are almost evenly divided between Chinese OTUs (7%) and European OTUs (9%). Out of the 6,227 shared OTUs, 663 OTUs (11%) consisted to at least 99% of Chinese reads and 744 OTUs (12%) consisted to at least 99% of European reads. Most OTUs (55%) were annotated to taxa assigned to the Oligotrichida, aloricate Choreotrichida, or Tintinnina, while the CONthreeP (e.g., peritrichs) were less often observed. Interestingly, 43% of all purely Chinese and European OTUs (8.4% of total reads) were annotated by the last common ancestor approach to the same taxon names, suggesting that there are considerable regional genetic deviations.

On closer inspection of the shared Swarm OTUs, three main patterns of geographic affiliation are distinguished for each enclosed amplicon (**Figure 2**): (i) the amplicon comprises reads from only one region, (ii) the vast majority of reads within the amplicon originate from one region, while only one or relatively few reads (<1%) originate from the respective other region and are interpreted as methodological artifacts (e.g., in the oligotrichid *Spirotontonia* sp.), and (iii) the amplicon contains a considerable number of reads from both regions, such that its occurrence in both regions is unlikely to be a methodological artifact (e.g., in the tintinnid *Tintinnopsis baltica*; **Figure 3**). The distinction of the different amplicon types was of utmost importance for the representative amplicons used in the phylogenetic analyses.

Phylogenetic Trees and Second-Level Clustering

The phylogenetic trees of the 21 oligotrichean taxa display a spectrum of topologies ranging from distinct geographic to heterogeneous distribution patterns generated by the representative amplicon sequences of the Swarm OTUs (**Figure 4**). Distinct patterns thereby suggest that the amount of geographically restricted genetic diversity is the result of past effective dispersal events in specific taxa as indicated by long and highly supported branches (**Supplementary Figure 1**). On the other hand, multiple effective dispersal events are repeatedly ongoing in several other taxa as indicated by heterogeneous distribution patterns and short branch lengths.

Most of the phylogenetic trees show various degrees of heterogeneous branching patterns with no clear split between Chinese and European OTUs. Several different branching patterns are exemplified in the tree of the tintinnid *T. baltica* (**Figure 3A**). Please, note that the last common ancestor approach assigned the V4 sequences only to the reference sequence of *T. baltica* although the reference sequences of *Tintinnopsis acuminata* and *Tintinnopsis nana* are identical in their V4 regions. Hence, the tree shown might actually comprise several species. The various subclades in the tree mainly consist of closely related Chinese, European, and shared OTUs, which display an alternating and irregular branching (**Figure 3B**). The representative sequences of the shared OTUs were assigned to one of the three types described above (**Figure 2**), depending on the percentages of reads from the particular regions in its representative amplicon (**Figure 3B**).

Distinct geographic distribution patterns are apparent in trees of four taxa (**Figure 4**), in which Chinese and European OTUs are entirely (the oligotrichids *Spirotontonia* sp. and *Strombidium* K sp.) or largely separated (the oligotrichid Strombidiidae K X sp. and the tintinnid *Tintinnidium* sp.). The representative sequences of shared OTUs are evenly distributed in the phylogenies of the four taxa and either fall into clades of European or Chinese OTUs. They belong to Type 2 of shared OTUs, and their representative amplicons can be assigned to the geographic region of their respective clade (**Figure 2**).

The bifurcation forming the conspicuous split between Chinese and European OTUs in the trees of the four abovementioned taxa (**Supplementary Figure 1**) exhibit high support values (Shimodaira–Hasegawa test $\geq$ 0.9; Shimodaira, 2002) and are further corroborated by signature nucleotides (see section "Materials and Methods"). In general, the number of signature nucleotides greatly varies (**Supplementary Figure 3**).

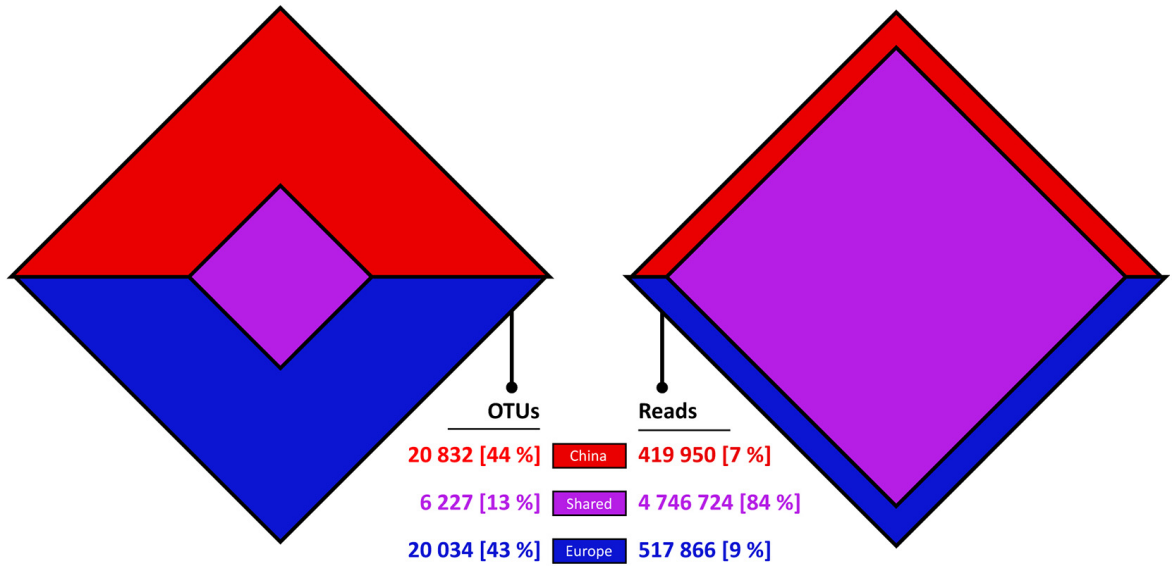

FIGURE 1 | Venn-diamonds displaying the comparison between Chinese, European, and shared Swarm OTUs and their respective read numbers.

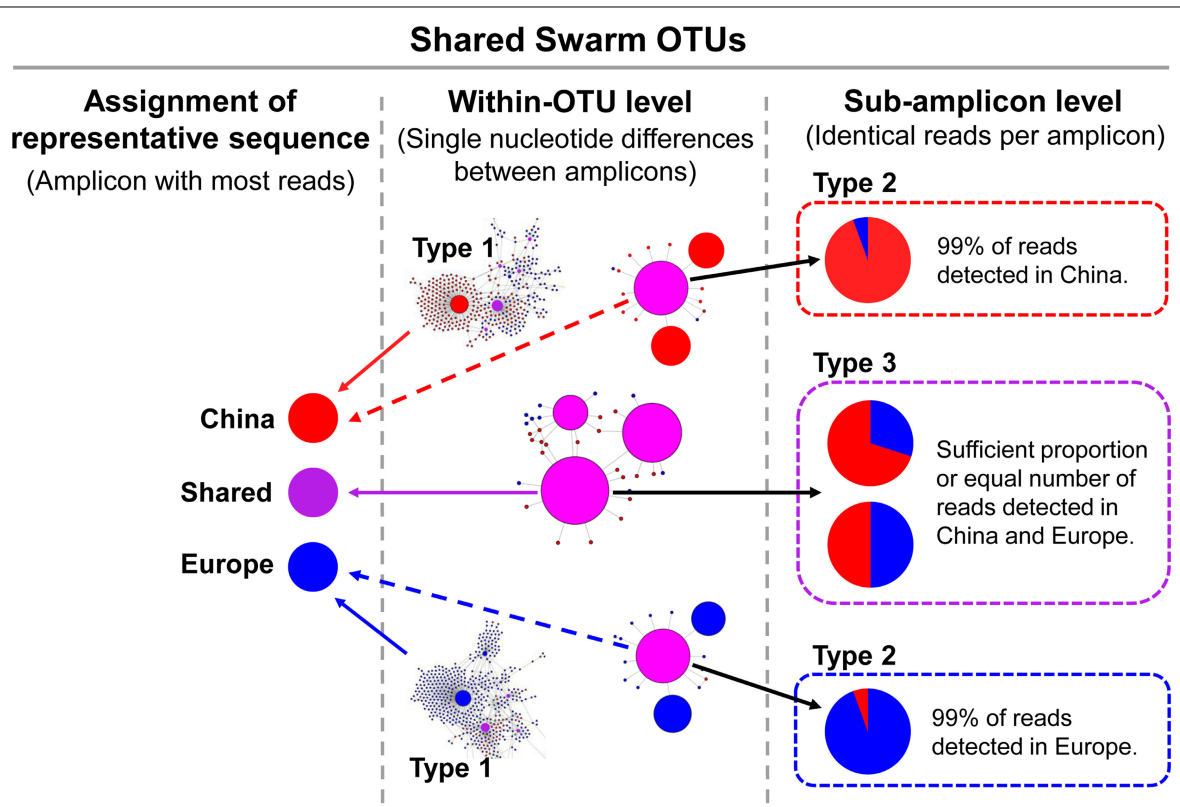

FIGURE 2 | Types of shared Swarm OTUs. The circle sizes in the within-OTU networks correspond to the read numbers of the respective amplicons. The representative amplicons (with highest read number) of the shared OTUs might comprise reads from China and Europe in different proportions. In Type 1 of shared OTUs, the representative amplicon consists of reads only detected in China or in Europe. In Type 2 of shared OTUs, only a minute proportion of reads was detected in the respective other region and is attributed to methodological artifacts (sample bleeding; Mitra et al., 2015). Accordingly, Type 2 of shared OTUs is interpreted as purely consisting of reads from the dominating region. In Type 3 of shared OTUs, similar read numbers from China and Europe constitute the representative amplicon.

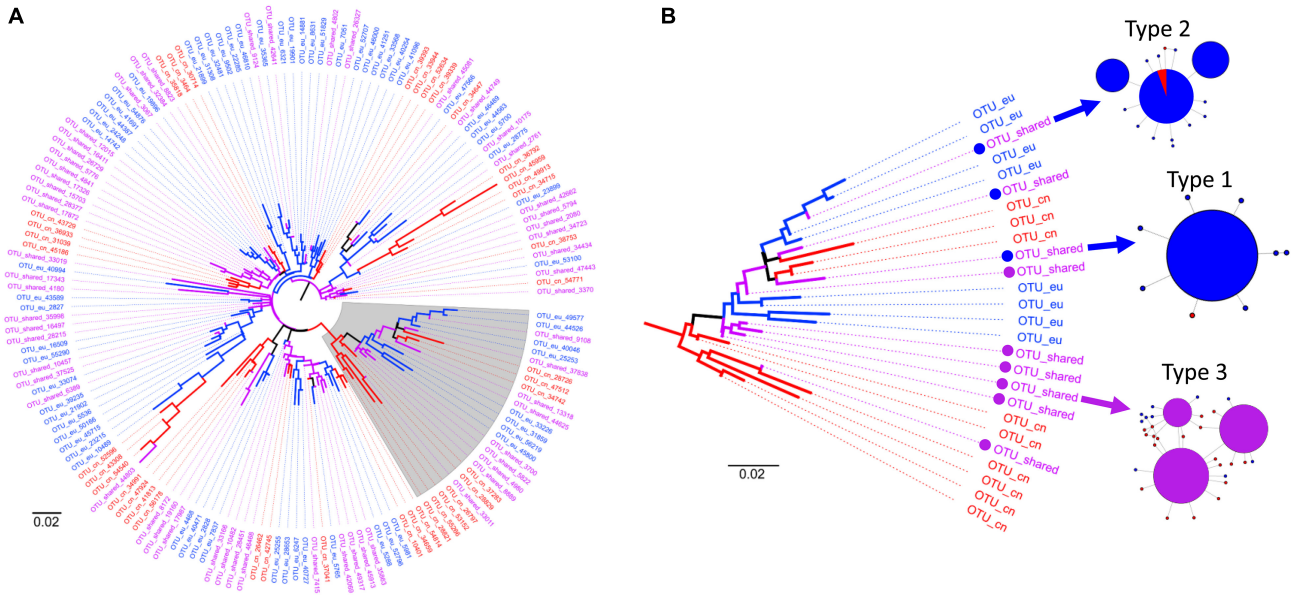

FIGURE 3 | Phylogenetic tree of the tintinnid *Tintinnopsis baltica* **(A)** and highlighted sub-clade **(B)** displaying various branching patterns with different types of shared Swarm OTUs. In Type 1, the representative amplicon of the shared OTUs was exclusively detected in one region but is associated to one or more amplicons from the respective other region. In Type 2, the representative amplicon consists of many reads from one region and only one or very few reads from the respective other region, which are interpreted as methodological artifacts (cp. **Figure 2**). In Type 3, the representative amplicon comprises a considerable number of reads from both regions.

Further geographic patterns emerged, e.g., in *Strombidium* sp.; yet, they are not supported by signature nucleotides. In the individual alignments, all signature nucleotides are restricted to an otherwise conserved section of the V4 (positions 59–152; **Supplementary Figure 2**), which comprises the highest read quality scores for each nucleotide position. In the same V4 section, signature nucleotides also occurred in other taxa (e.g., the oligotrichids *Strombidium* sp., Strombidiida XX sp., and the aloricate choreotrichid *Pelagostrobilidium* sp.; data not shown). However, they are not signature nucleotides characteristic for either geographic region as the separation of the OTUs is ambiguous; they represent phylogenetic signatures. These findings demonstrate the significance of this particular section of the V4 for ascribing amplicons to a certain geographic region.

In the two trees with nearly complete geographic separation (the oligotrichids *Spirotontonia* sp. and *Strombidium* K sp.), the majority of OTUs originate from China. The genealogy of *Spirotontonia* sp. including reference sequences (**Supplementary Figures 1A,B**) shows that a single shared OTU in the European clade (OTU 1377; 472 reads) is identical to one unidentified environmental sequence collected from the East Pacific Rise (KF129779) and nearly identical to another unidentified environmental sequence collected in the South China Sea (KJ760553). On the other hand, the reference sequences of *Spirotontonia turbinata* (FJ422994) and *Spirotontonia taiwanica* (FJ715634) described from coastal waters of China and north-eastern Taiwan, respectively, group closely together with a few basally branching Chinese OTUs, while the remaining Chinese OTUs are more distantly related to any reference sequence and display an intense radiation. Each reference sequence shares the signature nucleotides of the respective European or Chinese OTU clades they are assigned to. Interestingly, the reference sequence of *Spirotontonia grandis* from the South China Sea (KU525755) branching between both clades is not closely related to any particular OTU. Further, it shares 13 binary signature nucleotides with the European OTUs and two binary signature nucleotides with the Chinese OTUs.

The PR^2 reference sequences of the oligotrichid "taxa" *Strombidium* K sp. and Strombidiidae K X sp. are unidentified environmental sequences, but are related with sequences of two species sampled from Chinese coastal waters and deposited as *Strombidium triquetrum* (KJ609052; Gao et al., 2016) and *Strombidium capitatum* (KP260510; Song et al., 2015) in GenBank. The sequences of the four "taxa" are aggregated into the "Strombidiidae K cluster" in the PR^2 database. In the phylogenetic tree of the *Strombidium* K sp. OTUs and reference sequences (**Supplementary Figures 1C,D**), the *S. capitatum* sequence is related with the clade of European OTUs, while the sequence of *S. triquetrum* groups together with two PR^2 sequences in the cluster of Chinese OTUs. Both clades feature a huge genetic diversity as indicated by the numerous branches and partially considerable branch lengths. Signature nucleotides for the Chinese or European clades are shared by the respective reference sequences, except for the sequence of *S. capitatum*, which shares one binary signature with each of the two clades and two asymmetric signatures with the European clade.

In the phylogenetic tree of Strombidiidae K X sp. (**Supplementary Figures 1E,F**), two reference sequences

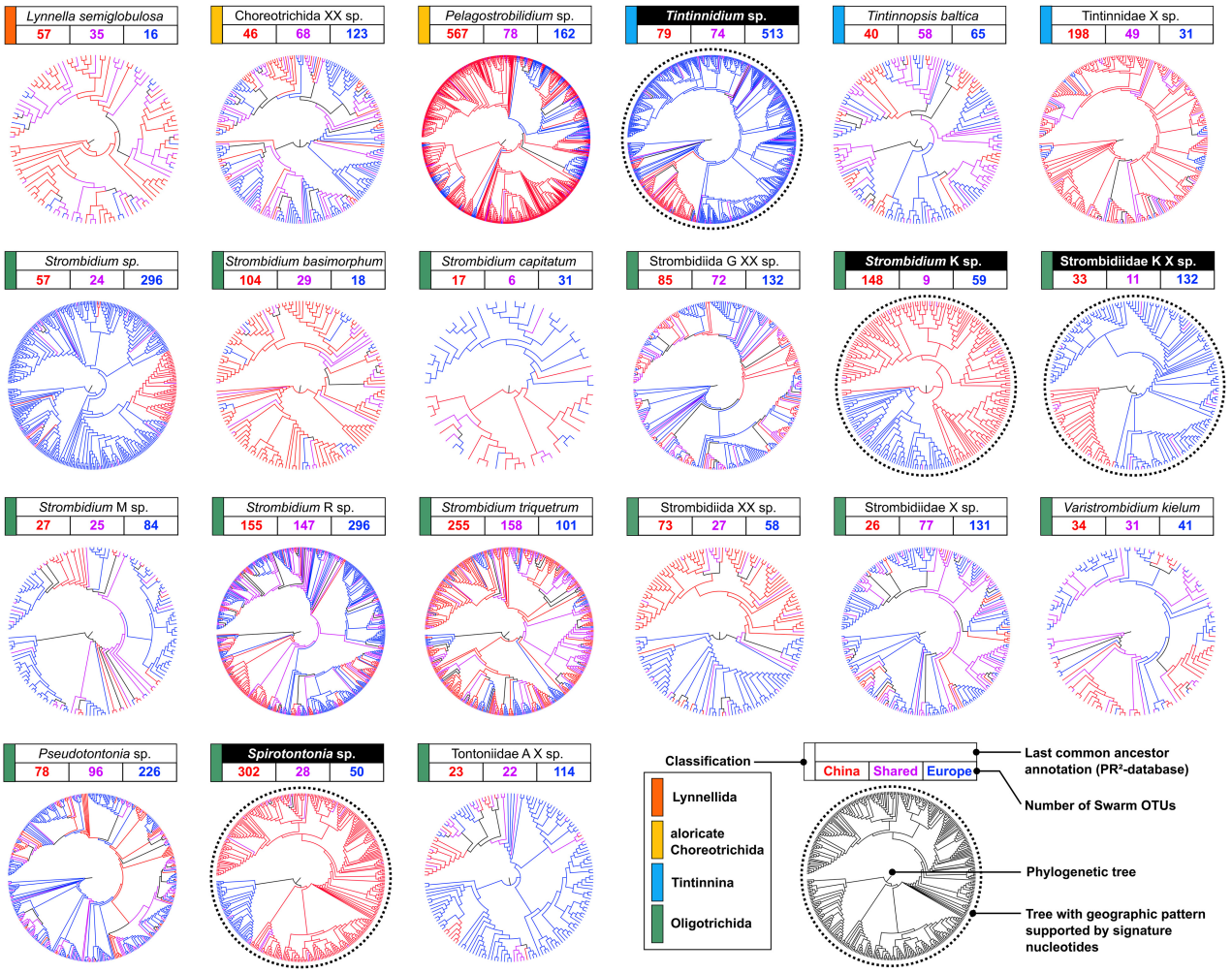

FIGURE 4 | Phylogenetic trees based on the representative sequences of the Swarm OTUs. Only trees that display a distinct geographic pattern supported by signature nucleotides are marked by "taxon" names highlighted in black and dotted circles.

from the eastern North Pacific (AF372790 and AF372789) and one sequence from the Mediterranean Sea (HQ394045) fall within the clade of Chinese OTUs, while one reference sequence from the eastern North Pacific (KJ762996) as well as one sequence from the North Atlantic (KC488382) are highly similar to a shared OTU (OTU 409) in the clade of mainly European OTUs. The latter clade comprises most sequences (including a single Chinese OTU) and is clearly separated from the clade of mostly Chinese OTUs by a long bifurcation. Additionally, both clades are characterized by 14 binary signatures.

The phylogenetic tree of *Tintinnidium* sp. (**Supplementary Figures 1G,H**) was complemented by reference sequences of known morphospecies belonging to the family Tintinnidiidae plus relevant sequences from the PR^2 database and an outgroup sequence belonging to the choreotrichid family Strobilidiidae (*Rimostrombidium lacustre*). The majority of OTUs form a predominantly Chinese and an exclusively European clade. Shared OTUs that group within these two clades contain 99% of reads from the respective geographic clade affiliation (Type 2 cp. **Figure 2**). Several OTUs branch between the outgroup sequence and the first reference sequences. The representative sequences of these OTUs are highly different from sequences of the Chinese and European clades (e.g., partly containing gap regions), indicating that they do not belong to the Tintinnidiidae at all and were thus excluded from the subsequent analysis of signature nucleotides. The clade of Chinese OTUs also contains eight European OTU sequences. Both the Chinese and European clades are supported by seven binary signatures. Interestingly, all reference sequences of known morphospecies (*Antetintinnidium mucicola*, *Tintinnidium fluviatile*, *Tintinnidium pusillum*, and *Tintinnidium balechi*) exclusively fall into the Chinese clade. The latter therefore comprises most of the currently known diversity of the Tintinnidiidae. Four unidentified environmental sequences, namely, from the Baltic Sea (FN690031), from two freshwater lakes in France and Germany (EU162620 and HM135052), and from the Columbia River estuary at the north-eastern Pacific coast (KJ925310), fall into a rather basally branching group of the European clade, while the

remaining European and related shared OTUs display a broad diversification into numerous subclades.

Those phylogenetically analyzed representative amplicons of Swarm OTUs that displayed clear geographical distribution patterns were subjected to a second-level clustering via sequence similarity networks (SSNs) along with reference sequences of the PR^2 database and closely related sequences of known morphospecies (**Figures 5**, **6**). The cut-off divergence at which the morphospecies separated into different network sequence clusters (NSCs) was determined for elucidating the number of NSCs without reference sequences; these may represent new species or ones lacking genetic data and await further validation, for example, by targeted recovery approaches (Gimmler and Stoeck, 2015). In both the oligotrichid *Spirotontonia* and the tintinnid *Tintinnidium,* a threshold of 98.5% sequence similarity was determined for separating the reference sequences of known morphospecies in the SSNs. The *Spirotontonia* network (**Figure 5**) contained five NSCs, which comprised 369 Swarm OTUs and 39,113 reads, indicating potential species. The largest of these NSCs was associated with *S. turbinata*; the smallest was associated with *S. grandis*. Both of these NSCs as well as two NSCs without any reference sequence predominantly included sequence data from Chinese samples. Only one NSC of a potential species included sequences predominantly from European samples as well as two unidentified environmental sequences.

The *Tintinnidium* network (**Figure 6**) contained at least six NSCs that indicated potential species. Four of these NSCs included unidentified congeneric environmental sequences, while two NSCs were not affiliated with any reference sequence. While the largest NSC and one without reference sequences predominantly included sequences from Europe, three smaller NSCs with reference sequences and the other NSC without affiliated reference sequences contained mostly sequences from China. One of the latter NSCs persistently contained reference sequences of the marine *T. balechi* and the freshwater *T. fluviatile* above thresholds of 98% because these two reference sequences share 99.5% V4 18S rDNA sequence similarity to another. The largest NSC of the *Tintinnidium* network consisted of two nearly separated groups of nodes (separation at 98.7% sequence similarity): one group with affiliations to reference sequences (*Tintinnidium* sp.), the other without affiliations to reference sequences. This pattern might indicate further potential species in the *Tintinnidium* network in addition to the six potential ones mentioned above.

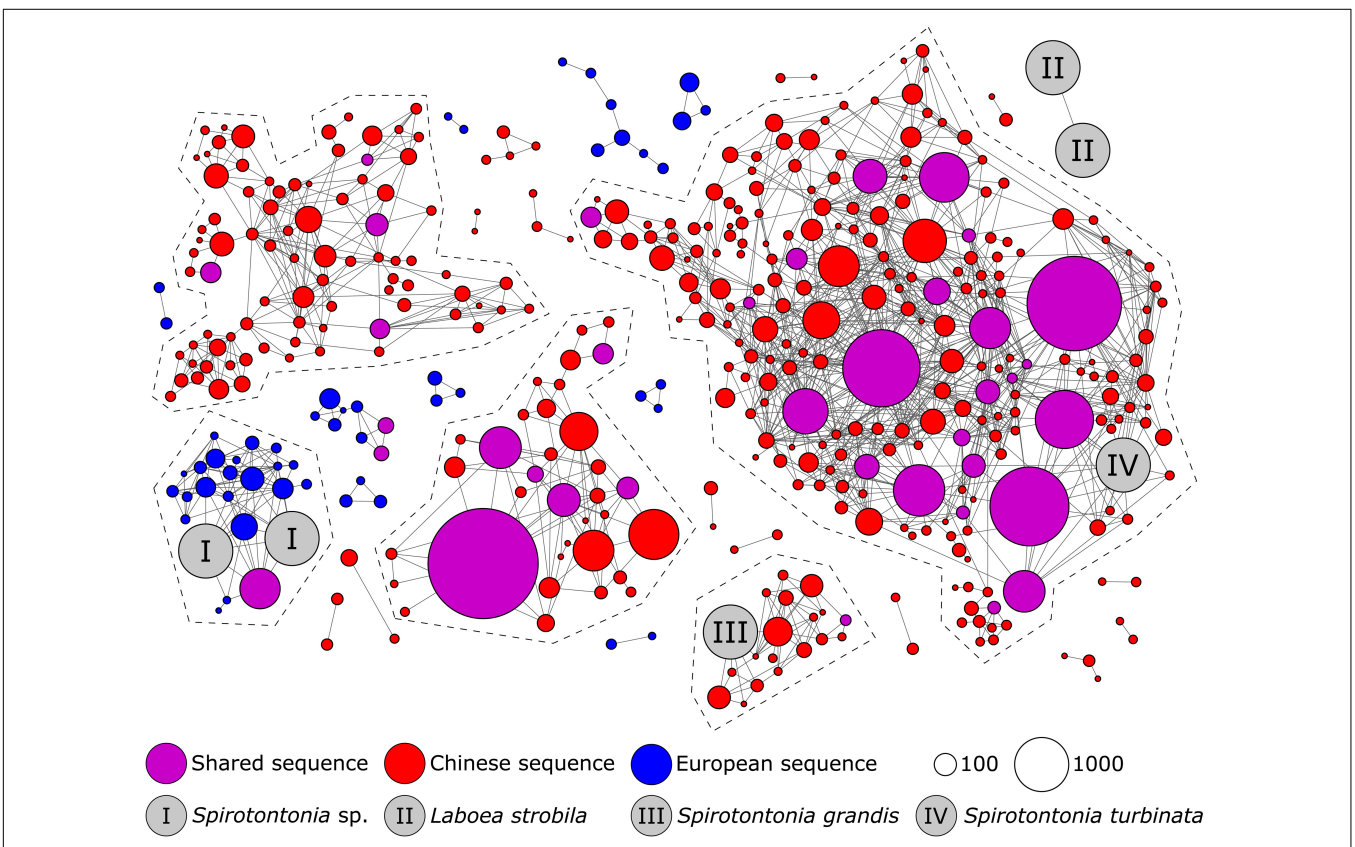

FIGURE 5 | Second-level clustering of the representative amplicons of Swarm OTUs detected in the present study and reference sequences from the PR^2 database assigned to *Spirotontonia* oligotrichids. At a threshold of 98.5%, the OTUs clustered into five network sequence clusters (NSC), two of which did not contain a reference sequence. *Laboea strobila*, a supposedly secondarily tail-less tontoniid with a somatic ciliary pattern identical to that in *Spirotontonia* species, remains separate. The circle sizes correspond to the read numbers of the representative amplicon sequences of the Swarm OTUs. NSCs which indicate potential species are framed by a dashed line.

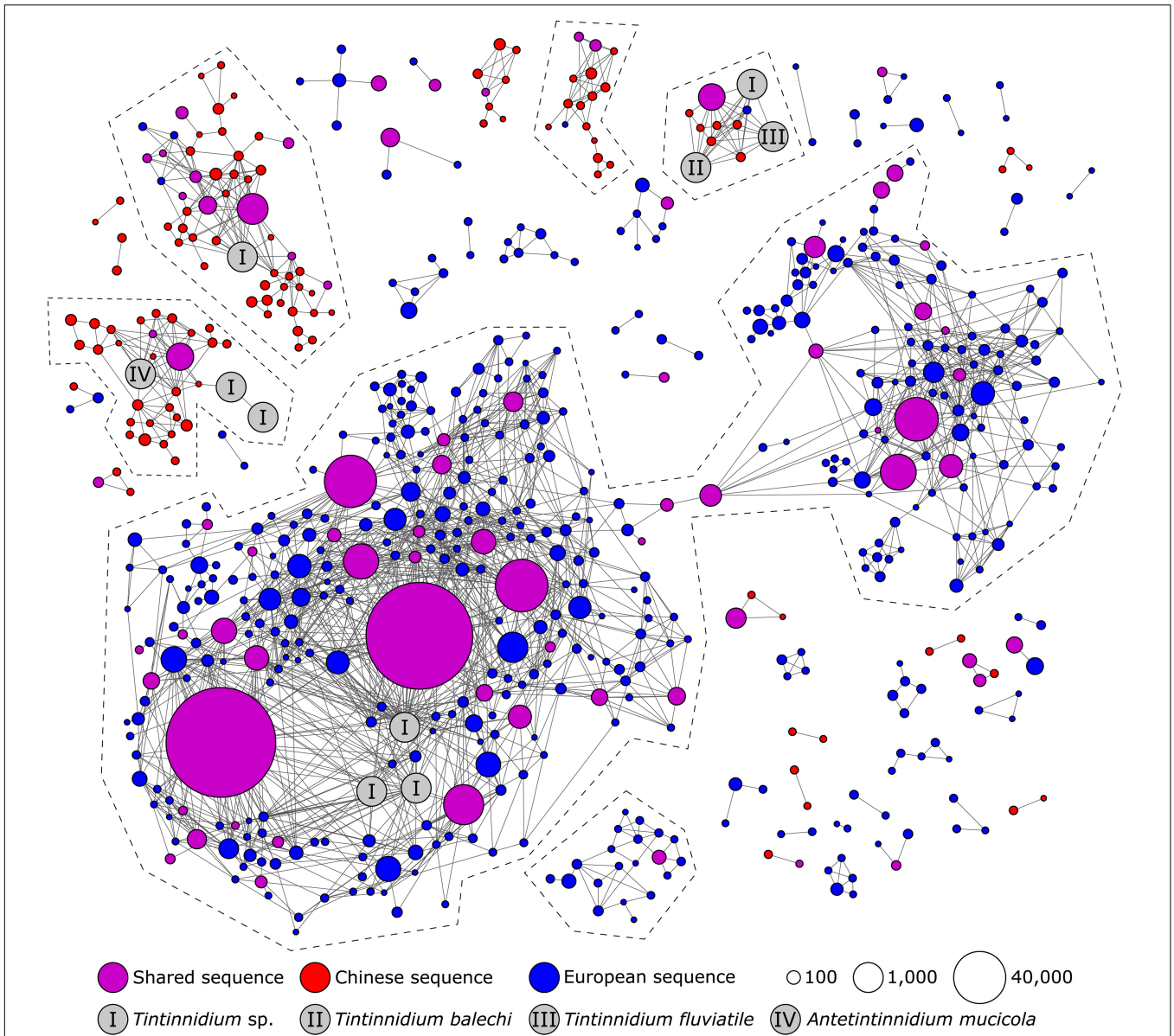

FIGURE 6 | Second-level clustering of the representative amplicons of Swarm OTUs detected in the present study and reference sequences from the PR^2 database assigned to the Tintinnidiidae tintinnids. At a threshold of 98.5%, the OTUs grouped into six larger network sequence clusters (NSCs), two of which did not contain any reference sequences and another two NSCs which contained unidentified congeneric reference sequences (*Tintinnidium* sp.). The circle sizes correspond to the read numbers of the representative amplicon sequences of the Swarm OTUs. NSCs which indicate potential species are framed by a dashed line.

Within Swarm OTU Assortativity Analyses

For 700 widespread (occurring in Chinese and European coastal waters) and abundant (comprising $\geq$ 0.0001% of the reads in the dataset) Swarm OTUs, assortativity analyses on the internal network structures were conducted. In 149 of these OTUs, assortativity values that were significantly higher than expected by chance for amplicons detected in Chinese samples were observed. Furthermore, 166 OTUs with assortativity values that were significantly higher than expected by chance for amplicons detected in European samples were found.

In another 211 of the 700 OTUs analyzed, the assortativity values were significantly higher than expected by chance for each geographic region simultaneously. Only patterns within these 211 OTUs are considered in the following and their results are displayed in **Figure 7**. Besides these significantly higher assortativity values, a disassortative grouping (assortativity $\leq$ 0) of amplicons from either region was discovered in 12 out of the 211 OTUs, most of which were taxonomically affiliated to the CONthreeP clade. In these OTUs, the slight tendency of amplicons to be connected to amplicons from the respective other region indicates that the effective dispersal between China

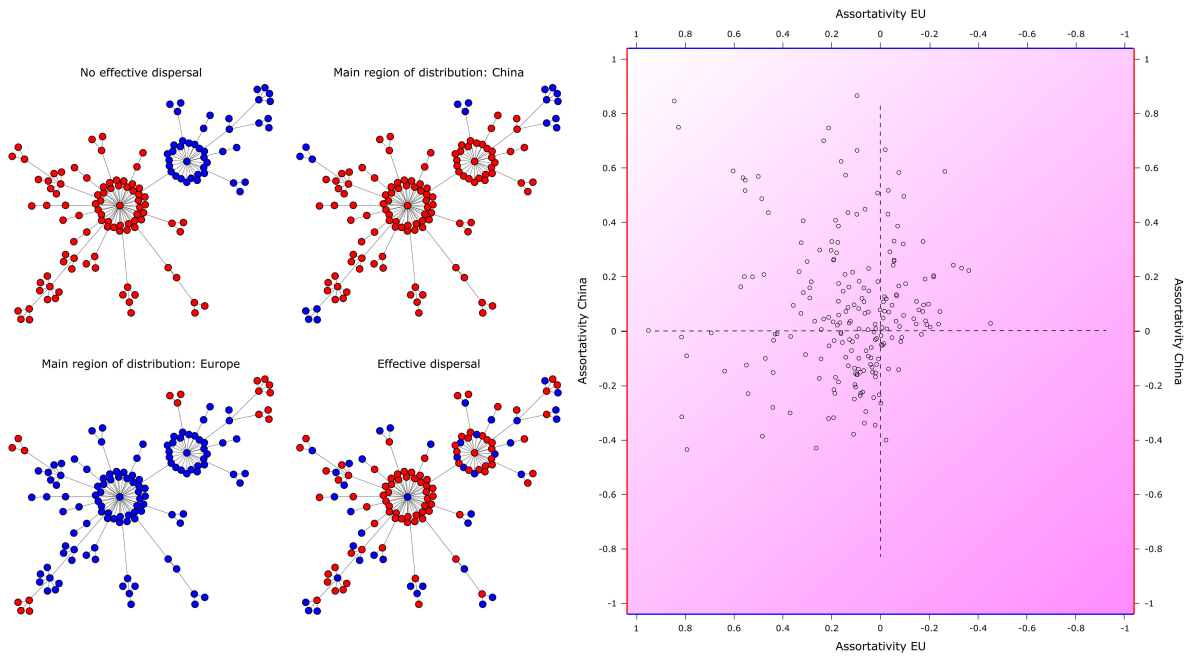

FIGURE 7 | Significant assortativity patterns of amplicons within 211 shared Swarm OTUs detected in Chinese and European (EU) coastal waters. **(Left panel)** Mock shared Swarm OTUs representing the four combinations of assortative and disassortative patterns (in these mock Swarms, node sizes were not scaled to read abundances). **(Right panel)** Each data point refers to a shared OTU and the respective assortativity values of its amplicons determine its placement in one of the four quadrants. **(Upper left)** Assortative grouping of amplicons from each region (indicating limited effective dispersal; 77 OTUs); **(upper right)** assortative grouping of Chinese amplicons, disassortative grouping of European amplicons (China main distribution area; 49 OTUs); **(lower left)** assortative grouping of European amplicons, disassortative grouping of Chinese amplicons (Europe main distribution area; 73 OTUs); **(lower right)** disassortative grouping of amplicons from each region (unlimited effective dispersal; 12 OTUs). Data points in the latter quadrant are scarce, since our analyses focused on OTUs which exhibited significantly higher assortativity values than expected by chance for sequences of both regions.

and Europe does not seem to be strongly limited (**Figure 7**; lower right quadrant).

There were 49 out of the 211 OTUs in which amplicons detected in China displayed a significant assortative grouping (assortativity > 0), but for which amplicons detected in Europe displayed a disassortative grouping (assortativity ≤ 0). For these OTUs (for an example see **Supplementary Figure 4A**), the assortativity of the amplicons in the internal OTU structure indicates a main area of distribution regarding genetic diversity in Chinese waters (**Figure 7**; upper right quadrant). Of those 49 OTUs, 23 were taxonomically affiliated to the Oligotrichida, eight to each the aloricate Choreotrichida and members of the CONthreeP, and four to the Tintinnina; taxonomic groups with less than three affiliated OTUs are not mentioned.

By contrast, there were 73 out of the 211 OTUs in which amplicons detected in Europe displayed a significant assortative grouping, but for which amplicons detected in China displayed a disassortative grouping. For these OTUs (for an example see **Supplementary Figure 4B**), the assortativity results indicate a main area of distribution regarding genetic diversity in European waters (**Figure 7**; lower left quadrant). The Oligotrichida were again the most abundant group among them, contributing 26 OTUs. Other abundant groups were the CONthreeP (23 OTUs), aloricate Choreotrichida (six OTUs), and Tintinnina (four OTUs).

Significant assortative groupings of amplicons from both Chinese and European waters occurred in 77 out of the 211 OTUs. Since the amplicons were mostly connected to amplicons detected in the same region, we suppose a limited effective dispersal between the regions for all these OTUs (**Figure 7**; upper left quadrant). Once more, the Oligotrichida were by far the most abundant group (42 OTUs), followed by the CONthreeP (14 OTUs), by OTUs that could not be assigned further than to the class Spirotrichea (nine OTUs), and by the aloricate Choreotrichida and the Tintinnina (four OTUs each).

DISCUSSION

Motivations for Coastal Sites and Sampling Strategy

Coasts are the ideal region for combining knowledge on ciliate plankton obtained by various methodological approaches. Apart from their easy accessibility, coastal habitats are characterized by high temporal dynamics and spatial heterogeneity, both of which are assumed to foster speciation (Norris, 2000). Climate variation and sea level changes severely affect the highly productive shallow coastal areas with their brackish water habitats. Sea level changes cause dramatic shifts in the distribution, the dimensions, and the connectivity of these regions (Palumbi, 1994). A drop in

sea level would thus restrict the neritic region to a narrow strip along the upper continental slope and thus reduce the habitat for specialized communities of coastal planktonic ciliates. Therefore, such regions are predestined for a bridge building approach like ours that aims to reconcile morphospecies, barcoded reference sequences, and OTUs in investigating geographic distribution patterns and their evolution, focusing on the community of oligotrichean ciliates. A comprehensive body of literature exists on neritic oligotrichean morphospecies (Cariou et al., 1999; Agatha, 2011; Liu et al., 2017; Hu et al., 2019). Furthermore, the majority of barcodes are from neritic taxa (Doherty et al., 2007; Bachy et al., 2012; Zhang et al., 2017; Santoferrara et al., 2018), and metabarcoding data are available (Santoferrara et al., 2014; Massana et al., 2015; Tucker et al., 2017).

Previous metabarcoding studies analyzed the genetic material obtained from entire microzooplankton or ciliate plankton communities and investigated community changes on higher taxonomic ranks (e.g., Massana et al., 2015). In our interdisciplinary multi-species approach, we combined the expertises of molecular ecologists and ciliate taxonomists to focus on the geographic patterns of particular ciliophoran Swarm OTUs and the interpretation of these patterns under evolutionary aspects. Thereby, our sampling strategy stands out from commonly applied approaches. In contrast to previous studies, our dataset is based on a material collection that complements a high temporal resolution (seasonal and daytime shifts) and large geographic distances between samples. Since the sea and the neritic regions are dynamic (Abboud-Abi Saab and Owaygen, 1998; Marteinsson et al., 2016; Huang et al., 2021) and highly structured horizontally and vertically (McManus and Woodson, 2012), environmental patchiness is a question of scale. Additionally, these regions are very heterogeneous for protists effecting together with community assembly processes a patchy distribution highly likely prone to undersampling. Previous data from our sampling regions indicate a pronounced seasonality in the ciliate community compositions (Mozetič et al., 1998; Witek, 1998; Gómez and Gorsky, 2003; Jiang et al., 2013; Yang et al., 2014). Despite the comparatively intensive sampling, however, only a small part of the pronounced seasonality with short abundance peaks and a rapid turnover of the dominating taxa could be caught. Likewise, the limitation to Chinese and European sites prevents an investigation of the entire taxon ranges.

Considerations for Innovative Pattern Inference on Between- and Within-OTU Level

Metabarcoding is a powerful complement to taxonomic surveys, especially when comprehensive and taxonomically validated reference databases enable unequivocal species identification. In this study, we contribute a novel approach combining phylogenetics, signature nucleotide analyses, and network analyses to enable an unprecedented investigation of genetic diversity patterns on multiple scales. Swarm is an ideal *de novo* clustering method to generate OTUs from metabarcoding data based on single nucleotide differences while retaining the underlying diversity in the amplicon networks. Different timescales can be investigated on between- and within-OTU levels: phylogenetic trees of the representative amplicon sequences (between-OTU level) visualize comparatively older processes (e.g., past effective dispersal and speciation events), whereas the internal network structure of Swarm OTUs (within-OTU level) may display more recent divergences on sub-species level. Albeit we are pretty sure to have ascertained genetic differentiations that evolved on different time scales, the distinction between intra- and interspecific sequence deviations remains blurry (Santoferrara et al., 2020).

In Swarm OTUs, those sequences resulting from natural genetic variation as well as some artificially created ones (see discussion below) group around the amplicon with the highest read number (the 'representative,' 'seed,' or 'dominant' amplicon). We interpret the numerous amplicons with much fewer reads (the 'minor' amplicons) than the 'dominant' one as intraspecific V4 variants generated by imperfect concerted evolution of the ribosomal DNA tandem repeats (Ganley and Kobayashi, 2007). In marine planktonic diatoms, Gaonkar et al. (2020) found a general correlation between the number of haplotypes comprising a taxon and the number of reads in its 'dominant' haplotype. Interestingly, the 'minor' amplicons of our dataset frequently displayed some peculiarities, namely, some were exclusively detected either in China or in Europe and thus exhibited a clear affiliation to one geographic region. It is unclear whether they originated from an ongoing splitting process or a recent merging of conspecific populations; yet, we favor a diverging scenario in cases where the dominant amplicon is truly shared. Estimating the extent of this intraspecific variation is crucial for metabarcoding studies, in which the 'minor' amplicons might indicate a considerable rare diversity. In the present study, the number of supposed 'minor' amplicon variants surpasses by far the findings obtained from sequencing up to three conspecific specimens and subsequent cloning steps in most major ciliate groups (Gong et al., 2013; Wang et al., 2017, 2019). We agree with these and previous studies that most genetic diversity originates from the high number of low-divergent sequence variants present in individuals of single ciliate species (Forster et al., 2019; Zhao et al., 2019). OTU clustering by Swarm in combination with second-level clustering turned out to represent an elegant solution to this problem, since the approach allows for inferring species-specific thresholds (Forster et al., 2019; Wang et al., 2019; Zhao et al., 2019).

Nevertheless, not all low-divergent ('minor') amplicons necessarily originate from real biological variation, but may instead reflect artificial sequences caused by methodological errors. A perfect distinction between these two types of sequences is currently impossible, but, of course, important for accurate diversity estimations (Brown et al., 2015). Potential error sources that generate non-biological sequences occur in the PCR amplification process, for instance, by a decrease in polymerase fidelity, thermal damage (Pienaar et al., 2006), or by the formation of chimeric sequences from two or multiple parental sequences (Lahr and Katz, 2009). Artificial sequences may also be generated during high-throughput sequencing (HTS) by erroneous base calls (Bokulich et al., 2013). Another often ignored error source in

HTS is sample bleeding, which is caused by incorrect assignment of small numbers of reads to multiplexed samples processed on the same sequencing lane (Mitra et al., 2015). Because of the fine-scaled resolution in our approach, we could observe events of sample bleeding and attribute Swarm OTUs with more than 99% of reads from one region and less than 1% of reads from the other region to this phenomenon.

To exclude artificially generated sequences from potential HTS error sources, we took several precautions and followed advices for best practices in sequence quality filtering[4]. Thus, except for sample bleeding (which may assign real biological sequences to the wrong sample), we conclude that only a negligible part of the genetic variation in our dataset is of non-biological origin. As a consequence, we further presume that the effect of artificial sequences on assortativity analyses will be of minor relevance. Since artificially generated sequences are highly unlikely to be generated from scratch, but rather from a dominant parental amplicon, both the artificial and dominant sequence will carry the same geographic information. This scenario is therefore not altering results of Swarm OTUs that consist completely or nearly completely of amplicons from the same region. In Swarm OTUs that include amplicons from different regions, artificial sequences might increase the number of edges between amplicons from the same region and therefore lead to more assortative patterns. Regarding the latter, though, we refer again to our quality filtering strategy, which removes low-quality sequences before clustering in Swarm is conducted. In addition, the patterns observed by within-OTU analyses were further corroborated by between-OTU analyses, which imply that they are not the result of artificially created sequences.

Denoising algorithms are an alternative to our sequence quality filtering strategy and have gained in popularity for analyzing metabarcoding datasets (e.g., Callahan et al., 2017). While denoising metabarcoding data prior to OTU clustering in Swarm is possible, too many of the low-abundant 'minor' sequence variants are aggregated into central consensus sequences or discarded by the denoising algorithms (Antich et al., 2021). The denoised dataset thus contains only few amplicons that can be further clustered by Swarm. Instead, the majority of these denoised amplicons are placed in standalone Swarm OTUs (i.e., singleton OTUs of high read abundance) without any other amplicon. Denoising a dataset before clustering in Swarm is therefore counter-effective for evaluating underlying network topologies of Swarm OTUs and exploring distribution patterns of genetic diversity with our newly introduced strategy.

Geographic Patterns and Diversity at Swarm OTU Level

The vast majority of Swarm OTUs in the present study were detected either in China or in Europe, whereas only a small proportion represents shared OTUs, admittedly, though, with high read numbers. Several phylogenetic relationships between the OTUs confirmed the occurrence of geographic patterns and indicate continuing limitations of effective dispersal. Some of the highly diversified clusters found only in one region branch basally and suggest historic cladogeneses with a high degree of genetic divergence possibly due to large population sizes. The geographic patterns are further corroborated by region-specific signature nucleotides detected by means of DeSignate (Hütter et al., 2020). The analyses focused on the most abundant ciliates in coastal waters, namely, the Oligotrichea. Four of them displayed geographic patterns, namely, the oligotrichid *Spirotontonia* sp., two further oligotrichids of the genus *Strombidium* (*Strombidium* K sp. and Strombidiidae K X sp.), and the tintinnid *Tintinnidium* sp.

The genus *Spirotontonia* Agatha, 2004 currently comprises three species (*S. grandis*, *S. taiwanica*, and *S. turbinata*). Like all Tontoniidae Agatha, 2004, it is characterized by a highly contractile tail. The single somatic kinety forms a sinistral spiral around the cell. The genus *Laboea* Lohmann, 1908 shares this somatic ciliary pattern and is considered a secondarily tail-less tontoniid based on ribosomal DNA phylogenies (Gao et al., 2009). Based on literature data about morphospecies, the genus is distributed in the Arctic Sea, the Mediterranean Sea, the North Atlantic, the North Pacific, and the Indian Ocean (SA, unpubl. data). Although no Chinese OTU grouped within the clade of European OTUs, the close relation between reference sequences from China and few European OTUs with identical signature nucleotides indicates that similar sequences occur in China, but were not detected in the present study. Yet, Chinese OTUs could not be detected in Europe, considering that the single or few reads from the respective other region in the shared OTUs are methodological artifacts caused by sample bleeding. The Chinese OTUs probably represent more than the currently known species (*S. turbinata* and *S. taiwanica*) given the numerous short branches, which suggest a radiation with a high diversification rate. *Spirotontonia grandis* might be of hybrid origin as its reference sequence shares signature nucleotides with amplicon sequences from both the Chinese and European clades. In the related euplotid ciliates, hybridization for instance caused by an overlap in the pheromone structures and inter-specific mating further increases the complexity of the interpretations (Luporini et al., 2016). The phylogenetic tree features a high diversity beyond reference sequences of known morphospecies, which is corroborated by the second-level clustering proposing at least two new *Spirotontonia* species in Chinese coastal waters.

The *Strombidium* K cluster contains numerous reference sequences labeled as *Strombidium* K sp. and Strombidiidae K X sp., respectively, and two reference sequences of morphologically identified species. Considering the original descriptions, however, the identification of these morphospecies is doubtful, and their sequences probably belong to different species. *Strombidium capitatum* (Leegaard, 1915) Kahl, 1932 was discovered in the Northeast Atlantic (reported as *Laboea capitata*). *Seravinella pectinata* Alekperov and Mamaeva, 1992 is based on a completely deformed and destroyed *S. capitatum* cell as revealed by the reinvestigation of the type slide. Further reports of the morphospecies come from the Arctic Sea, the North Atlantic, the Mediterranean Sea, the South Atlantic, the North Pacific, the Indian Ocean, and the Antarctic Sea (SA, unpubl. data). The GenBank sequence KP260510 was linked to a specimen identified as *Strombidium capitatum* sampled from

[4]https://github.com/frederic-mahe/swarm/wiki/Fred's-metabarcoding-pipeline

Chinese coastal waters (Song et al., 2015). The gene sequence is accompanied by a short description, line drawings, and micrographs. The line drawings and one micrograph come from a previous study on *S. capitatum*; the remaining micrographs do not provide many details and primarily depict a conspicuous apical protrusion. Conspecificity of the sequenced specimens with *S. capitatum* is questioned by a much larger cell size (90–135 μm × 70–100 μm vs. 45–70 μm × 40–60 μm) and much longer extrusomes (22–24 μm vs. about 15 μm; Song et al., 2015). Hence, a cryptic species different from *S. capitatum* might have been sequenced. *Strombidium triquetrum* Agatha and Riedel-Lorjé, 1997 was described from the North Sea; further reports of this morphospecies do not exist. Gao et al. (2016) sequenced specimens identified as *Strombidium* cf. *capitatum*; the sequences were deposited in GenBank and included in the PR^2 database under the name *S. triquetrum*. Since the associated stamp-sized micrograph merely displays the anterior cell portion of a protargol-stained specimen, conspecificity is uncertain. The high amount of genetic diversity present in the *Strombidium* K cluster, which was partly restricted to one region, suggests several potentially new species. Nevertheless, attention should be paid to the reliable identification of species, using original descriptions or authoritative redescriptions to avoid an incorrect linkage of reference sequences and morphospecies.

The family Tintinnidiidae currently comprises the genera *Antetintinnidium* Ganser and Agatha, 2019, *Membranicola* Foissner et al., 1999, and *Tintinnidium* Kent, 1881 with in total 16 species (SA, own data). Considering the genetic divergence between known morphospecies (*Antetintinnidium mucicola*, *T. fluviatile*, *T. pusillum*, and *T. balechi*), the enormous genetic diversity recognizable in the European clade of the *Tintinnidium* sp. phylogeny suggests the presence of several as yet unknown species, which very likely differ distinctly in their cell morphologies. Likewise, the second-level clustering of *Tintinnidium* sp. yielded two network sequence clusters (NSC) with known morphospecies and additionally three clusters of probably novel Tintinnidiidae taxa. In addition, the NSC which contained the most amplicons and reads could only be linked to *Tintinnidium* sp. reference sequences, suggesting another unknown morphospecies. The relationships in the phylogenetic trees propose several independent introductions of Tintinnidiidae from brackish waters into freshwater (Ganser and Agatha, 2019).

In contrast to the abovementioned taxa, the majority did not display distinct geographic patterns. Exemplary for these taxa, OTU sequences assigned to the tintinnid *Tintinnopsis baltica* Brandt, 1896 were analyzed. The species had been established based on material from the Baltic Sea. Further reports of the morphospecies are from the Antarctic/Sub-Antarctic Sea, the North Atlantic, the Mediterranean Sea, the Black Sea, the Sea of Azov, the Southwest Atlantic, the North Pacific, the Southeast Pacific, and the Indian Ocean (SA, unpubl. data). Its tree topology might be interpreted as alternating multiple invasions, suggesting that this species belongs to a group of organisms with effective long-distance dispersal. Thus, allopatric speciation is probably a slow process in this tintinnid which might be indicated by the identical V4 regions in *T. baltica*, *T. acuminata*, and *T. nana*.

All phylogenetic analyses corroborate each other and shed light on previously undetected aspects of diversity. On the one hand, novel diversity, i.e., potentially new species or ones for which genetic data are not available, emerged in both the phylogenetic trees and the second-level clustering. On the other hand, geographical distribution patterns of OTUs in Chinese and European coastal waters were revealed by phylogenetic trees and second-level clustering and, in several cases, were further underpinned by signature nucleotides. In the future, 'dominant' amplicon sequences that are not closely related to sequences of a known morphospecies may enable the identification and proper description of new species, following a 'reverse taxonomy' or 'targeted recovery' approach (Markmann and Tautz, 2005; Gimmler and Stoeck, 2015). The sampling site and season at which the amplicon sequence was recorded together with the signature nucleotides detected by DeSignate (see above) further facilitate this aim.

Geographic Patterns and Diversification Within Widespread Swarm OTUs

Magnifying the resolution of sequence analyses from between Swarm OTU-level to within Swarm OTU-level further emphasized the existence of distribution patterns. Compared to results from phylogenetic analyses, which focus on sequences between which a sufficiently high sequence divergence has led to the establishment of genetically distinct units (OTUs), the assortativity analyses explore relatively recent or even ongoing processes (e.g., effective dispersal and gene flow), in which the genetic divergence is momentarily insufficient for establishing distinct OTUs.

Since our network analyses aimed at revealing dispersal limitations, the interpretations focused on those 211 widespread and abundant Swarm OTUs within which amplicons from each region had a significantly higher assortativity value than expected by chance. Using our novel approach, we distinguish three different scenarios by interpreting the assortative and disassortative patterns of amplicons within these shared OTUs. (i) No effective dispersal takes place. The assortative grouping of both the Chinese and the European amplicons indicates genetically different amplicon clusters that presumably experience limited gene flow. With increasing genetic divergence, it may eventuate in an allopatric speciation. One or very few edges (connections) between distinct clusters of amplicons from different regions suggest founder events followed by bottlenecks and genetic drift. This scenario was observed in 77 OTUs. (ii) The main area of distribution is apparently restricted to one particular region. This distribution pattern might be attributed to species sorting, i.e., the presence or absence of an appropriate niche, a rather recent dispersal limitation, or an extinction event without considerable resettlement. This scenario dominated in the present dataset on planktonic ciliates from European and Chinese coastal waters. It was observed in 122 OTUs: 49 OTUs with main area of distribution in China and 73 OTUs with main area of distribution in Europe. (iii) Effective dispersal takes place. The disassortative grouping of amplicons in the OTUs does not follow a clear geographic pattern owing to the lack

of a strong genetic separation between Chinese and European amplicons. Possibly because the ciliates are capable of effective dispersal or because their evolution rates are so low that they did not genetically diverge after spatial separation. This scenario was rarely found owing to our selection of OTUs (see section "Materials and Methods"). Although the patterns perceived are highly interesting, they necessitate further interpretations by intertwining them with future data, for instance, on the species' autecology (see section "Outlook"). By demonstrating geographic patterns on within-OTU level, we contradict Caron and Hu (2019) in that the knowledge far beyond species-level distinctions has no practical value.

Potential Causes for Geographic Patterns and Diversification

The "everything is everywhere, but the environment selects" tenet states that protist taxa are dispersed globally, but form populations only where the environmental conditions (abiotic and biotic) are suitable for them; otherwise, they might be present merely as resting cysts (see below). Since the autecology (including dispersal rates) and thus the niche parameters are unknown for the majority of Oligotrichea (Maselli et al., 2020), it is impossible to tell apart ecological and historical effects that cause distribution patterns (Bass and Boenigk, 2011).

Studies on the effective dispersal capabilities of marine planktonic ciliates are currently missing. The sparse evidence are records of identical marker gene sequences at the east and west coasts of the North Atlantic plus adjacent sea regions and in the Northwest Atlantic and Northeast Pacific (see section "Introduction"). For pelagic cyanobacteria, copepods, and foraminifera (Darling et al., 1999, 2000; de Vargas et al., 1999), genetic data indicate a strong effective dispersal across ocean basins as well as between them (Norris, 2000). Interestingly, almost identical gene sequences (three base pairs difference in the 18S) of planktonic foraminifera were detected in the Northeast Pacific and Mediterranean Sea, and a transport from east to west is supposed owing to the prevailing surface currents (Darling et al., 1999). These data imply that many foraminiferan genotypes have either evolved only slightly after their spatial separation or they are still capable of an effective dispersal. Molecular data on bipolar planktonic foraminifera and benthic ciliates as well as morphologic data on a planktonic tintinnid (*Acanthostomella norvegica*) suggest a *trans*-tropical effective dispersal (Darling et al., 2000; Di Giuseppe et al., 2013; Dolan and Pierce, 2013).

The metacommunity structure of small organisms with relatively high dispersal rates is probably dominated by species sorting and mass effects rather than by dispersal limitation and patch dynamics (De Meester, 2011). Likewise, Norris (2000) concluded that ranges of many pelagic groups are much more limited by their ability to maintain viable populations than by any inability to disperse across tectonic and hydrographic barriers. Oceanographic and climatic changes may create new habitats with new niches instead of preventing dispersal. Such shifting selective regimes have been found to generate large genetic differences very quickly, even between large populations that are not completely isolated (Palumbi, 1994). Three scenarios of species-niche interactions were discussed (Weiner et al., 2014). (i) Dispersal is limited. Bottlenecks, genetic drift, and abiotic boundaries may cause in concert the differentiation of allopatric sister lineages. (ii) Dispersal is rather unlimited and species interaction are negligible; the distribution of species thus probably reflects the spatial realization of appropriate niches. (iii) Species interactions are considerable; competitive exclusion hence influences the pattern of niche occupation. The present heterogeneous data on marine planktonic ciliates from Chinese and European coastal waters propose that all three scenarios are realized.

Dispersal limitation can, however, not be concluded from the absence of an active ciliate species at a particular site, i.e., a more intensive sampling might prove at least some of the Oligotrichea to be more widely dispersed and distributed, resulting in an increased number of shared amplicons in the Swarm OTUs. In non-random processes, planktonic Oligotrichea might be dispersed as active states by water currents over large areas or possibly even globally; but, the timespans are long compared to their generation times, questioning whether it is possible for a species to be cosmopolitan. In response to external triggers, many protists are, however, capable to form more or less resistant resting cysts (Foissner, 2011). Actually, some oligotricheans are known to generate at least occasionally resting cysts, and several similar shaped, but unidentified forms had been described (Meunier, 1910; Kim et al., 2002; Rubino et al., 2002; Agatha et al., 2005). Yet, the viability of the cysts and hence the ability to excyst decreases with time (Kim and Taniguchi, 1997). The factors controlling encystment, excystment, and viability of cysts may differ among closely related protist species and probably even between clones of the same species (Weisse, 2008). Since cysts also seem to sediment rather rapidly (Kim et al., 2008), they are very rarely found in plankton samples collected in the upper 2 m of the water column (SA, own observ.). Therefore, long-distance dispersal of suspended cysts and a subsequent population growth are probably rare events for oceanic taxa (Agatha, 2011), while cysts might easily be resuspended in shallow coastal waters during storm events. In the present study, the probability is low that considerable quantities of vital resting cysts were among the sequenced material, which was confirmed by microscopic inspection of some samples.

In the phylogenies based on our data, we detected comparatively deep and more recent splits; in addition, the assortativity values of some shared OTUs indicated ongoing divergence, possibly speciation. The origin of the Choreotrichida and Oligotrichida took place ca. 462 million years ago (mya) after an extreme boost on speciation rates in the stem branch linking these taxa to the hypotrichs (Fernandes and Schrago, 2019). Based on the ribosomal data set comprising the 18S, 5.8S, and 28S rDNA, the divergence time of the oligotrichids was calculated to 199–443 mya and that of the choreotrichids to 256–447 mya. A significant diversification rate shift commenced at the stem branch leading to the Perilemmaphora (= hypotrichs + oligotrichids + choreotrichids) at the Ediacaran period (about 550–650 mya) with the development of numerous new lineages. While the mean rate of nucleotide substitutions per 100 million years is rather low (μ = 0.0185) for the

ciliate ribosomal dataset, the substitution and speciation rates are markedly higher in the Perilemmaphora with on average 0.779 (0.635–0.956) species per million years (my). Their extinction rates were distinctly (5×) lower compared to the speciation rates and have remained nearly constant throughout time (0.011–0.396 species/my). At that time, the climate and the water currents were totally different from those prevailing today. Generally, the combination of high speciation rates with cladogenesis and low extinction rates generates an accumulation of lineages with long branches. However, the ribosomal time-calibrated tree of Fernandes and Schrago (2019) demonstrated an exceptional pattern in the cluster of hypotrichs, oligotrichids, and choreotrichids with several radiation events concentrated at the tips of the tree. The cladogenetic success of the Perilemmaphora is thus probably most likely a consilience of accelerated speciation rates and lineage accumulation. The combination of sexual reproduction and cell divisions might strongly promote the generation of local adaptations according to De Meester et al. (2002). The first reliable tintinnid fossils are from the Jurassic. Since they seem to be fully developed, the tintinnids apparently have an even longer history (Lipps et al., 2013), matching the abovementioned calculations by Fernandes and Schrago (2019).

In contrast to the conception that long-distance dispersal mitigates speciation by swamping the gene pool of the resident population, Norris (2000) suggests that long-distance dispersal may actually promote evolution by regularly carrying variants of a species across major oceanic fronts and thus exposing them to very different selection pressures than those occurring in their home range. Accordingly, large populations may accumulate mutations beneficial in particular environments in which natural selection and further adaptation take place, resulting in a differentiation from the parental population and finally a speciation (Shapiro et al., 2016). The experimental evolution of dispersal and movement in the freshwater ciliate *Tetrahymena* illustrated an increase in individual movement velocity and overall dispersal rates of populations at the margins of their distribution range over time (Fronhofer and Altermatt, 2015). Soft hydrographic barriers might cause populations to experience selection sufficiently strong on either side that speciation may take place, although they do not inhibit dispersal completely (Martín et al., 2020). Actually, individual populations might be more isolated than currently accepted as patterns of dispersal and connectivity could be highly structured (McManus and Woodson, 2012). Even sympatric speciation is possibly more widespread than previously assumed and is facilitated by environmental gradients of intermediate slope (Dieckmann and Doebeli, 1999; Doebeli and Dieckmann, 2003). An isolation by ecology, namely, regarding the depth or season of reproduction, had been described in planktonic foraminifera. In euplotid and hypotrich ciliates, any mutations in the coding sequence of a pheromone results in a new pheromone and a new pheromone receptor and thus in a new mating type (Luporini et al., 2016). Likewise, shifts in the seasonal occurrence or isolation in confined coastal areas may have been involved in the observed rapid speciation of the Oligotrichea.

Studies on the marine biogeography date back to more than 150 years and described a close linkage between faunistic and hydrogeographic features of the major oceanic water masses, resulting in a circumglobal warm water region with subtropical and tropical provinces and Northern and Southern cold water regions with polar and subpolar provinces (Zeitzschel, 1990). Van der Spoel and Heyman (1983) defined planktonic faunal centers with taxa sharing the same ecological preferences or ancestral forms, which simultaneously represent the main spots of speciation and dispersal. Many studies based on morphospecies discovered rather similar patterns in the distribution of planktonic organisms (Zeitzschel, 1990). In contrast, the Longhurst (2007) ecological provinces are primarily based on the primary production and frontal systems. Likewise, the preliminary metabarcoding studies revealed geographic patterns on community level. Yet, the rationales differ: some publications ascribe the observed patterns to abundance-dependent dispersal, while others regard species sorting, community interactions, or dispersal limitations as crucial. The present findings covering data from three Longhurst provinces suggest that marine planktonic ciliates, specifically, the Oligotrichea, might display similar geographic zonations as other planktonic organisms.

With the present study, a new perspective to this discussion is added by analyzing distribution patterns on within-OTU level down to single nucleotide differences. The impressive number of Swarm OTUs with records restricted to China or Europe and the geographical distribution patterns of sequences within OTUs revealed by assortativity analyses suggest an inverted scenario of the moderate endemicity model concerning the distribution of planktonic ciliates in coastal waters. This implies that the majority of marine planktonic ciliates has a restricted distribution, while only few have a wide, potentially cosmopolitan distribution.

Outlook

While we discovered a considerable variation in geographic distribution patterns of planktonic ciliates in Chinese and European coastal waters, the causes remain unknown. It is crucial to bring life-history traits into play, which are highly likely linked to (effective) dispersal. Much more experiments have to be conducted for comprehending the dispersal of active and resting stages, the formation of resting cysts and their viability, as well as the autecology regarding abiotic factors, food items and preferences, functional, numerical and thermal traits. For addressing these topics, we have to go beyond the simple assumption that geographical patterns are size-dependent (Jenkins et al., 2011). Nevertheless, our novel approach can uncover variational patterns at a resolution up to single nucleotide differences and is applicable to investigate any group of interest.

DATA AVAILABILITY STATEMENT

The datasets generated for this study can be found in online repositories. The names of the repository/repositories and accession number(s) can be found in the article/**Supplementary Material**.

AUTHOR CONTRIBUTIONS

MG, DF, and SA conceived the study and wrote the manuscript. MG, SA, and XL selected the sampling sites. WL performed the DNA extraction. MG and DF analyzed the data. WL, XL, and TS helped to improve the manuscript. All authors approved the final version of the manuscript.

FUNDING

This study was financially supported by the FWF project I3268 given to SA and the NSFC project 31761133001 given to XL. DF was supported by a postdoctoral research grant of the Carl Zeiss Foundation.

ACKNOWLEDGMENTS

Thanks go to Michael Gruber, Margit Kagerer, and Yong Zhang for taking samples. Further thanks go to John Dolan at the Observatoire Océanologique de Villefranche (France), Mona Hoppenrath at the German Centre for Marine Biodiversity Research in Wilhelmshaven (Germany), and Klaus Jürgens at the Leibniz Institute for Baltic Sea Research in Warnemünde (Germany) for providing lab space during the sampling campaign.

SUPPLEMENTARY MATERIAL

The Supplementary Material for this article can be found online at: https://www.frontiersin.org/articles/10.3389/fmars.2021.643822/full#supplementary-material

Supplementary Figure 1 | Phylogenetic analyses of the oligotrichids *Spirotontonia* sp. **(A,B)**, *Strombidium* K sp. **(C,D)**, Strombidiidae K X sp. **(E,F)**, and the tintinnid *Tintinnidium* sp. **(G,H)**. **(A,C,E,G)** Phylogenetic trees based on the representative Swarm OTU amplicons obtained in the present study. The green dots mark the branches selected as query (Q) and reference groups (R) in the DeSignate analyses for identifying signature nucleotides. **(B,D,F,H)** Phylogenetic trees based on the representative Swarm OTU amplicons obtained by the present study and reference sequences from GenBank and the PR^2 database.

Supplementary Figure 2 | Distribution of signature nucleotides detected by DeSignate (Hütter et al., 2020) in the Swarm OTU sequence alignments of the four taxa displaying distinct geographic patterns.

Supplementary Figure 3 | Signature nucleotides identified by DeSignate (Hütter et al., 2020). The upper line displays the V4 sequence with the position of the signature nucleotides. The middle and lower left portions demonstrate the entropy plot (blue line) of the alignment shown below. The upper portion of the alignment comprises the query group sequences, the lower portion the reference group sequences. In the lower right portion, the alignment positions are ranked according to their relevance. Green, binary signatures; orange, asymmetric signatures; gray, noisy characters.

Supplementary Figure 4 | Examples of Swarm OTU networks. The networks display the internal structure of Swarm OTUs, in which nodes represent amplicons and edges represent one nucleotide differences between the amplicons. The node size was scaled to the read abundance comprised within an amplicon. **(A)** Swarm OTU with main area of distribution in Chinese coastal waters. **(B)** Swarm OTU with main area of distribution in European coastal waters.

Supplementary Table 1 | Sampling data.

Supplementary Table 2 | List of the 21 oligotrichean taxa included in the phylogenetic analyses (1); signature nucleotides detected in the four taxa with distinct geographic patterns (2); list of reference sequences obtained from GenBank and the PR^2 database (3).

Supplementary Data 1 | Modifications to the DNA extraction protocol and details on the nested-PCR.

Supplementary Data 2 | Alignments and tree files of the 21 oligotrichean taxa included in the phylogenetic analyses.

REFERENCES

Abboud-Abi Saab, M., and Owaygen, M. (1998). Day-to-day fluctuations of microplankton during an autumnal period at a fixed station off the Lebanese coast. *Leb. Sci. Bull.* 11, 45–65.

Adl, S. M., Bass, D., Lane, C. E., Lukeš, J., Schoch, C. L., Smirnov, A., et al. (2019). Revisions to the classification, nomenclature, and diversity of eukaryotes. *J. Eukaryot. Microbiol.* 66, 4–119.

Agatha, S. (2011). Global diversity of aloricate Oligotrichea (*Protista*, *Ciliophora*, *Spirotricha*) in marine and brackish sea water. *PLoS One* 6:e22466. doi: 10.1371/journal.pone.0022466

Agatha, S., Strüder-Kypke, M. C., and Beran, A. (2004). Morphologic and genetic variability in the marine planktonic ciliate *Laboea strobila* Lohmann, 1908 (*Ciliophora*, *Oligotrichia*), with notes on its ontogenesis. *J. Eukaryot. Microbiol.* 51, 267–281. doi: 10.1111/j.1550-7408.2004.tb00567.x

Agatha, S., Strüder-Kypke, M. C., Beran, A., and Lynn, D. H. (2005). *Pelagostrobilidium neptuni* (Montagnes and Taylor, 1994) and *Strombidium biarmatum* nov. spec. (*Ciliophora*, *Oligotrichea*): phylogenetic position inferred from morphology, ontogenesis, and gene sequence data. *Eur. J. Protistol.* 41, 65–83. doi: 10.1016/j.ejop.2004.09.005

Antich, A., Palacín, C., Cebrian, E., Golo, R., Wangensteen, O. S., and Turon, X. (2020). Marine biomonitoring with eDNA: can metabarcoding of water samples cut it as a tool for surveying benthic communities? *Mol. Ecol.* (early view). doi: 10.1111/mec.15641

Antich, A., Palacin, C., Wangensteen, O. S., and Turon, X. (2021). To denoise or to cluster? That is not the question. optimizing pipelines for COI metabarcoding and metaphylogeography. *bioRxiv [preprint]* doi: 10.1101/2021.01.08.425760

Bachy, C., Dolan, J. R., López-García, P., Deschamps, P., and Moreira, D. (2013). Accuracy of protist diversity assessments: morphology compared with cloning and direct pyrosequencing of 18S rRNA genes and ITS regions using the conspicuous tintinnid ciliates as a case study. *ISME J.* 7, 244–255. doi: 10.1038/ismej.2012.106

Bachy, C., Gómez, F., López-García, P., Dolan, J. R., and Moreira, D. (2012). Molecular phylogeny of tintinnid ciliates (*Tintinnida*, *Ciliophora*). *Protist* 163, 873–887. doi: 10.1016/j.protis.2012.01.001

Bakker, J., Wangensteen, O. S., Baillie, C., Buddo, D., Chapman, D. D., Gallagher, et al. (2019). Biodiversity assessment of tropical shelf eukaryotic communities via pelagic eDNA metabarcoding. *Ecol. Evol.* 9, 14341–14355. doi: 10.1002/ece3.5871

Bass, D., and Boenigk, J. (2011). "Everything is everywhere: a twenty-first century de-/reconstruction with respect to protists," in *Biogeography of Microscopic Organisms: is Everything Small Everywhere?*, ed. D. Fontaneto (Cambridge: Cambridge University Press), 88–110. doi: 10.1017/cbo9780511974878.007

Bokulich, N. A., Subramanian, S., Faith, J. J., Gevers, D., Gordon, J. I., Knight, R., et al. (2013). Quality-filtering vastly improves diversity estimates from Illumina amplicon sequencing. *Nat. Methods* 10, 57–59. doi: 10.1038/nmeth.2276

Brown, S. P., Veach, A. M., Rigdon-Huss, A. R., Grond, K., Lickteig, S. K., Lothamer, K., et al. (2015). Scraping the bottom of the barrel: are rare high

throughput sequences artifacts? *Fungal Ecol.* 13, 221–225. doi: 10.1016/j.funeco.2014.08.006

Callahan, B. J., McMurdie, P. J., and Holmes, S. P. (2017). Exact sequence variants should replace operational taxonomic units in marker-gene data analysis. *ISME J.* 11, 2639–2643. doi: 10.1038/ismej.2017.119

Cariou, J.-B., Dolan, J. R., and Dallot, S. (1999). A preliminary study of tintinnid diversity in the NW Mediterranean Sea. *J. Plankton Res.* 21, 1065–1075. doi: 10.1093/plankt/21.6.1065

Caron, D. A., and Hu, S. K. (2019). Are we overestimating protistan diversity in nature? *Trends Microbiol.* 27, 197–205. doi: 10.1016/j.tim.2018.10.009

Csárdi, G., and Nepusz, T. (2005). The igraph software package for complex network research. *InterJ. Complex Syst.* 1695, 1–9.

Darling, K. F., Wade, C. M., Kroon, D., Brown, A. J. L., and Bijma, J. (1999). The diversity and distribution of modern planktic foraminiferal small subunit ribosomal RNA genotypes and their potential as tracers of present and past ocean circulations. *Paleoceanography* 14, 3–12. doi: 10.1029/1998pa900002

Darling, K. F., Wade, C. M., Stewart, I. A., Kroon, D., Dingle, R., and Brown, A. J. L. (2000). Molecular evidence for genetic mixing of Arctic and Antarctic subpolar populations of planktonic foraminifers. *Nature* 405, 43–47. doi: 10.1038/35011002

De Meester, L. (2011). "A metacommunity perspective on the phylo- and biogeography of small organisms," in *Biogeography of Microscopic Organisms: is Everything Small Everywhere?*, ed. D. Fontaneto (Cambridge: Cambridge University Press), 324–334. doi: 10.1017/cbo9780511974878.017

De Meester, L., Gómez, A., Okamura, B., and Schwenk, K. (2002). The monopolization hypothesis and the dispersal-gene flow paradox in aquatic organisms. *Acta Oecologica* 23, 121–135. doi: 10.1016/s1146-609x(02)01145-1

de Vargas, C., Audic, S., Henry, N., Decelle, J., Mahé, F., Logares, R., et al. (2015). Eukaryotic plankton diversity in the sunlit ocean. *Science* 348, 1–11. doi: 10.1126/science.1261605

de Vargas, C., Norris, R., Zaninetti, L., Gibb, S. W., and Pawlowski, J. (1999). Molecular evidence of cryptic speciation in planktonic foraminifers and their relation to oceanic provinces. *Proc. Natl. Acad. Sci. USA* 96, 2864–2868. doi: 10.1073/pnas.96.6.2864

DeSalle, R., Egan, M. G., and Siddall, M. (2005). The unholy trinity: taxonomy, species delimitation and DNA barcoding. *Phil. Trans. R. Soc. B* 360, 1905–1916. doi: 10.1098/rstb.2005.1722

Di Giuseppe, G., Barbieri, M., Vallesi, A., Luporini, P., and Dini, F. (2013). Phylogeographical pattern of *Euplotes nobilii*, a protist ciliate with a bipolar biogeographical distribution. *Mol. Ecol.* 22, 4029–4037. doi: 10.1111/mec.12363

Dieckmann, U., and Doebeli, M. (1999). On the origin of species by sympatric speciation. *Nature* 400, 354–357. doi: 10.1038/22521

Doebeli, M., and Dieckmann, U. (2003). Speciation along environmental gradients. *Nature* 421, 259–264. doi: 10.1038/nature01274

Doherty, M., Costas, B. A., McManus, G. B., and Katz, L. A. (2007). Culture-independent assessment of planktonic ciliate diversity in coastal northwest Atlantic waters. *Aquat. Microb. Ecol.* 48, 141–154. doi: 10.3354/ame048141

Doherty, M., Tamura, M., Costas, B. A., Ritchie, M. E., McManus, G. B., and Katz, L. A. (2010). Ciliate diversity and distribution across an environmental and depth gradient in Long Island Sound. *USA. Environ. Microbiol.* 12, 886–898. doi: 10.1111/j.1462-2920.2009.02133.x

Dolan, J. R., and Pierce, R. W. (2013). "Diversity and distributions of tintinnids," in *The Biology and Ecology of Tintinnid Ciliates: Models for Marine Plankton*, eds J. R. Dolan, D. J. S. Montagnes, S. Agatha, D. W. Coats, and D. K. Stoecker (Oxford: John Wiley & Sons, Ltd), 214–243. doi: 10.1002/9781118358092.ch10

Dunthorn, M., Klier, J., Bunge, J., and Stoeck, T. (2012). Comparing the hyper-variable V4 and V9 regions of the small subunit rDNA for assessment of ciliate environmental diversity. *J. Eukaryot. Microbiol.* 59, 185–187. doi: 10.1111/j.1550-7408.2011.00602.x

Edgar, R. C. (2010). Search and clustering orders of magnitude faster than BLAST. *Bioinformatics* 26, 2460–2461. doi: 10.1093/bioinformatics/btq461

Edgar, R. C. (2016). SINTAX: a simple non-Bayesian taxonomy classifier for 16S and ITS sequences. *bioRxiv [Preprint]* doi: 10.1101/074161

Edgar, R. C., Haas, B. J., Clemente, J. C., Quince, C., and Knight, R. (2011). UCHIME improves sensitivity and speed of chimera detection. *Bioinformatics* 27, 2194–2200. doi: 10.1093/bioinformatics/btr381

Fernandes, N. M., and Schrago, C. G. (2019). A multigene timescale and diversification dynamics of Ciliophora evolution. *Mol. Phylogenet. Evol.* 139:106521. doi: 10.1016/j.ympev.2019.106521

Foissner, W. (2011). "Dispersal of protists: the role of cysts and human interactions," in *Biogeography of Microscopic Organisms: is Everything Small Everywhere?*, ed. D. Fontaneto (Cambridge: Cambridge University Press), 61–87. doi: 10.1017/cbo9780511974878.006

Foissner, W., Chao, A., and Katz, L. A. (2008). Diversity and geographic distribution of ciliates (*Protista*: *Ciliophora*). *Biodivers. Conserv.* 17, 345–363. doi: 10.1007/s10531-007-9254-7

Forster, D., Bittner, L., Karkar, S., Dunthorn, M., Romac, S., Audic, S., et al. (2015). Testing ecological theories with sequence similarity networks: marine ciliates exhibit similar geographic dispersal patterns as multicellular organisms. *BMC Biol.* 13:16. doi: 10.1186/s12915-015-0125-5

Forster, D., Lentendu, G., Filker, S., Dubois, E., Wilding, T. A., and Stoeck, T. (2019). Improving eDNA-based protist diversity assessments using networks of amplicon sequence variants. *Environ. Microbiol.* 21, 4109–4124. doi: 10.1111/1462-2920.14764

Forster, D., Lentendu, G., Wilson, M., Mahé, F., Leese, F., Andersen, T., et al. (2020). Evaluating geographic variation within molecular operational taxonomic units (OTUs) using network analyses in Scandinavian lakes. *bioRxiv [preprint]* doi: 10.1101/2020.08.06.240267

Fronhofer, E. A., and Altermatt, F. (2015). Eco-evolutionary feedbacks during experimental range expansions. *Nat. Commun.* 6:6844. doi: 10.1038/ncomms7844

Ganley, A. R. D., and Kobayashi, T. (2007). Highly efficient concerted evolution in the ribosomal DNA repeats: total rDNA repeat variation revealed by whole-genome shotgun sequence data. *Genome Res.* 17, 184–191. doi: 10.1101/gr.5457707

Ganser, M. H., and Agatha, S. (2019). Redescription of *Antetintinnidium mucicola* (Claparède and Lachmann, 1858) nov. gen., nov. comb. (*Alveolata*, *Ciliophora*, *Tintinnina*). *J. Eukaryot. Microbiol.* 66, 802–820. doi: 10.1111/jeu.12728

Gao, F., Li, J., Song, W., Xu, D., Warren, A., Yi, Z., et al. (2016). Multi-gene-based phylogenetic analysis of oligotrich ciliates with emphasis on two dominant groups: cyrtostrombidiids and strombidiids (*Protozoa*, *Ciliophora*). *Mol. Phylogenet. Evol.* 105, 241–250. doi: 10.1016/j.ympev.2016.08.019

Gao, S., Gong, J., Lynn, D., Lin, X., and Song, W. (2009). An updated phylogeny of oligotrich and choreotrich ciliates (*Protozoa*, *Ciliophora*, Spirotrichea) with representative taxa collected from Chinese coastal waters. *Syst. Biodivers.* 7, 235–242. doi: 10.1017/s1477200009002989

Gaonkar, C. C., Piredda, R., Sarno, D., Zingone, A., Montresor, M., and Kooistra, W. H. C. F. (2020). Species detection and delineation in the marine planktonic diatoms *Chaetoceros* and *Bacteriastrum* through metabarcoding: making biological sense of haplotype diversity. *Environ. Microbiol.* 22, 1917–1929. doi: 10.1111/1462-2920.14984

Gimmler, A., and Stoeck, T. (2015). Mining environmental high-throughput sequence data sets to identify divergent amplicon clusters for phylogenetic reconstruction and morphotype visualization. *Environ. Microbiol. Rep.* 7, 679–686. doi: 10.1111/1758-2229.12307

Gimmler, A., Korn, R., de Vargas, C., Audic, S., and Stoeck, T. (2016). The Tara Oceans voyage reveals global diversity and distribution patterns of marine planktonic ciliates. *Sci. Rep.* 6:33555. doi: 10.1038/srep33555

Giner, C. R., Balagué, V., Krabberød, A. K., Ferrera, I., Reñé, A., Garcés, et al. (2019). Quantifying long-term recurrence in planktonic microbial eukaryotes. *Mol. Ecol.* 28, 923–935. doi: 10.1111/mec.14929

Gómez, F., and Gorsky, G. (2003). Annual microplankton cycles in Villefranche Bay, Ligurian Sea, NW Mediterranean. *J. Plankton Res.* 25, 323–339. doi: 10.1093/plankt/25.4.323

Gong, J., Dong, J., Liu, X., and Massana, R. (2013). Extremely high copy numbers and polymorphisms of the rDNA operon estimated from single cell analysis of oligotrich and peritrich ciliates. *Protist* 164, 369–379. doi: 10.1016/j.protis.2012.11.006

Grattepanche, J.-D., Santoferrara, L. F., McManus, G. B., and Katz, L. A. (2015). Distinct assemblage of planktonic ciliates dominates both photic and deep waters on the New England shelf. *Mar. Ecol. Prog. Ser.* 526, 1–9. doi: 10.3354/meps11256

Guillou, L., Bachar, D., Audic, S., Bass, D., Berney, C., Bittner, L., et al. (2013). The Protist Ribosomal Reference database (PR2): a catalog of unicellular eukaryote small sub-unit rRNA sequences with curated taxonomy. *Nucleic Acids Res.* 41, D597–D604. doi: 10.1093/nar/gks1160

Hada, Y. (1938). Studies on the Tintinnoinea from the western tropical Pacific. *J. Fac. Sci. Hokkaido Imp. Univ. Ser. VI Zool.* 6, 87–190.

Hanson, C. A., Fuhrman, J. A., Horner-Devine, M. C., and Martiny, J. B. H. (2012). Beyond biogeographic patterns: processes shaping the microbial landscape. *Nat. Rev. Microbiol.* 10, 497–506. doi: 10.1038/nrmicro2795

Hofker, J. (1931). Studien über Tintinnoidea. *Arch. Protistenk.* 75, 315–402.

Hu, X., Lin, X., and Song, W. (2019). *Ciliate Atlas: Species Found in the South China Sea*. Singapore: Science Press & Springer Nature.

Huang, H., Yang, J., Huang, S., Gu, B., Wang, Y., Wang, L., et al. (2021). Spatial distribution of planktonic ciliates in the western Pacific Ocean: along the transect from Shenzhen (China) to Pohnpei (Micronesia). *Mar. Life Sci. Technol.* 3, 103–115. doi: 10.1007/s42995-020-00075-7

Hütter, T., Ganser, M. H., Kocher, M., Halkic, M., Agatha, S., and Augsten, N. (2020). DeSignate: detecting signature characters in gene sequence alignments for taxon diagnoses. *BMC Bioinformatics* 21:151. doi: 10.1186/s12859-020-3498-6

Jenkins, D. G., Medley, K. A., and Franklin, R. B. (2011). "Microbes as a test of biogeographic principles," in *Biogeography of Microscopic Organisms: is Everything Small Everywhere?*, ed. D. Fontaneto (Cambridge: Cambridge University Press), 309–323. doi: 10.1017/cbo9780511974878.016

Jiang, Y., Xu, H., Zhu, M., and Al-Rasheid, K. A. S. (2013). Temporal distributions of microplankton populations and relationships to environmental conditions in Jiaozhou Bay, northern China. *J. Mar. Biol. Ass. U.K.* 93, 13–26. doi: 10.1017/s0025315412001324

Jung, J.-H., Moon, J. H., Park, K.-M., Kim, S., Dolan, J. R., and Yang, E. J. (2018). Novel insights into the genetic diversity of *Parafavella* based on mitochondrial CO1 sequences. *Zool. Scr.* 47, 743–755. doi: 10.1111/zsc.12312

Katoh, K., and Standley, D. M. (2013). MAFFT Multiple Sequence Alignment Software Version 7: improvements in performance and usability. *Mol. Biol. Evol.* 30, 772–780. doi: 10.1093/molbev/mst010

Katz, L. A., McManus, G. B., Snoeyenbos-West, O. L. O., Griffin, A., Pirog, K., Costas, B., et al. (2005). Reframing the 'everything is everywhere' debate: evidence for high gene flow and diversity in ciliate morphospecies. *Aquat. Microb. Ecol.* 41, 55–65. doi: 10.3354/ame041055

Kim, S. Y., Xu, D., Jung, J.-H., and Choi, J. K. (2020). Phylogeny and genetic/morphological variation of *Strombidinopsis minima*-like species (*Ciliophora*: *Choreotrichia*). *J. Eukaryot. Microbiol.* 67, 115–124. doi: 10.1111/jeu.12761

Kim, Y.-O., and Taniguchi, A. (1997). Seasonal variation of excystment pattern of the planktonic oligotrich ciliate *Strombidium conicum*. *Mar. Biol.* 128, 207–212. doi: 10.1007/s002270050084

Kim, Y.-O., Ha, S., and Taniguchi, A. (2008). Morphology and in situ sedimentation of the cysts of a planktonic oligotrich ciliate, *Strombidium capitatum*. *Aquat. Microb. Ecol.* 53, 173–179. doi: 10.3354/ame01241

Kim, Y.-O., Suzuki, T., and Taniguchi, A. (2002). A new species in the genus *Cyrtostrombidium* (*Ciliophora*, *Oligotrichia*, *Oligotrichida*): its morphology, seasonal cycle and resting stage. *J. Eukaryot. Microbiol.* 49, 338–343. doi: 10.1111/j.1550-7408.2002.tb00380.x

Laackmann, H. (1910). Die Tintinnodeen der Deutschen Südpolar-Expedition 1901-1903. Deutsche Südpolar-Expedition 1901-1903 im Auftrage des Reichsamtes des Innern. XI. *Zoologie* 3, 342–496.

Lahr, D. J. G., and Katz, L. A. (2009). Reducing the impact of PCR-mediated recombination in molecular evolution and environmental studies using a new-generation high-fidelity DNA polymerase. *BioTechniques* 47, 857–866. doi: 10.2144/000113219

Lara, E., Berney, C., Harms, H., and Chatzinotas, A. (2007). Cultivation-independent analysis reveals a shift in ciliate 18S rRNA gene diversity in a polycyclic aromatic hydrocarbon-polluted soil. *FEMS Microbiol. Ecol.* 62, 365–373. doi: 10.1111/j.1574-6941.2007.00387.x

Lipps, J. H., Stoeck, T., and Dunthorn, M. (2013). "Fossil tintinnids," in *The Biology and Ecology of Tintinnid Ciliates: Models for Marine Plankton*, eds J. R. Dolan, D. J. S. Montagnes, S. Agatha, D. W. Coats, and D. K. Stoecker (Oxford: John Wiley & Sons, Ltd), 186–197. doi: 10.1002/9781118358092.ch8

Liu, W., Jiang, J., Xu, Y., Pan, X., Qu, Z., Luo, X., et al. (2017). Diversity of free-living marine ciliates (*Alveolata*, *Ciliophora*): faunal studies in coastal waters of China during the years 2011-2016. *Eur. J. Protistol.* 61, 424–438. doi: 10.1016/j.ejop.2017.04.007

Logares, R., Audic, S., Bass, D., Bittner, L., Boutte, C., Christen, R., et al. (2014). Patterns of rare and abundant marine microbial eukaryotes. *Curr. Biol.* 24, 813–821. doi: 10.1016/j.cub.2014.02.050

Logares, R., Deutschmann, I. M., Junger, P. C., Giner, C. R., Krabberød, A. K., Schmidt, et al. (2020). Disentangling the mechanisms shaping the surface ocean microbiota. *Microbiome* 8:55. doi: 10.1186/s40168-020-00827-8

Longhurst, A. (2007). *Ecological Geography of the Sea*. Burlington: Academic Press.

Luporini, P., Alimenti, C., Pedrini, B., and Vallesi, A. (2016). "Ciliate communication via water-borne pheromones," in *Biocommunication of Ciliates*, eds G. Witzany and M. Nowacki (Cham: Springer), 159–174. doi: 10.1007/978-3-319-32211-7_10

Mahé, F., Rognes, T., Quince, C., de Vargas, C., and Dunthorn, M. (2015). Swarm v2: highly-scalable and high-resolution amplicon clustering. *PeerJ* 3:e1420. doi: 10.7717/peerj.1420

Markmann, M., and Tautz, D. (2005). Reverse taxonomy: an approach towards determining the diversity of meiobenthic organisms based on ribosomal RNA signature sequences. *Philos. Trans. R. Soc. B* 360, 1917–1924. doi: 10.1098/rstb.2005.1723

Marteinsson, V. Þ., Groben, R., Reynisson, E., and Vannier, P. (2016). "Biogeography of marine microorganisms," in *The Marine Microbiome*, eds L. J. Stal and M. S. Cretoiu (Cham: Springer), 187–207. doi: 10.1007/978-3-319-33000-6_6

Martin, M. (2011). Cutadapt removes adapter sequences from high-throughput sequencing reads. *EMBnet J.* 17, 10–12. doi: 10.14806/ej.17.1.200

Martín, P. V., Bucek, A., Bourguignon, T., and Pigolotti, S. (2020). Ocean currents promote rare species diversity in protists. *bioRxiv [preprint]* doi: 10.1101/2020.01.10.901165

Maselli, M., Altenburger, A., Stoecker, D. K., and Hansen, P. J. (2020). Ecophysiological traits of mixotrophic *Strombidium* spp. *J. Plankton Res.* 42, 485–496. doi: 10.1093/plankt/fbaa041

Massana, R., Gobet, A., Audic, S., Bass, D., Bittner, L., Boutte, C., et al. (2015). Marine protist diversity in European coastal waters and sediments as revealed by high-throughput sequencing. *Environ. Microbiol.* 17, 4035–4049. doi: 10.1111/1462-2920.12955

McManus, G. B., and Santoferrara, L. F. (2013). "Tintinnids in microzooplankton communities," in *The Biology and Ecology of Tintinnid Ciliates: Models for Marine Plankton*, eds J. R. Dolan, D. J. S. Montagnes, S. Agatha, D. W. Coats, and D. K. Stoecker (Oxford: John Wiley & Sons, Ltd), 198–213. doi: 10.1002/9781118358092.ch9

McManus, G. B., Xu, D., Costas, B. A., and Katz, L. A. (2010). Genetic identities of cryptic species in the *Strombidium stylifer/apolatum/oculatum* cluster, including a description of *Strombidium rassoulzadegani* n. sp. *J. Eukaryot. Microbiol.* 57, 369–378. doi: 10.1111/j.1550-7408.2010.00485.x

McManus, M. A., and Woodson, C. B. (2012). Plankton distribution and ocean dispersal. *J. Exp. Biol.* 215, 1008–1016. doi: 10.1242/jeb.059014

Merkle, H. (1909). Untersuchungen an Tintinnodeen der Ost- und Nordsee. *Wiss. Meeresunters., Abt. Kiel* 11, 139–186 + Plates II, III.

Meunier, A. (1910). *Microplankton des Mers de Barents et de Kara. Campagne Arctique de 1907*. Bruxelles: C. Bulens.

Minicante, S. A., Piredda, R., Quero, G. M., Finotto, S., Aubry, F. B., Bastianini, M., et al. (2019). Habitat heterogeneity and connectivity: effects on the planktonic protist community structure at two adjacent coastal sites (the Lagoon and the Gulf of Venice, Northern Adriatic Sea, Italy) revealed by metabarcoding. *Front. Microbiol.* 10:2736.

Mitra, A., Skrzypczak, M., Ginalski, K., and Rowicka, M. (2015). Strategies for achieving high sequencing accuracy for low diversity samples and avoiding sample bleeding using Illumina platform. *PLoS One* 10:e0120520. doi: 10.1371/journal.pone.0120520

Moritz, C., and Cicero, C. (2004). DNA barcoding: promise and pitfalls. *PLoS Biol.* 2:e354. doi: 10.1371/journal.pbio.0020354

Mozetič, P., Fonda Umani, S., Cataletto, B., and Malej, A. (1998). Seasonal and inter-annual plankton variability in the Gulf of Trieste (northern Adriatic). *ICES J. Mar. Sci.* 55, 711–722. doi: 10.1006/jmsc.1998.0396

Newman, M. E. J. (2003). Mixing patterns in networks. *Phys. Rev. E* 67:026126. doi: 10.1103/PhysRevE.67.026126

Norris, R. D. (2000). *Pelagic Species Diversity, Biogeography, and Evolution*. Cambridge: Cambridge University Press

Palumbi, S. R. (1994). Genetic divergence, reproductive isolation, and marine speciation. *Annu. Rev. Ecol. Syst.* 25, 547–572. doi: 10.1146/annurev.es.25.110194.002555

Pienaar, E., Theron, M., Nelson, M., and Viljoen, H. J. (2006). A quantitative model of error accumulation during PCR amplification. *Comput. Biol. Chem.* 30, 102–111. doi: 10.1016/j.compbiolchem.2005.11.002

Pierce, R. W., and Turner, J. T. (1992). Ecology of planktonic ciliates in marine food webs. *Rev. Aquat. Sci.* 6, 139–181.

Pierce, R. W., and Turner, J. T. (1993). Global biogeography of marine tintinnids. *Mar. Ecol. Prog. Ser.* 94, 11–26. doi: 10.3354/meps094011

Piredda, R., Tomasino, M. P., D'Erchia, A. M., Manzari, C., Pesole, G., Montresor, R., et al. (2017). Diversity and temporal patterns of planktonic protist assemblages at a Mediterranean Long Term Ecological Research site. *FEMS Microbiol. Ecol.* 93:fiw200. doi: 10.1093/femsec/fiw200

Price, M. N., Dehal, P. S., and Arkin, A. P. (2010). FastTree 2 - approximately maximum-likelihood trees for large alignments. *PLoS One* 5:e9490. doi: 10.1371/journal.pone.0009490

R Core Team (2018). *R: a Language and Environment for Statistical Computing*. Vienna: R Foundation for Statistical Computing.

Rognes, T., Flouri, T., Nichols, B., Quince, C., and Mahé, F. (2016). VSEARCH: a versatile open source tool for metagenomics. *PeerJ* 4:e2584. doi: 10.7717/peerj.2584

Rubino, F., Moscatello, S., Saracino, O. D., Fanelli, G., Belmonte, G., and Boero, F. (2002). Plankton-derived resting stages in marine coastal sediments along the Salento Peninsula (Apulia, south-eastern Italy). *Mar. Ecol.* 23(Suppl. 1), 329–339. doi: 10.1111/j.1439-0485.2002.tb00031.x

Santoferrara, L. F., Alder, V. V., and McManus, G. B. (2017). Phylogeny, classification and diversity of Choreotrichia and Oligotrichia (*Ciliophora*, *Spirotrichea*). *Mol. Phylogenet. Evol.* 112, 12–22. doi: 10.1016/j.ympev.2017.03.010

Santoferrara, L. F., Bachy, C., Alder, V. A., Gong, J., Kim, Y.-O., Saccà, A., et al. (2016a). Updating biodiversity studies in loricate protists: the case of the tintinnids (*Alveolata*, *Ciliophora*, *Spirotrichea*). *J. Eukaryot. Microbiol.* 63, 651–656. doi: 10.1111/jeu.12303

Santoferrara, L. F., Grattepanche, J.-D., Katz, L. A., and McManus, G. B. (2014). Pyrosequencing for assessing diversity of eukaryotic microbes: analysis of data on marine planktonic ciliates and comparison with traditional methods. *Environ. Microbiol.* 16, 2752–2763. doi: 10.1111/1462-2920.12380

Santoferrara, L. F., Grattepanche, J.-D., Katz, L. A., and McManus, G. B. (2016b). Patterns and processes in microbial biogeography: do molecules and morphologies give the same answers? *ISME J.* 10, 1779–1790. doi: 10.1038/ismej.2015.224

Santoferrara, L. F., Rubin, E., and McManus, G. B. (2018). Global and local DNA (meta)barcoding reveal new biogeography patterns in tintinnid ciliates. *J. Plankton Res.* 40, 209–221. doi: 10.1093/plankt/fby011

Santoferrara, L. F., Tian, M., Alder, V. A., and McManus, G. B. (2015). Discrimination of closely related species in tintinnid ciliates: new insights on crypticity and polymorphism in the genus *Helicostomella*. *Protist* 166, 78–92. doi: 10.1016/j.protis.2014.11.005

Santoferrara, L., Burki, F., Filker, S., Logares, R., Dunthorn, M., and McManus, G. B. (2020). Perspectives from ten years of protist studies by high-throughput metabarcoding. *J. Eukaryot. Microbiol.* 67, 612–622. doi: 10.1111/jeu.12813

Schmidt, T. S. B., Matias Rodrigues, J. F., and von Mering, C. (2015). Limits to robustness and reproducibility in the demarcation of operational taxonomic units. *Environ. Microbiol.* 17, 1689–1706. doi: 10.1111/1462-2920.12610

Shapiro, B. J., Leducq, J.-B., and Mallet, J. (2016). What is speciation? *PLoS Genet.* 12:e1005860. doi: 10.1371/journal.pgen.1005860

Sherr, E., and Sherr, B. (1988). Role of microbes in pelagic food webs: a revised concept. *Limnol. Oceanogr.* 33, 1225–1227. doi: 10.4319/lo.1988.33.5.1225

Shimodaira, H. (2002). An approximately unbiased test of phylogenetic tree selection. *Syst. Biol.* 51, 492–508. doi: 10.1080/10635150290069913

Siegenthaler, A., Wangensteen, O. S., Soto, A. Z., Benvenuto, C., Corrigan, L., and Mariani, S. (2019). Metabarcoding of shrimp stomach content: harnessing a natural sampler for fish biodiversity monitoring. *Mol. Ecol. Resour.* 19, 206–220. doi: 10.1111/1755-0998.12956

Song, W., Zhao, X., Liu, W., Hu, X., Al-Farraj, S. A., Al-Rasheid, K. A. S., et al. (2015). Biodiversity of oligotrich ciliates in the South China Sea: description of three new *Strombidium* species (*Protozoa*, *Ciliophora*, *Oligotrichia*) with phylogenetic analyses. *Syst. Biodivers.* 13, 608–623. doi: 10.1080/14772000.2015.1081992

Stamatakis, A. (2006). RAxML-VI-HPC: maximum likelihood-based phylogenetic analyses with thousands of taxa and mixed models. *Bioinformatics* 22, 2688–2690. doi: 10.1093/bioinformatics/btl446

Stoeck, T., Bass, D., Nebel, M., Christen, R., Jones, M. D. M., Breiner, H.-W., et al. (2010). Multiple marker parallel tag environmental DNA sequencing reveals a highly complex eukaryotic community in marine anoxic water. *Mol. Ecol.* 19(Suppl. 1), 21–31. doi: 10.1111/j.1365-294x.2009.04480.x

Stoecker, D. K., and Capuzzo, J. M. (1990). Predation on protozoa: its importance to zooplankton. *J. Plankton Res.* 12, 891–908. doi: 10.1093/plankt/12.5.891

Sun, P., Huang, L., Xu, D., Warren, A., Huang, B., Wang, Y., et al. (2019). Integrated space-time dataset reveals high diversity and distinct community structure of ciliates in mesopelagic waters of the northern South China Sea. *Front. Microbiol.* 10:2178. doi: 10.3389/fmicb.2019.02178

Sun, Y., Cai, Y., Huse, S. M., Knight, R., Farmerie, W. G., Wang, X., et al. (2012). A large-scale benchmark study of existing algorithms for taxonomy-independent microbial community analysis. *Brief. Bioinform.* 13, 107–121. doi: 10.1093/bib/bbr009

Tavaré, S. (1986). Some probabilistic and statistical problems in the analysis of DNA sequences. *Lectures Math. Life Sci.* 17, 57–86.

Tucker, S. J., McManus, G. B., Katz, L. A., and Grattepanche, J.-D. (2017). Distribution of abundant and active planktonic ciliates in coastal and slope waters off New England. *Front. Microbiol.* 8:2178.

Van der Spoel, S., and Heyman, R. P. (1983). *A Comparative Atlas of Zooplankton - Biological Patterns in the Oceans*. Berlin: Springer-Verlag.

Wang, C., Zhang, T., Wang, Y., Katz, L. A., Gao, F., and Song, W. (2017). Disentangling sources of variation in SSU rDNA sequences from single cell analyses of ciliates: impact of copy number variation and experimental error. *Proc. R. Soc. London Ser. B* 284:20170425. doi: 10.1098/rspb.2017.0425

Wang, Y., Wang, C., Jiang, Y., Katz, L. A., Gao, F., and Yan, Y. (2019). Further analyses of variation of ribosome DNA copy number and polymorphism in ciliates provide insights relevant to studies of both molecular ecology and phylogeny. *Sci. China Life Sci.* 62, 203–214. doi: 10.1007/s11427-018-9422-5

Warren, A., Patterson, D. J., Dunthorn, M., Clamp, J. C., Achilles-Day, U. E. M., Aescht, E., et al. (2017). Beyond the "Code": a guide to the description and documentation of biodiversity in ciliated protists (*Alveolata*, *Ciliophora*). *J. Eukaryot. Microbiol.* 64, 539–554. doi: 10.1111/jeu.12391

Weiner, A. K. M., Weinkauf, M. F. G., Kurasawa, A., Darling, K. F., Kucera, M., and Grimm, G. W. (2014). Phylogeography of the tropical planktonic foraminifera lineage *Globigerinella* reveals isolation inconsistent with passive dispersal by ocean currents. *PLoS One* 9:e92148. doi: 10.1371/journal.pone.0092148

Weisse, T. (2008). Distribution and diversity of aquatic protists: an evolutionary and ecological perspective. *Biodivers. Conserv.* 17, 243–259. doi: 10.1007/s10531-007-9249-4

Will, K. W., and Rubinoff, D. (2004). Myth of the molecule: DNA barcodes for species cannot replace morphology for identification and classification. *Cladistics* 20, 47–55. doi: 10.1111/j.1096-0031.2003.00008.x

Witek, M. (1998). Annual changes of abundance and biomass of planktonic ciliates in the Gdańsk basin, southern Baltic. *Int. Rev. Hydrobiol.* 83, 163–182. doi: 10.1002/iroh.19980830207

Xu, D., Sun, P., Shin, M. K., and Kim, Y. O. (2012). Species boundaries in tintinnid ciliates: a case study - morphometric variability, molecular characterization, and temporal distribution of *Helicostomella* species (*Ciliophora*, *Tintinnina*). *J. Eukaryot. Microbiol.* 59, 351–358. doi: 10.1111/j.1550-7408.2012.00625.x

Yang, J., Löder, M. G. J., and Wiltshire, K. H. (2014). A survey of ciliates at the long-term sampling station "Helgoland Roads", North Sea. *Helgol. Mar. Res.* 68, 313–327. doi: 10.1007/s10152-014-0392-5

Zeitzschel, B. (1966). Die Verbreitung der Tintinnen im Nordatlantik. *Veröff. Inst. Meeresforsch. Bremerh. Sonderbd.* 2, 293–300.

Zeitzschel, B. (1969). Tintinnen des westlichen Arabischen Meeres, ihre Bedeutung als Indikatoren für Wasserkörper und Glied der Nahrungskette. *"Meteor". Forschungsergeb* 4, 47–101.

Zeitzschel, B. (1990). "Zoogeography of marine protozoa: an overview emphasizing distribution of planktonic forms," in *Ecology of Marine Protozoa*, ed. G. M. Capriulo (Oxford: Oxford University Press), 139–185.

Zhang, Q., Agatha, S., Zhang, W., Dong, J., Yu, Y., Jiao, N., et al. (2017). Three rDNA loci-based phylogenies of tintinnid ciliates (*Ciliophora*, *Spirotrichea*, *Choreotrichida*). *J. Eukaryot. Microbiol.* 64, 226–241. doi: 10.1111/jeu.12354

Zhao, F., Filker, S., Xu, K., Li, J., Zhou, T., and Huang, P. (2019). Effects of intragenomic polymorphism in the SSU rRNA gene on estimating marine microeukaryotic diversity: a test for ciliates using single-cell high-throughput DNA sequencing. *Limnol. Oceanogr. Meth.* 17, 533–543. doi: 10.1002/lom3.10330

Conflict of Interest: The authors declare that the research was conducted in the absence of any commercial or financial relationships that could be construed as a potential conflict of interest.

frontiers in Marine Science

ORIGINAL RESEARCH
published: 23 April 2021
doi: 10.3389/fmars.2021.627879

Molecular Evolutionary Analyses of *Euplotes* Species Living in Freshwater and Marine Habitats: A Mitogenomic Perspective

Ning Huang[1], Shuai Chen[1], Ming He[1], Qi Song[1], Lina Hou[1], Yan Zhao[2], Shuo Zhao[3]* and Miao Miao[1]**

[1] Savaid Medical School, University of Chinese Academy of Sciences, Beijing, China, [2] College of Life Sciences, Capital Normal University, Beijing, China, [3] College of Resources and Environment, University of Chinese Academy of Sciences, Beijing, China

OPEN ACCESS

Edited by:
Xiaoshou Liu,
Ocean University of China, China

Reviewed by:
Daode Ji,
Yantai Nanshan University, China
Wenzhe Xu,
Tianjin University of Science and Technology, China

***Correspondence:**
Miao Miao
miaomiao@ucas.ac.cn
Shuo Zhao
zhaoshuo@ucas.ac.cn
Yan Zhao
yanzhao@cnu.edu.cn

Specialty section:
This article was submitted to Marine Evolutionary Biology, Biogeography and Species Diversity, a section of the journal Frontiers in Marine Science

Received: *10 November 2020*
Accepted: *02 March 2021*
Published: *23 April 2021*

Citation:
Huang N, Chen S, He M, Song Q, Hou L, Zhao Y, Zhao S and Miao M (2021) Molecular Evolutionary Analyses of Euplotes Species Living in Freshwater and Marine Habitats: A Mitogenomic Perspective. Front. Mar. Sci. 8:627879. doi: 10.3389/fmars.2021.627879

Ciliates are the most complex unicellular eukaryotic organisms, which play important roles in various ecosystems. The *Euplotes* is a dominant genus in the ciliates Euplotida and consists of approximate one hundred species. They distribute widely in environments with various salinity levels including freshwater, brackish, seawater as well as hypersaline. In this study, we obtained four mitochondrial genomes of *Euplotes* species, using both high throughput sequencing and Sanger sequencing. Combined with two previously reported *Euplotes* mitochondrial genomes, we analyzed their gene structure, codon usage pattern as well as phylogenetic relationship. We found that gene rearrangement exists in *Euplotes* and codon usage bias is different among these species. Phylogenetic analyses based on both mitochondrial and nuclear genes further unveiled that *Euplotes* spp. living in similar salinity levels tend to be clustered together. Moreover, we found that the *dN/dS* ratios of two mitochondrial genes, *cox1* and *cox2*, are significantly different between marine and freshwater species, indicating the salinity could act as a barrier for the *Euplotes* species distribution. We also recommended mitochondrial genes to discriminate the species with highly similarity of *Euplotes* which could not be easily distinguished by nuclear gene marker and morphological characteristics. This study provides novel resources to improve our understanding of *Euplotes* evolution and also its adaptation to habitats with different salinity levels.

Keywords: codon usage bias, *Euplotes*, gene rearrangement, mitochondrial genome, phylogeny, salinity adaptation

INTRODUCTION

Ciliates play important ecological roles in natural environments and become one of the most prevailing model territory in unicellular eukaryotes (Graziano et al., 2010; Gentekaki et al., 2014). They are more diverse and highly differentiated than multicellular eukaryotes (Graziano et al., 2010) and able to survive in various types of environments (Giuseppe et al., 2011). The genus *Euplotes* is one of hypotrichous ciliates which contains approximately one hundred species (Pedrini et al., 2017). Recent studies have been focus on *Euplotes* diversity and

phylogeny based on morphological characters and molecular data (Yi et al., 2009; Syberg-Olsen et al., 2016). However, different opinions by taxonomists may result in identification confusion, also lack of enough molecular sequences could lead to misestimating the inner relationship among the increasing taxa. Besides, as species in the genus *Euplotes* have a wide distribution from freshwater to marine water, more genetic traits are needed to provide the relation between salinity and *Euplotes* clusters. Mitochondrial genome analyses have been playing a growing important role in phylogenetic and evolutionary studies. Mitochondrial genome contains multiple vital genes and has a higher evolutionary rate than nuclear gene markers (Gray et al., 1999; Zhang et al., 2016). The inheritance of mitochondrial DNA occurs in a unique and heritably separate manner that is spatially different from nuclear DNA, which may provide a new perspective for the phylogenetics of the *Euplotes*. Moreover, its small size makes it to be more accessible than nuclear genome. Therefore, mitochondrial genomes have been widely used to study biogeography, phylogeny as well as evolutionary biology (Ballard, 2000; Sivasankaran et al., 2017). Until now, mitochondrial genomes from only three species have been sequenced in ciliated species (de Graaf et al., 2009; Serra et al., 2019).

This research aims to revisit the phylogenetic relationship among the representative *Euplotes* species, as well as to explore the correlation between *Euplotes* evolution and salinity of their habitats from the perspective of mitochondria. We obtained the mitogenomes of two freshwater species (*E. aediculatus* and *E. otocarinatus*) and two seawater species (*E. vannus* and *E. focardii*) by Sanger sequencing and high throughput sequencing. Then the structure feature and codon usage were compared among all *Euplotes* mitogenomes. We also identified the major force influencing codon usage pattern. By constructing phylogenetic trees based on both nuclear and mitochondrial genes, we investigated the correlation between phylogenetic diversity and salinity of habitats. Finally, two mitochondrial genes (*cox1* and *cox2*) were speculated to be related to salinity adaptation. These data provided new clues to explore the genetic basis on how *Euplotes* adapts to diverse habitats.

MATERIALS AND METHODS

Cultivation and DNA Extraction

E. aediculatus and *E. vannus* were obtained from Qingdao Agricultural University (Qingdao, China) and Ocean University of China (Qingdao, China), respectively. The former was cultured in sterilized freshwater at the room temperature, while the latter was cultured in sterilized seawater with concentration of 30‰ at the room temperature. When the density of cells reached 600 per milliliter (ml), we used a 15-μm-pore-size nylon filter membrane to harvest them from the medium and washed by sterilized water to reduce bacterial contamination (Kodama and Fujishima, 2005). The cells were starved and incubated with 1 × penicillin-streptomycin antibiotics (Invitrogen, Carlsbad, CA, United States) for 24 h to further eliminate the contamination of bacteria (McGrath et al., 2014; Slabodnick et al., 2017; He et al., 2019). We collected cells by centrifugation at 8,000 rpm/min for 10 min and extracted DNA using the DNeasy Blood & Tissue Kit (Qiagen, Düsseldorf, Germany).

Sequencing and Assembly

We obtained the mitochondrial sequences of *E. vannus* by Sanger sequencing. Conserved regions between *E. minuta* and *E. crassus* were selected to design several pairs of degenerate primers (**Supplementary Table 1**), then we amplified corresponding regions by degenerate Polymerase Chain Reaction (PCR) (de Graaf et al., 2009; Barth and Berendonk, 2011). The long range PCR was performed to acquire connection between conserved regions. Seqman in DNAstar 7.1 was used to assemble the amplified sequences.

Approximately 2 μg DNA from *E. aediculatus* was used to construct a DNA library with 500 bp insert size and then sequenced on an Illumina HiSeq 2500 platform. Ultimately, 1858120 read pairs were acquired (PE250). Adaptors and low quality bases were removed by Trimmomatic with default parameters (Bolger et al., 2014). We employed SPAdes to assemble the mitochondrial genome with an option of "careful" (Bankevich et al., 2012; Zhang et al., 2016; Serra et al., 2019) and obtained *E. aediculatus* mitochondrial contigs by TBLASTN (E value < 1e-5). We further used the same approach to assemble the mitogenomes from two published genomic DNA-seq datasets of *E. focardii* (SRR3929761) and *E. ocatocarinatus* (SRR2474557), respectively. The processes of verifying and concatenating the assembled contigs from *E. aediculatus* were accomplished by PCR.

Annotation

Firstly, we predicted all possible open reading frames (ORFs) from the assembled mitochondrial genomes. If there were multiple ORFs in one position, only the longest one was kept. Besides, ORFs shorter than 150 bp were also removed (Swart et al., 2012). BLASTX was employed to align these ORFs to non-redundant (nr) protein database and Swiss-prot database to detect homologous mitochondrial protein coding sequences. As for the protein coding genes with high divergence, a more sensitive homology detection approach HHpred was used to search against the protein families (Soding et al., 2005), which can detect homology based on HMM-HMM-comparison. The tRNA genes were identified with tRNAscan-SE version 2.0 (Lowe and Chan, 2016). The boundaries of rRNA genes were determined using clustalW by aligning to known *Euplotes* mitochondrial rRNA genes. The tandem repeat region was determined by Tandem Repeats Finder (Benson, 1999).

AT and GC Skew Profiling

We divided the upstream and downstream sequences of the tandem repeat region into 50 bins, respectively. The cumulative AT skew and cumulative GC skew were calculated by the

following formula, where i indicate i-th bin of mitochondrial genome (Grigoriev, 1998).

$$\text{Cumulative AT skew} = \sum_{i=1}^{100} \left(\frac{A-T}{A+T}\right)_i$$

$$\text{Cumulative GC skew} = \sum_{i=1}^{100} \left(\frac{G-C}{G+C}\right)_i$$

Codon Usage Bias Analysis

The relative synonymous codon usage (RSCU), effective number of codons (ENC), aromaticity (AROMO) as well as general average hydropathicity (GRAVY) were calculated by CodonW (v1.4.4)[1]. GC12 represents the mean GC content of the first and second sites of codons, and GC3 represents GC content of the third site of codons. The expect ENC value was calculated according to the previous study (Wright, 1990). Principal component analysis (PCA) and correlation analysis were carried out using R studio (Wei et al., 2014).

Phylogenetic Analysis

SSU-rRNA genes of *E. vannus* and *E. aediculatus* were obtained by PCR with degenerated primers Euk-A (5′-AACCTGGTTGATCCTGCCAGT-3′) and EukB (5′- GATCC TTCTGCAGGTTCACCTAC-3′) (Medlin et al., 1988). SSU-rRNA sequences of *E. focardii* and *E. ocatocarinatus* were extracted from the assembled contigs by BLASTN, and SSU-rRNA genes of other species were downloaded from GenBank (**Supplementary Table 4**). These sequences were aligned and manually edited using BioEdit (Hall, 1999). After curation, a total of 1984 positions of SSU-rRNA genes were kept for subsequent phylogenetic analyses. According to MrModeltest (version 2.4)[2] with Akaike Information Criterion (AIC), GTR + I + G was the best-fit model for SSU-rRNA genes. The datasets were then analyzed using two phylogenetic methods, Maximum Likelihood (ML) and Bayesian Inference (BI), under the best-fit model. ML analyses with 1000 non-parametric bootstrap replicates were carried out using RAxML (Stamatakis, 2014). BI analyses were performed using MrBayes (Ronquist et al., 2012). Four Markov Chain Monte Carlo (MCMC) were run twice with 10^6 generations and sampled every 100th cycle, while the first 2500 trees were discarded as burn-in (Fernandes et al., 2016; Shazib et al., 2016).

In order to construct phylogenetic trees using mitochondrial genes, we downloaded mitochondrial genomes of another eleven species in ciliates and *Durinskia baltica* (outgroup) from GenBank. GET_HOMOLOGUES was employed to identify orthologs genes among these mitogenomes (Contreras-Moreira and Vinuesa, 2013). The selected genes were aligned using MAFFT (Katoh and Standley, 2013) and then combined by SequenceMatrix (Vaidya et al., 2011). Conserved regions in the alignments were determined by Gblocks and all gaps were removed (Castresana, 2000; He et al., 2019). The best-fit model LG + G + F amino acid replacement matrix according to AIC was determined by the ProtTest 3 (Darriba et al., 2011). The phylogenetic tree based on the concatenated mitochondrial genes was constructed by the same method as that based on SSU-rRNA genes.

Analysis of Selection

The ratio of non-synonymous to synonymous substitutions (dN/dS) is usually used to measure strength and mode of natural selection (Jeffares et al., 2015). If dN/dS > 1, positive Darwinian selection (positive selection) is acting on PCGs, whereas dN/dS < 1 suggests purifying selection, and dN/dS = 1 indicates neutral selection. The ω represents estimate dN/dS value. Branch model test was used to test whether ω between *Euplotes* G1 and G2 is significantly different. The branch model test based on protein coding genes was carried out by the program CODEML of PAML Version 4.8a (Yang, 2007). We set CodonFreq equal to 1. The one ratio model (icode = 3, model = 0) assumes that ω across all branches is identical. For two ratio model (icode = 3, model = 2), *Euplotes* G2 was selected as the foreground branch, ω0 was for *Euplotes* G2 species while ω1 was for *Euplotes* G1 species. The likelihood ratio test was used to compare and test the significance between two models by jModelTest 2 (Darriba et al., 2012).

RESULTS

Structure Feature of Mitochondrial Genomes

Similar to previous reports, the four new mitochondrial genomes in this study also have a linear structure, with the length ranging from 32.6 kb to 43.6 kb (**Table 1**). All *Euplotes* mitogenomes have considerably high AT content, especially for *E. aediculatus* (80.2%) and *E. otocarinatus* (82.0%). In this study, we used the reannotation of *E. minuta* (Swart et al., 2012) and reannotated *E. crassus* through the same strategy (**Supplementary Table 2**). We found that *Euplotes* mitochondrial genomes have all protein-coding genes (PCGs) that have been reported in other ciliate mitochondria. Regardless of the ORFs with unknown function, gene order among *E. minuta*, *E. crassus*, *E. vannus* as well as *E. focardii* is almost the same with exception of *nad6*, which is absent in *E. crassus*. Here, we classified these four species as group one, termed as *Euplotes* G1. Likewise, the arrangements of PCGs in mitochondria of the other two *Euplotes* species are completely consistent, which could be classified as group two (*Euplotes* G2). However, there are inversion and translocation of PCGs between these two groups. For species in *Euplotes* G1, *cob* locates between *ccmF* and *trnM* but it interposes between *nad3* and *trnH* in *Euplotes* G2. In *E. octocarinatus*, we also found that *nad5-ccmf* is translocated to the end of *nad1a*, but the orientation of transcription remains unchanged (**Figure 1**).

Compared with mitochondrial genomes of *Euplotes* G1, there are no *trnM* and *trnE* but two *trnQs* (*Q1* and *Q2* in **Figure 1**) in *Euplotes* G2 mitogenomes. The *trnQ1* in *Euplotes* G2 owns the same anticodon (UUG) as *trnQ* in *Euplotes* G1, while the anticodon of *trnQ2* is CUG (**Supplementary Figure 1A**). Besides,

[1] http://codonw.sourceforge.net/

[2] https://github.com/nylander/MrModeltest2

TABLE 1 | Summary of *Euplotes* mitochondrial genomes.

Species	Habitats	Sequencing length (bp)	Effective number of codons (ENC)	AT content	Publication date
E. crassus	Seawater	33,273	48.96	65.5%	2009
E. minuta	Seawater	40,382	51.46	64.7%	
E. vannus	Seawater	33,603	51.76	63.6%	In this study
E. focardii	Seawater	43,620	51.88	66.3%	
E. octocarinatus	Freshwater	40,133	33.93	82.0%	
E. aediculatus	Freshwater	32,628	33.11	80.2%	

the sequence similarity between *Euplotes* G2 *trnQ1* and *Euplotes* G1 *trnQ* is higher than that between *Euplotes* G2 *trnQ2* and *Euplotes* G1 *trnQ* (**Supplementary Figure 1B**). The interspecific divergence of *trnQ1* (between *E. aediculatus* and *E. octocarinatus*) is smaller than that of *trnQ2* both in sequence and structure (**Supplementary Figures 1A,B**). The disparity of *trnQ2* mainly reflects on both D arm and anticodon arms.

Asymmetric Nucleotide Composition Flanking the Tandem Repeat Regions

Although the sequences of the tandem repeat region are not completely consistent within the existing *Euplotes* mitochondrial genomes, their AT content is obviously higher than that of the entire mitogenome. We calculated AT skew and GC skew of upstream and downstream by regarding the tandem repeat region as midpoint. The AT skew of the non-overlapping windows of all species in upstream are mostly positive while windows in the downstream are opposite, which means there are more A than T in the upstream and more T than A in the downstream. However,

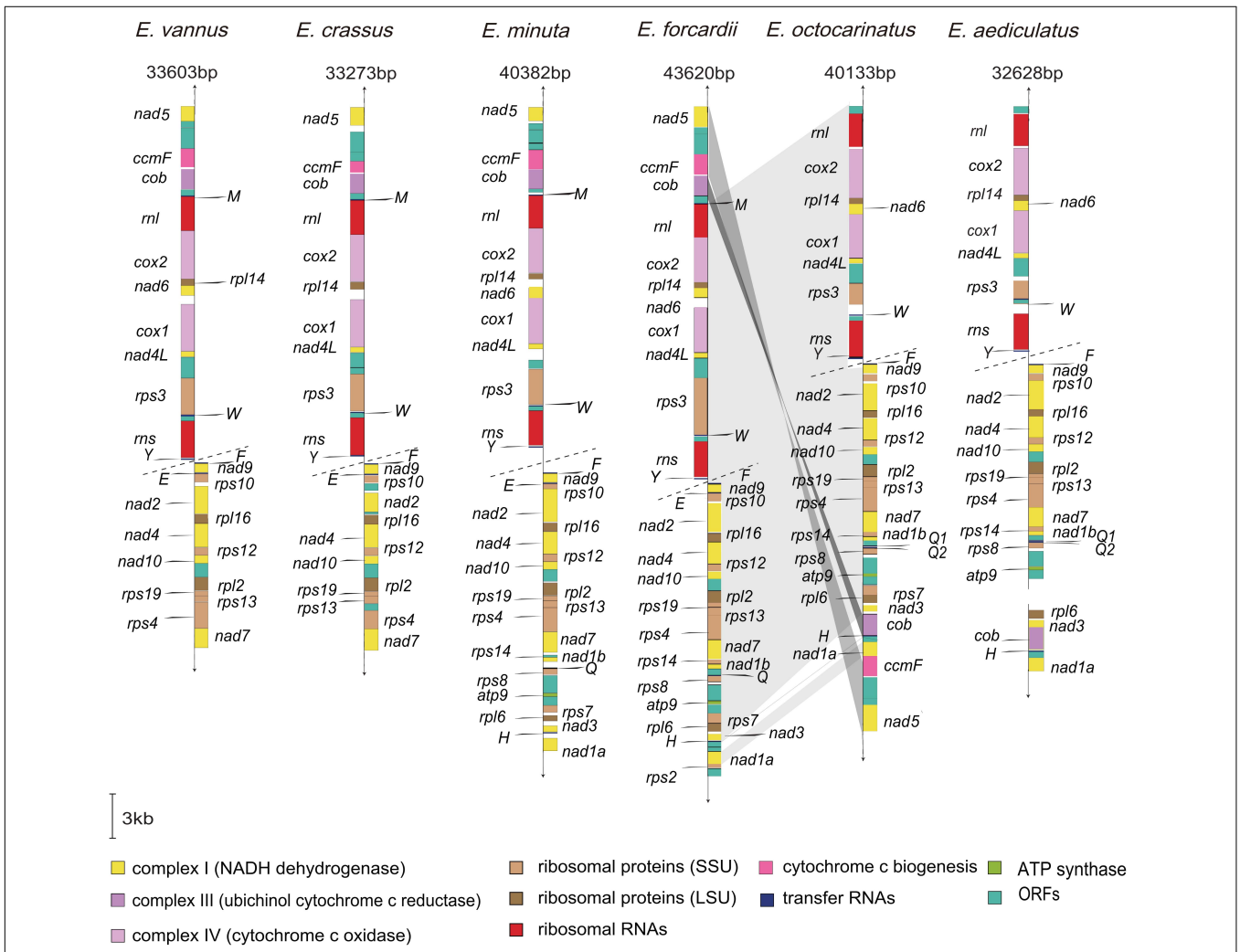

FIGURE 1 | Mitochondrial gene maps in *Euplotes*. Different colors are used to distinguish genes with different functions. Gray-colored regions represent the collinearity between the two groups of mitochondrial genomes. The dot line indicates the tandem repeat region with unknown length located in mitogenomes. Arrow shows the transcriptional direction of genes. The length of *Euplotes* mitochondrial genomes is labeled excluding the central tandem repeat region. For *E. aediculatus*, we obtained two segments from mitochondria and failed to connect them.

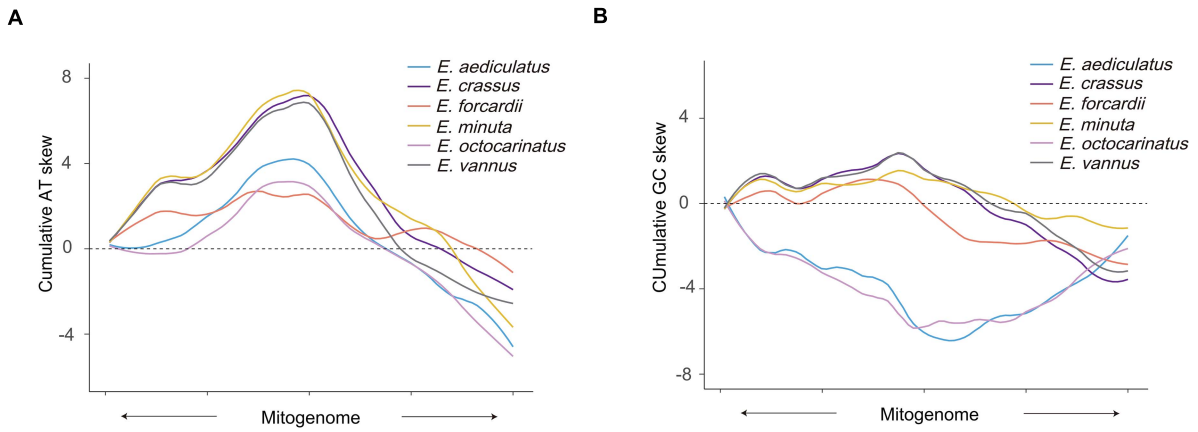

FIGURE 2 | Cumulative AT skew and GC skew of *Euplotes* mitogenomes. **(A)** Cumulative AT skew of upstream and downstream of the tandem repeat regions. Upstream and downstream sequences of all mitochondrion are scaled to the same length, respectively. The midpoint of *X*-axis shows the position of the tandem repeat region. The arrow shows the transcriptional direction. **(B)** Cumulative GC skew of upstream and downstream of the tandem repeat regions. The meaning of the diagram marks are the same as panel **(A)**.

the GC skew of *Euplotes* G1 and *Euplotes* G2 has different tendencies regardless of upstream or downstream, which means there are more G than C in the upstream and more C than G in the downstream of *Euplotes* G1 but completely different for *Euplotes* G2 (**Supplementary Figure 2**). In order to facilitate the observation of their trend, we calculated cumulative AT skew and cumulative GC skew and found turning points near the tandem repeat region (**Figures 2A,B**).

Codon Usage Bias

The effective number of codons which ranges from 20 to 61 is an index used to measure codon usage bias level (Wright, 1990). A value of 20 indicates that there exists extreme bias - only one codon is used for each amino acid, while a value of 61 indicates no bias that all codons are equally used (Fuglsang, 2006). We found that *Euplotes* species in G2 have a higher degree of codon usage bias than those in G1 (**Table 1**). Then, we calculated the relative synonymous codon usage (RSCU) of 61 codons (except two stop codons and ATG) in all *Euplotes* species and found that *Euplotes* G1 and G2 exhibit different codon usage patterns but both prefer codons ending with AT. Compared with species belonging to G1, species in G2 seem to use more AT-ending codons (**Figure 3A**).

Factors Influencing Codon Usage

To explore the potential factor that shapes the codon usage bias in *Euplotes* mitogenomes, the neutrality plot analysis and ENC-plot analysis were carried out using all PCGs as well as ORFs in six *Euplotes*. The correlation between GC12 and GC3 is statistically significant ($r = 0.722$, $p < 2.2e^{-16}$) and the slope of the regression line is 0.549 ($R^2 = 0.518$, $p < 2.2e^{-16}$) (**Figure 3B**). We further calculated the expected ENC values by GC3 with the assumption that codon usage bias is only subject to mutation bias. Subsequently, we plotted the standard curve by GC3 and the corresponding expected ENC values. As shown in **Figure 3C**, most genes distributed near the standard curve and the Pearson correlation coefficient between actual ENC values and expected ENC values is 0.877 ($p < 2.2e^{-16}$). It should be mentioned that the ENC values of several genes deviated from the standard curve by more than 20%, most of which have shorter length compared to the remaining genes. However, there is no significant difference on gene length between the genes deviated from the standard values by more than 10% and less than 20% and those deviated from the standard values by less than 10% (**Supplementary Figure 3**).

Principal component analysis was carried out based on 61 synonymous codons. The first principal component (PC1) and the second principal component (PC2) can explain 73.06% and 5.04% of the total variation, respectively. The positions of codon were marked in two-dimensional coordinates and codons ending with AT and GC could be clearly separated (**Figure 4A**). Both PC1 and PC2 were significantly correlated with GC3 and GC content but only slightly correlated with protein aromaticity (**Figure 4B**). There is no correlation between these principal components and protein hydrophily.

Phylogenetic Analysis

We selected conserved genes that are shared in all sequenced ciliate mitochondrial genomes (**Supplementary Table 3**), including *cox1*, *cox2*, *nad4*, *nad7*, *rpl2*, *rps12*, to construct phylogenetic trees based on the concatenated sequence of these genes. The phylogenetic trees using ML and BI method have similar topologies so we only present the ML tree with support values of both methods labeling on branches. The sequenced ciliates come from two classes and *Euplotes* belongs to Spirotrichea. Six *Euplotes* species were clustered into two groups, G1 and G2 (**Figure 5A**), which is consistent to the classification based on gene order. We further investigated the evolutionary history of the genus *Euplotes* based on SSU-rRNA genes (**Supplementary Table 4**). The phylogentic tree can classify species into five clades, with G1 and G2 belonging to two main clades respectively. Unlike phylogenetic tree

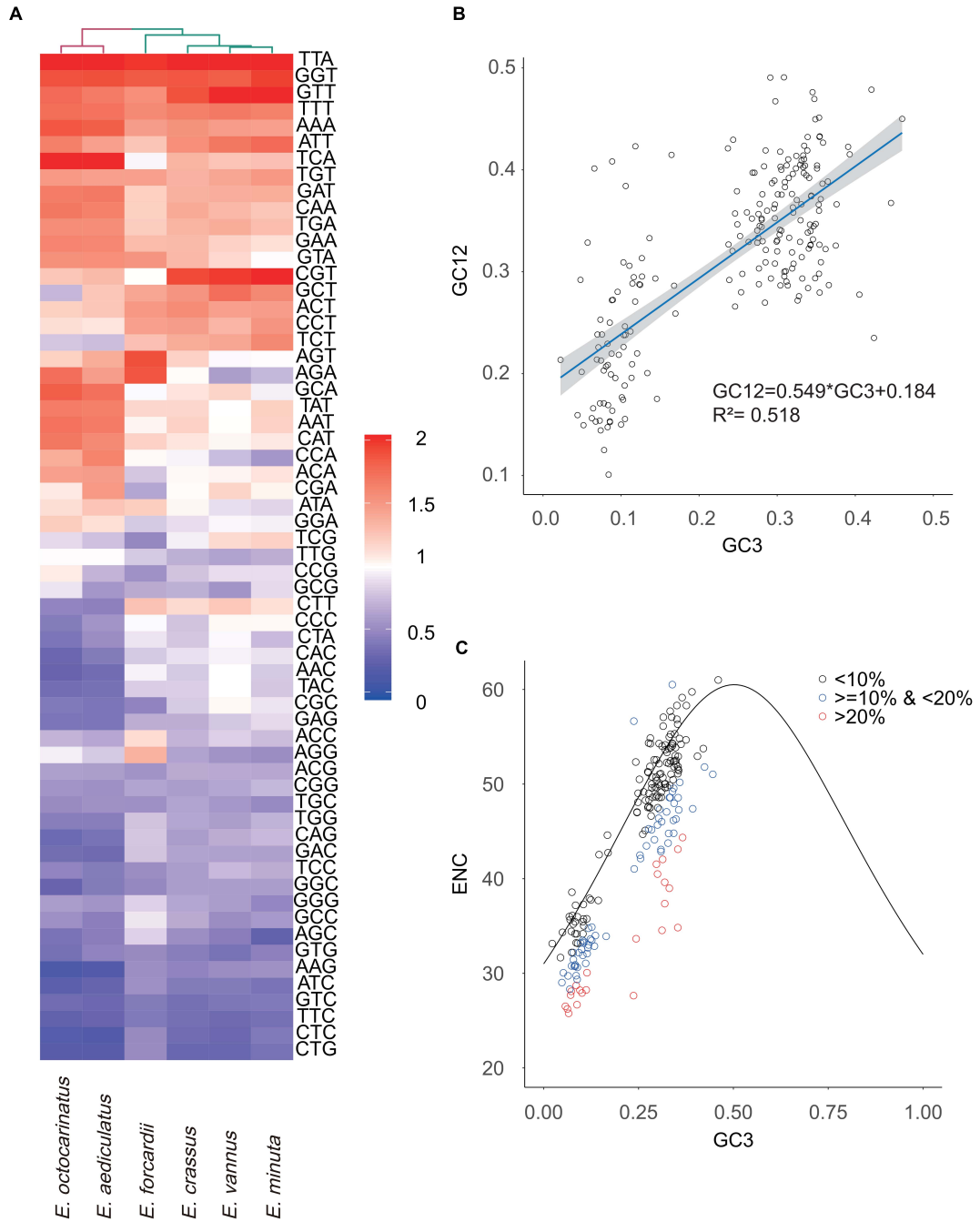

FIGURE 3 | Analysis of codon usage bias. **(A)** The heatmap shows RSCU values of 61 codons used in *Euplotes* mitochondrial genomes. **(B)** Neutrality plot analysis. GC3 refers to GC content of the third codon site, GC12 means GC content of the first and second codon sites. The dark blue line represents the regression line and the gray area represents 95% confidence interval. **(C)** ENC-plot analysis. We divided genes into three levels (<10%, <20% & >10%, >20%) based on the degree of the actual ENC values deviating from the standard curve.

based on mitochondrial genes, *E. vannus* is closer to *E. crassus* rather than *E. minuta*. Since salinity was often absent in previous studies, we defined the description of freshwater, brackish water and habitats less than 25‰ salinity to be low salinity while the description of seawater, hypersaline water and habitats more than 25‰ salinity as high salinity (Syberg-Olsen et al., 2016). Both two main clades contain species habitat in low salinity and high salinity and clustered *Euplotes* species tend to live in similar salinity level (**Figure 5B**). However, some species, including *E. encysticus*, *E. harpa*, *E. curdsi* and *E. petzi*, could survive in both high salinity and low salinity environments (Syberg-Olsen et al., 2016).

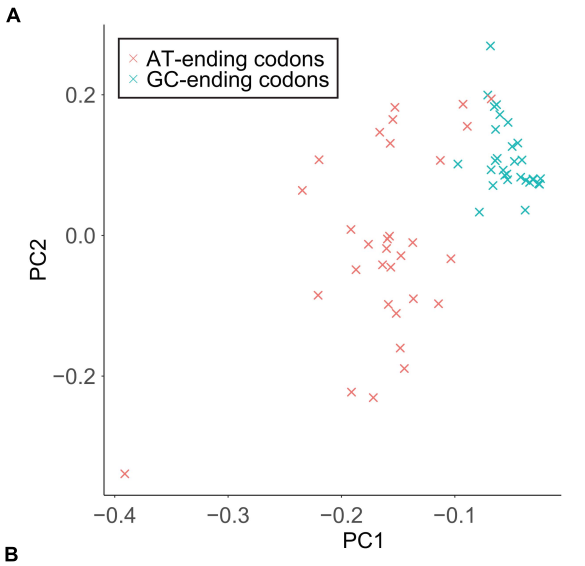

B

	GC3	GC content	AROMO	GRAVY
PC1	0.825***	0.618***	- 0.330***	- 0.08
PC2	0.937***	0.786***	- 0.459***	- 0.201**

FIGURE 4 | Principal component analysis of codon usage. **(A)** The first principal component (PC1) and the second principal component (PC2) form two-dimensional coordinate and 61 codons are marked on it. **(B)** Correlation between principal components and potential factors that may affect codon usage. *** indicates $p < 0.001$, and ** indicates $p < 0.01$.

Selection on Mitochondrial Genes

The branch that represents *Euplotes* G2 is selected as the foreground branch for all mitochondrial protein coding genes. ω of all genes present are much less than 1, indicating they are under strong purifying selection. The one-ratio model assumes that foreground branch and background branch have the same ω value, while two-ratio model is opposite. The result of likelihood-ratio test indicates that most genes fit the one-ratio model, while *cox1, cox2* and *rps3* seem to better fit to the two-ratio model (**Table 2**) ($p < 0.05$). It is likely that ω of these three genes are significant different between *Euplotes* G1 and G2, indicating different degree of purifying selection pressure may occur on the speciation of the two clades.

DISCUSSION

Gene Rearrangement and Putative Origin in *Euplotes* Mitochondrial Genomes

There is a long tandem repeat region with high level of AT content in *Euplotes* mitochondrial genomes, which makes it difficult to acquire complete sequences by high-throughput sequencing techniques. Despite the incompleteness of mitogenomes, we found gene rearrangement events present in *Euplotes* mitochondrion. Genes involved in rearrangement include tRNA genes as well as protein-coding genes. In general, the tRNA genes rearrange more frequently than PCGs and rRNA genes within the mitogenome (Wu et al., 2014). In 2007, a pseudo-tRNA gene, which was absent in other *Tetrahymena* species, had been detected in *Tetrahymena paravorax* (Moradian et al., 2007). We noticed that species in *Euplotes* G1 are from the marine water, while *Euplotes* G2 species live in freshwater. Interestingly, *E. vannus* living in low salinity stress could activated an extra pathway related to the glutamine (Gln, Q) metabolic process (Chen et al., 2019). The extra *trnQ* in *Euplotes* G2 mitogenome which has different anticodons might be related to salinity of habitats.

Previous study shows that the AT rich region usually plays an important role in regulating the process of transcription and replication (Boore, 1999). In two genera *Paramecium* and *Tetrahymena*, the AT-rich region coincides with the DNA replication origin (Moradian et al., 2007). Due to the difference in replication mechanisms of leading strand and lagging strand, there should be a positive GC skew and negative AT skew in the leading strand, a negative GC skew and a positive AT skew in the lagging strand in prokaryote genomes (Charneski et al., 2011). AT skew or GC skew in prokaryotes can switch at the origin and terminus of replication (Fellenberg et al., 2001). Considering that both cumulative AT skew and cumulative GC skew have a turning point near the tandem repeat region, it suggests that this interval may be the replication origin of *Euplotes* mitochondrion. The origin of replication in *Paramecium* mitochondria is at one terminus, whereas it is near the center in *Tetrahymena* (Pritchard and Cummings, 1981; Pritchard et al., 1990; Burger et al., 2000). The fact that the sequence flanking the tandem repeat region transcribes in the opposite directions increases the possibility that this region may be involved in transcription and replication initiation.

Mutation Bias as the Major Driving Force of Codon Usage Bias

It is generally acknowledged that codon usage pattern reflects a balance between mutation bias and natural selection for translational efficiency (Sharp et al., 1993; Liu et al., 2004). The neutrality plot analysis is a classical method to compare the influences of these two factors by plotting the GC12 of the synonymous codons against the GC3. Considering that base composition of three codon positions should be similar without natural selection, the closer the slope of their regression curve is to 1, the greater the influence of mutational bias. In *Euplotes* mitogenomes, GC12 and GC3 are highly correlated with a slope of 0.549, indicating that mutation bias might be the major driving force of codon usage bias. For ENC-plot analysis, if genes distribute near the standard curve, their codon usage is more likely affected by mutation bias. In this study, we found that most genes in the ENC-plot locate near the standard curve and the correlation between actual ENC and expected ENC is highly significant, which further confirm mutation bias as the major driving force. Genes which are deviated from the standard curve (>20% deviation) are mostly

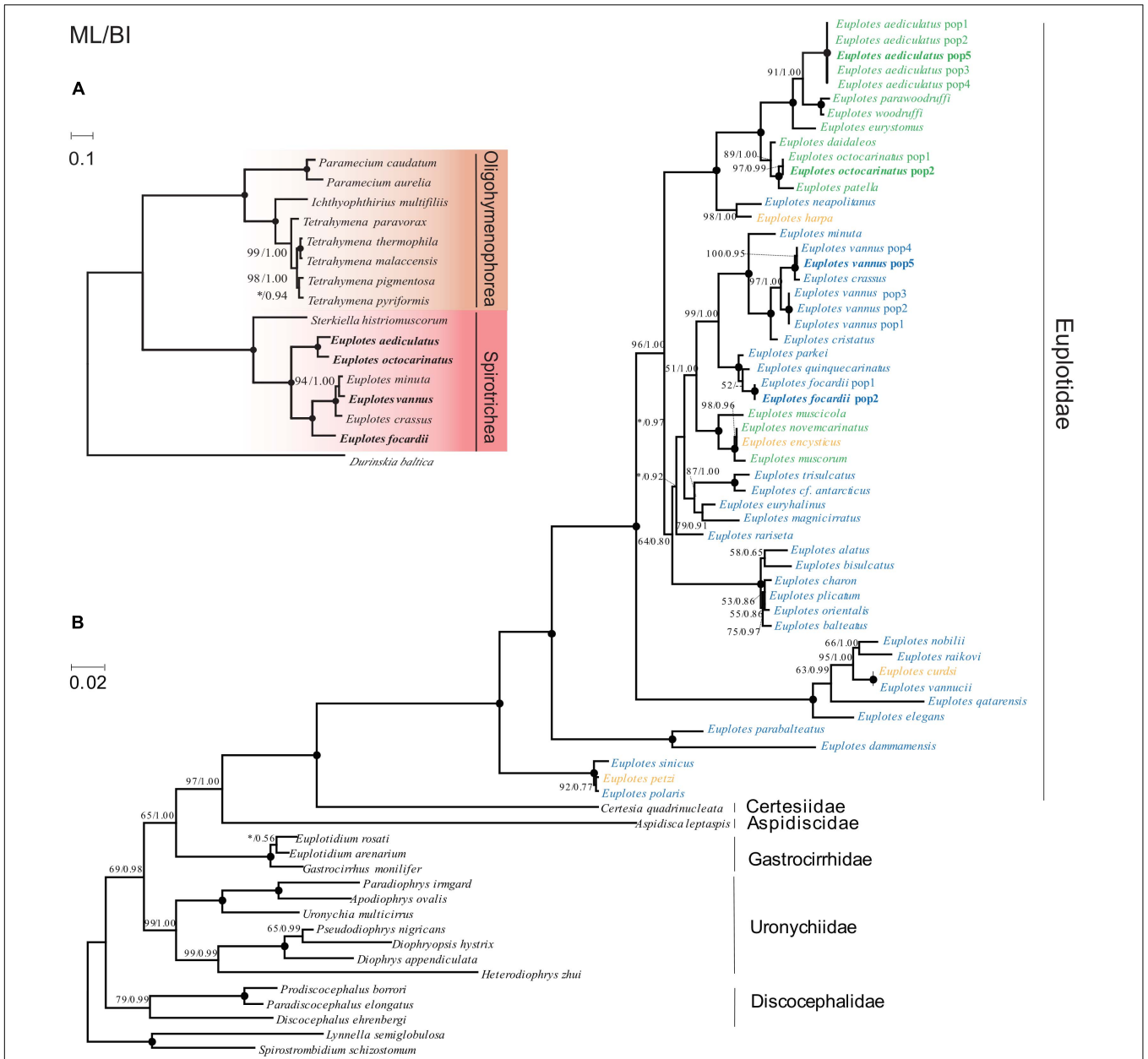

FIGURE 5 | Phylogenetic trees based on mitochondrial genes and nuclear genes. BP values for ML tree and PP values for BI tree are given near nodes and separated by slash. The asterisks represent BP values lower than 50 or PP values lower than 0.7. Solid circles indicate fully supported branches (100%/1.00). Species sequenced in the present study are shown in bold. **(A)** Phylogenetic trees constructed based on multiple mitochondrial genes. The scale bar represents 10 substitutions per 100 nucleotide positions. **(B)** Phylogenetic tree constructed based on SSU-rRNA genes. *Euplotes* living in environment with low salinity are shown in green, while those in high salinity are shown in blue. Species surviving in both high salinity and low salinity environments are marked with yellow. The "pop" represents different strains within a specific species. The scale bar corresponds to 2 substitutions per 100 nucleotide positions.

shorter than 500 bp (**Supplementary Figure 3**), it is likely the short length rather than actual codon usage bias lead to the extremely low ENC values.

There are various factors contributing to codon usage bias, including gene function (Chiapello et al., 1998), composition of bases and amino acid, gene length (Duret and Mouchiroud, 1999), gene expression (Liu et al., 2004; Wei et al., 2014), abundance of tRNA (Duret, 2000). Codons ending with AT and GC form two clusters by plotting PC1 against PC2, indicating that GC3 has great impact on codon usage. Although the effect is not as strong as GC3, GC content also affects codon usage. Protein aromaticity is negatively related to codon usage, as protein aromaticity depends on the composition of amino acid and gene function, which is considered to be the result of natural selection (Wei et al., 2014). Therefore, the codon usage bias in *Euplotes* mitogenomes is mainly

TABLE 2 | Branch test performed on protein coding genes of mitochondrion.

Gene	One-ratio model	Two-ratio model	Degrees of freedom	2ΔLnL	*P* value	ω
nad2	−5962.9931	−5962.9301	1	0.1262	0.7225	0.0375
nad4	−7047.9516	−7046.2576	1	3.3880	0.0656	0.0381
nad4L	−1609.1080	−1608.8552	1	0.5056	0.4771	0.0329
nad9	−2938.0647	−2937.6186	1	0.8921	0.3449	0.0628
nad10	−1728.2985	−1727.5019	1	1.5931	0.2069	0.0140
cox1	−12309.4543	−12307.0436	1	4.8213	0.0281	ω0 = 0.03141 ω1 = 0.00010
cox2	−16276.0915	−16271.2973	1	9.5884	0.0019	ω0 = 0.07228 ω1 = 0.00325
cob	−3950.7519	−3949.7568	1	1.9903	0.1583	0.0080
rps3	−8518.2443	−8513.7291	1	9.0304	0.0027	ω0 = 0.07138 ω1 = 0.00603
rps4	−6703.6457	−6702.7679	1	1.7558	0.1852	0.0365
rps10	−1230.8911	−1230.3573	1	1.0677	0.3015	0.0087
rps12	−2131.4662	−2131.4081	1	0.1161	0.7333	0.0079
rps13	−1778.7224	−1777.9087	1	1.6274	0.2021	0.0238
rps19	−1073.4163	−1072.9863	1	0.8601	0.3537	0.0056
rpl2	−4227.5063	−4226.9362	1	1.1402	0.2856	0.0522
rpl14	−1865.2229	−1864.4274	1	1.5910	0.2072	0.0340
rpl16	−2256.9874	−2256.7256	1	0.5235	0.4694	0.0216

shaped by mutations bias, whereas natural selection is only the minor driving force.

Phylogeny and Habitat Salinity

For aquatic organisms, salinity are one of the most important environmental factors which determine the community composition (Crump et al., 2004; Herlemann et al., 2016). Previous studies suggest that the *Euplotes* species and subclades in phylogenetic tree based on SSU-rRNA gene are more uniform in term of habitat salinity (Petroni et al., 2002; Yi et al., 2009; Syberg-Olsen et al., 2016). It is still be true when we carried out phylogenetic analysis by SSU-rRNA gene from more species in *Euplotes*. When constructing the phylogenetic tree by multiple mitochondrial genes, we found the six species in *Euplotes* were divided into two branches, corresponding to *Euplotes* G1 (seawater) and *Euplotes* G2 (freshwater), respectively. These results indicate that salinity might act as a barrier for the distribution of *Euplotes* species. The salinity barrier seems not be strict as the euryhaline species might be the intermediate stage of immigration from ancestrally marine to freshwater (Zhao et al., 2018).

Mitochondrial Genes Used for Discriminating Closely Related *Euplotes* Species

There is a long standing species classification problem in the *vannus-crassus* group (Caprette and Gates, 1994; Zhao et al., 2018). One view point is that *E. vannus* and *E. crassus* experienced separated evolution and speciation (Giannì and Piras, 1990), while another is that *E. vannus* and *E. crassus* form a highly polymorphic species (Caprette and Gates, 1994). *E. vannus* and *E. crassus* have similar morphological characteristics and high sequence identity (SSU-rRNA: average 97.78%), which makes it difficult to distinguish them. Sequence identity in mitochondrial genes between *E. vannus* and *E. crassus* is relatively low (e.g., 78.1% in *cox1*), which can help distinguish *E. vannus* from *E. crassus* and other species with highly similarity. In phylogenetic trees based on mitochondrial genes (both single and concatenated genes), phylogenetic relationship among *E. vannus, E. crassus* and *E. minuta* is slightly different from that based on nuclear genes, which may be due to incongruent evolutionary rates between mitochondrial and nuclear genes in these species.

Adaptations From Marine to Freshwater

Immigration from marine to freshwater require specific adaptive mechanism to adjust osmoregulation (Alverson et al., 2007). Evolutionary divergence between marine and freshwater *Euplotes* might be caused by this kind of physiological adaptations. We found that ω of all mitochondrial genes are far less than 1, indicating strong purifying selection acting on these genes in *Euplotes*. The result of branch-specific test indicates that *cox1*, *cox2* and *rps3* have inconsistent ω value along the branch of *Euplotes* G1 and G2, which means their evolutionary rate is different. The *rps3* encodes ribosomal protein small subunit and it shows a relatively low sequence similarity in the middle of gene and is of great difference in length among *Euplotes* species. Previous study reported that the mitochondrial *rps3* is variable in size and position as well as gene arrangement due to insertions, microsatellite expansions (Sethuraman et al., 2009). These may result in inconsistent ω values of *rps3* between *Euplotes* G1 and G2. Both *cox1* and *cox2* encode cytochrome *c* oxidase which play crucial roles in ATP production by participating in oxidative phosphorylation (OXPHOS pathway). The strategy for osmotic adjustment rely on energy-depend mechanism (Harding et al., 2016; Weinisch et al., 2018). The two genes of *Euplotes* G1 and *Euplotes* G2 may undergo diversifying evolutionary process for physiological adaptations from marine to freshwater.

CONCLUSION

The current study mainly acquired four mitogenomes of *Euplotes* and help to provide valuable resources and new insights into the evolution process of *Euplotes* genus. Mitochondrial genes of *Euplotes* including PCGs and tRNA genes undergo rearrangement events but the position of putative origin of transcription and replication is conserved. Though the codon usage patterns of mitochondrion are different in *Euplotes* genus, mutation bias is always the major driving force resulting in the codon usage bias. Interestingly, both gene order and codon usage bias seem to be uniform with habitat salinity level. Phylogenetic analyses based on both mitochondrial and nuclear genes further confirm that species living in similar salinity habitat tend to cluster together. Salinity does present a barrier to the distribution of *Euplotes*. However, some of the ancestrally marine species could adapt to the freshwater. Physiological adaptations may happen to regulate osmotic pressure regulation participated in this process. The *cox1* and *cox2* which participate in OXPHOS pathway might be the key genes for physiological adaptations from marine to freshwater. Besides, mitochondrial genes have higher evolutionary rate compared with traditional nuclear gene markers, so they are more effective for discriminating species with highly similarity.

DATA AVAILABILITY STATEMENT

The datasets presented in this study can be found in online repositories. The names of the repository/repositories and accession number(s) can be found below: https://www.ncbi.nlm.nih.gov/, MT665958; https://www.ncbi.nlm.nih.gov/, MT665959.

AUTHOR CONTRIBUTIONS

MM designed and guided the study. NH, SC, MH, and LH conducted sampling and performed laboratory work. NH and SC performed the evolutionary and phylogenetic analyses. NH drafted the manuscript. MM, SZ, YZ, and QS made further revisions. All authors read and approved this manuscript.

FUNDING

This work was supported by Natural Science Foundation of China (32070432, 31672279, 41702385, 32070461), and the Fundamental Research Funds for the Central Universities.

ACKNOWLEDGMENTS

Our thanks are due to Prof. Weibo Song (Ocean University of China, China) for supplying samples and technical support.

SUPPLEMENTARY MATERIAL

The Supplementary Material for this article can be found online at: https://www.frontiersin.org/articles/10.3389/fmars.2021.627879/full#supplementary-material

Supplementary Figure 1 | Secondary structure and identity of *trn*Qs. **(A)** The secondary structure of *trn*Qs in *Euplotes*. The short lines mean there are two hydrogen bonds between the bases, the round dots are used to denote three hydrogen bonds between G and C. Mismatched base pairs are marker by green solid circle. **(B)** Pairwise identity of *trnQs* in *Euplotes*. The order of *trnQs* from top to bottom is exactly the same as the order from left to right.

Supplementary Figure 2 | AT skew and GC skew of *Euplotes* mitogenomes. AT skew and GC shew of upstream and downstream of the tandem repeat regions. Upstream and downstream sequences of all mitochondrion are scaled to the same length respectively. The midpoint of x-coordinate represents the position of the tandem repeat region. The arrows show the transcriptional directions.

Supplementary Figure 3 | Relationship between gene length and degree of actual ENC values deviating from the standard values. The x-coordinate represents the percentage of deviation from the standard, while y-coordinate is gene length. Three asterisks indicate *p* value is less than 0.001 (*t*-test).

Supplementary Table 1 | Degenerate primers for *E. vannus*.

Supplementary Table 2 | The previous annotation refers to earliest annotation of *E. minuta* and *E. crassus* done by de Graaf et al. (2009). The new annotation of *E. minuta* represents result of reannotation done by Swart et al. (2012). We reannotated *E. crassus* as the new annotation of *E. crassus*. In this study, we used new annotation results uniformly.

Supplementary Table 3 | Accession numbers of all sequenced ciliate mitochondrial genomes.

Supplementary Table 4 | Accession numbers of SSU-rRNA genes used to construct phylogenetic tree.

REFERENCES

Alverson, A. J., Jansen, R. K., and Theriot, E. C. (2007). Bridging the Rubicon: phylogenetic analysis reveals repeated colonizations of marine and fresh waters by thalassiosiroid diatoms. *Mol. Phylogenet. Evol.* 45, 193–210. doi: 10.1016/j.ympev.2007.03.024

Ballard, J. W. (2000). Comparative genomics of mitochondrial DNA in *Drosophila simulans*. *J. Mol. Evol.* 51, 64–75. doi: 10.1007/s002390010067

Bankevich, A., Nurk, S., Antipov, D., Gurevich, A. A., Dvorkin, M., Kulikov, A. S., et al. (2012). SPAdes: a new genome assembly algorithm and its applications to single-cell sequencing. *J. Comput. Biol.* 19, 455–477. doi: 10.1089/cmb.2012.0021

Barth, D., and Berendonk, T. U. (2011). The mitochondrial genome sequence of the ciliate *Paramecium caudatum* reveals a shift in nucleotide composition and codon usage within the genus *Paramecium*. *BMC Genomics* 12:272. doi: 10.1186/1471-2164-12-272

Benson, G. (1999). Tandem repeats finder: a program to analyze DNA sequences. *Nucleic Acids Res.* 27, 573–580. doi: 10.1093/nar/27.2.573

Bolger, A. M., Lohse, M., and Usadel, B. (2014). Trimmomatic: a flexible trimmer for Illumina sequence data. *Bioinformatics* 30, 2114–2120. doi: 10.1093/bioinformatics/btu170

Boore, J. L. (1999). Animal mitochondrial genomes. *Nucleic Acids Res.* 27, 1767–1780. doi: 10.1093/nar/27.8.1767

Burger, G., Zhu, Y., Littlejohn, T. G., Greenwood, S. J., Schnare, M. N., Lang, B. F., et al. (2000). Complete sequence of the mitochondrial genome of *Tetrahymena pyriformis* and comparison with *Paramecium aurelia* mitochondrial DNA. *J. Mol. Biol.* 297, 365–380. doi: 10.1006/jmbi.2000.3529

Caprette, C. L., and Gates, M. A. (1994). Quantitative analyses of interbreeding in populations of *E. vannus*-Morphotype *Euplotes*, with special attention to the

nominal species *E. vannus and E. crassus*. *J. Eukaryot. Microbiol.* 41, 316–324. doi: 10.1111/j.1550-7408.1994.tb06084.x

Castresana, J. (2000). Selection of conserved blocks from multiple alignments for their use in phylogenetic analysis. *Mol. Biol. Evol.* 17, 540–552. doi: 10.1093/oxfordjournals.molbev.a026334

Charneski, C. A., Honti, F., Bryant, J. M., Hurst, L. D., and Feil, E. J. (2011). Atypical AT skew in Firmicute genomes results from selection and not from mutation. *PLoS Genet.* 7:e1002283. doi: 10.1371/journal.pgen.1002283

Chen, X., Jiang, Y., Gao, F., Zheng, W., Krock, T. J., Stover, N. A., et al. (2019). Genome analyses of the new model protist *Euplotes* vannus focusing on genome rearrangement and resistance to environmental stressors. *Mol. Ecol. Resour.* 19, 1292–1308. doi: 10.1111/1755-0998.13023

Chiapello, H., Lisacek, F., Caboche, M., and Hénaut, A. (1998). Codon usage and gene function are related in sequences of *Arabidopsis thaliana*. *Gene* 209, GC1–GC38. doi: 10.1016/s0378-1119(97)00671-9

Contreras-Moreira, B., and Vinuesa, P. (2013). GET_HOMOLOGUES, a versatile software package for scalable and robust microbial pangenome analysis. *Appl. Environ. Microbiol.* 79, 7696–7701. doi: 10.1128/aem.02411-13

Crump, B. C., Hopkinson, C. S., Sogin, M. L., and Hobbie, J. E. (2004). Microbial biogeography along an estuarine salinity gradient: combined influences of bacterial growth and residence time. *Appl. Environ. Microbiol.* 70, 1494–1505. doi: 10.1128/aem.70.3.1494-1505.2004

Darriba, D., Taboada, G. L., Doallo, R., and Posada, D. (2011). ProtTest 3: fast selection of best-fit models of protein evolution. *Bioinformatics* 27, 1164–1165. doi: 10.1093/bioinformatics/btr088

Darriba, D., Taboada, G. L., Doallo, R., and Posada, D. (2012). jModelTest 2: more models, new heuristics and parallel computing. *Nat. Methods* 9, 772–772. doi: 10.1038/nmeth.2109

de Graaf, R. M., van Alen, T. A., Dutilh, B. E., Kuiper, J. W., van Zoggel, H. J., Huynh, M. B., et al. (2009). The mitochondrial genomes of the ciliates *Euplotes minuta* and *Euplotes crassus*. *BMC Genomics* 10:514. doi: 10.1186/1471-2164-10-514

Duret, L. (2000). tRNA gene number and codon usage in the *C. elegans* genome are co-adapted for optimal translation of highly expressed genes. *Trends Genet.* 16, 287–289. doi: 10.1016/s0168-9525(00)02041-2

Duret, L., and Mouchiroud, D. (1999). Expression pattern and, surprisingly, gene length shape codon usage in *Caenorhabditis*, *Drosophila*, *Arabidopsis*. *Proc. Natl. Acad. Sci. U.S.A.* 96, 4482–4487. doi: 10.1073/pnas.96.8.4482

Fellenberg, K., Hauser, N. C., Brors, B., Neutzner, A., Hoheisel, J. D., and Vingron, M. (2001). Correspondence analysis applied to microarray data. *Proc. Natl. Acad. Sci. U.S.A.* 98, 10781–10786. doi: 10.1073/pnas.181597298

Fernandes, N. M., Paiva, T., da Silva-Neto, I. D., Schlegel, M., and Schrago, C. G. (2016). Expanded phylogenetic analyses of the class Heterotrichea (Ciliophora, Postciliodesmatophora) using five molecular markers and morphological data. *Mol. Phylogenet. Evol.* 95, 229–246. doi: 10.1016/j.ympev.2015.10.030

Fuglsang, A. (2006). Estimating the "effective number of codons": the Wright way of determining codon homozygosity leads to superior estimates. *Genetics* 172, 1301–1307. doi: 10.1534/genetics.105.049643

Gentekaki, E., Kolisko, M., Boscaro, V., Bright, K. J., Dini, F., Di Giuseppe, G., et al. (2014). Large-scale phylogenomic analysis reveals the phylogenetic position of the problematic taxon *Protocruzia* and unravels the deep phylogenetic affinities of the ciliate lineages. *Mol. Phylogenet. Evol.* 78, 36–42. doi: 10.1016/j.ympev.2014.04.020

Giannì, A., and Piras, L. (1990). Autoecological and molecular approach to the species problem in the *Euplotes vannus-crassus-minuta* group (Ciliophora, Hypotrichida). *Eur. J. Protistol.* 26, 142–148. doi: 10.1016/s0932-4739(11)80108-2

Giuseppe, G. D., Erra, F., Dini, F., Alimenti, C., Vallesi, A., Pedrini, B., et al. (2011). Antarctic and Arctic populations of the ciliate *Euplotes nobilii* show common pheromone-mediated cell-cell signaling and cross-mating. *Proc. Natl. Acad. Sci. U.S.A.* 108, 3181–3186. doi: 10.1073/pnas.1019432108/-/DCSupplemental

Gray, M. W., Burger, G., and Lang, B. F. (1999). Mitochondrial evolution. *Science* 283, 1476–1481. doi: 10.1126/science.283.5407.1476

Graziano, G., Danielle, S., Graziano, D. G., and Fernando, D. (2010). Structures, biological activities and phylogenetic relationships of terpenoids from marine ciliates of the genus *Euplotes*. *Mar. Drugs* 8, 2080–2116. doi: 10.3390/md8072080

Grigoriev, A. (1998). Analyzing genomes with cumulative skew diagrams. *Nucleic Acids Res.* 26, 2286–2290. doi: 10.1093/nar/26.10.2286

Hall, T. A. (1999). BioEdit: a user-friendly biological sequence alignment editor and analysis program for Windows 95/98/NT. *Nucleic Acids Symp. Ser.* 41, 95–98. doi: 10.14601/Phytopathol_Mediterr-14998u1.29

Harding, T., Brown, M. W., Simpson, A. G., and Roger, A. J. (2016). Osmoadaptative strategy and its molecular signature in obligately halophilic heterotrophic protists. *Genome Biol. Evol.* 8, 2241–2258. doi: 10.1093/gbe/evw152

He, M., Wang, J., Fan, X., Liu, X., Shi, W., Huang, N., et al. (2019). Genetic basis for the establishment of endosymbiosis in *Paramecium*. *ISME J.* 13, 1360–1369. doi: 10.1038/s41396-018-0341-4

Herlemann, D. P., Lundin, D., Andersson, A. F., Labrenz, M., and Jurgens, K. (2016). Phylogenetic signals of salinity and season in bacterial community composition across the salinity gradient of the Baltic Sea. *Front. Microbiol.* 7:1883. doi: 10.3389/fmicb.2016.01883

Jeffares, D., Tomiczek, B., Sojo, V., and dos Reis, M. (2015). A beginners guide to estimating the non-synonymous to synonymous rate ratio of all protein-coding genes in a genome. *Methods Mol. biol.* 1201, 65–90. doi: 10.1007/978-1-4939-1438-8_4

Katoh, K., and Standley, D. M. (2013). MAFFT multiple sequence alignment software version 7: improvements in performance and usability. *Mol. Biol. Evol.* 30, 772–780. doi: 10.1093/molbev/mst010

Kodama, Y., and Fujishima, M. (2005). Symbiotic *Chlorella* sp. of the ciliate *Paramecium bursaria* do not prevent acidification and lysosomal fusion of host digestive vacuoles during infection. *Protoplasma* 225, 191–203. doi: 10.1007/s00709-005-0087-5

Liu, Q. P., Feng, Y., and Xue, Q. Z. (2004). Analysis of factors shaping codon usage in the mitochondrion genome of *Oryza sativa*. *Mitochondrion* 4, 313–320. doi: 10.1016/j.mito.2004.06.003

Lowe, T. M., and Chan, P. P. (2016). tRNAscan-SE On-line: integrating search and context for analysis of transfer RNA genes. *Nucleic Acids Res.* 44, W54–W57. doi: 10.1093/nar/gkw413

McGrath, C. L., Gout, J. F., Doak, T. G., Yanagi, A., and Lynch, M. (2014). Insights into three whole-genome duplications gleaned from the *Paramecium caudatum* genome sequence. *Genetics* 197, 1417–1428. doi: 10.1534/genetics.114.163287

Medlin, L., Elwood, H. J., Stickel, S., and Sogin, M. L. (1988). The characterization of enzymatically amplified eukaryotic 16S-like rRNA-coding regions. *Gene* 71, 491–499. doi: 10.1016/0378-1119(88)90066-2

Moradian, M. M., Beglaryan, D., Skozylas, J. M., and Kerikorian, V. (2007). Complete mitochondrial genome sequence of three *Tetrahymena* species reveals mutation hot spots and accelerated nonsynonymous substitutions in *Ymf* genes. *PLoS One* 2:e650. doi: 10.1371/journal.pone.0000650

Pedrini, B., Suter-Stahel, T., Vallesi, A., and Luporinic, C. A. P. (2017). Molecular structures and coding genes of the water-borne protein pheromones of *Euplotes petzi*, an early diverging polar species of *Euplotes*. *J. Eukaryot. Microbiol.* 64, 164–172. doi: 10.1111/jeu.12348

Petroni, G., Dini, F., Verni, F., and Rosati, G. (2002). A molecular approach to the tangled intrageneric relationships underlying phylogeny in *Euplotes* (Ciliophora, Spirotrichea). *Mol. Phylogenet. Evol.* 22, 118–130. doi: 10.1006/mpev.2001.1030

Pritchard, A. E., and Cummings, D. J. (1981). Replication of linear mitochondrial DNA from *Paramecium*: sequence and structure of the initiation-end crosslink. *Proc. Natl. Acad. Sci. U.S.A.* 78, 7341–7345. doi: 10.1073/pnas.78.12.7341

Pritchard, A. E., Seilhamer, J. J., Mahalingam, R., Sable, C. L., Venuti, S. E., and Cummings, D. J. (1990). Nucleotide sequence of the mitochondrial genome of *Paramecium*. *Nucleic Acids Res.* 18, 173–180. doi: 10.1093/nar/18.1.173

Ronquist, F., Teslenko, M., van der Mark, P., Ayres, D. L., Darling, A., Hohna, S., et al. (2012). MrBayes 3.2: efficient Bayesian phylogenetic inference and model choice across a large model space. *Syst. Biol.* 61, 539–542. doi: 10.1093/sysbio/sys029

Serra, V., Gammuto, L., Nitla, V., Castelli, M., Lanzoni, O., Sassera, D., et al. (2019). Next generation taxonomy: integrating traditional species description with the holobiont concept and genomic approaches – the in-depth characterization of a novel *Euplotes* species as a case study. *bioRxiv* [Preprint]. doi: 10.1101/666461

Sethuraman, J., Majer, A., Iranpour, M., and Hausner, G. (2009). Molecular evolution of the mtDNA encoded *rps3* gene among filamentous ascomycetes fungi with an emphasis on the Ophiostomatoid fungi. *J. Mol. Evol.* 69, 372–385. doi: 10.1007/s00239-009-9291-9

Sharp, P. M., Stenico, M., Peden, J. F., and Lloyd, A. T. (1993). Codon usage: mutational bias, translational selection, or both? *Biochem. Soc. Trans.* 21, 835–841. doi: 10.1042/bst0210835

Shazib, S. U., Vdacny, P., Kim, J. H., Jang, S. W., and Shin, M. K. (2016). Molecular phylogeny and species delimitation within the ciliate genus *Spirostomum* (Ciliophora, Postciliodesmatophora, Heterotrichea), using the internal transcribed spacer region. *Mol. Phylogenet. Evol.* 102, 128–144. doi: 10.1016/j.ympev.2016.05.041

Sivasankaran, K., Mathew, P., Anand, S., Ceasar, S. A., Mariapackiam, S., and Ignacimuthu, S. (2017). Complete mitochondrial genome sequence of fruit-piercing moth *Eudocima phalonia* (Linnaeus, 1763) (Lepidoptera: Noctuoidea). *Genom. Data* 14, 66–81. doi: 10.1016/j.gdata.2017.09.004

Slabodnick, M. M., Ruby, J. G., Reiff, S. B., Swart, E. C., Gosai, S., Prabakaran, S., et al. (2017). The macronuclear genome of *Stentor coeruleus* reveals tiny introns in a giant cell. *Curr. Biol.* 27, 569–575. doi: 10.1016/j.cub.2016.12.057

Soding, J., Biegert, A., and Lupas, A. N. (2005). The HHpred interactive server for protein homology detection and structure prediction. *Nucleic Acids Res.* 33, W244–W248. doi: 10.1093/nar/gki408

Stamatakis, A. (2014). RAxML version 8: a tool for phylogenetic analysis and post-analysis of large phylogenies. *Bioinformatics* 30, 1312–1313. doi: 10.1093/bioinformatics/btu033

Swart, E. C., Nowacki, M., Shum, J., Stiles, H., Higgins, B. P., Doak, T. G., et al. (2012). The *Oxytricha trifallax* mitochondrial genome. *Genome Biol. Evol.* 4, 136–154. doi: 10.1093/gbe/evr136

Syberg-Olsen, M. J., Irwin, N. A., Vannini, C., Erra, F., Di Giuseppe, G., Boscaro, V., et al. (2016). Biogeography and character evolution of the ciliate genus *Euplotes* (Spirotrichea, Euplotia), with description of *Euplotes curdsi* sp. nov. *PLoS One* 11:e0165442. doi: 10.1371/journal.pone.0165442

Vaidya, G., Lohman, D. J., and Meier, R. (2011). SequenceMatrix: concatenation software for the fast assembly of multi-gene datasets with character set and codon information. *Cladistics* 27, 171–180. doi: 10.1111/j.1096-0031.2010.00329.x

Wei, L., He, J., Jia, X., Qi, Q., Liang, Z., Zheng, H., et al. (2014). Analysis of codon usage bias of mitochondrial genome in *Bombyx mori* and its relation to evolution. *BMC Evol. Biol.* 14:262. doi: 10.1186/s12862-014-0262-4

Weinisch, L., Kuhner, S., Roth, R., Grimm, M., Roth, T., Netz, D. J. A., et al. (2018). Identification of osmoadaptive strategies in the halophile, heterotrophic ciliate Schmidingerothrix salinarum. *PLoS Biol.* 16:e2003892. doi: 10.1371/journal.pbio.2003892

Wright, F. (1990). The 'effective number of codons' used in a gene. *Gene* 87, 23–29. doi: 10.1016/0378-1119(90)90491-9

Wu, X. Y., Xiao, S., Li, X. L., Li, L., Shi, W., and Yu, Z. N. (2014). Evolution of the tRNA gene family in mitochondrial genomes of five *Meretrix clams* (Bivalvia, Veneridae). *Gene* 533, 439–446. doi: 10.1016/j.gene.2013.09.077

Yang, Z. (2007). PAML 4: phylogenetic analysis by maximum likelihood. *Mol. Biol. Evol.* 24, 1586–1591. doi: 10.1093/molbev/msm088

Yi, Z. Z., Song, W. B., Clamp, J. C., Chen, Z. G., Gao, S., and Zhang, Q. Q. (2009). Reconsideration of systematic relationships within the order Euplotida (Protista, Ciliophora) using new sequences of the gene coding for small-subunit rRNA and testing the use of combined data sets to construct phylogenies of the Diophrys-complex. *Mol. Phylogenet. Evol.* 50, 599–607.

Zhao, Y., Yi, Z. Z., Warren, A., and Song, W. B. (2018). Species delimitation for the molecular taxonomy and ecology of the widely distributed microbial *Eukaryote* genus Plotters (Alveolata, Ciliophora). *Proc. Biol. Sci.* 285:20172159. doi: 10.1098/rspb.2017.2159

Zhang, H. L., Liu, B. B., Wang, X. Y., Han, Z. P., Zhang, D. X., and Su, C. N. (2016). Comparative mitogenomic analysis of species representing six subfamilies in the family Tenebrionidae. *Int. J. Mol. Sci.* 17:841. doi: 10.3390/ijms17060841

Conflict of Interest: The authors declare that the research was conducted in the absence of any commercial or financial relationships that could be construed as a potential conflict of interest.

Advantages of publishing in Frontiers

OPEN ACCESS
Articles are free to read for greatest visibility and readership

FAST PUBLICATION
Around 90 days from submission to decision

HIGH QUALITY PEER-REVIEW
Rigorous, collaborative, and constructive peer-review

TRANSPARENT PEER-REVIEW
Editors and reviewers acknowledged by name on published articles

Frontiers
Avenue du Tribunal-Fédéral 34
1005 Lausanne | Switzerland

Visit us: www.frontiersin.org
Contact us: frontiersin.org/about/contact

REPRODUCIBILITY OF RESEARCH
Support open data and methods to enhance research reproducibility

DIGITAL PUBLISHING
Articles designed for optimal readership across devices

FOLLOW US
@frontiersin

IMPACT METRICS
Advanced article metrics track visibility across digital media

EXTENSIVE PROMOTION
Marketing and promotion of impactful research

LOOP RESEARCH NETWORK
Our network increases your article's readership